frontiers
RESEARCH TOPICS

# THE NEURAL CIRCUIT FOR SPATIAL REPRESENTATION

Hosted by
Yasser Roudi and Lisa M. Giocomo

frontiers in
NEURAL CIRCUITS

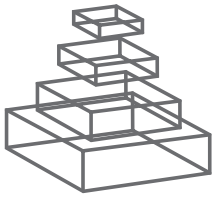

# frontiers




Cover image provided by Ibbl sarl, Lausanne CH

**ISSN** 1664-8714
**ISBN** 978-2-88919-050-8
**DOI** 10.3389/978-2-88919-050-8


## ABOUT FRONTIERS

Frontiers is more than just an open-access publisher of scholarly articles: it is a pioneering approach to the world of academia, radically improving the way scholarly research is managed. The grand vision of Frontiers is a world where all people have an equal opportunity to seek, share and generate knowledge. Frontiers provides immediate and permanent online open access to all its publications, but this alone is not enough to realize our grand goals.

## FRONTIERS JOURNAL SERIES

The Frontiers Journal Series is a multi-tier and interdisciplinary set of open-access, online journals, promising a paradigm shift from the current review, selection and dissemination processes in academic publishing.
All Frontiers journals are driven by researchers for researchers; therefore, they constitute a service to the scholarly community. At the same time, the Frontiers Journal Series operates on a revolutionary invention, the tiered publishing system, initially addressing specific communities of scholars, and gradually climbing up to broader public understanding, thus serving the interests of the lay society, too.

## DEDICATION TO QUALITY

Each Frontiers article is a landmark of the highest quality, thanks to genuinely collaborative interactions between authors and review editors, who include some of the world's best academicians. Research must be certified by peers before entering a stream of knowledge that may eventually reach the public - and shape society; therefore, Frontiers only applies the most rigorous and unbiased reviews.
Frontiers revolutionizes research publishing by freely delivering the most outstanding research, evaluated with no bias from both the academic and social point of view.
By applying the most advanced information technologies, Frontiers is catapulting scholarly publishing into a new generation.

## WHAT ARE FRONTIERS RESEARCH TOPICS?

Frontiers Research Topics are very popular trademarks of the Frontiers Journals Series: they are collections of at least ten articles, all centered on a particular subject. With their unique mix of varied contributions from Original Research to Review Articles, Frontiers Research Topics unify the most influential researchers, the latest key findings and historical advances in a hot research area!
Find out more on how to host your own Frontiers Research Topic or contribute to one as an author by contacting the Frontiers Editorial Office: researchtopics@frontiersin.org

# THE NEURAL CIRCUIT FOR SPATIAL REPRESENTATION

Hosted By:
**Yasser Roudi**, Norwegian University of Science and Technology, Norway
**Lisa M. Giocomo**, Norwegian University of Science and Technology, Norway

How do we find our way? The discovery of medial entorhinal cortex grid cells in 2005 stimulated a wide variety of experimental, theoretical and computational work aimed at elucidating the neural circuit underlying spatial representations in the entorhinal cortex. However, grid cells act in concert with place cells, head direction cells and border cells, each playing a part in the spatial navigation circuit. The aim of this Research Topics is to solicit contributions from leading researchers in the field of spatial navigation and spatial memory to present new experimental data, computational modeling or discussion on mechanisms underlying the neural encoding of space in the parahippocampal cortices.

# Table of Contents

frontiers in
NEURAL CIRCUITS

EDITORIAL
published: 17 August 2012
doi: 10.3389/fncir.2012.00053

# The neural encoding of space in parahippocampal cortices

***Lisa M. Giocomo* and Yasser Roudi***

*Kavli Institute for Systems Neuroscience and Centre for the Biology of Memory, Norwegian University of Science and Technology, Trondheim, Norway*
**Correspondence: giocomo@gmail.com*

***Edited by:***
*Rafael Yuste, Columbia University, USA*

***Reviewed by:***
*Rafael Yuste, Columbia University, USA*

As animals navigate through the environment, they use internal and external sensory cues to update their movements and successfully locate food or nest sites. The rich repertoire of spatial behaviors characteristic of many species has spurred intense research into the neural basis for representing external space. For many years, the mammalian hippocampus has been considered a structure crucial for supporting the creation or storage of spatial information (O'Keefe and Dostrovsky, 1971; Eichenbaum et al., 1999). Yet recent research on other functionally specialized neurons, such as medial entorhinal grid cells, has indicated a wider brain circuit is likely involved in the neurobiology of spatial encoding. Grid cells are neurons that fire in spatially specific locations and form a hexagonal pattern of firing activity that covers the entire environment (Fyhn et al., 2004; Hafting et al., 2005). Despite frequent changes in the animal's running speed and direction, the grid pattern remains periodic, suggesting that the grid population may enable a coordinate system for metric based navigation (Hafting et al., 2005; McNaughton et al., 2006). The discovery of grid cells stimulated a wide variety of experimental and theoretical work aimed at elucidating the neural circuit underlying spatial representations in parahippocampal cortices. In this Research Topic new experimental data, computational modeling, and discussion are presented with a focus on the mechanisms underlying the neural encoding of space. Here, we provide a brief overview of the different types of neurons in the spatial circuit and the relevant context for the papers included in this Topic.

Since the discovery of grid cells, computational modeling has been a key tool in generating hypotheses and theories to explain the origin of periodic and hexagonal firing patterns (For a review see Giocomo et al., 2011; Zilli, 2012). Generally, computational models of grid formation have been grouped into one of two classes; oscillatory interference models and network attractor models. Oscillatory interference models propose that multiple, velocity driven oscillators combine to generate periodic patterns. Attractor network models depend on excitatory or inhibitory recurrent activity and use velocity signals to move a bump of activity across a neural sheet of grid cells. Models in both of these broadly defined categories have significantly evolved since their first inception (O'Keefe and Burgess, 2005; Fuhs and Touretzky, 2006; McNaughton et al., 2006; Burgess et al., 2007) and recent computational models have integrated a combination of elements from oscillatory interference and network attractor classes (see Hasselmo and Brandon, 2012). As computational work on grid cell formation continues to evolve, classification into two broadly defined groups may oversimplify the complexity of various models. As proposed by Zilli (2012), an alternative perspective may be to classify models based on the mechanisms they use to encode, update, and read out position locations.

A prominent feature of grid cells is their spatial scale, which is organized topographically, increasing progressively from dorsal to ventral medial entorhinal cortex (mEC; Hafting et al., 2005). Grid scale is characterized by two spatial measures; the distance between the grid nodes (spacing) and the size of the grid nodes (field size; Hafting et al., 2005). Soon after the discovery of the topographical organization in grid scale, a series of complementary *in vitro* studies described a myriad of biophysical properties which also showed a strong dorsal-ventral organization in mEC (Giocomo et al., 2007; Garden et al., 2008; Giocomo and Hasselmo, 2008; Boehlen et al., 2010 and for a review see Pastoll et al., 2012). The correlative changes in entorhinal cells at the systems and cellular level has resulted in several computational models utilizing single-cell mechanisms to determine the organization of grid scale (Hasselmo et al., 2007; Burgess, 2008; Navratilova et al., 2011). Some versions of oscillatory interference models have focused specifically on the *in vitro* finding that theta band oscillations measured in single mEC neurons decrease in frequency along the dorsal-ventral axis (Giocomo et al., 2007). These oscillatory interference models utilize elements of the intrinsic oscillatory activity, such as the oscillation frequency, to directly determine grid size and spacing. Barry et al. (2012) reviews how a cholinergic decrease in the frequency of theta band oscillations may mediate the expansion of grid scale observed in novel environments (Barry, et al., 2012), an idea supported by *in vitro* slice recordings showing a decrease in the frequency of the theta band resonance after the application of cholinergic agonists (Heys et al., 2010). However, as an alternative or even complementary mechanism, cholinergic activation may induce a change in grid scale by modulating the temporal spiking or integrative properties of layer II mEC neurons (see Pastoll et al., 2012; Yoshida et al., 2012).

Spatial representations are thought to depend not only on grid cells but also on a multitude of other functionally specialized neurons in the parahippocampus. One of these specialized neuronal classes is head direction cells, which respond strongest when an animal faces a particular direction in the environment, irrespective of their behavior or location at the time (Taube et al., 1990; for a review see Clark and Taube, 2012). In mEC, head direction cells exist independently and co-localized with grid cells (Sargolini et al., 2006). This co-localization of head direction signals with grid cells raises the possibility that these

two neural populations may interact to some degree. A paper by Kubie and Fenton (2012) proposes that the head direction signal may support the computation, by grid cells, of serial locations in the direction the animal is facing. While the "prospective coding" modeled by Kubie and Fenton highlights a potential influence of head direction signals onto grid cells, experimental data suggests this relationship may be unidirectional. Whitlock and Derdikman (2012) present new data suggesting that the encoding of direction by head direction cells does not depend on the calculation of position by grid cells. The authors demonstrate that, while the fragmentation of the spatial environment results in a break-down of the hexagonal firing patterns of grid cells, head direction cells retain their preferred tuning direction. The stability of head direction with spatial fragmentation may reflect the hierarchical nature of directional signals, which potentially arise from deep brain structures where vestibular cues, rather than spatial cues, dominate the neural response (see Clark and Taube, 2012).

The apparent flexibility in grid scale under conditions of novelty, experience, or fragmentation of the spatial environment may be reflected by hippocampal place cell signals, which have been proposed as downstream targets for the grid cell output (Solstad et al., 2006). Place cells are neurons in the hippocampus that tend to have higher firing rates when the rat is located in a specific portion of the environment (O'Keefe and Dostrovsky, 1971). Navratilova et al. (2012) presents experimental work showing that the directional selectivity of hippocampal place cells develops with experience. Initially, place cell firing on a linear track is determined by allocentric position. With continued experience however, firing changes to respond to sensory information or behavioral cues, raising the possibility that these place cell representations undergo experience-dependent plasticity.

One way to gain a deeper understanding of how these different spatial signals interact in the parahippocampal circuit is to study and compare their developmental time course. Work in very young animals has already demonstrated that specific features of place cells reach adult levels at an earlier age than grid cells (Langston et al., 2010; Wills et al., 2010). However, once grid cells are present, they contain all of the essential features of the adult grid cell population (Wills et al., 2012). The developmental timeline of place and grid cells is also consistent with new data, in this Topic, suggesting that different types of spatial memories follow dissociated timelines. While memory for objects alone develops at a very young age, memory for more complex associations between objects and spatial locations comes online at a later age (Ainge and Langston, 2012).

This Research Topic provides a unique collection of new data and discussion covering a broad scope of questions aimed at understanding the neural representation of external space. We encourage the reader to sample the full range of articles.

## REFERENCES


Ainge, J. A., and Langston, R. F. (2012). Ontogeny of neural circuits underlying spatial memory in the rat. *Front. Neural Circuits* 6:8. doi: 10.3389/fncir.2012.00008

Barry, C., Heys, J. G., and Hasselmo, M. E. (2012). Possible role of acetylcholine in regulating spatial novelty effects on theta rhythm and grid cells. *Front. Neural Circuits* 6:5. doi: 10.3389/fncir.2012.00005

Boehlen, A., Heinemann, U., and Erchova, I. (2010). The range of intrinsic frequencies represented by medial entorhinal cortex stellate cells extends with age. *J. Neurosci.* 30, 4585–4589.

Burgess, N. (2008). Grid cells and theta as oscillatory interference: theory and predictions. *Hippocampus* 18, 1157–1174.

Burgess, N., Barry, C., and O'Keefe, J. (2007). An oscillatory interference model of grid cell firing. *Hippocampus* 17, 801–812.

Clark, B. J., and Taube, J. S. (2012). Vestibular and attractor network basis of the head direction cell signal in subcortical circuits. *Front. Neural Circuits* 6:7. doi: 10.3389/fncir.2012.00007

Eichenbaum, H., Dudchenko, P., Wood, E., Shapiro, M., and Tanila, H. (1999). The hippocampus, memory, and place cells: is it spatial memory or a memory space. *Neuron* 23, 209–226.

Fuhs, M. C., and Touretzky, D. S. (2006). A spin glass model of path integration in rat medial entorhinal cortex. *J. Neurosci.* 26, 4266–4276.

Fyhn, M., Molden, S., Witter, M. P., Moser, E. I., and Moser, M. B. (2004). Spatial representation in the entorhinal cortex. *Science* 305, 1258–1264.

Garden, D. L., Dodson, P. D., O'Donnell, C., White, M. D., and Nolan, M. F. (2008). Tuning of synaptic integration in the medial entorhinal cortex to the organization of grid cell firing fields. *Neuron* 60, 875–889.

Giocomo, L. M., and Hasselmo, M. E. (2008). Time constants of h current in layer II stellate cells differ along the dorsal to ventral axis of medial entorhinal cortex. *J. Neurosci.* 28, 9414–9425.

Giocomo, L. M., Moser, M. B., and Moser, E. I. (2011). Computational models of grid cells. *Neuron* 71, 589–603.

Giocomo, L. M., Zilli, E. A., Fransen, E., and Hasselmo, M. E. (2007). Temporal frequency of subthreshold oscillations scales with entorhinal grid cell field spacing. *Science* 315, 1719–1722.

Hafting, T., Fyhn, M., Molden, S., Moser, M. B., and Moser, E. I. (2005). Microstructure of a spatial map in the entorhinal cortex. *Nature* 436, 801–806.

Hasselmo, M. E., and Brandon, M. P. (2012). A model combining oscillations and attractor dynamics for generation of grid cell firing. *Front. Neural Circuits* 6:30. doi: 10.3389/fncir.2012.00030

Hasselmo, M. E., Giocomo, L. M., and Zilli, E. A. (2007). Grid cell firing may arise from interference of theta frequency membrane potential oscillations in single neurons. *Hippocampus* 17, 1252–1271.

Heys, J. G., Giocomo, L. M., and Hasselmo, M. E. (2010). Cholinergic modulation of the resonance properties of stellate cells in layer II of medial entorhinal cortex. *J. Neurophysiol.* 104, 258–270.

Kubie, J. L., and Fenton, A. A. (2012). Linear look-ahead in conjunctive cells: an entorhinal mechanism for vector-based navigation. *Front. Neural Circuits* 6:20. doi: 10.3389/fncir.2012.00020

Langston, R. F., Ainge, J. A., Couey, J. J., Canto, C. B., Bjerknes, T. L., Witter, M. P., Moser, E. I., and Moser, M. B. (2010). Development of the spatial representation system in the rat. *Science* 328, 1576–1580.

McNaughton, B. L., Battaglia, F. P., Jensen, O., Moser, E. I., and Moser, M. B. (2006). Path integration and the neural basis of the "cognitive map." *Nat. Rev. Neurosci.* 7, 663–678.

Navratilova, Z., Giocomo, L. M., Fellous, J. M., Hasselmo, M. E., and McNaughton, B. L. (2011). Phase precession and variable spatial scaling in a periodic attractor map model of medial entorhinal grid cells with realistic after-spike dynamics. *Hippocampus* 22, 772–789.

Navratilova, Z., Hoang, L. T., Schwindel, C. D., Tatsuno, M., and McNaughton, B. L. (2012). Experience-dependent firing rate remapping generates directional selectivity in hippocampal place cells. *Front. Neural Circuits* 6:6. doi: 10.3389/fncir.2012.00006

O'Keefe, J., and Burgess, N. (2005). Dual phase and rate coding in hippocampal place cells: theoretical significance and relationship to entorhinal grid cells. *Hippocampus* 15, 853–866.

O'Keefe, J., and Dostrovsky, J. (1971). The hippocampus as a spatial map. Preliminary evidence from unit activity in the freely-moving rat. *Brain Res.* 34, 171–175.

Pastoll, H., Ramsden, H. L., and Nolan, M. F. (2012). Intrinsic electrophysiological properties of entrohinal cortex stellate cells and their contribution to grid cell firing fields. *Front. Neural Circuits* 6:17. doi: 10.3389/fncir.2012.00017

Sargolini, F., Fyhn, M., Hafting, T., McNaughton, B. L., Witter, M. P.,

Moser, M. B., and Moser, E. I. (2006). Conjunctive representation of position, direction, and velocity in entorhinal cortex. *Science* 312, 758–762.

Solstad,T., Moser, E. I., and Einvoll, G. T. (2006). From grid cells to place cells: a mathematical model. *Hippocampus* 16, 1026–1031.

Taube, J. S., Muller, R. U., and Ranck, J. B. J. (1990). Head-direction cells recorded from the postsubiculum in freely moving rats. I. Description and quantitative analysis. *J. Neurosci.* 10, 420–435.

Whitlock, J. R., and Derdikman, D. (2012). Head direction maps remain stable despite grid map fragmentation. *Front. Neural Circuits* 6:9. doi: 10.3389/fncir.2012.00009

Wills, T. J., Barry, C., and Cacucchi, F. (2012). The abrupt development of adult-like grid firing in the medial entorhinal cortex. *Front. Neural Circuits* 6:21. doi: 10.3389/fncir.2012.00021

Wills, T. J., Cacucci, F., Burgess, N., and O'Keefe, J. (2010). Development of the hippocampal cognitive map in preweanling rats. *Science* 328, 1573–1576.

Yoshida, M., Knauer, B., and Jochems, A. (2012). Cholinergic modulation of the CAN current may adjust neural dynamics for active memory maintenance, spatial navigation and time-compressed replay. *Front. Neural Circuits* 6:10. doi: 10.3389/fncir. 2012.00010

Zilli, E. A. (2012). Models of grid cell spatial firing published 2005–2011. *Front. Neural Circuits* 6:16. doi: 10.3389/fncir.2012.00016

*Received: 28 June 2012; accepted: 27 July 2012; published online: 17 August 2012.*
*Citation: Giocomo LM and Roudi Y (2012) The neural encoding of space in parahippocampal cortices. Front. Neural Circuits* ***6****:53. doi: 10.3389/fncir.2012.00053*

frontiers in
NEURAL CIRCUITS

REVIEW ARTICLE
published: 18 April 2012
doi: 10.3389/fncir.2012.00016

# Models of grid cell spatial firing published 2005–2011

***Eric A. Zilli****

*Department of Psychology, Center for Memory and Brain, Boston University, Boston, MA, USA*

***Edited by:***
*Yasser Roudi, Norwegian University of Science and Technology, Norway*

***Reviewed by:***
*Nestor Parga, Columbia University, USA*
*Yoram Burak, Harvard University, USA*

****Correspondence:***
*Eric A. Zilli, Department of Psychology, Center for Memory and Brain, Boston University, 2 Cummington Street, Boston, MA 02215, USA.*
*e-mail: zilli@bu.edu*

Since the discovery of grid cells in rat entorhinal cortex, many models of their hexagonally arrayed spatial firing fields have been suggested. We review the models and organize them according to the mechanisms they use to encode position, update the positional code, read it out in the spatial grid pattern, and learn any patterned synaptic connections needed. We mention biological implementations of the models, but focus on the models on Marr's algorithmic level, where they are not things to individually prove or disprove, but rather are a valuable collection of metaphors of the grid cell system for guiding research that are all likely true to some degree, with each simply emphasizing different aspects of the system. For the convenience of interested researchers, MATLAB implementations of the discussed grid cell models are provided at ModelDB accession 144006 or http://people.bu.edu/zilli/gridmodels.html.

**Keywords: medial temporal lobe, path integration, place cell, ring attractor, self-organization**

## 1. INTRODUCTION

The puzzling grid cell has become a popular topic in neuroscience due to its simultaneously simple behavioral firing correlate (the animal's position) and complex spatial activity (a nearly regular hexagonal arrangement of spatial fields; **Figure 1**).

From their spatial-coordinate–like appearance, persistence in darkness, head direction preference (in a subset of grid cells), and anatomical position in the medial temporal lobe (Hafting et al., 2005; Sargolini et al., 2006), all accounts of the hexagonal firing pattern assume grid cell firing is a function of the animal's internal sense of its position. Most models specifically assume the grid cells are performing or reflecting path integration: the process of continuously updating an estimate of position with each movement made (McNaughton et al., 1996; Redish, 1999; Etienne and Jeffery, 2004). The current models of the hexagonal field arrangement therefore all start with path integration and then translate the path integrated information into the grid pattern through additional trickery (e.g., modifying the path integration mechanism to produce a hexagonal grid as a side effect or path integrating along directions in 60° or 120° increments and combining the separate integrated positions into a hexagonal pattern).

Existing grid cell models use a variety of different mechanisms, but similarities among models have led to a rough classification scheme (Burgess et al., 2007; Burgess, 2008; Giocomo and Hasselmo, 2008; Jeewajee et al., 2008; Kropff and Treves, 2008; Moser and Moser, 2008; Welinder et al., 2008; Burak and Fiete, 2009; Zilli et al., 2009; Milford et al., 2010; Zilli and Hasselmo, 2010; Giocomo et al., 2011; Yartsev et al., 2011; Mhatre et al., 2012) into the groups of continuous attractor network (CAN) models or of interference models, with some suggesting the true mechanism may involve both (Burgess, 2008; Hasselmo, 2008; Jeewajee et al., 2008). This terminology is somewhat misleading, though. For example, a number of models (Blair et al., 2007, 2008; Welday et al., 2011; Mhatre et al., 2012) use both CANs as well as the mechanism of interference (and see Discussion). The models can be better understood and compared when considered in terms of their subcomponents:

- How is the positional information encoded and maintained?
- How is the positional information updated when the animal moves?
- How is the encoded information read out as a hexagonal spatial pattern?
- How do any structured synaptic connections in the model self-organize?

As an example, Burgess et al. (2007) encoded positional information as the phase difference between oscillators, updated that position by modulating the oscillator frequencies, and used temporal interference to read that code out into the grid pattern. In these terms the space of models described in the literature becomes much clearer. For example, CANs are mechanisms for encoding and maintaining positional information, whereas interference is a read-out mechanism, so strictly the two are independent properties of a model.

Information-processing tasks (e.g., path integration) can be understood on multiple levels, three of which were emphasized by Marr (1982). On the highest level, tasks can be characterized by their goal (e.g., accumulate spatial displacements). A system can also be characterized by the way it represents the relevant data (e.g., phase differences, population activity patterns, etc.) and the algorithm that transforms the data (e.g., frequency modulation). Finally, a system has an implementation, mapping the representation and algorithm to physical systems. **Tables 1** and **2** summarize the models with respect to the subcomponents above on the algorithmic and implementational levels, respectively. Though not all models fit perfectly into this system nor do all publications attempt to examine each of these aspects, this approach allows a useful overview of the field.

Below we discuss current approaches to the above questions before discussing each of the individual models. We hope our

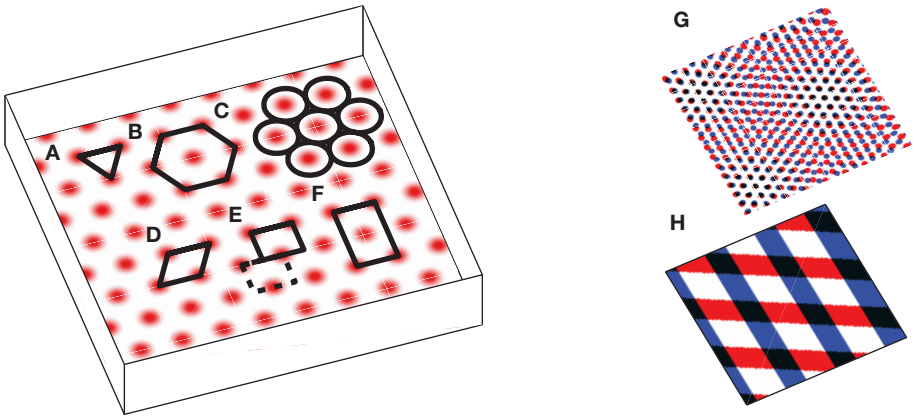


**FIGURE 1 | The grid cell spatial pattern.** Different descriptions of the grid suggest different underlying mechanisms. The simplest descriptions as **(A)** an equilateral triangular tessellation or **(B)** a hexagonal grid suggest no obvious mechanism. **(C)** The pattern can be thought of as inactivity-surrounded place fields packed as closely as possible, which leads to Kropff and Treves (2008). Alternatively, the regularity of the pattern suggests that perhaps only a small segment, e.g., **(D)** a rhombus (skewed rectangle) or a rectangle large enough for **(E)** only one or **(F)** two or more appropriately spaced fields, is represented and when the animal walks off the segment it re-enters from the other side. If a rectangle containing only one field is used, it must be twisted so that walking off the bottom on the left brings the animal to the top on the right (the top edge is shifted by half its width, see dashed rectangle), while walking off the left or right sides wraps around normally. The grid can also be thought of as the overlap or interference between other spatial patterns, such as **(G)** smaller scale grids or **(H)** sinusoid-like gratings, not unlike a Fourier decomposition of the grid, and this produces the temporal interference models when generalized to the temporal domain. Note that in all figures spatial plots are shown in perspective to distinguish them from 2D plots of neural activities or synaptic weights.

tight focus on model mechanisms complements other recent reviews (e.g., Welinder et al., 2008; Giocomo et al., 2011) that considered wider ranges of grid cell topics. For the convenience of interested researchers, we have also implemented in MATLAB most of the models of grid cells we are aware of and have shared them as a collection at ModelDB accession 144006 or http://people.bu.edu/zilli/gridmodels.html

## 2. RESULTS

### 2.1. ENCODING POSITIONS

The starting point of all path integration models is a mechanism that allows neurons to represent and maintain a spatial position. These mechanisms can be divided into those that independently represent 1D positions and recombine them to form the 2D grid (linear-coding: Burgess et al., 2007; Gaussier et al., 2007; Giocomo et al., 2007; Blair et al., 2008; Burgess, 2008; Hasselmo, 2008; Hasselmo and Brandon, 2008; Zilli and Hasselmo, 2010; Welday et al., 2011; Mhatre et al., 2012) and those that directly represent 2D positions (planar-coding: Conklin and Eliasmith, 2005; O'Keefe and Burgess, 2005; Fuhs and Touretzky, 2006; McNaughton et al., 2006; Blair et al., 2007; Guanella et al., 2007; Kropff and Treves, 2008; Burak and Fiete, 2009; Navratilova et al., 2012). So far these suffice since grid cells seem to ignore height in simple 3D environments (Hayman et al., 2011).

#### *2.1.1. Linear-coding*

We first examine ways 1D positions can be encoded.

Perhaps the most obvious way of encoding a linear position is as a coordinate in a single cell's firing rate. This mechanism was used by Gaussier et al. (2007) and Hasselmo and Brandon (2008), where respective scaling factors $\alpha$ or $\beta$ Hz/cm translated distance moved along a cell's preferred direction into a change in its firing rate. An advantage to directly storing distances from the starting position is that the return vector to the starting position can be easily calculated (e.g., Burgess et al., 1993; Touretzky et al., 1993; Hasselmo and Brandon, 2008), but since coordinates can be arbitrarily large (or negative) while cells can only fire over a limited frequency range, most models represent position less explicitly.

On linear tracks, grid cells have fairly regular field spacing (Brun et al., 2008). The fields seem to repeat endlessly so the animal's 1D location can be encoded as a single number that gives its position relative to the nearest field (**Figure 2A**, top). Such a position is conveniently described in circular terms as a phase (an angle) in radians or degrees. A number of mechanisms for storing a phase have been used in grid cell models.

A ring attractor is a CAN of neurons arranged in a circle, like the hours on an analog clock (illustrated in **Figure 2A**). In a simple ring attractor, any cell (e.g., 6 o'clock) strongly excites nearby cells (e.g., 4, 5, 7, and 8 o'clock) and weakly excites or even inhibits distant cells (e.g., 12 o'clock). When a small group of nearby cells is active (e.g., 6 and 7 o'clock) we call it a bump of activity. The cells mutually excite each other to continue firing while inhibiting the rest of the cells and so can store any phase value indefinitely by maintaining a bump of activity on the ring at that phase. We call this an unbiased ring attractor. Though our example used only one bump of activity, a larger network could easily support multiple bumps spaced out over the cells (see below and **Figure 2B**).

If the strongest output from each cell were systematically shifted in one direction, we could call it a biased ring attractor, cyclic attractor (Eliasmith, 2005), or ring oscillator (Blair et al., 2008). The bias causes the bump of activity to rotate around the ring at a fixed frequency that depends on the size of the network and the distance the peak output is shifted (Zhang, 1996). This asymmetry in

**Table 1 | The models on Marr's algorithmic level.**

| Grid cell model | Position representation | Updating mechanism | Read-out mechanism | Learning mechanism |
|---|---|---|---|---|
| Conklin and Eliasmith (2005) | Torus attractor, single bump | Direction-conjunctive cells | Direct | – |
| O'Keefe and Burgess (2005) | [Torus attractor, single bump] | [Direction-modulated recurrent connections] | Direct | – |
| Fuhs and Touretzky (2006) | Aperiodic attractor, multi-bump | Direction-conjunctive cells | Direct | Wave packets in development for symmetric weights |
| McNaughton et al. (2006) | [Torus attractor, single bump] | [Direction-conjunctive cells] | Direct | Learn toroidal topology through grid pattern in a teaching layer |
| Blair et al. (2007) | [Theta grids] | – | Spatial interference | – |
| Burgess et al. (2007) | Sinusoid phase difference | Frequency modulation | Temporal interference | [Self-organization of directional velocity to oscillators] |
| Gaussier et al. (2007) | Firing rates as coordinates | Firing rate modulation | Spatial interference | Self-organization of stripe cell spatial phases to grid cells |
| Giocomo et al. (2007) | Sinusoid phase difference | Frequency modulation | Temporal interference | – |
| Guanella et al. (2007) | Twisted-torus attractor, single bump | Dynamic recurrent connections | Direct | – |
| Blair et al. (2008) | [Biased ring attractor phase difference] | [Direction-conjunctive cells] | Temporal interference | – |
| Burgess (2008) | Sinusoid phase difference | Frequency modulation | Temporal interference | – |
| Hasselmo (2008) | Sinusoid phase difference | Frequency modulation | Temporal interference | – |
| Hasselmo and Brandon (2008) | Firing rate | Frequency modulation | Spatial interference | – |
| Kropff and Treves (2008) | Place cells | [Place cell updating] | Direct via place-to-grid synapses | Self-organization of place Cell inputs |
| Burak and Fiete (2009) | Torus and aperiodic attractors, multi-bump | Direction-conjunctive cells | Direct | – |
| Mhatre et al. (2012) | [Unbiased ring attractor] | [Direction-conjunctive cells] | Spatial interference | Self-organization of stripe cell spatial phases and orientations to grid cells |
| Zilli and Hasselmo (2010) | Spiking population phase difference | Spiking frequency modulation | Temporal interference | – |
| Navratilova et al. (2012) | Unbiased ring attractor | Direction-conjunctive cells | Direct or spatial interference | – |
| Welday et al. (2011) | [Biased ring attractor phase difference] | [Direction-conjunctive cells] | Temporal interference | – |

*"–" Indicates no specific mechanism given in reference. Gray rows are planar-coding models, white linear-coding. Square brackets indicate the mechanism was suggested but not simulated.*

the synaptic connections turns the network into an oscillator and so precludes storing a phase as a fixed bump of activity. Instead, a pair of biased ring attractors with identical frequencies can be used to store a phase in the difference between the phases of the rings (Blair et al., 2008). As the bumps move in the same direction and speed, the networks can maintain the phase difference indefinitely (**Figure 2**).

This mechanism of storing a phase with a pair of identical oscillators works with any oscillator imaginable (**Figure 2A**) as long as the oscillator can precisely and indefinitely maintain a specified frequency. Some early grid models (Burgess et al., 2007; Giocomo et al., 2007) interpreted the model oscillations as narrow-band oscillations in a cell's membrane potential or in the local field potential (LFP; e.g., theta rhythm), though they were modeled abstractly as sinusoids. Other approaches manipulated the sinusoids to treat them as a rough approximation of repeating single spikes or burst of spikes (Burgess, 2008; Hasselmo, 2008). Unfortunately, data suggest biological oscillators like these are highly irregular (Welinder et al., 2008; Zilli et al., 2009; Dodson et al., 2011) and so unsuited for use in these models. One solution to this problem used synchronized networks of coupled, noisy, spiking neurons, which produce much more regular oscillations on the population level (Zilli and Hasselmo, 2010).

Using any of these mechanisms, a linear position can be represented neurally, but these mechanisms cannot represent a 2D position, which requires storing at least two values. Instead, to represent 2D positions, two or more independent linear-coding mechanisms can be used to encode linear position along two different directions (**Figure 2B**, top), requiring a read-out stage as described below.

An alternative is provided by planar-coding models.

**Table 2 | The models' biological implementations, though somewhat arbitrary, allow for concrete experimental predictions.**

| Grid cell model | Position representation | Updating mechanism | Read-out mechanism |
|---|---|---|---|
| Conklin and Eliasmith (2005) | [Subiculum or MEC population activity] | [Excitatory and inhibitory recurrents] | Direct |
| O'Keefe and Burgess (2005) | [MEC population activity] | [Head direction modulated weights or direction conjunctive cells] | Direct |
| Fuhs and Touretzky (2006) | [Dorsal MEC population activity] | [Inhibitory recurrents] | Direct |
| McNaughton et al. (2006) | [Dorsal MEC population activity] | [Head direction and grid conjunctive cells] | Direct |
| Blair et al. (2007) | [Mammillary complex population activity] | – | Interfering inputs to grid cell |
| Burgess et al. (2007) | MECII stellate dendritic SMPOs vs. theta-rhythmic MS input phase differences | Body velocity/voltage-dependent SMPO frequency | Interference in soma |
| " | MECII stellate somatic SMPO vs. theta-rhythmic MS input phase difference | " | Synapses among band cells create grid cells |
| Gaussier et al. (2007) | [Retrosplenial or parietal spiking activity] | – | Interfering inputs to grid cell |
| Giocomo et al. (2007) | MECII stellate dendritic vs. somatic SMPO phase differences | Body velocity/voltage-dependent SMPO frequency | Interference in soma |
| Guanella et al. (2007) | [MEC population activity] | [Velocity-modulated excit. and inhib. recurrents] | Direct |
| Blair et al. (2008) | Theta cells in raphe nuclei, mammillary bodies | [Body-direction-conjunctive cells] | Interfering inputs to grid cell |
| Burgess (2008) | MECII stellate or MECV pyramidal somatic vs. dendritic SMPO phase differences | Body velocity/voltage-dependent SMPO or spiking frequency | Interfering inputs to soma |
| " | MECII stellate or MECV pyramidal spiking vs. [theta-rhythmic input] phase differences | " | Interference in ECIII pyramidals |
| Hasselmo (2008) | ECV pyramidal spiking phase differences | Body–velocity–dependent spiking frequency | Interfering inputs to grid cell |
| Hasselmo and Brandon (2008) | ECII pyramidal firing rates | Body velocity/$Ca^{2+}$-dependent spiking frequency | Interfering inputs to grid cell |
| Kropff and Treves (2008) | [CA1 place cells, MECV/VI grid cells] | – | Direct via CA1 to MEC projection |
| Burak and Fiete (2009) | [MEC population activity] | [Inhibitory recurrents] | Direct |
| Mhatre et al. (2012) | [ECII, III, V/VI population activities] | [ECIII to ECII synaptic connections] | Interfering inputs to grid cell |
| Zilli and Hasselmo (2010) | [Spiking neurons] | [Velocity-modulated firing rate] | Interfering inputs to grid cell |
| Navratilova et al. (2012) | ECII stellate, ECIII pyramidal population activities | ECIII to ECII synaptic connections | Direct or interfering inputs to grid cell |
| Welday et al. (2011) | Theta cells in medial septum, hippocampus, and anterior thalamus | – | Interfering inputs to grid cell |

*"–" Indicates no specific implementation given in reference. Gray rows are planar-coding models, white linear-coding. [Square brackets indicate a mechanism not specifically identified with a known cell type, synaptic connection, etc. below the level of e.g. a grid cell in a general region.] MECII, medial entorhinal cortex layer II; MS, medial septum; SMPO, subthreshold membrane potential oscillation.*

#### *2.1.2. Planar-coding*

The planar-coding models represent the 2D position directly within one population of cells.

The simplest way of encoding a 2D position is through a Cartesian coordinate $(x, y)$. A natural neural code for specific $(x, y)$ positions is provided by the place cell: a cell that is nearly silent in all locations except in its place field, a small region of the environment where it fires at an elevated rate (O'Keefe, 1976; Skaggs et al., 1996). Place cells are used as the position code in Kropff and Treves (2008), the only non-path-integrating model of grid cells (though place cells could be driven by path integration).

Since grid cells themselves appear to code 2D positions, Blair et al. (2007) used high–spatial-frequency grid cells (**Figure 1H**) to encode and maintain 2D positional information. While they reported interesting results, using grid cells to produce grid cells somewhat lacks in explanatory power.

Just as 1D positions are identified with respect to the nearest two grid fields, 2D positions only need to be encoded in terms of position within, e.g., a rhombus whose corners are four adjacent fields (**Figure 1D**). So by analogy with an unbiased ring attractor in the linear-coding case, a 2D position can be encoded as a bump on a rectangular sheet of cells (Zhang, 1996; Samsonovich

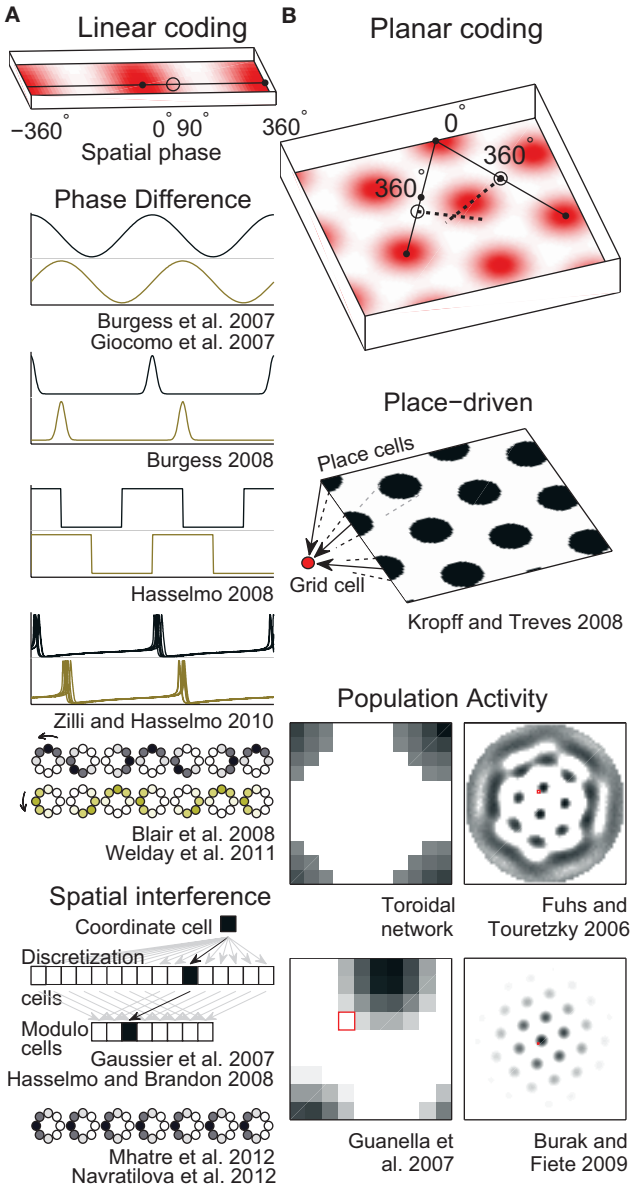


**FIGURE 2 | Spatial position codes. (A)** Linear-coding models. Top. A linear track environment with three grid fields. Positions can be identified as a spatial phase between 0° in the center of one field and 360° (0°) at neighboring fields. One-quarter of the distance between the field centers, 90°, is indicated. Some models (Burgess et al., 2007; Giocomo et al., 2007; Blair et al., 2008; Burgess, 2008; Hasselmo, 2008; Zilli and Hasselmo, 2010; Welday et al., 2011) store the 90° linear position as a 90° phase difference between two oscillators. An unbiased (stationary) ring attractor (Mhatre et al., 2012; Navratilova et al., 2012) can also directly store the 90° phase as a bump of activity centered on cells in the ring at a corresponding angle. Instead of encoding position as a phase, the animal's actual position or coordinate could be stored as the firing rate of a single cell (Gaussier et al., 2007). Hasselmo and Brandon (2008) described one model using only coordinate cells and another using only modulo cells. **(B)** Top. A square environment with many grid fields. Linear-coding models can encode 2D positions as two spatial phases, now measured between rows of grids, not neighboring grid fields (so only alternate 0° points are field centers). For example, a position at 0° along one direction and 90° along the other is *(Continued)*

**FIGURE 2 | Continued**
indicated. Alternatively, place cells can represent 2D positions (Kropff and Treves, 2008) or a 2D position can be represented by the relative position of a fixed activity pattern on a sheet of cells (Fuhs and Touretzky, 2006; Guanella et al., 2007; Burak and Fiete, 2009). Early toroidal models, however, would produce a rectangular rather than a hexagonal grid. In continuous attractor network models each circle (Blair et al., 2008; Mhatre et al., 2012; Navratilova et al., 2012) or pixel (Fuhs and Touretzky, 2006; Guanella et al., 2007; Burak and Fiete, 2009) represents one cell and darker colors indicate higher activities. Red squares on the right indicate one cell that might produce the grid fields shown in the spatial environment.

and McNaughton, 1997; Conklin and Eliasmith, 2005; O'Keefe and Burgess, 2005; McNaughton et al., 2006; Guanella et al., 2007; **Figure 2B**, right). Just as the ring attractor is essentially a string of cells with the ends connected to each other, the bump on the 2D sheet must be allowed to move off one edge of the sheet and reappear on the opposite edge.

A 2D sheet with opposite edges connected in this manner is called a torus. Such a network will generally produce rectangular, not hexagonal patterns. One solution (Guanella et al., 2007) that produces a hexagonal pattern is to twist the torus in such a way that the edges wrap around normally in one direction (e.g., left/right), but when a bump moves past, e.g., the top edge, it reappears on the bottom edge shifted by half the width of the torus (see **Figures 1E** and **2B**, bottom). Strictly, though, this twist is not necessary and a normal torus can produce the hexagonal pattern if the velocity inputs are skewed (see below and our online model code for an example).

Rather than encoding position with a single bump of activity, a sheet of cells can maintain multiple bumps of activity, **Figure 2B**, arrayed hexagonally on the sheet of cells like each grid cell's fields in space (Fuhs and Touretzky, 2006; Burak and Fiete, 2009). A cell's adjacent fields occur not because a bump of activity wraps around one edge and returns to the cell, but rather because while the first bump moves off behind the cell, another bump comes from ahead. Bumps moving off one edge simply disappear while new bumps are created at the opposite edge. For this reason, a multi-bump CAN can produce the hexagonally arrayed fields without the need for synaptic connections wrapping around the edges. This is called an aperiodic network.

A multi-bump 2D CAN can also produce a hexagonal grid on an untwisted torus (a periodic network). In that case the bump spacing must be consistent with the size of the torus (Burak and Fiete, 2009).

### 2.2. UPDATING

With the above mechanisms a position can be represented and maintained, but the key to path integration is updating that representation of position as an animal moves from one place to another. In all models except (Kropff and Treves, 2008), changes in position are provided as a body velocity signal. Guanella et al. (2007) uses the 2D velocity signal directly, but the other models first pre-process 2D velocity into 1D directional velocity signals. The directional velocity $v_\phi(t)$ along a preferred direction $\phi$ is defined as $v_\phi(t) = s(t)\cos(d(t) - \phi)$, where $s(t)$ and $d(t)$ are the animal's speed and direction at time $t$. Linear-coding models

usually use two to six of these directional velocity inputs with preferred directions at increments of 60° or 120°, while planar-coding models generally assume four inputs at 90° increments (but would work with as few as three at 120° or up to a continuous distribution of all directions). Clear directional body velocity signals have not yet been found (but see Welday et al., 2011), but an analogous representation of reaching movements has been reported (Kalaska et al., 1983; van Hemmen and Schwartz, 2008).

Each mechanism for representing position has a corresponding updating mechanism. For example, since position is the integral of velocity, a cell that maintains a position in its firing rate can update its encoded position by perfectly integrating its velocity input.

If two oscillators encode a phase difference (e.g., oscillator A is 90° ahead of oscillator B), the phase difference can be modified by momentarily changing the frequency of either or both oscillators. Generally oscillator A is an active oscillator whose frequency can change and oscillator B is a baseline oscillator whose frequency never changes. An oscillator's frequency $w$ is the rate of change of its phase $\phi$, or $\mathrm{d}\phi/\mathrm{d}t = w$, so, given two oscillators, the derivative of the encoded position (their phase difference) is the difference in their frequencies: $\mathrm{d}(\phi_1 - \phi_2)/\mathrm{d}t = \mathrm{d}\phi_1/\mathrm{d}t - \mathrm{d}\phi_2/\mathrm{d}t = w_1 - w_2$. If $w_1 - w_2$ is always proportional to an animal's speed in some direction, then $\phi_1 - \phi_2$ is proportional to its distance moved in that direction, which is the basis for path integration in these models.

The exact mechanism for modulating an oscillator's frequency depends on the nature of the oscillator. The frequency of abstract oscillators like sinusoids can be controlled directly. When the oscillator is a network of cells, changing the level of injected current or synaptic inputs to the cells will cause their firing frequency to increase or decrease. In a biased ring attractor, the frequency is related to the amount of bias (the distance of the offset in the synaptic weights) and the activity level of the biased cells, and either can be changed to control the frequency.

In unbiased attractor networks, balanced symmetric connectivity maintains a position as a bump of activity in a fixed location, so, to update the stored position, the velocity inputs must introduce a bias to shift the bump in the desired direction. Broadly this has been done in two ways.

Guanella et al. (2007) gave a simple solution to this problem. In their model the synaptic output resembles the unbiased attractor weight matrix given above when the animal stands still (**Figure 3**). Each cell's output is centered on itself, so the bump is stationary. When the animal moves, the network becomes biased: the weight matrix changes dynamically so that the output of each cell is shifted in a direction according to the animal's movement direction and by a distance proportional to the animal's speed. When the animal moves north, all cells shift their output in the north direction on the sheet (**Figure 3**, right) and the bump begins to move in that direction. Dynamically changing the weights this way is an effective but seemingly biologically implausible mechanism. With this mechanism cells do not have a fixed preferred direction (they are pure grid cells).

A more common and biologically plausible solution used in other grid cell models (O'Keefe and Burgess, 2005; Fuhs and Touretzky, 2006; McNaughton et al., 2006; Burak and Fiete, 2009; Navratilova et al., 2012) assigns a directional velocity input to some or all cells in the network, producing direction-conjunctive grid cells. The synaptic outputs of a conjunctive cell have a shift in a corresponding direction: the same or opposite direction, depending on whether the output is respectively excitatory (Navratilova et al., 2012) or inhibitory (Fuhs and Touretzky, 2006; Burak and Fiete, 2009), **Figure 3**. While standing still the velocity inputs to all cells are equal, so the synaptic output is symmetrical and the bump remains stationary. When velocity input increases to a subset of cells, their relative influence on the synaptic activity in the network increases, producing a momentarily biased network and allowing the network to path integrate. Two more-or-less equivalent variations of this mechanism are used: one simple arrangement (O'Keefe and Burgess, 2005; McNaughton et al., 2006; Navratilova et al., 2012) considers the pure grid cells as one population and assumes the existence of separate, parallel populations of conjunctive cells that are interconnected with the grid cells and responsible for shifting the pattern about. The other models (Fuhs and Touretzky, 2006; Burak and Fiete, 2009) do away with the pure grid cells and simply interconnect the conjunctive populations into one large network.

### 2.3. READ-OUT

With the previously discussed mechanisms, an animal's movements can be integrated into a running estimate of its position, and presumably this information is sent to many areas of the brain to support many processes, but our current interest is the way the information comes to appear as a hexagonal arrangement of spatial fields.

In Kropff and Treves (2008), the read-out mechanism is particularly simple: synaptic connections from place cells with fields arranged in a hexagonal grid directly drive a common grid cell.

In the 2D CAN models (Conklin and Eliasmith, 2005; O'Keefe and Burgess, 2005; Fuhs and Touretzky, 2006; McNaughton et al., 2006; Guanella et al., 2007; Burak and Fiete, 2009; Navratilova et al., 2012), the spatial grid pattern is a direct consequence of the positional code and no transformation is needed: the bump(s) of activity simply move in concert with the animal's movements, and the networks are shaped so that bumps activate any given cell when the animal enters positions arranged in a hexagonal pattern.

The other models, however, break up the encoding of position into multiple networks, and these must be recombined with a read-out mechanism to produce the hexagonal field arrangement. Blair et al. (2007), for instance, stored a 2D position in multiple grid networks and, in a process of spatial interference, produced a larger scale grid pattern where the smaller grids overlap (**Figure 1H**). This is a planar-coding model, so the read-out is not needed to produce a 2D pattern *per se*, but rather to produce one of the necessary scale.

Read-out is mandatory, however, to produce a 2D hexagonal pattern in a linear-coding model. In such models the grid pattern is irrelevant to path integration and occurs as just one of many ways the encoded position may be read-out (Welday et al., 2011). Some models (Burgess et al., 2007; Gaussier et al., 2007; Hasselmo and Brandon, 2008; Mhatre et al., 2012) contain stripe or band cells (**Figure 1G**) that in 1D could look like repeating fields, but their firing pattern is clearly striped rather than a grid in 2D environments. However, when two or more of these patterns at 60° angles are overlaid, their intersections produce a 2D hexagonal grid. This is essentially the same process of spatial interference as

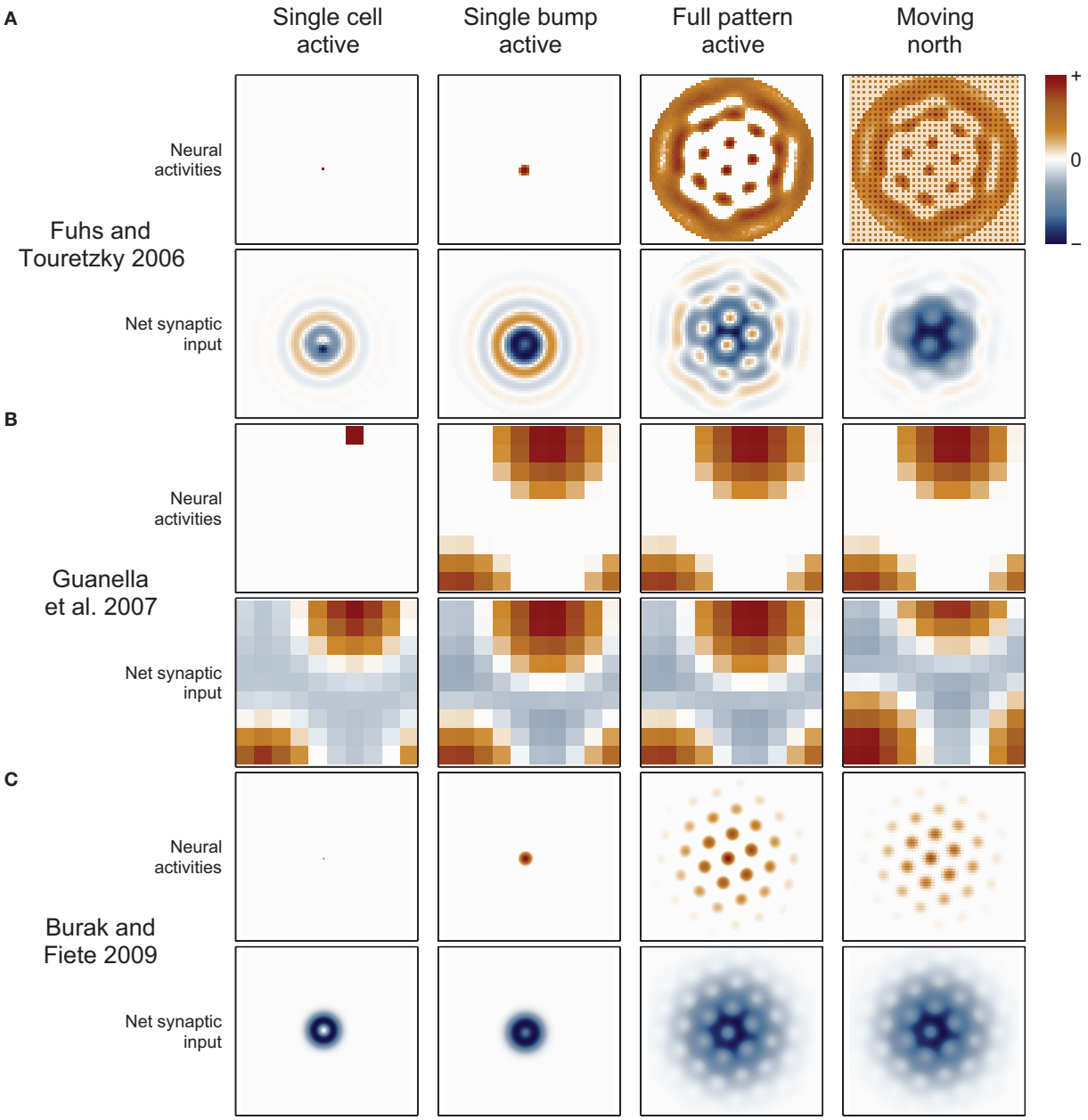


**FIGURE 3 | Synaptic connections play a major role in continuous attractor networks.** For each of three 2D attractor models, we plot the activity of the sheet of neurons (top in each row) and the synaptic input to each cell caused by that activity (bottom in each row). **(A)** Each cell in the Fuhs and Touretzky (2006) model projects symmetrically outward in alternating rings of excitatory and inhibitory synapses. Just offset from the center, in this case downward, is an asymmetric inhibitory region (dark blue). When this cell fires, it inhibits the nearby cells except in a small region just above it where other cells are free to fire. Cells have different offset directions, so a bump of activity can form in a small group of cells that each inhibit a different direction around the bump, surrounding it in a ring of inhibition. All the cells here are driven to fire, creating new bumps spontaneously, and the excitatory ring surrounded by inhibition on each side encourages the new bumps to maintain a particular spacing. When the animal moves north, north-conjunctive cells increase in activity (producing the checker boarding of activity), increasing the inhibition on one side of each bump and causing the pattern to shift. **(B)** In Guanella et al. (2007) each cell has an identical synaptic output: an excitatory Gaussian bump that is inhibitory at long distances. The model has only one bump of activity, which wraps around on all sides, but with a "twist" in the up-down direction (see **Figure 1A**). The synapses change dynamically with velocity: e.g., when moving north the synaptic output is offset upward on the sheet of cells, which causes the bump to slide in that direction. **(C)** In Burak and Fiete (2009) the output of each cell is a ring of inhibition, the center offset in the direction the cell tries to move activity bumps (in this case offset two cells upward). The space inside the ring allows a bump to form, each active cell contributing to a strong ring of inhibition around the bump. The cells are driven to fire spontaneously so as many bumps form as is possible. Under the repulsive effects of the inhibitory rings, the bumps pack as tightly as possible, which is in a hexagonal grid. While moving north, north-conjunctive cells are driven strongly, slightly shifting the pattern of the synaptic drive and so shifting the bumps as well.

in Blair et al. (2007). A natural neural implementation of spatial interference is given by the thresholded sum of inputs from the cells producing the stripes or grids (and see **Figure 4**).

Temporal interference is another commonly used mechanism (Burgess et al., 2007; Giocomo et al., 2007; Blair et al., 2008; Burgess, 2008; Hasselmo, 2008; Zilli and Hasselmo, 2010; Welday et al., 2011). Whereas in spatial interference models, the grid cell inputs are either active or inactive at any time, in temporal interference models the inputs are always active (they fire at all locations) but their spike timing changes with respect to a baseline oscillation as a function of position. In these models the grid cell must become active when all of the inputs are sufficiently close in time to the baseline. In particular, grid field width is usually around one-half the field spacing, so the cell must fire when all active oscillators are within 90° of the baseline. Any mechanism that can perform this sort of coincidence detection will work. In the more abstract models (Burgess et al., 2007; Blair et al., 2008; Burgess, 2008; Hasselmo, 2008), various combinations of multiplying, adding, and thresholding the various inputs have been used successfully (**Figure 4**). A more realistically modeled grid cell must spike to reflect coincidence detection of its synaptic inputs, which can be can be difficult to carry out over an extended window with three or more inputs (two active and one baseline inputs). A simple approach (Zilli and Hasselmo, 2010; Welday et al., 2011) is to use inhibitory connections from the oscillators to the grid cell, and to drive the grid cell so it spikes spontaneously when not inhibited. The result is that when the oscillators are not sufficiently similar in phase, the grid cell receives tonic inhibition (**Figure 4**, bottom),

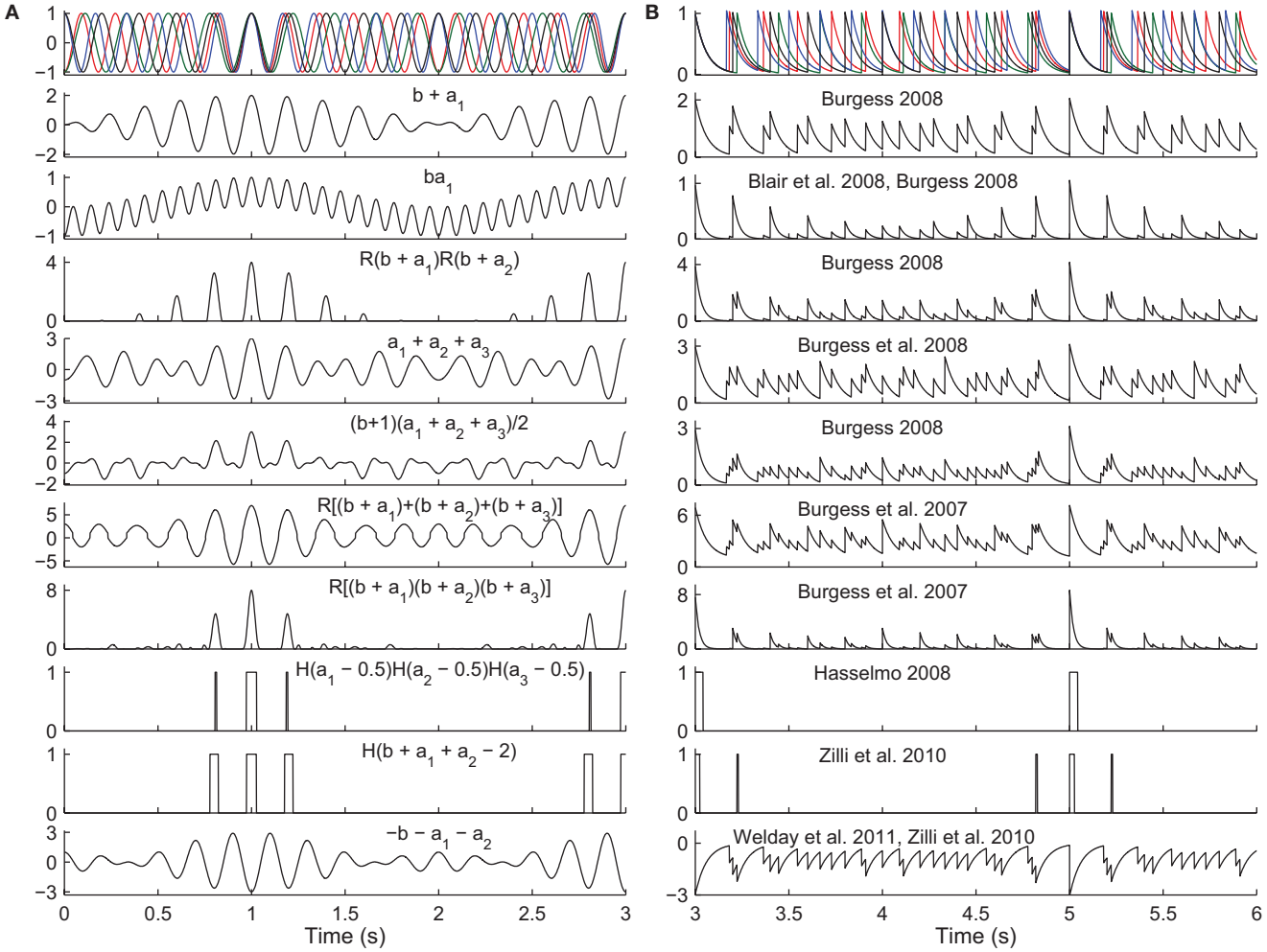


**FIGURE 4 | Read-out in temporal interference models.** Top. A 5-Hz baseline oscillation (black) and three active oscillators (colors) path integrating while receiving a constant velocity input. The oscillator outputs are **(A)** sinusoids or **(B)** exponentially decaying synaptic potentials (50 ms time constant). The simulated animal begins between grid fields at time $t = 0$ s and enters fields at times $t = \{1,3,5\}$ s. The remaining rows show the output of various models in response to the input oscillations (some using fewer than three active oscillator inputs). The rules all aim to produce maximal activity when the oscillators are all closely aligned in phase. The activity would then be thresholded (grid field width *in vivo* is about one-half the field spacing). Most of these rules were not intended to work with synaptic potentials (right column), but we show them to illustrate the difficulty of performing coincidence detection with spiking inputs: with some rules there is no threshold that would produce realistic field widths. Abbreviations: $b$, baseline oscillation; $a_i$, active oscillations; $H(x)$, the Heaviside step function ($H(x) = 0$ if $x < 0$ and $H(x) = 1$ if $x \geq 0$), and $R(x)$ the ramp function ($R(x) = 0$ if $x < 0$ and $R(x) = x$ if $x \geq 0$).

but when the oscillators move into phase with each other, the grid cell is able to spike in the time between volleys of inhibition.

### 2.4. LEARNING

All of the grid cell models require specifically structured connectivity. Depending on the model, the connections may include: connections from specific directional velocity inputs to specific oscillators or cells, from specific oscillators or place cells to specific grid cells, or connections among grid and direction-conjunctive cells. The models only work if the synaptic connections and weights are close enough to their optimal values (Zhang, 1996; Burgess et al., 2007), so some mechanism must exist that allows the necessary connectivity to be learned (though at least one model has been shown to be robust to high levels of noise in the weights; Conklin and Eliasmith, 2005).

The following subsections describe the mechanisms that have been suggested for learning connections from one region or cell type to another.

#### *2.4.1. Velocity to network oscillators*

When a ring attractor or population of phase-synchronized spiking cells acts as a velocity-controlled oscillator, each of the cells must develop the same preferred input direction, and this learning problem has not been addressed for either type of oscillator. Standard self-organization methods may work when the oscillator is a network of phase-synchronized cells, as the co-activity of the cells may cause them all to select the same direction (though this suggestion is untested). For ring attractors, though, the problem is compounded because not only must all the conjunctive cells for one direction learn the same directional preference, but cells conjunctive for the other direction must all learn the opposite preferred direction.

#### *2.4.2. Velocity to planar CANs*

The complexity of the velocity to direction-conjunctive cell problem just mentioned is most clear in 2D attractor models. To control the bump of activity, conjunctive cells in at least three directions (and more commonly four) are required. Because the synaptic outputs of the conjunctive cells are shifted in some direction (see below regarding learning those connections), those cells have both a velocity input direction and a synaptic output direction, and not only must all cells with the same output direction learn to prefer the same input direction, but cells with different output directions must learn to prefer consistent input directions. If the cells with output direction up all develop a preference for north velocities, then the down output cells must develop a preference for south velocities, and this further constrains the input preferences that left and right cells can have. This problem has not yet been solved.

#### *2.4.3. Place cells to grid cells*

In place-driven models (Kropff and Treves, 2008), no learning of velocity inputs is required. Instead the grid cells must develop connections from place cells whose fields are arranged in a hexagonal pattern. Kropff and Treves (2008) gave a solution to this problem that can be thought of in two stages. In the first stage, grid cells develop place fields surrounded by rings of inactivity, and in the second stage these fields shift around to minimize their distance from each other, which produces the hexagonal field arrangement (**Figure 1C**).

This behavior comes from the combination of the learning rule and grid cell dynamics in the model. Grid cells undergo an inactivating adaptation, so a steady input makes a cell fire at a high rate, then adapt down to a lower rate, then return to a high rate as adaptation inactivates. The place-to-grid learning rule, roughly, increases the strength of active synapses when the grid cell's activity is high, but weakens active synapses when the grid cell's activity is low. The place-to-grid synaptic weights begin with random values, so as the animal explores, a grid cell will receive enough input to fire at random places. The learning rule strengthens the synapses that started the firing (reinforcing the firing field), but as the animal continues to move and adaptation lowers the grid cell's activity, synapses from subsequently active place cells will decrease in weight onto the grid cell. With repeated passes through a grid field, the learning rule reinforces the strongest cells and then weakens surrounding cells, carving out an area of inactivity around the field. As the animal continues, adaptation inactivates and place cell inputs can again be strengthened, encouraging fields to appear or stabilize at that distance. The time or distance it takes for adaptation to inactivate roughly sets the scale of the grid pattern in this model.

However, place cells randomly remap in new environments while grid cells appear to maintain consistent relative spatial phases to each other (Leutgeb et al., 2005; Fyhn et al., 2007), while this mechanism must slowly re-learn the grid pattern in each new environment the animal is exposed to, unless a large number of maps have all been pre-learned (Samsonovich and McNaughton, 1997). The adaptation is also based on fixed time constants in the model, so the grid cell spacing depends on the history of velocities an animal has experienced in an environment.

#### *2.4.4. Directional integrators to grid cells*

Linear-coding models (Burgess et al., 2007; Gaussier et al., 2007; Giocomo et al., 2007; Blair et al., 2008; Burgess, 2008; Hasselmo, 2008; Hasselmo and Brandon, 2008; Zilli and Hasselmo, 2010; Welday et al., 2011; Mhatre et al., 2012) only produce the classic hexagonal field arrangement if the displacement is integrated along directions at 60° increments. One possibility is that the directional integrators only exist at 60° or 120° angles. Gaussier et al. (2007) gave a self-organizing map for learning spatial phases in a simplified version of this case.

Alternatively, directional integrators may exist for many directions and the grid cells must somehow learn to prefer input from specific directional integrators at appropriate angles. Burgess et al. (2007) showed in preliminary simulations that a cell's activity was highest if it received three inputs at angles producing a hexagonal grid, suggesting that this could be the basis for self-organization of the 60° directional inputs. Mhatre et al. (2012) gave a model of grid cells as a self-organizing map that does just that. Input to their grid cells came in the form of a set of stripe cells (**Figure 1G**), which fire spatially in parallel lines of constant spacing but with systematically varied phases and directions. In their model the amount of plasticity increases with the activity level of the grid cell, and these stripe cell inputs compete for a limited total synaptic weight onto each grid cell.

As a result, input patterns that occur frequently and produce the highest level of activity use up the most of the available synaptic weights, and Mhatre et al. (2012) argued geometrically that these inputs will be near 60°. Simulations show this mechanism produces fairly grid-like firing patterns, though the orientation of each cell in the network is not identical, in contradiction to the pattern observed *in vivo*. As this mechanism is experience-dependent, the grids develop slowly and require extended exposure to environments larger than the largest scale of the grids present in an animal's brain for the grid to properly develop. Like the Kropff and Treves (2008) model, this mechanism is also velocity-dependent.

#### 2.4.5. Grid cells to grid cells

When encoding position in attractor networks, synaptic connections among the grid and direction-conjunctive cells are needed to both maintain and update the pattern of activity. As suggested above, conjunctive cells must not only learn to prefer a common input direction, but their output must be directed to cells offset in a corresponding direction. A useful starting point may be analogous learning mechanisms used in head direction network models (Hahnloser, 2003; Stringer and Rolls, 2006).

In some models (Fuhs and Touretzky, 2006; McNaughton et al., 2006; Guanella et al., 2007; Navratilova et al., 2012), additional, symmetric synaptic connections are used to establish and maintain the pattern of activity. Fuhs and Touretzky (2006) gave a developmental model for learning the Mexican-hat–like connectivity shown in **Figure 3**. In their model, packets of activity randomly flowed over the network (by analogy with retinal waves in the developing eye). These packets were shaped like a sinusoidal grating, with alternating peaks of excitation and inhibition where the distance between peaks of excitation was the desired spacing of the rings in the synaptic matrix. Burak and Fiete (2006) reported that the symmetry of this Mexican-hat shape means it can maintain a grid at any orientation, so unfortunately the network has a tendency to drift in orientation.

McNaughton et al. (2006) suggested a mechanism that could solve this rotation problem, where the cells were directly connected to other cells hexagonally arranged in the sheet of cells, rather than having rotationally symmetric synaptic output in the form of rings. They showed that if entorhinal cells were driven by a sheet of cells with a drifting (in position but not rotation) hexagonal pattern of spiking, associative plasticity would connect co-active entorhinal cells into a toroidal topology, though Burak and Fiete (2006) reported this mechanism fails because the undesired rotations do occur.

### 2.5. MODELS

Having reviewed the individual components used in the models, we now briefly discuss each of the models themselves (summarized in **Tables 1** and **2**). The models are separated into linear- and planar-coding categories, because these two strands seemed to develop rather independently. Further technical details can be found in the comments in our online implementations of these models or in the papers themselves.

#### 2.5.1. Linear-coding

O'Keefe and Burgess (2005), though focused on CAN models, called attention to earlier models that produced place cell theta phase precession through interfering oscillators (O'Keefe and Recce, 1993; Lengyel et al., 2003; Huhn et al., 2005). These models produced a series of equally spaced place fields, providing a fruitful starting point for later models.

Burgess et al. (2007) described subsequent work that generalized those models to two dimensions. In the basic temporal interference model, one grid cell received inputs from (or contained all of) the active oscillators, reading out the grid pattern in its activity. The main focus was on one biological implementation where LFP theta provided the baseline oscillation to a neuron's soma, while SMPOs in the dendrites acted as active oscillators.

Giocomo et al. (2007) simulated a variant of the Burgess et al. (2007) modified to be consistent with their *in vitro* data (but see Burgess et al., 2007) showing that the resonant frequency and peak subthreshold membrane potential oscillation (SMPO) frequency of entorhinal cortical layer II stellate cells decreased in a dorsal to ventral gradient. In this model the baseline frequency scaled the speed inputs, so a lower frequency produced larger field spacing. As in Burgess et al. (2007), SMPOs were suggested to be the biological form of the model's oscillators, but SMPOs within a cell cannot store arbitrary phase differences (Remme et al., 2009), and if they could, SMPOs are far too irregular to store one for long enough to create a stable grid (Welinder et al., 2008; Zilli et al., 2009; Dodson et al., 2011).

In Gaussier et al. (2007), linear positions were first encoded in the firing rates of two cells with preferred directions 60° apart. By integrating respective directional velocities, their activities gave the total displacement along the respective directions. The firing rate of these cells was discretized in a separate population E, e.g., one cell in E fires only when the animal has moved 10 cm in the $x$ direction from its starting $x$ coordinate (like stripe or band cells, except these have only a single band rather than repeating bands). E cells with firing bands at equal increments were synaptically connected to a modulo cell which then fired in a set of equally spaced parallel stripes. Finally, grid cells were created by adding or multiplying the activity of one modulo cell from each of the two directions. They also gave a simple learning mechanism that allowed grid cells to select a unique input from each of six different modulo populations at 60° increments. The learning was fairly trivial, however, creating a new grid cell for each novel combination of modulo cell activities experienced by the animal.

Blair et al. (2008) used temporal interference to read out linear positions stored between biased ring attractors rather than abstract, sinusoidal oscillators. The authors examined the firing phases of various cells in the network and found some cells precess (their **Figures 4B,C** show less than 180° of precession, not the 360° claimed) with respect to a baseline oscillation while other pairs of cells could show procession, shifting phases, or phase locking. Only the 1D case was modeled, the 2D case later appearing in Welday et al. (2011).

Burgess (2008) expanded on the Burgess et al. (2007) model, still using frequency-modulated sinusoids to perform path integration (also considering a slightly more spike-like shape from transforming the sinusoids), and examined the behavior of the

model using various read-out mechanisms. He emphasized the importance of the baseline oscillation in reducing out-of-field spatial firing when oscillations are summed rather than multiplied. He also gave the first temporal interference model of grid cell phase precession that always precessed on every pass through a field. The precession mechanism used six oscillators at 60° increments: their frequencies increased or decreased normally, but at any time only the three oscillators that were firing faster than baseline were allowed to influence (through an unspecified mechanism) the grid cell, which then always fired faster than the baseline and so precessed.

Hasselmo (2008) gave a variation on the Burgess et al. (2007) model that interpreted the oscillator outputs as trains of spikes, represented artificially by thresholding a sinusoidal oscillation into a train of rectangular pulses. The model still path integrated through frequency modulation, but it did not use a baseline oscillator. The role of the baseline oscillator was played by an additional active oscillator along a third direction. Just as with a baseline oscillation, the third oscillator only moved into phase with the two others at positions arranged hexagonally. The lack of a baseline oscillation means that the model does not produce correct phase precession (and see Figure 7A left in Burgess, 2008). This paper also considered how place-based resetting of the grid system could explain context-dependent firing in the hippocampus and the non-grid pattern observed from grid cells in the hairpin maze (Derdikman et al., 2009), giving resetting mechanisms that would work with any path integration model.

Hasselmo and Brandon (2008) discussed multiple models including a spatial interference model they called a cyclical persistent firing model. Linear position was encoded in the firing rate of an individual cell, and that cell's velocity input caused the firing rate to cycle such that the cell's spatial firing occurred in parallel bands across the environment. In essence this is a temporal interference model with a baseline frequency of 0 Hz (like a single-cell analog of the cells found in a ring attractor), but it assumed an unspecified mechanism by which a constant input could modulate a cell's firing rate in a sinusoidal manner.

Mhatre et al. (2012) addressed the issue of learning velocity inputs at 60° or 120° increments. They gave a self-organizing map (Grossberg, 1976a,b) receiving inputs in the form of increased activity along parallel lines at various orientations (their stripe cells, but possibly also Turing stripes, McNaughton et al., 2006, or band cells, Burgess et al., 2007) that could select for inputs at 60° increments and so eventually produce grid cells. The learning, however, produces grid cells at various orientations instead of one common orientation, seems to be sensitive to the velocity of the training trajectory, and requires early experience in large environments to learn the large-scale grids.

Zilli and Hasselmo (2010) addressed another concern in temporal interference models: the biological oscillators (SMPOs, LFP, and neuronal inter-spike or inter-burst intervals) considered in earlier models are highly noisy, which prevents them from stably storing a position on behavioral time scales (Welinder et al., 2008; Zilli et al., 2009). Zilli and Hasselmo (2010) showed that connecting a large enough number of cells in each oscillator allowed the synchronizing effect of coupling to overcome the independent noise injected into each cell. This produced spatial grid patterns that were fairly stable on the order of minutes, though such a large number of cells were needed as to seem wasteful. Other issues likely to recur in other increasingly biophysical interference grid cell models were discussed, including a lagging frequency response of neuronal oscillators, the non-linear frequency response of spiking neurons, and the difficulty performing coincidence detection on three or more inputs (especially when their magnitudes change stochastically). However, use of inhibitory inputs from oscillators (**Figure 4**) made coincidence detection easier (later confirmed by Welday et al., 2011).

Welday et al. (2011) continued the work of Blair et al. (2008), showing how arbitrary spatial firing patterns (including many seen in the medial temporal lobe) can be created by combining the outputs of biased ring attractors. They provided a valuable theoretical approach (carrying on from Blair et al., 2008) that focused on the spatial envelope of the interference of two oscillators, allowing questions of temporal interference to be treated as simpler spatial interference problems.

#### *2.5.2. Planar-coding*

Early path integration models that considered or used single-bump toroidal CANs (Zhang, 1996; Samsonovich and McNaughton, 1997) recognized that the place fields produced by the network would repeat as a rectangular grid in large environments, and the relationship between this pattern and grid cells was quickly noticed (Hafting et al., 2005).

Conklin and Eliasmith (2005) gave such a toroidal (rectangular grid) CAN and was the first modeling work to link it to the firing patterns of cells that would later be called grid cells (Fyhn et al., 2004; Hafting et al., 2005). This model featured improvements over earlier 2D CAN place cell models such as requiring fewer cells and tolerating heterogeneity in the cells and errors in the weight matrix.

Fuhs and Touretzky (2006) described a planar CAN model producing a hexagonal pattern of multiple bumps that could be moved over a circular sheet of cells. The rate-based grid cells were connected to nearby cells with concentric rings of excitatory and inhibitory synapses (**Figure 3**). With this pattern of connectivity, bumps of activity formed in a hexagonal pattern where the excitatory bands intersect (**Figure 3**). A conjunctive cell's asymmetric output was an inhibitory region near the center of the concentric rings, offset opposite the direction that the cell would shift the population (each cell has one of four preferred directions). The recurrent weights faded out to 0 toward the edge of the network to prevent bumps of activity from forming lines parallel to the edges, creating cells at the edge that were barely spatially modulated and resembled head direction cells. Fuhs and Touretzky (2006) also described a developmental mechanism to learn the concentric rings component of the synaptic weights inspired by retinal waves observed in the developing eye. Later simulations (Burak and Fiete, 2006) showed that, due to uncontrollable rotations of the spatial pattern and a non-linear velocity response, this model fails to produce a stable spatial hexagonal grid.

McNaughton et al. (2006) further discussed the use of attractor dynamics, reviewing the basic functioning of ring and planar attractor networks (see also Zhang, 1996; Eliasmith, 2005). Their preliminary simulations (no details given) dealt with the problem

of learning the toroidal synaptic connections needed for a single-bump 2D CAN like the one outlined in O'Keefe and Burgess (2005). McNaughton et al. (2006) reasoned that grid pattern development must be experience-independent because lab rats are unlikely to have been exposed to environments larger than the ventral grid spacing (a challenge to experience-dependent models like Kropff and Treves, 2008; Mhatre et al., 2012).

Blair et al. (2007) formed the hexagonal spatial pattern through spatial interference. Assuming the existence of small-scale, planar-coding "theta grids" (generated through unspecified attractor dynamics), they showed two ways two small-scale grids could interfere to produce the large-scale grid pattern (one hinted at in Figure 6A in McNaughton et al., 2006). By scaling-up or rotating one of the theta grids, its firing peaks would respectively phase precess or maintain a relatively fixed relationship with the fields of the other theta grid. If the spiking of one theta grid produced the LFP theta rhythm, spikes from the other grid could precess relative to theta. Blair et al. (2007) suggested this could relate to the difference between the theta phase profiles of cells in different layers of entorhinal cortex (Hafting et al., 2008). With this mechanism theta frequency would vary linearly with running speed, so they had to assume that the spacing of the grid producing LFP theta would vary with speed to keep theta frequency nearly constant. Consequently, the second grid had to dynamically scale or rotate to account for the changes in the first grid to maintain constant spacing in the large-scale grid.

Guanella et al. (2007) gave the first planar CAN model that produced a stable hexagonal spatial firing pattern. No conjunctive cells were used to update the stored position. Instead, the recurrent connections changed dynamically to shift the bump of activity smoothly and perfectly in any direction. The mechanism is conveniently simple, but not particularly biologically plausible. The authors introduced a twisted-torus topology to remedy the rectangular pattern produced by previous toroidal proposals (Conklin and Eliasmith, 2005; O'Keefe and Burgess, 2005; McNaughton et al., 2006). A twist in the torus is not strictly necessary: a hexagonal pattern results from an untwisted torus if the velocity input directions of certain conjunctive cells are skewed relative to their synaptic output directions (see online code). For example, the cells shifting the activity left and right still receive east and west velocity inputs, but the cells shifting the activity up and down receive velocity input along a direction 60° from the east/west direction (rather than the expected 90°). This modification produces elliptical rather than circular fields (a different solution to the toroidal problem is given by Burak and Fiete, 2009).

Kropff and Treves (2008) described a model that relied on place cell inputs rather than path integration. Their focus was on a developmental model that allowed a grid cell to develop its spatial pattern by slowly learning to prefer inputs from place cells whose fields are arranged in a hexagonal pattern. As described, the model produced grid cells that vary in orientation (unlike neighboring grid cells *in vivo* which appear to have the same orientation, Hafting et al., 2005). Also, distinct environments have distinct place field maps (Thompson and Best, 1989), so grid pattern would have to be relearned in each new environment, which is contrary to experimental reports that the grid pattern appears immediately on entry to a new environment (Hafting et al., 2005).

Burak and Fiete (2009) gave a multi-bump planar CAN, building on the work of Fuhs and Touretzky (2006) and Guanella et al. (2007), and studied many problems that can occur in this type of model. Their main focus was on the effects of periodic (i.e., toroidal) versus aperiodic (the network fades out to the edges which do not wrap around) networks. Edges produced detrimental effects in their aperiodic network, including noise-induced rotations of the pattern and inaccurate responses of the network to low velocity inputs. Fading out the velocity inputs to cells at the edges of the network (rather than fading out the synaptic weights as in Fuhs and Touretzky, 2006) lessened these effects. Those distortions also decreased in larger networks, so their large network with faded inputs path integrated successfully. Periodic networks, having no edges, had none of these problems, though finer tuning of the grid spacing was required so that the pattern perfectly fit the dimensions of the sheet of cells. The authors also showed that an attractor network of stochastically spiking cells is considerably more robust to small amounts of noise than models (Burgess et al., 2007; Gaussier et al., 2007; Giocomo et al., 2007; Burgess, 2008; Hasselmo, 2008; Hasselmo and Brandon, 2008) where only a single noisy cell encodes position (and see Zilli et al., 2009).

Navratilova et al. (2012) extended CAN models to address theta phase precession, focusing on the 1D case. The model included an 8 Hz theta oscillation injected into the conjunctive cells and an artificial ADP and mAHP injected into the grid cells after a spike. The grid cells formed an unbiased ring attractor and projected to corresponding cells in the conjunctive populations (6 o'clock grid cells to 6 o'clock conjunctive cells). The two populations of conjunctive cells projected back to the grid cells, but offset in each direction. Thus an input from one spiking grid cell drove activity in the conjunctive populations at the same position, which drove grid cells on either side of the first grid cell. Biased by velocity input, one conjunctive population has greater activity, asymmetrically driving the grid cells and nudging the bump in one direction. When the newly active grid cells fire, the cycle repeats and the bump continues moving. The ADP, mAHP, and NMDA time constants in the grid cell determine how quickly the grid cell bump can re-fire, setting how many times the bump can nudge forward in any unit of time, and so influencing grid field spacing. This process occurs with the conjunctive cells depolarized to near threshold by the theta input, but at the trough of the theta input, the conjunctive cells fire much less. At those times the ADP currents of recently active grid cells caused them to fire again, making the bump of activity jump back to an earlier point. Theta phase precession arises from this alternation of the bump moving forward under the influence of velocity followed by the bump jumping back. Only a 1D version of the model was given, but the model might be extended to 2D either via spatial interference of two rings or by expanding it to be a planar-coding CAN (Guanella et al., 2007; Burak and Fiete, 2009).

## 3. DISCUSSION

### 3.1. SUMMARY

Rather than the common division of continuous attractor vs. interference models, we suggest alternative categorizations.

The positional codes in the models fall into linear-coding and planar-coding categories. The key difference is that linear-coding

models *independently* encode linear positions along different directions such that changing the position encoded along one direction may not affect encoded positions along other directions. In planar-coding models, although individual cells have preferred directions, the position coded by the set of cells with one preferred direction is also changed by movements along any other direction. The models can also be distinguished according to the mechanisms used to encode and maintain positions. Unbiased attractor networks or oscillator phase differences are most commonly used, though some models use more direct positional codes like place cells or encoding coordinates as firing rates.

A more fine-grained, but non-exclusive categorization of the models is given by the mechanism used to update the encoded position. Positions stored using abstract oscillators or phase-synchronized spiking cells are updated by modulating the frequency or firing rate of the oscillators, and positions stored in unbiased continuous attractor networks are updated through direction-conjunctive cells. Biased attractor networks, however, can be understood as both: inputs modulate the frequency of the networks, but this is done via conjunctive cells.

Finally, the models can be categorized by their read-out mechanisms, a distinction loosely related to the linear vs. planar distinction. Planar models do not generally require a read-out mechanism to produce a 2D grid (but see Blair et al., 2007), while read-out mechanisms are required for linear-coding models. For simplicity we divided the read-out mechanisms into temporal interference and spatial interference, though they are essentially equivalent because temporal interference models become spatial interference models when the baseline oscillation frequency is set to 0 Hz.

### 3.2. EXPERIMENTS AND MODELS

The publications we have reviewed all give models on Marr's algorithmic level (**Table 1**), and many also specify an implementation (**Table 2**). The two levels have different values and uses.

On the algorithmic level, simulations have theoretical value as proofs-of-concept demonstrating that a solution can actually work, but these make fairly limited experimental predictions regarding only phenomena that might be observed. For example, algorithmically Burgess et al.'s (2007) model can only predict that somewhere in the brain there are oscillatory processes being modulated by the animal's body velocity. Similarly, Burak and Fiete's (2009) model can only predict that somewhere there are velocity-sensitive (i.e., conjunctive) grid cells whose gain changes when an environment is deformed or which always maintain a perfect spatial phase relationship.

This limitation arises because a single algorithmic model or prediction can have many different biological implementations and experiments can only directly support or oppose specific implementational predictions. For example, spatial position in CAN models should be perturbed if the direction-conjunctive cells are perturbed, but some cells may inherit the direction signal without partaking in network dynamics and perturbing such a cell may have no effect. That null result should not be evidence against the algorithmic model, but would be evidence against a particular implementation.

As a result, the valuable experimental predictions of a model generally come from the implementational level where specific properties are attributed to specific anatomical or electrophysiological elements. This is a valuable step because predictions become concrete and easily tested, though there is a degree of arbitrariness in selecting an implementation and only this arbitrary implementation can actually be evaluated (rather than the algorithmic model itself).

Temporal interference models that include theta-rhythmic (spiking or subthreshold oscillations or external input modulated at a theta frequency) elements provide one example of the value of distinguishing among these levels.

There are many oscillatory processes in the rodent medial temporal lobe that show rhythmicity in the 6 to 10 Hz theta band, including fluctuations in the local field potential (LFP), subthreshold fluctuations in neuronal membrane potentials, and bursting or modulation of firing rate of many cells types (and so also rhythmic synaptic input to cells over recurrent connections). The prominence of these oscillations has led to their use in many implementation-level models that have made explicit predictions about how the scale of the grid pattern may be reflected in rhythmic processes (O'Keefe and Burgess, 2005; Burgess et al., 2007; Burgess, 2008). Many predictions have been confirmed (Giocomo et al., 2007; Giocomo and Hasselmo, 2008; Jeewajee et al., 2008; Welday et al., 2011; Navratilova et al., 2012). At the same time, experimental (Welinder et al., 2008; Zilli et al., 2009; Dodson et al., 2011) and theoretical (Remme et al., 2009, 2010) arguments have been raised against the same implementations.

Recently Yartsev et al. (2011) provocatively claimed to have disproven the entire class of "oscillatory interference" models based on the fact that the LFP in bats contained no strong theta signal nor did the grid cells show theta modulation in their spike time autocorrelations. If theta is the same frequency in bats as rats (though the functional role, not the numerical frequency value is what is important in the models), this would be good evidence against an implementation that involves theta, but no more evidence against the whole class of interference models than any of the earlier experimental results identifying flaws in those implementations. Algorithmically, no model requires any regular rhythmic components nor necessarily produces them as output (see our online code; although the bat data seems to contain a low frequency rhythmic component around 1/3–1 Hz that would still be consistent with the temporal interference models).

The interesting result of making explicit predictions is that models that make them have been quite successful in guiding experiments that have discovered new results, and the experiments have been quite consistent in revealing flaws with the originally specified implementations.

#### 3.2.1. *Distinguishing linear from planar-coding*

It is natural to ask how experiments might distinguish linear- from planar-coding models. A direct approach would be a time consuming, systematic search for linear coding (either cells with stripe-like firing patterns or oscillators whose phase relative to a baseline varies with directional position) in the inputs to grid cells. Locating such a code would provide great support to linear-coding models, though the challenge would remain to show those inputs are in fact used to create the grid.

Alternatively, the effects of linear-coding inputs may be visible in intracellular recordings of grid cells *in vivo*. The linear position inputs may be fairly strong because few such inputs are required in these models (though out-of-field inputs might be hidden by dendritic non-linearities). Spatial interference models predict strong, tonic subthreshold inputs at positions along the lines between adjacent fields, but not in the central spaces of triangles of fields. Temporal interference models predict grid cells should receive multiple inputs (modulated around a common baseline frequency) with relative phases that vary systematically with position, and subsets of these should move into alignment at positions along the lines connecting adjacent fields (**Figure 4**).

These predictions are in contrast to planar-coding models, where there might be spatially correlated (e.g., sensory) subthreshold inputs or even inputs that repeat systematically with the grid (e.g., from flaws in a synaptic weight matrix), but most models would not predict consistent inputs only along lines of a particular orientation connecting adjacent fields. One exception is the Fuhs and Touretzky (2006) model, which contains cells near the network edge that might produce such stripe-y grid cells if the model accurately path integrated. Though the case of subthreshold inputs may be easier to detect, *in vivo* intracellular recording is still in its infancy, so these predictions might also be examined in the positions of out-of-field grid cell spiking (i.e., out-of-field firing primarily along lines connecting neighboring fields may suggest linear-coding).

The linear/planar distinction, however, should not be thought of as necessarily intrinsic to a model. In theory any of the planar-coding CAN models could be reduced down to a ring attractor and a pair used in a linear-coding model. Linear-coding approaches can also be merged into a planar code (e.g., an unbiased ring attractor where the bump position indicates spatial position along one direction and the phase relative to a baseline of bursts of bump activity encodes position along a second direction).

#### *3.2.2. Questions for future work*

A number of questions about grid cells arise from studying the models in detail.

First, path integration requires the body's movements as inputs, but the grid cell literature largely focuses on the existence of head direction cells in the medial temporal lobe. Do head direction cells actually encode body movement direction, or, if not, do path integration errors consistently occur if the animal moves forward with its head rotated to one side? Also, when a grid cell has a directional preference, is the preference always along a direction connecting adjacent fields (and if so, along three or all six directions?) or are all directions represented?

Grid cells often show firing at positions along environmental edges that does not conform to the overall hexagonal pattern. Though grid cell models allow for sensory inputs on the grid cell, no model specifically tries to explain this edge firing. In particular, if the regularity of grid fields is key to the use of grid cells as a spatial code, are spatial abilities impaired at environmental boundaries?

It has sometimes been suggested that local flaws in grid field spacing can create pentagons or heptagons rather than hexagons (Fuhs and Touretzky, 2006). Does this actually occur or is it due to edge effects or undersampling of animal positions? If it does occur, are spatial abilities impaired in environments where it is observed?

Is the amount of phase precession observed within a field correlated with the ratio of field width to field spacing? Temporal interference models predict that firing phase range is $360^\circ \cdot$ (field width)/(field spacing). This phase range applies only to the range where the spikes are truly precessing, not the second component (Yamaguchi et al., 2001) as the animal exits the field, where the cell fires across most phases.

Are grid fields firmly established immediately on entry into a new environment and does a grid cell always fire on every pass through each field? Both during the course of development and on exposure to a novel environment, do dorsal grid cells appear or stabilize before ventral grid cells? Experience-dependent learning models must reform the grid pattern in new environments, but they might be able to more quickly organize grid cells with smaller field spacing.

In the event that the environment is stretched or deformed such that place cells stretch their place fields, the grid pattern would also be expected to stretch or deform to match (Blair et al., 2007; Burgess et al., 2007). A stretched grid pattern due to place influences can be distinguished from a stretched grid due to changes in input gain along different directions (an alternative explanation) by comparing the velocity-modulation and firing fields of pairs of simultaneously recorded grid cells (Burak and Fiete, 2009).

Does a grid cell's firing rate slow down in the middle of a field? Models like Kropff and Treves (2008) and Mhatre et al. (2012) require adaptation or habituation dynamics that decrease the activity of tonically active cells.

### 3.3. ATTRACTORS AND INTERFERENCE

A common division of grid cell models is into continuous attractor network and oscillatory interference models. As we have already suggested, this distinction is misleading because it contrasts independent qualities. To distinguish their general meanings from the classes of models the terms have come to represent, additional points about attractors and interference are worth mentioning.

An attractor is a state (or region of state space) that a system moves toward if the system's state is nearby. All neurons have attractors: both the stable equilibrium of a neuron at rest and the consistent voltage trajectory (limit cycle) maintained by a steadily spiking cell are attractors. A system can have multiple simultaneous attractors: bistable cells can have both a resting equilibrium and a spiking limit cycle at the same time, and others (Hughes et al., 1999; Izhikevich, 2007) have two simultaneously stable voltage attractors (e.g., with no applied current, the voltage can remain at $-75$ or at $-59$ mV, and brief inputs can move it back and forth). A system can even have infinitely many attractors (e.g., a hypothetical cell that could stably maintain any voltage in between $-75$ and $-59$ mV). This is called a continuous attractor (continuous meaning there is always a third attractor between any two nearby attractors). A similar continuous attractor is used in Gaussier et al. (2007) and Hasselmo and Brandon (2008) in their cells that store a coordinate in their firing rates. Similarly, networks of cells have attractors, and such networks are called attractor networks when the attractor aspect is emphasized. The phase-synchronized state of a population of cells can be an attractor (Izhikevich, 2007), so

Zilli and Hasselmo (2010) used (non-continuous) attractor networks in their model. Continuous attractors can also occur in networks, as in the many ring and 2D attractor models described above. In these the attractors are patterns of neural activities containing one or more localized bumps. Continuous attractor networks are less generic than other attractors since they require patterned synaptic connections, but as Conklin and Eliasmith (2005) showed, imperfect networks can behave as CANs. The CAN metaphor is thus a matter of degree, not a binary property of a system.

Interference refers to the signal produced by combining two other signals, with emphasis on the large peaks in the output where the inputs constructively interfere and the low points where the inputs are out of phase and destructively interfere. This is not a special mechanism, but rather a simple physical fact that two inputs to a cell that co-occur will produce a larger net effect than if they had occurred separately. Even in planar CANs, each conjunctive cell has a slightly different synaptic output pattern and the final activity of the cells is given by the sum of all of these patterns, producing a sort of synaptic spatial interference [e.g., in Fuhs and Touretzky (2006), the arrangement of bumps is the interference pattern of the synaptic rings of excitatory and inhibitory outputs]. In grid cell models, the term oscillatory interference is generally used, suggesting more specifically the interference of regular oscillations (presumably temporal or spatial) rather than simply identifying the overlap of multiple synaptic inputs, but any signal can be considered a complex oscillation in some sense.

Attractors and interference appear not only in the grid cell models named after them, but also in the other grid cell models, and are general properties of every circuit in the brain. This is clear from their widespread occurrence in other models. For example, a focus on interference of oscillations arose in models of place cell precession (O'Keefe and Recce, 1993; Lengyel et al., 2003; Huhn et al., 2005; O'Keefe and Burgess, 2005), but also, e.g., models of timing (Miall, 1989; Hopfield and Brody, 2001). Attractor networks have been used to model both place cells (Samsonovich and McNaughton, 1997; Conklin and Eliasmith, 2005) and head direction cells (Skaggs et al., 1995; Zhang, 1996), and many other systems (Eliasmith, 2005).

### 3.4. NOISE

As path integration models require that a position be both stably encoded and accurately updated, successful models must account for the high levels of noise observed in biological systems. All of the path integration models are equally susceptible to noise in the velocity inputs themselves (Burak and Fiete, 2009; Zilli et al., 2009), so the noise intrinsic to the system is most commonly studied. Noise is also assumed to have a mean of zero, as non-zero mean noise introduces a constant bias that strongly disrupts the stable grid pattern (Giocomo and Hasselmo, 2008).

Early models encoding positions as phase differences were considered particularly susceptible to noise (Burgess et al., 2007; Giocomo and Hasselmo, 2008; Hasselmo, 2008; Welinder et al., 2008), though later work showed that the use of multiple, redundant oscillators allowed for robustness to small levels of noise (Zilli et al., 2009). Considerably greater robustness to noise was provided by subsequent work in which each oscillator comprised many coupled spiking neurons (Zilli and Hasselmo, 2010).

This is a general effect of coupled cells, so all CANs automatically attain robustness to noise (including those used to encode phase differences; e.g., Blair et al., 2008). Burak and Fiete (2009) examined the behavior of CANs with intrinsic noise and showed that toroidal networks are robust to noise, with the pattern drifting in a diffusion process, while aperiodic networks were less robust, showing the same translational diffusion but also a more damaging rotational drifting of the pattern. The same diffusive process producing error in the encoded position occurs with noise in phase difference models (Zilli et al., 2009), suggesting it is likely the generic behavior of path integration models with internal noise. To deal with the drifting pattern that occurs with noise, Guanella et al. (2007) simulated connections from place cells to grid cells that could reset the grid network. Navratilova et al. (2012) showed that phase precession in their model was also robust to the presence of noise.

### 3.5. "BEST" MODEL

It is possible exactly one current model or mechanism fully explains the grid pattern to the complete exclusion of all other models or alternative mechanisms, but grid cells are part of a messy biological system created through natural selection and individual development. Grid cell models are designed specifically to produce the grid in as simple a manner as possible, but the biological system is unlikely to have evolved with the goal of finding the simplest way to produce a grid. Grid cells individually or as a population likely perform a complex and perhaps context-sensitive processing on inputs that may themselves reflect various complex, context-sensitive mechanisms, and so the models may better be considered collectively as a set of metaphors that guide research by describing how grid cells may possibly be driven at various times or in different states, rather than as things to be proven or disproven. For example, the place-driven metaphor of Kropff and Treves (2008) may be true in familiar environments, and linear-coding or planar-coding used respectively in 1D or 2D environments, or perhaps both 1D and 2D environments are coded linearly, while incidental (e.g., standing on a moving platform or pushing against a wall and sliding backward) or illusory(e.g., the bus next to your car backs up slightly, creating the illusion of forward motion) movements might be understood as updating the position representation through conjunctive cells as in CANs.

These are meant as examples, not predictions, but it is easy to see that, given the variety of ways that spatial position could change, and the distinct systems that may encode or produce different types of movements, there is much room for a variety of mechanisms to be involved in the unitary representation of position that grid cells are thought to reflect.

## ACKNOWLEDGMENTS

I thank Mark Brandon, Jason Climer, Michael Hasselmo, Jim Heys, Caitlin Monaghan, and Yusuke Tsuno for comments and discussion, and Yoram Burak, Stephen Grossberg, Michael Hasselmo, Himanshu Mhatre, Zaneta Navratilova, Praveen Pilly, and Bailu Si for discussions, information, and materials helpful in implementing various models. Supported by grants to Michael Hasselmo (ONR MURI award N00014-10-1-0936, NIMH Silvio O. Conte grant P50 MH094263, and NIMH R01 MH60013).

## REFERENCES


Blair, H. T., Gupta, K., and Zhang, K. (2008). Conversion of a phase- to rate-coded position signal by a three-stage model of theta cells, grid cells, and place cells. *Hippocampus* 18, 1239–1255.

Blair, H. T., Welday, A. W., and Zhang, K. (2007). Scale-invariant memory representations emerge from moiré interference between grid fields that produce theta oscillations: a computational model. *J. Neurosci.* 27, 3211–3229.

Brun, V. H., Solstad, T., Kjelstrup, K. B., Fyhn, M., Witter, M. P., Moser, E. I., and Moser, M.-B. (2008). Progressive increase in grid scale from dorsal to ventral medial entorhinal cortex. *Hippocampus* 18, 1200–1212.

Burak, Y., and Fiete, I. R. (2006). Do we understand the emergent dynamics of grid cell activity? *J. Neurosci.* 26, 9352–9354.

Burak, Y., and Fiete, I. R. (2009). Accurate path integration in continuous attractor network models of grid cells. *PLoS Comput. Biol.* 5, e1000291. doi:10.1371/journal.pcbi.1000291

Burgess, N. (2008). Grid cells and theta as oscillatory interference: theory and predictions. *Hippocampus* 18, 1157–1174.

Burgess, N., Barry, C., and O'Keefe, J. (2007). An oscillatory interference model of grid cell firing. *Hippocampus* 17, 801–812.

Burgess, N., O'Keefe, J., and Recce, M. (1993). "Using hippocampal 'place cells' for navigation, exploiting phase coding," in *Advances in Neural Information Processing Systems 5*, eds S. J. Hanson, C. L. Giles, and J. D. Cowan (San Mateo: Morgan Kaufmann Publishers Inc.), 929–936.

Conklin, J., and Eliasmith, C. (2005). A controlled attractor network model of path integration in the rat. *J. Comput. Neurosci.* 18, 183–203.

Derdikman, D., Whitlock, J. R., Tsao, A., Fyhn, M., Hafting, T., Moser, M.-B., and Moser, E. I. (2009). Fragmentation of grid cell maps in a multicompartment environment. *Nat. Neurosci.* 12, 1325–1332.

Dodson, P., Pastoll, H., and Nolan, M. (2011). Dorsal-ventral organization of theta-like activity intrinsic to entorhinal stellate neurons is mediated by differences in stochastic current fluctuations. *J. Physiol. (Lond.)* 589, 2993–3008.

Eliasmith, C. (2005). A unified approach to building and controlling spiking attractor networks. *Neural Comput.* 17, 1276–1314.

Etienne, A. S., and Jeffery, K. J. (2004). Path integration in mammals. *Hippocampus* 14, 180–192.

Fuhs, M. C., and Touretzky, D. S. (2006). A spin glass model of path integration in rat medial entorhinal cortex. *J. Neurosci.* 26, 4266–4276.

Fyhn, M., Hafting, T., Treves, A., Moser, M.-B., and Moser, E. I. (2007). Hippocampal remapping and grid realignment in entorhinal cortex. *Nature* 446, 190–194.

Fyhn, M., Molden, S., Witter, M. P., Moser, E. I., and Moser, M.-B. (2004). Spatial representation in the entorhinal cortex. *Science* 305, 1258–1264.

Gaussier, P., Banquet, J. P., Sargolini, F., Giovannangeli, C., Save, E., and Poucet, B. (2007). A model of grid cells involving extra hippocampal path integration, and the hippocampal loop. *J. Integr. Neurosci.* 6, 447–476.

Giocomo, L. M., and Hasselmo, M. E. (2008). Computation by oscillations: implications of experimental data for theoretical models of grid cells. *Hippocampus* 18, 1186–1199.

Giocomo, L. M., Moser, M.-B., and Moser, E. I. (2011). Computational models of grid cells. *Neuron* 71, 589–603.

Giocomo, L. M., Zilli, E. A., Fransén, E., and Hasselmo, M. E. (2007). Temporal frequency of subthreshold oscillations scales with entorhinal grid cell field spacing. *Science* 23, 1719–1722.

Grossberg, S. (1976a). Adaptive pattern classification and universal recoding, II: feedback, expectation, olfaction, and illusions. *Biol. Cybern.* 23, 187–202.

Grossberg, S. (1976b). Adaptive pattern classification and universal recoding, I: parallel development and coding of neural feature detectors. *Biol. Cybern.* 23, 121–134.

Guanella, A., Kiper, D., and Verschure, P. (2007). A model of grid cells based on a twisted torus topology. *Int. J. Neural Syst.* 17, 231–240.

Hafting, T., Fyhn, M., Bonnevie, T., Moser, M. B., and Moser, E. I. (2008). Hippocampus-independent phase precession in entorhinal grid cells. *Nature* 453, 1248–1252.

Hafting, T., Fyhn, M., Molden, S., Moser, M. B., and Moser, E. I. (2005). Microstructure of a spatial map in the entorhinal cortex. *Nature* 436, 801–806.

Hahnloser, R. H. R. (2003). Emergence of neural integration in the head-direction system by visual supervision. *Neuroscience* 120, 877–891.

Hasselmo, M. E. (2008). Grid cell mechanisms and function: contributions of entorhinal persistent spiking and phase resetting. *Hippocampus* 18, 1213–1229.

Hasselmo, M. E., and Brandon, M. P. (2008). Linking cellular mechanisms to behavior: entorhinal persistent spiking and membrane potential oscillations may underlie path integration, grid cell firing and episodic memory. *Neural Plast.* 2008, 658323.

Hayman, R., Verriotis, M., Jovalekic, A., Fenton, A., and Jeffery, K. J. (2011). Anisotropic encoding of three-dimensional space by place cells and grid cells. *Nat. Neurosci.* 14, 1182–1188.

Hopfield, J. J., and Brody, C. D. (2001). What is a moment? Transient synchrony as a collective mechanism for spatiotemporal integration. *Proc. Natl. Acad. Sci. U.S.A.* 98, 1282–1287.

Hughes, S. W., Cope, D. W., Toth, T. L., Williams, S. R., and Crunelli, V. (1999). All thalamocortical neurones possess a T-type $Ca^{2+}$ 'window' current that enables the expression of bistability-mediated activities. *J. Physiol. (Lond.)* 517, 805–815.

Huhn, Z., Orbán, G., Érdi, P., and Lengyel, M. (2005). Theta oscillation-coupled dendritic spiking integrates inputs on a long time scale. *Hippocampus* 15, 950–962.

Izhikevich, E. M. (2007). *Dynamical Systems in Neuroscience: The Geometry of Excitability and Bursting.* Cambridge, MA: MIT Press.

Jeewajee, A., Barry, C., O'Keefe, J., and Burgess, N. (2008). Grid cells and theta as oscillatory interference: electrophysiological data from freely moving rats. *Hippocampus* 18, 1175–1185.

Kalaska, J. F., Caminiti, R., and Georgopoulos, A. P. (1983). Cortical mechanisms related to the direction of two-dimensional arm movements: relations in parietal area 5 and comparison with motor cortex. *Exp. Brain Res.* 51, 247–260.

Kropff, E., and Treves, A. (2008). The emergence of grid cells: intelligent design or just adaptation. *Hippocampus* 18, 1256–1269.

Lengyel, M., Szatmáry, Z., and Érdi, P. (2003). Dynamically detuned oscillations account for the coupled rate and temporal code of place cell firing. *Hippocampus* 13, 700–714.

Leutgeb, S., Leutgeb, J. K., Barnes, C. A., Moser, E. I., McNaughton, B. L., and Moser, M.-B. (2005). Independent codes for spatial and episodic memory in hippocampal neuronal ensembles. *Science* 309, 619–623.

Marr, D. (1982). *Vision: A Computational Investigation into the Human Representation and Processing of Visual Information.* New York: Freeman.

McNaughton, B. L., Barnes, C. A., Gerrard, J. L., Gothard, K., Jung, M. W., Knierim, J. J., Kudrimoti, H., Qin, Y., Skaggs, W. E., Suster, M., and Weaver, K. L. (1996). Deciphering the hippocampal polyglot: the hippocampus as a path integration system. *J. Exp. Biol.* 199, 173–185.

McNaughton, B. L., Battaglia, F. P., Jensen, O., Moser, E. I., and Moser, M. B. (2006). Path integration and the neural basis of the 'cognitive map'. *Nat. Rev. Neurosci.* 7, 663–678.

Mhatre, H., Gorchetchnikov, A., and Grossberg, S. (2012). Grid cell hexagonal patterns formed by fast self-organized learning within entorhinal cortex. *Hippocampus* 22, 320–334.

Miall, C. (1989). The storage of time intervals using oscillating neurons. *Neural Comput.* 1, 359–371.

Milford, M. J., Wiles, J., and Wyeth, G. F. (2010). Solving navigational uncertainty using grid cells on robots. *PLoS Comput. Biol.* 6, e1000995. doi:10.1371/journal.pcbi.1000995

Moser, E. I., and Moser, M.-B. (2008). A metric for space. *Hippocampus* 18, 1142–1156.

Navratilova, Z., Giocomo, L. M., Fellous, J.-M., Hasselmo, M. E., and McNaughton, B. L. (2012). Phase precession and variable spatial scaling in a periodic attractor map model of medial entorhinal grid cells with realistic after-spike dynamics. *Hippocampus* 22, 772–789.

O'Keefe, J. (1976). Place units in the hippocampus of the freely moving rat. *Exp. Neurol.* 51, 78–109.

O'Keefe, J., and Burgess, N. (2005). Dual phase and rate coding in hippocampal place cells: theoretical significance and relationship to entorhinal grid cells. *Hippocampus* 15, 853–866.

O'Keefe, J., and Recce, M. L. (1993). Phase relationship between hippocampal place units and the EEG theta rhythm. *Hippocampus* 3, 317–330.

Redish, A. D. (1999). *Beyond the Cognitive Map: From Place Cells to Episodic Memory.* Cambridge, MA: MIT Press.

Remme, M. W. H., Lengyel, M., and Gutkin, B. S. (2009). The role of ongoing dendritic oscillations in single-neuron dynamics. *PLoS Comput. Biol.* 5, e1000493. doi:10.1371/journal.pcbi.1000493

Remme, M. W. H., Lengyel, M., and Gutkin, B. S. (2010). Democracy-independence trade-off in oscillating dendrites and its implications for grid cells. *Neuron* 66, 429–437.

Samsonovich, A., and McNaughton, B. L. (1997). Path integration and cognitive mapping in a continuous attractor neural network model. *J. Neurosci.* 17, 5900–5920.

Sargolini, F., Fyhn, M., Hafting, T., McNaughton, B. L., Witter, M. P., Moser, M. B., and Moser, E. I. (2006). Conjunctive representation of position, direction, and velocity in entorhinal cortex. *Science* 312, 758–762.

Skaggs, W. E., Knierim, J. J., Kudrimoti, H., and McNaughton, B. L. (1995). A model of the neural basis of the rat's sense of direction. *Adv. Neural Inf. Process. Syst.* 7, 173–180.

Skaggs, W. E., McNaughton, B. L., Wilson, M. A., and Barnes, C. A. (1996). Theta phase precession in hippocampal neuronal populations and the compression of temporal sequences. *Hippocampus* 6, 149–172.

Stringer, S. M., and Rolls, E. T. (2006). Self-organizing path integration using a linked continuous attractor and competitive network: path integration of head direction. *Network* 17, 419–445.

Thompson, L. T., and Best, P. J. (1989). Place cells and silent cells in the hippocampus of freely-behaving rats. *J. Neurosci.* 9, 2382–2390.

Touretzky, D. S., Redish, A. D., and Wan, H. S. (1993). Neural representation of space using sinusoidal arrays. *Neural Comput.* 5, 869–884.

van Hemmen, J. L., and Schwartz, A. B. (2008). Population vector code: a geometric universal as actuator. *Biol. Cybern.* 98, 509–518.

Welday, A. C., Shlifer, I. G., Bloom, M. L., Zhang, K., and Blair, H. T. (2011). Cosine directional tuning of theta cell burst frequencies: evidence for spatial coding by oscillatory interference. *J. Neurosci.* 31, 16157–16176.

Welinder, P. E., Burak, Y., and Fiete, I. R. (2008). Grid cells: the position code, neural network models of activity, and the problem of learning. *Hippocampus* 18, 1283–1300.

Yamaguchi, Y., Aota, Y., McNaughton, B. L., and Lipa, P. (2001). Bimodality of theta phase precession in hippocampal place cells in freely running rats. *J. Neurophysiol.* 87, 2629–2642.

Yartsev, M. M., Witter, M. P., and Ulanovsky, N. (2011). Grid cells without theta oscillations in the entorhinal cortex of bats. *Nature* 479, 103–107.

Zhang, K. (1996). Representation of spatial orientation by the intrinsic dynamics of the head-direction cell ensemble: a theory. *J. Neurosci.* 16, 2112–2126.

Zilli, E. A., and Hasselmo, M. E. (2010). Coupled noisy spiking neurons as velocity-controlled oscillators in a model of grid cell spatial firing. *J. Neurosci.* 30, 13850–13860.

Zilli, E. A., Yoshida, M., Tahvildari, B., Giocomo, L. M., and Hasselmo, M. E. (2009). Evaluation of the oscillatory interference model of grid cell firing through analysis and measured period variance of some biological oscillators. *PLoS Comput. Biol.* 5, e1000573. doi:10.1371/journal.pcbi.1000573

**Conflict of Interest Statement:** The author declares that the research was conducted in the absence of any commercial or financial relationships that could be construed as a potential conflict of interest.

*Received: 10 December 2011; accepted: 22 March 2012; published online: 18 April 2012.*

*Citation: Zilli EA (2012) Models of grid cell spatial firing published 2005–2011. Front. Neural Circuits* ***6****:16. doi: 10.3389/fncir.2012.00016*

frontiers in
NEURAL CIRCUITS

ORIGINAL RESEARCH ARTICLE
published: 28 May 2012
doi: 10.3389/fncir.2012.00030

# A model combining oscillations and attractor dynamics for generation of grid cell firing

***Michael E. Hasselmo* and Mark P. Brandon***

*Graduate Program for Neuroscience, Department of Psychology, Center for Memory and Brain, Boston University, Boston, MA, USA*

***Edited by:***
*Lisa Marie Giocomo, Norwegian University of Science and Technology, Norway*

***Reviewed by:***
*Hugh T. Blair, University of California Los Angeles, USA*
*Yuanquan Song, University of California San Francisco, USA*

****Correspondence:***
*Michael E. Hasselmo, Department of Psychology, Center for Memory and Brain, Graduate Program for Neuroscience, Boston University, 2 Cummington Street, Boston, 02215 MA, USA.*
*e-mail: hasselmo@bu.edu*

Different models have been able to account for different features of the data on grid cell firing properties, including the relationship of grid cells to cellular properties and network oscillations. This paper describes a model that combines elements of two major classes of models of grid cells: models using interactions of oscillations and models using attractor dynamics. This model includes a population of units with oscillatory input representing input from the medial septum. These units are termed heading angle cells because their connectivity depends upon heading angle in the environment as well as the spatial phase coded by the cell. These cells project to a population of grid cells. The sum of the heading angle input results in standing waves of circularly symmetric input to the grid cell population. Feedback from the grid cell population increases the activity of subsets of the heading angle cells, resulting in the network settling into activity patterns that resemble the patterns of firing fields in a population of grid cells. The properties of heading angle cells firing as conjunctive grid-by-head-direction cells can shift the grid cell firing according to movement velocity. The pattern of interaction of oscillations requires use of separate populations that fire on alternate cycles of the net theta rhythmic input to grid cells.

**Keywords: entorhinal cortex, stellate cells, whole-cell patch recording, spatial navigation, oscillatory interference**

## INTRODUCTION

Neurophysiological recordings from the entorhinal cortex of rats foraging in an open field environment have demonstrated neurons termed grid cells (Moser and Moser, 2008). Grid cells exhibit spiking activity when the rat visits specific locations in the environment that are laid out in a regular array of locations that fall on the vertices of tightly packed equilateral triangles (Fyhn et al., 2004; Hafting et al., 2005; Moser and Moser, 2008). This regular firing pattern of grid cells indicates that these neurons effectively encode the location of the rat as it moves along a complex trajectory. Grid cells at different dorsal to ventral positions in the medial entorhinal cortex show differences in the size and spacing between their firing fields (Hafting et al., 2005; Sargolini et al., 2006).

A number of models have addressed potential mechanisms for the firing pattern of grid cells that can be categorized based on different features (see Zilli, 2012, this special issue, for review). Among other things, models can be categorized in terms of how they code location. Many attractor models code location with sustained fixed-point attractor states (Fuhs and Touretzky, 2006; McNaughton et al., 2006; Guanella et al., 2007; Burak and Fiete, 2009). In contrast, another class of models code location by the relative phase of oscillations (Blair et al., 2007; Burgess et al., 2007; Hasselmo et al., 2007; Burgess, 2008; Hasselmo, 2008; Zilli and Hasselmo, 2010; Welday et al., 2011). The second class of models is commonly referred to as oscillatory interference models (Burgess et al., 2007), though the oscillatory interference in these models is involved in generating the model output, and the relative phase code itself does not require interference (Zilli, 2012). Both classes of models address certain features of the experimental data.

Many continuous attractor models generate the hexagonal array of firing based on synaptic connectivity between neurons in the entorhinal cortex. The synaptic connectivity is circularly symmetric on average and depends on the distance between the environmental locations coded by individual grid cells. The firing can be updated by velocity input shifting the network attractor. Attractor models can account for the shared orientation of grid cells recorded close to each other in entorhinal cortex (Hafting et al., 2005; Fyhn et al., 2007), for the discrete quantal jumps in grid cell spacing (Barry et al., 2007), and for the sometimes irregular distribution of grid cell firing fields.

In contrast, oscillatory interference models generate the spatial pattern of firing due to interference between oscillations of different frequency (Burgess et al., 2007; Blair et al., 2008; Burgess, 2008; Hasselmo, 2008). In existing implementations of this model, the difference in frequency is driven by the running velocity of the animal, coded by neurons sensitive to head direction and to running speed. Oscillatory interference models provide a framework for generating the theta phase precession of grid cells (Hafting et al., 2008) in models (Burgess, 2008), and for linking the spacing of grid cells to the intrinsic frequency of these neurons as measured with both extracellular recording *in vivo* (Jeewajee et al., 2008) and with intracellular recording of the resonance frequencies of membrane potential dynamics *in vitro* (Giocomo et al., 2007; Giocomo and Hasselmo, 2008). The link to intrinsic properties is supported by recent data showing that changes in intrinsic properties due to knockout of the HCN1 subunit of the h current channel alters the spacing and size of entorhinal grid cell firing fields (Giocomo et al., 2011).

None of the existing models yet account for the full range of data on grid cells. Most initial attractor dynamic models did not require theta rhythm oscillations (Fuhs and Touretzky, 2006; McNaughton et al., 2006; Burak and Fiete, 2009), did not show theta phase precession, and did not link grid cell properties to intrinsic properties. However, a recent model using attractor dynamics does address all of these issues (Navratilova et al., 2011). Continuous attractor models rely on structured circularly symmetric synaptic connectivity to create the pattern of grid cell firing fields. A difference in the gain of velocity input on frequency could generate the change in firing patterns observed with changes in environment size (Barry et al., 2007) or shape (Derdikman et al., 2009). Oscillatory interference models have less dependence on synaptic connectivity, but they require velocity controlled oscillators regulated by speed and with preferred movement direction at intervals distributed at multiples of 60° in order to generate hexagonal patterns of interference. The continuous attractor models do not require this fixed interval of head direction input. Instead, continuous attractor models generate hexagons due to the interaction of circularly symmetric connectivity, consistent with theorems showing that hexagons provide the densest packing of circles (Fuhs and Touretzky, 2006).

The initial proposal of oscillatory interference models addressed both network and single cell implementations (Burgess et al., 2005, 2007; Burgess, 2008). Recent oscillatory interference models have used interactions of network oscillations (Zilli and Hasselmo, 2010) to overcome the issues preventing implementation with single neurons, including the variability of the temporal period of membrane potential oscillations or bistable persistent spiking (Zilli et al., 2009), the tendency of oscillations within single neurons to synchronize (Remme et al., 2009, 2010) and the lack of a linear relationship between membrane potential oscillations and depolarization (Yoshida et al., 2011). However, models using network oscillations (Zilli and Hasselmo, 2010), do not yet explain the link of grid cell spacing to the intrinsic membrane current properties of entorhinal neurons (Giocomo et al., 2007, 2011).

Recent data shows a loss of the spatial periodicity of grid cells when network theta rhythm oscillations are reduced by inactivation of the medial septum (Brandon et al., 2011; Koenig et al., 2011). These recent results along with the data on the cellular frequency of medial entorhinal neurons (Giocomo et al., 2007; Jeewajee et al., 2008) provide impetus for trying to understand how network theta oscillations and single cell intrinsic frequency contribute to the mechanism of grid cell generation. As a step in this direction, the model presented here combines oscillations and attractor dynamics to generate simulations of grid cell firing fields.

## MATERIALS AND METHODS

### OVERVIEW OF MODEL

The model uses two populations of neurons inspired by experimental data. One population represents grid cells without head direction selectivity in medial entorhinal cortex, as described initially in the Moser laboratory (Fyhn et al., 2004; Moser and Moser, 2008). Cells in the second population are termed heading angle cells, and they are inspired by conjunctive cells that combine sensitivity to head direction with the spatially periodic firing of grid cells, as discovered in the Moser laboratory (Sargolini et al., 2006) and replicated in later work (Hafting et al., 2008; Brandon et al., 2011). Similar to conjunctive cells, this second population in the model contains cells that increase their activity when the rat is moving and the current head direction angle matches their preferred head direction, but they also have a background level of activity for all current head directions. This population has fixed, unchanging connections to the grid cell population with a pattern of connections that depends on each cells preferred heading angle in the environment. The rationale for these neurons is that the ability to shift the grid cell representation for movement in any arbitrary heading could arise from transitions between heading angle cells coding sequential spatial phases along that heading. The grid cell population has fixed, unchanging connections back to the heading angle cells such that grid cells coding a specific spatial phase of locations connect to an array of heading angle cells coding that same spatial phase.

### HEADING ANGLE CELLS

In the model, the heading angle cells are divided into separate sub-populations referred to here as arrays. Each array of heading angle cells codes a specific spatial phase designated by spatial phase indices $x$ and $y$. Spatial phases have integer values $x = [1, 2...30]$ and $y = [1,2...30]$ for a total of 900 arrays of heading angle cells. Within each heading angle cell array there are cells coding a full range of 24 heading angles (at 15° intervals), and each heading angle is coded by 10 cells that oscillate with different temporal phases. These cells have fixed, unchanging matrices of synaptic connections to a population of grid cells that contains a single grid cell coding each spatial phase (i.e., 900 total grid cells).

The fixed pattern of synaptic connections from heading angle cells to grid cells is based on the allocentric heading angle $\phi$ coded by individual heading angle cells, for example toward the East (0° heading angle), or the Northeast (45° heading angle). The structure of the model is summarized in **Figures 1** and **2**. In the figures, the activity of the heading angle cells is usually shown as the pattern of synaptic output to the grid cell population from individual heading angle arrays, filtered by the fixed pattern of synaptic connectivity between the heading angle array and the grid cell population. In the figures, the neurons will be plotted according to how their spatial phase maps to the environment, but this does not imply that neurons are laid out with anatomical topography within the entorhinal cortex, as data shows they are not (Hafting et al., 2005).

Note that the model equates head direction with the direction of movement by the rat, making the assumption that when the rat is moving its head direction is usually in the direction of movement. In contrast to many oscillatory interference models, this model does not focus on heading angles that fall at intervals of 60°. Instead, this model utilizes neurons coding a large number of heading angles at regular intervals (at 15° intervals). The spatial phases of each array of heading angle cells are similar to the spatial phases of the firing fields of conjunctive cells (Sargolini et al., 2006; Brandon et al., 2011). This corresponds to the relative position coded by the heading angle cell in the environment, but because the coding is periodic it does not limit the spatial range that can be coded by the network.

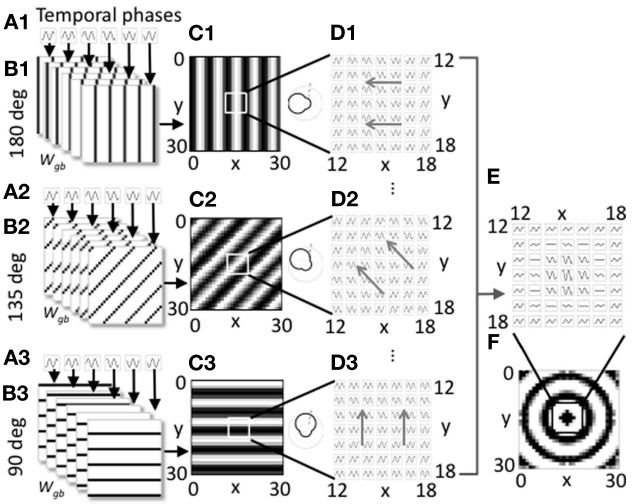


**FIGURE 1 | Overview of model components for a single spatial phase.** **(A1–A3)**. Three groups of heading angle cells described by Eq. 1 show oscillations over time with different temporal phases (six phases shown). **(B1–B3)** The three groups project to grid cells with synaptic connectivity that depends on the six different temporal phases and the heading angles of 180° **(B1)**, 135° **(B2)**, and 90° **(B3)**. Only 3 of 24 heading angles are shown. Connectivity also depends upon spatial phase. The groups shown all code a single spatial phase. **(C1–C3)** At a single time *t*, the synaptic input to the grid cell population from a full set of temporal phases coding an individual heading angle and spatial phase contains bands of higher amplitude (black). The polar plots on the right show how the output amplitude for each heading angle will change dependent on the direction of movement. **(D1–D3)** The full time course plotted for a 7 by 7 array of synaptic inputs shows that they oscillate over time with different temporal phases and align to form different spatial bands. Different spatial phases reach the peak of the oscillation at different times resulting in a shift in the bands over time in the direction of the gray arrows. **(E)** Synaptic input to a 7 by 7 array of grid cells is shown summed across all heading angles for a group of cells coding the spatial phase in the center of the grid cell plane ($x = 15$, $y = 15$). **(F)** At a single point in time, for this single spatial phase, the distribution of synaptic input to the full 30 by 30 array of the grid cell plane when summed over all heading angles has a circularly symmetric pattern.

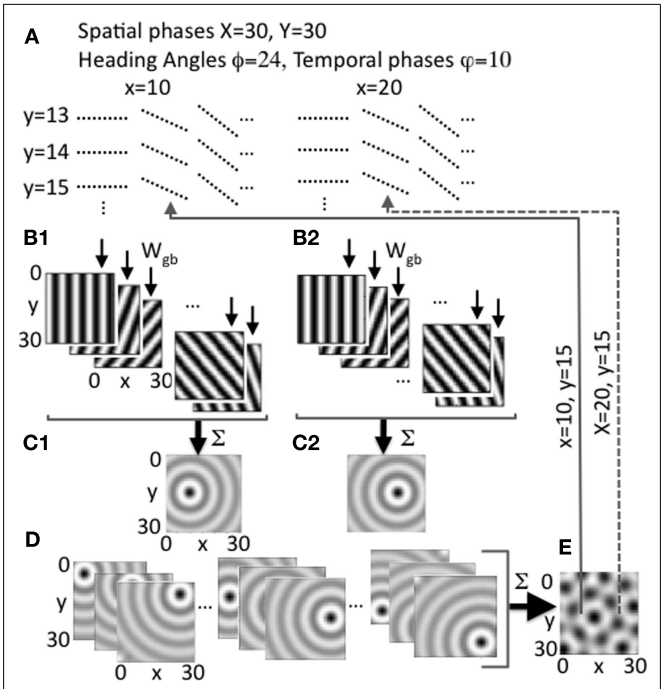


**FIGURE 2 | Heading angle input across the full range of spatial phases.** **(A)** Each spatial phase (*x, y*) is coded by a heading angle array that includes 24 different heading angles with 10 different temporal phases in each heading angle. Examples show 3 out of 24 angles for individual spatial phases $y = 13$, 14, 15 and $x = 10$, 20, with 10 temporal phases (dashed lines) for each angle. **(B1,B2)** Examples show synaptic output to the grid cell plane from different heading angle cell groups coding 5 out of 24 angles for a single spatial phase at a single point in time *t*, with bands of higher amplitude synaptic input shown in black. **(B1)** Shows example output for a single pair of spatial phases $x = 10$, $y = 15$, and **(B2)** shows output for $x = 20$, $y = 15$. **(C1)** Sum of all heading angle output plotted at a single time *t* for a single spatial phase ($x = 10$, $y = 15$). The sum over heading angles creates an amplitude pattern of circles in the grid cell plane centered on the grid cell spatial phase $x = 10$, $y = 15$. **(C2)** The sum of the synaptic output over all heading angles for spatial phase $x = 20$, $y = 15$. **(D)** Examples show synaptic output for a range of different spatial phases (left: $y = 5$, $x = 5$, 15, 25; center: $y = 15$, $x = 5$, 15, 25; right: $y = 25$, $x = 5$, 15, 25). **(E)** The synaptic output from heading angles is summed across all spatial phases in the grid cell plane. The example shows that differences in the relative amplitude of the heading angle input will result in a grid cell pattern. Arrows show examples of feedback from individual grid cells in the grid cell plane that project back to regulate input from heading angle cell arrays coding $x = 10$, $y = 15$ (solid line) and $x = 20$, $y = 15$ (dashed line).

The heading angle cells at each spatial phase *x, y*, and each heading angle $\phi_i$ have temporal dynamics of their membrane potential $b(t)$ described by a difference equation:

$$b_{\phi,\varphi,x,y}(t) = \tau b(t-1) + \sin\left(2\pi\left(ft + \varphi_k\right)\right) \times \left[g_{x,y}(t) - \lambda_g\right]_+ / \max_{x,y}\left(g\left(t\right)\right) \quad (1)$$

This difference equation models the persistence of activity from the previous time step according to tau ($\tau = 0.2$). The equation also includes oscillatory input from the medial septum with a temporal frequency *f* which was set to 4 Hz to replicate properties of theta cycle skipping, so that the grid cell population would generate a frequency of 8 Hz as described below. For each pair of spatial phases *x, y*, and heading angle $\phi_i$ (with index i) there is a full array of neurons with different temporal phases $\varphi_k$ described by the index *k*. The temporal phase $\varphi_k$, the spatial phases *x, y*, and the heading angle $\phi_i$ all determine the pattern of connectivity of a given heading angle cell to the array of grid cells. The temporal phase determines the position along each heading angle for connections to the grid cell array. The oscillatory activity described by equation 1 is shown for different temporal phases in **Figures 1A1–A3.** The figure also shows the synaptic output of these cells that is described below in the section on Connectivity with Grid Cells.

Equation 1 for heading angle cell activity also includes feedback from the grid cell population $g(t)$, where each array of heading angle cells coding a specific spatial phase *x, y* have their oscillatory input multiplied by the corresponding activity of the grid cell $g_{x,y}$. That is, the grid cell with spatial phase coordinates *x,y* regulates the activity of the array of heading angle cells with spatial phase coordinates *x,y*. If the activity of both regions were laid out as vectors, the connectivity would be an identity matrix. The feedback from

grid cells has a threshold linear input-output function designated by $[]_+$ that takes the value of the grid cell activity $g(t) - \lambda_g$ when it is above the threshold $\lambda_g = 0.6$ and stays at zero below threshold. In addition, the grid cell output was sometimes normalized to the maximum activity level of individual grid cells $\max_{x,y}(g(t))$ at time $t$ measured over all spatial phases $x,y$. This normalization helps to prevent the system from exploding or dying out in activity. This normalization was used in **Figure 5** to provide greater stability during movement, but was not used in the other figures in order to allow the time courses to be more visible in the plots in **Figure 7**. This effect could be mediated by feedback inhibition.

#### CONNECTIVITY WITH GRID CELLS

The heading angle cells project to the grid cells via patterns of synaptic connections that depend upon the heading angle cell properties including assigned spatial phase, heading angle and temporal phase. As shown in **Figure 1B**, each heading angle cell sends connections to grid cells arranged in lines in the grid cell plane with angles across the plane that depend upon the heading angle of the originating cell. The connections from the heading angle cell array $b$ to the grid cell population $g$ is described by a multi-dimensional matrix $W_{gb}$. This can be considered as an array of individual matrices, each of which connects a vector of heading angle cells with different temporal phases (but the same spatial phase and heading angle) to grid cells with different spatial phases $x$, $y$. The synaptic weights have values of 0 or 1. The index $k$ for weights to be set to 1 is determined by the following equation:

$$W_{gb}\left(x, y, px, py, k, i\right) = 1 \tag{2}$$

if:

$$k = \text{round}(K(\text{mod}\,(f_s(\cos(\phi_i)(x - px)/X + \sin(\phi_i)(y - py)/Y), 1)))$$

where $x$, $y$ describe the spatial phase in the grid cell population. For computing connectivity from the heading angle cell population, px and py describe the spatial phase in this equation, $\phi_i$ describes the heading angle. The value $k$ is the index for the heading angle cell with temporal phase $\varphi_k$ and $K$ is the total number of different temporal phases of the heading angle cells coding a specific spatial phase $px$, $py$, and heading angle $\phi_i$. The value $f_s$ is the spatial frequency which in the simulations shown here ranged between three and five cycles across the full range of spatial phases in the population. $X$ is the total number of discrete spatial phases along the spatial phase dimension indexed by $x$ (and $px$), and $Y$ is the total number of discrete spatial phases along the dimension of spatial phase indexed by $y$ (and $py$). The use of the mod function mod() ensures that values beyond the range of the matrix are mapped back into the matrix.

Equation 2 is not particularly intuitive, but the connectivity pattern is relatively simple as shown in **Figure 1B**. Each heading angle cell connects to the plane of grid cells in bands that have heading angle $\phi_i$, a spatial phase offset $px$, $py$, and a position within each cycle of spatial phase that depends upon temporal phase $\varphi_k$. The connections for six heading angle cells with different temporal phases are shown in **Figure 1B1** (for cells with heading angle 180), in part B2 for cells with heading angle of 135° and in part B3 for cells with heading angle of 90°. This results in synaptic output with bands of shared phase to the grid cell plane (**Figures 1C,D**).

**Figure 1** shows how the individual sets of heading angle cells have different temporal phases for different relative positions along an individual heading angle. The position of these temporal phases is offset for neurons with different two-dimensional spatial phases. As shown in **Figure 1C**, each set of active cells multiplied by the fixed synaptic connectivity matrix $W_{gb}$ produces synaptic output with temporal phases of oscillation that appear in bands across the environment that are perpendicular to the preferred heading angle. Each square in **Figure 1C** shows the result of multiplying the synaptic connectivity matrices in **Figure 1B** with the vector of heading angle cells with different temporal phases that code an individual spatial phase with an individual heading angle. For a single snapshot in time, as shown in **Figure 1C**, the differences in temporal phase result in bands of higher amplitude that are perpendicular to the preferred heading angle. A movie of this activity over time shows waves of activity that move across the plane of spatial phases in the direction of the heading angle, as indicated by the gray arrows in **Figure 1D**. When the output of heading angle cells is summed across all heading angles, this results in a standing wave pattern of concentric circles as shown across time in **Figure 1E** and at a single point in time in **Figure 1F**. The polar plots in **Figure 1C** show that the amplitude of the oscillations depends upon the heading direction of the virtual rat. There is a background oscillation of amplitude one for all heading angles regardless of the heading of the virtual rat, but this amplitude is increased when the rat runs in a heading that matches the heading angle for individual heading angle cells. The heading angle cell amplitude is also influenced by the feedback from the grid cells which show spatial periodicity, so these heading angle cells have properties of spatial periodicity, theta rhythmicity, and heading angle sensitivity similar to conjunctive cells (but with a baseline response during all directions of movement).

#### INTERACTION BETWEEN HEADING ANGLE CELLS AND GRID CELLS

The array of heading angle cells sends input to the array of grid cells via the connectivity matrix $W_{gb}$. The activation of the grid cells is described by:

$$g_{x,y}(t) = \tau g(t-1) + \sum_{\phi,px,py} W_{gb} b_{px,py,\phi,\varphi}(t) / \max_{x,y}\left(W_{gb} b\,(t)\right) \tag{3}$$

Where $g_{x,y}(t)$ represents the activation of an individual grid cell with spatial phase described by $x$, $y$. The activity of the grid cell shows persistence of activity from the previous timestep according to the parameter tau ($\tau = 0.3$). As described above, for each group of heading angle cells with a specific spatial phase $px$, $py$ and heading angle $\phi$, individual heading angle cells with temporal phase $\varphi$ send output to grid cells at periodic spatial phases $x$, $y$. The number of spatial bands of this periodic output are determined by the spatial frequency $f_s$ of the synaptic connectivity and the total number of spatial phases $X$ and $Y$ being simulated. As shown

in Eq. 3, the inputs to the grid cell are summed over the array of heading angles ϕ (**Figures 1F** and **2C,D**) and are also summed over the different spatial phases *px,py* and of the heading angle cell population (**Figure 2E**). In most simulations, the activity is normalized to the spatial phase *x,y* with maximum value at time *t* of the synaptic input from the heading angle plane that was summed across angles (the maximum is taken from the full set of possible combinations of postsynaptic spatial phases *x,y* and presynaptic spatial phases *px,py*). The activity in the grid cell plane starts out with random activity drawn from a uniform distribution between 0 and 1.

As shown previously in Eq. 1, the heading angle cells receive feedback from the grid cells via direct one to one connections from grid cells coding the corresponding spatial phase $x = px$ and $y = py$. Thus, if we consider only the spatial phase index *px, py* of the heading angle cells and lay them out in a single vector, then the feedback connectivity matrix from grid cells to heading angle cells would be an identity matrix. The normalization of the feedback from the grid cell layer in Eq. 1 is sufficient to keep the network within a stable range of activity when implemented alone, but in most simulations normalization to a maximum was used in both Eqs 1 and 3.

The input arising from the heading angle population is summarized in **Figure 2** which shows examples of the synaptic output for different heading angles. Note that **Figures 1C** and **2B** plot the amplitudes at one point in time of the full set of synaptic inputs from each heading angle to the grid cell plane. This results in input to the grid cell population that constantly shifts in phase in the direction of heading angle over time (see **Figure 6** below), similar to rotating ring attractors in models by Blair (Blair et al., 2007; Welday et al., 2011). The different temporal phases result in a constant shift in amplitude of synaptic input in all 24 directions across the grid cell plane. Summation of these waves of activity over all 24 different directions results in a circularly symmetric standing wave of synaptic input to the grid cell plane, as illustrated in **Figures 1F** and **2C,D**. However, the model is not proposing cells with circularly symmetric firing fields in medial entorhinal cortex. This is just the pattern of synaptic activation arising from summation across all heading angles of the synaptic input from heading angle cells coding a single spatial phase. This resembles the mechanism used to create synaptic weights in one of the models using continuous attractors (Fuhs and Touretzky, 2006), but the synaptic connectivity used here is not circular but organized in bands. The center of the circle of synaptic output depends upon the spatial phase coded by the active cells in the heading angle population. Thus, the sum of the input from heading angle neurons with the correct phase creates synaptic input that peaks at the center of the circle with coordinates *x, y*.

At a single point in time, heading angle synaptic output can have different relative spatial phases as shown in **Figures 2B1,B2**. Close inspection of the figure will reveal that the bands for each angle have spatial phases that differ between 2B1 ($x = 10$, $y = 15$) and 2B2 ($x = 20$, $y = 15$). As shown in **Figures 2C1,C2**, and **2D**, when the synaptic outputs for different angles in the heading angle array are summed together they generate input to the grid cell population that appears as concentric circle patterns with different spatial phases. **Figure 2C1** is centered on spatial phase $x = 10$, $y = 15$, and **Figure 2C2** is centered on spatial phase $x = 20$, $y = 15$. All the interactions in the model involve summing over both heading angles and spatial phases, but to help understanding of the model the summation over heading angles is shown alone in **Figures 1E,F** and in **Figures 2C,D** before the synaptic output is summed over all spatial phases to generate the activity in the grid cell population (e.g., **Figure 2E**). Each grid cell coding an individual spatial phase *x, y* then sends feedback that regulates input from the full array of heading angle cells (including all angles and temporal phases) that code that individual spatial phase.

To summarize, at a single point in time, the amplitude of synaptic input from the population of heading angle cells has a band like pattern that may seem analogous to a population of band cells from oscillatory interference models (Burgess et al., 2007). However, this is just at a single point in time. Due to the differences in temporal phases, the activity shifts through spatial phases along the direction of each separate heading angle plane. Thus, these neurons have a specific temporal phase dependent upon their one-dimensional spatial phase, like the cells used in spiking versions of the oscillatory interference model (Burgess, 2008; Hasselmo, 2008) or the ring attractors in models by Blair (Blair et al., 2007; Welday et al., 2011). These waves of temporal phase shifts move simultaneously in the direction of all heading angles. Summation over all heading angles results in standing waves that have the concentric circle pattern shown in **Figures 1** and **2**. These patterns are then summed across all spatial phases to drive the activity of the grid cell population (e.g., **Figure 2E**). The grid cell population then sends feedback to regulate the magnitude of input based on the spatial phase.

## RESULTS

### GENERATION OF GRID CELL ACTIVITY

The feedback interaction between the population of heading angle cells and the population of grid cells results in activity in the grid cell plane settling into a pattern resembling the distribution of grid cells. As shown in **Figures 3A1–A5**, this iterative process results in a gradual evolution of the activity in the grid cell population and heading angle cell from an initial random distribution with regions of higher activity to a regular hexagonal array of active regions. This evolution results from the iterative interaction of the grid cell population with the heading angle cell population. This interaction is similar in effect and mathematical structure to the generation of grid cells in attractor dynamics models, but instead of using circularly symmetric synaptic connectivity, the interaction depends upon feedback to groups of heading angle cells receiving oscillatory input from medial septum that project to the grid cells based on different heading angle preferences. The summation across all heading angles results in circularly symmetric patterns of input to the grid cell population.

If the network is balanced properly, the activity converges to a stable pattern of activity in the grid cell population (**Figure 3C**, same as **Figure 3A5**). This results from a stable pattern of synaptic output from heading angle arrays including the components shown in **Figure 3B**. In **Figure 3B**, each pattern that looks like concentric circles shows synaptic output from an array of heading angle cells coding an individual spatial phase, after the vector of temporal phases is multiplied by the synaptic connectivity matrix

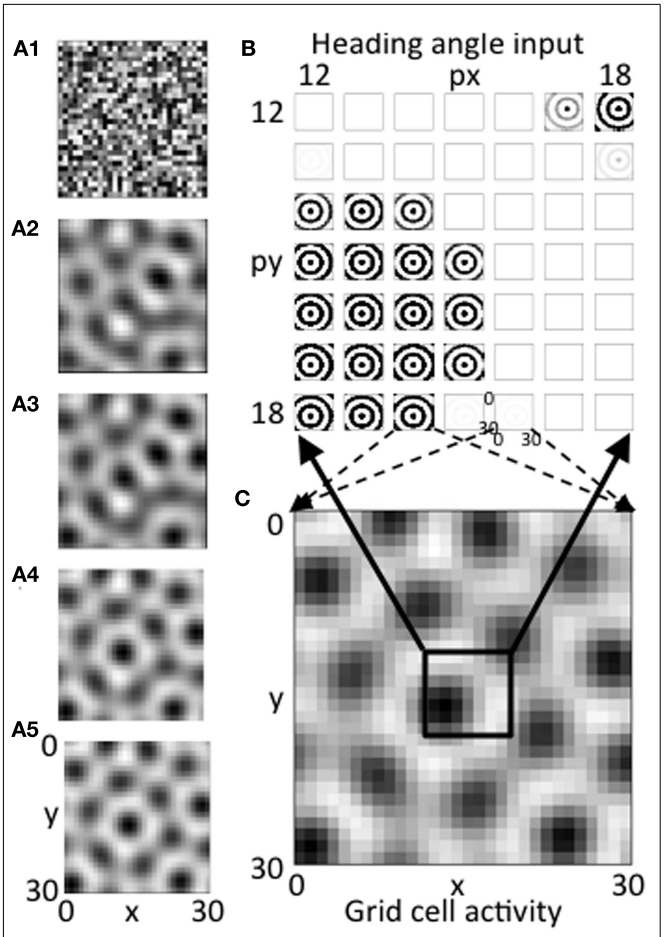


**FIGURE 3 | (A1–A5)** The evolution of activity in the grid cell plane at different stages during the iterative interaction. The network starts with random activity that then evolves into a hexagonal array of firing fields in a manner similar to continuous attractor dynamics models of grid cells. **(B)** Example of the magnitude of synaptic input at a single time step at the end of the simulation for a 7 by 7 set of heading angle cell arrays. The full simulation contains 30 spatial phases in the *px* dimension and 30 in the *py* dimension, but only a 7 by 7 array of spatial phases from the center is shown (phases 12–18). The input from heading angle cells at a specific spatial phase is determined by feedback from the grid cell plane. **(C)** The pattern of activity in the full grid cell plane with 30 by 30 spatial phases showing how feedback regulation of the pattern of summed activity from the heading angle plane produces a grid cell firing pattern that is stable. The pattern is stable because the pattern created by summing the 30 by 30 pattern of synaptic input from the 30 by 30 array of spatial phases of heading angles **(B)** matches the pattern of feedback activation of the heading angle array from active cells in the 30 by 30 array of grid cells **(C)**.

$W_{bg}$ and summed across all heading angles. The population of grid cells coding 30 by 30 different spatial phases have different levels of activity that provide feedback to 30 by 30 different groups of heading angle cells representing different spatial phases. For each grid cell that is highly active (e.g., black region in lower left of black box in **Figure 3C**), the corresponding input to the whole grid cell population from the heading angle array coding that same spatial phase is strong (e.g., black concentric circles in lower left portion of **Figure 3B**). Thus, the feedback from the grid cells to the heading angle cells causes them to have spatial periodicity similar to the grid cell population.

**Figure 3B** shows synaptic inputs to the grid cell plane from a 7 by 7 selection of heading angle cell arrays (spatial phases $x = 12$–18 and $y = 12$–18) driven by the active grid cells in the 7 by 7 central spatial phases of the 30 by 30 population. This smaller 7 by 7 selection is shown to enhance visibility of the synaptic output arising from each of the heading angle arrays, because this synaptic output projects to the full 30 by 30 population of grid cells (the dashed arrows show this projection for a pair of example phases). The summed synaptic input from the heading angle cells to the grid cells consists of circularly symmetric standing waves that extend across the full population of 900 grid cells. If all heading angle cells are equally active, the input is uniform. But the random initial activity in the grid cell population (**Figure 3A1**) causes feedback that results in non-uniform activity in heading angle arrays coding different spatial phases. Each input interacts with input from all the other heading angle cells with different phases to generate activity that converges to a hexagonal pattern. The ongoing interaction results in the individual arrays of heading angle cells that code different spatial phases having activity that is strongest when they match the grid cell activity pattern driven by heading angle input summed over different angles and spatial phases. The feedback interaction results in a hexagonal pattern of activity in the grid cell plane (**Figures 3A5,C**) and results in corresponding patches of activity in the heading angle arrays (shown for the 7 by 7 set of spatial phases in **Figure 3B**).

The network that generated the simulations shown in **Figure 3A** was run multiple times with different random initial conditions. The network converged to a grid-like pattern each time and generated grid-like patterns with a range of different spatial phases and orientations, similar to what occurs in continuous attractor dynamic models.

### FEEDBACK INTERACTION FROM GRID CELL TO HEADING ANGLE CELLS

The network involves an interaction between the sum of a wide range of heading angle inputs and the plane of grid cells. As an example in the absence of feedback, the heading angle output with a full array of spatial phases are shown in **Figure 4A**, illustrating the coding of output starting from a wide range of different spatial phases. Close inspection of the figure will reveal that the concentric circles are centered on different spatial phases (different spatial phases $x$ and $y$). **Figure 4A** shows a 7 by 7 array of summed outputs from heading angle groups representing central spatial phases within a larger simulation with a full array of heading angle inputs with 30 different spatial phases in the $x$ dimension and 30 different spatial phases in the $y$ dimension.

The grid cell population begins with initial random magnitudes of activity in different spatial locations as shown in **Figure 4B**. This initial spatially random activity in the plane of grid cell activity has a multiplicative influence on the activity in the heading angle cell populations, as shown by the synaptic input from the 7 by 7 selection of central spatial phases for the heading angle cell arrays shown together in **Figure 4C**. Multiplicative interactions in neural circuits have been proposed to be mediated by interactions in the dendritic tree involving depolarizing input that activates NMDA receptors (Mel, 1993) or gating of dendritic spike

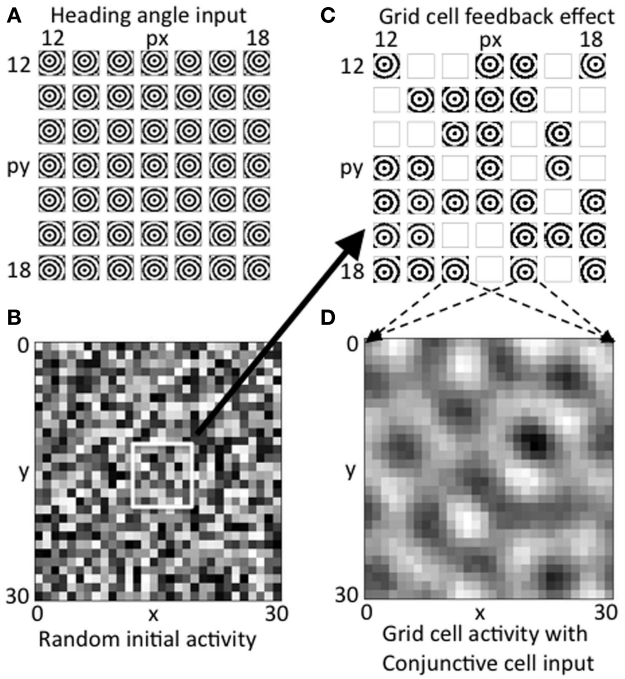


**FIGURE 4 | Activity on first two time steps. (A)** The array of concentric circles due to summation of synaptic input from all heading angle cells at a 7 by 7 array of heading angle spatial phases. The centers fall at different locations dependent on the different spatial phases of the heading angle cells. **(B)** Initial random activity in the grid cell population shown for all 30 by 30 spatial phases of grid cells. **(C)** Feedback from the random grid cell activity in **(B)** interacts with the corresponding array of heading angle cells at the same spatial phases. Where there is high activity in the grid cell initial random activity, the summation of synaptic input from heading angle planes yields a strong concentric circle input. Where random activity in the grid cells falls below threshold the synaptic input from heading angle cells is absent. **(D)** The heading angle synaptic input in **(C)** regulated by random feedback is summed together across the grid cell plane to generate a pattern of activity that already shows peaks of activity falling in a hexagonal pattern due to the overlap of concentric circles.

propagation (Jarsky et al., 2005). This could involve input from grid cells that influence the dendritic integration of cells receiving particular heading angle inputs and particular phases of oscillation. Where the magnitude of random activity in the grid cell population is larger, this causes stronger synaptic input from the corresponding set of heading angle cells in **Figure 4C** (for example, grid cells that appear as active black squares in **Figure 4B** correspond to stronger concentric standing waves in the heading angle synaptic inputs in **Figure 4C**). There is a threshold on the feedback from the grid cell plane in **Figure 4B**, so grid cell units at spatial phases with low magnitude in 4B give a mean output of zero, resulting in the absence of activity (white boxes) for the corresponding spatial phases of heading angle arrays in **Figure 4C**. Overall, this results in random activation of the heading angle input shown in **Figure 4C**.

The heading angle planes in **Figure 4C** are then summed together in **Figure 4D**. Synaptic output from the entire range of 30 by 30 spatial phases of heading angle arrays are summed up (for visibility only a 7 by 7 subset of summed heading angle inputs to the grid cell population are shown in **Figure 4C**). The summation across all spatial phases of heading angle arrays yields the distributed pattern of grid cell activity shown in **Figure 4D**. This already shows elements of a hexagonal distribution of activity due to the properties of interacting heading angle synaptic input. This provides the start of a feedback cycle that involves iterative interaction. On each cycle, the summed activity at each time step in the grid cell population (**Figure 4D**) is multiplied by the activity at each time step in the corresponding spatial phases of heading angle arrays shown summed across heading angle in **Figure 4C**, resulting in a varying magnitude of these inputs back to the grid cell plane. This then results in the progression of iterations in grid cell activity shown in **Figures 3A1–A5**, and ends with the final state of activity in heading angle cells in **Figure 3B** and in the grid cell population shown in **Figure 3C**.

### SHIFT IN GRID CELL ACTIVITY WITH MOVEMENT

The network has the capability of representing the influence of movement on the grid cell representation. This was implemented in the model by adding to the amplitude of oscillations in the heading angle cells in proportion to the cosine of the difference between the cell heading angle and the simulated movement heading angle (as shown in **Figure 5D**). The tuning shown in **Figure 5D** could represent heading angle cells that have the properties of speed-modulated conjunctive grid-by-head direction cells with baseline activity for all headings. Alternately, this could represent two separate populations of heading angle cells, one of which is active for all heading angles, and the other that would contain neurons that are only active when the rat is moving with non-zero speed in specific heading directions. During movement, the cells with heading angle preference angle $\phi_i$ closest to the current heading angle $\phi(t)$ produced the strongest synaptic output to the grid cell plane. Other cells increased their amplitude of oscillation in proportion to the cosine of the angle between their heading angle and the current movement direction of the virtual rat and speed S, as described in the following modified version of Eq. 1.

$$b_{\phi,\varphi,x,y}(t) = \tau b(t-1) + (1 + S\cos(\phi(t) - \phi_k)) \times \sin\left(2\pi\left(ft + \varphi_k\right)\right)\left[g_{x,y}(t) - \lambda_g\right]_+ / \max_{x,y}\left(g(t)\right) \quad (4)$$

The effect of this input on the pattern of activity in the model is shown in **Figure 5**. This figure shows the effect of sustained movement in the direction West (angle $\phi(t) = \pi$) starting at time step 10 and continuing at constant level (intervals of 5 time steps are shown). As shown in **Figure 5A**, the grid cell population settles to a pattern of activity corresponding to multiple fields in a hexagonal distribution at time step 10. As the movement input continues, this pattern of grid cell activity progressively shifts to the West over subsequent time steps 15–35. Note that this would result in individual grid cells that increase and decrease in activity similar to experimental data. There was not sufficient space in the figure to show individual time steps, but at the level of single time steps, there is a small scale forward and backward shift on each cycle of the theta rhythm oscillation in the model similar to that observed previously for place cells.

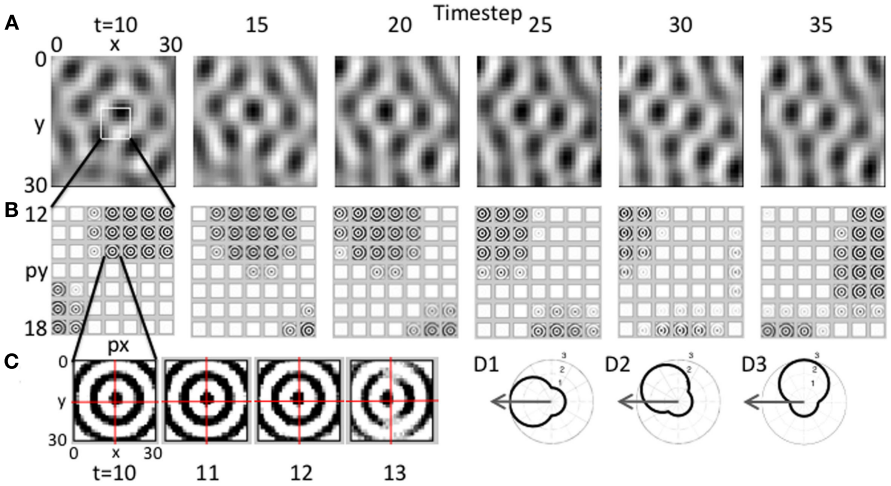


**FIGURE 5 | Movement of the grid cell activity induced by speed modulation of head direction input. (A)** With constant speed and with head direction facing West, the network receives greater input from the heading angle line coding West. This causes a progressive shift in the population activity of the grid cell plane, resulting in the hexagonal pattern shifting to the West. **(B)** This shift occurs because of the distortion in the circular pattern of synaptic input. The synaptic weights do not change, but the greater amplitude of oscillations in heading angle cells coding angles closer to West distorts the magnitude of synaptic input from each array of heading angle cells, resulting in a progressive shift of grid cell activity to the West. Feedback from the grid cell plane to the heading angle plane causes a progressive shift in the synaptic input. **(C)** Expansion of the synaptic input from the heading angle neurons coding a single spatial phase shows that on successive time steps 11–13 the circles show a distortion toward the West. Rhythmic regulation of the network prevents activity during the period when the same heading angle input would distort the pattern toward the East. **(D1)** A polar plot shows the amplitude of response of a heading angle cell with an angle of 180° (West). The arrow shows how the input velocity causes a maximum change in amplitude (3.0) for this heading angle cell. **(D2)** A heading angle cell with angle of 135° (Northwest) has a smaller change in amplitude (2.4). **(D3)** A heading angle cell with angle of 90° (North) shows no change in response for this velocity, but maintains the background amplitude (1.0).

This shift in the pattern of activity is due to the interaction of the grid cell population with the heading angle population, resulting in a progressive Westward shift in the synaptic input from the heading angle cells as shown in **Figure 5B**. This is driven by an increase in amplitude of a subset of oscillations causing a shift in the synaptic input from heading angle cells to grid cells. There is no change in synaptic connectivity, but the distribution of synaptic input to the grid cells is skewed by the larger amplitude of oscillations in one set of heading angle cells. This shift in the distribution of input is visible in the overall distribution of activity in **Figure 5B**, time step 30.

To make the shift in synaptic input clearer, the input from one set of heading angle cells across the full set of heading angles is shown in **Figure 5C**. This shows the circularly symmetric synaptic input from a set of heading angle cells coding an individual spatial phase. On time steps 10–13 in **Figure 5C**, there is a progressive shift in distribution of the synaptic activity from East to West. This shift is what drives the overall shift in grid cell activity in A that then shifts the magnitude of synaptic input from heading angle cells in B so that the new position is held and movement continues. Note that if the full cycle of oscillation interactions were included, the network would shift back due to oscillations with different temporal phase shifting the activity backward. This is prevented by regulation of activity so that heading angle cells are only active on a specific set of phases, as described below.

#### REGULATION OF PHASE OF HEADING ANGLE ACTIVITY

The effective function of the model required regulation of the phase of activity in the heading angle cells providing synaptic input to the grid cell population. There are two reasons this regulation was necessary: (1) to allow oscillations to drive activity in one direction, and (2) to prevent opposite distributions of spatial activity. In the simulations, the regulation of activity took the form of oscillatory gating of input at different phases. This could represent the effects of rhythmic inhibition in the entorhinal cortex. The oscillatory gating depended on a periodic Heaviside step function with timing determined by an oscillation with a phase offset $2\pi/8$ and a threshold $\lambda = 0.24$, as follows:

$$b_{\phi,\varphi,x,y}(t) = \tau b(t-1) + (1 + S\cos(\phi(t) - \phi_k)) \times \left[\sin\left(2\pi\left(ft + 1/8\right)\right)\right]_H \sin\left(2\pi\left(ft + \varphi_k\right)\right) \times \left[g_{x,y}(t) - \lambda_g\right]_+ / \max_{x,y}\left(g(t)\right) \quad (5)$$

The selection of the threshold and phase offset was partly determined by the parameters that allowed effective movement of the grid cell firing fields (reason #1 above). The phase offset meant that oscillations with a particular temporal phase would influence the synaptic output of the network (**Figure 5C**), without different phases causing a corresponding shift in the opposite direction. Thus, this allowed the network to show effective movement without being counteracted by different oscillatory phases.

As noted above, the second reason for regulation of the phase of heading angle activity was to avoid the opposite pattern of spatial activity. The gate shown above in the equation was used for one population of heading angle cells (Group A) and the same gate offset by an additional phase shift of $\pi$ was used to gate the activity of a different population of heading angle cells (Group B).

The need for this regulation of opposite spatial activity is shown in **Figures 6A,B**. **Figure 6A** shows the temporal dynamics of heading angle cells and the synaptic input to grid cells. This shows the synaptic output of heading angle cells coding one spatial phase ($x = 15$, $y = 15$). Each column shows the distribution of synaptic output from 6 out of the 24 different heading angles for each of the 10 time steps (the other 18 heading angles are not shown). The spatial frequency is 3, so there are three cycles across the full range of 30 by 30 spatial phases. As the sinewave oscillations of each heading angle cell evolve in time, the difference in temporal phase of the heading angle cells means that the pattern of synaptic input to the grid cell population shifts in the direction of the heading angle on each time step. **Figure 6B** shows that the progressive shift in all directions of the heading angles causes the sum of synaptic input to the grid cells to be a standing wave of oscillations with a circularly symmetric pattern. On timesteps 1–4, the standing wave pattern has maximal activity in the center (spatial phase $x = 15$, $y = 15$) and one ring outside the center. The cross-hairs are there to enhance visibility of the center. On timesteps 5–7, the sum of heading angle outputs results in minimal activity in the center, and a ring just outside of the center, in an opposite pattern from timesteps 1–4. In full simulations, this opposite pattern of activity would disrupt the grid cell firing pattern in the grid cell population.

A number of techniques were tested to overcome this problem, to obtain more stable patterns of activity in the grid cell population. One method that proved effective was used in all of the simulations shown in **Figures 3–5**. As shown in **Figures 6C,D**, these simulations all used two separate populations of heading angle cells that are active during opposite phase time periods. During one period, the gating of activity favored output from Group A (on timesteps 1–4), which then shows synaptic output activity with a maximum in the center ($px = 15$, $py = 15$). Then on timesteps 5–9, Group A is reduced in activity, and Group B is increased in activity to give a similar synaptic input to the grid cell population. The figure shows that the periodic gating then results in the cycle repeating, as shown in timestep 10. As shown in **Figure 6D**, this ensures that the pattern of synaptic input from the heading angle cells is essentially equivalent at most times.

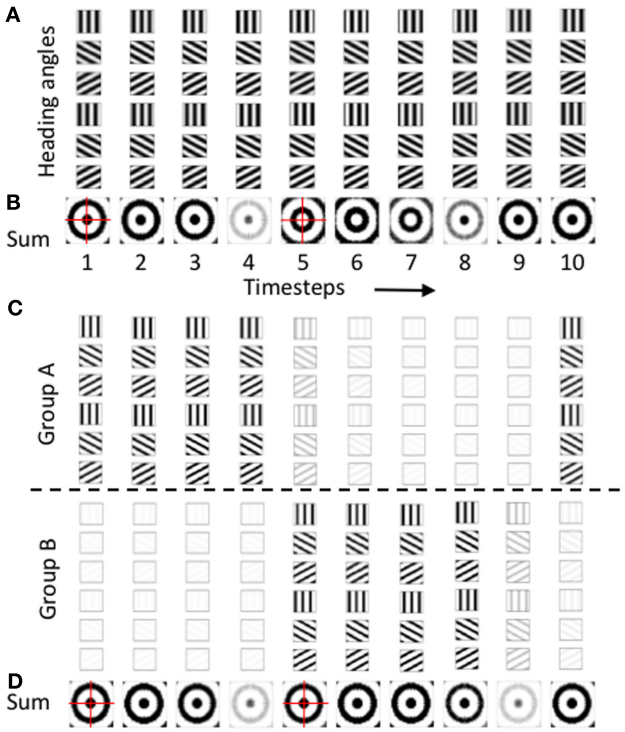


**FIGURE 6 | Temporal dynamics of heading angle cells and synaptic input to grid cells. (A)** The synaptic output of heading angle cells coding one spatial phase ($px = 15$, $py = 15$) are shown for each of 10 time steps, with each column showing the same 6 headings (18 out of 24 headings are not shown). Note that due to the different temporal phases, the pattern of activity shifts in the direction of the heading angle on each time step. **(B)** Sum of synaptic input results in a standing wave of oscillations with a circularly symmetric pattern. On timesteps 1–4, the pattern has maximal activity in the center (spatial phase $px = 15$, $py = 15$) and has one ring outside the center. On timesteps 5–7, the sum of heading angle outputs results in the opposite pattern. **(C)** Use of two separate populations of heading angle cells overcomes this problem. On timesteps 1–4, Group **(A)** shows output activity with a maximum in the center ($px = 15$, $py = 15$). On timesteps 5–9, Group **(A)** is decreased and group **(B)** is increased in activity to give a similar synaptic input to the grid cell population. **(D)** With two groups, the synaptic input from the heading angle cells is similar in pattern at most times.

## RELATIONSHIP TO DIFFERENT CYCLES OF ACTIVITY

Though the pattern of activity is similar on different timesteps in **Figure 6D**, it is clearly evident that the amplitude of the inputs increases and decreases in cycles dependent upon the regulation of heading angle cell activity as well as the magnitude of the oscillations at different temporal phases. **Figure 6D** shows two cycles of periodic changes in activity in the synaptic input to the grid cell population, whereas **Figure 6C** shows a single cycle in each group of heading angle cells providing input (Group A and Group B). If we consider the changes in overall synaptic input to the grid cells to be at theta rhythm frequency (i.e., 8 Hz), then the activity of each of the two groups providing input to the grid cell population would be at half of that frequency (4 Hz), and would show activity on opposite phases of the theta rhythm oscillation. This pattern of activity resembles recent experimental data from unit recordings in awake behaving animals in our laboratory (Brandon et al., 2011; Brandon et al., in review) as well as previously observed experimental data (King et al., 1998; Deshmukh et al., 2010). In the data, head direction cells and conjunctive grid-by-head direction cells in the medial entorhinal cortex show theta cycle skipping, defined as firing on alternate cycles of the network theta rhythm oscillations.

The activity on alternate theta cycles in the model is illustrated further in **Figure 7**. The top of **Figure 7** shows the pattern of activity in the two different populations of heading angle cells, Group A (**Figure 7A**) and Group B (**Figure 7B**). This shows the time-course of activity during the simulation shown in **Figures 3** and **4**. **Figure 7C** shows the time course of the sum of synaptic input to the grid cell population. Note that because the time course of synaptic input includes input from both populations, the frequency of this input is double that of the individual populations. In subsequent discussion, the frequency of the total synaptic input to the grid cell

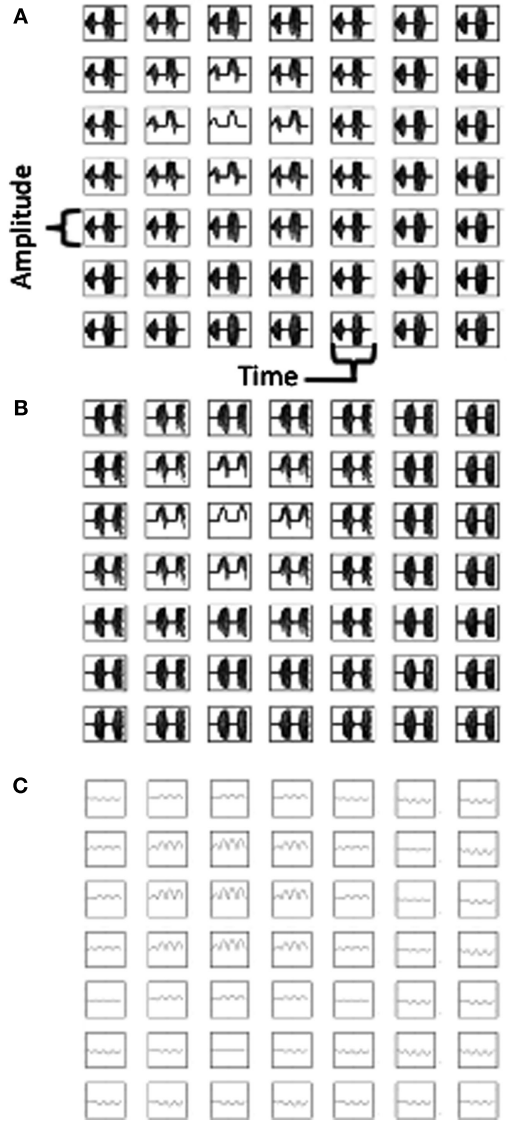


**FIGURE 7 | Plots of neural activity over time. (A)** Time course of activity of the heading angle cells in Group **(A)** representing different angles for a 7 by 7 array of heading angle spatial phases from the center of the population used in **Figures 3–4**. **(B)** Time course of activity of the heading angle cells in Group **(B)** representing the same angles and spatial phases, but regulated to be active at different temporal phase (see text). **(C)** Time course of total synaptic input to the grid cell population showing oscillations that are double the frequency of the oscillations in Group **(A)** and Group **(B)**. The activity in **(A,B)** shows theta cycle skipping relative to activity in **(C)**.

population will be considered as theta rhythm frequency (8 Hz) and the frequency of the individual populations will be considered to be half that frequency (4 Hz).

The two different populations of heading angle cells in **Figures 7A,B** each show activity on two cycles during the full time period of the simulation. Note that the period of activity of Group B is the opposite of the period of activity of Group A. This means that simultaneous recording of one neuron from Group A and one neuron from Group B would result in non-overlapping spiking activity, that would show up as a low cross-correlation at zero delay between the cell. In contrast, there would be a large cross-correlation at the interval of one theta cycle (i.e., 125 ms) to either side. In contrast, two cells recorded from Group A (or both from Group B) would have a high cross-correlation at zero delay between the cells, with a lower cross-correlation at one theta cycle. In addition, each individual neuron would have an autocorrelation with a peak at two theta cycles rather than a single theta cycle, whereas the grid cells would be expected to have an autocorrelation with a peak at a single theta cycle.

## DISCUSSION

The model of grid cell firing presented here was designed to combine the oscillations that are prominent in one set of grid cell models (Burgess et al., 2007; Giocomo et al., 2007; Hasselmo et al., 2007; Blair et al., 2008; Burgess, 2008; Hasselmo, 2008; Hasselmo and Brandon, 2008; Zilli and Hasselmo, 2010; Welday et al., 2011) as well as the attractor dynamics prominent in a different set of grid cell models (Fuhs and Touretzky, 2006; McNaughton et al., 2006; Guanella and Verschure, 2007; Guanella et al., 2007; Burak and Fiete, 2009).

The model uses a population of heading angle cells (Eq. 1) that are motivated by the theory that movement in any given heading could involve transitions between neurons with different temporal phases that code different spatial phases along that heading. This component was inspired by transitions in phase due to frequency modulation of oscillating neurons (Burgess, 2008; Hasselmo, 2008) or oscillating ring attractors (Blair et al., 2007; Welday et al., 2011), but here the transition is triggered by changes in the amplitude of oscillations coding one heading direction rather than changes in frequency.

The population of heading angle cells has synaptic connections with a population of grid cells that are periodic in spatial phase along each heading angle (Eq. 2). Simulations of the model arrays that code 24 different heading angles (see **Figure 2B**). The synaptic input from the heading angle cells with different temporal phases can be pictured as waves of activity propagating across the grid cell plane in the direction of each heading angle (see **Figures 1** and **6**). For heading angle cells with a particular spatial phase, the sum of this synaptic input across all angles corresponds to a standing wave of concentric circles centered on the individual spatial phase of that set of heading angle cells in the environment (**Figures 1** and **2**). Different heading angle cells with different spatial phases will provide standing waves centered on different spatial phases.

The synaptic input influences the activity of a population of grid cells (Eq. 3) that send feedback to the heading angle cells to influence their amplitude of oscillation. The interaction of the synaptic input from heading angle cells with the grid cell activity plane generates grid-like patterns of activity as shown in **Figures 3–5**. This pattern of activity varies dependent upon initial conditions and spatial frequency of synaptic connectivity. The spatial periodicity of firing occurs in both the grid cell population and across different arrays of heading angle cells. Thus, the heading angle cells would show grid cell periodicity similar to that of conjunctive grid-by-head-direction cells in medial entorhinal

cortex (Sargolini et al., 2006; Hafting et al., 2008; Brandon et al., 2011). These same heading angle cells show different amplitudes of activity dependent upon the heading direction of movement (**Figure 1C** and **Figure 5D**), similar to the head direction selectivity of conjunctive cells, but with stronger background for all headings.

As shown in **Figure 5**, the model can shift the locus of firing of the grid cell activity under the influence of head direction input that selectively activates a subset of heading angle cells. This causes an increase in the amplitude of input from one oscillation versus the others. Without any change in synaptic connectivity, this shifts the predominant activity of the grid cells along the direction of movement, thereby shifting the heading angle cell activity in that same direction (**Figure 5**). The shift in locus of firing depends upon heading angle cells responding to the direction of movement, as shown in **Figure 5D**. The model is similar to other models using attractor dynamics in that it requires either that there be a set of speed-modulated conjunctive cells that have zero activity when the rat is stationary, or that it have cells that have a uniform baseline response to all heading directions and then increase from this uniform baseline response for the preferred heading angle. Both of these features differ from most head direction cells and conjunctive cells in medial entorhinal cortex (Sargolini et al., 2006; Brandon et al., 2011), which have very low baseline responses to non-preferred headings, but do not reduce to zero activity when the rat is stationary.

The simulations used regulation of heading angle activity on different phases of the theta rhythm oscillations in order to allow the shift in activity with movement. In addition, this regulation of heading angle activity also reduced the disruptive influence of spatial activity during opposite temporal phases, which would cause grid cell activity to activate a mismatching input from the heading angle cells. This problem was avoided by setting up two groups of heading angle cells that were active on different cycles, to allow the grid cells to receive consistent input across all cycles. As shown in **Figure 7**, the two groups of heading angle cells were active at delta frequencies (e.g., 4 Hz), whereas the total synaptic input to the grid cells showed cycles at twice that frequency (e.g., 8 Hz). This appears to be consistent with neurophysiological data showing theta cycle skipping in a subset of head direction cells and conjunctive grid-by-head direction cells in the medial entorhinal cortex (Deshmukh et al., 2010; Brandon et al., 2011). Theta cycle skipping in the autocorrelogram indicates more interspike intervals corresponding to 4 Hz frequencies compared to 8 Hz frequencies.

An alternate mechanism for avoiding the problem of opposite phases could be the resonance properties of medial entorhinal neurons, as shown in a number of studies (Haas and White, 2002; Erchova et al., 2004; Giocomo et al., 2007; Giocomo and Hasselmo, 2009; Boehlen et al., 2010). These resonance properties when implemented in the grid cell population in the model can allow the neurons to be active during one period and then less active (due to decreases in the hyperpolarization activated cation current) on a subsequent period. This prevents the problem of opposite phase input, but results in a pattern of anti-grid firing that has been observed in some preliminary neurophysiological recordings, but not alternating with a grid pattern. The resonance properties of neurons could also contribute to shifts in frequency with depolarization that could alter the phase relationship of grid cells and heading angle cells and contribute to shifting of the grid representation during movement. Experimental data shows that depolarization does shift the resonance frequency of individual medial entorhinal neurons to lower frequencies in a linear manner with depolarization between −70 mV and threshold (Shay et al., 2010).

The model presented here uses interactions of theta-frequency oscillations with attractor dynamics to generate the spatial firing pattern of grid cells. Theta-frequency oscillations have been the primary frequency used in oscillatory interference models (Blair et al., 2007; Burgess et al., 2007; Burgess, 2008; Hasselmo, 2008; Zilli and Hasselmo, 2010). However, another early model showed that lower frequency oscillations can simulate grid cell firing patterns (Hasselmo and Brandon, 2008) based on data showing cyclical changes in bistable persistent spiking (Klink and Alonso, 1997). These spiking phenomenon could occur based on acceleration of spiking due to buildup of calcium activation of the CAN current, and deceleration of spiking due to calcium inactivation of the CAN current or due to the calcium-activated potassium current (AHP). The Hasselmo and Brandon (2008) model can be implemented with the following equations: $dV_i/dt = c_i(t)Hv(t)$, $dc_i/dt = -\omega^2 V_i(t)Hv(t)$, $g(t) = \prod_i V_i(t)$. Where $V$ represents membrane potential, c represents the net activation of calcium activated currents including both the CAN current and the AHP current, $H$ represents the head direction matrix that transforms the velocity at each time point $v(t)$ into a speed-modulated head direction signal, and the frequency of oscillations depends upon $\omega^2$. These dynamics generate bands of activity that sum together to create grid cells, showing how slower oscillations based on a different set of cellular mechanisms could generate grid cell firing. This mechanism could use head direction input with preference angles at 60° intervals, or could interact with attractor dynamic properties to generate grid cell firing with head direction input at a wide range of preference angles.

In the model presented here, the use of neurons with oscillatory phase driven by the medial septum resembles features of the oscillatory interference models that code location by relative phase of different velocity controlled oscillators (VCOs; Burgess et al., 2007; Giocomo et al., 2007; Hasselmo et al., 2007; Blair et al., 2008; Burgess, 2008; Hasselmo, 2008; Hasselmo and Brandon, 2008; Zilli and Hasselmo, 2010; Welday et al., 2011). The loss of input from the medial septum would remove this phase signal, thereby blocking the spatial periodicity of grid cells. The loss of grid cell spatial periodicity has been shown during pharmacological inactivation of the medial septum (Brandon et al., 2011; Koenig et al., 2011), and this loss of periodicity could underlie the spatial memory impairments associated with inactivation of the medial septum (Chrobak et al., 1989). The use of an interactive feedback process with circular symmetry resembles features of the continuous attractor dynamic models of grid cells that have the grid cell activity interacting with circularly symmetric synaptic connectivity (Fuhs and Touretzky, 2006; McNaughton et al., 2006; Guanella and Verschure, 2007; Guanella et al., 2007; Burak and Fiete, 2009). The iterative process of interaction of the grid

cell plane with the summed heading angle plane is mathematically analogous to the interaction of the grid cell plane with the circularly symmetric synaptic connectivity matrix in attractor dynamic models.

## ACKNOWLEDGMENTS

This work was supported by National Institute of Mental Health R01 MH61492, R01 MH60013, P50 MH094263, and the Office of Naval Research MURI grant N00014-10-1-0936.

## REFERENCES

Barry, C., Hayman, R., Burgess, N., and Jeffery, K. J. (2007). Experience-dependent rescaling of entorhinal grids. *Nat. Neurosci.* 10, 682–684.

Blair, H. T., Gupta, K., and Zhang, K. (2008). Conversion of a phase- to a rate-coded position signal by a three-stage model of theta cells, grid cells, and place cells. *Hippocampus* 18, 1239–1255.

Blair, H. T., Welday, A. C., and Zhang, K. (2007). Scale-invariant memory representations emerge from moire interference between grid fields that produce theta oscillations: a computational model. *J. Neurosci.* 27, 3211–3229.

Boehlen, A., Heinemann, U., and Erchova, I. (2010). The range of intrinsic frequencies represented by medial entorhinal cortex stellate cells extends with age. *J. Neurosci.* 30, 4585–4589.

Brandon, M. P., Bogaard, A. R., Libby, C. P., Connerney, M. A., Gupta, K., and Hasselmo, M. E. (2011). Reduction of theta rhythm dissociates grid cell spatial periodicity from directional tuning. *Science* 332, 595–599.

Burak, Y., and Fiete, I. R. (2009). Accurate path integration in continuous attractor network models of grid cells. *PLoS Comput. Biol.* 5, e1000291. doi:10.1371/journal.pcbi.1000291

Burgess, N. (2008). Grid cells and theta as oscillatory interference: theory and predictions. *Hippocampus* 18, 1157–1174.

Burgess, N., Barry, C., Jeffery, K. J., O'Keefe, J. (2005). "A grid and place cell model of path integration utilizing phase precession versus theta," in *Computational Cognitive Neuroscience Meeting*, Washington, DC.

Burgess, N., Barry, C., and O'Keefe, J. (2007). An oscillatory interference model of grid cell firing. *Hippocampus* 17, 801–812.

Chrobak, J. J., Stackman, R. W., and Walsh, T. J. (1989). Intraseptal administration of muscimol produces dose-dependent memory impairments in the rat. *Behav. Neural Biol.* 52, 357–369.

Derdikman, D., Whitlock, J. R., Tsao, A., Fyhn, M., Hafting, T., Moser, M. B., and Moser, E. I. (2009). Fragmentation of grid cell maps in a multicompartment environment. *Nat. Neurosci.* 12, 1325–1332.

Deshmukh, S. S., Yoganarasimha, D., Voicu, H., and Knierim, J. J. (2010). Theta modulation in the medial and the lateral entorhinal cortices. *J. Neurophysiol.* 104, 994–1006.

Erchova, I., Kreck, G., Heinemann, U., and Herz, A. V. (2004). Dynamics of rat entorhinal cortex layer II and III cells: characteristics of membrane potential resonance at rest predict oscillation properties near threshold. *J. Physiol. (Lond.)* 560(Pt 1), 89–110.

Fuhs, M. C., and Touretzky, D. S. (2006). A spin glass model of path integration in rat medial entorhinal cortex. *J. Neurosci.* 26, 4266–4276.

Fyhn, M., Hafting, T., Treves, A., Moser, M. B., and Moser, E. I. (2007). Hippocampal remapping and grid realignment in entorhinal cortex. *Nature* 446, 190–194.

Fyhn, M., Molden, S., Witter, M. P., Moser, E. I., and Moser, M. B. (2004). Spatial representation in the entorhinal cortex. *Science* 305, 1258–1264.

Giocomo, L. M., and Hasselmo, M. E. (2008). Computation by oscillations: implications of experimental data for theoretical models of grid cells. *Hippocampus* 18, 1186–1199.

Giocomo, L. M., and Hasselmo, M. E. (2009). Knock-out of HCN1 subunit flattens dorsal-ventral frequency gradient of medial entorhinal neurons in adult mice. *J. Neurosci.* 29, 7625–7630.

Giocomo, L. M., Hussaini, S. A., Zheng, F., Kandel, E. R., Moser, M.-B., and Moser, E. I. (2011). Increased spatial scale in grid cells of HCN1 knockout mice. *Cell* 147, 1159–1170.

Giocomo, L. M., Zilli, E. A., Fransen, E., and Hasselmo, M. E. (2007). Temporal frequency of subthreshold oscillations scales with entorhinal grid cell field spacing. *Science* 315, 1719–1722.

Guanella, A., Kiper, D., and Verschure, P. (2007). A model of grid cells based on a twisted torus topology. *Int. J. Neural Syst.* 17, 231–240.

Guanella, A., and Verschure, P. F. (2007). Prediction of the position of an animal based on populations of grid and place cells: a comparative simulation study. *J. Integr. Neurosci.* 6, 433–446.

Haas, J. S., and White, J. A. (2002). Frequency selectivity of layer II stellate cells in the medial entorhinal cortex. *J. Neurophysiol.* 88, 2422–2429.

Hafting, T., Fyhn, M., Bonnevie, T., Moser, M. B., and Moser, E. I. (2008). Hippocampus-independent phase precession in entorhinal grid cells. *Nature* 453, 1248–1252.

Hafting, T., Fyhn, M., Molden, S., Moser, M. B., and Moser, E. I. (2005). Microstructure of a spatial map in the entorhinal cortex. *Nature* 436, 801–806.

Hasselmo, M. E. (2008). Grid cell mechanisms and function: contributions of entorhinal persistent spiking and phase resetting. *Hippocampus* 18, 1213–1229.

Hasselmo, M. E., and Brandon, M. P. (2008). Linking cellular mechanisms to behavior: entorhinal persistent spiking and membrane potential oscillations may underlie path integration, grid cell firing, and episodic memory. *Neural Plast.* 2008, 658323.

Hasselmo, M. E., Giocomo, L. M., and Zilli, E. A. (2007). Grid cell firing may arise from interference of theta frequency membrane potential oscillations in single neurons. *Hippocampus* 17, 1252–1271.

Jarsky, T., Roxin, A., Kath, W. L., and Spruston, N. (2005). Conditional dendritic spike propagation following distal synaptic activation of hippocampal CA1 pyramidal neurons. *Nat. Neurosci.* 8, 1667–1676.

Jeewajee, A., Barry, C., O'Keefe, J., and Burgess, N. (2008). Grid cells and theta as oscillatory interference: electrophysiological data from freely moving rats. *Hippocampus* 18, 1175–1185.

King, C., Reece, M., and O'Keefe, J. (1998). The rhythmicity of cells of the medial septum/diagonal band of Broca in the awake freely moving rat: relationships with behaviour and hippocampal theta. *Eur. J. Neurosci.* 10, 464–477.

Klink, R., and Alonso, A. (1997). Muscarinic modulation of the oscillatory and repetitive firing properties of entorhinal cortex layer II neurons. *J. Neurophysiol.* 77, 1813–1828.

Koenig, J., Linder, A. N., Leutgeb, J. K., and Leutgeb, S. (2011). The spatial periodicity of grid cells is not sustained during reduced theta oscillations. *Science* 332, 592–595.

McNaughton, B. L., Battaglia, F. P., Jensen, O., Moser, E. I., and Moser, M. B. (2006). Path integration and the neural basis of the "cognitive map." *Nat. Rev. Neurosci.* 7, 663–678.

Mel, B. W. (1993). Synaptic integration in an excitable dendritic tree. *J. Neurophysiol.* 70, 1086–1101.

Moser, E. I., and Moser, M. B. (2008). A metric for space. *Hippocampus* 18, 1142–1156.

Navratilova, Z., Giocomo, L. M., Fellous, J. M., Hasselmo, M. E., and McNaughton, B. L. (2011). Phase precession and variable spatial scaling in a periodic attractor map model of medial entorhinal grid cells with realistic after-spike dynamics. *Hippocampus* 22, 772–789.

Remme, M. W., Lengyel, M., and Gutkin, B. S. (2009). The role of ongoing dendritic oscillations in single-neuron dynamics. *PLoS Comput. Biol.* 5, e1000493. doi:10.1371/journal.pcbi.1000493

Remme, M. W., Lengyel, M., and Gutkin, B. S. (2010). Democracy-independence trade-off in oscillating dendrites and its implications for grid cells. *Neuron* 66, 429–437.

Sargolini, F., Fyhn, M., Hafting, T., McNaughton, B. L., Witter, M. P., Moser, M. B., and Moser, E. I. (2006). Conjunctive representation of position, direction, and velocity in entorhinal cortex. *Science* 312, 758–762.

Shay, C. F., Boardman, I. S., and Hasselmo, M. E. (2010). Comparison of resonance and subthreshold membrane potential oscillation properties in whole cell patch recordings in slices of rat medial and lateral entorhinal cortex. *Abstr. Soc. Neurosci.* 36, 101.23.

Welday, A. C., Shlifer, I. G., Bloom, M. L., Zhang, K., and Blair, H. T. (2011). Cosine directional tuning of theta cell burst frequencies: evidence for spatial coding by oscillatory interference. *J. Neurosci.* 31, 16157–16176.

Yoshida, M., Giocomo, L. M., Boardman, I., and Hasselmo, M. E. (2011). Frequency of subthreshold oscillations at different membrane potential voltages in neurons at different anatomical positions on the dorsoventral axis in the rat medial entorhinal cortex. *J. Neurosci.* 31, 12683–12694.

Zilli, E. A. (2012). Models of grid cell spatial firing published 2005–2011. *Front. Neural Circuits* 6:16. doi: 10.3389/fncir.2012.00016

Zilli, E. A., and Hasselmo, M. E. (2010). Coupled noisy spiking neurons as velocity-controlled oscillators in a model of grid cell spatial firing. *J. Neurosci.* 30, 13850–13860.

Zilli, E. A., Yoshida, M., Tahvildari, B., Giocomo, L. M., and Hasselmo, M. E. (2009). Evaluation of the oscillatory interference model of grid cell firing through analysis and measured period variance of some biological oscillators. *PLoS Comput. Biol.* 5, e1000573. doi:10.1371/journal.pcbi.1000573

**Conflict of Interest Statement:** The authors declare that the research was conducted in the absence of any commercial or financial relationships that could be construed as a potential conflict of interest.

*Received: 10 December 2011; accepted: 04 May 2012; published online: 28 May 2012.*

*Citation: Hasselmo ME and Brandon MP (2012) A model combining oscillations and attractor dynamics for generation of grid cell firing. Front. Neural Circuits* ***6****:30. doi: 10.3389/fncir.2012.00030*

frontiers in
NEURAL CIRCUITS

ORIGINAL RESEARCH ARTICLE
published: 24 April 2012
doi: 10.3389/fncir.2012.00017

# Intrinsic electrophysiological properties of entorhinal cortex stellate cells and their contribution to grid cell firing fields

***Hugh Pastoll*[1]*, Helen L. Ramsden*[1] *and Matthew F. Nolan*[2]****

[1] *Neuroinformatics Doctoral Training Centre, University of Edinburgh, Edinburgh, UK*
[2] *Centre for Integrative Physiology, University of Edinburgh, Edinburgh, UK*

***Edited by:***
*Lisa M. Giocomo, Norwegian University of Science and Technology, Norway*

***Reviewed by:***
*John A. White, University of Utah, USA*
*Christoph Schmidt-Hieber, University College London, UK*

****Correspondence:***
*Matthew F. Nolan, Centre for Integrative Physiology, University of Edinburgh, Edinburgh, Scotland, EH8 9XD, UK.*
*e-mail: mattnolan@ed.ac.uk*

The medial entorhinal cortex (MEC) is an increasingly important focus for investigation of mechanisms for spatial representation. Grid cells found in layer II of the MEC are likely to be stellate cells, which form a major projection to the dentate gyrus. Entorhinal stellate cells are distinguished by distinct intrinsic electrophysiological properties, but how these properties contribute to representation of space is not yet clear. Here, we review the ionic conductances, synaptic, and excitable properties of stellate cells, and examine their implications for models of grid firing fields. We discuss why existing data are inconsistent with models of grid fields that require stellate cells to generate periodic oscillations. An alternative possibility is that the intrinsic electrophysiological properties of stellate cells are tuned specifically to control integration of synaptic input. We highlight recent evidence that the dorsal-ventral organization of synaptic integration by stellate cells, through differences in currents mediated by HCN and leak potassium channels, influences the corresponding organization of grid fields. Because accurate cellular data will be important for distinguishing mechanisms for generation of grid fields, we introduce new data comparing properties measured with whole-cell and perforated patch-clamp recordings. We find that clustered patterns of action potential firing and the action potential after-hyperpolarization (AHP) are particularly sensitive to recording condition. Nevertheless, with both methods, these properties, resting membrane properties and resonance follow a dorsal-ventral organization. Further investigation of the molecular basis for synaptic integration by stellate cells will be important for understanding mechanisms for generation of grid fields.

**Keywords: ion channel, grid cell, HCN, synaptic integration, oscillation, theta, resonance**

## INTRODUCTION

Stellate cells in layer II of the medial entorhinal cortex (MEC) are a crucial component of the neural circuit for representation of space. These neurons receive synaptic input from diverse cortical areas and send axonal projections to the dentate gyrus of the hippocampus (Steward and Scoville, 1976; Schwartz and Coleman, 1981; Ruth et al., 1982; Ruth and Collier, 1988; Insausti et al., 1997; Dolorfo and Amaral, 1998; Burwell, 2000; van Groen et al., 2003; Witter, 2007). They are defined by a stellate dendritic architecture and distinctive electrophysiological properties (Ramón y Cajal, 1995; Alonso and Llinás, 1989; Alonso and Klink, 1993; Jones, 1994; Klink and Alonso, 1997a; Heinemann et al., 2000; Erchova et al., 2004; Burton et al., 2008; Garden et al., 2008). Stellate cells received considerable attention initially because of their possible role in theta-frequency (4–12 Hz) oscillations that are associated with exploratory spatial behaviors (Mitchell and Ranck, 1980; Alonso and García-Austt, 1987; Dickson et al., 1995; Buzsáki, 1996; White et al., 1998; Hasselmo et al., 2002).

The discovery that cells in layer II of the MEC have grid-like spatial firing fields has given further motivation to investigation of the functional properties of stellate cells (Fyhn et al., 2004; Hafting et al., 2005). Several observations suggest that grid cells in layer II of the MEC are stellate cells. Stellate cells are the main excitatory neuron type in the layer where grid cells are most frequently found (Alonso and Klink, 1993; Hafting et al., 2005; Sargolini et al., 2006), and they were recently shown to encode spatial information during navigation on linear tracks (Burgalossi et al., 2011). The topographical organization of the spatial resolution of grid firing fields along the dorsal-ventral axis of the MEC (Hafting et al., 2005; Sargolini et al., 2006; Barry et al., 2007; Brun et al., 2008; Fyhn et al., 2008) is mirrored by differences between stellate cells in their intrinsic theta-frequency activity and resonance (Giocomo et al., 2007; Boehlen et al., 2010; Dodson et al., 2011; Yoshida et al., 2011), and in their integration of synaptic responses (Garden et al., 2008). The intrinsic electrophysiological properties of stellate cells may, therefore, offer vital clues and experimental targets for the investigation of cellular mechanisms involved in the neuronal representation of space (Giocomo et al., 2011b; O'Donnell and Nolan, 2011).

With this goal in mind we review the known intrinsic electrophysiological properties of stellate cells in layer II of the MEC and introduce new data obtained using perforated patch-clamp methods. We begin by considering the identity and nature of the ion channels that stellate cells express. We then examine how these channels influence membrane properties of stellate cells typically measured with recordings from brain slices. We compare the voltage dependence of key membrane properties of stellate cells (**Figures 1A,B**) with that of their ion channels (**Figure 1C**). We show that new data obtained with the perforated patch-clamp method can reconcile differences between results obtained with whole-cell and sharp electrode recordings (**Figures 2–9**). Finally, we consider evidence for how the intrinsic properties of stellate cells influence neuronal computations important for the representation of space in behaving animals. We argue that models that require stellate cells to generate periodic oscillations are not consistent with existing data. We suggest that establishing how stellate cells integrate their synaptic input (Garden et al., 2008) will be crucial for understanding the cellular basis for grid cell firing fields.

## RESULTS AND DISCUSSION

### ION CHANNELS DETERMINING THE INTRINSIC EXCITABILITY OF STELLATE CELLS

#### *Sodium channels*

Three types of sodium conductance have been identified in stellate cells (**Figure 1C**). Depolarization to membrane potentials above approximately –50 mV activates a transient sodium current ($Na_T$) with rapid kinetics (White et al., 1993; Magistretti and Alonso, 1999b, 2007; Magistretti et al., 1999b). This current consists of a component that is sensitive to the classic $Na^+$ channel blocker tetrodotoxin (TTX) and a component that is relatively insensitive (White et al., 1993). The kinetics and voltage dependence of these two components are indistinguishable, but the TTX-resistant component of $Na_T$ is more sensitive to block by $Cd^{2+}$, $La^{3+}$, and $Zn^{2+}$ (White et al., 1993). The sensitivity to $Zn^{2+}$ may be of functional relevance as $Zn^{2+}$ is found at high levels in the neuropil of the MEC (Haug, 1976; Holm and Geneser, 1989; Slomianka, 1992). The TTX-insensitive component of $Na_T$ is smaller than the TTX-sensitive component (White et al., 1993).

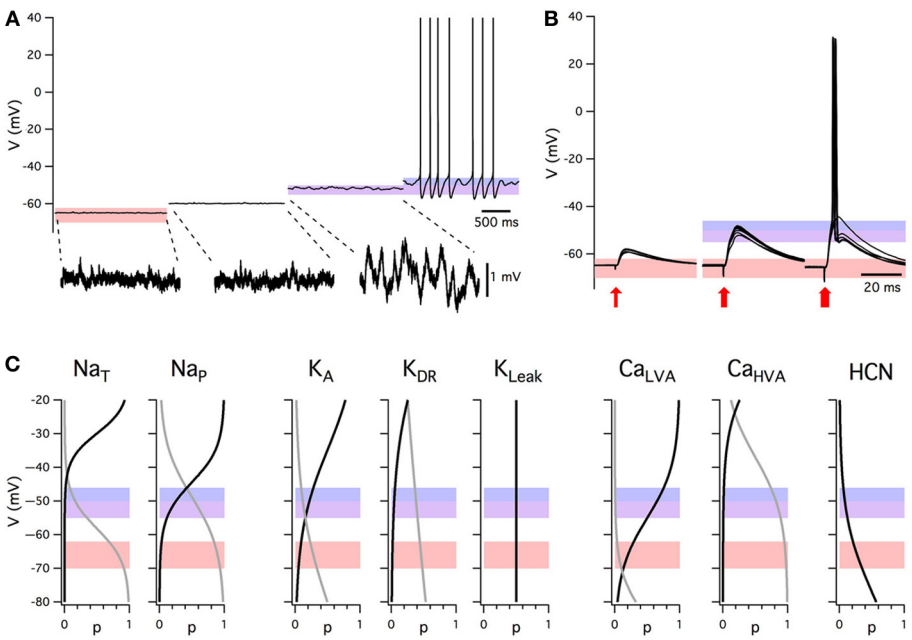


**FIGURE 1 | Summary of intrinsic electrophysiological properties of stellate cells from layer II of the medial entorhinal cortex.** **(A)** Example of membrane potential activity at rest and during injection of constant current. Shading indicates the range of typical resting membrane potentials (orange), peri-threshold theta-frequency activity (purple), and threshold for initiation of action potential firing (blue). Subthreshold activity is shown on an expanded voltage-scale below. **(B)** Examples of excitatory post-synaptic potentials evoked by stimuli of increasing amplitude (left to right). Each block shows five consecutive responses to stimuli of identical intensity. Data in **A** and **B** are obtained with whole-cell patch-clamp recordings from the same stellate cell in the presence of picrotoxin (50 μM) and CGP55845 (1 μM) to block inhibitory synaptic transmission. **(C)** Voltage dependence of stellate cell conductances. Boltzmann fits for activation (black) and inactivation (gray). From left: $Na_T$: activation ($V_{1/2} = -29.9$ mV, $k = 3.9$ mV) and inactivation ($V_{1/2} = -58.2$ mV, $k = -5$ mV) [Magistretti and Alonso (1999a)]; $Na_P$: activation ($V_{1/2} = -44.4$ mV, $k = 5.2$ mV), inactivation ($V_{1/2} = -48.8$ mV, $k = -10$ mV) [Magistretti and Alonso (1999a)]; $K_A$: activation ($V_{1/2} = -34.7$ mV, $k = 12$ mV), inactivation ($V_{1/2} = -80.3$ mV, $k = -12$ mV) where $V_{1/2}$ parameters were calculated in [Eder and Heinemann (1996)] and the slopes were estimated from Figure 2A [Eder and Heinemann (1996)]; $K_{DR}$: activation ($V_{1/2} = -34.8$ mV, $k = 11$ mV), inactivation ($V_{1/2} = -74.3$ mV, $k = -15$ mV) where $V_{1/2}$ given in [Eder and Heinemann (1996)] and the slopes were estimated from Figure 2B [Eder and Heinemann (1996)]; $K_{Leak}$; $Ca_{LVA}$ activation ($V_{1/2} = -45$ mV, $k = 8$ mV), estimated from threshold and peak amplitude data in [Bruehl and Wadman (1999)], inactivation ($V_{1/2} = -89$ mV, $k = -6.9$ mV) [Bruehl and Wadman (1999)]; $Ca_{HVA}$ activation ($V_{1/2} = -11.1$ mV, $k = 8.4$ mV) [Castelli and Magistretti (2006)], inactivation ($V_{1/2} = -37$ mV, $k = -8.7$ mV) [Bruehl and Wadman (1999)]. HCN activation ($V_{1/2} = -83.1$ mV, $k = -8.1$ mV) [Nolan et al. (2007)].

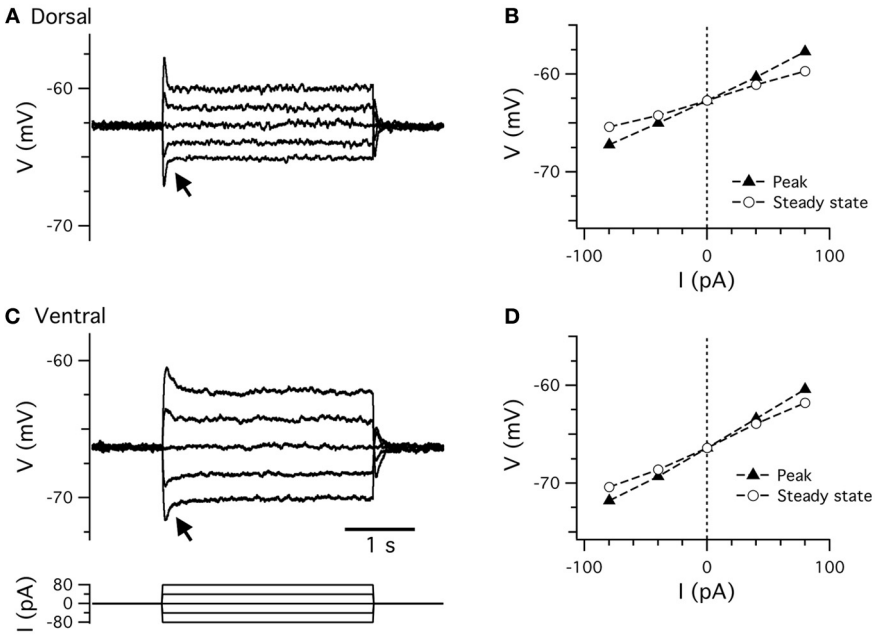


**FIGURE 2 | Resting membrane properties. (A,C)** Examples of perforated patch-clamp recordings of membrane potential responses to current steps (**C**, lower) recorded from dorsal **(A)** and ventral **(C)** stellate cells. Arrows indicate the membrane potential "sag." **(B,D)** Peak (closed triangles) and steady-state (open circles) membrane potential responses plotted as a function of current step amplitude for data from dorsal **(B)** and ventral **(D)** stellate cells in **(A,C)**.

In addition to $Na_T$, stellate cells express a prominent voltage-gated, persistent sodium current ($Na_P$) (Alonso and Llinás, 1989; Jones, 1994; Magistretti and Alonso, 1999a,b, 2002, 2007; Magistretti et al., 1999a,b, 2003). The threshold for activation of $Na_P$ is approximately 10–15 mV lower than $Na_T$ (Magistretti et al., 1999b) and in contrast to $Na_T$ it inactivates relatively slowly with a half-maximal inactivation voltage of approximately −60 mV (Magistretti and Alonso, 1999a,b) (**Figure 1C**). These properties suggest that in stellate cells $Na_P$ is active at membrane potentials below the threshold for action potential firing (**Figures 1A,B**).

A series of elegant studies have investigated the properties of $Na_P$ using single channel recordings (Magistretti and Alonso, 1999a, 2002, 2007; Magistretti et al., 1999a,b, 2003). This approach has the advantages that it is not subject to voltage errors associated with whole-cell recordings, provides information about channel location and gives useful insights into channel gating mechanisms. Single channels with properties of $Na_P$ and $Na_T$ are found on the dendrites as well as the cell bodies of stellate cells (Magistretti et al., 1999a). $Na_P$ is mediated by relatively high conductance single channels (∼20 pS) compared to $Na_T$ (∼16 pS) (Magistretti et al., 1999b). The voltage-dependence of activation of the macroscopic $Na_P$ current appears to depend on the strong voltage dependence of single channel opening times during bursts of channel activity (Magistretti and Alonso, 2002). Increases in closure duration between such bursts may underlie the slow inactivation of the current (Magistretti and Alonso, 2002). Further detailed analysis suggests that ion channels mediating $Na_P$ exist in one of two preferred gating modes (Magistretti et al., 2003) and have at least six different sub-states between fully open and closed (Magistretti and Alonso, 2007). Given the likely importance of stochastic gating of $Na_P$ for computation by stellate cells (White et al., 1998; Dorval and White, 2005), it will be important in the future to generate complete kinetic schemes of $Na_P$ gating that fully account for these observations.

### *Potassium channels*

Stellate cells express at least four major types of potassium current: leak, delayed rectifier, A-type, and calcium-activated (**Figure 1C**). They are distinguished by their kinetics, voltage dependence, and pharmacology. An M-type current has also been investigated (Yoshida and Alonso, 2007; Heys et al., 2010), but is yet to be isolated with voltage-clamp experiments.

A substantial potassium leak conductance found in stellate cells is relatively independent of membrane potential and is at least in part blocked by $Ba^{2+}$, low pH, and quinidine (Deng et al., 2007; Garden et al., 2008), suggesting that it is mediated by two-pore domain ($K_{2P}$) potassium channels. Consistent with this idea, immunohistochemical data demonstrate that the two-pore-domain channels TASK-1 (Kcnk3), TASK-3 (Kcnk9), TWIK-1 (Kcnk1), TREK-1 (Kcnk2), and TREK-2 (Kcnk10) are all present in layer II of MEC (Deng et al., 2009). At present it is not completely clear which of these channels are open at rest, but pharmacological data point to a role for TASK channels (Deng et al., 2007). Two-pore domain channels are likely to be important targets for modulation of stellate cells (Deng et al., 2007, 2009).

A delayed rectifier potassium current ($K_{DR}$) activates in stellate cells on depolarization to potentials above approximately

−45 mV (Eder et al., 1991; Eder and Heinemann, 1996) (**Figure 1C**). $K_{DR}$ shows considerable rundown (∼80% within 60 min) in the whole-cell recording configuration, with small shifts in steady-state activation and much larger shifts in steady-state inactivation, suggesting that it is under metabolic control. Rundown can be avoided with the use of perforated patch-clamp techniques (Eder et al., 1991). This current has a greater density in stellate cells than pyramidal cells (Eder and Heinemann, 1994). Its molecular basis is unclear.

An A-type current ($K_A$) recorded from stellate cells is distinguished from $K_{DR}$ by its strong inactivation (Eder et al., 1991; Eder and Heinemann, 1996) (**Figure 1C**). Consequently, activation of $K_A$ first requires removal of inactivation by hyperpolarization of the membrane to potentials below −60 mV. Depolarization to voltages positive to −50 mV then activates $K_A$. The density of $K_A$ is lower in stellate cells than in neighboring pyramidal cells (Eder and Heinemann, 1994). Its molecular basis is again not clear.

Other voltage-gated potassium channels are much less prominent in stellate cells. M-current blockade has small effects on stellate cell properties (Yoshida and Alonso, 2007; Heys et al., 2010). Nevertheless, there is reasonably high expression of mRNA for Kv7 subunits in layer II in Allen Brain Atlas data (Garden et al., 2008), although this could be due to expression in non-stellate cells, where M current blockade has a greater effect (Yoshida and Alonso, 2007). There is evidence that stellate cells express inward-rectifying potassium channels. This comes from a small, $Ba^{2+}$-sensitive rectification in the instantaneous current-voltage relationship at voltages negative to −80 mV (Dickson et al., 2000b). However, this current has not been studied further and these findings could also be consistent with properties of some $K_{2P}$ channels.

Stellate cells also express calcium-activated potassium channels ($K_{Ca}$) (Khawaja et al., 2007). These channels are activated indirectly following depolarization as a result of $Ca^{2+}$ influx through voltage-gated $Ca^{2+}$ channels. The $K_{Ca}$ current recorded from stellate cells has a large relatively fast component and a smaller slow component (Khawaja et al., 2007). Neither component is sensitive to apamin, which blocks small conductance $K_{Ca}$ channels, but the slow component can be modulated by the cAMP pathway, as forskolin reduces the amplitude of $K_{Ca}$ currents (Khawaja et al., 2007). The molecular basis for these currents is unclear. MEC layer II neurons express RNA for apamin-sensitive $K_{Ca}2.2$ (SK2) and $K_{Ca}2.3$ (SK3) subunits and the apamin-insensitive $K_{Ca}2.1$ (SK1) subunit of small-conductance channels (Stocker and Pedarzani, 2000; D'Hoedt et al., 2004). It is either possible that the apamin-sensitive subunits are expressed by non-stellate cells, or that they are expressed by stellate cells, but have functions that have not yet been investigated in stellate cells, for example to control local synaptic depolarizations (Ngo-Anh et al., 2005).

### *Calcium channels*

Two calcium currents have been described in MEC stellate cells (**Figure 1C**). A high-voltage-activated calcium current ($Ca_{HVA}$) is mediated by channels that open on depolarization to potentials positive to approximately −50 mV (Bruehl and Wadman, 1999; Visan et al., 2002; Castelli and Magistretti, 2006), whereas a low-voltage activated current ($Ca_{LVA}$) is mediated by channels that open with depolarization above approximately −60 mV (Bruehl and Wadman, 1999; Visan et al., 2002). The two channel populations are further distinguished by the membrane potentials at which they inactivate. Both currents slowly inactivate on depolarization, but $Ca_{HVA}$ inactivates at more depolarized potentials compared with $Ca_{LVA}$ (Bruehl and Wadman, 1999; Visan et al., 2002). This difference is important as it means that depolarization from potentials in the region of −50 mV will activate $Ca_{HVA}$, but not $Ca_{LVA}$. In contrast, depolarization from more hyperpolarized voltages will activate both currents. $Ca_{HVA}$ currents appear to have similar properties in stellate and pyramidal cells (Bruehl and Wadman, 1999; Castelli and Magistretti, 2006), suggesting that they are not responsible for the distinct electrophysiological properties of stellate cells (Castelli and Magistretti, 2006). There is some evidence that the density of $Ca_{HVA}$ currents is larger in pyramidal cells (Bruehl and Wadman, 1999), but this may be specific to older animals and could be confounded by inclusion of layer III cells in the analysis (Castelli and Magistretti, 2006).

Several calcium channel types appear to contribute to the $Ca_{HVA}$ current. These include L-type channels (∼50%), N-type (∼23–30%), P/Q-type (∼22–24%) and a component that is insensitive to pharmacological block of these channel types (11–13%) (Castelli and Magistretti, 2006). This residual current is reduced by 57–62% by the $Ca_v2.3$ channel blocker SNX-482 (Castelli and Magistretti, 2006). $Ca_{LVA}$ has properties consistent with T-type channels, but again the molecular identity of the current remains to be established.

### *HCN channels*

Hyperpolarization activated cation currents ($I_h$) have been extensively studied in stellate cells. Unlike most other voltage-gated currents, $I_h$ activates when the membrane is hyperpolarized and de-activates on depolarization (Robinson and Siegelbaum, 2003). Its presence in stellate cells was initially established from the observation of a sag-like response during injection of negative current steps (Alonso and Llinás, 1989; Jones, 1994). Subsequent voltage-clamp experiments have investigated the kinetics, voltage dependence, and pharmacology of $I_h$ in stellate cells (Richter et al., 1997, 2000; Dickson et al., 2000b; Nolan et al., 2007; Giocomo and Hasselmo, 2008). Interestingly, the density of $I_h$ increases with age from newborn to adult (Richter et al., 1997), with a peak approximately three weeks after birth (Burton et al., 2008), suggesting its importance for function of the mature MEC circuit.

Typically, $I_h$ in stellate cells activates at voltages negative to −50 mV (Dickson et al., 2000b; Richter et al., 2000; Nolan et al., 2007), shows half-maximal activation at −80 mV (Dickson et al., 2000b; Nolan et al., 2007) and has a reversal potential of approximately −20 mV (Dickson et al., 2000b). It is blocked by ZD7288 (Richter et al., 1997; Dickson et al., 2000b; Nolan et al., 2007) and $Cs^+$ (Alonso and Llinás, 1989; Klink and Alonso, 1993; Dickson et al., 2000b; Richter et al., 2000). $I_h$ in stellate cells, but not MEC pyramidal cells, can be activated by the cAMP analog 8-Bromo-c-AMP (Richter et al., 2000). The kinetics of $I_h$ are relatively slow compared to transient potassium and sodium currents. The time

course of activation of $I_h$ is best fit with a sum of two exponentials (Dickson et al., 2000b; Nolan et al., 2007). When measured at room temperature to better isolate currents, the fast component has a time constant of approximately ∼80 ms on hyperpolarization to −90 mV, whereas the slow component has a time constant of approximately ∼400 ms (Dickson et al., 2000b; Nolan et al., 2007). The relative amplitude of the fast component increases with hyperpolarization (Dickson et al., 2000b; Nolan et al., 2007). Deactivation is also relatively slow, with kinetics that speed-up on depolarization (Dickson et al., 2000b; Nolan et al., 2007). While these kinetics are accelerated at physiological temperatures (Nolan et al., 2007), it is important to recognize that they are nevertheless much slower than the voltage-gated channels underlying the action potential. These kinetics are important for certain models of grid cell firing fields discussed further below.

The molecular basis for $I_h$ has been investigated in more detail than that of other ion channels expressed by stellate cells. Four genes (HCN1–4) encode channels with properties of $I_h$ (Robinson and Siegelbaum, 2003). A direct role for HCN1 is evident from experiments using mice in which the HCN1 gene is deleted. This deletion reduces the amplitude of $I_h$ in stellate cells by approximately two-thirds and abolishes the fast activation of the current (Nolan et al., 2007). The residual $I_h$ has slower kinetics and a more negative voltage-dependence than the wild-type current (Nolan et al., 2007). This suggests that the two components of the wild-type current are unlikely to be a simple arithmetic sum of independent currents mediated by HCN1 and other HCN subunits. Rather, a substantial fraction of the wild-type current is likely to be mediated by heteromers containing HCN1 and one or more additional subunits. The kinetics of the wild-type current most closely resemble those of heteromers of HCN1 and HCN2 (Santoro et al., 2000; Chen et al., 2001; Ulens and Tytgat, 2001). Nevertheless, more direct experiments will be required to clearly establish the molecular identity of the additional HCN subunits expressed by stellate cells.

Consistent with these electrophysiological data, gene expression data from the Allen Brain Atlas indicates that mRNA levels of HCN1 and HCN2 are particularly high in layer II of the MEC. Antibody labeling also suggests strong HCN1 expression in superficial layers of the MEC (Notomi and Shigemoto, 2004; Nolan et al., 2007), whilst HCN2 and HCN3 show moderate expression (Notomi and Shigemoto, 2004). However, antibody labeling could reflect HCN1 channels expressed in the dendrites of pyramidal cells with somata in layers III and V (Shah et al., 2004; Rosenkranz, 2006). The use of HCN1 channel knockout mice to establish links between cellular properties of neurons and spatial behavior (Nolan et al., 2004; Giocomo et al., 2011a) is discussed below.

### *Other ion channels*

A non-specific cation current, $I_{NCM}$, has also been identified as a potentially important contributor to stellate cell function. It is activated during muscarinic receptor-dependent depolarization and is sensitive to $Ca^{2+}$ influx through voltage-gated channels (Klink and Alonso, 1997a; Shalinsky et al., 2002; Magistretti et al., 2004). It possesses a transient tail and sustained plateau component (Magistretti et al., 2004), the former of which may be of functional relevance to action potential firing patterns (Yoshida and Alonso, 2007). Interestingly, this current is analogous to that mediated by TRP channels (Shalinsky et al., 2002) and there is evidence that TRP channels mediate $I_{NCM}$ in layer V neurons (Zhang et al., 2011). Immunohistochemical analysis shows that the TRPC5 and TRPC1 channels are present in layer II of MEC (Bohlen und Halbach et al., 2005).

## INTRINSIC EXCITABLE PROPERTIES OF STELLATE CELLS

Since initial pioneering investigations (Alonso and Llinás, 1989), it has been clear that intrinsic voltage-gated ion channels play an important role in determining the membrane potential trajectory of stellate cells prior to initiation of action potential firing. Ion channels that activate at membrane potentials below the threshold for action potential firing may contribute to the generation of intrinsic activity that is independent of synaptic input (**Figures 1A,C**), and will also shape integration of synaptic responses as the membrane potential moves toward the action potential threshold (**Figures 1B,C**). Ion channels that open at more depolarized voltages influence action potential initiation and repolarization (**Figures 1A–C**). We will consider below key integrative properties of stellate cells at sub-threshold and suprathreshold membrane potentials.

Because there are differences between data obtained from stellate cells with the two techniques most frequently used for investigating their membrane properties—sharp electrode and whole-cell patch-clamp recording (Erchova et al., 2004; Nolan et al., 2007; Boehlen et al., 2010)—we will also introduce new data obtained with the perforated patch-clamp recording method (**Figures 2–9**). With this technique a high resistance seal is formed between a patch-clamp electrode and the recorded cell. Electrical access to the inside of the cell is then obtained through small pores in the membrane formed by an antibiotic included in the pipette solution (Horn and Marty, 1988; Mathias et al., 1991). Perforated patch-clamp recordings overcome a potential limitation of whole-cell recording by avoiding dialysis of the cell and possible rundown or washout of membrane currents (Horn and Marty, 1988). At the same time, because a tight seal is maintained between the recording electrode and the cell membrane, errors associated with sharp electrode recordings are also avoided (Spruston and Johnston, 1992).

### *Resting properties*

In the absence of significant synaptic input stellate cells do not fire action potentials and have a stable resting membrane potential. At physiological temperatures in brain slices from mature (>30 day) rodents the resting membrane potential of a stellate cell is typically in the range of −60 mV to −70 mV (Alonso and Llinás, 1989; Alonso and Klink, 1993; Jones, 1994; Erchova et al., 2004; Nolan et al., 2007; Garden et al., 2008; Boehlen et al., 2010). In anesthetized rats the resting potential is approximately −70 mV (Quilichini et al., 2010). Input resistance is typically between 20 and 80 MΩ and the membrane time constant is in the range 5–15 ms (Alonso and Llinás, 1989; Alonso and Klink, 1993; Jones, 1994; Erchova et al., 2004; Nolan et al., 2007; Garden et al., 2008; Boehlen et al., 2010). These properties appear similar in rats and mice [cf. (Nolan et al., 2007; Garden et al., 2008;

Boehlen et al., 2010)], change during development (Burton et al., 2008) and are substantially different when measured at room temperature (Dickson et al., 2000b). A large part of the within-study variation in input resistance and time constant can be explained by differences in neuronal location along the dorsal-ventral axis of the MEC (Garden et al., 2008; Boehlen et al., 2010) (see below).

A further source of variation between studies is the recording method used to investigate stellate cell properties. After accounting for a neuron's position, it appears that sharp electrode recordings produce membrane potentials that are typically more negative, input resistance that is lower and membrane time constants that are shorter compared with data from whole-cell recordings (Boehlen et al., 2010). We find that the direction of the difference between perforated patch-clamp and whole-cell measures of resting potential and input resistance (**Table 1**) is opposite to that between sharp electrode and whole-cell measures (Boehlen et al., 2010). Therefore, as for hippocampal neurons (Spruston and Johnston, 1992), sharp electrode recordings may under-estimate input resistance and the membrane time constant of stellate cells. Nevertheless, whole-cell recordings also appear to modify the resting membrane potential and input resistance of stellate cells, suggesting the importance of validating key results with perforated patch-clamp methods.

The ionic basis for the stellate cell resting potential involves a balance between a depolarizing drive from $I_h$ and a hyperpolarizing drive from leak potassium channels. $I_h$ depolarizes the resting membrane potential by approximately 10 mV (Dickson et al., 2000b; Haas et al., 2007; Nolan et al., 2007) and appears to contribute approximately 50% of the resting membrane conductance, with a large component requiring HCN1 channels (Nolan et al., 2007). Leak potassium channels that are open at rest in stellate cells have properties consistent with the $Ba^{2+}$- and acid-sensitive TASK sub-type of $K_{2P}$ channel and may account for the majority of the remaining resting membrane conductance (Deng et al., 2007; Garden et al., 2008). It is possible that the resting membrane potential is also influenced by a depolarizing leak $Na^+$ conductance (Garden et al., 2008).

Control of the resting potential by leak potassium currents is important for actions of neuromodulators on stellate cells. Serotonin and GABA modulate $K_{2P}$ channels through 5-$HT_{1A}$ and $GABA_B$ receptors, respectively. $GABA_B$ receptors are highly expressed in stellate cells (Mizukami et al., 2002). Baclofen, a $GABA_B$ receptor agonist, hyperpolarizes stellate cells and reduces their input resistance by activating TREK-2 channels (Deng et al., 2009). This modulation may be critical in spatial learning (Deng et al., 2009). Serotonin modulation occurs through activation of the quinidine-sensitive channel TWIK-1, which depends on 5-$HT_{1A}$ receptor activation (Deng et al., 2007). HCN channels may also be targets for modulation (Heys et al., 2010).

#### *Membrane potential sag*

Small perturbations of the membrane potential of a stellate cell are opposed after a short delay, leading to a characteristic "sag" response (Alonso and Llinás, 1989; Alonso and Klink, 1993; Klink and Alonso, 1993, 1997b; Jones, 1994; van der Linden and Lopes da Silva, 1998; Dickson et al., 2000b; Nolan et al., 2007). The sag response is prominent in previous whole-cell and sharp electrode recordings, and using perforated patch-clamp recordings (**Figure 2** and **Table 1**). The sag response is due to a change in the depolarizing inward current provided by $I_h$ (Dickson et al., 2000b; Nolan et al., 2007). During responses to negative current steps the membrane potential hyperpolarizes and $I_h$ slowly activates, thus causing a return depolarization. Conversely, when the membrane potential depolarizes $I_h$ slowly deactivates, causing the membrane potential to then hyperpolarize. $I_h$ block by $Cs^+$ or ZD7288 abolishes the sag (Klink and Alonso, 1993; Jones, 1994; Dickson et al., 2000b; Haas et al., 2007; Nolan et al., 2007), while deletion of HCN1 reduces the amplitude and slows the kinetics of the sag (Giocomo and Hasselmo, 2009; Nolan et al., 2007).

#### *Theta-frequency resonance*

A complementary approach to investigating the integrative properties of stellate cells is through their response to sinusoidally modulated current inputs. Membrane potential responses are largest to inputs that vary at frequencies in the theta range (4–12 Hz) (Haas and White, 2002; Erchova et al., 2004; Schreiber et al., 2004) (**Figure 3**). This theta-frequency resonance distinguishes stellate cells from other nearby neurons (Erchova et al., 2004). At lower frequencies the membrane potential response also has a small phase advance relative to the injected current, whereas at higher frequencies the membrane potential lags behind the injected current (Erchova et al., 2004; Nolan et al., 2007; Heys et al., 2010) (**Figure 3**).

Resonant properties also appear to be sensitive to recording method. Two properties are often used to describe resonance: the frequency of the resonance peak (F) and the relative amplitude of the peak (Q) (Hutcheon et al., 1996). Previous studies indicate that F is greater for sharp-electrode compared (Erchova et al., 2004; Boehlen et al., 2010) with whole-cell recordings (Nolan

**Table 1 | Sub-threshold membrane properties.**

| | Perforated patch ($n = 11$) | Whole-cell ($n = 14$) | $p$ | Test |
|---|---|---|---|---|
| Resting membrane potential (mV) | $-64.2 \pm 0.7$ | $-67.1 \pm 0.8$ | 0.047 | ANCOVA |
| Input resistance (+ve) (MΩ) | $55.5 \pm 9.6$ | $34.9 \pm 3.5$ | 0.0002 | ANCOVA |
| Input resistance (−ve) (MΩ) | $53.8 \pm 9.4$ | $32.5 \pm 3.0$ | 0.0004 | ANCOVA |
| Membrane time constant (ms) | $11.2 \pm 0.9$ | $12.7 \pm 0.9$ | 0.64 | ANCOVA |
| Sag coefficient | $0.66 \pm 0.02$ | $0.58 \pm 0.01$ | 0.0005 | ANCOVA |
| Location (μm) | $1096 \pm 192$ | $1114 \pm 206$ | 0.92 | *t*-test |

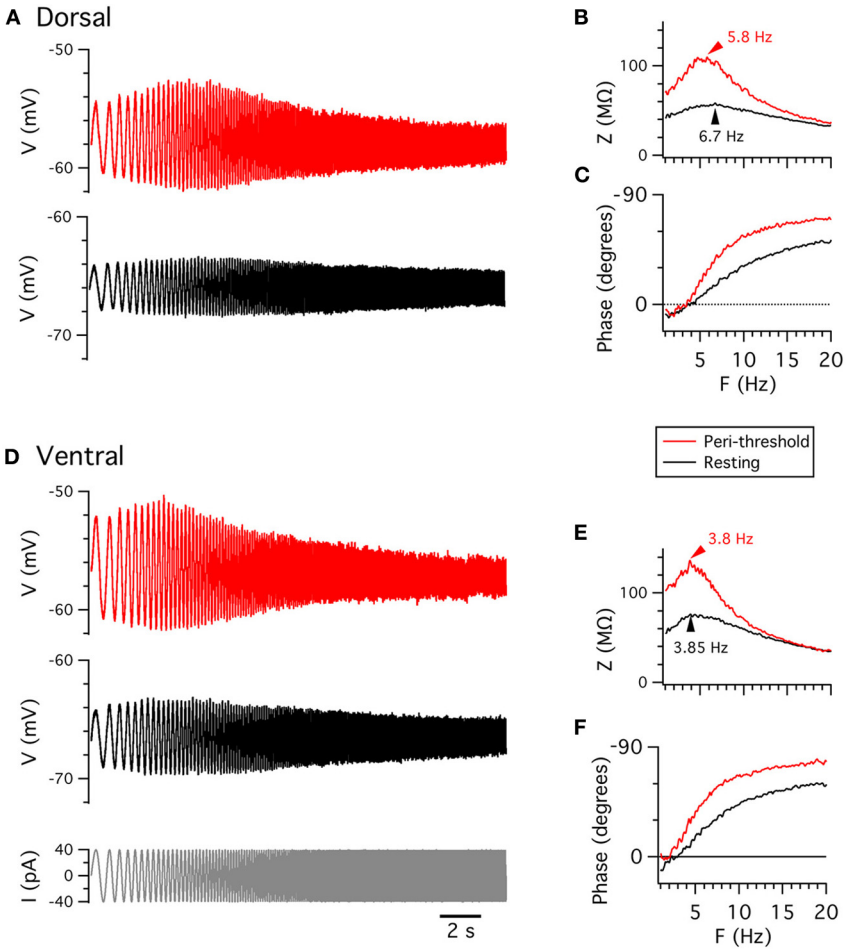


**FIGURE 3 | Membrane potential resonance. (A,D)** Examples of perforated patch-clamp recordings of membrane potential responses from resting potential (black) and from depolarized membrane potential (red) to ZAP current waveforms (**D**, lower), from dorsal **(A)** and ventral **(D)** stellate cells. **(B,E)** Membrane impedance plotted as a function of frequency. **(C,F)** Membrane phase plotted as a function of frequency. **B,C** and **E,F** are calculated from data in **A** and **D**, respectively.

et al., 2007; Boehlen et al., 2010; Heys et al., 2010). We find that F is similar, at either resting membrane potentials or peri-threshold potentials (approximately −50 to −55 mV), when measured with whole-cell or perforated patch-clamp methods (**Table 2**). Q also does not differ significantly between the two methods (**Table 2**), although with perforated patch-clamp recordings Q is significantly smaller at peri-threshold compared to resting membrane potentials (**Table 3**). Our finding here that with whole-cell recordings Q is similar when measured at resting potential (−65 mV) and peri-threshold potentials (−50 to −55 mV), while previous results indicate that Q is reduced on depolarization from −70 to −60 mV (Nolan et al., 2007), may be explained by resonance at peri-threshold potentials resulting from a different mechanism to that observed at resting potentials. Together, these data suggest that sharp electrode recordings may over-estimate the F at both resting and peri-threshold potentials, while whole-cell methods appear to provide estimates of resonant properties that are comparable to perforated patch-clamp data.

At resting membrane potentials the attenuation of low frequency signals that is essential for resonance in stellate cells requires HCN1 channels (Nolan et al., 2007). Deletion of HCN1 or pharmacological block of $I_h$ abolishes resonance by increasing the amplitude of responses to current inputs with frequencies less than 4 Hz (Haas et al., 2007; Nolan et al., 2007). The phase advance is also abolished (Nolan et al., 2007). Thus, resonance at resting membrane potentials can be explained by $I_h$ opposing slow changes in the membrane potential (Hutcheon and Yarom, 2000; Nolan et al., 2007; Dudman and Nolan, 2009; Dodson et al., 2011). Roles for other ion channels in resonance are less clear. In other cell types persistent sodium currents and M-type potassium currents can contribute to resonance at more depolarized voltages (Hu et al., 2007). In stellate cells the M-current blocker XE991 reduces the frequency and amplitude of the resonance peak at more depolarized voltages, but not at resting membrane potentials, although the frequency shift is on average less than 1 Hz and the reduction in amplitude appears quite small (Heys et al., 2010).

**Table 2 | Resonant properties.**

| | Perforated patch ($n = 5$) | Whole-cell ($n = 14$) | $p$ | Test |
|---|---|---|---|---|
| Q (resting) | 2.0 ± 0.2 | 1.7 ± 0.1 | 0.1 | ANCOVA |
| Q (peri-threshold) | 1.6 ± 0.1 | 1.8 ± 0.1 | 0.3 | ANCOVA |
| $F_{Z\text{-}max}$ (Hz) (resting) | 5.9 ± 1.0 | 6.1 ± 0.5 | 0.84 | ANCOVA |
| $F_{Z\text{-}max}$ (Hz) (peri-threshold) | 4.7 ± 0.9 | 4.4 ± 0.4 | 0.56 | ANCOVA |
| | **Resting** | **Peri-threshold** | $p$ | **Test** |
| Q (perforated patch) | 2.0 ± 0.2 | 1.6 ± 0.1 | 0.03 | Paired *t*-test |
| Q (whole-cell) | 1.7 ± 0.1 | 1.8 ± 0.1 | 0.4 | Paired *t*-test |
| $F_{Z\text{-}max}$ (Hz) (perforated patch) | 5.9 ± 1.0 | 4.7 ± 0.9 | 0.02 | Paired *t*-test |
| $F_{Z\text{-}max}$ (Hz) (whole-cell) | 6.1 ± 0.5 | 4.4 ± 0.4 | 2.8e-6 | Paired *t*-test |

**Table 3 | Action potential properties.**

| | Perforated. patch ($n = 11$) | Whole-cell ($n = 13$) | $p$ | Test |
|---|---|---|---|---|
| Proportion spikes in clusters (*Pc*) | 0.85 ± 0.06 | 0.26 ± 0.1 | 1.1e-5 | ANCOVA |
| Intra-cluster spike frequency (Hz) | 11.8 ± 1.3 | 7.8 ± 0.3 | 0.004 | ANCOVA |
| Overall spiking frequency (Hz) | 2.1 ± 0.1 | 2.3 ± 0.1 | 0.17 | ANCOVA |
| Spikes per cluster | 2.6 ± 0.1 | 3.8 ± 0.7 | 0.1 | ANCOVA |
| Rheobase (pA) | 181.8 ± 18.8 | 246.2 ± 21.6 | 0.005 | ANCOVA |
| Spike max (mV) | 41.9 ± 1.7 | 45.8 ± 1.0 | 0.06 | ANCOVA |
| Spike width at half-height (ms) | 0.59 ± 0.02 | 0.6 ± 0.01 | 0.65 | ANCOVA |
| Spike threshold (mV) | −44.7 ± 1.45 | −42.5 ± 0.7 | 0.16 | ANCOVA |
| AHP minimum (mV) | −60.9 ± 0.7 | −59.2 ± 0.6 | 0.08 | ANCOVA |
| AHP width at half-height (ms) | 64.3 ± 3.9 | 74.9 ± 4.1 | 0.03 | ANCOVA |

Theta-frequency resonance is also observed when stellate cells are probed with non-periodic frozen-noise inputs (Schreiber et al., 2004). However, the relationship between resonance and stellate cell responses to more physiological inputs is not fully understood. For excitatory glutamatergic synaptic input, stimulation at theta frequency produces little or no temporal summation of the response, whereas stimulation at gamma frequencies (40–80 Hz) causes strong temporal summation (Garden et al., 2008). This frequency dependence may reflect the fact that glutamatergic synaptic currents are very short compared with the membrane time constant (Garden et al., 2008) and so fast synaptic inputs will have very different temporal structure to the continuous sinusoidal inputs that are typically used to investigate resonant properties.

#### *Peri-threshold theta-frequency membrane potential activity*

When the membrane potential of a stellate cell is depolarized from rest to close to the threshold for action potential firing it becomes unstable, appearing to oscillate with frequency in the theta range (4–12 Hz) (**Figure 1A**) (Alonso and Llinás, 1989; Alonso and Klink, 1993; Dickson et al., 2000b; Erchova et al., 2004; Nolan et al., 2007; Dodson et al., 2011; Yoshida et al., 2011). This is of considerable interest first because it suggests a cellular correlate of the network theta rhythm recorded from the MEC and other hippocampal regions *in vivo* (Stewart et al., 1992; Dickson et al., 2000a; Mizuseki et al., 2009), and second because it has been argued that theta-frequency oscillations may be a substrate for encoding of spatial information by grid cells (Burgess et al., 2007; Giocomo et al., 2007).

Peri-threshold theta-frequency activity is consistently recorded from stellate cells with both sharp electrode and whole-cell techniques. However, the frequency of membrane potential activity during whole-cell recordings (Giocomo et al., 2007; Nolan et al., 2007; Giocomo and Hasselmo, 2009; Boehlen et al., 2010; Dodson et al., 2011) appears to be lower than during sharp electrode recordings (Alonso and Llinás, 1989; Klink and Alonso, 1993; White et al., 1998; Erchova et al., 2004; Boehlen et al., 2010). We find with perforated patch-clamp recordings that all stellate cells generate significant theta-frequency activity at membrane potentials close to spike threshold (**Figure 4**). In spectrograms the activity is characterized by brief epochs of power at theta frequencies (**Figures 4B,G**). Use of long windows for spectrograms as in some previous studies (Yoshida et al., 2011) may cause transient activity to appear sustained, whereas with shorter windows spectral peaks are revealed as non-stationary (cf **Figures 4B–C, G–H**). When activity is analyzed with Lomb periodograms of adjacent segments of activity (see Dodson et al., 2011 for details), the instability is manifest as variability in the frequency of the most significant activity peak and as multiple peaks in each segment (**Figures 4D,I**). This variability is clear from representative data (**Figures 4E,J**). Variability in the frequency of activity is also apparent during periods between action potential clusters (**Figure 4K**). Considering only the most significant peak in each of five epochs of duration 3 s, the

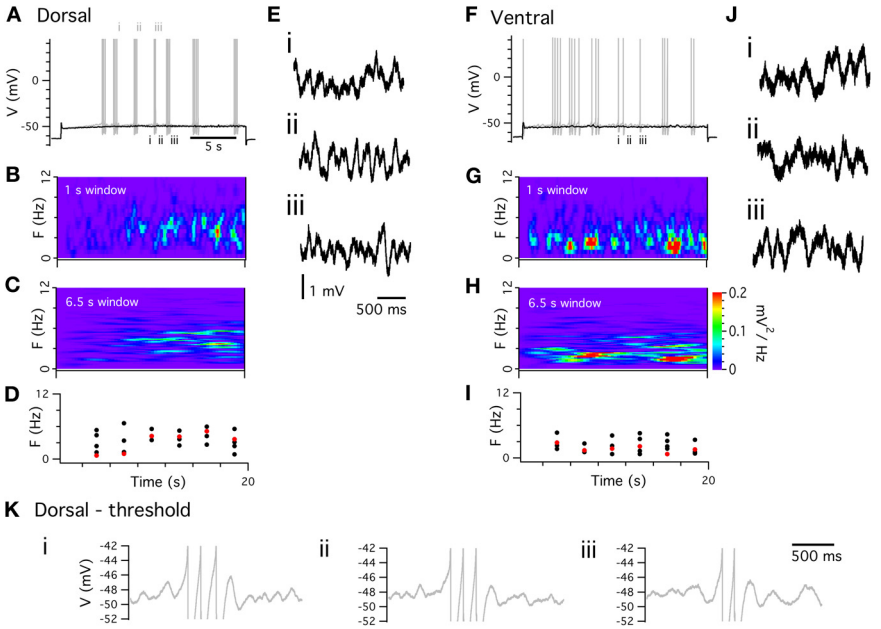


**FIGURE 4 | Peri-threshold theta-frequency activity.**
**(A,F)** Examples of perforated patch-clamp recordings of peri-threshold (black) and threshold (gray) membrane potential responses to current steps. **(B,G)** Spectograms from peri-threshold responses in **A,F**, calculated with 1 s windows. **(C,H)** Spectrograms from the same traces calculated using 6.5 s windows. **(D,I)** Frequency of most significant component (red) and all other significant frequencies (black) of peri-threshold membrane potential activity in **A,F**. Frequencies are obtained from Lomb periodograms of contiguous 3 s segments of data. **(E,J)** Examples of consecutive 2 s segments of data from peri-threshold activity in **A,F (K)** Examples of 1.5 s segments of membrane potential activity triggered by final spikes of three consecutive clusters of action potentials in **A**. Note the different frequency of the theta activity following each spike cluster.

mean frequency is 3.6 ± 0.5 Hz, while the range of significant frequencies across all five epochs is 3.2 ± 0.55 Hz. These results are similar to data from previous whole-cell recordings (Dodson et al., 2011).

The mechanism responsible for peri-threshold theta-frequency activity has been subject to debate. One class of ionic mechanism proposes that theta-frequency activity is generated by a periodic oscillator. This follows from the consideration that addition of an amplifying conductance, such as $Na_P$, to a resonator can lead to the generation of oscillations (Hutcheon and Yarom, 2000). Consistent with this idea, models of stellate cells that include $Na_P$ and $I_h$ can produce periodic membrane potential oscillations at peri-threshold potentials (Dickson et al., 2000b; Fransén et al., 2004). An important test of this oscillator model is whether the theta activity is periodic. In this case power spectra of the activity will have a single spectral peak that will have a stable frequency in consecutive analysis windows (Hajimiri and Lee, 1998; Dodson et al., 2011). The theta-frequency activity, recorded with perforated patch-clamp methods (**Figure 4**), and in previous whole-cell recordings (Nolan et al., 2007; Dodson et al., 2011), does not match this prediction (**Figures 4B–D, G–I**). Instead, the theta activity during sub-threshold sweeps and between spikes during suprathreshold sweeps (**Figure 4K**) has a frequency that changes apparently unpredictably. These observations are evidence against some models of grid cell firing fields that we discuss below. While these properties could perhaps be explained by variation in the period of an oscillator (Zilli et al., 2009), the variation would be so high that this would amount to an oscillatory system with dynamics that are essentially swamped by stochastic fluctuations.

A second class of ionic mechanism that can account for peri-threshold theta-frequency activity is based on evidence that stochastic gating of membrane ion channels can cause the membrane potential to fluctuate at theta frequencies (White et al., 1998). Direct support for this mechanism comes from experiments in which theta-frequency activity is abolished by pharmacologically blocking $Na_P$. When a dynamic clamp is then used to reintroduce a purely deterministic version of $Na_P$ theta-frequency fluctuations remain absent (Dorval and White, 2005). In contrast, reintroduction of stochastic $Na_P$ channels restores theta-frequency activity (Dorval and White, 2005). Consistent with this mechanism, detailed models of stellate cells, in which all ion channels gate stochastically, reproduce spectral properties of theta-frequency activity (Dudman and Nolan, 2009; Dodson et al., 2011). Nevertheless, because these models represent stellate cells as a single compartment, whereas the electrical properties of stellate cells are primarily determined by their dendrites (Garden et al., 2008), it will be important to establish whether theta-frequency activity is also accounted for by models that include stochastic gating of dendritic ion channels (Cannon et al., 2010).

Considering these data together, it is unlikely that theta-frequency membrane potential fluctuations reflect the output of a periodic oscillatory process. Instead, they appear most

consistent with filtering of membrane potential noise resulting from stochastic ion channel gating. In this scenario, resonance due to voltage-gated ion channels likely plays an important role in shaping the frequency of the noise-driven membrane potential activity (White et al., 1998; Haas et al., 2007). It remains to be determined whether this intrinsic theta-frequency activity originates in the cell body or dendrites of stellate cells. For example, membrane potential changes at the cell body may reflect much larger stochastic events originating in the dendrites (Cannon et al., 2010).

### *The action potential and its after-polarization*

Stellate cells generate action potentials when their membrane potential is depolarized above approximately −50 mV (Alonso and Klink, 1993; Jones, 1994). When action potentials are initiated during injection of constant positive current they are followed immediately by an after-polarization with several components (**Figure 5**). First, there is a shallow and rapid AHP, which is followed by a brief after-depolarization (ADP). Finally, at typical physiological spiking rates (<∼20 Hz) (Sargolini et al., 2006), there is a slower AHP which maintains the membrane potential below its peri-threshold value (Alonso and Klink, 1993). These properties are seen with whole-cell and sharp electrode recordings, but their relative prominence may differ (Boehlen et al., 2010). We find that with perforated patch-clamp recordings these characteristic features of the action potential and its AHP are also maintained (**Figure 5**). We note that when action potentials are triggered by brief synaptic input, the waveform of the after-polarization differs (**Figure 1B**), but while this difference may be important for physiological activation of stellate cells it has so far received very little attention.

Initiation of the action potential is blocked by TTX (Alonso and Llinás, 1989), but not by riluzole (Dorval and White, 2005), indicating that it requires $Na_T$, but not $Na_P$. As for many other neuron types, the duration of the action potential is increased by blocking voltage-gated potassium channels (Klink and Alonso, 1993). This is consistent with $K_{DR}$ channels mediating rapid repolarization. $Ca^{2+}$-dependent activation of $K_{Ca}$ is important for the later stages of repolarization and for the AHP (Klink and Alonso, 1993; Khawaja et al., 2007). The recovery of the membrane potential to rest following the peak of the AHP is accelerated by activation of $I_h$ mediated by HCN1 channels (Nolan et al., 2007). Further experimental investigation of the action potential AHP is likely to be important, particularly as the AHP and ADP are difficult to fully account for in current biophysical models of stellate cells (Fransén et al., 2004; Dudman and Nolan, 2009) and may play important roles in generation of grid cell firing fields (Navratilova et al., 2012).

### *Clustering of action potentials*

Compared with other neuron types, stellate cells generate distinctive clustered patterns of action potentials during maintained supra-threshold depolarization (Alonso and Klink, 1993; Klink and Alonso, 1993; Nolan et al., 2007; Engel et al., 2008; Fernandez and White, 2008) (**Figures 1A, 5**). During whole-cell recordings, spikes within a cluster have similar inter-spike intervals that are independent of the overall firing frequency and that are often in the high theta range (about 8–12 Hz) (Nolan et al., 2007; Fernandez and White, 2008). Clustered patterns of spikes are most robust when the overall spike frequency is less than 5 Hz, with the inter-cluster interval sometimes being a second or longer (Nolan et al., 2007). At higher overall spike frequencies clustered patterns of spikes are no longer detectable. Spike trains show very little frequency adaptation at firing rates below the typical physiological maximum (∼20 Hz) (Alonso and Klink, 1993; Sargolini et al., 2006). Importantly, while clustered patterns of action potential firing have peaks in their power spectra in the theta-frequency range, the underlying mechanism is distinct from

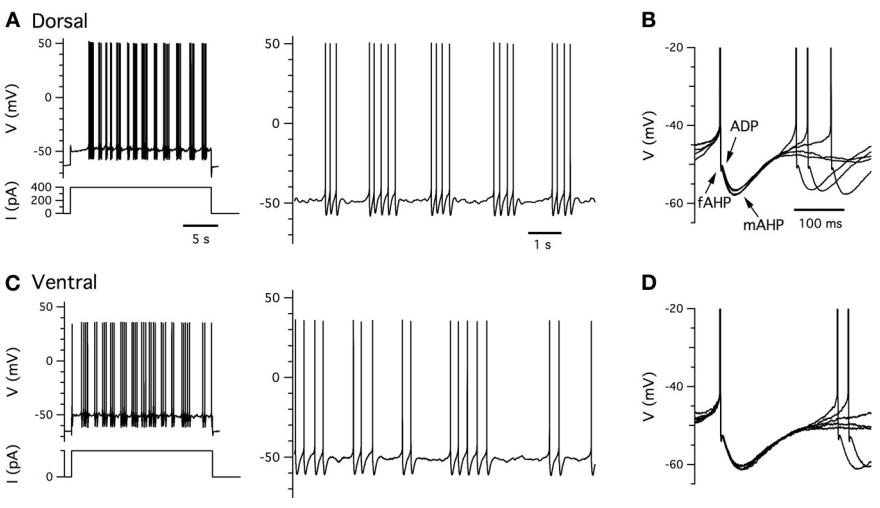


**FIGURE 5 | Clustered firing patterns. (A,C)** Examples of perforated patch-clamp recordings of supra-threshold membrane potential responses (upper left) to positive current steps (lower left) from dorsal **(A)** and ventral **(C)** stellate cells. Action potentials on an expanded time base are shown to the right. **(B,D)** Examples of five consecutive action potential afterhyperpolarizations captured from traces in **(A,C)**. Arrows indicate components of the after polarization.

that of sub-threshold theta-frequency resonance (Nolan et al., 2007; Fernandez and White, 2008).

When recorded with perforated-patch methods clustered firing is exceptionally robust (**Figures 5A,C**). The probability that a spike is within a cluster is substantially greater when recorded with perforated patch compared to whole-cell methods (**Table 3**). The frequency of spikes within clusters is also higher for perforated patch recordings, whereas the number of spikes per cluster is similar to measurements with whole-cell recordings (Nolan et al., 2007). These data suggest that during whole-cell recordings there may be washout of a conductance that is not necessary for clustered firing patterns, but that increases their probability of occurrence.

We took advantage of the relatively large differences between whole-cell and perforated patch-clamp methods in the duration of the AHP and the probability that a spike is part of a cluster to estimate the time course of changes that takes place during intracellular dialysis associated with whole-cell recording from stellate cells (**Figure 6**). We found that even within 2 min of break in to the whole-cell configuration—the shortest interval within which we could reliably estimate the threshold current to trigger spike firing—the probability that spikes are part of a cluster differed significantly from that measured with perforated patch-clamp recording (**Figure 6**). This property and the AHP half-duration continued to change during the first 30 min following break-in (**Figure 6**). These data suggest that signaling pathways sensitive to washout during whole-cell recording regulate the firing properties of stellate cells.

Ion channels that determine the amplitude and duration of the AHP appear to be critical for determining the pattern of spiking activity generated by stellate cells (Fransén et al., 2004; Nolan et al., 2007; Fernandez and White, 2008; Dudman and Nolan, 2009). Deletion of HCN1 or block of $I_h$ greatly reduces spike clustering (Nolan et al., 2007). This can be explained by a model in which action potentials are triggered by stochastic fluctuations in membrane potential (Dudman and Nolan, 2009). In this model HCN channels engaged during the AHP provide a depolarizing drive that transiently increases the probability that membrane potential noise will trigger an action potential (Dudman and Nolan, 2009). Alternatively, termination of spike clusters could be achieved through incremental elevation of intracellular $Ca^{2+}$ following each action potential (Fransén et al., 2004). However, with this mechanism it is difficult to explain the probabilistic properties of clustered spike firing that are accounted for by stochastic models (Dudman and Nolan, 2009). A model based on inductor-dependent resonance can also reproduce statistics of clustered spiking trains (Engel et al., 2008). However, this model appears inconsistent with experiments showing that the dominant frequency of spike train power spectral densities can be manipulated independently from that of peri-threshold membrane potential activity (Fernandez and White, 2008).

## SYNAPTIC INTEGRATION

A typical stellate cell has 6–10 primary dendrites that are densely populated with dendritic spines (Klink and Alonso, 1997b; Buckmaster et al., 2004; Garden et al., 2008). These spines are likely to be the main sites of excitatory synaptic input to stellate cells, but while the experiments considered so far evaluate stellate cell output in response to current injected through an experimental electrode, much less are known about how stellate cells respond to synaptic inputs. Stimulation of layer I evokes excitatory postsynaptic potentials (EPSPs) in stellate cells that can trigger action potentials (**Figure 1B**) (Alonso et al., 1990; Garden et al., 2008). The origin of these inputs is not clear, but

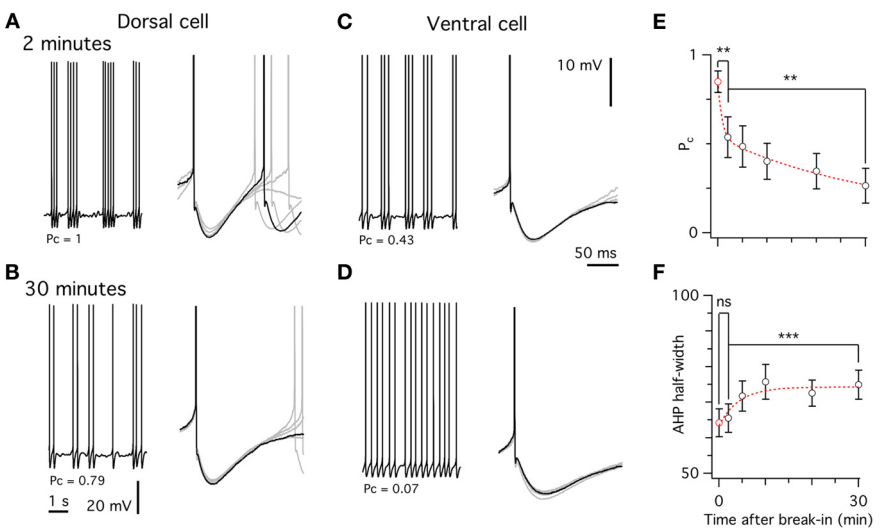


**FIGURE 6 | Washout of spiking properties during whole-cell recording.** **(A,C)** Spiking pattern (left) and after-hyperpolarization (right) in a dorsal **(A)** and ventral **(C)** stellate cell approximately 2 min after break in. **(B,D)** Spiking pattern and after-hyperpolarization from the same cells as in **A,C**, 30 min after break-in. **(E)** Decrease of the probability of spikes occurring in a cluster (*Pc*) over time after break-in. **(F)** Increase in the after-hyperpolarization width at half-height over time. In **E,F** the red data point at time zero is from the perforated patch data. ANCOVA was used for comparisons between data obtained using different recording methods and Student's paired *t*-test to test differences within cells at different time points.

might include axons from neurons in the neocortex (Dolorfo and Amaral, 1998; Burwell, 2000). Synaptic potentials can also be evoked in stellate cells by stimulation in the parasubiculum or deeper layers of the MEC (Jones, 1994). Recent experiments using localized photo-uncaging of glutamate to activate inputs from neurons at anatomically defined locations have begun to establish principles for the organization of local microcircuits containing stellate cells (Kumar et al., 2007; Beed et al., 2010). These experiments suggest that stellate cells receive local excitatory input from neurons in layer II of the MEC as well as from deeper layers. However, dual intracellular recordings from over 100 pairs of layer II principle cells did not find evidence for excitatory connections between stellate cells, suggesting that if recurrent excitation is present within layer II it is very sparse (Dhillon and Jones, 2000). The neurotransmitter receptors that mediate synaptic responses of stellate cells appear to have properties similar to other central neurons. EPSPs have fast components mediated by AMPA (non-NMDA) receptors and slower NMDA receptor components (Alonso et al., 1990; Jones, 1994). Fast synaptic inhibition is mediated by $GABA_A$ receptors (Jones, 1994), while slower synaptic inhibition is through $GABA_B$ receptors (Jones, 1994; Deng et al., 2009). Inputs from different locations can differentially activate plasticity mechanisms in stellate cells (Ma et al., 2008), but it is unclear whether they also engage distinct integrative mechanisms.

How do non-synaptic ion channels modify the responses of stellate cells to synaptic input? As the main ion channels open at rest (**Figure 1C**), leak potassium channels and HCN channels are important determinants of integration of sub-threshold synaptic responses (Garden et al., 2008). Both channel types determine the time window for detection of coincident inputs and summation of inputs activated at gamma frequencies (Garden et al., 2008). If either channel is blocked the coincidence detection time window becomes wider and summation of gamma frequency inputs increases. In contrast, the interval between synaptic responses evoked at theta frequency is too long for interactions between successive responses to be influenced by these integrative mechanisms (Garden et al., 2008). Unlike for some other neuron types (Stuart and Sakmann, 1994; Schiller et al., 2000), it is not yet clear whether synaptic input to dendrites of stellate cells can initiate local spikes. The role of $Na_P$ is also unclear, although experiments in other neuron types suggest it may be important for amplification of EPSPs (Stuart and Sakmann, 1995).

## DORSAL-VENTRAL ORGANIZATION OF MEMBRANE PROPERTIES

Grid cells are organized topographically according to the spatial resolution of their firing fields, such that more dorsal cells have smaller firing fields that are spaced closer together compared with more ventral cells (Hafting et al., 2005; Sargolini et al., 2006; Barry et al., 2007; Brun et al., 2008; Fyhn et al., 2008). Several of the integrative properties of stellate cells that we describe above follow a similar dorsal-ventral organization. This correlation is of potential importance as it may reflect cellular computations important for generation of grid fields (Giocomo et al., 2011b; O'Donnell and Nolan, 2011). However, to test whether such correlations play a causal role in establishing grid cell firing fields, it is essential to first understand their underlying mechanisms. We describe below evidence for dorsal-ventral organization of ion channel properties, resting membrane properties, frequency selectivity, action potential clustering, and synaptic integration. We will suggest how these observations can be explained by increasing density of currents mediated by HCN and leak potassium channels in stellate cells located at dorsal compared to more ventral locations (Garden et al., 2008).

### *Ion channel function*

There is evidence for a dorsal-ventral gradient in the density of a leak potassium conductance (Garden et al., 2008) and in either the density (Garden et al., 2008) or kinetics of $I_h$ (Giocomo and Hasselmo, 2008). In one study, when pharmacologically isolated $I_h$ was measured by two independent methods—from tail currents and from currents sensitive to the blocker ZD7288—the amplitude of $I_h$ appeared to be smaller for neurons located at progressively more ventral locations (Garden et al., 2008). Differences in morphology between cells at different locations were insufficient to explain the differences in the measured currents (Garden et al., 2008). These data are consistent with *in situ* hybridization data in the Allen Brain Atlas, which suggests that mRNA levels of HCN1 and HCN2 follow a dorsal-ventral gradient in expression in layer II of the MEC. In this study there was very little variability in the time constant of $I_h$ (Garden et al., 2008). In contrast to these data, a different study suggests that time constants, but not the amplitude of $I_h$, vary across the dorsal-ventral extent of the MEC (Giocomo and Hasselmo, 2008). Because these differences lead to very different functional predictions for the roles of $I_h$ in stellate cells, it will be important for future work to clarify their cause, for example young (Giocomo and Hasselmo, 2008) vs. mature animals (Garden et al., 2008), or rats (Giocomo and Hasselmo, 2008) vs. mice (Garden et al., 2008).

### *Resting membrane properties*

Stellate cells at dorsal locations have lower input resistance and faster membrane time constants than those at ventral locations (Garden et al., 2008; Boehlen et al., 2010). Consistent with these data, in perforated patch-clamp experiments we also find a significant dorsal-ventral organization of the input-resistance and membrane time constant, but not the resting membrane potential (**Figures 7A–C**). This organization can be accounted for by differences in the density of both leak potassium channels and HCN channels that mediate $I_h$ (Garden et al., 2008). Thus, in dorsal neurons a greater density of leak potassium and HCN conductances lowers the input resistance and membrane time constant compared with more ventral neurons.

### *Frequency selectivity*

Stellate cells exhibit a gradient in their frequency selectivity, with dorsal cells having a resting resonance peak at higher frequencies than cells from more ventral locations (Giocomo et al., 2007; Boehlen et al., 2010). Results from perforated patch-clamp experiments are consistent with these data (**Figures 7D–E**). Differences in the density of currents through HCN channels could account for this organization of resonance frequencies, as greater $I_h$ amplitude in dorsal cells will more effectively oppose slow changes

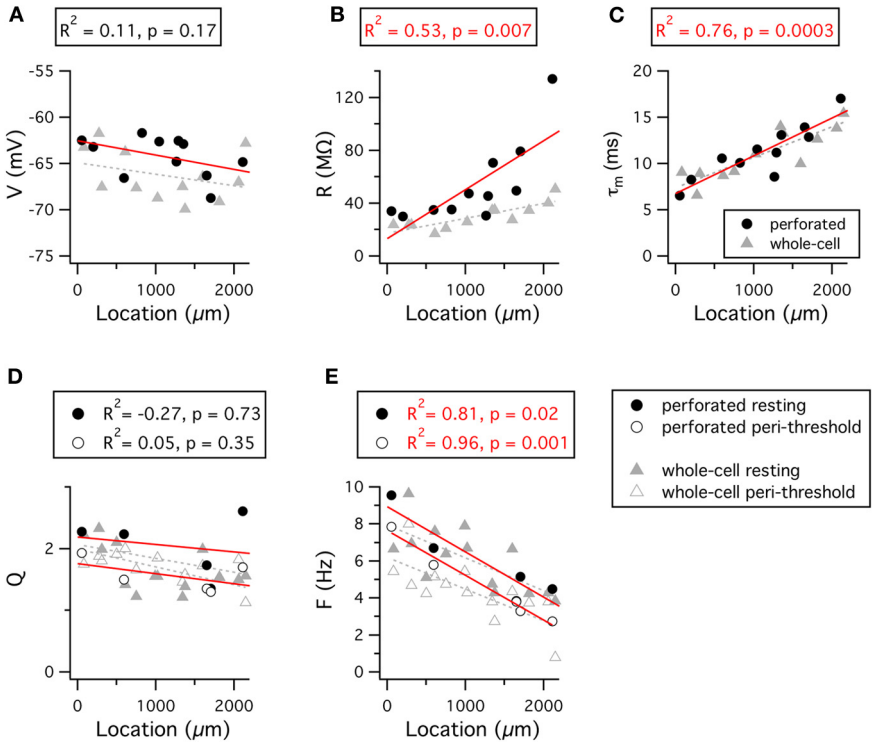


**FIGURE 7 | Dorsal-ventral organization of resting and resonant membrane properties. (A–E)** Resting membrane potential **(A)**, input resistance **(B)**, membrane time constant **(C)**, resonance amplitude **(D)** and resonant frequency **(E)** are plotted as a function of the location of the recorded stellate cell. Red lines indicate fits to the perforated patch-clamp data. Grey dashed lines indicate fits to the whole-cell data. Adjusted $R^2$ value and significance of the fit for the perforated patch-clamp data are stated above each plot. The $R^2$ and significance values for fits of the whole-cell data are as follows: *V*, $R^2 = 0.04$, $p = 0.24$; *R*, $R^2 = 0.59$, $p = 0.0009$; $\tau_m$, $R^2 = 0.64$, $p = 0.0003$; $Q_{rest}$, $R^2 = 0.22$, $p = 0.052$; $Q_{peri}$, $R^2 = 0.006$, $p = 0.32$; $F_{rest}$, $R^2 = 0.46$, $p = 0.005$; $F_{peri}$, $R^2 = 0.5$, $p = 0.003$. Location refers to distance from the dorsal border of the MEC.

in membrane potential, thus causing greater attenuation of low frequency inputs (Nolan et al., 2007; Heys et al., 2010). While not found in mature neurons (Garden et al., 2008), differences in the kinetics of $I_h$ could in principle also account for the dorsal-ventral organization of membrane resonance (Giocomo and Hasselmo, 2008), but this would not explain the dorsal-ventral organization of input resistance (Garden et al., 2008).

Just as for the resonant response to injected current, the properties of peri-threshold theta-frequency activity also follow a dorsal-ventral gradient (Giocomo et al., 2007; Giocomo and Hasselmo, 2008, 2009; Dodson et al., 2011; Yoshida et al., 2011). With perforated patch-clamp recordings the frequency of the most significant peak in a 15 s window varies steeply as a function of location (**Figures 8A–C**). These data are consistent with previous observations from whole-cell and sharp electrode recordings (Giocomo et al., 2007; Giocomo and Hasselmo, 2008, 2009; Dodson et al., 2011; Yoshida et al., 2011). The dependence of the significant frequencies on the length of the analysis time window (**Figures 8A–B**) and their variability between consecutive time windows (**Figure 8C**) is consistent with the idea that theta-frequency activity reflects filtering of a noise source (Dodson et al., 2011).

The ionic basis for the dorsal-ventral organization of theta-frequency activity appears to involve differences in $I_h$. Knockout of the HCN1 subunit flattens the frequency gradient of the fluctuations (Giocomo and Hasselmo, 2009), although following pharmacological block of $I_h$ a gradient nevertheless remains (Dodson et al., 2011). If the theta-frequency activity was periodic then these differences could be explained by models in which ion channels gate deterministically and the kinetics of $I_h$ vary with location (Yoshida et al., 2011). However, as we discuss above, models of this kind do not appear to account for the stochastic nature of theta-frequency activity. In contrast, both the variability and the frequency of the largest amplitude activity are accounted for by models in which all ion channels gate stochastically and in which the density of HCN and leak potassium channels follows a dorsal-ventral organization (Dodson et al., 2011). It is, therefore, possible that the dorsal-ventral organization of intrinsic theta-frequency activity is a secondary consequence of control of the resting integrative properties of stellate cells by these ion channels.

### *Clustering of action potentials*

Stellate cells also demonstrate a dorsal-ventral gradient in their pattern of action potential firing (**Figures 9A–C**). This organization of stellate cell firing patterns has not previously been described. With perforated patch-clamp recordings we find that, although spike clustering remains high in stellate neurons along

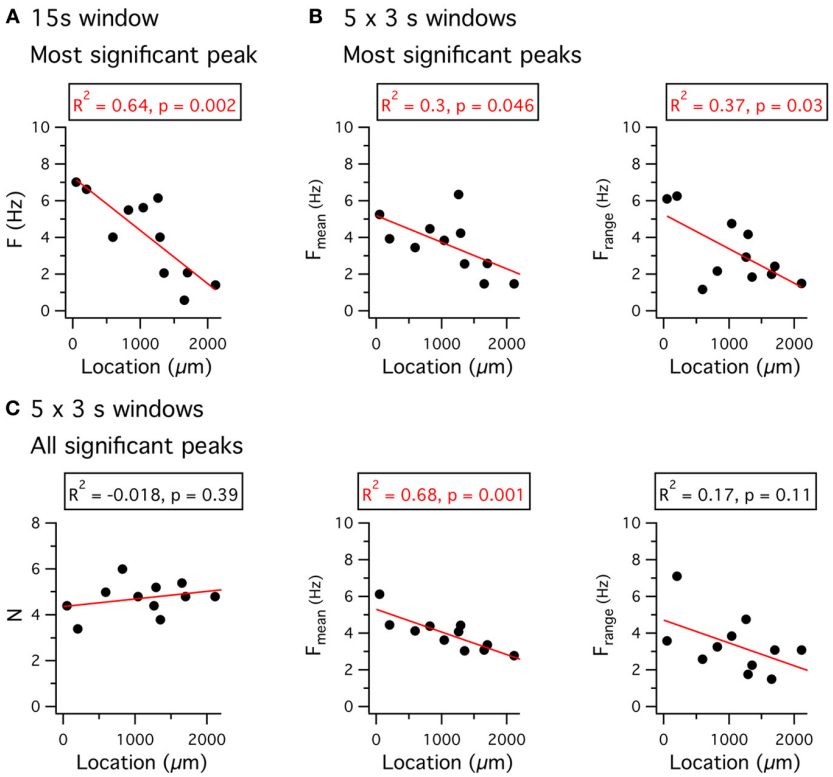


**FIGURE 8 | Dorsal-ventral organization of theta-frequency activity. (A)** The frequency of the most significant peak in a Lomb periodogram of 15 s of peri-threshold membrane potential activity is plotted as a function of the location of the recorded neuron. **(B)** The mean frequency (left) and the range of frequencies (right) of the most significant peak of Lomb periodograms, obtained from five consecutive 3 s duration segments of peri-threshold activity, is plotted as a function of the location of the recorded neuron. **(C)** The number of significant peaks (left), the mean frequency (middle) of all significant peaks, and the range of frequencies of all significant peaks (right), obtained from five consecutive 3 s duration segments of peri-threshold activity, plotted as a function of the location of the recorded neuron. Data analyzed were from 5 s to 20 s after the onset of the largest amplitude current step that did not trigger action potential firing. Adjusted $R^2$ value and significance of the fit for the perforated patch-clamp data are stated above each plot. Location refers to distance from the dorsal border of the MEC.

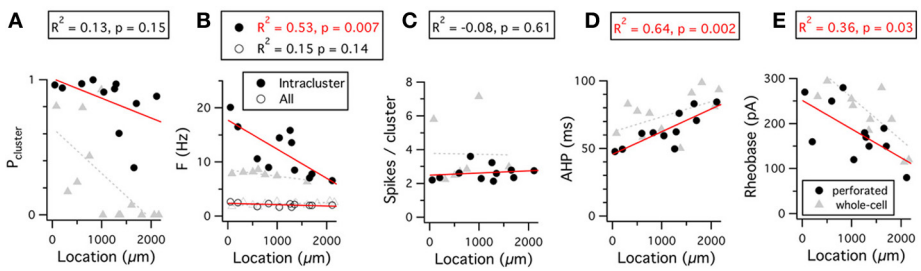


**FIGURE 9 | Dorsal-ventral organization of firing properties. (A–E)** Probability that a spike is part of a cluster **(A)**, frequency of spikes throughout the 15 s duration analysis window (open circles) or within a cluster (closed circles) **(B)**, number of spikes per cluster **(C)**, duration of the action potential after-hyperpolarization **(D)**, and rheobase **(E)**, are plotted as a function of the location of the recorded neuron. Data analyzed were from 5 s to 20 s after the onset of the current steps that triggered action potential firing at frequencies in the range 1–3 Hz. Adjusted $R^2$ value and significance of the fit for the perforated patch-clamp data are stated above each plot. The $R^2$ and significance values for fits of the whole-cell data are as follows: $P_{cluster}$, $R^2 = 0.35$, $p = 0.02$; $F_{intracluster}$, $R^2 = 0.56$, $p = 0.03$; $F_{all}$, $R^2 = 0.19$, $p = 0.08$; Spikes/cluster, $R^2 = 0.38$, $p = 0.08$; AHP, $R^2 = 0.19$, $p = 0.08$; Rheobase, $R^2 = 0.61$, $p = 0.0009$. Location refers to distance from the dorsal border of the MEC.

the full dorsal-ventral extent of the MEC (**Figure 9A**), the frequency with which spikes occur within clusters follows a gradient (**Figure 9B**). In contrast, in our whole-cell recordings clustering appears to be reduced in more ventral cells, leading to the emergence of a gradient in the probability that an action potential is part of a clustered firing pattern (**Figure 9A**). The number of spikes per cluster is independent of location and recording method.

This organization of the pattern of spike firing by stellate cells can be explained by differences in the density of current through HCN channels (Garden et al., 2008) and their influence on the action potential AHP (Nolan et al., 2007; Dudman and Nolan, 2009). Because activation of HCN channels accelerates repolarization following the peak of the action potential AHP (Nolan et al., 2007; Dudman and Nolan, 2009), the greater density of HCN channels in dorsal cells will reduce the duration of the AHP and, therefore, increase the intra-cluster spike frequency. Consistent with this explanation, the AHP duration is shortest in more dorsal cells and increases for cells at progressively more ventral locations (**Figure 9D**) (Boehlen et al., 2010). The dependence of the probability of clustered firing on location found with whole-cell recordings is consistent with a strong correlation between these parameters in whole-cell recording conditions (Nolan et al., 2007; Fernandez and White, 2008). The absence of this gradient from perforated-patch recordings suggests wash-out during whole-cell recordings of a factor that promotes clustered patterns of activity in ventral cells. One possible explanation is that wash-out during whole-cell recordings causes a shift in the voltage dependence of HCN channels that reduces their influence on the AHP.

The threshold-current required to initiate action potential firing also follows a dorsal-ventral organization (Garden et al., 2008; Boehlen et al., 2010). This organization is maintained in perforated patch-clamp and whole-cell recordings (**Figure 9E**). The organization of the threshold-current is at least in part explained by the lower input resistance of dorsal compared to more ventral neurons, resulting from their higher density of leak potassium and HCN channels (Garden et al., 2008).

#### *Synaptic integration*

The waveforms of evoked and spontaneous excitatory synaptic potentials recorded from stellate cells follow a dorsal-ventral organization that is also explained by the density of currents through HCN and leak potassium channels. For neurons located more dorsally, EPSPs are shorter than for neurons located more ventrally (Garden et al., 2008). One consequence is that gamma frequency inputs to stellate cells at ventral locations sum more effectively relative to cells at more dorsal locations (Garden et al., 2008). Another is that dorsal cells have narrower time windows for detection of coincident synaptic activity than ventral cells and may, therefore, be better at temporal discrimination (Garden et al., 2008). Importantly, either leak potassium channels or HCN channels alone can support the gradient in integrative properties, although block of either channel increases the duration of EPSPs (Garden et al., 2008). Simulations suggest that gradients in the amplitude of the currents that organize synaptic integration are sufficient to also account for the dorsal-ventral organization of peri-threshold theta-frequency activity (Dodson et al., 2011).

## FROM ION CHANNELS TO GRID FIRING FIELDS

The electrophysiological investigations of stellate cells described above provide a foundation to begin addressing questions about cellular mechanisms for spatial computations carried out within the MEC. For example, what is the relationship between computational properties evaluated with *in vitro* experiments and generation of grid firing fields? What are the roles in generation of grid firing fields of particular ion channels expressed by stellate cells? Does modulation of the intrinsic electrophysiological properties of stellate cells play roles in firing during spatial behaviors? Answering these and related questions will require integration of cellular data with predictive models for computation carried out during spatial behaviors, and testing of these models using recordings from behaving animals and specific manipulation of cellular properties of stellate cells.

#### *Constraining models based on intrinsic electrophysiological properties*

Two general classes of abstract model have been proposed to account for generation of grid firing fields (Burgess and O'Keefe, 2011; Giocomo et al., 2011b). In one, grid fields are produced by interference between oscillations with frequency sensitive to an animal's velocity (Burgess et al., 2007; Giocomo et al., 2007; Blair et al., 2008; Burgess, 2008; Hasselmo, 2008). In the second, grid fields result from bumps in an attractor network that are shifted by velocity inputs (Fuhs and Touretzky, 2006; McNaughton et al., 2006; Burak and Fiete, 2009; Navratilova et al., 2012). We consider below how known intrinsic electrophysiological properties of stellate cells constrain the ways in which each class of abstract model can be implemented, and how knowledge of ion channel function in stellate cells can be used to distinguish between different models.

Models that compute location through oscillatory interference rely on periodic oscillators that are sensitive to velocity. Initial versions of these models proposed that theta-frequency activity of stellate cells reflected one or more oscillations of this kind (Burgess et al., 2007; Giocomo et al., 2007). However, several cellular properties argue against this mechanism. First, while theta-frequency activity can be interpreted as the output of a periodic oscillator (Dickson et al., 2000a; Fransén et al., 2004), the data discussed above suggests it is more likely to reflect filtered stochastic noise (White et al., 1998; Nolan et al., 2007; Dodson et al., 2011). This is a substantial problem as filtered noise signals are not periodic and computation by oscillatory interference mechanisms is extremely sensitive to noise (Burak and Fiete, 2009). Second, models that require independent oscillators in different dendrites appear to be impossible to implement given known cable properties of dendrites (Remme et al., 2010). Third, theta-frequency activity is abolished by synaptic conductances that mimic activity that might occur *in vivo* (Fernandez and White, 2008).

Alternative implementations of oscillatory interference models assume that neurons that act as velocity-sensitive oscillators are located upstream of grid cells (Blair et al., 2008; Burgess, 2008; Hasselmo, 2008). Recent evidence suggests that firing of "theta cells" in the anterior thalamus, hippocampus and medial septum may perform this function (Welday et al., 2011). In these cells theta-frequency bursts of action potentials are modulated by both movement speed and movement direction. For further evaluation of this theory it will be important to determine if these cells synapse with stellate cells and how the intrinsic properties of stellate cells influence responses to these inputs. For example, dorsal-ventral gradients in theta-frequency resonance or synaptic

integration might contribute to decoding of inputs from velocity sensitive oscillators.

In models of grid cell firing that rely on network attractor states the influence of stellate cell integrative properties has received less direct attention. While these models are typically implemented using abstract neurons, in all cases tuning of neuronal gain is necessary for the network to produce attractor states (Fuhs and Touretzky, 2006; McNaughton et al., 2006; Burak and Fiete, 2009; Navratilova et al., 2012). Therefore models of this kind can also be used to make predictions for how intrinsic properties of stellate cells might influence grid firing fields. A recent attractor model predicts possible roles for the AHP and ADP, along with synaptic NMDA conductances, in grid cell firing, periodicity, and phase precession (Navratilova et al., 2012). This model assumes dorsal-ventral tuning of NMDA kinetics, but observations of dorsal-ventral organization of synaptic integration (Garden et al., 2008) would likely also predict experimentally observed dorsal-ventral spacing of grid firing fields using models of this kind (Navratilova et al., 2012). Dorsal-ventral gradients in the AHP waveform are also consistent with this model (**Figure 9**) (Boehlen et al., 2010).

#### *Ion channel manipulation in behaving animals*

One of the most promising approaches for understanding the contribution of the intrinsic electrical properties of hippocampal and entorhinal neurons to spatial behavior is using animals in which key ion channels are genetically deleted. So far most attention has been directed toward the HCN1 ion channel (Nolan et al., 2004; Giocomo et al., 2011a; Hussaini et al., 2011). When the HCN1 channel is deleted from forebrain neurons spatial memory is enhanced (Nolan et al., 2004). Removal of HCN1 also increases the amplitude of the theta rhythm recorded in the hippocampus (Nolan et al., 2004). Consistent with these results and the effects of HCN1 deletion on the intrinsic properties of stellate cells (Nolan et al., 2007), grid-like firing fields of neurons in layer II of the MEC and place fields of hippocampal CA1 neurons are maintained in mice with deletion of HCN1 from forebrain neurons (Giocomo et al., 2011a; Hussaini et al., 2011). Together, these observations provide strong evidence against models for neuronal representation of space that require functions attributed to HCN1, including models based on interference between intrinsic oscillations. These results also argue against the view that HCN channels in the entorhinal cortex are pacemakers of theta-frequency activity.

Recent experiments that record from grid cells in mice with deletion of HCN1 from forebrain neurons are of further interest because they suggest that HCN1 plays important regulatory roles in the encoding of space (Giocomo et al., 2011a; Hussaini et al., 2011). Most intriguingly, grid cells and place cells observed following deletion of HCN1 appear to be larger and are more stable than in control animals (Giocomo et al., 2011a; Hussaini et al., 2011). The spacing between grid fields is also increased, while the dorsal-ventral organization of grid fields is maintained, so that on average firing fields at all locations are larger and further apart in HCN1 knockout compared to control mice (Giocomo et al., 2011a). While a potential caveat in interpretation of these observations is that deletion of HCN1 is throughout the forebrain, including neurons upstream of grid cells, they nevertheless raise important new questions. For example, why does deletion of HCN1 make grid fields larger and wider? One possibility is that this reflects the increased time-window for synaptic integration or summation of synaptic responses in stellate cells (Garden et al., 2008). Another is that it reflects place field expansion in CA1 (Hussaini et al., 2011), possibly in turn resulting from increased synaptic plasticity of CA1 pyramidal cells (Nolan et al., 2004). What mechanisms maintain the dorsal-ventral organization of grid field properties in the absence of HCN1? A possibility is that control of synaptic integration by the dorsal-ventral organization of leak potassium channels is sufficient to coordinate these properties of grid fields (Garden et al., 2008). What aspects of HCN1 channel function are critical to the behavioral roles of the channel? On the one hand, these behavioral roles may reflect control of sub-threshold resonant or oscillatory dynamics of stellate cells through voltage-dependent gating of HCN1 (Nolan et al., 2007; Giocomo and Hasselmo, 2009). On the other hand, the pattern of spike output from stellate cells may be independent of sub-threshold resonant properties (Fernandez and White, 2008), and instead the key function of HCN1 may be simply through its contribution to the resting membrane potential and conductance (Nolan et al., 2007). Further experimental investigation will be required to address these and other questions about the relationship between HCN1 channels, leak potassium channels and grid firing fields.

A further possible caveat in interpretation of behavioral results from knockout mice is that adaptation may mask roles of the deleted protein. For example, while data from knockout mice indicates that HCN1 is not required for generation of grid firing fields, this does not rule out the possibility that in wild-type animals HCN1 plays a central role that can nevertheless be compensated for when the channel is deleted. Comparison of intrinsic electrophysiological properties of stellate cells from control and HCN1 deletion mice during block of $I_h$ does not reveal evidence of adaptation (Nolan et al., 2007). However, in pyramidal neurons from the somatosensory cortex there is strong evidence for up-regulation of a tonic $GABA_A$ receptor conductance following deletion of HCN1 (Chen et al., 2010). This up-regulation is not found in hippocampal neurons (Nolan et al., 2004; Chen et al., 2010), and is not consistent with data from stellate neurons (Nolan et al., 2007), suggesting it may be specific to neocortical neurons. Nevertheless, these results highlight the need for additional approaches to corroborate results from knockout mice. New pharmacological tools that discriminate between HCN subunits may be of use [e.g., (Del Lungo et al., 2011; McClure et al., 2011)], although interpretation of *in vivo* effects of existing HCN channel blockers is difficult because of their off-target effects (Chevaleyre and Castillo, 2002). Viruses that knockdown HCN1 in mature mice may in the future also have important experimental roles (White et al., 2011).

#### *Stellate cells across species*

Comparison of stellate cell properties between species may give additional insights into their roles in generation of grid firing fields. Grid fields have so far been directly observed in neurons from layer II of the MEC of rats, mice and bats (Hafting et al.,

2005; Fyhn et al., 2008; Yartsev et al., 2011). There is also strong evidence that neurons in the human entorhinal cortex have grid firing fields (Doeller et al., 2010). Given that the anatomical organization of entorhinal and hippocampal circuits is similar in each species it is likely that cellular mechanisms critical for representation of space will also be conserved across species. Consistent with this notion, basic electrophysiological properties of stellate cells in rats and mice, including their prominent sag response, theta-frequency peri-threshold activity and clustered spike firing, are also found in primates (Buckmaster et al., 2004). However, primate stellate cells have more primary dendrites, more dendritic branches and a greater total dendritic length (Buckmaster et al., 2004). They also have a less pronounced sag, and slower and less robust sub-threshold theta-frequency activity (Buckmaster et al., 2004). Stellate cells in humans (Mikkonen et al., 2000) are larger than in rats (Klink and Alonso, 1997b). While there are differences between studies in properties of stellate cells from mouse and rat, it seems likely that they could reflect technical differences such as experimental preparation and age of the animals. Nevertheless, more systematic study of this issue and comparison with species differences in spatial encoding may lead to useful insights.

## CONCLUSION

Stellate cells in layer II of the MEC are a striking example of neurons in which single-cell computations are controlled by voltage-gated ion channels that open prior to initiation of action potentials. We have highlighted in this review that $Na_P$, HCN, and $K_{2P}$ ion channels in particular influence properties such as resonance and temporal summation of synaptic inputs, suggesting they will be important for computation in behaving animals. We suggest that the influence of these ion channels on integration of synaptic input may be central to the computation carried out by stellate cells. We believe this will be a particularly important area for future investigation. In contrast, one of the most studied aspects of stellate cell activity, the theta-frequency activity, may be a secondary consequence of tuning ion channels to control integration of synaptic inputs.

To establish how stellate cell ion channels influence computations that underlie spatial representation, it will be important in the future to manipulate channels such as $Na_P$, HCN, and $K_{2P}$ specifically in stellate cells while recording membrane potential or spiking activity in behaving animals. This will help demonstrate which of the intrinsic electrophysiological properties are critical for behavior. An important step toward this goal is the demonstration that forebrain HCN1 channels are not required for generation or dorsal-ventral organization of grid firing fields, but instead may be critical modulators of grid field size, spacing, and stability (Giocomo et al., 2011a). Correspondence between these results and previous cellular data suggests the importance of tuning of synaptic integration for grid cell computation (Garden et al., 2008). It also highlights the significance of ion channels in addition to HCN1, for example the $K_{2P}$ ion channels, in the topographic organization of stellate cell integrative properties (Garden et al., 2008). These studies point toward the exciting prospect of a cellular and molecular level understanding of the neural representation of space.

## MATERIALS AND METHODS

### SLICE PREPARATION AND MAINTENANCE

Sagittal brain slices with thickness of 400 μm were prepared from 30 to 53 day old mice using previously described procedures (Garden et al., 2008; Dodson et al., 2011). Slices were maintained in physiological artificial cerebrospinal fluid of the following composition (mM): NaCl 124, $NaH_2PO_4$ 1.2, KCl 2.5, $NaHCO_3$ 25, Glucose 20, $CaCl_2$ 2, $MgCl_2$ 1. Patch electrodes were filled with an intracellular solution of the following composition (mM): K Gluconate 130; KCl 10, HEPES 10, $MgCl_2$ 2, EGTA 0.1, $Na_2ATP$ 2, $Na_2GTP$ 0.3, NaPhosphoCreatine 10. Excitatory glutamate receptor-mediated and inhibitory GABA receptor-mediated synaptic transmission was blocked with NBQX (5 μM), D-APV (50 μM), picrotoxin (50 μM) and CGP55845 (1 μM).

### DATA COLLECTION

All recordings were made at 34–37°C. Recording electrodes had a tip resistance of 3–7 MΩ. All membrane seals had resistance of >2 GΩ as calculated by the current response to 10 mV pulses in voltage-clamp. A liquid junction potential of 8.1 mV (bath relative to pipette) was not corrected for. Stellate cells were identified in the superficial part of layer II by their large soma, the presence of multiple similar sized primary dendrites and their characteristic electrophysiological properties including the presence of prominent sag potentials and bi-phasic spike after-hyperpolarization (AHP).

For the perforated patch recordings the electrodes were front-filled with standard intracellular solution and then back-filled with an intracellular solution containing the antibiotic amphotericin B (final concentration 0.075–0.15 mg/ml) dissolved in DMSO (final concentration 3–6 μl/ml). For these recordings, after rapidly establishing a cell-attached configuration, rather than rupturing the membrane to achieve a whole-cell configuration, we waited for the antibiotic to permeabilize the membrane. We confirmed that spontaneous break-in did not occur by including a fluorescent label (Alexa 488) in the intracellular solution. Using this technique, access resistances of 24–85 MΩ were achieved after a delay lasting from 20 min to an hour after seal formation. Whole-cell patch recordings had access resistances <30 MΩ. All access resistances were fully compensated for using the bridge-balance technique. All signals were recorded in current clamp using a Multiclamp 700B amplifier (Molecular Devices), low pass filtered at 10 kHz (two pole Bessel filter), converted with an ADC (National Instruments ITC-18) and sampled at 20 kHz.

### DATA ANALYSIS

Data analysis was performed as previously described (Nolan et al., 2007; Garden et al., 2008; Dodson et al., 2011) using Axograph and custom written MATLAB routines. Statistical calculations were done using R (www.r-project.org). All results are reported as mean ± standard error.

#### *Time frequency analysis*

To examine the persistence of spectral components across time we used Lomb analysis to identify significant frequencies in contiguous 3 s segments perithreshold recordings as previously described (Dodson et al., 2011). Spectrograms (in **Figure 4**) had windows of 1 s or 6.5 s, with 32768 or 131072 points and had 90% or

95% overlap. The first second of each 20 s trace was ignored to eliminate high frequency transients associated with current injection steps.

### *Spike clustering*

We used a previously described algorithm (Nolan et al., 2007) to calculate the spike clustering coefficient, *Pc*, the proportion of spikes occurring in a cluster. Briefly, a group of spikes was considered a cluster if no inter-spike interval in the group exceeded 250 ms and if the inter-cluster interval was at least 300 ms.

## ACKNOWLEDGMENTS

This work was supported by the Biotechnology and Biological Sciences Research Council (Matthew F. Nolan), the Engineering and Physical Sciences Research Council (Hugh Pastoll and Helen Ramsden) and the Commonwealth Scholarships Commission (Hugh Pastoll).

## REFERENCES

Alonso, A., de Curtis, M., and Llinás, R. (1990). Postsynaptic Hebbian and non-Hebbian long-term potentiation of synaptic efficacy in the entorhinal cortex in slices and in the isolated adult guinea pig brain. *Proc. Natl. Acad. Sci. U.S.A.* 87, 9280–9284.

Alonso, A., and García-Austt, E. (1987). Neuronal sources of theta rhythm in the entorhinal cortex of the rat. II. Phase relations between unit discharges and theta field potentials. *Exp. Brain Res.* 67, 502–509.

Alonso, A., and Klink, R. (1993). Differential electroresponsiveness of stellate and pyramidal-like cells of medial entorhinal cortex layer II. *J. Neurophysiol.* 70, 128.

Alonso, A., and Llinás, R. R. (1989). Subthreshold Na+-dependent theta-like rhythmicity in stellate cells of entorhinal cortex layer II. *Nature* 342, 175–177.

Barry, C., Hayman, R., Burgess, N., and Jeffery, K. J. (2007). Experience-dependent rescaling of entorhinal grids. *Nat. Neurosci.* 10, 682–684.

Beed, P., Bendels, M. H. K., Wiegand, H. F., Leibold, C., Johenning, F. W., and Schmitz, D. (2010). Analysis of excitatory microcircuitry in the medial entorhinal cortex reveals cell-type-specific differences. *Neuron* 68, 1059–1066.

Blair, H. T., Gupta, K., and Zhang, K. (2008). Conversion of a phase- to a rate-coded position signal by a three-stage model of theta cells, grid cells, and place cells. *Hippocampus* 18, 1239–1255.

Boehlen, A., Heinemann, U., and Erchova, I. (2010). The range of intrinsic frequencies represented by medial entorhinal cortex stellate cells extends with age. *J. Neurosci.* 30, 4585–4589.

Bohlen und Halbach, O., Hinz, U., Unsicker, K., and Egorov, A. V. (2005). Distribution of TRPC1 and TRPC5 in medial temporal lobe structures of mice. *Cell Tissue Res.* 322, 201–206.

Bruehl, C., and Wadman, W. J. (1999). Calcium currents in acutely isolated stellate and pyramidal neurons of rat entorhinal cortex. *Brain Res.* 816, 554–562.

Brun, V. H., Solstad, T., Kjelstrup, K. B., Fyhn, M., Witter, M. P., Moser, E. I., and Moser, M-B. (2008). Progressive increase in grid scale from dorsal to ventral medial entorhinal cortex. *Hippocampus* 18, 1200–1212.

Buckmaster, P. S., Alonso, A., Canfield, D. R., and Amaral, D. G. (2004). Dendritic morphology, local circuitry, and intrinsic electrophysiology of principal neurons in the entorhinal cortex of macaque monkeys. *J. Comp. Neurol.* 470, 317–329.

Burak, Y., and Fiete, I. R. (2009). Accurate path integration in continuous attractor network models of grid cells. *PLoS Comput. Biol.* 5:e1000291. doi: 10.1371/journal.pcbi.1000291

Burgalossi, A., Herfst, L., von Heimendahl, M., Förste, H., Haskic, K., Schmidt, M., and Brecht, M. (2011). Microcircuits of functionally identified neurons in the rat medial entorhinal cortex. *Neuron* 70, 773–786.

Burgess, N. (2008). Grid cells and theta as oscillatory interference: theory and predictions. *Hippocampus* 18, 1157–1174.

Burgess, N., Barry, C., and O'Keefe, J. (2007). An oscillatory interference model of grid cell firing. *Hippocampus* 17, 801–812.

Burgess, N., and O'Keefe, J. (2011). Models of place and grid cell firing and theta rhythmicity. *Curr. Opin. Neurobiol.* 21, 734–744.

Burton, B. G., Economo, M. N., Lee, G. J., and White, J. A. (2008). Development of theta rhythmicity in entorhinal stellate cells of the juvenile rat. *J. Neurophysiol.* 100, 3144–3157.

Burwell, R. D. (2000). The parahippocampal region: corticocortical connectivity. *Ann. N.Y. Acad. Sci.* 911, 25–42.

Buzsáki, G. (1996). The hippocampo-neocortical dialogue. *Cereb. Cortex* 6, 81–92.

Cannon, R. C., O'Donnell, C., and Nolan, M. F. (2010). Stochastic ion channel gating in dendritic neurons: morphology dependence and probabilistic synaptic activation of dendritic spikes. *PLoS Comput. Biol.* 6:e1000886. doi: 10.1371/journal.pcbi.1000886

Castelli, L., and Magistretti, J. (2006). High-voltage-activated $Ca^{2+}$ currents show similar patterns of expression in stellate and pyramidal cells from rat entorhinal cortex layer II. *Brain Res.* 1090, 76–88.

Chen, S., Wang, J., and Siegelbaum, S. A. (2001). Properties of hyperpolarization-activated pacemaker current defined by coassembly of HCN1 and HCN2 subunits and basal modulation by cyclic nucleotide. *J. Gen. physiol.* 117, 491–504.

Chen, X., Shu, S., Schwartz, L. C., Sun, C., Kapur, J., and Bayliss, D. A. (2010). Homeostatic regulation of synaptic excitability: tonic GABA(A) receptor currents replace I(h) in cortical pyramidal neurons of HCN1 knock-out mice. *J. Neurosci.* 30, 2611–2622.

Chevaleyre, V., and Castillo, P. E. (2002). Assessing the role of Ih channels in synaptic transmission and mossy fiber LTP. *Proc. Natl. Acad. Sci. U.S.A.* 99, 9538–9543.

D'Hoedt, D., Hirzel, K., Pedarzani, P., and Stocker, M. (2004). Domain analysis of the calcium-activated potassium channel SK1 from rat brain. Functional expression and toxin sensitivity. *J. Biol. Chem.* 279, 12088–12092.

Del Lungo, M., Melchiorre, M., Guandalini, L., Sartiani, L., Mugelli, A., Koncz, I., Szel, T., Varro, A., Romanelli, M. N., and Cerbai, E. (2011). Novel blockers of hyperpolarization-activated current with isoform selectivity in recombinant cells and native tissue. *Br. J. Pharmacol.* doi: 10.1111/j.1476-5381.2011.01782.x. [Epub ahead of print].

Deng, P-Y., Poudel, S. K. S., Rojanathammanee, L., Porter, J. E., and Lei, S. (2007). Serotonin inhibits neuronal excitability by activating two-pore domain k+ channels in the entorhinal cortex. *Mol. Pharmacol.* 72, 208–218.

Deng, P.-Y., Xiao, Z., Yang, C., Rojanathammanee, L., Grisanti, L., Watt, J., Geiger, J. D., Liu, R., Porter, J. E., and Lei, S. (2009). GABA(B) receptor activation inhibits neuronal excitability and spatial learning in the entorhinal cortex by activating TREK-2 K+ channels. *Neuron* 63, 230–243.

Dhillon, A., and Jones, R. S. (2000). Laminar differences in recurrent excitatory transmission in the rat entorhinal cortex *in vitro*. *Neuroscience* 99, 413–422.

Dickson, C. T., Kirk, I. J., Oddie, S. D., and Bland, B. H. (1995). Classification of theta-related cells in the entorhinal cortex: cell discharges are controlled by the ascending brainstem synchronizing pathway in parallel with hippocampal theta-related cells. *Hippocampus* 5, 306–319.

Dickson, C. T., Magistretti, J., Shalinsky, M., Hamam, B., and Alonso, A. (2000a). Oscillatory activity in entorhinal neurons and circuits. Mechanisms and function. *Ann. N.Y. Acad. Sci.* 911, 127–150.

Dickson, C. T., Magistretti, J., Shalinsky, M. H., Fransén, E., Hasselmo, M. E., and Alonso, A. (2000b). Properties and role of I(h) in the pacing of subthreshold oscillations in entorhinal cortex layer II neurons. *J. Neurophysiol.* 83, 2562–2579.

Dodson, P. D., Pastoll, H., and Nolan, M. F. (2011). Dorsal-ventral organization of theta-like activity intrinsic to entorhinal stellate neurons is mediated by differences in stochastic current fluctuations. *J. Physiol.* 589, 2993–3008.

Doeller, C. F., Barry, C., and Burgess, N. (2010). Evidence for grid cells in a human memory network. *Nature* 463, 657–661.

Dolorfo, C. L., and Amaral, D. G. (1998). Entorhinal cortex of the rat:

organization of intrinsic connections. *J. Comp. Neurol.* 398, 49–82.

Dorval, A. D., and White, J. A. (2005). Channel noise is essential for perithreshold oscillations in entorhinal stellate neurons. *J. Neurosci.* 25, 10025–10028.

Dudman, J. T., and Nolan, M. F. (2009). Stochastically gating ion channels enable patterned spike firing through activity-dependent modulation of spike probability. *PLoS Comput. Biol.* 5:e1000290. doi: 10.1371/journal.pcbi.1000290

Eder, C., Ficker, E., Gündel, J., and Heinemann, U. (1991). Outward currents in rat entorhinal cortex stellate cells studied with conventional and perforated patch recordings. *Eur. J. Neurosci.* 3, 1271–1280.

Eder, C., and Heinemann, U. (1994). Current density analysis of outward currents in acutely isolated rat entorhinal cortex cells. *Neurosci. Lett.* 174, 58–60.

Eder, C., and Heinemann, U. (1996). Potassium currents in acutely isolated neurons from superficial and deep layers of the juvenile rat entorhinal cortex. *Pflügers Arch.* 432, 637–643.

Engel, T. A., Schimansky-Geier, L., Herz, A. V. M., Schreiber, S., and Erchova, I. (2008). Subthreshold membrane-potential resonances shape spike-train patterns in the entorhinal cortex. *J. Neurophysiol.* 100, 1576–1589.

Erchova, I., Kreck, G., Heinemann, U., and Herz, A. V. M. (2004). Dynamics of rat entorhinal cortex layer II and III cells: characteristics of membrane potential resonance at rest predict oscillation properties near threshold. *J. Physiol.* 560, 89–110.

Fernandez, F. R., and White, J. A. (2008). Artificial synaptic conductances reduce subthreshold oscillations and periodic firing in stellate cells of the entorhinal cortex. *J. Neurosci.* 28, 3790.

Fransén, E., Alonso, A. A., Dickson, C. T., Magistretti, J., and Hasselmo, M. E. (2004). Ionic mechanisms in the generation of subthreshold oscillations and action potential clustering in entorhinal layer II stellate neurons. *Hippocampus* 14, 368–384.

Fuhs, M. C., and Touretzky, D. S. (2006). A spin glass model of path integration in rat medial entorhinal cortex. *J. Neurosci.* 26, 4266–4276.

Fyhn, M., Hafting, T., Witter, M. P., Moser, E. I., and Moser, M.-B. (2008). Grid cells in mice. *Hippocampus* 18, 1230–1238.

Fyhn, M., Molden, S., Witter, M. P., Moser, E. I., and Moser, M. B. (2004). Spatial representation in the entorhinal cortex. *Science* 305, 1258–1264.

Garden, D. L. F., Dodson, P. D., O'Donnell, C., White, M. D., and Nolan, M. F. (2008). Tuning of synaptic integration in the medial entorhinal cortex to the organization of grid cell firing fields. *Neuron* 60, 875–889.

Giocomo, L. M., and Hasselmo, M. E. (2008). Time constants of h current in layer ii stellate cells differ along the dorsal to ventral axis of medial entorhinal cortex. *J. Neurosci.* 28, 9414–9425.

Giocomo, L. M., and Hasselmo, M. E. (2009). Knock-out of HCN1 subunit flattens dorsal-ventral frequency gradient of medial entorhinal neurons in adult mice. *J. Neurosci.* 29, 7625–7630.

Giocomo, L. M., Hussaini, S. A., Zheng, F., Kandel, E. R., Moser, M. B., and Moser, E. I. (2011a). Grid cells use HCN1 channels for spatial scaling. *Cell* 147, 1159–1170.

Giocomo, L. M., Moser, M. B., and Moser, E. I. (2011b). Computational models of grid cells. *Neuron* 71, 589–603.

Giocomo, L. M., Zilli, E. A., Fransén, E., and Hasselmo, M. E. (2007). Temporal frequency of subthreshold oscillations scales with entorhinal grid cell field spacing. *Science* 315, 1719–1722.

Haas, J. S., Dorval, A. D., and White, J. A. (2007). Contributions of Ih to feature selectivity in layer II stellate cells of the entorhinal cortex. *J. Comput. Neurosci.* 22, 161–171.

Haas, J. S., and White, J. A. (2002). Frequency selectivity of layer II stellate cells in the medial entorhinal cortex. *J. Neurophysiol.* 88, 2422–2429.

Hafting, T., Fyhn, M., Molden, S., Moser, M.-B., and Moser, E. I. (2005). Microstructure of a spatial map in the entorhinal cortex. *Nature* 436, 801–806.

Hajimiri, A., and Lee, T. H. (1998). A general theory of phase noise in electrical oscillators. *Solid-State Circuits, IEEE J.* 33, 179–194.

Hasselmo, M. E. (2008). Grid cell mechanisms and function: contributions of entorhinal persistent spiking and phase resetting. *Hippocampus* 18, 1213–1229.

Hasselmo, M. E., Hay, J., Ilyn, M., and Gorchetchnikov, A. (2002). Neuromodulation, theta rhythm and rat spatial navigation. *Neural Netw.* 15, 689–707.

Haug, F. M. (1976). Sulphide silver pattern and cytoarchitectonics of parahippocampal areas in the rat. Special reference to the subdivision of area entorhinalis (area 28) and its demarcation from the pyriform cortex. *Adv. Anat. Embryol. Cell Biol.* 52, 3–73.

Heinemann, U., Schmitz, D., Eder, C., and Gloveli, T. (2000). Properties of entorhinal cortex projection cells to the hippocampal formation. *Ann. N.Y. Acad. Sci.* 911, 112–126.

Heys, J. G., Giocomo, L. M., and Hasselmo, M. E. (2010). Cholinergic modulation of the resonance properties of stellate cells in layer II of medial entorhinal cortex. *J. Neurophysiol.* 104, 258–270.

Holm, I. E., and Geneser, F. A. (1989). Histochemical demonstration of zinc in the hippocampal region of the domestic pig: I. Entorhinal area, parasubiculum, and presubiculum. *J. Comp. Neurol.* 287, 145–163.

Horn, R., and Marty, A. (1988). Muscarinic activation of ionic currents measured by a new whole-cell recording method. *J. Gen. Physiol.* 92, 145–159.

Hu, H., Vervaeke, K., and Storm, J. F. (2007). M-channels (Kv7/KCNQ channels) that regulate synaptic integration, excitability, and spike pattern of CA1 pyramidal cells are located in the perisomatic region. *J. Neurosci.* 27, 1853–1867.

Hussaini, S. A., Kempadoo, K. A., Thuault, S. J., Siegelbaum, S. A., and Kandel, E. R. (2011). Increased size and stability of CA1 and CA3 Place Fields in HCN1 knockout mice. *Neuron* 72, 643–653.

Hutcheon, B., Miura, R. M., and Puil, E. (1996). Subthreshold membrane resonance in neocortical neurons. *J. Neurophysiol.* 76, 683–697.

Hutcheon, B., and Yarom, Y. (2000). Resonance, oscillation and the intrinsic frequency preferences of neurons. *Trends Neurosci.* 23, 216–222.

Insausti, R., Herrero, M. T., and Witter, M. P. (1997). Entorhinal cortex of the rat: cytoarchitectonic subdivisions and the origin and distribution of cortical efferents. *Hippocampus* 7, 146–183.

Jones, R. S. (1994). Synaptic and intrinsic properties of neurons of origin of the perforant path in layer II of the rat entorhinal cortex *in vitro*. *Hippocampus* 4, 335–353.

Khawaja, F. A., Alonso, A. A., and Bourque, C. W. (2007). Ca(2+)-dependent K(+) currents and spike-frequency adaptation in medial entorhinal cortex layer II stellate cells. *Hippocampus* 17, 1143–1148.

Klink, R., and Alonso, A. (1993). Ionic mechanisms for the subthreshold oscillations and differential electroresponsiveness of medial entorhinal cortex layer II neurons. *J. Neurophysiol.* 70, 144–157.

Klink, R., and Alonso, A. (1997a). Ionic mechanisms of muscarinic depolarization in entorhinal cortex layer II neurons. *J. Neurophysiol.* 77, 1829–1843.

Klink, R., and Alonso, A. (1997b). Morphological characteristics of layer II projection neurons in the rat medial entorhinal cortex. *Hippocampus* 7, 571–583.

Kumar, S. S., Jin, X., Buckmaster, P. S., and Huguenard, J. R. (2007). Recurrent circuits in layer II of medial entorhinal cortex in a model of temporal lobe epilepsy. *J. Neurosci.* 27, 1239–1246.

Ma, L., Alonso, A., and Dickson, C. T. (2008). Differential induction of long-term potentiation in the horizontal versus columnar superficial connections to layer II cells of the entorhinal cortex. *Neural plast.* 2008, 814815.

Magistretti, J., and Alonso, A. (1999a). Biophysical properties and slow voltage-dependent inactivation of a sustained sodium current in entorhinal cortex layer-II principal neurons. *J. Gen. physiol.* 114, 491.

Magistretti, J., and Alonso, A. (1999b). Slow voltage-dependent inactivation of a sustained sodium current in stellate cells of rat entorhinal cortex layer II. *Ann. N.Y. Acad. Sci.* 868, 84–87.

Magistretti, J., and Alonso, A. (2002). Fine gating properties of channels responsible for persistent sodium current generation in entorhinal cortex neurons. *J. Gen. Physiol.* 120, 855–873.

Magistretti, J., and Alonso, A. (2007). Multiple conductance substates in pharmacologically untreated $Na^+$ channels generating persistent openings in rat entorhinal cortex neurons. *J. Membr. Biol.* 214, 165–180.

Magistretti, J., Ma, L., Shalinsky, M. H., Lin, W., Klink, R., and Alonso, A. (2004). Spike patterning by $Ca^{2+}$-dependent regulation of a muscarinic cation current in entorhinal cortex layer II neurons. *J. Neurophysiol.* 92, 1644–1657.

Magistretti, J., Ragsdale, D. S., and Alonso, A. (1999a). Direct demonstration of persistent $Na^+$ channel activity in dendritic processes

of mammalian cortical neurones. *J. Physiol.* 521(Pt 3), 629–636.

Magistretti, J., Ragsdale, D. S., and Alonso, A. (1999b). High conductance sustained single-channel activity responsible for the low-threshold persistent Na(+) current in entorhinal cortex neurons. *J. Neurosci.* 19, 7334–7341.

Magistretti, J., Ragsdale, D. S., and Alonso, A. (2003). Kinetic diversity of single-channel burst openings underlying persistent Na(+) current in entorhinal cortex neurons. *Biophys. J.* 85, 3019–3034.

Mathias, R. T., Riquelme, G., and Rae, J. L. (1991). Cell to cell communication and pH in the frog lens. *J. Gen. Physiol.* 98, 1085–1103.

McClure, K. J., Maher, M., Wu, N., Chaplan, S. R., Eckert, W. A. III, Lee, D. H., Wickenden, A. D., Hermann, M., Allison, B., Hawryluk, N., Breitenbucher, J. G., and Grice, C. A. (2011). Discovery of a novel series of selective HCN1 blockers. *Bioorg. Med. Chem. Lett.* 21, 5197–5201.

McNaughton, B. L., Battaglia, F. P., Jensen, O., Moser, E. I., and Moser, M.-B. (2006). Path integration and the neural basis of the "cognitive map". *Nat. Rev. Neurosci.* 7, 663–678.

Mikkonen, M., Pitkänen, A., Soininen, H., Alafuzoff, I., and Miettinen, R. (2000). Morphology of spiny neurons in the human entorhinal cortex: intracellular filling with lucifer yellow. *Neuroscience* 96, 515–522.

Mitchell, S. J., and Ranck, J. B. (1980). Generation of theta rhythm in medial entorhinal cortex of freely moving rats. *Brain Res.* 189, 49–66.

Mizukami, K., Ishikawa, M., Hidaka, S., Iwakiri, M., Sasaki, M., and Iritani, S. (2002). Immunohistochemical localization of GABAB receptor in the entorhinal cortex and inferior temporal cortex of schizophrenic brain. *Prog. Neuropsychopharmacol. Biol. Psychiatry* 26, 393–396.

Mizuseki, K., Sirota, A., Pastalkova, E., and Buzsáki, G. (2009). Theta oscillations provide temporal windows for local circuit computation in the entorhinal-hippocampal loop. *Neuron* 64, 267–280.

Navratilova, Z., Giocomo, L. M., Fellous, J-M., Hasselmo, M. E., and McNaughton, B. L. (2012). Phase precession and variable spatial scaling in a periodic attractor map model of medial entorhinal grid cells with realistic after-spike dynamics. *Hippocampus*. 22, 772–789.

Ngo-Anh, T., Bloodgood, B., Lin, M., Sabatini, B., Maylie, J., and Adelman, J. (2005). SK channels and NMDA receptors form a $Ca^{2+}$-mediated feedback loop in dendritic spines. *Nat. Neurosci.* 8, 642–649.

Nolan, M. F., Dudman, J. T., Dodson, P. D., and Santoro, B. (2007). HCN1 channels control resting and active integrative properties of stellate cells from layer II of the entorhinal cortex. *J. Neurosci.* 27, 12440.

Nolan, M. F., Malleret, G., Dudman, J. T., Buhl, D. L., Santoro, B., Gibbs, E., Vronskaya, S., Buzsáki, G., Siegelbaum, S. A., Kandel, E. R., and Morozov, A. (2004). A behavioral role for dendritic integration: HCN1 channels constrain spatial memory and plasticity at inputs to distal dendrites of CA1 pyramidal neurons. *Cell* 119, 719–732.

Notomi, T., and Shigemoto, R. (2004). Immunohistochemical localization of Ih channel subunits, HCN1–4, in the rat brain. *J. Comp. Neurol.* 471, 241–276.

O'Donnell, C., and Nolan, M. F. (2011). Tuning of synaptic responses: an organizing principle for optimization of neural circuits. *Trends Neurosci.* 34, 51–60.

Quilichini, P., Sirota, A., and Buzsáki, G. (2010). Intrinsic circuit organization and theta-gamma oscillation dynamics in the entorhinal cortex of the rat. *J. Neurosci.* 30, 11128–11142.

Ramón y Cajal, S. (1995). *Histology of the Nervous System, vol. II*. (Trans. N. Swanson and L. W. Swanson). New York, NY: Oxford University Press.

Remme, M. W. H., Lengyel, M., and Gutkin, B. S. (2010). Democracy-independence trade-off in oscillating dendrites and its implications for grid cells. *Neuron* 66, 429–437.

Richter, H., Heinemann, U., and Eder, C. (2000). Hyperpolarization-activated cation currents in stellate and pyramidal neurons of rat entorhinal cortex. *Neurosci. Lett.* 281, 33–36.

Richter, H., Klee, R., Heinemann, U., and Eder, C. (1997). Developmental changes of inward rectifier currents in neurons of the rat entorhinal cortex. *Neurosci. Lett.* 228, 139–141.

Robinson, R. B., and Siegelbaum, S. A. (2003). Hyperpolarization-activated cation currents: from molecules to physiological function. *Annu. Rev. Physiol.* 65, 453–480.

Rosenkranz, J. A. (2006). Dopaminergic regulation of neuronal excitability through modulation of Ih in layer V entorhinal cortex. *J. Neurosci.* 26, 3229–3244.

Ruth, R. E., and Collier, T. J. (1988). Topographical relationship between the entorhinal cortex and the septotemporal axis of the dentate gyrus in rats: II. Cells projecting from lateral entorhinal subdivision. *J. Comp. Neurol.* 270, 506–516.

Ruth, R. E., Collier, T. J., and Routtenberg, A. (1982). Topography between the entorhinal cortex and the dentate septotemporal axis in rats: I. Medial and intermediate entorhinal projecting cells. *J. Comp. Neurol.* 209, 69–78.

Santoro, B., Chen, S., Luthi, A., Pavlidis, P., Shumyatsky, G. P., Tibbs, G. R., and Siegelbaum, S. A. (2000). Molecular and functional heterogeneity of hyperpolarization-activated pacemaker channels in the mouse CNS. *J. Neurosci.* 20, 5264–5275.

Sargolini, F., Fyhn, M., Hafting, T., McNaughton, B. L., Witter, M. P., Moser, M-B., and Moser, E. I. (2006). Conjunctive representation of position, direction, and velocity in entorhinal cortex. *Science* 312, 758–762.

Schiller, J., Major, G., Koester, H. J., and Schiller, Y. (2000). NMDA spikes in basal dendrites of cortical pyramidal neurons. *Nature* 404, 285–289.

Schreiber, S., Erchova, I., Heinemann, U., and Herz, A. V. M. (2004). Subthreshold resonance explains the frequency-dependent integration of periodic as well as random stimuli in the entorhinal cortex. *J. Neurophysiol.* 92, 408–415.

Schwartz, S. P., and Coleman, P. D. (1981). Neurons of origin of the perforant path. *Exp. Neurol.* 74, 305–312.

Shah, M. M., Anderson, A. E., Leung, V., Lin, X., and Johnston, D. (2004). Seizure-induced plasticity of h channels in entorhinal cortical layer III pyramidal neurons. *Neuron* 44, 495–508.

Shalinsky, M. H., Magistretti, J., Ma, L., and Alonso, A. A. (2002). Muscarinic activation of a cation current and associated current noise in entorhinal-cortex layer-II neurons. *J. Neurophysiol.* 88, 1197–1211.

Slomianka, L. (1992). Neurons of origin of zinc-containing pathways and the distribution of zinc-containing boutons in the hippocampal region of the rat. *Neuroscience* 48, 325–352.

Spruston, N., and Johnston, D. (1992). Perforated patch-clamp analysis of the passive membrane properties of three classes of hippocampal neurons. *J. Neurophysiol.* 67, 508–529.

Steward, O., and Scoville, S. A. (1976). Cells of origin of entorhinal cortical afferents to the hippocampus and fascia dentata of the rat. *J. Comp. Neurol.* 169, 347–370.

Stewart, M., Quirk, G. J., Barry, M., and Fox, S. E. (1992). Firing relations of medial entorhinal neurons to the hippocampal theta rhythm in urethane anesthetized and walking rats. *Exp. Brain Res.* 90, 21–28.

Stocker, M., and Pedarzani, P. (2000). Differential distribution of three Ca(2+)-activated K(+) channel subunits, SK1, SK2, and SK3, in the adult rat central nervous system. *Mol. Cell. Neurosci.* 15, 476–493.

Stuart, G., and Sakmann, B. (1995). Amplification of EPSPs by axosomatic sodium channels in neocortical pyramidal neurons. *Neuron* 15, 1065–1076.

Stuart, G. J., and Sakmann, B. (1994). Active propagation of somatic action potentials into neocortical pyramidal cell dendrites. *Nature* 367, 69–72.

Ulens, C., and Tytgat, J. (2001). Functional heteromerization of HCN1 and HCN2 pacemaker channels. *J. Biol. Chem.* 276, 6069–6072.

van der Linden, S., and Lopes da Silva, F. H. (1998). Comparison of the electrophysiology and morphology of layers III and II neurons of the rat medial entorhinal cortex *in vitro*. *Eur. J. Neurosci.* 10, 1479–1489.

van Groen, T., Miettinen, P., and Kadish, I. (2003). The entorhinal cortex of the mouse: organization of the projection to the hippocampal formation. *Hippocampus* 13, 133–149.

Visan, V., Heinemann, U., Volynets, A., and Müller, W. (2002). Calcium currents in rat entorhinal cortex layer II stellate and layer III pyramidal neurons in acute brain slice. *Neurosci. Lett.* 327, 153–156.

Welday, A. C., Shlifer, I. G., Bloom, M. L., Zhang, K., and Blair, H. T. (2011). Cosine directional tuning of theta cell burst frequencies: evidence for spatial coding by oscillatory interference. *J. Neurosci.* 31, 16157–16176.

White, J. A., Alonso, A., and Kay, A. R. (1993). A heart-like Na+ current in the medial entorhinal cortex. *Neuron* 11, 1037–1047.

White, J. A., Klink, R., Alonso, A., and Kay, A. R. (1998). Noise from voltage-gated ion channels may influence neuronal dynamics in the entorhinal cortex. *J. Neurophysiol.* 80, 262–269.

White, M. D., Milne, R. V., and Nolan, M. F. (2011). A molecular

toolbox for rapid generation of viral vectors to Up- or Down-Regulate neuronal gene expression *in vivo*. *Front. Mol. Neurosci.* 4:8. doi: 10.3389/fnmol.2011.00008

Witter, M. P. (2007). The perforant path: projections from the entorhinal cortex to the dentate gyrus. *Prog. Brain Res.* 163, 43–61.

Yartsev, M. M., Witter, M. P., and Ulanovsky, N. (2011). Grid cells without theta oscillations in the entorhinal cortex of bats. *Nature* 479, 103–107.

Yoshida, M., and Alonso, A. (2007). Cell-type specific modulation of intrinsic firing properties and subthreshold membrane oscillations by the M(Kv7)-current in neurons of the entorhinal cortex. *J. Neurophysiol.* 98, 2779–2794.

Yoshida, M., Giocomo, L. M., Boardman, I., and Hasselmo, M. E. (2011). Frequency of subthreshold oscillations at different membrane potential voltages in neurons at different anatomical positions on the dorsoventral axis in the rat medial entorhinal cortex. *J. Neurosci.* 31, 12683–12694.

Zhang, Z., Reboreda, A., Alonso, A., Barker, P. A., and Séguéla, P. (2011). TRPC channels underlie cholinergic plateau potentials and persistent activity in entorhinal cortex. *Hippocampus* 21, 386–397.

Zilli, E. A., Yoshida, M., Tahvildari, B., Giocomo, L. M., and Hasselmo, M. E. (2009). Evaluation of the oscillatory interference model of grid cell firing through analysis and measured period variance of some biological oscillators. *PLoS Comput. Biol.* 5:e1000573. doi: 10.1371/journal.pcbi.1000573

**Conflict of Interest Statement:** The authors declare that the research was conducted in the absence of any commercial or financial relationships that could be construed as a potential conflict of interest.

*Received: 10 December 2011; accepted: 25 March 2012; published online: 24 April 2012.*

*Citation: Pastoll H, Ramsden HL and Nolan MF (2012) Intrinsic electrophysiological properties of entorhinal cortex stellate cells and their contribution to grid cell firing fields. Front. Neural Circuits* ***6****:17. doi: 10.3389/fncir.2012.00017*

frontiers in
NEURAL CIRCUITS

REVIEW ARTICLE
published: 20 February 2012
doi: 10.3389/fncir.2012.00005

# Possible role of acetylcholine in regulating spatial novelty effects on theta rhythm and grid cells

***Caswell Barry*[1,2]*, *James G. Heys*[1] *and Michael E. Hasselmo*[1]***

[1] *Department of Psychology, Center for Memory and Brain, Boston University, Boston, MA, USA*
[2] *Institute of Neurology, University College London, London, UK*

***Edited by:***
*Lisa M. Giocomo, Norwegian University of Science and Technology, Norway*

***Reviewed by:***
*Dori Derdikman, Technion, Israel*
*James Ainge, University of St Andrews, UK*

***Correspondence:**
*Caswell Barry, ICN, Alexandra House, 17 Queen Square, WC1N 3AR, London, UK.*
*e-mail: caswell.barry@ucl.ac.uk*

*Michael E. Hasselmo, Department of Psychology, Center for Memory and Brain, Boston University, Boston, 02215 MA, USA.*
*e-mail: hasselmo@bu.edu*

Existing pharmacological and lesion data indicate that acetylcholine plays an important role in memory formation. For example, increased levels of acetylcholine in the hippocampal formation are known to be associated with successful encoding while disruption of the cholinergic system leads to impairments on a range of mnemonic tasks. However, cholinergic signaling from the medial septum also plays a central role in generating and pacing theta-band oscillations throughout the hippocampal formation. Recent experimental results suggest a potential link between these distinct phenomena. Environmental novelty, a condition associated with strong cholinergic drive, has been shown to induce an expansion in the firing pattern of entorhinal grid cells and a reduction in the frequency of theta measured from the LFP. Computational modeling suggests the spatial activity of grid cells is produced by interference between neuronal oscillators; scale being determined by theta-band oscillations impinging on entorhinal stellate cells, the frequency of which is modulated by acetylcholine. Here we propose that increased cholinergic signaling in response to environmental novelty triggers grid expansion by reducing the frequency of the oscillations. Furthermore, we argue that cholinergic induced grid expansion may enhance, or even induce, encoding by producing a mismatch between expanded grid cells and other spatial inputs to the hippocampus, such as boundary vector cells. Indeed, a further source of mismatch is likely to occur between grid cells of different native scales which may expand by different relative amounts.

**Keywords: grid cell, place cell, acetylcholine, theta, stellate cell**

## INTRODUCTION

Compelling evidence from several fields indicates that acetylcholine enhances the dynamics of memory encoding. Pharmacological studies in humans, primates, and other animals show that blockade of cholinergic receptors compromises memory formation whereas cholinergic agonists can promote mnemonic function. In particular, impairment of the parahippocampal cholinergic system produces deficits in recognition, spatial, and working memory apparently limited to encoding but not retrieval (Aigner and Mishkin, 1986; Tang et al., 1997). Electrophysiological investigations suggest this enhancement is due to several factors including an augmentation of long-term potentiation (LTP) as well as suppression of feedback connectivity, which may reduce interference between existing memories and incoming stimuli (Hasselmo et al., 1995; Hasselmo, 2006). However, a parallel body of work implicates acetylcholine in the generation and pacing of theta-band oscillations observed in the local field potential (LFP) throughout the hippocampal formation. For example, disruption of cholinergic transmission from the medial septum to the hippocampus severely attenuates theta power (Lee et al., 1994), impairs spatial learning (Rogers and Kesner, 2003; Elvander et al., 2004) [but also see Baxter et al. (1995)], and reduces the spatial specificity of hippocampal place cells (Shapiro et al., 1989; Brazhnik et al., 2003). Conversely systemic application of physostigmine, which leads to elevated levels of acetylcholine, promotes a constant theta state in the LFP of anesthetized animals (Yoder and Pang, 2005).

The significance of this dual role exhibited by acetylcholine remains unclear; to what extent are common systems involved and what role might modulation of theta-band oscillations have in memory encoding? A recent theory linking theta-band frequencies of intrinsic oscillations in entorhinal stellate cells with the generation of spatial firing produced by grid cells provides a potential resolution. Briefly, the scale of the grid firing pattern is believed to depend on the relative frequency of theta-band neuronal oscillators in the entorhinal cortex (Burgess et al., 2007), which are subject to cholinergic modulation. In response to environmental novelty, a condition known to increase intrahippocampal acetylcholine, the frequency of the theta-band network oscillations is seen to decrease (Jeewajee et al., 2008b) and is matched by an increase in grid scale (Barry et al., *Soc. Neurosci. Abstr.* 101.25, 2009). We anticipate the expansion of the grid firing pattern will likely lead to a mismatch between grids and other spatial inputs to the hippocampus [see also, (Burgess et al., 2007; Burgess, 2008)] and potentially also between grids of different native scales (Monaco and Abbott, 2011). It is likely then that this orthogonalized input promotes the formation of spatial memories in the form of distinct, stable place cell representations. In this document we first describe how acetylcholine has been proposed to modulate learning in the hippocampal formation before

focusing on its role in the generation of theta. Finally, we argue that the reduction in theta frequency observed in response to environmental novelty is mediated by acetylcholine and drives hippocampal remapping.

## ACETYLCHOLINE AND ITS ROLE IN THE MODULATION OF LEARNING

Extensive data indicates a role of acetylcholine in encoding of new memories. Multiple studies have shown impairments of encoding after systemic injections of scopolamine, an antagonist at muscarinic acetylcholine receptors. Subjects that encoded a list of words under the influence of scopolamine showed severe reductions in subsequent free recall of the word list (Ghoneim and Mewaldt, 1975; Peterson, 1977). The same subjects under the influence of scopolamine did not show impaired retrieval of words encoded before the injection. Scopolamine injections also impair performance in an n-back working memory task (Green et al., 2005). In monkeys, the encoding of visual stimuli for subsequent recognition is impaired by systemic injections of scopolamine (Aigner and Mishkin, 1986), and in rats systemic injections of muscarinic antagonists impair performance on the Morris water maze (Whishaw, 1985; Buresova et al., 1986) and eight-arm radial maze (McGurk et al., 1988).

## CHOLINERGIC MODULATION IN THE HIPPOCAMPAL FORMATION

Localized infusions suggest that these effects of acetylcholine receptor blockade are due to effects in the hippocampus and regions of parahippocampal cortex. Encoding for recognition memory in monkeys is impaired by local infusions of scopolamine into the perirhinal cortex but not the dentate gyrus (Tang et al., 1997). In rats, local infusions of scopolamine into the perirhinal cortex impair encoding of stimuli for subsequent recognition (Winters et al., 2006), and local infusions of cholinergic antagonists impair encoding of the association between tone stimuli and shock in a trace conditioning paradigm (Bang and Brown, 2009; Esclassan et al., 2009). Encoding of platform location in the Morris water maze is impaired by infusions of scopolamine in the hippocampus (Blokland et al., 1992) and the medial septum (Elvander et al., 2004). Encoding for subsequent recognition is also impaired by selective lesions of the cholinergic fibers in rats that innervate entorhinal cortex (McGaughy et al., 2005) and perirhinal cortex (Winters and Bussey, 2005) and recognition performance is also impaired by selective lesions of cholinergic fibers innervating perirhinal cortex in monkeys (Turchi et al., 2005).

The role of acetylcholine in the encoding of new information appears consistent with microdialysis studies of levels of acetylcholine in the hippocampus, which increase in novel environments (Acquas et al., 1996). Acetylcholine levels in the hippocampus and neocortex also increase during active exploration of the environment (Marrosu et al., 1995). Active exploration is also associated with theta rhythm oscillations in the hippocampus, and theta rhythm oscillations are associated with increases in acetylcholine levels measured with microdialysis (Monmaur et al., 1997) and amperometry (Zhang et al., 2010). The increase of acetylcholine during novelty is consistent with the evidence that cholinergic lesions appear to impair the increased exploration by rats encountering novel objects (Winters and Bussey, 2005) or novel associations of locations and context (Easton et al., 2011) though surprisingly not more complex episodic associations. In summary, the studies of local infusion effects and selective cholinergic lesions suggest a role for acetylcholine in the hippocampus and parahippocampal cortex for encoding of new memories. Further understanding of these behavioral effects can be obtained by considering the cellular effects of acetylcholine on neurons within these cortical structures.

## CHOLINERGIC MODULATION OF SYNAPTIC AND CELLULAR MECHANISMS FOR ENCODING

Acetylcholine could enhance encoding through a number of direct effects on the physiology of cortical principal cells. Acetylcholine directly enhances the induction of LTP in cortical regions including the hippocampus (Blitzer et al., 1990), the entorhinal cortex (Yun et al., 2000), and other structures including piriform cortex (Patil et al., 1998) and primary visual cortex (Brocher et al., 1992). The induction of Hebbian synaptic modification could also be enhanced by muscarinic enhancement of postsynaptic spiking activity due to direct depolarization of cortical pyramidal cells (Cole and Nicoll, 1984; Barkai and Hasselmo, 1994) as well as suppression of spike frequency accommodation (Madison and Nicoll, 1984; Madison et al., 1987; Barkai and Hasselmo, 1994).

Acetylcholine may also enhance encoding by augmenting the influence of external afferent input relative to the internal spread of activity within cortical structures (see **Figure 1**). Acetylcholine causes direct nicotinic enhancement of afferent fiber synaptic transmission at thalamocortical synapses (Gil et al., 1997). Acetylcholine also enhances the response of the dentate gyrus to afferent input (Foster and Deadwyler, 1992), and these responses also increase during behavioral states associated with increased acetylcholine such as REM sleep (Winson and Abzug, 1977). At the same time as it enhances input, acetylcholine reduces the synaptic transmission at excitatory glutamatergic recurrent feedback synapses within cortical structures. For example,

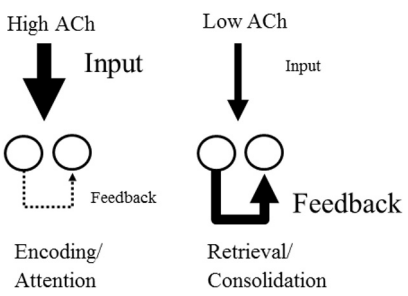


**FIGURE 1 | Effect of acetylcholine on cortical processing.** High acetylcholine (ACh) enhances encoding by increasing the efficacy of afferent input to the cortex via the action of nicotinic receptors. At the same time high acetylcholine suppresses transmission at glutamatergic recurrent feedback synapses within cortical regions. Conversely, lower acetylcholine favors the retrieval of stored memories by enhancing the influence of recurrent connections relative to afferent input.

acetylcholine suppresses excitatory feedback synapses in the piriform cortex (Hasselmo and Bower, 1992, 1993), in neocortical structures (Gil et al., 1997; Kimura and Baughman, 1997) and in region CA3 of the hippocampal formation (Hasselmo et al., 1995; Vogt and Regehr, 2001; Kremin and Hasselmo, 2007). Computational models of cortical structures show that this selective muscarinic presynaptic inhibition of glutamatergic synaptic transmission prevents retrieval of previously encoded memories from interfering with the encoding of new memories in the hippocampus (Hasselmo et al., 1992; Hasselmo and Schnell, 1994), while the cholinergic enhancement of input and LTP can enhance encoding.

In contrast, cortical circuits have different dynamics during slow wave sleep, when levels of acetylcholine in the hippocampus and neocortex drop to less than 1/3 of waking levels (Marrosu et al., 1995). Slow wave sleep has been proposed to provide dynamics for consolidation of previously encoded information (Buzsaki, 1989; Wilson and McNaughton, 1994). The lower levels of acetylcholine mean less presynaptic inhibition of glutamatergic transmission, allowing the spread of activity at feedback synapses within the hippocampus and from hippocampus back to neocortical structures (Hasselmo, 1999). Consistent with this, scopolamine blockade of acetylcholine enhances consolidation (Rasch et al., 2006) whereas cholinergic agonists impair consolidation in rats (Bunce et al., 2004) and humans (Gais and Born, 2004).

## MAINTENANCE OF BISTABLE PERSISTENT SPIKING AT THE LEVEL OF INPUTS TO HIPPOCAMPUS

In addition to enhancing dynamics for encoding, acetylcholine also appears to be important for the maintenance of working memory (Green et al., 2005). This is consistent with cellular effects of acetylcholine that enhance the maintenance of presented activity by enhancing bistable persistent spiking or plateau potentials (Klink and Alonso, 1997) that allows depolarization to persist after the end of an input stimulus. In addition to enhancing mechanisms of working memory, these effects may also favor long-term encoding by prolonging specific input patterns to the hippocampus, acting as a buffer to hold recently presented novel information during encoding (Hasselmo, 2006; Hasselmo and Stern, 2006).

The effects described above provide a coherent framework for understanding the enhancement of encoding. However, they focus on a static view of the role of acetylcholine in the hippocampal formation, as if the representations for working memory and long-term encoding were all stable fixed-point attractors. To fully understand the role of acetylcholine, we must address the full range of dynamics, including transient activity and oscillations. Acetylcholine also has a well-defined role in the generation and pacing of theta, which is itself linked to memory formation.

## HIPPOCAMPAL THETA

Theta-band modulations of the LFP are among the most distinct and easily visualized electrophysiological phenomena in the brain. In the moving rat theta is evident in the hippocampus as a large amplitude (exceeding 1 mV) 6–12 Hz sinusoidal oscillation (Vanderwolf, 1969, 1971; Buzsaki, 2002) (see **Figure 2A**). Though less obvious, theta is also present in the hippocampal LFP of other animals including bats, rabbits, and humans (Winson, 1976; Kahana et al., 1999; Cantero et al., 2003; Ulanovsky and Moss, 2007). Work conducted in the 1960s and 1970s revealed that theta has distinct behavioral correlates which vary between animal species, as does the frequency and amplitude of the oscillation (Whishaw and Vanderwolf, 1973; Vanderwolf, 2001). These correlates are most clearly defined for the rat in which, based on behavioral and pharmacological grounds, two distinct forms of theta have been identified (Kramis et al., 1975; Vanderwolf et al., 1977). Type 1 theta, sometimes referred to as translational theta or *t*-theta, is apparent during voluntary movement, specifically any behavior that causes the animal's head to move through space (e.g., running, swimming, grooming) (Whishaw and Vanderwolf, 1973; O'Keefe and Nadel, 1978). In contrast, type 2 or attentional theta, can be identified during highly aroused states when the animal is immobile (e.g., in the presence of a predator or during fear conditioning) (Whishaw, 1972; Sainsbury et al., 1987).

While several subcortical nuclei are implicated in the pacing of theta, the medial septum-diagonal band of Broca seems particularly important and is necessary for the generation of both forms of theta; inactivation or lesion of the medial septum abolishes all theta (Rawlins et al., 1979; Mitchell et al., 1982; Mizumori et al., 1989). Pharmacological manipulation of the medial septum has revealed distinct neuromodulatory mechanisms supporting the two forms (Bland, 1986; Mizumori et al., 1990b). Hence, type 2 theta appears to be acetylcholine dependent, so intraseptal infusion of anti-cholinergic drugs, such as atropine, eliminate it but spare the acetylcholine independent type 1 theta (Kramis et al., 1975). Conversely, application of carbachol, a cholinergic agonist, to the septum promotes a constant type 2 theta state (Bunce et al., 2004). In turn, movement-related type 1 theta depends upon the entorhinal cortex as entorhinal lesions spare only type 2 theta (Kramis et al., 1975). In particular the glutamatergic layer II/III entorhinal afferents to the hippocampus seem to be a necessary component of the circuit generating movement-related theta; application of the NMDAR antagonist ketamine abolishes type 1 theta and coupled with scopolamine removes all theta (Buzsaki, 2002). Electrophysiological investigation of the medial septum revealed populations of GABAergic and cholinergic neurons, which exhibit phase locking to hippocampal theta, and project to interneurons in CA3 and CA1 (Freund and Antal, 1988; Stewart and Fox, 1990; King et al., 1998). Destruction of the cholinergic projections alone attenuates but does not eliminate theta during movement and as such is the complement of septal infusion of cholinergic antagonists (Lee et al., 1994). It is tempting then to simply equate these two cell types with the two forms of theta (Stewart and Fox, 1990). However, subsequent work has complicated the picture. For example, while the GABAergic septal cells are highly active and show strong theta phase locking, the cholinergic cells are less active and do not exhibit rhythmic activity (Simon et al., 2006). Furthermore, work in slices shows the application of cholinergic agonists to the hippocampus, in particular CA3, is sufficient to promote spontaneous oscillations (Fischer et al., 1999). Similarly, in the intact rat, non-phasic activation of acetylcholine receptors in the hippocampus and medial septum increases theta

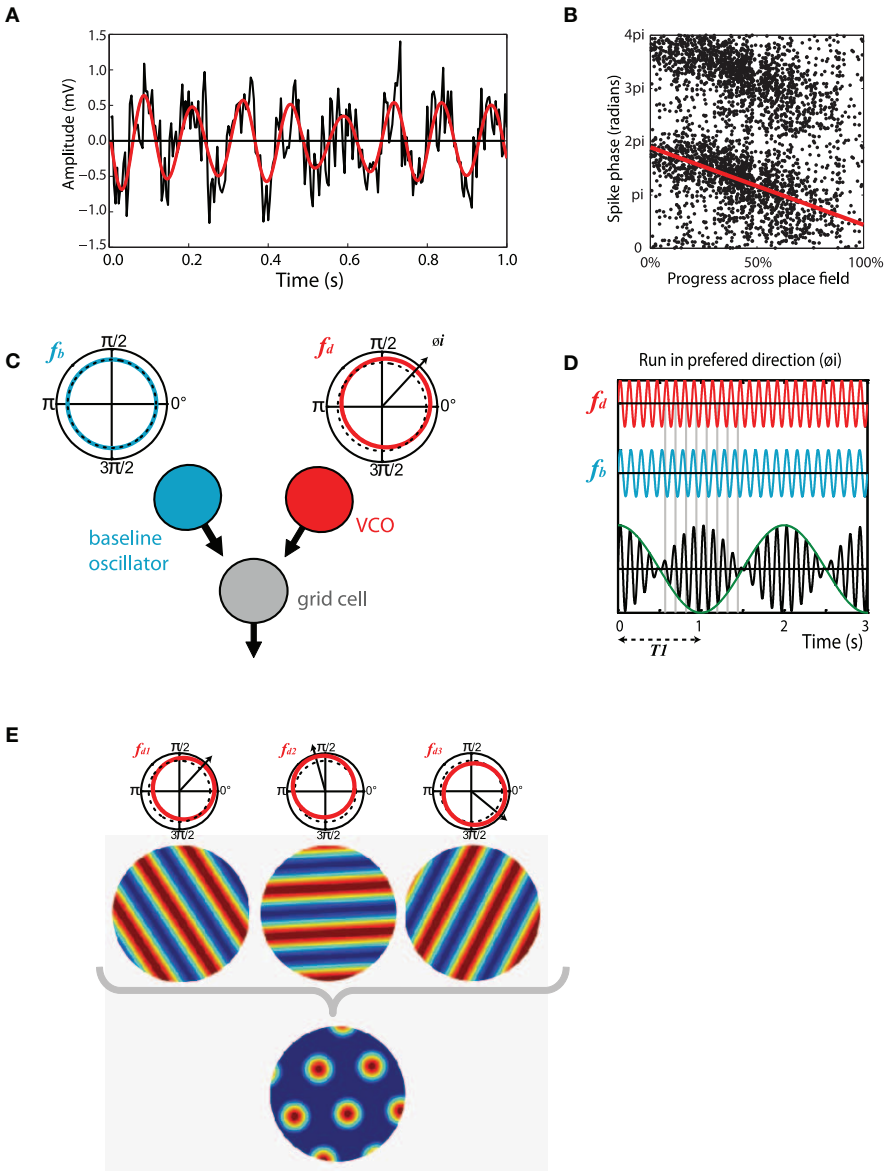


**FIGURE 2 | Theta-band oscillations play an important role in structuring spatial activity in the hippocampus and entorhinal cortex. (A)** Theta recorded from the entorhinal LFP of a moving rat. Black trace, raw LFP, mean normalized showing 1s of data. 8 Hz theta modulation is clearly visible, higher frequency gamma oscillations are also present. Red trace, same signal band pass filtered in 6–12 Hz range. **(B)** Phase precession in a CA1 place cell, the phase, and location of individual spikes is shown as follows: X-axis indicates the animal's progress across the place field, moving left to right. Y-axis indicates the phase of each spike relative to theta measured from the cell layer, two cycles are shown for completeness. Red line indicates best fit to data for linear-circular regression. **(C)** Schematic of the basic oscillatory interference model showing two components: a baseline oscillation (blue) with a constant frequency in the theta-band (*fb*) and; A velocity controlled component (red) the frequency (*fd*) of which increases proportionate to the animal's velocity in a preferred direction ($\varphi i$). **(D)** Interference pattern generated between the components described in **C**. Spikes are emitted at the peaks of the carrier (black) which has a frequency equal to the mean of *fb* and *fd*. Grid scale is determined by the envelope (green) which has a frequency equal to the difference between *fb* and *fd*. **(E)** Multiple velocity controlled components with preferred firing directions at increments of 60° are required to produce a grid interference pattern. A single baseline oscillator and velocity controlled component will produce a spatially stable stripped pattern similar to a sine grating.

power (Siok et al., 2006). A more accurate view then is that the GABAergic septal cells probably do function as a pacemaker, and so entrain oscillators in the EC and hippocampus. In contrast, the cholinergic projection has a permissive modulatory role (Buzsaki, 2002).

What then is the function of hippocampal theta? In addition to the behavioral correlates outlined above, manipulations that attenuate or abolish theta *in vivo* point to a role in learning and memory. Lesions made to the fornix or septum, which reduce theta power but also cholinergic drive to the hippocampus, impair

performance on a wide range of memory tasks including goal directed navigation (Winson, 1978; Hagan et al., 1988), delayed non-match to position (Markowska et al., 1989), and spatial alternation (Givens and Olton, 1990). More specifically, reversible medial septal inactivations show that the deficit is specific to the encoding and retrieval phases of a spatial alternation task, thus theta was not required for maintenance of a recent memory (Mizumori et al., 1990a). Similarly, theta power was found to correlate with performance on a non-spatial working memory task but not on a reference memory task, indicating a role in encoding of information (Givens and Olton, 1994). This behavioral link between theta and learning is supported by physiological studies that point to a modulation in the efficacy of hippocampal LTP with theta phase. As such, tetanic stimuli arriving at the peak of theta measured in the stratum radiatum (corresponding to trough of theta at the fissure), are more likely to result in potentiation, those arriving during the opposite phase produce depression (Huerta and Lisman, 1995; Holscher et al., 1997; Orr et al., 2001; Hyman et al., 2003). Theta can also provide a mechanism during which synaptic potentiation or synaptic depression can occur depending upon relative timing of the presynaptic input and separate modulatory input (Kwag and Paulsen, 2009). In this study, CA1 Schaeffer collaterals were stimulated relative to an induced theta input at the cell body. Either LTP or LTD could be induced in the Schaeffer collaterals depending upon which phase of theta the stimulation occurred and the relative timing of secondary stimulation of the tempero-ammonic pathway. This work highlights the fact that the hippocampus and entorhinal circuit must work in concert with theta to produce consistent learning rules.

## THETA-BAND MODULATION OF SPATIAL FIRING IN THE HIPPOCAMPUS: PLACE CELLS AND GRID CELLS

Perhaps the clearest evidence for the functional role of theta comes from studies of the spatially modulated cell types found in the hippocampus and surrounding regions; in these areas at least, theta-band oscillations seem to have an important role in structuring spatial activity. Working in the early 1970s O'Keefe and Dostrovsky (1971) first reported place cells, hippocampal pyramidal cells that exhibit spatially stable firing. Place cells seem to be a common feature of the mammalian hippocampus and have subsequently been found in bats, monkeys, humans, and even pigeons (Ekstrom et al., 2003; Hori et al., 2003; Bingman et al., 2006; Ulanovsky and Moss, 2007). In a familiar environment the firing field (place field) of a place cell is typically stable between visits to a location, even if those visits are separated by several days (Muller et al., 1987). However, if an animal is moved to a novel environment place cells change their relative firing positions and rates such that a new stable population code is generated, this effect is known as remapping and is considered to be part of the process by which the hippocampus encodes a new spatial memory (O'Keefe and Nadel, 1978; Muller and Kubie, 1987; Bostock et al., 1991). The timing of spikes emitted by place cells show an interesting relationship relative to the current phase of theta measured from the LFP, as follows: when an animal first enters the firing field of a cell, action potentials are emitted around the peak of theta (measured from the pyramidal cell layer). As the animal advances through the field spikes are emitted at progressive earlier phases, typically moving forwards by about 180° during a single run to be fired near the trough of theta as it exits the place field (O'Keefe and Recce, 1993) (see **Figure 2B**). This effect, known as phase precession, is equivalent to the spike train of the place cell being modulated at a frequency slightly greater than theta measured from the LFP (as measured in autocorrelations); this modulation is referred to as the intrinsic firing frequency of the cell. Because spike phase is linked to the proportion of the field traversed, cells with large place fields tend to have lower frequency modulation than those with smaller fields and similarly faster running is matched by higher firing frequencies (Huxter et al., 2003; Geisler et al., 2007). Phase precession is clearest for runs made on a linear track, in such conditions the phase of spikes relative to theta convey more information about the animal's position than the firing rate (Jensen and Lisman, 2000; Huxter et al., 2003). Phase precession is, however, evident in data collected during open field foraging (Burgess et al., 1994; Skaggs et al., 1996).

Recently a second class of spatial cells, grid cells, have been reported in the medial entorhinal cortex of rodents and humans, as well as in the pre and parasubiculum (Fyhn et al., 2004; Hafting et al., 2005; Boccara et al., 2010; Doeller et al., 2010). Grid cells, like place cells, have spatially stable fields but differ in that each grid cell has multiple circular firing fields arranged in a hexagonal lattice. Grid cells that neighbor each other in the brain typically exhibit a lattice of similar scale but a topographical gradient exists so those at more ventral locations tend to be of a larger scale, increasing in increments that possibly have a fixed ratio (Hafting et al., 2005; Barry et al., 2007; Stensland et al., 2010). The lattice of grids in each hemisphere, and possibly those in different hemispheres, appear to have the same orientation such that the hexagonal arrangement of their firing fields share the same three axes, albeit with some localized distortions (Hafting et al., 2005; Barry et al., 2007; Stensland et al., 2010). Significantly grid cells also exhibit phase precession, the effect being clearest in cells recorded from layer II of medial entorhinal cortex where all grids precess. In deeper layers a subset of grid cells phase precess, the others being phase locked or simply firing with no apparent relationship to theta phase (Hafting et al., 2008).

## THE OSCILLATORY INTERFERENCE MODEL OF GRID CELL FIRING

The regular firing of grid cells is particularly amenable to computational modeling and a number of ideas have been presented to account for the lattice-like activity of these cells. With a few exceptions [see Kropff and Treves (2008)] most of the models describe grid firing in terms of self-motion; updating an animal's representation of its location based on movement cues. Broadly, the models fall into two schools, those in which grid firing is a product of attractor dynamics (Fuhs and Touretzky, 2006; McNaughton et al., 2006; Burak and Fiete, 2009; Navratilova et al., 2011) and those which see grid activity as resulting from interference between multiple de-tuned neuronal oscillators (O'Keefe and Burgess, 2005; Blair et al., 2007; Burgess et al., 2007; Hasselmo et al., 2007; Giocomo and Hasselmo, 2008a; Welday et al., 2011; Hasselmo and Brandon, 2012, this issue). Attractor based models

provide a good account of some of the properties of grid cells, for example, the incremental steps in scale and apparently fixed phase offset between neighboring cells (Barry et al., 2007; Fyhn et al., 2007). This class of model requires a precise pattern of recurrent connectivity which would presumably have to be learnt in early life, and has yet to be identified in the medial entorhinal cortex. It is possible though that the necessary connectivity may be located in other brain regions, potentially the pre or parasubiculum. Alternatively it may be spatially localized, for example, being limited to the dense entorhinal cell islands (Burgalossi et al., 2011) and thus be hard to detect. For a detailed review of the relative merits of recurrent models of grid cell formation and oscillatory interference models see Giocomo et al. (2011b).

The oscillatory interference framework was first proposed as model of place cell activity with a place field described as the envelope of an interference pattern generated between two neuronal oscillators (O'Keefe and Recce, 1993; Lengyel et al., 2003). The lower frequency component oscillates at theta frequency and the higher frequency component increases in frequency above this proportionate with the animal's running speed (see **Figure 2C**). Spikes are emitted at the peaks of the carrier which is the combined activity of the two oscillators and has the mean frequency of the two component waves. Thus, spikes exhibit phase precession relative to the slower frequency theta oscillation (see **Figure 2D**). Though intended as a model of place cell activity, grid cells provide a more natural target for this type of model, the multiple regular fields of the grid lattice arising as the oscillators move repeatedly into and out of phase. Extension of the model to grid cells requires the addition of one or more velocity controlled oscillators (VCOs), the frequency of which tracks the animal's velocity in a preferred direction. So, the model consists of a single baseline oscillator and multiple (between two and six) VCOs with preferred directions that lie at increments of 60° to each other (O'Keefe and Burgess, 2005; Burgess et al., 2007) (see **Figure 2E**). The scale of grids generated by the model is determined by the difference in frequency between the baseline oscillator and the higher frequency VCOs; a large difference resulting in smaller spacing between firing fields of grid cells and vice versa. Early versions of the model supposed that the multiple oscillators required to form a grid might be present within individual stellate cells (Burgess et al., 2007). However, modeling shows this is unlikely as oscillators arranged in this way would quickly entrain each other (Remme et al., 2010), subsequent formulations of the model place the VCOs in individual cells upstream of the grid cells (Zilli and Hasselmo, 2010).

The interference model has found support from a number of directions. In the first instance, entorhinal layer II stellate cells exhibit sub-threshold membrane potential oscillations (MPOs) with frequencies in the theta-band (Alonso and Klink, 1993) and have been proposed as one of the components of the model (O'Keefe and Burgess, 2005; Burgess et al., 2007). These cells have been labeled after juxtacellular recording in moving rats, confirming that stellate cells do exhibit grid-like firing and are likely to be the layer II grid cells previously recorded with extracellular electrodes (Burgalossi et al., 2011). Second, a gradient in the frequency of the MPOs as well as the resonance of stellate cells has been shown to exist along the dorsal-ventral axis of the medial entorhinal cortex (Giocomo et al., 2007). This gradient mirrors grid scale which increases along the same axis (Hafting et al., 2005; Barry et al., 2007); this relationship is predicted by the model. MPO and resonance frequency is partly determined by the composition of the HCN channel, the HCN1 subunit being differentially expressed along the dorsal-ventral axis (Giocomo and Hasselmo, 2008b). Mice with the HCN1 subunit knocked out exhibit a reduction in the frequency of the MPOs as well as a flattening of the frequency gradient (Giocomo and Hasselmo, 2009). Significantly, grids recorded from these mice are of a larger scale than those found in wild type mice, indicating a causal link between the intrinsic frequency of neurons and the spatial firing of grid cells (Giocomo et al., 2011a). However, the relationship may be more complex than initially assumed because the dorsal-ventral gradient in grid scale was not flattened in the same way the frequency gradient was. Third, the model requires VCOs that track an animal's velocity, their firing frequency being modulated in the theta-band but increasing with the speed of travel along a preferred firing direction. Bursting theta cells with these properties, specifically a cosine-like directional tuning and speed modulation, have been found in the medial septum as well as the hippocampus and anterior thalamus (Welday et al., 2011). Finally, the model explicitly requires theta-band oscillations to generate grid firing, though once established firing may be maintained by sensory input from environmental cues, such as boundaries (Hartley et al., 2000; Burgess et al., 2007; Solstad et al., 2008). Accordingly, inactivation of the medial septum, which abolishes theta-band modulation in the entorhinal cortex, caused grid cells to temporarily lose their spatial firing, the grid lattice being reinstated when theta returns (Brandon et al., 2011; Koenig et al., 2011).

A possible criticism of the model is that the level of temporal precision necessary to maintain stable spatial firing is beyond that which can be expected of a biological system (Burak and Fiete, 2009; Zilli et al., 2009). Simulations suggest this is not the case, while independent realistically noisy oscillators would quickly decohere, a population of coupled oscillators would not (Zilli and Hasselmo, 2010; Welday et al., 2011). Furthermore, work by Fernandez and White (*Soc. Neurosci. Abstr.* 766.19, 2011) demonstrates that correlated excitatory and inhibitory synaptic background noise increases firing rate modulation to sinusoidal input which could help to maintain stable firing of grid cells. Recently, recordings from the medial entorhinal cortex of crawling fruit bats have added to the debate. These animals exhibit grid-like spatial firing in the absence of theta-band modulation of the cells' spike trains or of the hippocampal and entorhinal LFP (Yartsev et al., 2011). It remains to be seen if species specific differences, the unnatural nature of the foraging task, or possibly the low firing rate of the bat grid cells themselves might account for this discrepancy with the rodent data.

## GRID EXPANSION, THETA RHYTHM, AND ENVIRONMENTAL NOVELTY

It has been known for some time that when an animal enters a novel environment place cells remap; place fields change their relative positions and rates (Muller and Kubie, 1987; Bostock et al., 1991; Karlsson and Frank, 2008). Conditions that provoke place

cell remapping also cause grid firing to shift and rotate relative to the environment but not relative to grids of the same scale (Fyhn et al., 2007). Now, several new studies suggest a potential link between these phenomena and cholinergic signaling of novelty (Acquas et al., 1996; Thiel et al., 1998; Giovannini et al., 2001). Entorhinal recordings show that when a rat first enters a novel environment the regular grid lattice expands and becomes less regular (Barry et al., *Soc. Neurosci. Abstr.* 101.25, 2009), these effects occur in addition to the previously reported realignment. Individual fields increase in size and move further apart, at the same time becoming less circular and conform less well to a hexagonal structure. With repeated exposure to the environment the grid returns to the scale seen in a familiar environment, becoming more regular at the same time. The initial expansion, which is typically about 40% of the familiar scale, attenuates at a decreasing rate so that the "novel" grids come to resemble "familiar" grids after about four hours of experience. Environmental novelty is known to reduce theta frequency measured from the hippocampal LFP, which exhibits a similar recovery time course (Jeewajee et al., 2008b). Similarly, the theta-band modulation of expanded grids' spike trains were found to reduce in the novel environment, as did theta measured from the entorhinal LFP (Barry et al., *Soc. Neurosci. Abstr.* 101.25, 2009). More specifically, the reduction in intrinsic firing frequency was found to inversely correlate with the increase in scale, indicating a causal link between entorhinal oscillations and grid firing, as posited by the oscillatory interference model.

Increased cholinergic drive, such as that resulting from environmental novelty (Acquas et al., 1996; Thiel et al., 1998; Giovannini et al., 2001), reduces hippocampal theta frequency (Givens and Olton, 1995). Might cholinergic modulation contribute to the reduction in entorhinal theta and concomitant grid expansion? The potential link between increases in acetylcholine level and decreases in oscillation frequencies is supported by cellular data on the effects of acetylcholine on stellate cell resonance frequency. As noted above, intracellular recording from stellate cells in medial entorhinal cortex allows measurement of their intrinsic frequency. In particular, the resonance frequency of these neurons can be measured by delivering a current injection with a sinusoid oscillation that progressively increases in frequency from 0 Hz to 20 Hz over 20 s (Haas and White, 2002; Erchova et al., 2004; Heys et al., 2010). Stellate cells in medial entorhinal cortex show a clear change in amplitude of their membrane potential response to this current injection, increasing amplitude as frequency increases to theta frequencies, and then decreasing thereafter. In contrast, neurons in the lateral entorhinal cortex show a decrease in oscillation amplitude across the full range of frequencies (Shay et al., 2011). In recent experiments, the resonance frequency of stellate cells was measured before and during application of the cholinergic agonist carbachol (Heys et al., 2010). These experiments showed a clear decrease in the resonance frequency of stellate cells in the presence of carbachol. This decrease in resonance frequency appears to arise from a cholinergic reduction in the magnitude of the hyperpolarization activated cation current (h current), as shown by voltage clamp studies with carbachol in these same cells (Heys and Hasselmo, *Soc. Neurosci. Abstr.* 730.09, 2011). This decrease in resonance frequency could underlie the decrease in the intrinsic frequency of theta modulation of grid cells in novel environments (Barry et al., *Soc. Neurosci. Abstr.* 101.25, 2009). In addition to the decrease in the intrinsic resonance frequency, application of carbachol also decreased the resonance strength in stellate cells, which is consistent with reports from Barry et al. (*Soc. Neurosci. Abstr.* 101.25, 2009) demonstrating a decrease in the theta-band modulation of the grids' spike train. The reduction of intrinsic frequency could also contribute to the reduction in network theta frequency in the LFP. Cholinergic modulation of other cellular properties could also contribute to the change in network oscillations, as cholinergic modulation has been shown to induce oscillations in the hippocampus in interneurons in lacunosum-moleculare (Chapman and Lacaille, 1999) as well as interneurons in stratum oriens that synapse in lacunosum-moleculare (Lawrence et al., 2006). Cholinergic modulation also regulates rhythmicity in GABAergic cells of the medial septum projecting to the hippocampus (Alreja et al., 2000).

What then is the utility of reduced theta frequency and why should this occur in response to environmental novelty? One proposed function of the theta rhythm is to provide a distinction between the circuit dynamics of encoding and retrieval (Hasselmo et al., 2002); reducing interference between patterns being learnt and those already stored (see **Figure 3**). In this model, the encoding of new information involves a strong influence of external afferent input on cortical structures including the hippocampus and entorhinal cortex as well as neocortical regions (Hasselmo et al., 2002). In the hippocampus, this is consistent with the strong current sinks in stratum lacunosum-moleculare during the peak of theta recorded in the cell body layer (Brankack et al., 1993). Furthermore, studies of LTP show that stimulation delivered at this same phase are most effective at producing potentiation (Huerta and Lisman, 1995; Holscher et al., 1997; Orr et al., 2001; Hyman et al., 2003). In contrast, the opposite phase of theta is

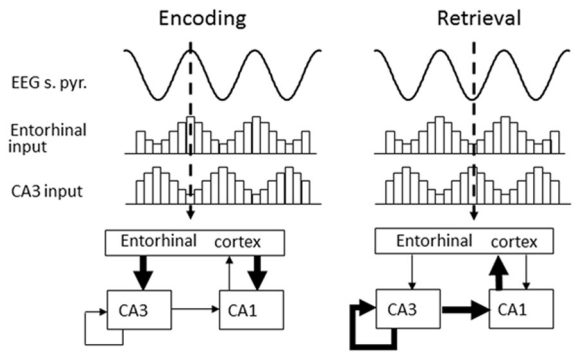


**FIGURE 3 | Theta phase is proposed to segment retrieval and encoding phases of mnemonic processing in the hippocampus.** Encoding (left) occurs around the peak of theta (measured from the cell-layer) when strong current sinks are evident in the lacunosum-moleculare where entorhinal inputs terminate. Retrieval (right) occurs during the trough of theta when internal connectivity within the hippocampus is more active, producing a strong current sink in the stratum radiatum.

proposed to play a role in retrieval. In this phase, the internal connections of the hippocampus cause a stronger current sink in stratum radiatum (Brankack et al., 1993), and stimulation on this phase (the trough of theta in stratum pyramidale) causes long-term depression instead of LTP. Thus, this model proposes a rapid transition between encoding and retrieval during individual cycles of theta (Hasselmo et al., 2002), but at the same time slower changes in acetylcholine levels may shift the overall tone of the network more toward encoding. Such a shift is consistent with unit recording studies that have shown a change in the phase of spiking with novel stimuli (Manns et al., 2007) or in novel environments (Lever et al., 2010). In fact, a possible mechanism for the shift may be an increase in the duration of the encoding phase of the theta cycle, which would allow more effective encoding and arise from the decrease in theta frequency observed in novel environments (Jeewajee et al., 2008a,b; Barry et al., *Soc. Neurosci. Abstr.* 101.25, 2009).

In addition to moving the network toward a state that favors encoding, increased cholinergic modulation may, as we have described, provoke the increase in grid scale seen in novel environments. Grid expansion is likely to induce a mismatch between the expanded firing pattern of grid cells and the more stable activity of other sensory inputs to the hippocampus, such as entorhinal boundary vector cells, which do not remap or expand in novel environments (Solstad et al., 2008; Lever et al., 2009), see also (Burgess et al., 2007; Burgess, 2008). Additionally, because grids of different native scales appear to expand by differing amounts (Barry et al., *Soc. Neurosci. Abstr.* 101.25, 2009) they may also produce a mismatch relative to one another (see **Figure 4**). This differential expansion may occur if populations of grid cell or VCOs exhibit different sensitivity to acetylcholine [e.g., Shulz et al. (2000)], alternatively it might simply be a product of local variations in the concentration of extracellular acetylcholine. A further source of mismatch may be the realignment of different scaled grids which occurs between distinct environments (Fyhn et al., 2007). Together these effects would result in a significant change in the medial entorhinal input to the hippocampus, essentially orthogonalizing the pattern of activity being presented to CA3 and CA1. It seems possible then that this change would drive remapping of the hippocampal place cells, causing a new

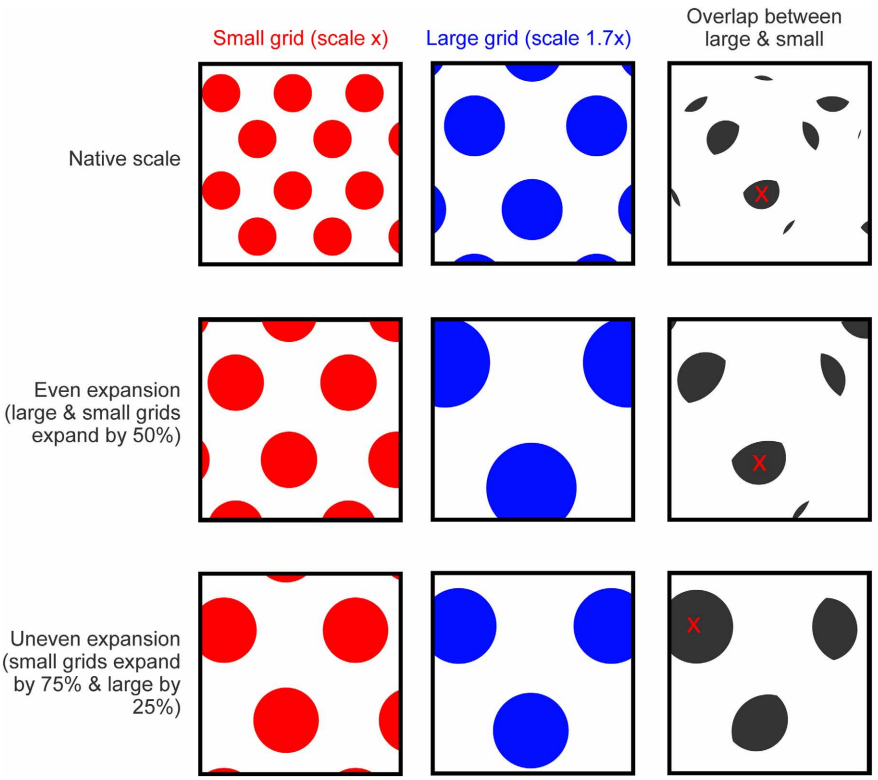


**FIGURE 4 | Grid expansion as a source of mismatch.** Top row, cartoon showing the spatial activity of two idealized grid cells in a square environment, a small-scale grid is shown in red and larger scale grid (1.7x larger than the small grid) in blue. Panel to the right shows areas where the firing of the two grids overlap (gray), the red cross indicates the area of largest overlap. Middle row, grid activity from the first row with a 50% expansion applied to both the small and large grid (expansion focused on the center of the environment). Fields from both grids are translocated relative to the environment and will likely "mismatch" with spatial inputs, such as boundary vector cells that do not expand or remap. However, the fields of the small and large grid do not shift relative to one another. The pattern of overlap is expanded (by 50%) relative to the first row but is otherwise unchanged; the area of largest overlap (red cross) is shifted only slightly relative to the unexpanded situation. Bottom row, an uneven expansion (small grid expands by 75% but large by only 25%, again focus is center of environment) causes fields from the two grids to move relative to the environment but also relative to one another, producing an additional source of mismatch. The pattern of overlap shown in gray is dissimilar to the previous rows and the site of maximum overlap is completely changed.

representation to be formed for the current environment. This view is supported by a recent computational study showing that distinct patterns of hippocampal activity could be generated by shifted or expanded grid inputs (Monaco and Abbott, 2011). As well as initiating hippocampal remapping, the orthogonalized input would also enhance the dynamics of encoding: Because the expanded pattern of entorhinal activity is distinct from stored patterns encoding familiar environments interference produced by inappropriate retrieval would be reduced further (Hasselmo et al., 2002; Hasselmo, 2005). After the initial expansion, subsequent exposure to a novel environment produces an incremental reduction in grid scale until, after several days, grids are the same size as those in a familiar environment (Barry et al., *Soc. Neurosci. Abstr.* 101.25, 2009). This contraction is accompanied by a gradual increase in theta frequency from the LFP and grid spike trains (Jeewajee et al., 2008b; Barry et al., *Soc. Neurosci. Abstr.* 101.25, 2009), and presumably is mediated by a reduction in cholinergic drive from the medial septum, which also attenuates with familiarity (Thiel et al., 1998). Unlike the sudden increase in scale provoked by environmental novelty, the gradual reversion to a native scale does not cause hippocampal remapping, although place fields do exhibit a slight reduction in scale with experience (Karlsson and Frank, 2008; Barry et al., *Soc. Neurosci. Abstr.* 101.25, 2009). It seems likely that the slower rate of change in the latter case does not generate a mismatch signal, possibly providing time for slow plastic processes to update the mapping between entorhinal grids and hippocampal place cells (Lever et al., 2002).

We have described a circuit for the detection and encoding of novelty, in particular environmental novelty, in which cholinergic modulation of theta frequency both triggers and augments the formation of new memories. In response to novel stimuli, cholinergic signaling from the medial septum to the entorhinal cortex and hippocampus is augmented (Acquas et al., 1996). Increased cholinergic tone causes a reduction in the frequency of theta-band oscillations in the hippocampal formation (Givens and Olton, 1995), a state which may favor encoding and likely contributes to the expansion and reorganization of grid firing seen in novel environments (Fyhn et al., 2007; Barry et al., *Soc. Neurosci. Abstr.* 101.25, 2009). In turn, this immediate and pronounced change in grid cell activity is expected to push the entorhinal input to the hippocampus away from previously learnt states, instigating remapping, and supporting accurate encoding (Hasselmo et al., 2002). This dynamic mechanism is consistent with the established view of acetylcholine as an important controller of mnemonic function and fits with the mechanisms that have already been proposed to support this role, for example, the enhancement of LTP (Blitzer et al., 1990; Huerta and Lisman, 1995; Patil et al., 1998; Adams et al., 2004), elevation of feedforward over feedback connectivity (Hasselmo and Bower, 1992; Gil et al., 1997), and maintenance of input patterns (Hasselmo and Stern, 2006). Similarly, existing research (Huerta and Lisman, 1995; Holscher et al., 1997; Hyman et al., 2003), in particular computational modeling (Hasselmo et al., 2002), suggests a role for hippocampal theta in the segmentation of encoding and retrieval. The mechanism proposed here builds on those existing ideas and demonstrates how they may be tailored to an animal's current conditions, for example, biasing the efficacy of encoding when confronted with a new or changed environment.

## ACKNOWLEDGMENTS

This work was supported by ONR MURI award N000141010936 and NIH R01 MH61492 and R01 MH60013, USA. Caswell Barry additionally supported by the Wellcome Trust and EU SPACEBRAIN.

## REFERENCES

Acquas, E., Wilson, C., and Fibiger, H. C. (1996). Conditioned and unconditioned stimuli increase frontal cortical and hippocampal acetylcholine release: effects of novelty, habituation, and fear. *J. Neurosci.* 16, 3089–3096.

Adams, S. V., Winterer, J., and Muller, W. (2004). Muscarinic signaling is required for spike-pairing induction of long-term potentiation at rat Schaffer collateral-CA1 synapses. *Hippocampus* 14, 413–416.

Aigner, T. G., and Mishkin, M. (1986). The effects of physostigmine and scopolamine on recognition memory in monkeys. *Behav. Neurosci.* 45, 81–87.

Alonso, A., and Klink, R. (1993). Differential electroresponsiveness of stellate and pyramidal-like cells of medial entorhinal cortex layer II. *J. Neurophysiol.* 70, 128–143.

Alreja, M., Wu, M., Liu, W., Atkins, J. B., Leranth, C., and Shanabrough, M. (2000). Muscarinic tone sustains impulse flow in the septohippocampal GABA but not cholinergic pathway: implications for learning and memory. *J. Neurosci.* 20, 8103–8110.

Bang, S. J., and Brown, T. H. (2009). Muscarinic receptors in perirhinal cortex control trace conditioning. *J. Neurosci.* 29, 4346–4350.

Barkai, E., and Hasselmo, M. E. (1994). Modulation of the input/output function of rat piriform cortex pyramidal cells. *J. Neurophysiol.* 72, 644–658.

Barry, C., Hayman, R., Burgess, N., and Jeffery, K. J. (2007). Experience-dependent rescaling of entorhinal grids. *Nat. Neurosci.* 10, 682–684.

Baxter, M. G., Bucci, D. J., Gorman, L. K., Wiley, R. G., and Gallagher, M. (1995). Selective immunotoxic lesions of basal forebrain cholinergic cells: effects on learning and memory in rats. *Behav. Neurosci.* 109, 714–722.

Bingman, V. P., Siegel, J. J., Gagliardo, A., and Erichsen, J. T. (2006). Representing the richness of avian spatial cognition: properties of a lateralized homing pigeon hippocampus. *Rev. Neurosci.* 17, 17–28.

Blair, H. T., Welday, A. C., and Zhang, K. (2007). Scale-invariant memory representations emerge from moire interference between grid fields that produce theta oscillations: a computational model. *J. Neurosci.* 27, 3211–3229.

Bland, B. H. (1986). The physiology and pharmacology of hippocampal-formation theta rhythms. *Prog. Neurobiol.* 26, 1–54.

Blitzer, R. D., Gil, O., and Landau, E. M. (1990). Cholinergic stimulation enhances long-term potentiation in the CA1 region of rat hippocampus. *Neurosci. Lett.* 119, 207–210.

Blokland, A., Honig, W., and Raaijmakers, W. G. M. (1992). Effects of intra-hippocampal scopolamine injections in a repeated spatial acquisition task in the rat. *Psychopharmacology* 109, 373–376.

Boccara, C. N., Sargolini, F., Thoresen, V. H., Solstad, T., Witter, M. P., Moser, E. I., and Moser, M. B. (2010). Grid cells in pre- and parasubiculum. *Nat. Neurosci.* 13, 987–994.

Bostock, E., Muller, R. U., and Kubie, J. L. (1991). Experience-dependent modifications of hippocampal place cell firing. *Hippocampus* 1, 193–206.

Brandon, M. P., Bogaard, A. R., Libby, C. P., Connerney, M. A., Gupta, K., and Hasselmo, M. E. (2011). Reduction of theta rhythm dissociates grid cell spatial periodicity from directional tuning. *Science* 332, 595–599.

Brankack, J., Stewart, M., and Fox, S. E. (1993). Current source density analysis of the hippocampal theta rhythm: associated sustained potentials and candidate synaptic generators. *Brain Res.* 615, 310–327.

Brazhnik, E. S., Muller, R. U., and Fox, S. E. (2003). Muscarinic blockade slows and degrades the location-specific firing of hippocampal pyramidal cells. *J. Neurosci.* 23, 611–621.

Brocher, S., Artola, A., and Singer, W. (1992). Agonists of cholinergic and noradrenergic receptors facilitate synergistically the induction of long-term potentiation in slices of rat visual cortex. *Brain Res.* 573, 27–36.

Bunce, J. G., Sabolek, H. R., and Chrobak, J. J. (2004). Intraseptal infusion of the cholinergic agonist carbachol impairs delayed-non-match-to-sample radial arm maze performance in the rat. *Hippocampus* 14, 450–459.

Burak, Y., and Fiete, I. R. (2009). Accurate path integration in continuous attractor network models of grid cells. *PLoS Comput. Biol.* 5, e1000291. doi: 10.1371/journal.pcbi.1000291

Buresova, O., Bolhuis, J. J., and Bures, J. (1986). Differential effects of cholinergic blockade on performance of rats in the water tank navigation task and in a radial water maze. *Behav. Neurosci.* 100, 476–482.

Burgalossi, A., Herfst, L., von Heimendahl, M., Forste, H., Haskic, K., and Schmidt, M. B. M. (2011). Microcircuits of functionally identified neurons in the rat medial entorhinal cortex. *Neuron* 70, 773–786.

Burgess, N. (2008). Grid cells and theta as oscillatory interference: theory and predictions. *Hippocampus* 18, 1157–1174.

Burgess, N., Barry, C., and O'Keefe, J. (2007). An oscillatory interference model of grid cell firing. *Hippocampus* 17, 801–812.

Burgess, N., Recce, M., and O'Keefe, J. (1994). A model of hippocampal function. *Neural Netw.* 7, 1065–1081.

Buzsaki, G. (1989). Two-stage model of memory trace formation: a role for "noisy" brain states. *Neuroscience* 31, 551–570.

Buzsaki, G. (2002). Theta oscillations in the hippocampus. *Neuron* 33, 325–340.

Cantero, J. L., Atienza, M., Stickgold, R., Kahana, M. J., Madsen, J. R., and Kocsis, B. (2003). Sleep-dependent theta oscillations in the human hippocampus and neocortex. *J. Neurosci.* 23, 10897–10903.

Chapman, C. A., and Lacaille, J. C. (1999). Cholinergic induction of theta-frequency oscillations in hippocampal inhibitory interneurons and pacing of pyramidal cell firing. *J. Neurosci.* 19, 8637–8645.

Cole, A. E., and Nicoll, R. A. (1984). Characterization of a slow cholinergic postsynaptic potential recorded *in vitro* from rat hippocampal pyramidal cells. *J. Physiol.* 352, 173–188.

Doeller, C. F., Barry, C., and Burgess, N. (2010). Evidence for grid cells in a human memory network. *Nature* 463, 657–661.

Easton, A., Fitchett, A. E., Eacott, M. J., and Baxter, M. G. (2011). Medial septal cholinergic neurons are necessary for context-place memory but not episodic-like memory. *Hippocampus* 21, 1021–1027.

Ekstrom, A. D., Kahana, M. J., Caplan, J. B., Fields, T. A., Isham, E. A., Newman, E. L., and Fried, I. (2003). Cellular networks underlying human spatial navigation. *Nature* 425, 184–188.

Elvander, E., Schott, P. A., Sandin, J., Bjelke, B., Kehr, J., Yoshitake, T., and Ogren, S. O. (2004). Intraseptal muscarinic ligands and galanin: influence on hippocampal acetylcholine and cognition. *Neuroscience* 126, 541–557.

Erchova, I., Kreck, G., Heinemann, U., and Herz, A. V. (2004). Dynamics of rat entorhinal cortex layer II and III cells: characteristics of membrane potential resonance at rest predict oscillation properties near threshold. *J. Physiol.* 560, 89–110.

Esclassan, F., Coutureau, E., Di Scala, G., and Marchand, A. R. (2009). A cholinergic-dependent role for the entorhinal cortex in trace fear conditioning. *J. Neurosci.* 29, 8087–8093.

Fischer, Y., Gahwiler, B. H., and Thompson, S. M. (1999). Activation of intrinsic hippocampal theta oscillations by acetylcholine in rat septo-hippocampal cocultures. *J. Physiol.* 519(Pt 2), 405–413.

Foster, T. C., and Deadwyler, S. A. (1992). Acetylcholine modulates averaged sensory evoked responses and perforant path evoked field potentials in the rat dentate gyrus. *Brain Res.* 587, 95–101.

Freund, T. F., and Antal, M. (1988). GABA-containing neurons in the septum control inhibitory interneurons in the hippocampus. *Nature* 336, 170–173.

Fuhs, M. C., and Touretzky, D. S. (2006). A spin glass model of path integration in rat medial entorhinal cortex. *J. Neurosci.* 26, 4266–4276.

Fyhn, M., Hafting, T., Treves, A., Moser, M. B., and Moser, E. I. (2007). Hippocampal remapping and grid realignment in the entorhinal cortex. *Nature* 446, 190–194.

Fyhn, M., Molden, S., Witter, M. P., Moser, E. I., and Moser, M. B. (2004). Spatial representation in the entorhinal cortex. *Science* 305, 1258–1264.

Gais, S., and Born, J. (2004). Low acetylcholine during slow-wave sleep is critical for declarative memory consolidation. *Proc. Natl. Acad. Sci. U.S.A.* 101, 2140–2144.

Geisler, C., Robbe, D., Zugaro, M., Sirota, A., and Buzsaki, G. (2007). Hippocampal place cell assemblies are speed-controlled oscillators. *Proc. Natl. Acad. Sci. U.S.A.* 104, 8149–8154.

Ghoneim, M. M., and Mewaldt, S. P. (1975). Effects of diazepam and scopolamine on storage, retrieval and organizational processes in memory. *Psychopharmacologia* 44, 257–262.

Gil, Z., Conners, B. W., and Amitai, Y. (1997). Differential regulation of neocortical synapses by neuromodulators and activity. *Neuron* 19, 679–686.

Giocomo, L. M., and Hasselmo, M. E. (2008a). Computation by oscillations: implications of experimental data for theoretical models of grid cells. *Hippocampus* 18, 1186–1199.

Giocomo, L. M., and Hasselmo, M. E. (2008b). Time constants of h current in layer II stellate cells differ along the dorsal to ventral axis of medial entorhinal cortex. *J. Neurosci.* 28, 9414–9425.

Giocomo, L. M., and Hasselmo, M. E. (2009). Knock-out of HCN1 subunit flattens dorsal-ventral frequency gradient of medial entorhinal neurons in adult mice. *J. Neurosci.* 29, 7625–7630.

Giocomo, L. M., Hussaini, S. A., Zheng, F., Kandel, E. R., Moser, M. B., and Moser, E. I. (2011a). Grid cells use HCN1 channels for spatial scaling. *Cell* 147, 1159–1170.

Giocomo, L. M., Moser, M. B., and Moser, E. I. (2011b). Computational models of grid cells. *Neuron* 71, 589–603.

Giocomo, L. M., Zilli, E. A., Fransen, E., and Hasselmo, M. E. (2007). Temporal frequency of subthreshold oscillations scales with entorhinal grid cell field spacing. *Science* 315, 1719–1722.

Giovannini, M. G., Rakovska, A., Benton, R. S., Pazzagli, M., Bianchi, L., and Pepeu, G. (2001). Effects of novelty and habituation on acetylcholine, GABA, and glutamate release from the frontal cortex and hippocampus of freely moving rats. *Neuroscience* 106, 43–53.

Givens, B., and Olton, D. S. (1994). Local modulation of basal forebrain: effects on working and reference memory. *J. Neurosci.* 14, 3578–3587.

Givens, B., and Olton, D. S. (1995). Bidirectional modulation of scopolamine-induced working memory impairment by muscarinic activation of the medial septal area. *Neurobiol. Learn. Mem.* 63, 269–276.

Givens, B. S., and Olton, D. S. (1990). Cholinergic and GABAergic modulation of the medial septal area: effect on working memory. *Behav. Neurosci.* 104, 849–855.

Green, A., Ellis, K. A., Ellis, J., Bartholomeusz, C. F., Ilic, S., Croft, R. J., Luan Phan, K., and Nathan, P. J. (2005). Muscarinic and nicotinic receptor modulation of object and spatial n-back working memory in humans. *Pharmacol. Biochem. Behav.* 81, 575–584.

Haas, J. S., and White, J. A. (2002). Frequency selectivity of layer II stellate cells in the medial entorhinal cortex. *J. Neurophysiol.* 88, 2422–2429.

Hafting, T., Fyhn, M., Bonnevie, T., Moser, M. B., and Moser, E. I. (2008). Hippocampus-independent phase precession in entorhinal grid cells. *Nature* 453, 1248–1252.

Hafting, T., Fyhn, M., Molden, S., Moser, M. B., and Moser, E. I. (2005). Microstructure of a spatial map in the entorhinal cortex. *Nature* 436, 801–806.

Hagan, J. J., Salamone, J. D., Simpson, J., Iversen, S. D., and Morris, R. G. M. (1988). Place navigation in rats is impaired by lesions of medial septum and diagonal band but not nucleus basalis magnocellularis. *Behav. Brain Res.* 27, 9–20.

Hartley, T., Burgess, N., Lever, C., Cacucci, F., and O'Keefe, J. (2000). Modeling place fields in terms of the cortical inputs to the hippocampus. *Hippocampus* 10, 369–379.

Hasselmo, M. E. (1999). Neuromodulation: acetylcholine and memory consolidation. *Trends Cogn. Sci.* 3, 351–359.

Hasselmo, M. E. (2005). What is the function of hippocampal theta rhythm? – Linking behavioral data to phasic properties of field potential and unit recording data. *Hippocampus* 15, 936–949.

Hasselmo, M. E. (2006). The role of acetylcholine in learning and memory. *Curr. Opin. Neurobiol.* 16, 710–715.

Hasselmo, M. E., Anderson, B. P., and Bower, J. M. (1992). Cholinergic modulation of cortical associative memory function. *J. Neurophysiol.* 67, 1230–1246.

Hasselmo, M. E., Bodelon, C., and Wyble, B. P. (2002). A proposed function for hippocampal theta rhythm: separate phases of encoding

and retrieval enhance reversal of prior learning. *Neural Comput.* 14, 793–817.

Hasselmo, M. E., and Bower, J. M. (1992). Cholinergic suppression specific to intrinsic not afferent fiber synapses in rat piriform (olfactory) cortex. *J. Neurophysiol.* 67, 1222–1229.

Hasselmo, M. E., and Bower, J. M. (1993). Acetylcholine and memory. *Trends Neurosci.* 6, 218–222.

Hasselmo, M. E., and Brandon, M. P. (2012). A model combining phase coding and continuous attractors for generation of grid cell firing. *Front. Neural Circuits*, this issue.

Hasselmo, M. E., Giocomo, L. M., and Zilli, E. A. (2007). Grid cell firing may arise from interference of theta frequency membrane potential oscillations in single neurons. *Hippocampus* 17, 1252–1271.

Hasselmo, M. E., and Schnell, E. (1994). Laminar selectivity of the cholinergic suppression of synaptic transmission in rat hippocampal region CA1: computational modeling and brain slice physiology. *J. Neurosci.* 14, 3898–3914.

Hasselmo, M. E., Schnell, E., and Barkai, E. (1995). Dynamics of learning and recall at excitatory recurrent synapses and cholinergic modulation in rat hippocampal region CA3. *J. Neurosci.* 15, 5249–5262.

Hasselmo, M. E., and Stern, C. E. (2006). Mechanisms underlying working memory for novel information. *Trends Cogn. Sci.* 10, 487–493.

Heys, J. G., Giocomo, L. M., and Hasselmo, M. E. (2010). Cholinergic modulation of the resonance properties of stellate cells in layer II of medial entorhinal cortex. *J. Neurophysiol.* 104, 258–270.

Holscher, C., Anwyl, R., and Rowan, M. J. (1997). Stimulation on the positive phase of hippocampal theta rhythm induces long-term potentiation that can be depotentiated by stimulation on the negative phase in area CA1 *in vivo*. *J. Neurosci.* 17, 6470–6477.

Hori, E., Tabuchi, E., Matsumura, N., Tamura, R., Eifuku, S., Endo, S., Nishijo, H., and Ono, T. (2003). Representation of place by monkey hippocampal neurons in real and virtual translocation. *Hippocampus* 13, 190–196.

Huerta, P. T., and Lisman, J. E. (1995). Bidirectional synaptic plasticity induced by a single burst during cholinergic theta oscillation in CA1 *in vitro*. *Neuron* 15, 1053–1063.

Huxter, J., Burgess, N., and O'Keefe, J. (2003). Independent rate and temporal coding in hippocampal pyramidal cells. *Nature* 425, 828–832.

Hyman, J. M., Wyble, B. P., Goyal, V., Rossi, C. A., and Hasselmo, M. E. (2003). Stimulation in hippocampal region CA1 in behaving rats yields long-term potentiation when delivered to the peak of theta and long-term depression when delivered to the trough. *J. Neurosci.* 23, 11725–11731.

Jeewajee, A., Barry, C., O'Keefe, J., and Burgess, N. (2008a). Grid cells and theta as oscillatory interference: electrophysiological data from freely moving rats. *Hippocampus* 18, 1175–1185.

Jeewajee, A., Lever, C., Burton, S., O'Keefe, J., and Burgess, N. (2008b). Environmental novelty is signaled by reduction of the hippocampal theta frequency. *Hippocampus* 18, 340–348.

Jensen, O., and Lisman, J. E. (2000). Position reconstruction from an ensemble of hippocampal place cells: contribution of theta phase coding. *J. Neurophysiol.* 83, 2602–2609.

Kahana, M. J., Sekuler, R., Caplan, J. B., Kirschen, M., and Madsen, J. R. (1999). Human theta oscillations exhibit task dependence during virtual maze navigation. *Nature* 399, 781–784.

Karlsson, M. P., and Frank, L. M. (2008). Network dynamics underlying the formation of sparse, informative representations in the hippocampus. *J. Neurosci.* 28, 14271–14281.

Kimura, F., and Baughman, R. W. (1997). Distinct muscarinic receptor subtypes suppress excitatory and inhibitory synaptic responses in cortical neurons. *J. Neurophysiol.* 77, 709–716.

King, C., Reece, M., and O'Keefe, J. (1998). The rhythmicity of cells of the medial septum/diagonal band of Broca in the awake freely moving rat: relationships with behaviour and hippocampal theta. *Eur. J. Neurosci.* 10, 464–477.

Klink, R., and Alonso, A. (1997). Muscarinic modulation of the oscillatory and repetitive firing properties of entorhinal cortex layer II neurons. *J. Neurophysiol.* 77, 1813–1828.

Koenig, J., Linder, A. N., Leutgeb, J. K., and Leutgeb, S. (2011). The spatial periodicity of grid cells is not sustained during reduced theta oscillations. *Science* 332, 592–595.

Kramis, R., Vanderwolf, C. H., and Bland, B. H. (1975). Two types of hippocampal rhythmical slow activity in both the rabbit and the rat: relations to behavior and effects of atropine, diethyl ether, urethane, and pentobarbital. *Exp. Neurol.* 49, 58–85.

Kremin, T., and Hasselmo, M. E. (2007). Cholinergic suppression of glutamatergic synaptic transmission in hippocampal region CA3 exhibits laminar selectivity: implication for hippocampal network dynamics. *Neuroscience* 149, 760–767.

Kropff, E., and Treves, A. (2008). The emergence of grid cells: intelligent design or just adaptation? *Hippocampus* 18, 1256–1269.

Kwag, J., and Paulsen, O. (2009). The timing of external input controls the sign of plasticity at local synapses. *Nat. Neurosci.* 12, 1219–1221.

Lawrence, J. J., Grinspan, Z. M., Statland, J. M., and McBain, C. J. (2006). Muscarinic receptor activation tunes mouse stratum oriens interneurones to amplify spike reliability. *J. Physiol.* 571, 555–562.

Lee, M. G., Chrobak, J. J., Sik, A., Wiley, R. G., and Buzsaki, G. (1994). Hippocampal theta activity following selective lesion of the septal cholinergic system. *Neuroscience* 62, 1033–1047.

Lengyel, M., Szatmary, Z., and Erdi, P. (2003). Dynamically detuned oscillations account for the coupled rate and temporal code of place cell firing. *Hippocampus* 13, 700–714.

Lever, C., Burton, S., Jeewajee, A., O'Keefe, J., and Burgess, N. (2009). Boundary vector cells in the subiculum of the hippocampal formation. *J. Neurosci.* 29, 9771–9777.

Lever, C., Burton, S., Jeewajee, A., Wills, T. J., Cacucci, F., Burgess, N., and O'Keefe, J. (2010). Environmental novelty elicits a later theta phase of firing in CA1 but not subiculum. *Hippocampus* 20, 229–234.

Lever, C., Wills, T., Cacucci, F., Burgess, N., and O'Keefe, J. (2002). Long-term plasticity in hippocampal place-cell representation of environmental geometry. *Nature* 416, 90–94.

Madison, D. V., Lancaster, B., and Nicoll, R. A. (1987). Voltage clamp analysis of cholinergic action in the hippocampus. *J. Neurosci.* 7, 733–741.

Madison, D. V., and Nicoll, R. A. (1984). Control of the repetitive discharge of rat CA 1 pyramidal neurones *in vitro*. *J. Physiol.* 354, 319– 331.

Manns, J. R., Zilli, E. A., Ong, K. C., Hasselmo, M. E., and Eichenbaum, H. (2007). Hippocampal CA1 spiking during encoding and retrieval: relation to theta phase. *Neurobiol. Learn. Mem.* 87, 9–20.

Markowska, A. L., Olton, D. S., Murray, E. A., and Gaffan, D. (1989). A comparative analysis of the role of fornix and cingulate cortex in memory: rats. *Exp. Brain Res.* 74, 187–201.

Marrosu, F., Portas, C., Mascia, M. S., Casu, M. A., Fa, M., Giagheddu, M., Imperato, A., and Gessa, G. L. (1995). Microdialysis measurement of cortical and hippocampal acetylcholine release during sleep-wake cycle in freely moving cats. *Brain Res.* 671, 329–332.

McGaughy, J., Koene, R. A., Eichenbaum, H., and Hasselmo, M. E. (2005). Cholinergic deafferentation of the entorhinal cortex in rats impairs encoding of novel but not familiar stimuli in a delayed nonmatch-to-sample task. *J. Neurosci.* 25, 10273–10281.

McGurk, S. R., Levin, E. D., and Butcher, L. L. (1988). Cholinergic-dopaminergic interactions in radial-arm maze performance. *Behav. Neural Biol.* 49, 234–239.

McNaughton, B. L., Battaglia, F. P., Jensen, O., Moser, E. I., and Moser, M. B. (2006). Path integration and the neural basis of the "cognitive map". *Nat. Rev. Neurosci.* 7, 663–678.

Mitchell, S. J., Rawlins, J. N., Steward, O., and Olton, D. S. (1982). Medial septal area lesions disrupt theta rhythm and cholinergic staining in medial entorhinal cortex and produce impaired radial arm maze behavior in rats. *J. Neurosci.* 2, 292–302.

Mizumori, S. J., Perez, G. M., Alvarado, M. C., Barnes, C. A., and McNaughton, B. L. (1990a). Reversible inactivation of the medial septum differentially affects two forms of learning in rats. *Brain Res.* 528, 12–20.

Mizumori, S. J. Y., Barnes, C. A., and Mcnaughton, B. L. (1989). Reversible inactivation of the medial septum-selective effects on the spontaneous unit-activity of different hippocampal cell-types. *Brain Res.* 500, 99–106.

Mizumori, S. J. Y., Barnes, C. A., and Mcnaughton, B. L. (1990b). Behavioral-correlates of theta-on and theta-off cells recorded from hippocampal-formation of mature young and aged rats. *Exp. Brain Res.* 80, 365–373.

Monaco, J. D., and Abbott, L. F. (2011). Modular realignment of entorhinal

grid cell activity as a basis for hippocampal remapping. *J. Neurosci.* 31, 9414–9425.

Monmaur, P., Collet, A., Puma, C., Frankel-Kohn, L., and Sharif, A. (1997). Relations between acetylcholine release and electrophysiological characteristics of theta rhythm: a microdialysis study in the urethane-anesthetized rat hippocampus. *Brain Res. Bull.* 42, 141–146.

Muller, R. U., and Kubie, J. L. (1987). The effects of changes in the environment on the spatial firing of hippocampal complex-spike cells. *J. Neurosci.* 7, 1951–1968.

Muller, R. U., Kubie, J. L., and Ranck, J. B. Jr. (1987). Spatial firing patterns of hippocampal complex-spike cells in a fixed environment. *J. Neurosci.* 7, 1935–1950.

Navratilova, Z., Giocomo, L. M., Fellous, J. M., Hasselmo, M. E., and McNaughton, B. L. (2011). Phase precession and variable spatial scaling in a periodic attractor map model of medial entorhinal grid cells with realistic after-spike dynamics. *Hippocampus* [Epub ahead of print].

O'Keefe, J., and Burgess, N. (2005). Dual phase and rate coding in hippocampal place cells: theoretical significance and relationship to entorhinal grid cells. *Hippocampus* 15, 853–866.

O'Keefe, J., and Dostrovsky, J. (1971). The hippocampus as a spatial map. Preliminary evidence from unit activity in the freely-moving rat. *Brain Res.* 34, 171–175.

O'Keefe, J., and Nadel, L. (1978). *The Hippocampus as a Cognitive Map*. Oxford, UK: Oxford University Press.

O'Keefe, J., and Recce, M. L. (1993). Phase relationship between hippocampal place units and the EEG theta rhythm. *Hippocampus* 3, 317–330.

Orr, G., Rao, G., Houston, F. P., McNaughton, B. L., and Barnes, C. A. (2001). Hippocampal synaptic plasticity is modulated by theta rhythm in the fascia dentata of adult and aged freely behaving rats. *Hippocampus* 11, 647–654.

Patil, M. M., Linster, C., Lubenov, E., and Hasselmo, M. E. (1998). Cholinergic agonist carbachol enables associative long-term potentiation in piriform cortex slices. *J. Neurophysiol.* 80, 2467–2474.

Peterson, R. C. (1977). Scopolamine-induced learning failures in man. *Psychopharmacologia* 52, 283–289.

Rasch, B. H., Born, J., and Gais, S. (2006). Combined blockade of cholinergic receptors shifts the brain from stimulus encoding to memory consolidation. *J. Cogn. Neurosci.* 18, 793–802.

Rawlins, J. N., Feldon, J., and Gray, J. A. (1979). Septo-hippocampal connections and the hippocampal theta rhythm. *Exp. Brain Res.* 37, 49–63.

Remme, M. W., Lengyel, M., and Gutkin, B. S. (2010). Democracy-independence trade-off in oscillating dendrites and its implications for grid cells. *Neuron* 66, 429–437.

Rogers, J. L., and Kesner, R. P. (2003). Cholinergic modulation of the hippocampus during encoding and retrieval. *Neurobiol. Learn. Mem.* 80, 332–342.

Sainsbury, R. S., Heynen, A., and Montoya, C. P. (1987). Behavioral correlates of hippocampal type 2 theta in the rat. *Physiol. Behav.* 39, 513–519.

Shapiro, M. L., Simon, D. K., Olton, D. S., Gage, F. H. 3rd., Nilsson, O., and Bjorklund, A. (1989). Intrahippocampal grafts of fetal basal forebrain tissue alter place fields in the hippocampus of rats with fimbria-fornix lesions. *Neuroscience* 32, 1–18.

Shay, C. F., Boardman, I. S., James, N. M., and Hasselmo, M. E. (2011). Comparison of resonance frequency at diffeent membrane potentials in rat medial and lateral entorhinal cortex. *Soc. Neurosci. Abstr.* 730.12.

Shulz, D. E., Sosnik, R., Ego, V., Haidarliu, S., and Ahissar, E. (2000). A neuronal analogue of state-dependent learning. *Nature* 403, 549–552.

Simon, A. P., Poindessous-Jazat, F., Dutar, P., Epelbaum, J., and Bassant, M. (2006). Firing properties of anatomically identified neurons in the medial septum of anestheized and unanesthetized restrained rats. *J. Neurosci.* 26, 9038–9046.

Siok, C. J., Rogers, J. A., Kocsis, B., and Hajos, M. (2006). Activation of alpha7 acetylcholine receptors augments stimulation-induced hippocampal theta oscillation. *Eur. J. Neurosci.* 23, 570–574.

Skaggs, W. E., McNaughton, B. L., Wilson, M. A., and Barnes, C. A. (1996). Theta phase precession in hippocampal neuronal populations and the compression of temporal sequences. *Hippocampus* 6, 149–172.

Solstad, T., Boccara, C. N., Kropff, E., Moser, M. B., and Moser, E. I. (2008). Representation of geometric borders in the entorhinal cortex. *Science* 322, 1865–1868.

Stensland, H., Kirkesola, T., Moser, M. B., and Moser, E. I. (2010). Orientational geometry of entorhinal grid cells. *Soc. Neurosci. Abstr.* 36, 101.14.

Stewart, M., and Fox, S. E. (1990). Do septal neurons pace the hippocampal theta rhythm? *Trends Neurosci.* 13, 163–168.

Tang, Y., Mishkin, M., and Aigner, T. G. (1997). Effects of muscarinic blockade in perirhinal cortex during visual recognition. *Proc. Natl. Acad. Sci. U.S.A.* 94, 12667–12669.

Thiel, C. M., Huston, J. P., and Schwarting, R. K. (1998). Hippocampal acetylcholine and habituation learning. *Neuroscience* 85, 1253–1262.

Turchi, J., Saunders, R. C., and Mishkin, M. (2005). Effects of cholinergic deafferentation of the rhinal cortex on visual recognition memory in monkeys. *Proc. Natl. Acad. Sci. U.S.A.* 102, 2158–2161.

Ulanovsky, N., and Moss, C. F. (2007). Hippocampal cellular network activity in freely moving echolocating bats. *Nat. Neurosci.* 10, 224–233.

Vanderwolf, C. H. (1969). Hippocampal electrical activity and voluntary movement in the rat. *Electroencephalogr. Clin. Neurophysiol.* 26, 407–418.

Vanderwolf, C. H. (1971). Limbic-diencephalic mechanisms of voluntary movement. *Psychol. Rev.* 78, 83–113.

Vanderwolf, C. H. (2001). The hippocampus as an olfacto-motor mechanism: were the classical anatomists right after all? *Behav. Brain Res.* 127, 25–47.

Vanderwolf, C. H., Kramis, R., and Robinson, T. E. (1977). Hippocampal electrical activity during waking behaviour and sleep: analyses using centrally acting drugs. *Ciba. Found. Symp.* 58, 199–226.

Vogt, K. E., and Regehr, W. G. (2001). Cholinergic modulation of excitatory synaptic transmission in the CA3 area of the hippocampus. *J. Neurosci.* 21, 75–83.

Welday, A. C., Shlifer, I. G., Bloom, M. L., Zhang, K., and Blair, H. T. (2011). Cosine directional tuning of theta cell burst frequencies: evidence for spatial coding by oscillatory interference. *J. Neurosci.* 31, 16157–16176.

Whishaw, I. Q. (1972). Hippocampal electroencephalographic activity in the Mongolian gerbil during natural behaviours and wheel running and in the rat during wheel running and conditioned immobility. *Can. J. Psychol.* 26, 219–239.

Whishaw, I. Q. (1985). Cholinergic receptor blockade in the rat impairs locale but not taxon strategies for place navigation in a swimming pool. *Behav. Neurosci.* 99, 979–1005.

Whishaw, I. Q., and Vanderwolf, C. H. (1973). Hippocampal EEG and behavior: changes in amplitude and frequency of RSA (theta rhythm) associated with spontaneous and learned movement patterns in rats and cats. *Behav. Biol.* 8, 461–484.

Wilson, M. A., and McNaughton, B. L. (1994). Reactivation of hippocampal ensemble memories during sleep. *Science* 265, 676–679.

Winson, J. (1976). Hippocampal theta rhythmn. II. Depth profiles in the freely moving rabbit. *Brain Res.* 103, 71–79.

Winson, J. (1978). Loss of hippocampal theta rhythm results in spatial memory deficit in the rat. *Science* 201, 160–163.

Winson, J., and Abzug, C. (1977). Gating of neuronal transmission in the hippocampus: efficacy of transmission varies with behavioral state. *Science* 196, 1223–1225.

Winters, B. D., and Bussey, T. J. (2005). Removal of cholinergic input to perirhinal cortex disrupts object recognition but not spatial working memory in the rat. *Eur. J. Neurosci.* 21, 2263–2270.

Winters, B. D., Saksida, L. M., and Bussey, T. J. (2006). Paradoxical facilitation of object recognition memory after infusion of scopolamine into perirhinal cortex: implications for cholinergic system function. *J. Neurosci.* 26, 9520–9529.

Yartsev, M. M., Witter, M. P., and Ulanovsky, N. (2011). Grid cells without theta oscillations in the entorhinal cortex of bats. *Nature* 479, 103–107.

Yoder, R. M., and Pang, K. C. (2005). Involvement of GABAergic and cholinergic medial septal neurons in hippocampal theta rhythm. *Hippocampus* 15, 381–392.

Yun, S. H., Cheong, M. Y., Mook-Jung, I., Huh, K., Lee, C., and Jung, M. W. (2000). Cholinergic modulation of synaptic transmission and plasticity in entorhinal cortex and hippocampus of the rat. *Neuroscience* 97, 671–676.

Zhang, H., Lin, S. C., and Nicolelis, M. A. (2010). Spatiotemporal coupling between hippocampal acetylcholine release and theta oscillations *in vivo*. *J. Neurosci.* 30, 13431–13440.

Zilli, E. A., and Hasselmo, M. E. (2010). Coupled noisy spiking neurons as velocity-controlled oscillators in a model of grid cell spatial firing. *J. Neurosci.* 30, 13850–13860.

Zilli, E. A., Yoshida, M., Tahvildari, B., Giocomo, L. M., and Hasselmo, M. E. (2009). Evaluation of the oscillatory interference model of grid cell firing through analysis and measured period variance of some biological oscillators. *PLoS Comput. Biol.* 5, e1000573. doi: 10.1371/journal.pcbi.1000573

**Conflict of Interest Statement:** The authors declare that the research was conducted in the absence of any commercial or financial relationships that could be construed as a potential conflict of interest.

*Received: 09 December 2011; accepted: 02 February 2012; published online: 20 February 2012.*

*Citation: Barry C, Heys JG and Hasselmo ME (2012) Possible role of acetylcholine in regulating spatial novelty effects on theta rhythm and grid cells. Front. Neural Circuits* ***6****:5. doi: 10.3389/fncir.2012.00005*

frontiers in
NEURAL CIRCUITS

REVIEW ARTICLE
published: 15 March 2012
doi: 10.3389/fncir.2012.00010

# Cholinergic modulation of the CAN current may adjust neural dynamics for active memory maintenance, spatial navigation and time-compressed replay

***Motoharu Yoshida*** [1,2]*, ***Beate Knauer*** [2] ***and Arthur Jochems*** [2]

[1] *Faculty of Psychology, Mercator Research Group - Structure of Memory, Ruhr-University Bochum, Bochum, Germany*
[2] *International Graduate School for Neuroscience, Ruhr-University Bochum, Bochum, Germany*

***Edited by:***
*Yasser Roudi, Norwegian University of Science and Technology, Norway*

***Reviewed by:***
*David J. Margolis, University of Zurich, Switzerland*
*Francesco P. Battaglia, Universiteit van Amsterdam, Netherlands*
*Cristina Savin, Cambridge University, UK*

***Correspondence:**
*Motoharu Yoshida, Faculty of Psychology, Mercator Research Group, Ruhr-University Bochum, GA 04/49, Universitatstrasse 150, 44801 Bochum, Germany.*
*e-mail: motoharu.yoshida@rub.de*

Suppression of cholinergic receptors and inactivation of the septum impair short-term memory, and disrupt place cell and grid cell activity in the medial temporal lobe (MTL). Location-dependent hippocampal place cell firing during active waking, when the acetylcholine level is high, switches to time-compressed replay activity during quiet waking and slow-wave-sleep (SWS), when the acetylcholine level is low. However, it remains largely unknown how acetylcholine supports short-term memory, spatial navigation, and the functional switch to replay mode in the MTL. In this paper, we focus on the role of the calcium-activated non-specific cationic (CAN) current which is activated by acetylcholine. The CAN current is known to underlie persistent firing, which could serve as a memory trace in many neurons in the MTL. Here, we review the CAN current and discuss possible roles of the CAN current in short-term memory and spatial navigation. We further propose a novel theoretical model where the CAN current switches the hippocampal place cell activity between real-time and time-compressed sequential activity during encoding and consolidation, respectively.

**Keywords: spatial navigation, short-term memory, calcium-activated non-specific cationic current, acetylcholine, encoding, consolidation, medial temporal lobe, hippocampus**

## INTRODUCTION

It has been suggested that the medial temporal lobe (MTL) supports memory formation through two distinct processes: encoding and consolidation (Buzsáki, 1989; McClelland et al., 1995; reviewed by McGaugh, 2000). Since the discovery of time-compressed "replay" of place cell activity during slow-wave-sleep (SWS) and the quiet waking state (Wilson and McNaughton, 1994; Lee and Wilson, 2002; Foster and Wilson, 2006), modeling studies have proposed that activity of place cells during active waking supports encoding, and time-compressed replay supports consolidation (Jensen and Lisman, 1996; Shen and McNaughton, 1996; Molter et al., 2007). In the encoding mode, hippocampal place cells fire sequentially with temporal overlap with adjacent place cells, depending on the location of the animal. This is believed to induce synaptic modifications which will, in the subsequent consolidation mode, activate the same set of place cells in the same sequence but with a highly (∼20 times) compressed time scale (Lee and Wilson, 2002).

The cholinergic system is believed to modulate the dynamics of the MTL between active waking, quiet waking, and SWS modes in the hippocampus, making the information flow suitable for encoding and consolidation (Hasselmo, 1999). This theory is based on the fact that the acetylcholine level is high during active waking, and lower during quiet waking and SWS (Kametani and Kawamura, 1990; Marrosu et al., 1995). Indeed, inactivation of the medial septum, which gives rise to major cholinergic projection to the MTL, reduces the activity and location-specificity of place cells and grid cells (Mizumori et al., 1989; Brandon et al., 2011; Koenig et al., 2011). In addition, infusion of a cholinergic receptor antagonist reduces the activity and location-specificity of hippocampal place cells (Brazhnik et al., 2003). This later study also shows that the cholinergic receptor antagonist reduced the theta activity period, which corresponds to active waking, and increased the large-amplitude irregular activity (ripple activity) period and the out-of-field firing, which corresponds to quiet waking. These observations suggest that cholinergic activation is crucial for physiological activity of the MTL spatial cells during active waking, and suppression of cholinergic activation contributes to switching the dynamical activities of place cells to replay mode. However, the underlying cellular mechanisms for the switch of dynamics by acetylcholine in the MTL are largely unknown.

Prior modeling studies on encoding and consolidation used sensory input to switch the time-scale of sequential activity between real-time and time-compressed activity (Jensen and Lisman, 1996; Molter et al., 2007). In Hasselmo (1999), synaptic suppression due to a high acetylcholine level was proposed to explain the encoding and consolidation functions. However, focus was not on the modulation of intrinsic dynamics. In this paper, we focus on how acetylcholine enables the network dynamics to switch within the MTL independently of the sensory input. We focus on the role of the calcium-activated non-specific cationic (CAN) membrane current which is found in the key areas for spatial navigation, such as the postsubiculum, the medial

entorhinal cortex (MEC) and the hippocampus (Gähwiler and Dreifuss, 1982; Benardo and Prince, 1982b; Caeser et al., 1993; Fraser and MacVicar, 1996; Klink and Alonso, 1997; Magistretti et al., 2004; Yoshida and Hasselmo, 2009a,b). The CAN current is activated through cholinergic receptor activation and through calcium entry to individual neurons, and it greatly excites the membrane, often depolarizing the membrane potential above the firing threshold.

In this paper, we (1) review the effect of the cholinergic modulation on single cells and synaptic transmission, focusing on the modulation by the CAN current. In short, CAN current enables single neurons to maintain information from the past through persistent firing, which is a repetitive neural spiking activity that outlasts triggering stimulation, (2) discuss the possible role of the CAN current in MTL-dependent short-term memory tasks, (3) discuss the possible role of the CAN current in spatial navigation, (4) propose a theoretical model of how the CAN current could support switching from time-compressed fast replay/preplay mode to slower real-time firing mode during active waking, and (5) discuss how the CAN current might be used to intentionally slow the network activity during encoding, to allow the network to perform future planning or sequential episodic memory recall in a speed faster than real-time. Furthermore, we discuss how our model could account for firing dynamics of "time cell" (MacDonald et al., 2011).

## EFFECTS OF ACETYLCHOLINE ON NEURONAL PROPERTIES: *IN VITRO* STUDIES

### ACTIVATION OF CAN CURRENT THROUGH CHOLINERGIC RECEPTOR

Application of acetylcholine or cholinergic receptor agonist mediates slow membrane potential depolarization, increased excitability and reduced firing frequency adaptation (Segal, 1982; Benardo and Prince, 1982a; Cole and Nicoll, 1983; Storm, 1989). This is partly due to the suppression of potassium currents such as the M-current and the calcium-activated potassium current (Halliwell and Adams, 1982; Cole and Nicoll, 1983; Madison et al., 1987). However, this slow depolarization was not fully blocked under the suppression of potassium channels and activation of calcium-activated non-specific cationic current (CAN current) was found to underlie this slow depolarization in the hippocampal pyramidal cells (Gähwiler and Dreifuss, 1982; Benardo and Prince, 1982b; Caeser et al., 1993; Fraser and MacVicar, 1996) and cortical pyramidal cells (Andrade, 1991). Because of the calcium dependency of the CAN current, a calcium channel blockade suppresses the depolarization (Fraser and MacVicar, 1996). On the other hand, spiking or depolarization of the membrane potential that increases calcium influx causes further activation of the CAN current under constant cholinergic activation (Caeser et al., 1993; Fraser and MacVicar, 1996; Kawasaki et al., 1999). In these studies, a brief current injection to the cell drove subthreshold or suprathreshold depolarization due to the CAN current for up to several seconds after the offset of the current injection. This depolarization triggered by a brief stimulation is called a "plateau potential." Persistent firing is often caused by the plateau potential which is large enough to depolarize the membrane potential above the spike threshold.

### CAN CURRENT DRIVEN PERSISTENT FIRING

Subsequent to the above-mentioned studies, the role of the CAN current in persistent firing was studied extensively in various MTL areas (reviewed in Major and Tank, 2004; Reboreda et al., 2011). The significance of the persistent firing found in the MTL areas was that firing often persisted for more than a few minutes without decreasing its firing frequency. **Figure 1** shows examples of persistent firing recorded *in vitro* from neurons in the postsubiculum (Yoshida and Hasselmo, 2009a) where head direction cells have been found *in vivo* (Ranck, 1984; Taube et al., 1990a,b). These recordings were done in an acute brain slice preparation using the cholinergic receptor agonist carbachol (10 μM). First, in a control condition without carbachol, a brief current injection (2 s) induced spiking of the neuron during the stimulation, but the neuron remained quiet once the stimulation was terminated (**Figure 1A**). In contrast, in the presence of carbachol, spikes induced by the same brief current stimulation drove stable persistent firing at a frequency of about 3–10 Hz (**Figure 1B**). In many cells, persistent firing continued for more than a few minutes, at which point persistent firing was terminated by the experimenter using a hyperpolarizing current injection. In this paper, we call this type of persistent firing "long-lasting persistent firing." In other neurons, persistent firing ended within 30 s (**Figure 1C**). We call this type of persistent firing "self-terminating persistent firing." Stable long-lasting persistent firing *in vitro* was found in layer II (Yoshida and Hasselmo, 2009b), in layer V (Egorov et al., 2002; Reboreda et al., 2007) neurons in the MEC, and in layer III neurons in the lateral entorhinal cortex (LEC; Tahvildari et al., 2007). Similar persistent firing has recently been shown in the perirhinal cortex (Navaroli et al., 2011). In addition, our preliminary observation shows long-lasting persistent firing in hippocampal CA1 and CA3 pyramidal cells in rats (unpublished observation by Beate Knauer and Arthur Jochems).

There is debate as to whether or not synaptic transmission is necessary for persistent firing (Major and Tank, 2004). For example, persistent firing observed as an "UP" state in a slice model of cortical SWS oscillation is dependent on intact AMPA and NMDA synaptic transmission (Shu et al., 2003). On the other hand, evidence suggests that persistent firing observed in brain slices from many of the MTL areas is driven by mechanisms intrinsic to individual neurons. Persistent firing can be observed in the presence of ionotoropic glutamatergic and $GABA_A$ synaptic blockers in the entorhinal cortex, postsubiculum, and perirhinal cortex (**Figure 2A**; Egorov et al., 2002; Yoshida and Hasselmo, 2009a; Navaroli et al., 2011). In addition, persistent firing is blocked in the absence of calcium (**Figure 2B**) or by the CAN current blocker flufenamic acid in these three areas (**Figure 2C**; Egorov et al., 2002; Tahvildari et al., 2008; Yoshida and Hasselmo, 2009a; Zhang et al., 2011; Navaroli et al., 2011). Furthermore, activation of muscarinic receptors (Egorov et al., 2002; Navaroli et al., 2011) and phospholipase Cβ (PLCβ; Zhang et al., 2011), which leads to CAN current activation, are shown to be necessary for the induction of persistent firing. As for the molecular correlates of the CAN current, it has been shown that transient receptor potential cation (TRPC) channels underlie the CAN current (Tai et al., 2010; Zhang et al., 2011; reviewed by Reboreda et al., 2011). These observations strongly suggest that

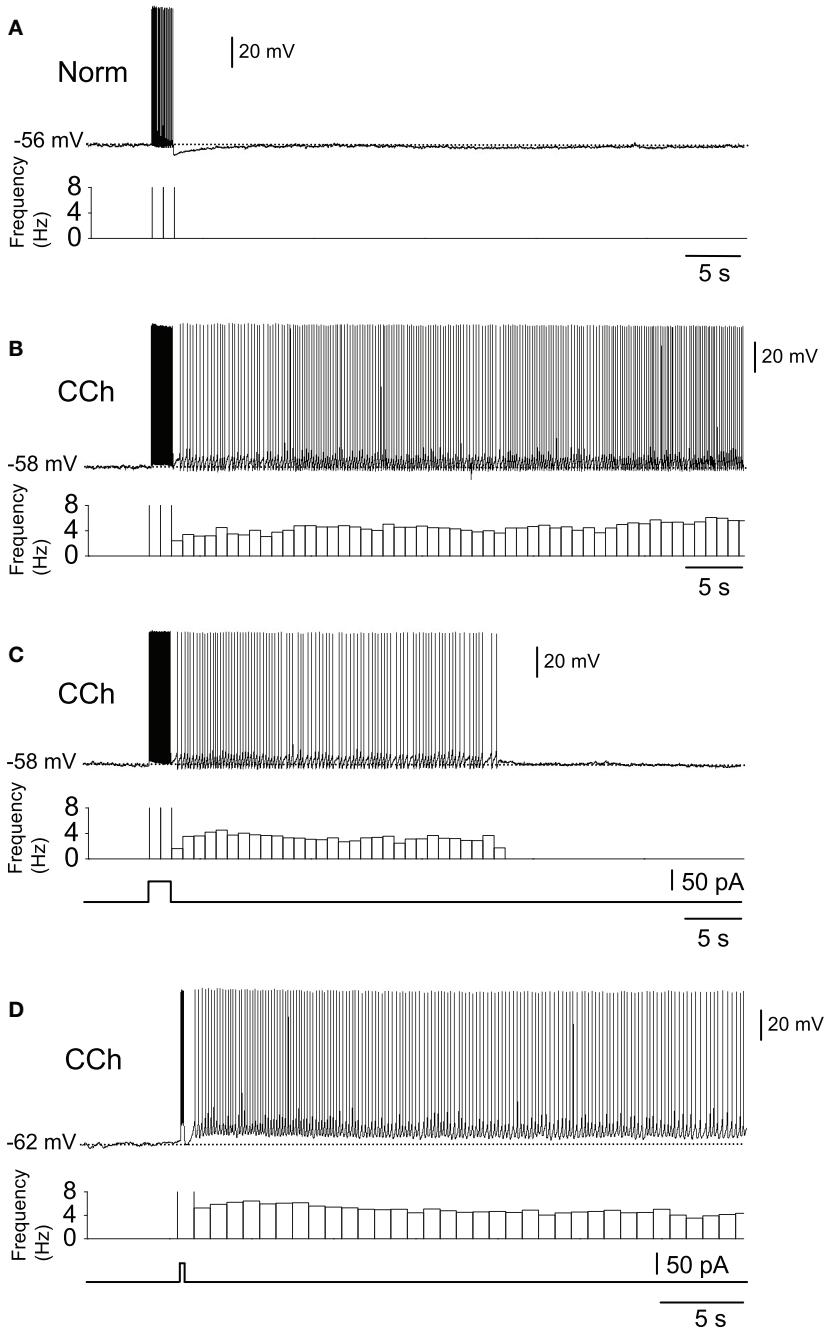


**FIGURE 1 |** ***In vitro*** **recordings of persistent firing in the rat postsubiculum. (A)** In the normal ACSF without the cholinergic receptor agonist carbachol, a brief current injection (2 s, 50 pA) elicited action potentials only during stimulation. **(B)** Long-lasting persistent firing. In the presence of carbachol (10 μM), the same current injection caused stable sustained firing lasting several minutes. **(C)** Self-terminating persistent firing. Under the same conditions as in **(B)**, some cells showed persistent firing that lasted for less than 30 s. **(D)** Persistent firing induced by shorter stimulation. In the postsubiculum, 200 ms of stimulation was often enough to elicit long-lasting persistent firing. Norm, Normal ACSF; Cch, carbachol. Modified from Yoshida and Hasselmo (2009a).

many MTL neurons can exhibit persistent firing through intrinsic cellular mechanisms. In an *in vivo* condition, both this intrinsic mechanism and the synaptic mechanism may contribute to persistent firing.

## MORE PHYSIOLOGICAL INDUCTION OF PERSISTENT FIRING

Several studies have tested detailed properties of persistent firing in the MTL to estimate its contribution to the function of the MTL. As described in detail in "Possible Roles of CAN Current

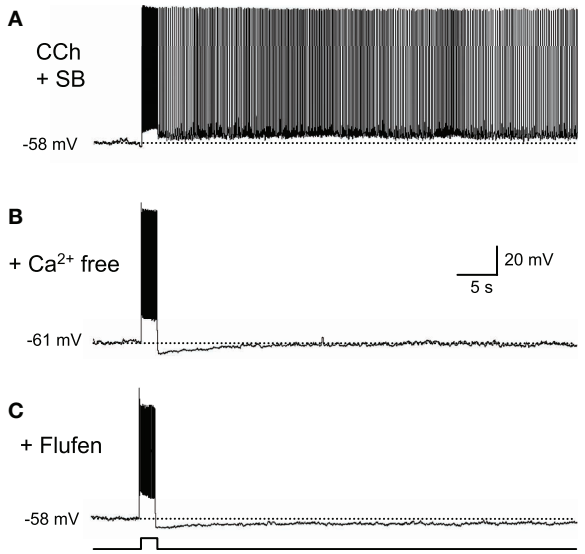


**FIGURE 2 | Intracellular mechanism supports persistent firing.** **(A)** Long-lasting persistent firing observed in synaptic blockers. Ionotropic glutamate (kynurenic acid) and $GABA_A$ (picrotoxin) blockers were used. **(B)** Persistent firing was not observed in the absence of calcium in ACSF. **(C)** CAN current blocker flufenamic acid blocked persistent firing. These results suggest that neurons in the postsubiculum have an ability to induce persistent firing with intrinsic mechanisms to the cells. SB, synaptic blockers; Flufen, flufenamic acid. Modified from Yoshida and Hasselmo (2009a).

in Active Maintenance of Memory in MTL," the MTL areas are important for trace conditioning tasks (Kim et al., 1995; Weiss et al., 1999; McEchron et al., 2000; Tseng et al., 2004; Kholodar-Smith et al., 2008; Esclassan et al., 2009) where an animal needs to associate two stimuli which are separated by a trace period (a few hundred milliseconds to tens of seconds). For the animal to acquire this task, information from the first stimulus (conditioned stimulus; CS) has to be maintained during the trace period until the second stimulus (unconditioned stimulus; US) is delivered. *In vivo* single unit recordings show persistent firing in a sub-population of hippocampal CA1 neurons during the trace period (Solomon et al., 1986; McEchron et al., 2001, 2003) and the intrinsic persistent firing supported by the CAN current has been suggested to underlie this *in vivo* persistent firing (Fransén et al., 2002).

Since the duration of the CS is only a few hundreds of milliseconds in some trace conditioning tasks, an induction of persistent firing by a stimulation with comparable duration was tested. It has been shown that in the entorhinal cortex and in the postsubiculum, a current pulse, as short as 300 and 200 ms, respectively, is sufficient to induce persistent firing (Egorov et al., 2002; Yoshida and Hasselmo, 2009a). In the case of the postsubiculum, a 200 ms current injection, which elicited only several spikes, drove persistent firing in more than 60% of cells (**Figure 1D**; Yoshida and Hasselmo, 2009a), suggesting that a physiological level of excitation is sufficient to induce persistent firing.

Persistent firing can also be initiated using synaptic stimulation instead of current injection in the entorhinal cortex (Egorov et al., 2002; Tahvildari et al., 2007; Yoshida et al., 2008). In addition, it has been suggested that an endogenous level of acetylcholine is sufficient for the induction of persistent firing in the amygdala (Egorov et al., 2006). In this study, cholinergic afferent fibers were stimulated instead of applying a cholinergic agonist to the brain slice preparation. Stimulation of the cholinergic afferent and subsequent brief current injection triggered persistent firing in principal neurons in the amygdala.

Persistent firing observed *in vivo* is typically terminated as the US is delivered. In *in vitro* studies, it has been shown that persistent firing can be terminated through hyperpolarization by current injection in layer V cells in the MEC and in cells in the perirhinal cortex (Egorov et al., 2002; Reboreda et al., 2007; Navaroli et al., 2011), suggesting that inhibitory synaptic input could be used to terminate persistent firing. Interestingly, in layer III of the LEC, persistent firing can be terminated by an application of a second positive current injection or synaptic stimulation (**Figure 4B**; Tahvildari et al., 2007) suggesting that different areas in the MTL might employ different means to terminate persistent firing.

An additional interesting feature of intrinsic persistent firing is the "integration" mechanism. In cells in the MEC layer V, perirhinal cortex and amygdala (Egorov et al., 2002, 2006; Navaroli et al., 2011), repeatedly applied current pulse stimulation increased the frequency of persistent firing in a step-like manner after each stimulation. Therefore, past sequences of stimulation in individual cells could be "integrated" into the current frequency of the persistent firing.

## LONG-LASTING PERSISTENT FIRING IN THE HIPPOCAMPUS

Although many earlier studies of the CAN current were performed in hippocampal pyramidal cells, there has been no clear evidence for long-lasting persistent firing in this type of cell. Fraser and MacVicar (1996) reported short-lasting plateau potential in CA1 pyramidal cells using relatively high (20 μM) concentration of carbachol and current injection. In this study, pyramidal cells typically showed strong depolarization beyond the spike threshold where action potentials were not repeatedly elicited, as a response to the current injection (800 ms). After the current injection, this plateau potential typically lasted for only several seconds before the membrane potential went back to the pre-stimulus level. In our laboratory we tested whether stable, long-lasting persistent firing could be elicited in hippocampal CA1 and CA3 pyramidal cells *in vitro*. In the presence of a lower concentration of carbachol (10 μM), a subset of CA1 and CA3 pyramidal neurons showed long-lasting persistent firing, up to a few minutes, similar to the persistent firing in the MEC (unpublished observation by Beate Knauer and Arthur Jochems).

Recently, long-lasting persistent firing has been found in hippocampal inhibitory interneurons (Sheffield et al., 2011). The mechanism for the induction of this persistent firing in interneurons seems to be very different from those in principal neurons. Persistent firing in interneurons does not require cholinergic receptor activation or calcium, indicating that the CAN current is not involved. However, this type of persistent firing requires intact gap junctions. In addition, induction of persistent firing requires repetitive stimulation for tens of seconds to minutes, suggesting

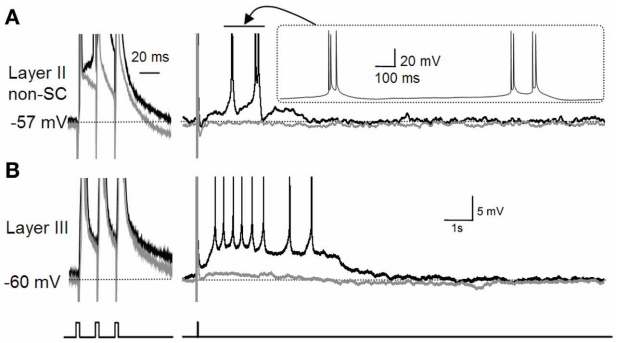


**FIGURE 3 | Effect of M-current suppression on persistent firing. (A)** The effect of the M-current in layer II non-stellate cells in the MEC. **(B)** The effect of the M-current in layer III pyramidal cells in the MEC. Suppression of the M-current by linopirdine revealed a plateau potential after three induced spikes in both types of neurons with different firing properties. Layer II non-stellate cells fired in a high-frequency burst while layer III cells fired regularly during plateau potential. Gray traces are control recordings and black traces are recordings in linopirdine. non-SC, non-stellate cell. Figures were modified from Yoshida and Alonso (2007).

that persistent firing in interneurons could be more suitable for excitability control than short-term maintenance of information.

### MODULATION OF OTHER NEURAL PROPERTIES BY ACETYLCHOLINE

It is worth noting that the effect of acetylcholine is not limited to the modulation of the CAN current. As briefly mentioned above, acetylcholine suppresses the M-current and the calcium-activated potassium current (Reviewed by Giocomo and Hasselmo, 2007). Suppression of the potassium currents may enhance the depolarization of the membrane potential by the CAN current. In fact, in the entorhinal cortex, suppression of the M-current revealed a plateau potential and self-terminating persistent firing (**Figure 3**; Yoshida and Alonso, 2007). This persistent firing was probably due to an endogenously active CAN current which was not visible in the presence of the M-current as the M-current was masking this inward current.

An additional well-established effect of cholinergic activation is the modulation of synaptic properties (Hasselmo, 1999; Giocomo and Hasselmo, 2007). First, synaptic plasticity is enhanced under cholinergic stimulation (Sugisaki et al., 2011). Second, synaptic conductance is suppressed in a systematic manner by acetylcholine (Hasselmo, 1999; Giocomo and Hasselmo, 2007). Interestingly, acetylcholine suppresses intrinsic synaptic transmission more strongly than afferent synapses. For example, excitatory synaptic connections within the hippocampus, such as the Schaffer collateral and CA3 recurrent connections, are strongly suppressed by cholinergic activation (Hasselmo and Schnell, 1994; Kremin and Hasselmo, 2007).

## POSSIBLE ROLES OF CAN CURRENT IN ACTIVE MAINTENANCE OF MEMORY IN MTL

### MTL SUPPORTS ACTIVE MAINTENANCE OF MEMORY

The MTL has long been known for its role in long-term memory (Squire, 1992). However, there are also many recent reports that support a role of the MTL in short-term memory retention, where the duration ranged from a few seconds to tens of seconds (Hannula et al., 2006; Olson et al., 2006; Hartley et al., 2007; Cashdollar et al., 2009). Some authors have suggested that such short-term retention might bridge the gap between two temporally separated events to form sequential memory (Wallenstein et al., 1998; Naya and Suzuki, 2011).

Although evidence for the involvement of the MTL in short-term memory in humans is relatively new, animal studies have long been suggesting its role in short-term memory retention. Strong evidence for this comes from the trace conditioning paradigm which is a subtype of classical conditioning. In this task, animals need to maintain the information about the CS until the US arrives in order to learn the association between the CS and the US. Animals with a lesion to the hippocampus, entorhinal cortex, or perirhinal cortex are impaired in this type of task (Kim et al., 1995; Weiss et al., 1999; McEchron et al., 2000; Tseng et al., 2004; Kholodar-Smith et al., 2008; Esclassan et al., 2009). More importantly, lesioned animals can learn the same conditioning task if the trace period is removed (delay task where CS and US were continuous in time; Kim et al., 1995; Weiss et al., 1999; McEchron et al., 2000; Tseng et al., 2004; Bangasser et al., 2006; Kholodar-Smith et al., 2008; Bang and Brown, 2009; Esclassan et al., 2009). These studies indicate that the MTL is necessary, particularly when a temporal gap exists between two stimuli (e.g., trace paradigm).

As with the trace conditioning task, the MTL, including the hippocampus and the entorhinal and perirhinal cortices, is crucial in delayed non-match to sample (DNMS) tasks in both non-human primates (Squire and Zola-Morgan, 1991) and rats (Otto and Eichenbaum, 1992a,b). The DNMS task is similar to the trace conditioning task in that the animal needs to maintain information of the first stimulus until the second stimulus arrives.

Involvement of the MTL in short-term memory retention can also be found in other experimental paradigms. In a spatial alternation task where rats were required to continuously turn right and left alternately in a T-shaped maze, both rats with and without hippocampal lesion performed well (Wood et al., 2000; Ainge et al., 2007). However, when a delay period of 2 or 10 s was introduced, during which the rats needed to wait before turning, this task required intact hippocampus (Ainge et al., 2007). Consistent with this, object-odor association task with temporal gap (10 s; Kesner et al., 2005), temporal sequence task (Gilbert et al., 2001), spatial choice task with 10 s of delay for rewards (Mikulka and Freeman, 1975; Rawlins et al., 1985), non-spatial sequence learning with 3 s and 10 s delay (Farovik et al., 2009), are all shown to be hippocampal-dependent. Many of these tasks become hippocampal-independent when the delay period is removed (Mikulka and Freeman, 1975; Rawlins et al., 1985; Gilbert and Kesner, 2002; Ainge et al., 2007). In summary, the MTL areas are crucial for tasks that require short-term memory.

### CHOLINERGIC DEPENDENCE OF SHORT-TERM MEMORY TASKS

Suppression of cholinergic transmission in the dorsal hippocampus and entorhinal cortex impairs trace conditioning task performance in rats, while the same task without trace period is not impaired (McGaughy et al., 2005; Bang and Brown, 2009;

Pang et al., 2010). Administration of a cholinergic antagonist impairs delayed-matching-to-sample task performance in monkeys (Penetar and McDonough, 1983). Moreover, Anagnostaras et al. (2003) have shown that M1 muscarinic cholinergic receptor KO mice are impaired in a working memory task with a delay period, but not in spatial learning which did not involve delay. In addition, a cholinergic blockade was found not only to impair the acquisition of these tasks, but also to reduce hippocampal activity during trace periods in humans (Schon et al., 2005). Finally, in rats, memory performance on a delay task was disrupted by lesion to the septum, which provides cholinergic afferent fiber to the MTL (Rawlins et al., 1985). These results suggest an important role of the cholinergic system in short-term memory retention.

## PERSISTENT FIRING MAY CONTRIBUTE TO SHORT-TERM MEMORY

Sustained increased activity in MTL areas has been observed in the trace period of trace conditioning tasks, or during the delay period of DNMS tasks, using *in vivo* electrophysiological recordings in animals, and using fMRI in humans. For example, hippocampal CA1 pyramidal cells show persistent firing over 30 s during the delay period in a DNMS task in monkeys and rats (**Figure 4A**; Colombo and Gross, 1994; Hampson et al., 2004; Deadwyler and Hampson, 2004). In addition, a similar increase in the firing rate during the delay period has been observed in the entorhinal cortex in rats and monkeys in a similar task (Suzuki et al., 1997; Young et al., 1997).

Similarly, increased firing frequency has been shown during the trace period of the trace conditioning paradigm in the hippocampus in rabbits (Solomon et al., 1986; McEchron et al., 2001, 2003). Interestingly, these studies have also shown that the number of cells that responded to the delay period decreased as the animals' performance improved, while the number of cells that responded to CS and US did not change (Solomon et al., 1986; McEchron et al., 2001). This suggests that the delay period activity, but not CS or US activity, may contribute to task performance improvement. Moreover, aged animals that were impaired in acquiring this trace conditioning task, showed significantly fewer cells responding during the delay period (McEchron et al., 2001). These results suggest that sustained firing activity of the hippocampal neurons is necessary for acquiring this type of task.

Finally, in humans, fMRI imaging studies showed increased neuronal activity during the delay period (Schon et al., 2004; Olsen et al., 2009), despite relatively poor temporal and spatial resolution compared to *in vivo* electrophysiological recordings. In a human MEG study, it has been suggested that the hippocampus plays a pivotal role in synchronizing multiple brain areas at theta frequency during the delay phase of delayed-match-to-sample (DMS) tasks (Cashdollar et al., 2009). In summary, persistent activity observed in the MTL seems to be important for short-term memory tasks.

## COMPUTATIONAL MODELS OF ACTIVE MAINTENANCE BY THE CAN CURRENT

Using computational simulation of a network of neurons with the CAN current, Fransén et al. (2002) have shown that the CAN current may allow sustained spiking in the entorhinal cortex which was robust to noise. Another line of research asked how multiple stimuli, that are presented sequentially one after another, can be stored as short-term memory without losing the sequence in which the stimuli were presented (Lisman and Idiart, 1995; Jensen and Lisman, 1996; Koene and Hasselmo, 2008). In these models, each memory trace was stored by one neuron that showed persistent firing in a theta frequency (4–14 Hz) due to the CAN current kinetics. Although each cell showed persistent firing at the same frequency, these neurons fired at slightly different timings from each other with a specific delay, which was equal to one gamma cycle (∼40 Hz; Lisman and Idiart, 1995; Jensen and Lisman, 1996). Koene and Hasselmo (2008) further suggested that memory items in the nested theta and gamma model can

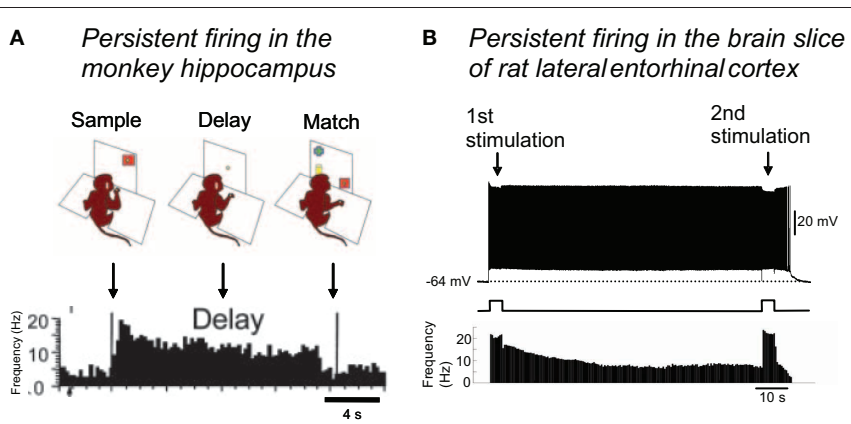


**FIGURE 4 | Persistent firing as the mechanism for short-term memory function of the MTL. (A)** Persistent firing recorded in monkey hippocampus during a delayed match-to-sample task. Some neurons in the hippocampus continued firing throughout the delay period, when the monkey needed to retain a piece of information presented at the sample phase. **(B)** In the brain slice preparation of lateral entorhinal cortex, brief (4 s) stimulation can trigger persistent firing supported by the CAN current. This persistent firing could be terminated by a second brief stimulation. Note the very similar time course of spike frequencies in *in vivo* and *in vitro* recordings. Single cell level persistent firing in the MTL could support short-term memory tasks. Figure in **(A)**: modified from Hampson et al. (2004). Figure in **(B)**: Tahvildari et al. (2007). Figure was re-drawn from original recording.

be updated with physiological mechanisms upon arrival of a new stimulation. In this model, CAN current activity set the persistent firing in the theta frequency range, and the gamma rhythm was set by an interneuron network. In these computational models, the persistent firing driven by the CAN current played an important role in short-term memory retention. These computational studies, therefore, support the idea that the CAN current driven persistent firing could support short-term memory function in the MTL.

## POSSIBLE ROLES OF CAN CURRENT IN SPATIAL NAVIGATION

In this section, we first introduce evidence that suggests requirement of short-term memory for spatial navigation. Second, we describe previously proposed and possible roles of CAN current-driven persistent firing in spatial navigation.

### SPATIAL NAVIGATION AND SHORT-TERM MEMORY

Since the discovery of place cells whose activity corresponds to the location of an animal (O'Keefe and Dostrovsky, 1971), studies in this field have revealed a vast amount of knowledge as to how spatial information is represented in the MTL (See Moser et al., 2008 for review). One may see the activity of head direction cells, grid cells, or place cells as a representation that is simply the sum of incoming sensory inputs. However, evidence suggests that this is not the case.

In daily life, we may need to walk into an underground subway station with very limited spatial cues, go through staircases with turns, come out through another exit and then resume walking in the direction in which we were originally going. To do this successfully, we need to maintain a sense of direction, even when we cannot see landmarks outside the station that could guide us. This issue has been explored in animal studies. Head direction cells in the postsubiculum in rats (Ranck, 1984; Taube et al., 1990a,b; Sharp, 1996; Boccara et al., 2010) continuously fire as long as the animal's head is pointed in the preferred direction of the cell. More importantly, they do not stop firing, even in total darkness, as long as the direction of the head points toward the preferred direction of the cell, although the direction tuning of the head direction cells gradually diverges from the original (Taube et al., 1990b; Goodridge et al., 1998). Therefore, the head direction system must have a means to actively maintain its firing to form an internal representation. This internal representation is thought to be updated by occasional self-motion cues such as angular velocity signals when spatial cues are absent (McNaughton et al., 1991; Skaggs et al., 1995; Redish et al., 1996; Goodridge and Touretzky, 2000; Boucheny et al., 2005; Song and Wang, 2005).

Similarly to the head direction cells, grid cells in the MEC, and place cells in the hippocampus, do not disappear in darkness for a certain duration (Quirk et al., 1990; Hafting et al., 2005; McNaughton et al., 2006). This suggests that animals can update their internal representation by self-motion cues. This ability is called path integration (McNaughton et al., 1991, 2006). Firing of grid cells and place cells cannot be explained solely by visual information, even under normal light conditions. Many grid cells in MEC layer II, and place cells in the hippocampus, are not sensitive to the current head direction of the animal (Muller et al., 1994; Sargolini et al., 2006). Since the animal's visual sensory inputs will differ, according to the head direction, even at the same location, firing of these cells cannot be a simple sum of sensory inputs. Rather, spatial representation seems to involve the integration of different types of sensory information, from the past and present, which leads to an allocentric representation of the space. In this sense, spatial representation is also based on short-term memory function (Bird and Burgess, 2008).

### POSSIBLE CONTRIBUTION OF CAN CURRENT IN COMPUTATIONAL MODELS OF SPATIAL REPRESENTATION

There are two distinct computational models of spatial representation: the oscillatory-interference model and the attractor-network model (reviewed by Giocomo et al., 2011). The oscillatory-interference model of place cells and grid cells uses multiple oscillators, with slightly different frequency within a theta frequency range, impinging on to a single neuron to give rise to a spatial representation (O'Keefe and Recce, 1993; O'Keefe and Burgess, 2005). When the oscillators are in phase, this neuron fires action potentials. When oscillators are not in phase, inputs from these oscillators will be subthreshold, and do not lead to action potentials. Spatial information in this model is, therefore, maintained in phases of these independent oscillators. As for the physiological correlates of the oscillators in this model, subthreshold membrane potential oscillations (SMPOs) or persistent firing has been shown to work in computational models (Hasselmo, 2007; Hasselmo et al., 2010). In the case of persistent firing, oscillatory frequency is defined as the frequency of persistent firing, driven by the CAN current. Oscillatory-interference models with SMPOs can replicate the increasing grid spacing along the dorso-ventral axis of the MEC found *in vivo* (Hafting et al., 2005), if the SMPO frequency gradient along the dorso-ventral axis found in *in vitro* intracellular recordings (Giocomo et al., 2007; Garden et al., 2008; Yoshida et al., 2011) is taken into account. On the other hand, the oscillatory-interference model is sensitive to disturbance, because a slight change in the phase of any of the oscillators affects spatial representation (Zilli et al., 2009). This sensitivity to noise, however, could be dramatically reduced if the oscillators are coupled by a synaptic network (Zilli and Hasselmo, 2010).

In contrast, the continuous attractor model does not require oscillators. Conceptually, activity of sub-population of cells in the network is a stable state in continuous attractor models. One way to implement this is to assume that neurons located close to each other in a network are connected with recurrent excitatory synapses, and that all cells receive global inhibition (e.g., Tsodyks and Sejnowski, 1995). This means that once a group of neurons starts firing, this firing can be maintained as a "bump" of activity, because the excitatory recurrent connections will keep this group of cells active, while inhibitory connections will keep the other neurons silent. The bump of activity is, therefore, a type of persistent firing supported by synaptic transmission, which will actively maintain the current location of the animal in the absence of sensory inputs in this model.

The head direction system in the postsubiculum is often modeled as a one dimensional attractor-network with excitatory synaptic connections among nearby head direction cells

(Skaggs et al., 1995; Redish et al., 1996; Zhang, 1996; Goodridge and Touretzky, 2000). However, based on the lack of strong support for excitatory connections, models with inhibitory connections alone have been proposed (Rubin et al., 2001; Boucheny et al., 2005; Song and Wang, 2005). These recent models assumed external excitatory inputs to ensure persistent firing of head direction cells. However, the origin of the spontaneous firing or the external inputs used in these models is unclear. Similarly to the head direction system in the postsubiculum, evidence for strong recurrent excitatory synaptic connections is lacking in the MEC layer II network, where grid cells were originally discovered, and in the hippocampal CA1 region, where place cells were originally discovered.

As described above, it has recently been shown that neurons in the postsubiculum have an ability to show persistent firing through the activation of the CAN current, independently from the synaptic connections (**Figures 1** and **2**; Yoshida and Hasselmo, 2009a). This mechanism could be used in the models of the head direction system with inhibitory synaptic connections alone (Rubin et al., 2001; Boucheny et al., 2005; Song and Wang, 2005). In addition, MEC layer II cells (Yoshida and Hasselmo, 2009b) and hippocampal CA1 cells (unpublished observation by Beate Knauer) both have the CAN current driven persistent firing. Therefore, the intrinsic persistent firing through the CAN current could be an ideal mechanism for the attractor model to work when recurrent excitation is limited.

## SWITCHING BETWEEN REAL-TIME AND TIME-COMPRESSED SEQUENTIAL ACTIVITY BY THE CAN CURRENT: A THEORETICAL MODEL

In this section, we first review evidence for the cholinergic system to switch brain states, and describe the firing pattern of hippocampal place cells in different brain states. We then propose a new model where the CAN current is used to switch the sequential firing speed from fast (time-compressed) to slow (real-time), upon activation. Finally, we discuss our model and our interpretation of the model.

### EVIDENCE THAT SUPPORTS SWITCHING OF INTERNAL DYNAMICS

The acetylcholine level is high during active waking and low during SWS in the rat hippocampus and in the cat cortex (Kametani and Kawamura, 1990; Marrosu et al., 1995). The level of acetylcholine is even higher during sustained attentional tasks (Himmelheber et al., 2001; Arnold et al., 2002) and lower during quiet waking (Kametani and Kawamura, 1990). The change in the level of acetylcholine is accompanied by changes in EEG activity, where low acetylcholine during sleep is associated with slow-wave activity, and high acetylcholine during the active waking state is associated with theta rhythm in the hippocampus (Green and Arduini, 1954; Winson, 1974). This clearly suggests that the level of acetylcholine modulates neural activity.

Modeling studies have suggested that the hippocampal synaptic network is modified during active waking in such a way that synaptic connections from place cells which fired earlier in the sequence, to those fired later, were potentiated (Jensen and Lisman, 1996; Wallenstein et al., 1998). Since the synaptic transmission usually takes from only a few milliseconds to tens of milliseconds, multiple place cells were activated in a time-compressed sequence during SWS.

A recent study by Dragoi and Tonegawa (2011) may have changed this traditional view that the sequence of place cells only exists after experiences in the maze. This study showed that time-compressed sequential activity of CA1 pyramidal cells during SWS, before the first run in a novel environment, matched well with the sequence of place cell activity during this first run. Such activity during SWS is called "preplay" and this result indicated that the sequential synaptic connections that favored a specific sequence existed even before the rats experienced the new environment, and this existing sequence was used to code the new environment. In other words, place cell firing was strongly influenced by existing synaptic connections, not only during SWS, but also during active waking.

Another line of research that suggests the importance of synaptic connections or internal dynamics during active waking is the "time cell" studies (Pastalkova et al., 2008; MacDonald et al., 2011). In these studies, recordings from sets of CA1 pyramidal cells showed sequential firing during the delay phase of memory tasks. During the delay period, rats were either running in a running wheel (Pastalkova et al., 2008) or waiting in a small confined area (MacDonald et al., 2011). In both tasks, each CA1 pyramidal cell always fired at a specific time after the onset of the delay period. The duration of the "field" was very similar to that of the place cells, and theta phase precession was also observed. Since there seems to be no particular sensory input that changes with time during the delay period, this sequential firing is believed to be generated internally. Although there is no experimental support for this, one hypothesis is that a synaptic network supports this sequential firing.

These recent studies suggest that sequential firing of hippocampal pyramidal cells can be supported by internal mechanisms such as synaptic connections, both in time-compressed scale during SWS and quiet waking, and in real-time scale during active waking. However, to date, it remains unclear how time-compressed (fast) and real-time (slow) sequential activity can be switched. In the next section of the paper, we propose that different levels of acetylcholine in active waking and SWS could modulate the CAN current and that the CAN current sets the temporal scale of sequential activity.

### CAN CURRENT-BASED TIME SCALE SWITCH MODEL

In this conceptual model, we aim to explain the switching between fast and slow sequential activity by taking two cholinergic modulations of cellular properties into account: (1) the modulation of the CAN current and (2) the modulation of synaptic strength. We consider four place cells (or groups of cells, A to D) which have overlapping place fields. **Figure 5** shows the activity of these place cells during SWS (**Figure 5A**) and while running (**Figure 5B**). Based on the observation by Dragoi and Tonegawa (2011) mentioned above, we assume that these four place cells are sequentially connected through excitatory synapses (A to B, B to C, etc.).

First, in the SWS condition where the acetylcholine level is low, synaptic potential will be relatively large due to the lack of synaptic suppression (Hasselmo, 1999). Therefore, when cell A elicits some action potentials due to random input, this will cause

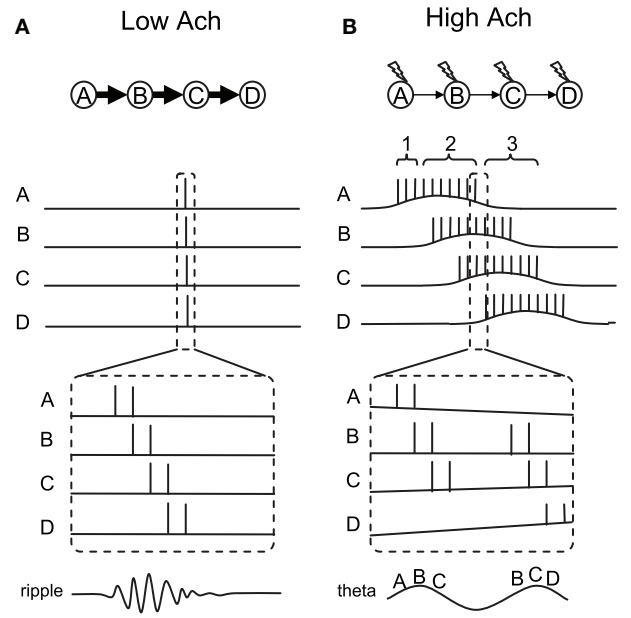


**FIGURE 5 | Conceptual model of dynamics switching.** Place cells A–D are sequentially connected by asymmetric synaptic connections. **(A)** Place cell firing in slow-wave-sleep and quiet waking with low acetylcholine. In this mode, strong synaptic transmission enables neural activity to propagate fast and activate all place cells sequentially within a few hundred milliseconds. **(B)** Place cell firing in active waking with high acetylcholine. In this mode, synaptic transmission is suppressed. However, a few spikes in each neuron activate the CAN current and drive persistent firing. Persistent firing will eventually cause enough temporal summation of EPSP in the cell downstream in the sequence. Sequential firing will occur at a much slower time scale compared to **(A)** because each neuron needs to activate the CAN current and drive persistent firing. Thick and thin arrows show strong and weak synaptic transmissions, respectively. Lightning signs in **(B)** show cholinergic receptor activation.

a large excitatory postsynaptic potential (EPSP) in cell B which receives synaptic input from cell A. This EPSP will trigger action potentials in cell B. Similarly, cell C and D will fire a couple of action potentials due to propagation of the activity through the synaptic connections. Since synaptic transmission by AMPA and NMDA components takes only from a few to tens of milliseconds, this sequential firing of cells A to D will occur within a few hundreds of milliseconds (duration of one or a few ripples). Because of the low acetylcholine level, action potentials in each cell will not activate the CAN current and, therefore, will not elicit persistent firing (**Figure 1A**). This fast sequential firing corresponds to replay or preplay during SWS.

Second, in the active waking condition when the acethylcholine level is relatively high, intrinsic synaptic transmission is suppressed (Giocomo and Hasselmo, 2007; Kremin and Hasselmo, 2007), even though the same synaptic connections exist. Therefore, when cell A fires a couple of spikes, this will not provide enough EPSP to immediately trigger firing of cell B (see time indicated by bracket 1 in **Figure 5B**). However, spikes of cell A will bring calcium into the cell, activate the CAN current and depolarize the membrane to trigger more spikes within cell A (time indicated by bracket 2 in **Figure 5B**). This does not happen in the absence of acetylcholine, because CAN current activation requires both cholinergic receptor activation and calcium entry, as described earlier. This repetitive firing will eventually cause enough temporal summation of EPSP for cell B to elicit action potentials. Similarly, cells C and D will be activated sequentially. In contrast to the SWS condition, activation of the CAN current in each cell is required for the activity to be propagated to the next cell in the sequence in the active waking stage. Therefore, the sequence is read out slower and each cell fires for a longer duration compared to that in the SWS condition.

As described above, persistent firing driven by the CAN current can be observed either as self-terminating persistent firing (**Figure 1C**), or long-lasting persistent firing (**Figure 1B**). If the cells develop self-terminating persistent firing, this model may not require any additional mechanism. However, if the cells develop long-lasting persistent firing, our model needs an additional mechanism to terminate the firing. As described above, long-lasting persistent firing can be terminated by hyperpolarization (Egorov et al., 2002; Navaroli et al., 2011). Such hyperpolarization could be provided by lateral inhibition. For example, for cell A in the model, cell B will not inhibit cell A, but cells C and D will inhibit cell A. This will terminate cell A's firing and deactivate the CAN current.

### THETA PHASE PRECESSION

*In vivo* electrophysiological recordings show that there is a particular relationship between the spike timing of place cells and the phase of local theta rhythm during active exploration. As the animal enters the place field, place cells initially fire in a late phase of the field theta rhythm, and progressively advance to an earlier phase as the animal goes through the place field (O'Keefe and Recce, 1993; Skaggs et al., 1996). This phenomenon is called "phase precession" and this can also be seen in our conceptual model. First of all, neurons tend to fire in a theta frequency range during CAN current-driven persistent firing. Therefore, we assume that neurons in our model fire in a theta frequency within its place field. Here, we explain the precession using **Figure 5B**, where one part of the activity within the dashed lines is magnified at the bottom.

Although synaptic connections are suppressed during active waking, EPSPs still exist to a smaller degree. Therefore, when two neurons (for example A and B) fire at locations where their fields overlap, neuron B will more likely spike on top of the EPSP due to the spiking of cell A. This causes cells that are in their overlapping place fields to fire sequentially within a theta cycle, in a time-compressed mode, as shown in *in vivo* data (Skaggs et al., 1996). This can be imagined as place cells A, B, and C firing sequentially in a time-compressed mode in every theta cycle as long as the animal's location is where those three fields overlap. However, as the animal walks toward the place field D, place cell D starts firing. At the same time, place cell A may stop firing since the animal is now outside the place field A. As a result, the time-compressed sequence of A-B-C will now change to B-C-D. The dashed lines in **Figure 5B** depict this shift from sequence A-B-C to B-C-D. The left half of the figure shows the activity of the cells at the end of the place field A, before the place cell D starts to fire. In this case, cells A-B-C fire sequentially as shown by the letters at the bottom of the

magnified traces. The right half of the figure shows the activity of the cells immediately after this, where place cell A stops firing and place cell D starts firing. In this case, cells B-C-D fire sequentially. As a result, the firing order of cell B, for example, precessed from second place in A-**B**-C to first place in **B**-C-D. This mechanism, therefore, allows place cells to shift their firing order toward an earlier position among the population of place cells that are currently firing, due to an overlap of place fields as the animal runs through the field.

We next argue that an earlier firing position in the population of cells is linked to theta phase precession, using the illustrated theta wave at the bottom of **Figure 5B**. As pointed out by Geisler et al. (2010), field theta rhythm could reflect population activity of neurons. This means that the population of place cells that is currently firing, due to overlapping place fields, sets the theta rhythm. In our model, this population of cells is, for example, cells A-B-C, where the firing timing of place cells A, B, and C correspond to early, mid and late phase of field theta rhythm, respectively. The illustrated theta rhythm in **Figure 5B** (bottom) reflects the population activity. Since place cells that are in the middle of their place fields fire more spikes than others, the resulting field potential increases toward the middle of the sequence. For example, when the animal is in the middle of place field B, place cell B fires with a higher frequency than other cells and causes a peak of the theta rhythm (**Figure 5B** bottom left). When the population of cells changes from A-B-C to B-C-D, firing of place cell B now corresponds to an early phase of the field theta rhythm (**Figure 5B**, bottom right). Firing of cell B, for example, therefore shifts from the later phase of theta to the earlier phase of theta. Our model shows theta phase precession in a similar way to that proposed by Geisler et al. (2010).

#### DIFFERENCE FROM ATTRACTOR-NETWORK MODEL

The active waking stage in our model is similar to the attractor-network model of place cells in that both models have an ability to maintain activity of groups of neurons. The means to maintain activity is, however, different. While most attractor-network models rely on an excitatory recurrent network among cells, our model relies on the CAN current activation, which is intrinsic to many types of cells in the MTL. While dense excitatory recurrent connections are found in the hippocampal CA3 area, such excitatory connection in CA1 or EC layer II does not seem to be abundant (Tamamaki and Nojyo, 1990; Witter and Amaral, 1991; Kumar et al., 2007; Quilichini et al., 2010). Our model does not rely on excitatory recurrent connections to produce a bump of activity; rather it uses recurrent connections to code sequences. Therefore, less excitatory recurrent connections available in the CA1 area may not be enough for the maintenance of the bump activity. However, it could still be enough to code the sequence when the maintenance of activity is done by the CAN current which is intrinsic to individual cells.

In addition, while the attractor model is prone to the problem of runaway excitation, and often needs global inhibition to keep the cellular activity in a reasonable firing frequency range, the CAN current bump could be relatively resistant to the problem of runaway excitation, since the amount of CAN current limits the maximum firing frequency in individual neurons.

#### AWAKE REPLAY

It has been shown that ripple activity occurs during quiet waking, as well as in SWS, and temporally compressed replay of either forward or backward sequence can be observed during ripples (Foster and Wilson, 2006). As described earlier, the acetylcholine level is reported to decrease during quiet waking. Recent observations of acetylcholine level measurements show that the acetylcholine level can be modulated in the order of seconds in the prefrontal cortex (Parikh et al., 2007). Network dynamics could, therefore, be set for time-compressed replay transiently during quiet waking. As for the direction of replay, our model can account for this if we assume that the synaptic connections are strengthened both in forward (A-B-C-D) and backward directions (D-C-B-A). Such connections could be realistic due to modified spike-timing-dependent synaptic plasticity (STDP) in high acetylcholine levels (Sugisaki et al., 2011). This study has shown that the STDP protocol causes LTP both at positive and negative spike timing in high acetylcholine levels. Such an STDP rule could possibly form a bi-directionally strengthened sequence of cells during a run, and support reversed replay in the quiet awake stage after the run.

#### INCREASED GRID CELL SPACING IN NOVEL ENVIRONMENTS

Preliminary data by Barry et al. (2009) has shown that grid cell spacing increases in a novel environment. As the concentration of acetylcholine is further elevated in a novel environment (Giovannini et al., 2001), a larger grid size could be related to higher cholinergic activation. Here we discuss this possibility in a grid cell model proposed by Navratilova et al. (2011) and in our own model.

The grid cell model by Navratilova et al. (2011) used an ADP current for activation of grid cells at different timings from that of field theta oscillation, in each theta cycle. As a result, the time constant of the ADP current defined the grid cell spacing. In this model, higher cholinergic activity in a novel environment may modulate the grid cell spacing through a modification of the ADP time constant in two possible ways. First, the slower membrane resonance frequency, due to the modulation of the H-current in higher cholinergic activity (Heys et al., 2010), may contribute to slowing the ADP time constant. Second, activation of the CAN current, which has delayed activation peak (Magistretti et al., 2004), could contribute to delaying the ADP peak. Both of these mechanisms could increase the grid spacing in this model.

In the model presented in this paper, however, the CAN current supported slow in-field depolarization, and the interaction between the CAN current and the theta rhythm was not considered. In our model, a larger CAN current conductance, and a greater suppression of excitatory synaptic connections, may cause greater grid cell spacing. First, the larger CAN current conductance may cause increased persistent firing of individual neurons, resulting in longer in-field firing duration. Second, further reduction of synaptic excitability may delay the activation of the next cell in the sequence. Even though our model is not a grid cell model, this mechanism could result in a larger grid cell spacing if our model is formed as a ring, as in the Navratilova et al. (2011) model.

## DISCUSSION

In this paper we have shown that activation of the CAN current supports persistent firing in many types of neurons in the MTL. Persistent firing enables each cell to maintain its previous input by sustained firing. We, and others, suggest this feature could be directly useful for the short-term memory function of the MTL. Furthermore, we suggest that persistent firing could be useful for the attractor-network model, especially when local excitatory recurrent synaptic connections are limited. We demonstrated that mechanisms for persistent firing may underlie activity of place cells during active waking. This is consistent with a study which has shown that cholinergic suppression greatly reduces the firing frequency of place cells (Brazhnik et al., 2003). Finally, we have proposed that the network activity switches from real-time to time-compressed replay mode as the acetylcholine level drops and suppresses the CAN current.

It has been proposed that the MTL, especially the hippocampus, is crucial for bridging the temporal gap (Wallenstein et al., 1998; Howard et al., 2005; Naya and Suzuki, 2011). In theory, it is possible to divide a linear maze, 1 m in length, into 1000 1 mm bins, and code all these locations with 1000 place cells, whose place fields are 1 mm long. This way, if a rat takes 5 s to walk through this maze, at least 1000 place cells will fire with a 5 ms interval between neurons. Since 5 ms is an optimal timing to induce LTP through STDP, this trajectory could be encoded successfully. In this case, the CAN current does not seem to be required.

However, a potential problem of this approach is costly and slow sequential recall ability. It has been reported that hippocampal CA3 place cells transiently encode paths forward of the animal at a choice point of a T-maze (Johnson and Redish, 2007). This is seen as a set of CA3 place cells that have place fields ahead of the animal to fire in a time-compressed mode, typically within one theta cycle (<200 ms). It is suggested that this activity is recalling possible future locations for planning future trajectories or for decision-making at a choice point (Johnson and Redish, 2007). If we assume that a 1 m long path is coded by 1000 sequentially connected place cells, without the aid of the CAN current, as described above, retrieval of the future 1 m long path, using the current location as the cue signal, will require activation of 1000 neurons. This will take 5 s, if we assume that glutamatergic synaptic transmission allows the propagation of activity in the chain of 1000 place cells with the delay of 5 ms in each pair of cells. Therefore, planning of the future trajectory may take the same amount of time as the animal actually takes to run along the trajectory. This would not be the best strategy, especially when the animal needs to plan a future path based on memory, to escape from a predator and to survive.

One way to solve this problem is to make the sequential firing during the encoding stage intentionally slow. This will provide the possibility to perform faster-than-real-time recall using a physiological mechanism. The model we proposed in this article used CAN current activation and synaptic suppression to achieve this slow dynamics during active waking. We believe that this is a physiologically plausible mechanism, particularly because the acetylcholine level is known to control the sequential firing speed (fast and slow), the CAN current and synaptic transmission.

Another possible benefit of this model comes from the longer duration firing of each place cell during active waking. Long-duration firing increases the chance for two place cells, with their center of field being far apart, to fire together, overlapping in time. This overlap will enable them to induce Hebbian synaptic plasticity. Therefore, there is no need to code location in 1 mm bins, which can reduce the number of place cells necessary to code 1 m of distance. Finally, this model could be applied to tasks other than spatial navigation. For example, we have an ability to recall a sequence of episodic memories, such as how we traveled from home to work in the morning, in a few seconds. This type of recall, which occurs faster than real-time, might be possible because of slowly changing hippocampal activity during acquisition of episodic memory.

As noted earlier, hippocampal CA1 cells show sequential firing during the delay period of some tasks that do not involve apparent spatial movements ("time cell," Pastalkova et al., 2008; MacDonald et al., 2011). Since animals perceive similar sensory input throughout the delay period, the existence of sequential firing indicates internal dynamics (Pastalkova et al., 2008). Our model, which requires only an initial cue to start sequential firing of cell A to D in active waking mode (**Figure 5B**), would also explain "time cell" firing. Although replay or preplay of time cells have not yet been reported, this model predicts that they would also show replay or preplay.

An interesting detail of time cell firing is that the "time field" for cells that fire later in the sequence tends to be longer than that of those that fire earlier in the sequence (MacDonald et al., 2011). Our model could explain this as follows: cells that fire early in the sequence are effectively inhibited by the lateral inhibition mechanism, described earlier, through activation of cells that fire later in the sequence. In contrast, cells that fire later in the sequence do not receive as much inhibition since fewer cells subsequently fire.

## REFERENCES


Ainge, J. A., van der Meer, M. A., Langston, R. F., and Wood, E. R. (2007). Exploring the role of context-dependent hippocampal activity in spatial alternation behavior. *Hippocampus* 17, 988–1002.

Anagnostaras, S. G., Murphy, G. G., Hamilton, S. E., Mitchell, S. L., Rahnama, N. P., Nathanson, N. M., and Silva, A. J. (2003). Selective cognitive dysfunction in acetylcholine M1 muscarinic receptor mutant mice. *Nat. Neurosci.* 6, 51–58.

Andrade, R. (1991). Cell excitation enhances muscarinic cholinergic responses in rat association cortex. *Brain Res.* 548, 81–93.

Arnold, H. M., Burk, J. A., Hodgson, E. M., Sarter, M., and Bruno, J. P. (2002). Differential cortical acetylcholine release in rats performing a sustained attention task versus behavioral control tasks that do not explicitly tax attention. *Neuroscience* 114, 451–460.

Bang, S. J., and Brown, T. H. (2009). Perirhinal cortex supports acquired fear of auditory objects. *Neurobiol. Learn. Mem.* 92, 53–62.

Bangasser, D. A., Waxler, D. E., Santollo, J., and Shors, T. J. (2006). Trace conditioning and the hippocampus: the importance of contiguity. *J. Neurosci.* 26, 8702–8706.

Barry, C., O'Keefe, J., and Burgess, N. (2009). Effect of novelty on grid cell firing. *Soc. Neurosci. Abstr.* 35, 101–124.

Benardo, L. S., and Prince, D. A. (1982a). Cholinergic excitation of

mammalian hippocampal pyramidal cells. *Brain Res.* 249, 315–331.

Benardo, L. S., and Prince, D. A. (1982b). Ionic mechanisms of cholinergic excitation in mammalian hippocampal pyramidal cells. *Brain Res.* 249, 333–344.

Bird, C. M., and Burgess, N. (2008). The hippocampus and memory: insights from spatial processing. *Nat. Rev. Neurosci.* 9, 182–194.

Boccara, C. N., Sargolini, F., Thoresen, V. H., Solstad, T., Witter, M. P., Moser, E. I., and Moser, M. B. (2010). Grid cells in pre- and parasubiculum. *Nat. Neurosci.* 13, 987–994.

Boucheny, C., Brunel, N., and Arleo, A. (2005). A continuous attractor network model without recurrent excitation: maintenance and integration in the head direction cell system. *J. Comput. Neurosci.* 18, 205–227.

Brandon, M. P., Bogaard, A. R., Libby, C. P., Connerney, M. A., Gupta, K., and Hasselmo, M. E. (2011). Reduction of theta rhythm dissociates grid cell spatial periodicity from directional tuning. *Science* 332, 595–599.

Brazhnik, E. S., Muller, R. U., and Fox, S. E. (2003). Muscarinic blockade slows and degrades the location-specific firing of hippocampal pyramidal cells. *J. Neurosci.* 23, 611–621.

Buzsáki, G. (1989). Two-stage model of memory trace formation: a role for "noisy" brain states. *Neuroscience* 31, 551–570.

Caeser, M., Brown, D. A., Gähwiler, B. H., and Knöpfel, T. (1993). Characterization of a calcium-dependent current generating a slow afterdepolarization of CA3 pyramidal cells in rat hippocampal slice cultures. *Eur. J. Neurosci.* 5, 560–569.

Cashdollar, N., Malecki, U., Rugg-Gunn, F. J., Duncan, J. S., Lavie, N., Duzel, E. (2009). Hippocampus-dependent and -independent theta-networks of active maintenance. *Proc. Natl. Acad. Sci. U.S.A.* 106, 20493–20498.

Cole, A. E., and Nicoll, R. A. (1983). Acetylcholine mediates a slow synaptic potential in hippocampalpyramidal cells. *Science* 221, 1299–1301.

Colombo, M., and Gross, C. G. (1994). Responses of inferior temporal cortex and hippocampal neurons during delayed matching to sample in monkeys (Macaca fascicularis). *Behav. Neurosci.* 108, 443–455.

Deadwyler, S. A., and Hampson, R. E. (2004). Differential but complementary mnemonic functions of the hippocampus and subiculum. *Neuron* 42, 465–476.

Dragoi, G., and Tonegawa, S. (2011). Preplay of future place cell sequences by hippocampal cellular assemblies. *Nature* 469, 397–401.

Egorov, A. V., Hamam, B. N., Fransén, E., Hasselmo, M. E., and Alonso, A. A. (2002). Graded persistent activity in entorhinal cortex neurons. *Nature* 420, 173–178.

Egorov, A. V., Unsicker, K., and von Bohlen und Halbach, O. (2006). Muscarinic control of graded persistent activity in lateral amygdala neurons. *Eur. J. Neurosci.* 24, 3183–3194.

Esclassan, F., Coutureau, E., Di Scala, G., and Marchand, A. R. (2009). A cholinergic-dependent role for the entorhinal cortex in trace fear conditioning. *J. Neurosci.* 29, 8087–8093.

Farovik, A., Dupont, L. M., and Eichenbaum, H. (2009). Distinct roles for dorsal CA3 and CA1 in memory for sequential nonspatial events. *Learn. Mem.* 17, 12–17.

Foster, D. J., and Wilson, M. A. (2006). Reverse replay of behavioural sequences in hippocampal place cells during the awake state. *Nature* 440, 680–683.

Fransén, E., Alonso, A. A., and Hasselmo, M. E. (2002). Simulations of the role of the muscarinic-activated calcium-sensitive nonspecific cation current INCM in entorhinal neuronal activity during delayed matching tasks. *J. Neurosci.* 22, 1081–1097.

Fraser, D. D., and MacVicar, B. A. (1996). Cholinergic-dependent plateau potential in hippocampal CA1 pyramidal neurons. *J. Neurosci.* 16, 4113–4128.

Garden, D. L., Dodson, P. D., O'Donnell, C., White, M. D., and Nolan, M. F. (2008). Tuning of synaptic integration in the medial entorhinal cortex to the organization of grid cell firing fields. *Neuron* 60, 875–889.

Gähwiler, B. H., and Dreifuss, J. J. (1982). Multiple actions of acetylcholine on hippocampal pyramidal cells in organotypic explant cultures. *Neuroscience* 7, 1243–1256.

Geisler, C., Diba, K., Pastalkova, E., Mizuseki, K., Royer, S., and Buzsáki, G. (2010). Temporal delays among place cells determine the frequency of population theta oscillations in the hippocampus. *Proc. Natl. Acad. Sci. U.S.A.* 107, 7957–7962.

Gilbert, P. E., and Kesner, R. P. (2002). Role of the rodent hippocampus in paired-associate learning involving associations between a stimulus and a spatial location. *Behav. Neurosci.* 116, 63–71.

Gilbert, P. E., Kesner, R. P., and Lee, I. (2001). Dissociating hippocampal subregions: double dissociation between dentate gyrus and CA1. *Hippocampus* 11, 626–636.

Giocomo, L. M., and Hasselmo, M. E. (2007). Neuromodulation by glutamate and acetylcholine can change circuit dynamics by regulating the relative influence of afferent input and excitatory feedback. *Mol. Neurobiol.* 36, 184–200.

Giocomo, L. M., Zilli, E. A., Fransén, E., and Hasselmo, M. E. (2007). Temporal frequency of subthreshold oscillations scales with entorhinal grid cell field spacing. *Science* 315, 1719–1722.

Giocomo, L. M., Moser, M. B., and Moser, E. I. (2011). Computational models of grid cells. *Neuron* 71, 589–603.

Giovannini, M. G., Rakovska, A., Benton, R. S., Pazzagli, M., Bianchi, L., and Pepeu, G. (2001). Effects of novelty and habituation on acetylcholine, GABA, and glutamate release from the frontal cortex and hippocampus of freely moving rats. *Neuroscience* 106, 43–53.

Goodridge, J. P., Dudchenko, P. A., Worboys, K. A., Golob, E. J., and Taube, J. S. (1998). Cue control and head direction cells. *Behav. Neurosci.* 112, 749–761.

Goodridge, J. P., and Touretzky, D. S. (2000). Modeling attractor deformation in the rodent head-direction system. *J. Neurophysiol.* 83, 3402–3410.

Green, J. D., and Arduini, A. A. (1954). Hippocampal electrical activity and arousal. *J. Neurophysiol.* 17, 533–557.

Hafting, T., Fyhn, M., Molden, S., Moser, M. B., and Moser, E. I. (2005). Microstructure of a spatial map in the entorhinal cortex. *Nature* 436, 801–806.

Halliwell, J. V., and Adams, P. R. (1982). Voltage-clamp analysis of muscarinic excitation in hippocampal neurons. *Brain Res.* 250, 71–92.

Hampson, R. E., Pons, T. P., Stanford, T. R., and Deadwyler, S. A. (2004). Categorization in the monkey hippocampus: a possible mechanism for encoding information into memory. *Proc. Natl. Acad. Sci. U.S.A.* 101, 3184–3189.

Hannula, D. E., Tranel, D., and Cohen, N. J. (2006). The long and the short of it: relational memory impairments in amnesia, even at short lags. *J. Neurosci.* 26, 8352–8359.

Hartley, T., Bird, C. M., Chan, D., Cipolotti, L., Husain, M., Vargha-Khadem, F., and Burgess, N. (2007). The hippocampus is required for short-term topographical memory in humans. *Hippocampus* 17, 34–48.

Hasselmo, M. E. (1999). Neuromodulation: acetylcholine and memory consolidation. *Trends Cogn. Sci.* 3, 351–359.

Hasselmo, M. E. (2007). Arc length coding by interference of theta frequency oscillations may underlie context-dependent hippocampal unit data and episodic memory function. *Learn. Mem.* 14, 782–794.

Hasselmo, M. E., Giocomo, L. M., Brandon, M. P., and Yoshida, M. (2010). Cellular dynamical mechanisms for encoding the time and place of events along spatiotemporal trajectories in episodic memory. *Behav. Brain Res.* 215, 261–274.

Hasselmo, M. E., and Schnell, E. (1994). Laminar selectivity of the cholinergic suppression of synaptic transmission in rat hippocampal region CA1: computational modeling and brain slice physiology. *J. Neurosci.* 14, 3898–3914.

Heys, J. G., Giocomo, L. M., and Hasselmo, M. E. (2010). Cholinergic modulation of the resonance properties of stellate cells in layer II of medial entorhinal cortex. *J. Neurophysiol.* 104, 258–270.

Himmelheber, A. M., Sarter, M., and Bruno, J. P. (2001). The effects of manipulations of attentional demand on cortical acetylcholine release. *Brain Res. Cogn. Brain Res.* 12, 353–370.

Howard, M. W., Fotedar, M. S., Datey, A. V., and Hasselmo, M. E. (2005). The temporal context model in spatial navigation and relational learning: toward a common explanation of medial temporal lobe function across domains. *Psychol. Rev.* 112, 75–116.

Jensen, O., and Lisman, J. E. (1996). Theta/gamma networks with slow NMDA channels learn sequences and encode episodic memory: role of NMDA channels in recall. *Learn. Mem.* 3, 264–278.

Johnson, A., and Redish, A. D. (2007). Neural ensembles in CA3 transiently encode paths forward of the animal at a decision point. *J. Neurosci.* 27, 12176–12189.

Kametani, H., and Kawamura, H. (1990). Alterations in acetylcholine release in the rat hippocampus during sleep-wakefulness detected by intracerebral dialysis. *Life Sci.* 47, 421–426.

Kawasaki, H., Palmieri, C., and Avoli, M. (1999). Muscarinic receptor activation induces depolarizing plateau potentials in bursting neurons of the rat subiculum. *J. Neurophysiol.* 82, 2590–2601.

Kesner, R. P., Hunsaker, M. R., and Gilbert, P. E. (2005). The role of CA1 in the acquisition of an object-trace-odor paired associate task. *Behav. Neurosci.* 119, 781–786.

Kholodar-Smith, D. B., Boguszewski, P., and Brown, T. H. (2008). Auditory trace fear conditioning requires perirhinal cortex. *Neurobiol. Learn. Mem.* 90, 537–543.

Kim, J. J., Clark, R. E., and Thompson, R. F. (1995). Hippocampectomy impairs the memory of recently, but not remotely, acquired trace eyeblink conditioned responses. *Behav. Neurosci.* 109, 195–203.

Klink, R., and Alonso, A. (1997). Muscarinic modulation of the oscillatory and repetitive firing properties of entorhinal cortex layer II neurons. *J. Neurophysiol.* 77, 1813–1828.

Koene, R. A., and Hasselmo, M. E. (2008). Reversed and forward buffering of behavioral spike sequences enables retrospective and prospective retrieval in hippocampal regions CA3 and CA1. *Neural Netw.* 21, 276–288.

Koenig, J., Linder, A. N., Leutgeb, J. K., and Leutgeb, S. (2011). The spatial periodicity of grid cells is not sustained during reduced theta oscillations. *Science* 332, 592–595.

Kremin, T., and Hasselmo, M. E. (2007). Cholinergic suppression of glutamatergic synaptic transmission in hippocampal region CA3 exhibits laminar selectivity: implication for hippocampal network dynamics. *Neuroscience* 149, 760–767.

Kumar, S. S., Jin, X., Buckmaster, P. S., and Huguenard, J. R. (2007). Recurrent circuits in layer II of medial entorhinal cortex in a model of temporal lobe epilepsy. *J. Neurosci.* 27, 1239–1246.

Lee, A. K., and Wilson, M. A. (2002). Memory of sequential experience in the hippocampus during slow wave sleep. *Neuron* 36, 1183–1194.

Lisman, J., and Idiart, M. (1995). Storage of 7 ± 2 short-term memories in oscillatory subcylces. *Science* 267, 1512–1515.

MacDonald, C. J., Lepage, K. Q., Eden, U. T., and Eichenbaum, H. (2011). Hippocampal "time cells" bridge the gap in memory for discontiguous events. *Neuron* 71, 737–749.

Madison, D. V., Lancaster, B., and Nicoll, R. A. (1987). Voltage clamp analysis of cholinergic action in the hippocampus. *J. Neurosci.* 7, 733–741.

Magistretti, J., Ma, L., Shalinsky, M. H., Lin, W., Klink, R., and Alonso, A. (2004). Spike patterning by Ca2+-dependent regulation of a muscarinic cation current in entorhinal cortex layer II neurons. *J. Neurophysiol.* 92, 1644–1657.

Major, G., and Tank, D. (2004). Persistent neural activity: prevalence and mechanisms. *Curr. Opin. Neurobiol.* 14, 675–684.

Marrosu, F., Portas, C., Mascia, M. S., Casu, M. A., Fà, M., Giagheddu, M., Imperato, A., and Gessa, G. L. (1995). Microdialysis measurement of cortical and hippocampal acetylcholine release during sleep-wake cycle in freely moving cats. *Brain Res.* 671, 329–332.

McClelland, J. L., McNaughton, B. L., and O'Reilly, R. C. (1995). Why there are complementary learning systems in the hippocampus and neocortex: insights from the successes and failures of connectionist models of learning and memory. *Psychol. Rev.* 102, 419–457.

McEchron, M. D., Tseng, W., and Disterhoft, J. F. (2000). Neurotoxic lesions of the dorsal hippocampus disrupt auditory-cued trace heart rate (fear) conditioning in rabbits. *Hippocampus* 10, 739–751.

McEchron, M. D., Tseng, W., and Disterhoft, J. F. (2003). Single neurons in CA1 hippocampus encode trace interval duration during trace heart rate (fear) conditioning in rabbit. *J. Neurosci.* 23, 1535–1547.

McEchron, M. D., Weible, A. P., and Disterhoft, J. F. (2001). Aging and learning-specific changes in single-neuron activity in CA1 hippocampus during rabbit trace eyeblink conditioning. *J. Neurophysiol.* 86, 1839–1857.

McGaugh, J. L. (2000). Memory–a century of consolidation. *Science* 287, 248–251.

McGaughy, J., Koene, R. A., Eichenbaum, H., and Hasselmo, M. E. (2005). Cholinergic deafferentation of the entorhinal cortex in rats impairs encoding of novel but not familiar stimuli in a delayed nonmatch-to-sample task. *J. Neurosci.* 25, 10273–10281.

McNaughton, B. L., Battaglia, F. P., Jensen, O., Moser, E. I., and Moser, M. B. (2006). Path integration and the neural basis of the 'cognitive map'. *Nat. Rev. Neurosci.* 7, 663–678.

McNaughton, B. L., Chen, L. L., and Markus, E. J. (1991). Dead reckoning, landmark learning, and the sense of direction-a neurophysiological and computational hypothesis. *J. Cogn. Neurosci.* 3, 192–202.

Mikulka, P. J., and Freeman, F. G. (1975). The effects of reinforcement delay and hippocampal lesions on the acquisition of a choice response. *Behav. Biol.* 15, 473–477.

Mizumori, S. J., McNaughton, B. L., Barnes, C. A., and Fox, K. B. (1989). Preserved spatial coding in hippocampal CA1 pyramidal cells during reversible suppression of CA3c output: evidence for pattern completion in hippocampus. *J. Neurosci.* 9, 3915–3928.

Molter, C., Sato, N., and Yamaguchi, Y. (2007). Reactivation of behavioral activity during sharp waves: a computational model for two stage hippocampal dynamics. *Hippocampus* 17, 201–209.

Moser, E. I., Kropff, E., and Moser, M. B. (2008). Place cells, grid cells, and the brain's spatial representation system. *Annu. Rev. Neurosci.* 31, 69–89.

Muller, R. U., Bostock, E., Taube, J. S., and Kubie, J. L. (1994). On the directional firing properties of hippocampal place cells. *J. Neurosci.* 14, 7235–7251.

Navratilova, Z., Giocomo, L. M., Fellous, J. M., Hasselmo, M. E., and McNaughton, B. L. (2011). Phase precession and variable spatial scaling in a periodic attractor map model of medial entorhinal grid cells with realistic after-spike dynamics. *Hippocampus.* (in print).

Navaroli, V. L., Zhao, Y., Boguszewski, P., and Brown, T. H. (2011). Muscarinic receptor activation enables persistent firing in pyramidal neurons from superficial layers of dorsal perirhinal cortex. *Hippocampus.* (in print).

Naya, Y., and Suzuki, W. A. (2011). Integrating what and when across the primate medial temporal lobe. *Science* 333, 773–776.

O'Keefe, J., and Burgess, N. (2005). Dual phase and rate coding in hippocampal place cells: theoretical significance and relationship to entorhinal grid cells. *Hippocampus* 15, 853–866.

O'Keefe, J., and Dostrovsky, J. (1971). The hippocampus as a spatial map. Preliminary evidence from unit activity in the freely-moving rat. *Brain Res.* 34, 171–175.

O'Keefe, J., and Recce, M. L. (1993). Phase relationship between hippocampal place units and the EEG theta rhythm. *Hippocampus* 3, 317–330.

Olsen, R. K., Nichols, E. A., Chen, J., Hunt, J. F., Glover, G. H., Gabrieli, J. D., and Wagner, A. D. (2009). Performance-related sustained and anticipatory activity in human medial temporal lobe during delayed match-to-sample. *J. Neurosci.* 29, 11880–11890.

Olson, I. R., Moore, K. S., Stark, M., and Chatterjee, A. (2006). Visual working memory is impaired when the medial temporal lobe is damaged. *J. Cogn. Neurosci.* 18, 1087–1097.

Otto, T., and Eichenbaum, H. (1992a). Neuronal activity in the hippocampus during delayed non-match to sample performance in rats: evidence for hippocampal processing in recognition memory. *Hippocampus* 2, 323–334.

Otto, T., and Eichenbaum, H. (1992b). Complementary roles of the orbital prefrontal cortex and the perirhinal-entorhinal cortices in an odor-guided delayed-nonmatching-to-sample task. *Behav. Neurosci.* 106, 762–775.

Pang, M. H., Kim, N. S., Kim, I. H., Kim, H., Kim, H. T., and Choi, J. S. (2010). Cholinergic transmission in the dorsal hippocampus modulates trace but not delay fear conditioning. *Neurobiol. Learn. Mem.* 94, 206–213.

Parikh, V., Kozak, R., Martinez, V., and Sarter, M. (2007). Prefrontal acetylcholine release controls cue detection on multiple timescales. *Neuron* 56, 141–154.

Pastalkova, E., Itskov, V., Amarasingham, A., and Buzsáki, G. (2008). Internally generated cell assembly sequences in the rat hippocampus. *Science* 321, 1322–1327.

Penetar, D. M., McDonough, J. H. Jr. (1983). Effects of cholinergic drugs on delayed match-to-sample performance of rhesus monkeys. *Pharmacol. Biochem. Behav.* 19, 963–967.

Quilichini, P., Sirota, A., and Buzsáki, G. (2010). Intrinsic circuit organization and theta-gamma oscillation dynamics in the entorhinal cortex of the rat. *J. Neurosci.* 30, 11128–11142.

Quirk, G. J., Muller, R. U., and Kubie, J. L. (1990). The firing of hippocampal place cells in the dark depends on the rat's recent experience. *J. Neurosci.* 10, 2008–2017.

Ranck, J. J. (1984). Head direction cells in the deep layer of dorsal presubiculum in freely moving rats. *Soc. Neurosci. Abstr.* 10, 599.

Rawlins, J. N., Feldon, J., and Butt, S. (1985). The effects of delaying reward on choice preference in rats with hippocampal or selective septal lesions. *Behav. Brain Res.* 15, 191–203.

Reboreda, A., Jiménez-Díaz, L., and Navarro-López, J. D. (2011). TRP channels and neural persistent activity. *Adv. Exp. Med. Biol.* 704, 595–613.

Reboreda, A., Raouf, R., Alonso, A., and Séguéla, P. (2007). Development of cholinergic modulation and graded persistent activity in layer v of medial entorhinal cortex. *J. Neurophysiol.* 97, 3937–3947.

Redish, A., Elga, A., and Touretzky, D. (1996). A coupled attractor model of the rodent head direction system. *Network* 7, 671–685.

Rubin, J., Terman, D., and Chow, C. (2001). Localized bumps of activity sustained by inhibition in a two-layer thalamic network. *J. Comput. Neurosci.* 10, 313–331.

Sargolini, F., Fyhn, M., Hafting, T., McNaughton, B. L., Witter, M. P., Moser, M. B., and Moser, E. I. (2006). Conjunctive representation of position, direction, and velocity in entorhinal cortex. *Science* 312, 758–762.

Schon, K., Atri, A., Hasselmo, M. E., Tricarico, M. D., LoPresti, M. L., and Stern, C. E. (2005). Scopolamine reduces persistent activity related to long-term encoding in the parahippocampal gyrus during delayed matching in humans. *J. Neurosci.* 25, 9112–9123.

Schon, K., Hasselmo, M. E., Lopresti, M. L., Tricarico, M. D., and Stern, C. E. (2004). Persistence of parahippocampal representation in the absence of stimulus input enhances long-term encoding: a functional magnetic resonance imaging study of subsequent memory after a delayed match-to-sample task. *J. Neurosci.* 24, 11088–11097.

Segal, M. (1982). Multiple action of acetylcholine at a muscarinic receptor studied in the rat hippocampal slice. *Brain Res.* 246, 77–87.

Skaggs, W. E., Knierim, J. J., Kudrimoti, H. S., and McNaughton, B. L. (1995). A model of the neural basis of the rat's sense of direction. *Adv. Neural Inf. Process. Syst.* 7, 173–180.

Skaggs, W. E., McNaughton, B. L., Wilson, M. A., and Barnes, C. A. (1996). Theta phase precession in hippocampal neuronal populations and the compression of temporal sequences. *Hippocampus* 6, 149–172.

Sharp, P. E. (1996). Multiple spatial/behavioral correlates for cells in the rat postsubiculum: multiple regression analysis and comparison to other hippocampal areas. *Cereb. Cortex* 6, 238–259.

Sheffield, M. E., Best, T. K., Mensh, B. D., Kath, W. L., and Spruston, N. (2011). Slow integration leads to persistent action potential firing in distal axons of coupled interneurons. *Nat. Neurosci.* 14, 200–207.

Shen, B., and McNaughton, B. L. (1996). Modeling the spontaneous reactivation of experience-specific hippocampal cell assembles during sleep. *Hippocampus* 6, 685–692.

Shu, Y., Hasenstaub, A., and McCormick, D. A. (2003). Turning on and off recurrent balanced cortical activity. *Nature* 423, 288–293.

Solomon, P. R., Vander Schaaf, E. R., Thompson, R. F., and Weisz, D. J. (1986). Hippocampus and trace conditioning of the rabbit's classically conditioned nictitating membrane response. *Behav. Neurosci.* 100, 729–744.

Song, P., and Wang, X. J. (2005). Angular path integration by moving "hill of activity": a spiking neuron model without recurrent excitation of the headdirection system. *J. Neurosci.* 25, 1002–1014.

Squire, L. R. (1992). Memory and the hippocampus: a synthesis from findings with rats, monkeys, and humans. *Psychol. Rev.* 99, 195–231.

Squire, L. R., and Zola-Morgan, S. (1991). The medial temporal lobe memory system. *Science* 253, 1380–1386.

Storm, J. F. (1989). An after-hyperpolarization of medium duration in rat hippocampal pyramidal cells. *J. Physiol.* 409, 171–190.

Sugisaki, E., Fukushima, Y., Tsukada, M., and Aihara, T. (2011). Cholinergic modulation on spike timing-dependent plasticity in hippocampal CA1 network. *Neuroscience* 192, 91–101.

Suzuki, W. A., Miller, E. K., and Desimone, R. (1997). Object and place memory in the macaque entorhinal cortex. *J. Neurophysiol.* 78, 1062–1081.

Tahvildari, B., Alonso, A. A., and Bourque, C. W. (2008). Ionic basis of ON and OFF persistent activity in layer III lateral entorhinal cortical principal neurons. *J. Neurophysiol.* 99, 2006–2011.

Tahvildari, B., Fransén, E., Alonso, A. A., and Hasselmo, M. E. (2007). Switching between "On" and "Off" states of persistent activity in lateral entorhinal layer III neurons. *Hippocampus* 17, 257–263.

Tai, C., Hines, D. J., Choi, H. B., and Macvicar, B. A. (2010). Plasma membrane insertion of TRPC5 channels contributes to the cholinergic plateau potential in hippocampal CA1 pyramidal neurons. *Hippocampus.* 21, 958–967.

Tamamaki, N., and Nojyo, Y. (1990). Disposition of the slab-like modules formed by axon branches originating from single CA1 pyramidal neurons in the rat hippocampus. *J. Comp. Neurol.* 291, 509–519.

Taube, J. S., Muller, R. U., Ranck, J. B. Jr. (1990a). Head-direction cells recorded from the postsubiculum in freely moving rats. I. Description and quantitative analysis. *J. Neurosci.* 10, 420–435.

Taube, J. S., Muller, R. U., and Ranck, J. B. Jr. (1990b). Head-direction cells recorded from the postsubiculum in freely moving rats. II. Effects of environmental manipulations. *J. Neurosci.* 10, 436–447.

Tseng, W., Guan, R., Disterhoft, J. F., and Weiss, C. (2004). Trace eyeblink conditioning is hippocampally dependent in mice. *Hippocampus* 14, 58–65.

Tsodyks, M. V., and Sejnowski, T. J. (1995). Associative memory and hippocampal place cells. *Int. J. Neural. Syst.* 6, 81–86.

Wallenstein, G. V., Eichenbaum, H., and Hasselmo, M. E. (1998). The hippocampus as an associator of discontiguous events. *Trends Neurosci.* 21, 317–323.

Weiss, C., Bouwmeester, H., Power, J. M., and Disterhoft, J. F. (1999). Hippocampal lesions prevent trace eyeblink conditioning in the freely moving rat. *Behav. Brain Res.* 99, 123–132.

Wilson, M. A., and McNaughton, B. L. (1994). Reactivation of hippocampal ensemble memories during sleep. *Science* 265, 676–679.

Winson, J. (1974). Patterns of hippocampal theta rhythm in the freely moving rat. *Electroencephalogr. Clin. Neurophysiol.* 36, 291–301.

Witter, M. P., and Amaral, D. G. (1991). Entorhinal cortex of the monkey: V. Projections to the dentate gyrus, hippocampus, and subicular complex. *J. Comp. Neurol.* 307, 437–459.

Wood, E. R., Dudchenko, P. A., Robitsek, R. J., and Eichenbaum, H. (2000). Hippocampal neurons encode information about different types of memory episodes occurring in the same location. *Neuron* 27, 623–633.

Yoshida, M., and Alonso, A. (2007). Cell-type specific modulation of intrinsic firing properties and subthreshold membrane oscillations by the M(Kv7)-current in neurons of the entorhinal cortex. *J. Neurophysiol.* 98, 2779–2794.

Yoshida, M., Fransén, E., and Hasselmo, M. E. (2008). mGluR-dependent persistent firing in entorhinal cortex layer III neurons. *Eur. J. Neurosci.* 28, 1116–1126.

Yoshida, M., Giocomo, L. M., Boardman, I., and Hasselmo, M. E. (2011). Frequency of subthreshold oscillations at different membrane potential voltages in neurons at different anatomical positions on the dorsoventral axis in the rat medial entorhinal cortex. *J. Neurosci.* 31, 12683–12694.

Yoshida, M., and Hasselmo, M. E. (2009a). Persistent firing supported by an intrinsic cellular mechanism in a component of the head direction system. *J. Neurosci.* 29, 4945–4952.

Yoshida, M., and Hasselmo, M. (2009b). Differences in persistent firing properties dependent upon anatomical location of neurons in rat medial entorhinal cortex. *Soc. Neurosci. Abstr.* 35, 193.19.

Young, B. J., Otto, T., Fox, G. D., and Eichenbaum, H. (1997). Memory representation within the parahippocampal region. *J. Neurosci.* 17, 5183–5195.

Zhang, K. (1996). Representation of spatial orientation by the intrinsic dynamics of the head-direction cell ensemble: a theory. *J. Neurosci.* 16, 2112–2126.

Zhang, Z., Reboreda, A., Alonso, A., Barker, P. A., and Séguéla, P. (2011). TRPC channels underlie cholinergic plateau potentials and persistent activity in

entorhinal cortex. *Hippocampus* 21, 386–397.

Zilli, E. A., and Hasselmo, M. E. (2010). Coupled noisy spiking neurons as velocity-controlled oscillators in a model of grid cell spatial firing. *J. Neurosci.* 30, 13850–13860.

Zilli, E. A., Yoshida, M., Tahvildari, B., Giocomo, L. M., and Hasselmo, M. E. (2009). Evaluation of the oscillatory interference model of grid cell firing through analysis and measured period variance of some biological oscillators. *PLoS Comput. Biol.* 5:e1000573. doi: 10.1371/journal.pcbi.1000573

**Conflict of Interest Statement:** The authors declare that the research was conducted in the absence of any commercial or financial relationships that could be construed as a potential conflict of interest.

*Received: 16 December 2011; accepted: 24 February 2012; published online: 15 March 2012.*

*Citation: Yoshida M, Knauer B and Jochems A (2012) Cholinergic modulation of the CAN current may adjust neural dynamics for active memory maintenance, spatial navigation and time-compressed replay. Front. Neural Circuits* ***6****:10. doi: 10.3389/fncir.2012.00010*

frontiers in
NEURAL CIRCUITS

REVIEW ARTICLE
published: 20 March 2012
doi: 10.3389/fncir.2012.00007

# Vestibular and attractor network basis of the head direction cell signal in subcortical circuits

***Benjamin J. Clark*** [†] ***and Jeffrey S. Taube*** [*]

*Department of Psychological and Brain Sciences, Center for Cognitive Neuroscience, Dartmouth College, Hanover, NH, USA*

***Edited by:***
*Yasser Roudi, Norwegian University of Science and Technology, Norway*

***Reviewed by:***
*Francesca Sargolini, Aix Marseille Université – CNRS, France*
*Douglas Nitz, University of California, San Diego, USA*

****Correspondence:***
*Jeffrey S. Taube, Department of Psychological and Brain Sciences, Dartmouth College, 6207 Moore Hall, Hanover, NH 03755, USA.*
*e-mail: jeffrey.taube@dartmouth.edu*

***[†] Present address:***
*Canadian Centre for Behavioural Neuroscience, University of Lethbridge, Lethbridge, AB, Canada T1K 3M4.*

Accurate navigation depends on a network of neural systems that encode the moment-to-moment changes in an animal's directional orientation and location in space. Within this navigation system are head direction (HD) cells, which fire persistently when an animal's head is pointed in a particular direction (Sharp et al., 2001a; Taube, 2007). HD cells are widely thought to underlie an animal's sense of spatial orientation, and research over the last 25+ years has revealed that this robust spatial signal is widely distributed across subcortical and cortical limbic areas. The purpose of the present review is to summarize some of the recent studies arguing that the origin of the HD signal resides subcortically, specifically within the reciprocal connections of the dorsal tegmental and lateral mammillary nuclei. Furthermore, we review recent work identifying "bursting" cellular activity in the HD cell circuit after lesions of the vestibular system, and relate these observations to the long held view that attractor network mechanisms underlie HD signal generation. Finally, we summarize anatomical and physiological work suggesting that this attractor network architecture may reside within the tegmento-mammillary circuit.

**Keywords: entorhinal, hippocampus, head direction, spatial orientation, navigation**

## INTRODUCTION

Accurate navigation depends on knowledge of current spatial position and direction (Gallistel, 1990). Precisely how this information is represented in the mammalian brain is not entirely understood, although it is widely believed that the basic structure of a map-like representation, which contains the spatial relationships between landmarks and objects within the immediate environment, is formed in the limbic system (O'Keefe and Nadel, 1978; McNaughton et al., 1996, 2006). An animal's position within this neural map is thought to arise from the reciprocal connections of areas within the parahippocampal-hippocampal region; a notion that follows from the fact that this circuitry contains neurons that represent an animal's location in an environment (Moser et al., 2008), as well as neurons that encode the animal's orientation (Taube, 2007). For instance, the hippocampal CA region contains neurons that discharge as an animal passes through specific locations within an environment (**Figure 1A**, left) (O'Keefe and Dostrovsky, 1971). In the parahippocampal cortex, neurons also encode an animal's environmental location, although these cells differ from hippocampal "place cells" because some cells discharge in multiple locations forming interlocking equilateral triangles (**Figure 1A**, middle) (Hafting et al., 2005), and others fire in relation to the boundaries of an environment (**Figure 1A**, right) (Savelli et al., 2008; Solstad et al., 2008). These parahippocampal neurons—referred to as "grid cells" and "border cells," respectively—were first identified within the medial entorhinal cortex (Hafting et al., 2005; Sargolini et al., 2006; Savelli et al., 2008; Solstad et al., 2008), but have also been identified within the subicular complex (subiculum, Lever et al., 2009; pre- and parasubiculum, Boccara et al., 2010).

In addition to the neural signals representing spatial location, a fourth class of spatially responsive cells, called "head direction (HD) cells" (**Figure 1B**), provide information regarding an animal's directional orientation in space, and are thought to underlie our sense of direction (Ranck, 1984; Taube et al., 1990a). This view is derived from the fact that because different HD cells are best-tuned to different directions, a small ensemble of these cells can accurately track the moment-to-moment changes in an animal's HD over time (Johnson et al., 2005). HD cells coexist with grid cells and border cells in parahippocampal (medial entorhinal, pre- and parasubicular) cortical areas (Sargolini et al., 2006; Boccara et al., 2010). In addition, HD cells have been identified throughout the limbic system including many structures within the classical Papez circuit (Papez, 1937; reviewed in Taube, 2007). Over the last two decades, a significant amount of research has broadened our understanding of the functional organization of this HD cell system, as well as how the HD signal is generated within subcortical and parahippocampal circuits. The purpose of the present review is to summarize these findings and specifically address some of the issues concerning their network organization and the mechanisms underlying their generation.

## HIERARCHICAL ORGANIZATION OF HD CELL CIRCUITRY

Although the HD cell signal is distributed across a wide range of brain regions, many of these structures are highly interconnected forming a complicated circuit with many reciprocal connections (see **Figure 2**). There is now considerable evidence that this interconnected circuit of HD cells is organized in a relatively hierarchical scheme (Taube, 2007). For instance, lesion studies have demonstrated that damage to cortical HD cell areas do not

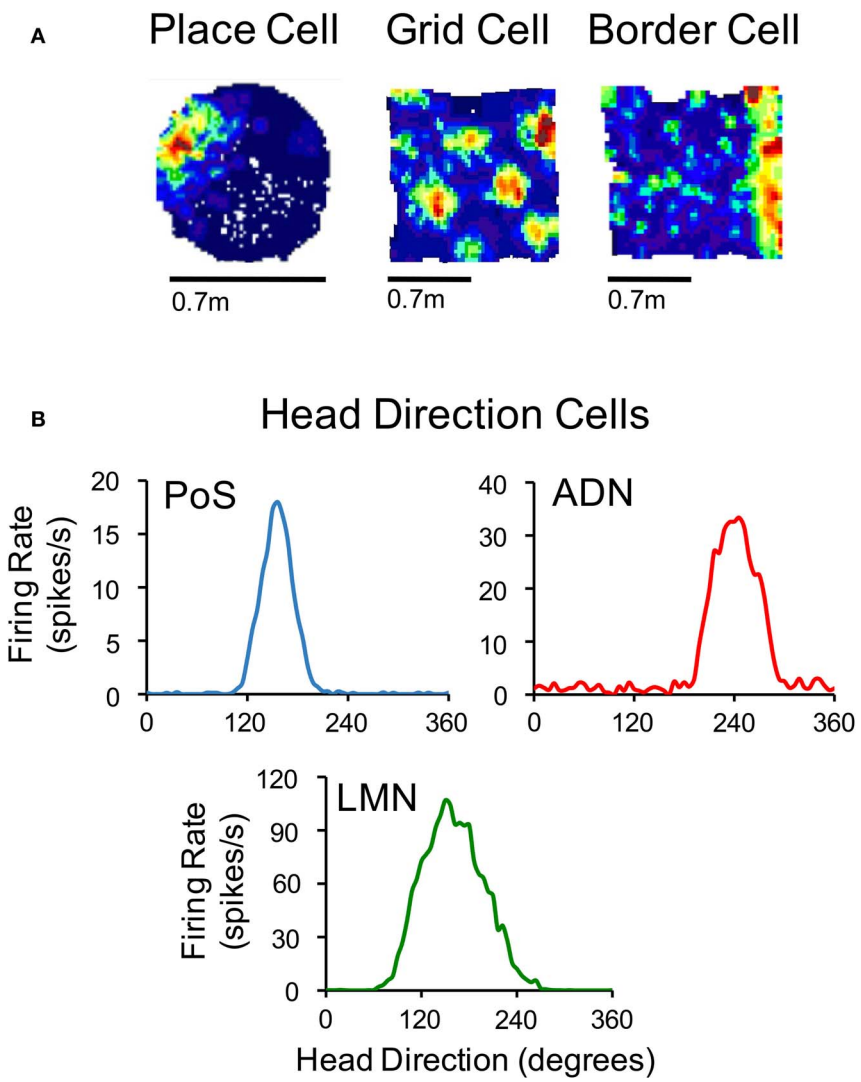


**FIGURE 1 | (A)** Color-coded rate maps for a hippocampal place cell, a medial entorhinal grid cell and a medial entorhinal border cell (Red, maximum firing rate; blue, minimum firing rate). **(B)** Firing rate by HD plots for representative HD cells recorded in the postsubiculum (PoS), anterodorsal thalamus (ADN), and lateral mammillary nuclei (LMN). The place cell in panel **(A)** is based on data from Calton et al. (2003), and the grid and border cells are from Clark et al. (2011). The plots in **(B)** are based on data from Clark et al. (2010) (for ADN), Stackman and Taube (1998) (for LMN), and Taube et al. (1990a) (for PoS).

abolish HD signal generation within subcortical structures, while lesions of subcortical HD cell regions generally abolish directional activity in cortical circuits (**Table 1**). The first study to provide evidence for this general principal of HD circuit organization came from Goodridge and Taube (1997) in which the anterodorsal thalamus was lesioned and cellular activity was recorded in the postsubiculum. In general, lesions of the anterodorsal thalamus completely abolished HD cell activity in the postsubiculum—a finding that has recently been replicated in preliminary work showing that similar lesions abolish HD cell activity in the parasubiculum and the superficial layers of the medial entorhinal cortex (Clark et al., 2011). In contrast, lesions of the postsubiculum do not disrupt HD signal generation in subcortical structures (Goodridge and Taube, 1997; Yoder and Taube, 2008), suggesting that descending cortical input to subcortical HD cell areas plays a more limited role in HD cell processing. Much of the work that has focused on lesioning cortical structures and monitoring HD cell activity in subcortical areas is consistent with this notion (see **Table 1**). However, the ability of visual landmark cues to control HD cell tuning is most significantly disrupted after damage to the postsubiculum (see Yoder et al., 2011a for review). The early work by Goodridge and Taube (1997) suggested that the postsibuculum might integrate this visual information into the HD circuit and more generally into the MEC and hippocampus (Calton et al., 2003). Recent preliminary work suggests (Yoder and Taube, 2008) that landmark information is also conveyed subcortically to HD cells in the lateral mammillary nuclei via direct projections from the postsubiculum. Indeed, the lateral mammillary nuclei may serve as one important node where landmark information is integrated with idiothetic information. In accordance with the

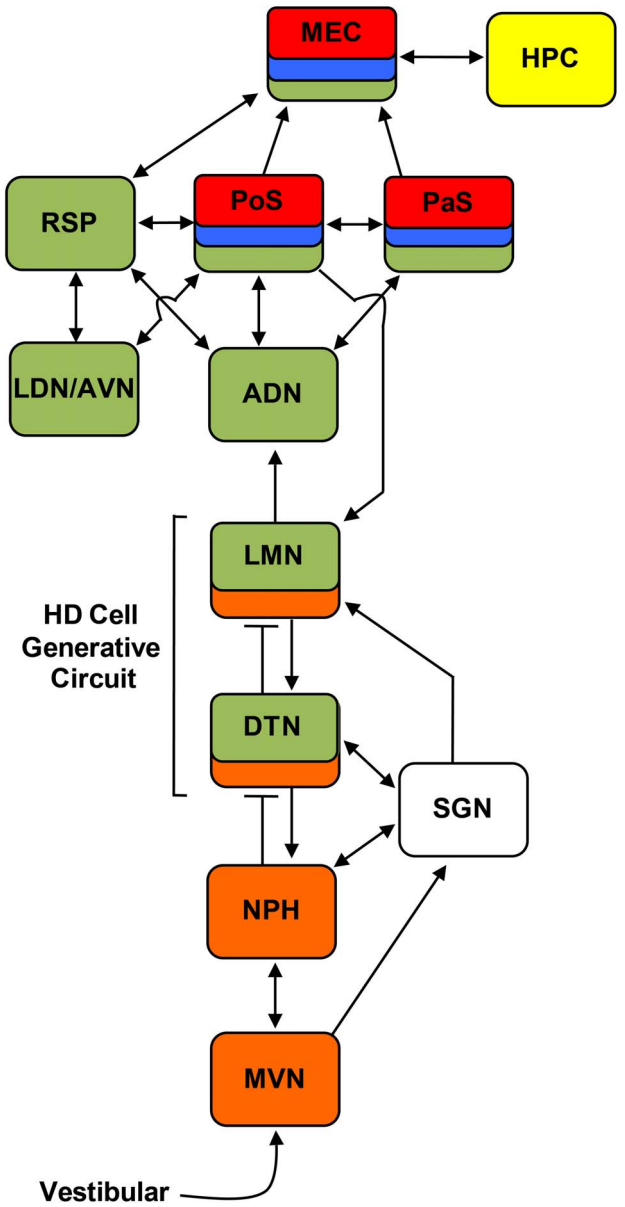


**FIGURE 2 | Circuit diagram showing the principle connections between brain regions containing place cells (yellow), grid cells (red), border cells (blue), HD cells (green), and angular velocity cells (orange) (Sharp et al., 2001a; Taube and Bassett, 2003; Taube, 2007).** Arrows indicate excitatory projections, and lines that end with a bar represent inhibitory projections. ADN, anterodorsal thalamus; AVN, anteroventral thalamus; DTN, dorsal tegmental nucleus; HPC, hippocampus; LDN, laterodorsal thalamus; LMN, lateral mammillary nuclei; MEC, medial entorhinal cortex; MVN, medial vestibular nuclei; NPH, nucleus prepositus hypoglossi; PaS, parasubiculum; PoS, postsubiculum; RSP, retrosplenial cortex; SGN, supragenual nucleus.

working model presented in **Figure 2**, damage to the postsubiculum may abolish directional activity in the medial entorhinal cortex as well as landmark control over other spatial signals within this region, given that it provides one of the most prominent inputs to this region (van Haeften et al., 1997; Kerr et al., 2007) and that postsubicular lesions disrupt landmark control in CA1 place cells (Calton et al., 2003).

Supporting the general conclusion that HD signal generation resides subcortically, several studies have shown that lesions centered on structures upstream of the anterior thalamus also eliminate directional tuning downstream (**Table 1**). Specifically, bilateral damage of the dorsal tegmental or lateral mammillary nuclei abolishes HD cell activity in the anterodorsal thalamus (Blair et al., 1998, 1999; Bassett et al., 2007). Further, lateral mammillary lesions abolish HD tuning in the postsubiculum, parasubiculum, and medial entorhinal cortex (Sharp and Koester, 2008). Again, lesions of the anterodorsal thalamus completely abolish directional tuning throughout the parahippocampal region, collectively indicating that given the known anatomy of these areas (see Taube, 2007 for review), the flow of information within the HD system likely follows a path from dorsal tegmental nucleus → lateral mammillary nuclei → anterodorsal thalamus → parahippocampal/retrosplenial cortex.

## VESTIBULAR INPUT, "BURSTY" CELLS, AND ATTRACTOR NETWORK HYPOTHESES OF HD SIGNAL GENERATION

HD cells are strongly influenced by external and internally generated sources of information (Taube, 2007). For instance, external cues such as visual landmarks can control HD cell tuning such that a change in the orientation of a landmark can induce a similar change in the preferred directions of HD cells. In other words, HD cell preferred firing directions tend to shift in the same direction and angular distance as landmarks (Taube et al., 1990b; Taube, 1995). Although landmark information exerts a strong influence on HD cells, the directional firing preference of HD cells can be maintained even when familiar external cues are eliminated, such as in darkness or in novel environments (Taube and Burton, 1995; Goodridge et al., 1998; Stackman et al., 2003; Yoder et al., 2011b). This finding suggests that internally generated information, or idiothetic cues (i.e., vestibular, proprioception, and motor efference), can be utilized to keep track of changes in directional heading over time, a process often referred to as angular path integration. The precise sensory mechanisms underlying angular path integration are unclear, however, it was suggested very early on that the vestibular system might play a particularly important role in this process (Potegal, 1982; Taube et al., 1990b; McNaughton et al., 1991). This view follows from the simple fact that angular head velocity—a product of the mechanical properties of the semicircular canals, which are sensitive to head acceleration—can be integrated over time to yield angular displacement, as has been demonstrated in occulomotor pathways (Robinson, 1989). An estimate of current HD can, therefore, be accomplished by a vector summation of the angular displacement and the animal's previous HD. McNaughton et al. (1991) provided the first computational model that captured this notion and subsequent models (e.g., Skaggs et al., 1995; Redish et al., 1996; Zhang, 1996) have expanded on this basic principal using continuous attractor networks (**Figure 3**). In these models, HD cells are conceptually arranged in a ring corresponding to their preferred firing directions. Cells with preferred directions that have overlapping directional firing ranges share excitatory connections and cells with greatly different preferred directions inhibit each other. This

**Table 1 | Summary of lesion results involving the HD cell circuit.**

| Lesion area | Recording location | HD signal | Landmark | Idiothetic | Reference |
|---|---|---|---|---|---|
| Vestibular labyrinth | Anterodorsal thalamus | No | – | – | Stackman and Taube, 1997 |
| | Postsubiculum | No | – | – | Stackman et al., 2002 |
| Supragenual nuclei | Anterodorsal thalamus | No | – | – | Clark et al., unpublished observations |
| Dorsal tegmental nuclei | Anterodorsal thalamus | No | – | – | Bassett et al., 2007 |
| Lateral mammillary nuclei | Anterodorsal thalamus | No | – | – | Blair et al., 1998; Bassett et al., 2007 |
| | Postsubiculum | No | – | – | Sharp and Koester, 2008 |
| | Parasubiculum | No | – | – | Sharp and Koester, 2008 |
| | Medial entorhinal cortex | No | – | – | Sharp and Koester, 2008 |
| Anterodorsal thalamus | Postsubiculum | No | – | – | Goodridge and Taube, 1997 |
| | Parasubiculum | No | – | – | Clark et al., 2011 |
| | Medial entorhinal cortex | No | – | – | Clark et al., 2011 |
| Laterodorsal thalamus | Postsubiculum | Yes | OK | Not tested | Golob et al., 1998 |
| Postsubiculum | Anterodorsal thalamus | Yes | Impaired | Mildly impaired | Goodridge and Taube, 1997 |
| | Lateral mammillary nuclei | Yes | Impaired | Not tested | Yoder and Taube, 2008 |
| Retrosplenial cortex | Anterodorsal thalamus | Yes | Mildly impaired | OK | Clark et al., 2010 |
| Medial entorhinal cortex | Anterodorsal thalamus | Yes | OK | OK | Clark and Taube, 2011 |
| Hippocampus | Anterodorsal thalamus | Yes | OK | Impaired | Golob and Taube, 1997, 1999 |
| | Postsubiculum | Yes | OK | Impaired | Golob and Taube, 1997, 1999 |
| Parietal cortex | Anterodorsal thalamus | Yes | OK | Mildly impaired | Calton et al., 2008 |
| | Medial entorhinal cortex | Yes | Not tested | Not tested | Whitlock et al., 2010 |

*For each lesion the table shows whether: (1) the HD signal is present, (2) landmark cue control is affected (as judged by the ability of the HD cell to shift its preferred direction following visual cue rotation), and (3) idiothetic cue processing (i.e., vestibular or motor) is affected (as judged by the ability of the HD cell to maintain a stable preferred direction as the animal locomotes in darkness and when locomoting from a familiar to a novel environment). Note: if no HD cells were identified following the lesion, then it was not possible to assess landmark or idiothetic cue processing.*

neural architecture forms a sustained "hill" of excitation centered on the animal's current HD. This activity hill is observed as a burst of firing when the animal's HD passes through the cell's preferred firing direction during a head turn. Angular head velocity information is commonly used to move the hill of activity around to different directions depending on changes to the animal's HD (this process is typically modeled through an additional ring of neurons that conjunctively encodes HD and angular head velocity; see **Figure 3**). A specific consequence of removing angular head velocity input is an activity hill that no longer moves along the ring in register with the animal's HD. Instead, the hill moves in different directions at different rates depending on the remaining inputs that convey information about current heading (e.g., visual and motor). In other words, neurons within the network would fire in bursts, as if the animal is passing its head through each cell's preferred firing direction. This latter feature of attractor networks, which we have termed "bursting" activity, forms an important prediction especially when considered with the lesion studies described below.

The hypothesis that vestibular information is critical for HD signal processing was first tested in a study conducted by Stackman and Taube (1997) in which anterodorsal thalamus HD cells were recorded before and after sodium arsanilate lesions of the vestibular system—a neurotoxic lesion technique that destroys hair cells throughout the vestibular labyrinth (Chen et al., 1986). In general, lesions of the peripheral vestibular system completely abolished directional activity in the anterodorsal thalamus of rats (**Figure 4A**). Surprisingly, the absence of HD cell activity persisted for up to 3 months (the post-lesion time period in which cell recording was monitored), strongly indicating that other sensory systems (e.g., vision or motor) were not capable of compensating for the loss of vestibular input, despite the fact that these cues can gain strong control over directional tuning (Goodridge et al., 1998; Stackman et al., 2003). An additional surprising result was the fact that Stackman and Taube did not detect burst firing in isolated units that had previously been modulated by HD. In other words, HD cells did not appear to "turn into" bursty cells following the neurotoxic lesions. As noted above, the significance of this result is derived from predictions of ring attractor models, in which an attractor that is uncoupled from its angular updating inputs should have the appearance of HD cell activity, but cell firing would be uncorrelated with the animal's HD. Because the activity hill would move around the ring attractor in random directions and at varying rates, the activity of a single cell recorded from such a network would resemble intermittent bursts of activity. Stackman and Taube identified some anterodorsal thalamus neurons that exhibited intermittent bursts of activity (e.g., **Figure 4C**), but because the spatial and behavioral correlates of these cells were not determined before the lesion, and because identified HD cells failed to display burst activity after lesions were produced, the authors argued against this interpretation.

Subsequent work by Stackman et al. (2002) replicated the general finding that vestibular input is necessary for HD cell

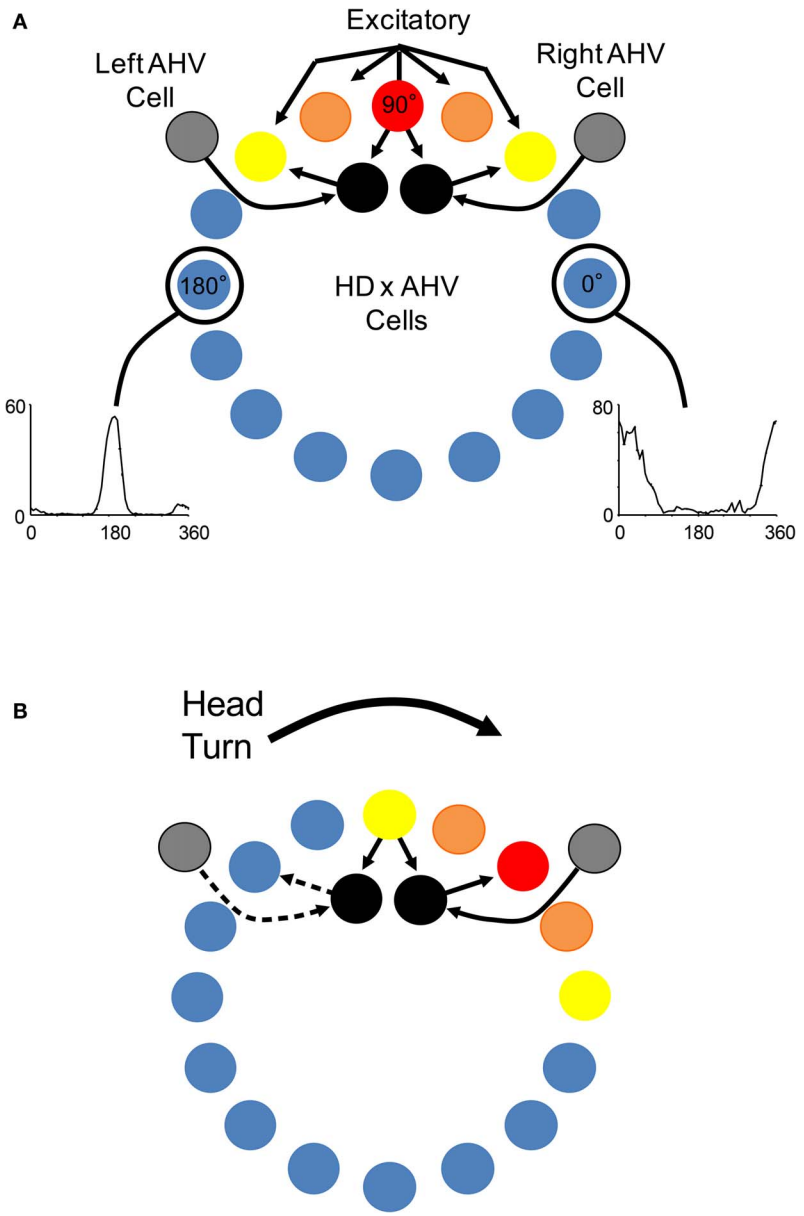


**FIGURE 3 | (A)** Components of a typical attractor network model of HD signal generation (e.g., Skaggs et al., 1995; Redish et al., 1996; McNaughton et al., 2006). In general, most attractor network models conceptually arrange HD cells in a circle or ring with each HD cell (colored circles) positioned according to their corresponding preferred tuning direction. Each HD cell sends strong excitatory axons to nearby neurons, and weaker excitatory inputs to more distant neurons. Inhibitory projections (not shown) within the network limit net activity resulting in a focused point, or a "hill," of high activity (warm colors). Movement of the activity hill corresponding to an animal's head movements is achieved by two additional neural signals: one that is sensitive to changes in an animal's angular head velocity (AHV) (gray circle), and another that conjunctively encodes current HD × AHV (black circle). These latter cells are either sensitive to right head turns and project to the right of the outer ring to which they receive input, or are sensitive to leftward head turns and project to the left of the ring to which they receive input. **(B)** Following a head turn, conjunctive HD × AHV cells drive the activity hill in the appropriate HD. For example, a right head turn would engage HD × AHV neurons that are specifically sensitive to clockwise head turns (solid arrows). These neurons would in turn activate HD cells to the right of the hill and drive activity to the animal's current HD.

generation, but instead utilized tetrodotoxin to temporarily inactivate vestibular hair cells. In short, postsubicular HD cells were recorded before and after vestibular inactivation, and consistent with the earlier study, were found to be completely non-directional during inactivation. Interestingly, vestibular inactivation also disrupted the location-specific firing of hippocampal place cells (see also Russell et al., 2003), indicating that both HD and place cell systems require vestibular input. Because it appears that grid cells require input from HD cells in the anterodorsal thalamus (Clark et al., 2011), disrupting the HD signal via vestibular manipulations would also likely disrupt grid cell firing patterns in MEC and other limbic areas. The results of

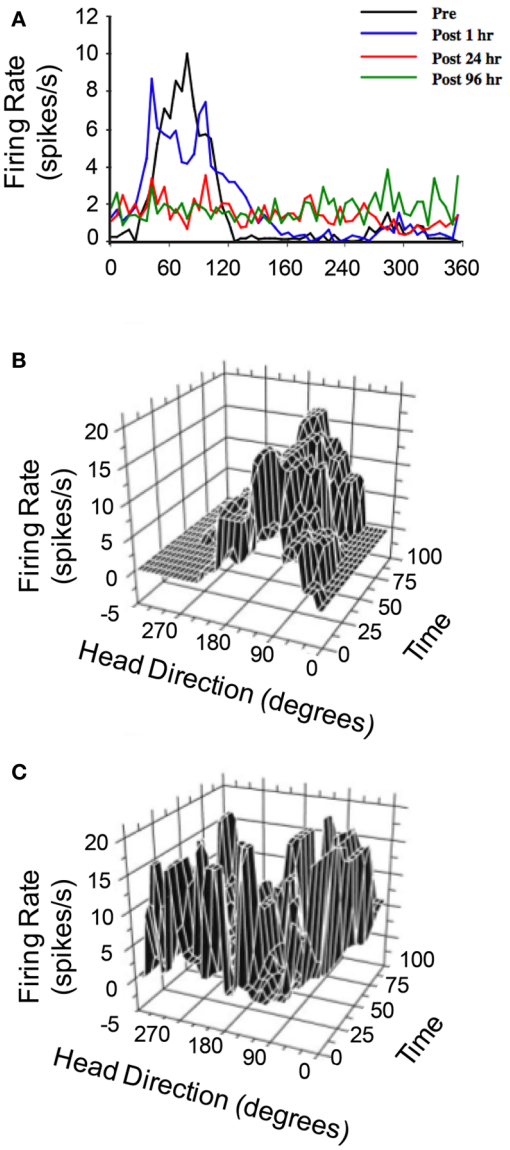


**FIGURE 4 | (A)** Responses of anterodorsal thalamic HD cells to sodium arsanilate lesions of the vestibular labyrinth (from Stackman and Taube, 1997). In general, disruption of the vestibular labyrinth abolished HD tuning shortly after the lesion and persisted up to 96 h after the lesion during which the cell was monitored. **(B,C)** 3D plot of firing rate and HD as a function of time in epochs of 5 s duration of a distinct anterodorsal thalamic HD cell recorded before vestibular lesion **(B)** and a non-directional anterodorsal thalamic burst cell recorded after vestibular lesion **(C)**. For both plots, unit activity was recorded over 8 min sessions, during which the rat foraged in a cylindrical apparatus. The post-lesion bursty cell depicted in **(C)** exhibited a characteristic pattern of intermittent high firing rate events that were neither related to the rat's HD nor temporally organized. Plots in **(A–C)** are modified from Stackman and Taube (1997).

Stackman et al. (2002), however, did not shed light on the issue of why burst activity was absent in their recordings after vestibular disruption. Moreover, because inactivation and permanent lesion techniques produce a general disruption to hair cells throughout the vestibular labyrinth (Chen et al., 1986), and even produce some damage to the 8th cranial nerve (Anniko and Wersäll, 1976), it remained unclear exactly where the origin of the impairments resided in the vestibular system.

The vestibular labyrinth is composed of the semicircular canals and the otolith organs, which provide information regarding angular and linear head acceleration, respectively. In an attempt to determine which of these vestibular components are essential for HD signal generation, Muir et al. (2009) occluded the semicircular canals bilaterally in chinchillas, a species of rodent that has large and easily accessible semicircular canals. Overall, the authors reported that anterodorsal thalamic HD cells recorded before semicircular canal occlusion lost all semblance of directional responding after occlusion. Importantly, and in contrast with the results of Stackman and Taube (1997), Muir et al. found that HD cells displayed bursty activity after semicircular canal occlusion. These "bursty" cells had the appearance of HD cells passing through their preferred directions when listened to through a loudspeaker, but unlike HD cells, they were completely uncorrelated with the animal's HD, even at brief time intervals (**Figure 5**). Bursty cells also showed very little accommodation, and were non-periodic; they fired in random intervals throughout the recording session. Thus, it was postulated that bursting activity represented HD cells that were disconnected from their primary driving input (i.e., vestibular), and in contrast to the results of Stackman and Taube (1997), these findings appeared to support the attractor network scheme of HD circuit organization. This general conclusion was also substantiated by a number of additional observations. First, the duration of bursting activity was dependent on movement velocity—with faster rotations resulting in shorter burst durations, a finding that corresponds to normal HD cells as they pass through their preferred firing directions. Second, the percentage of spikes during bursts and the percentage of samples that contained bursts were similar between bursty cells and HD cells. Finally, in sessions in which two bursty cells were recorded simultaneously, the temporal order in which the bursts occurred was contingent on the animal's direction of rotation (**Figures 5C** and **6**), just as an attractor network would predict. This latter observation is particularly interesting because it suggests that the general network organization remained intact following canal occlusion.

In a complimentary study conducted by Yoder and Taube (2009) that investigated the role of the otolith organs in HD cell activity, anterodorsal thalamic activity was monitored in otoconia deficient *tilted* mice (Lane, 1986), a transgenic mouse line that specifically have a disrupted sense of linear acceleration and head tilt. Surprisingly, Yoder and Taube (2009) identified a number of directionally tuned cells in the anterodorsal thalamus of *tilted* mice. For the most part, however, these HD cells demonstrated less robust directional firing compared to control mice, and were in many cases directionally unstable during recording sessions (i.e., the preferred direction of cells would drift over time). Consistent with Muir et al. a small number of bursty cells were identified in *tilted* mice, but not in control mice. Importantly, bursty cell activity was not observed simultaneously with neurons displaying sharp directional tuning, and the temporal order of simultaneously recorded bursty cells remained in register with one another depending on the direction of head rotation. This latter observation again supports the conclusion that the network

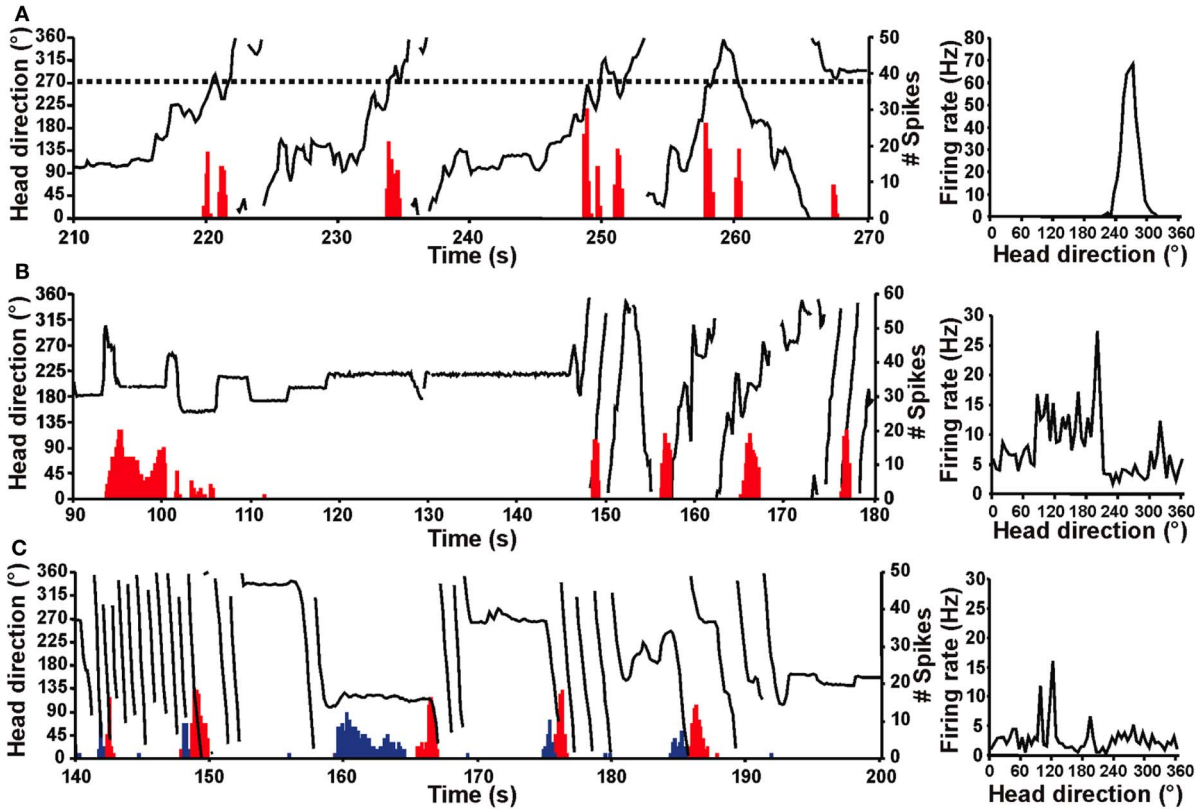


**FIGURE 5 | Firing of normal HD and bursty cells over time (red histogram) relative to the chinchilla's HD (black line) for portions of an 8 min recording session in a high-walled gray cylinder (left panels).** Corresponding firing rate × HD plots (right panels) for the cell shown at the left. **(A)** HD cell from a control chinchilla. The dotted line (left panel) represents the cell's preferred firing direction at ∼270° and this cell consistently fired at a high rate whenever the animal's head pointed at 270° (i.e., when the dotted line intersects the HD plot). The firing rate × HD plot for the control chinchilla (right panel) shows a clear, single-peaked function at ∼270° that matches the preferred firing direction in the plot at left. **(B,C)** Bursty cells from canal-plugged chinchillas. Note that the bursty cell in **(B)** fired in bursts similar to an HD cell in a control animal, but there was no consistent relationship between the animal's HD and the occurrence of bursts. This absence of a relationship is particularly evident in the bursty cell's irregular firing rate × HD function (right panel). **(C)** The plot on the left shows two simultaneously recorded bursty cells (cell 1, red; cell 2, blue). As in **(B)**, the duration of the burst was related to the velocity of the animal's head movement for both cells shown. In addition, the order of firing for the two cells was dependent upon the direction of movement (i.e., CW vs. CCW), where the animal was making almost exclusively CW movements during the periods of rapid rotation shown. The firing rate × HD plot for cell 2 is shown in the right panel. Panels **(A–C)** are from Muir et al. (2009).

organization remained intact, but accurate updating via velocity information was specifically impaired. Together, the results of Yoder and Taube suggested that the otolith organs were not necessary for the generation of the directional signal, but are critical for their stability and the robustness of the signal. Thus, when considered with the canal-plugging findings of Muir et al., the experiments suggest that only the semicircular canals are necessary for HD cell generation in the anterodorsal thalamus.

The bursty activity identified in the experiments by Muir et al. and in Yoder and Taube provided strong support for the attractor network hypothesis. Nevertheless, the failure to identify bursty activity in populations of HD cells after vestibular damage, as was the case in the Stackman and Taube (1997) study, has posed a challenge to this general conclusion. Muir et al. (2009) argued that the difference between these studies might be related to the amount of time between vestibular damage and cellular recording. While Stackman and Taube (1997) continued their recording sessions shortly after sodium arsanilate damage (1 h), Muir et al. waited 1–2 weeks for recovery before anterodorsal thalamic neurons were reassessed for directional activity. Stackman and Taube continued recording cellular activity within the anterodorsal thalamus for up to 96 h after the lesion, but in no cases were bursty cells recorded within this time period. This difference may be relevant because secondary vestibular neurons, which normally have high resting firing rates (mean: ∼35 spikes/s), return to only 50% of their baseline-firing rate after vestibular labyrinthectomy, and tonic activity of these neurons returns to pre-lesion levels only after 1 week (Ris and Godaux, 1998). Thus, Stackman and Taube monitored HD cell activity during a period of depressed tonic activity within the vestibular nuclei, suggesting that tonic firing by secondary vestibular neurons might underlie bursting activity.

## GENERATIVE CIRCUIT WITHIN THE HD CELL SYSTEM

The work summarized thus far suggests that HD cells likely adopt bursty firing characteristics following vestibular interventions (Muir et al., 2009; Yoder and Taube, 2009). Preliminary

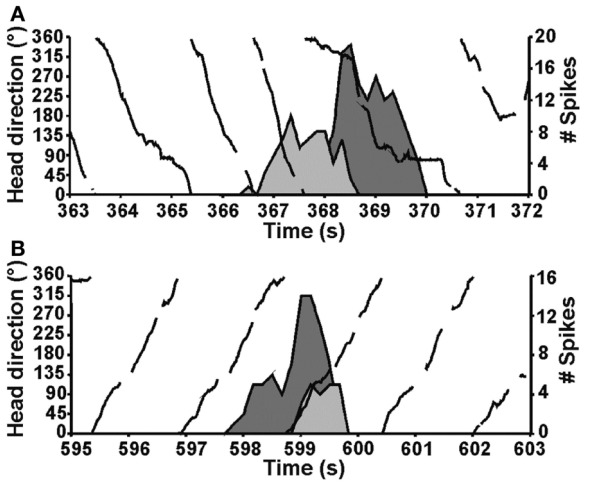


**FIGURE 6 | The direction of the animal's movement strongly predicted the order of cell firing when pairs of HD or bursty cells were recorded simultaneously (HD, solid black line).** Two different episodes are shown for the same pair of cells. During an episode when the animal made CCW turns (top), cell 1 (dark gray fill) fired a burst before cell 2 (light gray fill). In contrast, during an episode with CW head turns (bottom), cell 1 fired after cell 2. Plots in **(A,B)** are from Muir et al., 2009.

work from our laboratory has also corroborated these observations following lesions of putative vestibular relay centers such as the supragenual nucleus (Clark and Taube, unpublished observations). In contrast to these studies, however, Bassett et al. (2007) did not identify bursting activity in the anterodorsal thalamus of animals with bilateral lesions of the dorsal tegmental nuclei or lateral mammillary nuclei (see also Blair et al., 1998, 1999). Expanding on the interpretation that bursty activity after vestibular damage reflects an attractor network uncoupled from external vestibular input, these latter observations may constitute evidence that the HD signal and an attractor-based architecture resides in the reciprocal connectivity of the dorsal tegmental and lateral mammillary nuclei (Allen and Hopkins, 1989; Hayakawa and Zyo, 1989; Taube, 1998, 2007; Sharp et al., 2001a; Blair and Sharp, 2002).

The earliest support for the hypothesis above came from studies showing that both the lateral mammillary and dorsal tegmental nuclei contain populations of HD cells (Blair et al., 1998; Stackman and Taube, 1998; Sharp et al., 2001b), although with relatively smaller proportions reported in the dorsal tegmental nuclei compared to other diencephalic and telencephalic structures (reviewed in Taube and Bassett, 2003). Several anatomical studies also support the hypothesis, as both regions occupy a pivotal position between vestibular and landmark processing systems. Most notable among the vestibular system projections are the supragenual nuclei and nucleus prepositus hypoglossi (**Figure 2**; Brown et al., 2005; Biazoli et al., 2006); the latter of these two regions is thought to be the site of the neural integrator for the vestibulo-occular reflex (Robinson, 1989). Projections stemming from the nucleus prepositus hypoglossi are largely restricted to the dorsal tegmental nuclei (Brown et al., 2005; Biazoli et al., 2006), whereas output from the supragenual nuclei reaches all levels of the tegmento-mammillary pathway. These latter projections, however, are topographically organized such that output to the lateral mammillary nucleus is directed mostly ipsilateral, and output to the dorsal tegmental nucleus is directed largely to the contralateral side (Biazoli et al., 2006). The lateral mammillary nuclei also receive prominent projections from the postsubiculum (Shibata, 1989), suggesting that landmark information is integrated at this subcortical level (Yoder et al., 2011a).

Perhaps the strongest support for the hypothesis above comes from the findings that both the dorsal tegmental and lateral mammillary nuclei contain neurons sensitive to an animal's angular head velocity (**Figure 7**) (Blair et al., 1998; Stackman and Taube, 1998; Bassett and Taube, 2001; Sharp et al., 2001b). Indeed, ∼75% of the neurons in the dorsal tegmental nuclei code for angular head velocity, suggesting that the structure has a prominent role in self-movement cue processing. Bassett and Taube (2001) observed two types of angular velocity cells in this region: one that increased its firing rate proportionately to the speed to which the animal turned its head in either direction (**Figure 7A**) (i.e., clockwise or counterclockwise), and another that fires only when an animal turns its head in one direction (**Figures 7B,C**). These cells were termed symmetric and asymmetric angular velocity cells, respectively. While the symmetric subtype accounted for ∼50% of the total cells in the dorsal tegmental nuclei, asymmetric angular velocity neurons accounted for ∼25% of the total

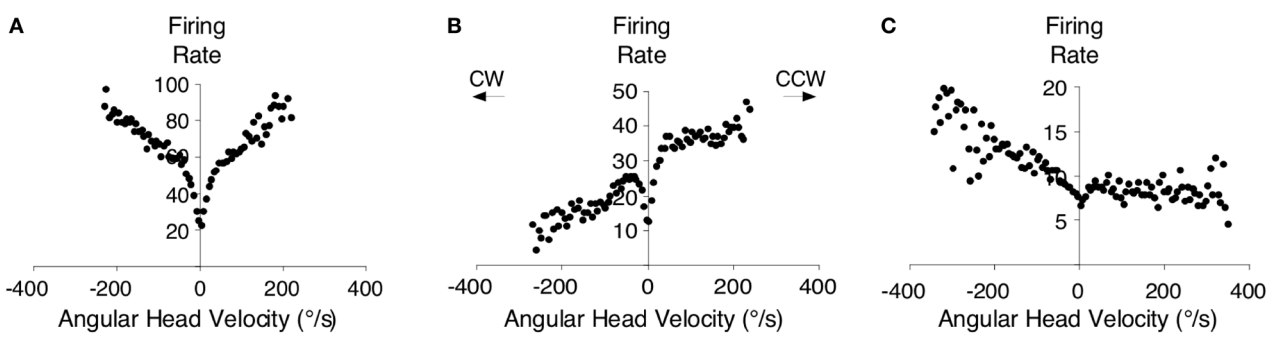


**FIGURE 7 | An example of a symmetric angular head velocity cell is shown in (A) and representative examples of asymmetric angular head velocity cells are shown in (B,C).** Clockwise (CW) and counter-clockwise (CCW) directions are as indicated. Plots in **(A–C)** are from Bassett and Taube (2001).

population. Interestingly, most asymmetric cells were localized in the hemisphere opposite the preferred tuning direction, suggesting some lateralization of cellular activity within the HD cell circuit. Angular velocity cells within the lateral mammillary nuclei constitute a smaller overall percentage (∼43%) compared to the dorsal tegmental nuclei (∼75%), however only the symmetric variety is found within this region. Furthermore, the properties of angular velocity cells are very similar between both brain regions. Asymmetric coding of angular velocity cells is consistent with the early ring attractor models, but the findings of symmetric subtypes have not received similar attention (but see Stratton et al., 2010). Given the high proportion of symmetric cells, future computational work should include networks with both asymmetric and symmetric subtypes.

One important issue to consider here is how the angular head velocity signal is derived within the tegmento-mammillary circuit? It is widely assumed that this signal is generated in large part from the vestibular system, and preliminary data from our laboratory appears to support this view, i.e., tetrodotoxin inactivation of the vestibular labyrinth significantly reduces angular head velocity sensitivity of neurons in the dorsal tegmental nucleus (Kosty and Taube, unpublished observations). Sharp et al. (2001b) demonstrated, however, that some angular velocity cells become "silent" when an animal is passively rotated while being handled by the experimenter. Although Sharp et al. reported that this was the case for only 5 of the 12 identified angular velocity cells in the study, this finding suggests that other sources of self-movement signals may play a role in generating angular velocity sensitivity. Subsequent work by Sharp et al. (2006) suggested that direct projections from the lateral habenula/interpeduncular nucleus to the dorsal tegmental nuclei might constitute a non-vestibular (motor) pathway. This possibility is supported by the identification of small proportions of angular and linear velocity modulated neurons in the habenula and interpeduncular nucleus (Sharp et al., 2006), as well as the finding that damage to the interpeduncular nucleus disrupts HD cell stability in the anterodorsal thalamus (Clark et al., 2009).

The possibility that the tegmento-mammillary circuit is the site of HD signal generation is also particularly attractive when considering the architecture of an attractor network. As noted above, network models typically rely on a set of recurrent excitatory connections to sustain the activity hill in a stable state (see **Figure 3**). They also rely on inhibitory connections to prevent the excitation of cells outside the current firing direction. The lateral mammillary and dorsal tegmental nuclei could conceivably contain this type of architecture because the dorsal tegmental nuclei to lateral mammillary nuclei projections are largely inhibitory (Gonzalo-Ruiz et al., 1993; Wirtshafter and Stratford, 1993), and the reciprocal projections are excitatory (**Figure 2**) (Hayakawa and Zyo, 1990). This pattern of connectivity has lent itself well to the interpretation that projecting neurons in the lateral mammillary region, presumably from HD cells, activate their inhibitory targets in the dorsal tegmental nuclei, which consequently inhibit their out-of-direction neighbors (Sharp et al., 2001a). Given that the reciprocal connections of the dorsal tegmental nuclei and nucleus prepositus hypoglossi also have an inhibitory/excitatory relationship, a similar conceptual scheme could be arranged between these nuclei as well. Nevertheless, very little is known about neural activity in the rodent nucleus prepositus in freely-moving animals [cf., McFarland and Fuchs, 1992, recorded from head fixed monkeys that were passively rotated sinusoidally and/or had to eye track a small target that moved horizontally. The authors found three types of neurons—two of which responded with eye movements, but were insensitive to vestibular stimulation, and a third type which was sensitive to both eye movement and vestibular stimulation]. Thus, whether this structure plays a significant role in HD signal computations is presently unclear.

Another theoretical prediction made by attractor models is the notion that conjunctive neurons that code for both HD and angular head velocity are responsible for driving the activity hill in the appropriate direction along the ring network (**Figure 3**). Consistent with this prediction, studies have identified small populations of these conjunctive neurons in the dorsal tegmental nuclei (11%, Bassett and Taube, 2001; 13%, Sharp et al., 2001b). However, it is important to point out that these putative conjunctive neurons fired across a broader range of directions and are, therefore, more coarsely modulated relative to the "classic" HD cell populations in other brain areas. Thus, it is unclear how such small populations of coarsely modulated conjunctive cells could be utilized to accurately update current HD within an attractor network.

One issue that has remained unexplored is the possibility that multiple generative circuits exist within the HD cell system. For instance, the connectivity within the postsubiculum and the inhibitory projections from this area could in principal support an attractor network (van Haeften et al., 1997). Arguing against this possibility, however, are the findings that neurons within the postsubiculum provide only a modest representation of angular head velocity, with ∼10% responding to this movement characteristic (Sharp, 1996). Neurons with angular head movement correlates have been identified in the rat parietal cortex (McNaughton et al., 1993), but as noted earlier, lesions of this region do not abolish directional tuning in the anterior thalamus (Calton et al., 2008), and inactivation of the structure does not impair directional firing "downstream" in the medial entorhinal cortex (Whitlock et al., 2010). Furthermore, lesions of the anterodorsal thalamus (Goodridge and Taube, 1997) or lateral mammillary nuclei (Sharp and Koester, 2008) completely abolish HD cell tuning in the postsubiculum, with no reports of bursting activity by postsubicular neurons after these lesions. This latter finding, in particular, suggests that HD cell generation most likely follows a path from the vestibular nuclei → supragenual/prepositus nuclei → dorsal tegmental nuclei → lateral mammillary nuclei → anterodorsal → thalamus parahippocampal/retrosplenial cortex.

One potential caveat to the hypotheses outlined above is the recent work that has identified populations of directionally tuned neurons in the anteroventral thalamus (Yoganarasimha et al., 2006; Tsanov et al., 2011); a thalamic region that does not receive direct input from the lateral mammillary nuclei (Shibata, 1992). The anteroventral thalamus receives one of its major inputs from the medial mammillary bodies (Shibata, 1992), which do not contain neurons with HD firing characteristics

(Sharp and Turner-Williams, 2005). One possibility is that anteroventral thalamic neurons receive their directional sensitivity through descending inputs from the retrosplenial cortex (Wyss and van Groen, 1992) or postsubiculum (van Groen and Wyss, 1990). In this scenario, the pathway would follow from anterodorsal thalamus → retrosplenial/postsubiculum → anteroventral thalamus. Alternatively, there could be a direct intra-thalamic projection from the anterodorsal to anteroventral region. Although there is no evidence for this latter projection, these connections are likely difficult to detect with current anatomical techniques, given that both nuclei lie adjacent to one another. HD cells have also been identified in the laterodorsal thalamus (Mizumori and Williams, 1993), but similar to the anteroventral thalamus, HD cells have not been identified in the subcortical afferents to the laterodorsal thalamus (Cooper et al., 1998) and lesions of the structure do not abolish HD cell activity in the postsubiculum (Golob et al., 1998). The laterodorsal nuclei receive large inputs from the retrosplenial cortex (Shibata, 2000) and postsubiculum (van Groen and Wyss, 1990), and again, it is possible that the HD signal within the laterodorsal thalamus is conveyed from these regions. Collectively, the studies summarized above suggest that a number of parallel processing pathways likely exist at the cortical-thalamic level of the HD cell circuit, which overlays the general hierarchical organization. Future work should be directed at identifying the critical pathways within these cortical-thalamic loops, and to better understand the precise role these parallel pathways play in shaping the HD cell signal.

## CONCLUSIONS

The present review summarized recent work that has been directed toward understanding the functional organization of the HD cell system, and much of this work supports three general conclusions. First, a large body of data strongly suggests that the HD cell signal is hierarchically organized and is primarily generated within subcortical circuits. This highly processed directional signal is then conveyed to cortical and parahippocampal regions through inputs from the anterior thalamus, including the anterodorsal thalamus and possibly the anteroventral region. A second general conclusion is that the identification of bursty activity within the HD cell network after vestibular damage appears to support the attractor network hypothesis of HD signal generation. The strongest evidence for this conclusion is derived from the fact that the temporal relationship between neurons is preserved after vestibular damage (Muir et al., 2009; Yoder and Taube, 2009) and is strongly correlated with an animal's direction of movement (i.e., right vs. left turns). Third, the observation of intermittent burst activity after vestibular damage, but not after dorsal tegmental or lateral mammillary damage is consistent with the hypothesis that the attractor architecture resides within the reciprocal connections of the tegmento-mammillary circuit.

## ACKNOWLEDGMENTS

This work was supported through grants from the National Institute of Health (NS053907, DC009318) to Jeffrey S. Taube and a postgraduate fellowship from the National Sciences and Engineering Research Council of Canada to Benjamin J. Clark.

## REFERENCES

Allen, G. V., and Hopkins, D. A. (1989). Mammillary body in the rat: topography and synaptology of projections from the subicular complex, prefrontal cortex, and midbrain tegmentum. *J. Comp. Neurol.* 286, 311–336.

Anniko, M., and Wersäll, J. (1976). Afferent and efferent nerve terminal degeneration in the guinea-pig cochlea following atoxyl administration. *Acta Otolaryngol.* 82, 325–336.

Bassett, J. P., and Taube, J. S. (2001). Neural correlates for angular head velocity in the rat dorsal tegmental nucleus. *J. Neurosci.* 21, 5740–5751.

Bassett, J. P., Tullman, M. L., and Taube, J. S. (2007). Lesions of the tegmentomammillary circuit in the head direction system disrupt the head direction signal in the anterior thalamus. *J. Neurosci.* 27, 7564–7577.

Biazoli, C. E. Jr., Goto, M., Campos, A. M., and Canteras, N. S. (2006). The supragenual nucleus: a putative relay station for ascending vestibular signs to head direction cells. *Brain Res.* 1094, 138–148.

Blair, H. T., and Sharp, P. E. (2002). "Functional organization of the rat head-direction circuit," in *The Neural Basis of Navigation*, ed P. E. Sharp (Boston: Kluwer), 163–182.

Blair, H. T., Cho, J., and Sharp, P. E. (1998). Role of the lateral mammillary nucleus in the rat head direction circuit: a combined single-unit recording and lesion study. *Neuron* 21, 1387–1397.

Blair, H. T., Cho, J., and Sharp, P. (1999). The anterior thalamic head-direction signal is abolished by bilateral but not unilateral lesions of the lateral mammillary nucleus. *J. Neurosci.* 19, 6673–6683.

Boccara, C. N., Sargolini, F., Thoresen, V. H., Solstad, T., Witter, M. P., Moser, E. I., and Moser, M. B. (2010). Grid cells in pre- and parasubiculum. *Nat. Neurosci.* 13, 987–994.

Brown, J. E., Card, J. P., and Yates, B. J. (2005). Polysynaptic pathways from the vestibular nuclei to the lateral mammillary nucleus of the rat: substrates for vestibular input to head direction cells. *Exp. Brain Res.* 161, 47–61.

Calton, J. L., Stackman, R. W., Goodridge, J. P., Archey, W. B., Dudchenko, P. A., and Taube, J. S. (2003). Hippocampal place cell instability after lesions of the head direction cell network. *J. Neurosci.* 23, 9719–9731.

Calton, J. L., Turner, C. S., Cyrenne, D. L., Lee, B. R., and Taube, J. S. (2008). Landmark control and updating of self-movement cues are largely maintained in head direction cells after lesions of the posterior parietal cortex. *Behav. Neurosci.* 122, 827–840.

Chen, Y. C., Pellis, S. M., Sirkin, D. W., Potegal, M., and Teitelbaum, P. (1986). Bandage backfall: labyrinthine and non-labyrinthine components. *Physiol. Behav.* 37, 805–814.

Clark, B. J., Bassett, J. P., Wang, S., and Taube, J. S. (2010). Impaired head direction cell representation in the anterodorsal thalamus after lesions of the retrosplenial cortex. *J. Neurosci.* 30, 5289–5302.

Clark, B. J., Sarma, A., and Taube, J. S. (2009). Head direction cell instability in the anterior dorsal thalamus after lesions of the interpeduncular nucleus. *J. Neurosci.* 29, 493–507.

Clark, B. J., and Taube, J. S. (2011). Intact landmark control and angular path integration by head direction cells in the anterodorsal thalamus after lesions of the medial entorhinal cortex. *Hippocampus* 21, 767–782.

Clark, B. J., Valerio, S., and Taube, J. S. (2011). *Disrupted grid and head direction cell signal in the entorhinal cortex and parasubiculum after lesions of the head direction system*. Program No. 729.11 2011 Neuroscience Meeting Planner. Washington, DC: Society for Neuroscience. [Online].

Cooper, B. G., Miya, D. Y., and Mizumori, S. J. (1998). Superior colliculus and active navigation: role of visual and non-visual cues in controlling cellular representations of space. *Hippocampus* 8, 340–372.

Gallistel, C. R. (1990). *The Organization of Learning*. Cambridge, MA: MIT Press.

Golob, E. J., and Taube, J. S. (1997). Head direction cells and episodic spatial information in rats without a hippocampus. *Proc. Natl. Acad. Sci. U.S.A.* 94, 7645–7650.

Golob, E. J., and Taube, J. S. (1999). Head direction cells in rats with hippocampal or overlying neocortical lesions: evidence for impaired angular path integration. *J. Neurosci.* 19, 7198–7211.

Golob, E. J., Wolk, D. A., and Taube, J. S. (1998). Recordings

of postsubiculum head direction cells following lesions of the laterodorsal thalamic nucleus. *Brain Res.* 780, 9–19.

Gonzalo-Ruiz, A., Sanz-Anquela, J. M., and Spencer, R. F. (1993). Immunohistochemical localization of GABA in the mammillary complex of the rat. *Neuroscience* 54, 143–156.

Goodridge, J. P., Dudchenko, P. A., Worboys, K. A., Golob, E. J., and Taube, J. S. (1998). Cue control and head direction cells. *Behav. Neurosci.* 112, 749–761.

Goodridge, J. P., and Taube, J. S. (1997). Interaction between postsubiculum and anterior thalamus in the generation of head direction cell activity. *J. Neurosci.* 17, 9315–9330.

Hafting, T., Fyhn, M., Molden, S., Moser, M. B., and Moser, E. I. (2005). Microstructure of a spatial map in the entorhinal cortex. *Nature* 436, 801–806.

Hayakawa, T., and Zyo, K. (1989). Retrograde double-labeling study of the mammillothalamic and the mammillotegmental projections in the rat. *J. Comp. Neurol.* 284, 1–11.

Hayakawa, T., and Zyo, K. (1990). Fine structure of the lateral mammillary projection to the dorsal tegmental nucleus of Gudden in the rat. *J. Comp. Neurol.* 298, 224–236.

Johnson, A., Seeland, K., and Redish, A. D. (2005). Reconstruction of the postsubiculum head direction signal from neural ensembles. *Hippocampus* 15, 86–96.

Kerr, K. M., Agster, K. L., Furtak, S. C., and Burwell, R. D. (2007). Functional neuroanatomy of the parahippocampal region: the lateral and medial entorhinal areas. *Hippocampus* 17, 697–708.

Lane, P. (1986). Tilted (tlt). *Mouse News Lett.* 75, 28.

Lever, C., Burton, S., Jeewajee, A., O'Keefe, J., and Burgess, N. (2009). Boundary vector cells in the subiculum of the hippocampal formation. *J. Neurosci.* 29, 9771–9777.

McFarland, J. L., and Fuchs, A. F. (1992). Discharge patterns in nucleus prepositus hypoglossi and adjacent medial vestibular nucleus during horizontal eye movement in behaving macaques. *J. Neurophysiol.* 68, 319–332.

McNaughton, B. L., Barnes, C. A., Gerrard, J. L., Gothard, K., Jung, M. W., Knierim, J. J., Kudrimoti, H., Qin, Y., Skaggs, W. E., Suster, M., and Weaver, K. L. (1996). Deciphering the hippocampal polyglot: the hippocampus as a path integration system. *J. Exp. Biol.* 199, 173–185.

McNaughton, B. L., Battaglia, F. P., Jensen, O., Moser, E. I., and Moser, M. B. (2006). Path integration and the neural basis of the 'cognitive map'. *Nat. Rev. Neurosci.* 7, 663–678.

McNaughton, B. L., Chen, L., and Markus, E. (1991). "Dead reckoning," landmark learning, and the sense of direction: a neurophysiological and computational hypothesis. *J. Cogn. Neurosci.* 3, 190–202.

McNaughton, B. L., Mizumori, S. J., Barnes, C. A., Leonard, B., Marquis, M., and Green, E. (1993). Cortical representation of motion during unrestrained spatial navigation in the rat. *Cereb. Cortex* 4, 27–39.

Mizumori, S. J., and Williams, J. D. (1993). Directionally selective mnemonic properties of neurons in the lateral dorsal nucleus of the thalamus of rats. *J. Neurosci.* 13, 4015–4028.

Moser, E. I., Kropff, E., and Moser, M. B. (2008). Place cells, grid cells, and the brain's spatial representation system. *Ann. Rev. Neurosci.* 31, 69–89.

Muir, G. M., Brown, J. E., Carey, J. P., Hirvonen, T. P., Della Santina, C. C., Minor, L. B., and Taube, J. S. (2009). Disruption of the head direction cell signal after occlusion of the semicircular canals in the freely moving chinchilla. *J. Neurosci.* 29, 14521–14533.

O'Keefe, J., and Dostrovsky, J. (1971). The hippocampus as a spatial map. Preliminary evidence from unit activity in the freely-moving rat. *Brain Res.* 34, 171–175.

O'Keefe, J., and Nadel, L. (1978). *The Hippocampus as a Cognitive Map*. Oxford, UK: Oxford University Press.

Papez, J. (1937). A proposed mechanism of emotion. *Arch. Neurol.* 38, 103–112.

Potegal, M. (1982). "Vestibular and neostriatal contributions to spatial orientation," in *Spatial Abilities: Development and Physiological Foundations,* ed M. Potegal (New York, NY: Academic Press), 361–387.

Ranck, J. B. Jr. (1984). Head direction cells in the deep layer of dorsal presubiculum in freely moving rats. *Soc. Neurosci. Abstr.* 10, 599.

Redish, A. D., Elga, A. N., and Touretzky, D. S. (1996). A coupled attractor model of the rodent head direction system. *Netw. Comput. Neural Syst.* 7, 671–685.

Ris, L., and Godaux, E. (1998). Neuronal activity in the vestibular nuclei after contralateral or bilateral labyrinthectomy in the alert guinea pig. *J. Neurophysiol.* 80, 2352–2367.

Robinson, D. A. (1989). Integrating with neurons. *Annu. Rev. Neurosci.* 12, 33–45.

Russell, N., Horii, A., Smith, P., Darlington, C., and Bilkey, D. (2003). Long-term effects of permanent vestibular lesions on hippocampal spatial firing. *J. Neurosci.* 23, 6490–6498.

Sargolini, F., Fyhn, M., Hafting, T., McNaughton, B. L., Witter, M. P., Moser, M. B., and Moser, E. I. (2006). Conjunctive representation of position, direction, and velocity in entorhinal cortex. *Science* 312, 758–762.

Savelli, F., Yoganarasimha, D., and Knierim, J. J. (2008). Influence of boundary removal on the spatial representations of the medial entorhinal cortex. *Hippocampus* 18, 1270–1282.

Sharp, P. E. (1996). Multiple spatial/behavioral correlates for cells in the rat postsubiculum: multiple regression analysis and comparison to other hippocampal areas. *Cereb. Cortex* 6, 238–259.

Sharp, P. E., and Koester, K. (2008). Lesions of the mammillary body region severely disrupt the cortical head direction, but not place cell signal. *Hippocampus* 18, 766–784.

Sharp, P. E., Blair, H. T., and Cho, J. (2001a). The anatomical and computational basis of the rat head-direction cell signal. *Trends Neurosci.* 24, 289–294.

Sharp, P. E., Tinkelman, A., and Cho, J. (2001b). Angular velocity and head direction signals recorded from the dorsal tegmental nucleus of Gudden in the rat: implications for path integration in the head direction cell circuit. *Behav. Neurosci.* 115, 571–588.

Sharp, P. E., and Turner-Williams, S. (2005). Movement-related correlates of single-cell activity in the medial mammillary nucleus of the rat during a pellet-chasing task. *J. Neurophysiol.* 94, 1920–1927.

Sharp, P. E., Turner-Williams, S., and Tuttle, S. (2006). Movement-related correlates of single cell activity in the interpeduncular nucleus and habenula of the rat during a pellet-chasing task. *Behav. Brain Res.* 166, 55–70.

Shibata, H. (1989). Descending projections to the mammillary nuclei in the rat, as studied by retrograde and anterograde transport of wheat germ agglutinin-horseradish peroxidase. *J. Comp. Neurol.* 285, 436–452.

Shibata, H. (1992). Topographic organization of subcortical projections to the anterior thalamic nuclei in the rat. *J. Comp. Neurol.* 323, 117–127.

Shibata, H. (2000). Organization of retrosplenial cortical projections to the laterodorsal thalamic nucleus in the rat. *Neurosci. Res.* 38, 303–311.

Skaggs, W. E., Knierim, J. J., Kudrimoti, H. S., and McNaughton, B. L. (1995). "A model of the neural basis of the rat's sense of direction," in *Advances in Neural Information Processing Systems*, Vol. 7, eds G. Tesauro, D. S. Touretzky, and T. K. Leen (Cambridge, MA: MIT Press), 173–180.

Solstad, T., Boccara, C. N., Kropff, E., Moser, M. B., and Moser, E. I. (2008). Representation of geometric borders in the entorhinal cortex. *Science* 322, 1865–1868.

Stackman, R. W., Clark, A. S., and Taube, J. S. (2002). Hippocampal spatial representations require vestibular input. *Hippocampus* 12, 291–303.

Stackman, R. W., Golob, E. J., Bassett, J. P., and Taube, J. S. (2003). Passive transport disrupts directional path integration by rat head direction cells. *J. Neurophysiol.* 90, 2862–2874.

Stackman, R. W., and Taube, J. S. (1997). Firing properties of head direction cells in rat anterior thalamic neurons: dependence upon vestibular input. *J. Neurosci.* 17, 4349–4358.

Stackman, R. W., and Taube, J. S. (1998). Firing properties of rat lateral mammillary single units: head direction, head pitch, and angular head velocity. *J. Neurosci.* 18, 9020–9037.

Stratton, P., Wyeth, G., and Wiles, J. (2010). Calibration of the head direction network: a role for symmetric angular head velocity cells. *J. Comput. Neurosci.* 28, 527–538.

Taube, J. S. (1995). Head direction cells recorded in the anterior thalamic nuclei of freely moving rats. *J. Neurosci.* 15, 70–86.

Taube, J. S. (1998). Head direction cells and the neurophysiological basis for a sense of direction. *Prog. Neurobiol.* 55, 225–256.

Taube, J. S. (2007). The head direction signal: origins and sensory-motor integration. *Annu. Rev. Neurosci.* 30, 181–207.

Taube, J. S., and Bassett, J. P. (2003). Persistent neural activity in head direction cells. *Cereb. Cortex* 13, 1162–1172.

Taube, J. S., and Burton, H. L. (1995). Head direction cell activity monitored in a novel environment and during a cue conflict situation. *J. Neurophysiol.* 74, 1953–1971.

Taube, J. S., Muller, R. U., and Ranck, J. B. Jr. (1990a). Head-direction cells recorded from the postsubiculum in freely moving rats. I. Description and quantitative analysis. *J. Neurosci.* 10, 420–435.

Taube, J. S., Muller, R. U., and Ranck, J. B. Jr. (1990b). Head-direction cells recorded from the postsubiculum in freely moving rats. II. Effects of environmental manipulations. *J. Neurosci.* 10, 436–447.

Tsanov, M., Chah, E., Vann, S., Reilly, R., Erichsen, J., Aggleton, J., and O'Mara, S. (2011). Theta-modulated head direction cells in the rat anterior thalamus. *J. Neurosci.* 31, 9489–9502.

van Groen, T., and Wyss, J. M. (1990). The postsubicular cortex in the rat: characterization of the fourth region of the subicular cortex and its connections. *Brain Res.* 529, 165–177.

van Haeften, T., Wouterlood, F., Jorritsma-Byham, B., and Witter, M. P. (1997). GABAergic presubicular projections to the medial entorhinal cortex of the rat. *J. Neurosci.* 17, 862–874.

Whitlock, J. R., Derdikman, D., Pfuhl, G., Moser, M. B., and Moser, E. I. (2010). *Effects of parietal cortical inactivation on representations in entorhinal cortex.* Program No. 101.13. 2010 Neuroscience Meeting Planner. San Diego, CA: Society for Neuroscience. [Online].

Wirtshafter, D., and Stratford, T. R. (1993). Evidence for GABAergic projections from the tegmental nuclei of Gudden to the mammillary body in the rat. *Brain Res.* 630, 188–194.

Wyss, J. M., and van Groen, T. (1992). Connections between the retrosplenial cortex and the hippocampal formation: a review. *Hippocampus* 1, 1–11.

Yoder, R., and Taube, J. S. (2008). *The postsubiculum provides visual landmark control to the head direction signal at the lateral mammillary nuclei.* Program No. 90.9. 2008 Neuroscience Meeting Planner. Washington, DC: Society for Neuroscience. [Online].

Yoder, R., and Taube, J. S. (2009). Head direction cell activity in mice: robust directional signal depends on intact otolith organs. *J. Neurosci.* 29, 1061–1076.

Yoder, R. M., Clark, B. J., and Taube, J. S. (2011a). Origins of landmark encoding in the brain. *Trends Neurosci.* 34, 561–571.

Yoder, R. M., Clark, B. J., Brown, J. E., Lamia, M. V., Valerio, S., Shinder, M. E., and Taube, J. S. (2011b). Both visual and idiothetic cues contribute to head direction cell stability during navigation along complex routes. *J. Neurophysiol.* 105, 2989–3001.

Yoganarasimha, D., Yu, X., and Knierim, J. J. (2006). Head direction cell representations maintain internal coherence during conflicting proximal and distal cue rotations: comparison with hippocampal place cells. *J. Neurosci.* 26, 622–631.

Zhang, K. (1996). Representation of spatial orientation by the intrinsic dynamics of the head-direction cell ensemble: a theory. *J. Neurosci.* 16, 2112–2126.

**Conflict of Interest Statement:** The authors declare that the research was conducted in the absence of any commercial or financial relationships that could be construed as a potential conflict of interest.

*Received: 13 December 2011; accepted: 14 February 2012; published online: 20 March 2012.*

*Citation: Clark BJ and Taube JS (2012) Vestibular and attractor network basis of the head direction cell signal in subcortical circuits. Front. Neural Circuits* ***6****:7. doi: 10.3389/fncir.2012.00007*

frontiers in
NEURAL CIRCUITS

ORIGINAL RESEARCH ARTICLE
published: 26 April 2012
doi: 10.3389/fncir.2012.00020

# Linear look-ahead in conjunctive cells: an entorhinal mechanism for vector-based navigation

***John L. Kubie[1]* and André A. Fenton[2,3]***

[1] *Department of Cell Biology, SUNY Downstate Medical Center, Brooklyn, NY, USA*
[2] *Center for Neural Science, New York University, New York, NY, USA*
[3] *Department of Physiology and Pharmacology, SUNY Downstate Medical Center, Brooklyn, NY, USA*

***Edited by:***
*Lisa Marie Giocomo, Norwegian University of Science and Technology, Norway*

***Reviewed by:***
*Michael E. Hasselmo, Boston University, USA*
*Benjamin Dunn, Kavli Institute for Systems Neuroscience, Norway*

****Correspondence:***
*John L. Kubie, Department of Cell Biology, SUNY Downstate Medical Center, 450 Clarkson Avenue, Brooklyn, NY 11203, USA.*
*e-mail: jkubie@downstate.edu*

The crisp organization of the "firing bumps" of entorhinal grid cells and conjunctive cells leads to the notion that the entorhinal cortex may compute linear navigation routes. Specifically, we propose a process, termed "linear look-ahead," by which a stationary animal could compute a series of locations in the direction it is facing. We speculate that this computation could be achieved through learned patterns of connection strengths among entorhinal neurons. This paper has three sections. First, we describe the minimal grid cell properties that will be built into our network. Specifically, the network relies on "rigid modules" of neurons, where all members have identical grid scale and orientation, but differ in spatial phase. Additionally, these neurons must be densely interconnected with synapses that are modifiable early in the animal's life. Second, we investigate whether plasticity during short bouts of locomotion could induce patterns of connections amongst grid cells or conjunctive cells. Finally, we run a simulation to test whether the learned connection patterns can exhibit linear look-ahead. Our results are straightforward. A simulated 30-min walk produces weak strengthening of synapses between grid cells that do not support linear look-ahead. Similar training in a conjunctive cell module produces a small subset of very strong connections between cells. These strong pairs have three properties: the pre- and post-synaptic cells have similar heading direction. The cell pairs have neighboring grid bumps. Finally, the spatial offset of firing bumps of the cell pair is in the direction of the common heading preference. Such a module can produce strong and accurate linear look-ahead starting in any location and extending in any direction. We speculate that this process may: (1) compute linear paths to goals; (2) update grid cell firing during navigation; and (3) stabilize the rigid modules of grid cells and conjunctive cells.

**Keywords: grid cell, conjunctive cell, entorhinal cortex, navigation, computation, place cell**

## INTRODUCTION

The discovery of place cells in the hippocampus over three decades ago led to the concept that the hippocampus was the critical structure in the brain's cognitive map (O'Keefe and Nadel, 1978). We now see this discovery as the first of several steps toward understanding how map-like properties are extracted. In subsequent years the elucidation of head-direction cells (Ranck, 1985), grid cells (Hafting et al., 2005), conjunctive cells (Sargolini et al., 2006), and barrier cells (Solstad et al., 2008) have contributed to an understanding of map construction. This paper will focus on the properties of grid cells and conjunctive cells in an effort to understand their utility for map construction. As with hippocampal place cells, these two cell types exhibit location-specific firing; that is, individual cells will fire in select locations of a given environment. In contrast to hippocampal place cells, individual conjunctive cells, and grid cells discharge in highly organized spatial patterns.

Time-averaged recordings from single grid cells reveals they express a dramatic spatial firing pattern composed of firing rate bumps that are spaced in a highly regular pattern. For a given cell, the bumps form a triangular lattice (grid) where the bumps are evenly spaced from nearest neighbors (scale), and extend along three axes, oriented 60° from each other (orientation). Individual patterns are also described as having a spatial "phase," the *x, y* offset of the set of bumps (**Figure 1**).

Although there is no direct evidence of the contribution of grid cells to place cells or navigation, the connectivity and firing patterns suggest several functions. First, layer II of the medial entorhinal cortex, where the greatest concentration of grid cells is found, projects directly to place cells in CA3 as well as indirectly to both CA3 and CA1 by way of the perforant path. This suggests that the spatial firing of grid cells may serve as input to place cells (O'Keefe and Burgess, 2005; Solstad et al., 2006). Second, the regular patterns of grid cell firing, where one bump location predicts the direction and distance to other bump locations, suggests that grid cells, at least in part, are driven by path integration (O'Keefe and Burgess, 2005; McNaughton et al., 2006). Third, the stability of grid cell firing patterns within and across sessions suggests that grid cell firing is also partially controlled by location-specific sensory cues (Hafting et al., 2005). Finally, the regular geometric firing patterns, characterized by straight lines and consistent angles, suggest

that the metrics of distance and direction are extractable features (Jeffery and Burgess, 2006).

The focus of the current study is to investigate potential mechanisms where the metric properties of grid cells could be used to predict locations directly ahead of the animal's nose: that is, the set of locations the animal would encounter if it walked on a direct path straight ahead. We call this process "linear look-ahead." We will explore how linear look-ahead can update an animal's location on the grid cell map to an adjacent location ahead of its nose, and how this process can be extrapolated to more distant locations, a process that can be exploited for selecting optimal straight line paths for navigation (**Figure 2**).

## THREE CRITICAL FEATURES

Three features of entorhinal cortex need to be elaborated before proceeding with the analysis. The first is that grid cells are not the only spatially tuned entorhinal neurons. Complementing grid cells found predominantly in layer II are conjunctive cells found predominantly in layer III (Sargolini et al., 2006). Like grid cells, conjunctive cells fire in the pattern of a regular triangular lattice. In contrast to grid cells, however, conjunctive cell firing is modulated by head-direction. An individual conjunctive cell will exhibit the spatial firing pattern of a grid cell, but, additionally, while the rat is in the location of the cell's firing bump, the cell will only fire if the rat's nose is pointed in the cell's preferred direction.

The second feature that is critical to our analysis is the dorsal-to-ventral increase in grid scale originally reported by Hafting et al. (2005). The scaling increase has been supported in subsequent work, and correlates both with differences in the membrane properties of grid cells (Sargolini et al., 2006; Giocomo et al., 2007) and differences in the scale of place cells at corresponding depths (Kjelstrup et al., 2008). The range of dorsal-to-ventral scale increase appears to be greater than a factor of 2 (Barry et al., 2007) but is presently unclear.

The third critical feature is the modular organization of grid cells. A grid cell module is a localized region where all cells share identical orientation and scale. That is, the characterization of individual grid cells within a module is determined solely by phase ($x$, $y$ offset of grid bumps). Hafting et al. (2005), in the initial grid cell study, reported that all grid cells recorded from a single tetrode had identical scale and modular properties. Barry et al. (2007) found discrete jumps in grid scale when driving electrodes from dorsal-to-ventral, suggesting large, discrete modules. The Moser group has preliminary evidence supporting large-scale modules (Stensola et al., 2011). It appears that medial entorhinal cortex is organized as a stack of horizontal slices, with each slice

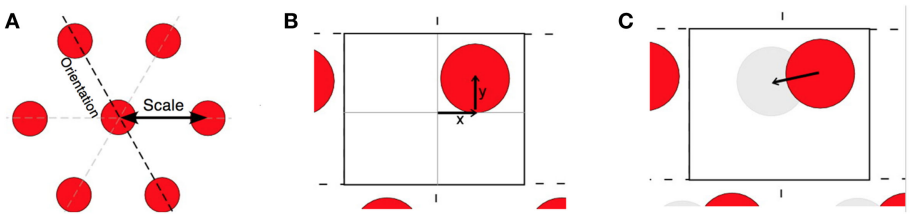


**FIGURE 1 | (A)** Idealized spatial excitability pattern of a single grid cell, illustrating grid scale, and orientation. **(B)** Closer view of the excitability map showing the boundaries of a single rectangular tile. The phase of one cell is illustrated as $x$ and $y$ offsets from the center. If this were from a rigid module, each cell in the module would have a single excitability bump within the tile. **(C)** The offset vector connecting the centers of two grid bumps within a tile.

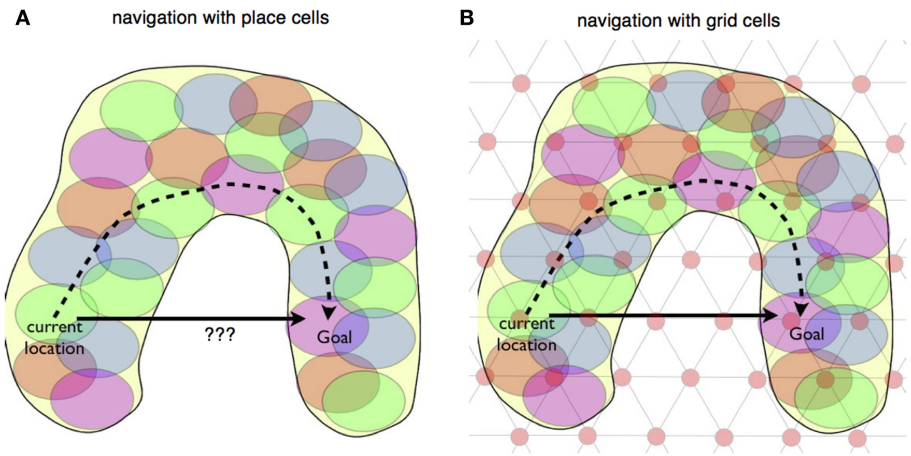


**FIGURE 2 | Place cell and grid cell navigation. (A)** An idealized *U*-shaped spatial terrain, covered with the firing fields of place cells. Many navigation models rely on the hippocampus computing a path between current location and goal that involves crossing a minimal number of firing fields, illustrated by the dashed arrow. **(B)** The terrain is overlaid with an idealized grid cell firing pattern, illustrating that grid cells, in principal contain information for a linear, shortest-path route between start location and goal. The path can cross unvisited space.

representing a module, and neighboring modules representing large steps in grid scale. Our presumption is that modules are real. Although evidence for modules has only been presented for grid cells, we will also assume that the layer III conjunctive cells have a modular organization that corresponds to the overlying grid cell module (predominantly found in layer II).

This paper is organized in three parts. The first is devoted to a concept we refer to as "rigid modules." Rigid modules are modules where the constraints of fixed grid scale and orientation are extremely tight. A "tile" is defined for a rigid module as a spatial region that contains a single grid bump for each neuron in the module. A tile is a repetitive unit that tessellates to cover all regions of accessible space. We will describe how understanding the organization of a tile is sufficient for understanding the collective properties of a rigid module, and how all between cell spatial firing relationships are represented in a tile. The final two parts will assume the existence of tile like organization in rigid modules. In part 2 we examine how regularities of movement may, through Hebbian synaptic plasticity, affect the connections amongst neurons in a rigid module. More specifically, we will show how Hebbian plasticity amongst conjunctive cells can produce small subsets of strong connections between-cell pairs where (a) the two cells have similar heading preferences and (b) the phases are such that the firing bump of the first cell is "upstream" to the firing bump of the second cell. Finally, in part 3, we will examine how several sets of rigid modules can, using linear look-ahead, identify a straight line path connecting the current location and a known goal, even if the path crosses unexplored regions of space.

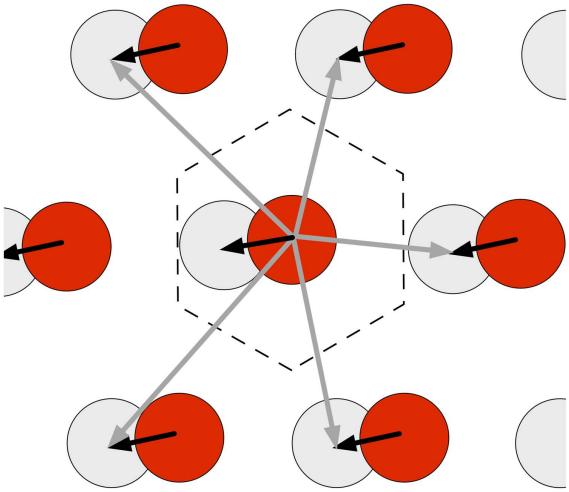


**FIGURE 3 | Shortest interbump vector (SIV).** In a rigid module, the vectors connecting the bump of a grid cell to the activity bumps of a second cell are fixed. The figure illustrates the activity pattern of a single grid cell (red) with a bump in the center, and the vectors to activity bumps of a second grid cell (gray). For the central red bump – and any red bump – there are six vectors to the nearest six bumps of the gray cell activity map: the shortest is black and the others are dark gray. The SIV is constant for all red cell activity bumps. A single gray bump falls within a hexagonal tile centered on the red bump.

## RESULTS

### PART 1: MODULAR ORGANIZATION AND RIGID MODULES

We call a module "rigid" if the orientation and scale of all of its members are identical. This strict criterion is intended to go beyond the similarity of orientation and scale in the description of modules. For example, while 5% variations in grid scale might be acceptable in a module, such a module would not be rigid. Are there true rigid modules in entorhinal cortex? There are three possibilities: (1) that the preliminary observations of horizontal slice modules are in fact rigid modules; (2) that the horizontal slice modules are not rigid and there are no rigid modules; and (3) that a single horizontal module contains several separate rigid subsets. Although we consider the answer unsettled, the model described in this manuscript makes the assumption that rigid modules exist and are the basis for information processing.

If rigid modules exist, then several interesting properties emerge. The first is that the vector connecting the nearest grid bumps of any two neurons in a rigid module is a constant. We call this vector the "shortest interbump vector" (SIV). Consider two grid cells A and B within a single rigid module (**Figure 3**). For all bumps of grid cell A the vector to the nearest bump of B is constant. The implication is that, if as an animal traverses space and one of its grid cells fires because the animal is at the location of one of the cell's grid bumps, then movement in a specific direction and distance will always result in the subject being at a grid bump location of a particular grid cell. The relationship holds for all regions in a large environment, no matter which of the cell's many grid bumps the subjects starts from. Moreover, this relationship is likely to be maintained across environments, given the observation that grid cells remap across different environments in a rigid manner, only by shifting the phase of all cells in a module by a constant amount (Fyhn et al., 2007). That is, in any environment, if cell A is firing and the rat moves a certain distance and direction it is likely that cell B will fire. Direction is determined with reference to the head-direction cell system.

A second property of rigid modules is a spatial pattern we will refer to as a "tile." In the initial paper describing grid cells, the authors introduced the concept that the firing pattern of a single grid cell will tessellate across the floor of any large apparatus (Hafting et al., 2005), where "tessellation" refers to laying out a repeated spatial bump pattern called a "tile." In a rigid module, a tessellating pattern can be described that includes all of the cells in the module. A tile for a rigid module is a contiguous region of space that contains one and only one bump from each neuron in the module. Regions that meet this condition can be laid out, edge-to-edge to cover all of accessible space (**Figure 4**). For any rigid grid cell set, several boundary shapes can outline a tile, including parallelograms (base = gridscale; height = 0.866 × gridscale), a rectangle (same base and height as parallelograms), and a regular hexagon (side = 0.577 × gridscale). If a shape successfully outlines a tile in one position, it will continue to define a tile through any translation (sliding $x$ and $y$) without rotation, no matter the magnitude of translation within the environment.

For a given tile shape, translation changes the relationship of specific grid bumps to the boundary, but leaves tile conformity intact. Consider the firing of a rigid set of grid cells whose bumps

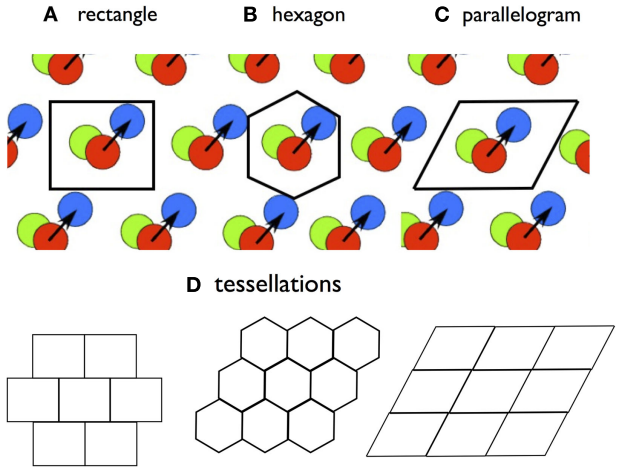


**FIGURE 4 | The tile concept.** A tile is a bounded region that contains one-and-only one activity bump from each grid cell in a rigid module. A tile boundary will tessellate, in that it can be placed edge-to-edge to cover a surface. Three possible tile boundary shapes are **(A)** rectangles; **(B)** hexagons; and **(C)** parallelograms. **(D)** shows tesselation patterns. No single tile boundary will contain all of the SIVs of a rigid module, but the hexagon contains all of the SIVs connecting to a grid cell with a bump at the center.

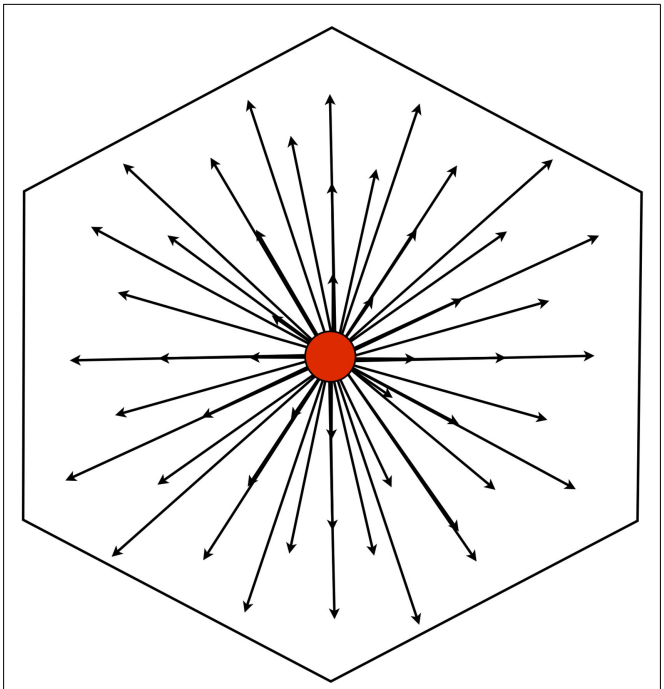

**FIGURE 5 | All of the shortest interbump vectors (SIVs) emanating from a grid bump A will describe a hexagonal tile with grid bump A at the center.** The horizontal width of a hexagonal tile is the grid scale; the side length is (grid scale)/[square root (3)]; the longest SIV is (grid scale)/[square root(3)].

are distributed across a large apparatus; add a boundary somewhere on this surface that defines a tile. If this boundary is lifted, translated in position and placed anywhere else, in a process similar to using a cookie cutter, the bumps enclosed in the second location will also define a tile. Although the new location changes the relationships of individual grid cell bumps to the tile boundaries, the boundary continues to enclose one-and-only one bump for each grid cell.

If we consider the interbump vectors between all bump pairs within a tile, we will find that many of these are SIVs, but, for any tile, some are longer. For example, consider bumps A and B from two different grid cells, with both lying within a rectangular tile, as in **Figure 5**. If bump A is adjacent to the left boundary and bump B is adjacent right boundary, the A–B distance measured within the tile will be long, approaching 1 grid bump unit. However, for each of these within-tile bumps, there is a shorter A–B vector to an outside-of-tile bump of the second cell. These shorter vectors are identical and are the SIVs for this bump cell pair. In brief, no tile will contain the SIVs connecting all of its bump pairs.

The set of SIVs originating from the bump of a single neuron, however, produces a surface bounded by a specific shape, the hexagon described above (**Figure 5**). This is a tile, since it includes one and only one grid bump for each neuron in the rigid set. Using different neurons as the origin produces translations of this tile. Thus, from the perspective of a grid bump of any grid cell, the set of SIVs extending from the bump forms a hexagon with the cell's grid bump at the center of the hexagon. This bump-centered tile is a construct that identifies all of the SIVs for the central cell. If we consider a continuously moving animal, we can define the "current effective tile" as the hexagon in which the center represents the current location of the animal.

### *Firing patterns in a rigid module*

The collective firing of a rigid module signals the animal's location within a tile, but contains no other location information. A simple network of neurons in a rigid module demonstrates this property. Since the tile of a rigid module contains one firing bump of each grid cell, a tile can be used to represent the spatial firing property of each neuron. We'll use a rigid module of grid cells, each with a grid scale of 60 cm and a rectangular tile covering 30 cm × 24 cm. Each cell's spatial firing correlate is represented as a 2D Gaussian centered at a position within a tile. The module contains 1800 neurons, that are assigned to 100 distinct "excitability maps," 18 neurons per map. Each excitability map covers a tile and has a single "firing bump." The firing bumps across the set of excitability maps are spread evenly across the tile. The tile representation is tessellated to cover the floor of a 1.8 m by 1.8 m square apparatus. A virtual rat's (vRat's) path, moving at 25 cm/s in 10 ms steps is constructed within the floor bounds. At every time step, each neuron's firing is calculated as a product of the vRat's location on the neuron's excitability map (within the current tile) and a random factor. For conjunctive cells, the vRat's head orientation is a third factor that governs firing. The result is straightforward and as predicted. For individual time samples the firing of the set of neurons is a two-dimensional firing bump, centered on the rat's location on a tile. As the rat moves, the center of the firing bump moves smoothly, but always remains within the tile. **Figure 6** illustrates single time samples, and the accompanying video (Movie S1 in Supplementary Material) illustrates movements of the firing

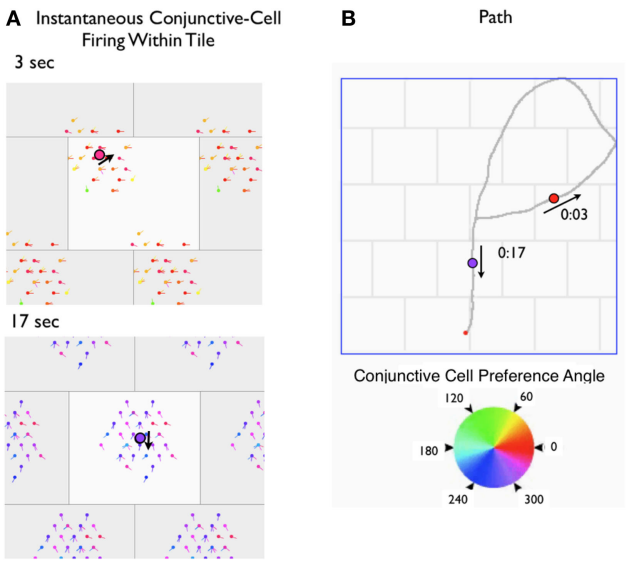


**FIGURE 6 | (A)** Video frames from a movie depicting the firing of conjunctive cells in a module during a 20 s path through a rectangular chamber. **(B)** The 20-s path is depicted on the right. In **(A)**, the rigid module is depicted as a rectangular tile, with each cell's phase mapped in the surface. A virtual neuron that has fired within the previous 200 ms is depicted with others invisible. Additionally, the color (and "nose") of the colored circle indicates the directional preference of a cell that fired. The black large circle is the virtual rat's location at the mid-point of the 200 ms sample. Gray boxes surrounding the central tile are half-replicas of the central tile. The three things to note are (1) the firing of cells is represented by a circular cluster, centered on the rat's location; (2) for conjunctive cells, a subset of head angles will fire together; and (3) the firing of the cells in a rigid module can only signal the rat's location and head orientation within the module.

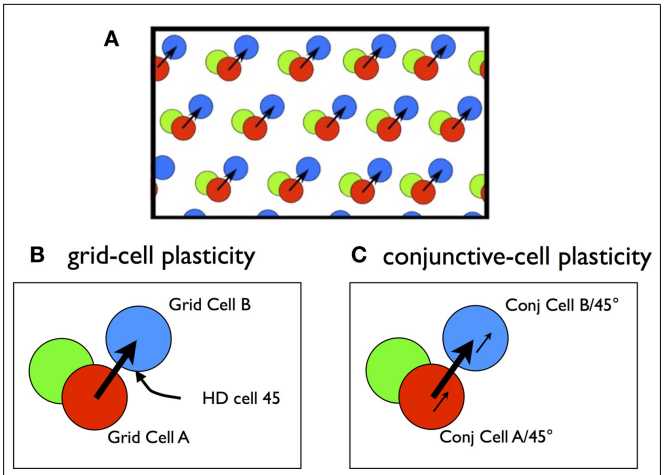


**FIGURE 7 | (A)** Fixed spatial relations between the activity bumps of three grid cells in a rigid module. **(B)** Preliminary Hebb model. Grid Cell A + Head-direction Cell 45, firing together, will predict the firing of Grid Cell B. While this is correct, the strengthening of these synapses will not be helpful in predicting the firing of Grid Cell B. The logic requires a conjunctive firing of the two upstream cells (see text). **(C)** Hebb model with conjunctive cells. In this case the firing of conjunctive cell A/45° predicts the firing of conjunctive cell B/45°. If the synapse has plasticity following Hebbian rules, the synapse ought to strengthen with experience and lead to predictive firing.

bump as a vRat traverses a virtual apparatus. Examining the collective firing of members of the module one could have a good estimate of the animal's location and movement within the tile, but would have no information about which tile in the apparatus the animal occupies.

## PART 2: LEARNING IN RIGID MODULES

A number of recent studies have proposed that grid cells are responsible for path-integration-based updates of the place cell representation of a rat's location (O'Keefe and Burgess, 2005; Fuhs and Touretzky, 2006; Sreenivasan and Fiete, 2011). A principal goal of our research program is to see if the cells of entorhinal cortex could perform other navigational calculations. Specifically, we wanted to see if the grid-modulated cells of entorhinal cortex could perform linear look-ahead," the process of projecting vectors to various distances directly ahead of the rat, in order to vicariously explore potential shortcuts. We speculated that linear look-ahead mechanisms might: (1) require rigid modules; and (2) be implemented by synaptic connections developed through experience-dependent plasticity.

Our reasoning is illustrated in **Figure 7**. Consider a rigid module of grid cells. A rat is at a particular location moving NE (45°). Firing correlates predict that one of the grid cells in the module (grid cell A) will fire and a head-direction cell tuned to 45° (HD 45) will fire. As the rat moves along this path, it will cross the firing bump of another cell (grid cell B) and it will fire. Since this is a rigid module, with fixed vectors connecting bump locations of pairs of cells, whenever the rat crosses the bump of Cell A at 45°, grid cell B will likely fire. If we imagine that these cells are connected with plastic Hebbian synapses (Grid Cell A and HD 45 → Grid Cell B), we suppose that with normal experience these synapses will strengthen. After the strengthening, we imagine that, when the rat is at the location of a firing bump of grid cell A and its nose in pointed 45°, the strengthened synapses will fire Grid Cell B, even if the rat is not moving. Grid Cell B firing along with HD 45 ought to lead to grid cell C firing, and so on, producing the sequential activation of a series of grid cells whose bumps form a straight line. This "linear chain reaction" would appear to be the linear look-ahead mechanism.

The problem is that this does not work. This is because HD 45 does not selectively predict the firing of Grid Cell B (or C). Since the firing bumps of all grid cells can be approached from a 45° angle, HD 45 equally well predicts the firing of all grid cells. Similarly, Grid Cell A does not predict the firing of Grid Cell B any more than the firing of other grid cells whose firing bumps surround it. While it is true that the conjunction of Grid Cell A firing and HD 45 predicts the firing of Grid Cell B, it is only the conjunction that is predictive. Knowledge of the firing of each cell alone is of little or no predictive value. Most importantly, the Hebbian process does not signal conjunction – the Hebbian strengthening rule does a poor job as a logical AND operator. This problem is logically identical to a problem with water-maze learning described by Brown and Sharp (1995). As the authors noted, the difficulty is due to the problem of "linear separability" or the "exclusive or" (XOR)

problem (Minsky and Papert, 1969). Predicting the firing of Grid Cell B requires a logical AND operator between the variables of grid cell firing and head-direction which simple rules of synaptic plasticity cannot provide. Below we use a simulation to show that applying a Hebbian learning rule between pairs of connected grid cells does not produce useful or selective patterns of synaptic strengthening.

The failure of useful association can be seen in a simulation. The simulation models a rat making a 1-h virtual path across 1.8 m × 1.8 m space. The path is created by having the rat move at constant speed (20 cm/s) and sampling at 10 ms intervals. At each sample the rat's heading direction is changed from the previous direction by a small random factor, within the range ±3°. When the rat encounters a wall, its heading changes in a random direction within accessible space.

The simulation involves a single grid cell that receives inputs from a large number of grid cells and head-direction cells. If we think of the single grid cell as "Grid Cell B" the useful association question boils down to whether during an extended random-walk training session we will see evidence of correlation between the firing of any of the upstream grid cells or head-direction cells and this cell. If Hebbian plasticity were in place, such correlated firing would lead to selectively strengthened synapses that in turn, might produce useful patterns of connection. In the simulation one group of afferents is a set of 882 grid cells with 49 distinct excitability maps whose peaks are evenly distributed over the tile. The second group of afferents is a set of 882 afferent head-direction cells with 18 distinct heading preferences, distributed in 20° increments. The firing of each afferent neuron and the single downstream neuron is determined for each 10 ms interval during the 1-h path. Firing of each grid cell is determined as a function of three factors: (1) the vRat's location in the cell's excitability map; (2) a random factor; and (3) a grid cell threshold factor (to achieve a mean firing rate of about 5 spikes/s). Firing of each head-direction cell is determined by (1) the vRat's heading direction relative to the cell's preferred direction; (2) a random factor; and (3) a head-direction threshold factor.

Each of the afferent cells has a connection to the target cell. For each connection the afferent cell is termed the "origin" and the single downstream cell is the "termination." To assess the correlated firing between the cells at each end of a connection, "hits" and "misses" were tabulated following each target cell spike. A hit was tabulated when the upstream cell fires within a 500 ms window preceding the downstream spike; a miss was recorded if there was no spike in the time window. At the conclusion of the 1-h path a hit ratio was calculated for each connection (e.g., between each pair of cells).

$$\text{Hit Ratio} = \text{hits}/(\text{hits} + \text{misses})$$

The results reveal little-to-no evidence that Hebbian mechanisms could contribute to look-ahead or other aspects of anticipatory firing. High hit ratios indicate co-active firing between the upstream cells and the single downstream grid cell. If there was a subset of connections with enhanced hit ratios, this would indicate, at least in principle, that selected synaptic connections could be strengthened by experience-dependent Hebbian mechanisms. The results are shown in **Figure 8**. The overall finding is that selective high hit ratios are barely present. There is a small tendency to observe high hit ratios for connections between grid cells with peak excitability maps in the region surrounding the peak excitability of the target grid cell. There is no tendency for high hit ratios among subsets of head-direction cells. In brief, high hit ratios, which, if Hebbian mechanisms were in place would lead to synaptic strengthening, could not lead to a linear look-ahead mechanism suggested above and in **Figure 8**. The reason for this is clear. The prediction made by **Figure 7** is that the conjoint firing of Grid Cell 1 and HD 45 predict the firing of grid cell 2. There is no suggestion that the firing of either of these cells alone will predict the firing of grid cell 2. The simulation shows that neither the firing of Grid Cell 1 nor HD 45 in isolation – or any grid cell or head-direction cell – will be of substantial predictive value.

### *The conjunctive cell solution*

The difficulty in using Hebbian rules to create networks that anticipate future locations is that anticipatory prediction requires a logical conjunction of grid cell firing and head-direction firing – a logical AND relation. Simple Hebbian learning rules cannot perform a conjunctive association. One solution might be a complex multi-compartmental synaptic morphology, that could perform logical AND operations (Alarcon et al., 2006). We considered the possibilities of patterned inputs to synaptic spines, or carefully arranged patterns of axo-axonic inputs. While exotic and un-documented patterns of neuronal connection might solve the "conjunctive" problem, a more parsimonious solution is known to exist in entorhinal cortex: conjunctive cells. Although we do not know how conjunctive cells acquire their basic firing properties, it is clear that they perform the conjunctive operation. A given conjunctive cell fires as if it is an AND gate for a head-direction cell and a grid cell. It will fire in a grid-like spatial pattern, but only when rat's head is pointed in the preferred direction (**Figure 7C**).

For the remainder of this paper we will examine the role of conjunctive cells in two steps. First, we will simulate a training session, where a vRat moves randomly through space, to show that the pattern of correlated firing between pairs of cells is precisely what is predicted above. In Part 3 we will use the strengthened connections to produce a series of activations simulating linear look-ahead.

### *Synaptic strengthening in conjunctive cells*

The simulation aimed at looking for patterns of synaptic strengthening was run separately on sets of conjunctive cells and grid cells in rigid modules. Each module contained 1800 all-to-all connected neurons (3,240,000 connections). The grid cell rigid module contained cells with 100 separate excitability maps, whose peaks were evenly spread across the tile. Eighteen grid cells shared a single excitability map. Their firing was individuated by the random excitability factor (0–1.0) for each cell at each time step along the path. Each conjunctive cell had a unique phase/heading preference combination. Each conjunctive cells was assigned 1 out of 100 phases (excitability maps) and one out of 18 evenly spaced heading preferences. At each 10 ms step, as the vRat moved along its path, the firing of a conjunctive cell was determined by phase,

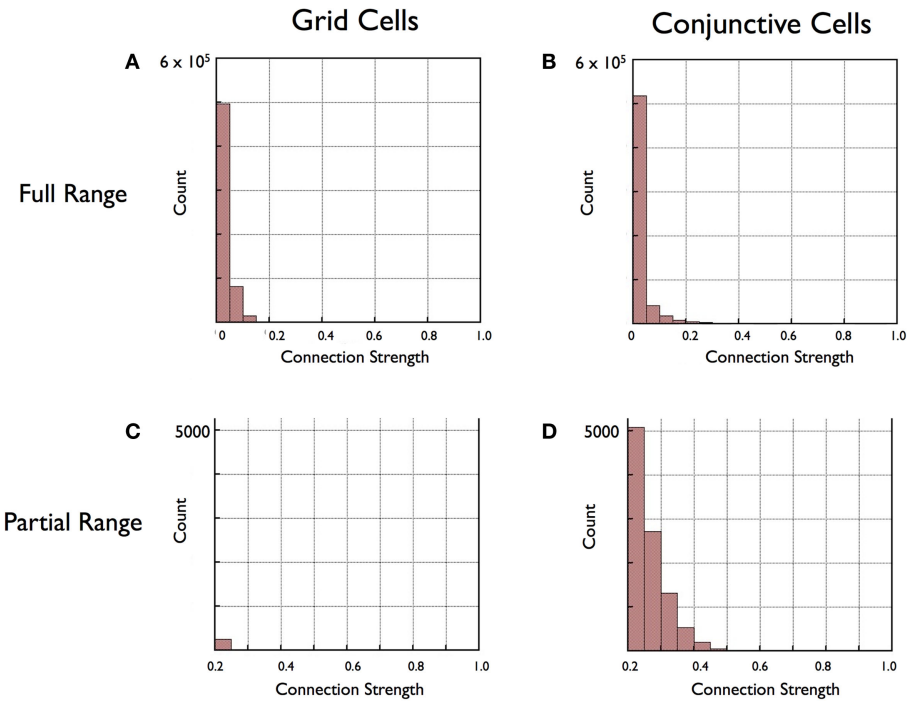


**FIGURE 8 | Histograms of results for connection strengths (co-activity indices) between all cell pairs in a rigid grid cell module (A,C) and conjunctive cell module (B,D). (A,B)** show that for both Grid Cells and Conjunctive cells that great majority of scores are low, roughly 80% of the strengths falling in the lowest bin. In **(C,D)** high-strength scores are selectively examined by eliminating values below 0.2 and rescaling. This close examination reveals a subset of strong connections found between pairs of conjunctive cells **(D)** but not grid cells **(C)**.

heading preference and a random factor. Connections between all pairs of grid cells and conjunctive cells were created.

The simulation was run using a single 30-min path with firing of each cell determined at each 10 ms interval. Although the conjunctive cell module and the grid cell module were run separately, both simulations were run on the same path, with identical input parameters. "Hits" and "misses" for each connection were updated during the run; at the end of the run "hit ratio" was computed for each connection.

The question these simulations investigated was whether specific patterns of correlated firing between pre- and post-synaptic cells develop within either rigid module. As before, we used the hit ratio from each cell pair connection to estimate co-active firing between cell pairs. High hit ratios are exclusively found in the conjunctive cell module, and, even there, the number of connections with high hit ratios is a small fraction of the total. As shown in the histograms of **Figure 8**, the great majority of connections in both the grid cell and the conjunctive cell modules have low hit ratios. If the higher end of the histograms are examined (**Figures 8C,D** apply a 0.2 strength cut-off), it is clear that virtually all of the high hit ratios, those above 0.2, are from the conjunctive cell modules. A chi-square test of the difference in proportion scores above 0.2 is significant at the 0.01 level.

Next we looked for distinctive features in the subset of conjunctive-to-conjunctive connections with high hit ratios. Since the vRat tended to move in straight lines, creating sequential firing of conjunctive cells with similar heading preferences, we examined the difference in heading preference in the origin and termination cells for each cell pair. **Figure 9** is a polar scatter plot of hit ratio as a function of the heading preference difference. As predicted, cell pairs with highly correlated activity (e.g., hit ratios above 0.2) were exclusively the cell pairs with close match in preferred headings.

Connection strength maps help to further identify the small set of strong connections among conjunctive cells (**Figure 10**). These maps are limited to connections between pairs of neurons with identical heading preferences. To construct the map, a single "origin" cell is placed at the center, and the co-activation score is displayed as a black circle, displaced from the center by the SIV between the two cells. With the size of each circle representing the co-activation score, the set of circles sits on a hexagonal tile, with the "origin" cell at the center. From the maps we see two further features of the connections with high scores. First, high-score connections are greatest for neurons with neighboring firing bumps (short SIVs). Second, the highest co-activation scores are found "downstream" to the origin cell; that is, with the center as origin, in the direction of the heading preference of both cells. This would be the most frequent direction of the vRat's movement.

The pattern on each map can be quantified by calculating the vector from the center of the tile to the centroid of the weighted connections (see Materials and Methods). When this is done for all 1800 maps, the mean difference between heading preference and centroid vectors is 0.3°, with a mean absolute value of 7.3° (**Figure 11A**). Doing the same computation on grid cells (with

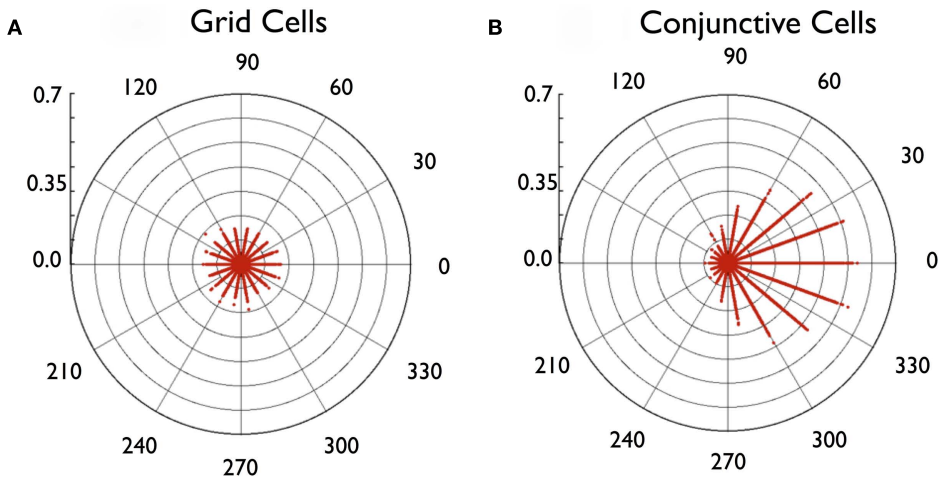


**FIGURE 9 | Circular scatter plots of connection strength as a function of the difference in heading preference of the connected cells. (A)** plots connection strengths between pairs of grid cells, where all values are low, and unmodulated by (pseudo) heading preference. **(B)** plots connection strengths between pairs of conjunctive cells, where high values are found between pairs with similar heading preference (i.e., difference values near zero).

heading preference randomly assigned) or a pure Monte Carlo distribution of 1800 angle pairs results in mean absolute deviations of ∼90°, the mean chance difference between two randomly selected angles (**Figures 11B,C**).

The connection strength maps of **Figure 10** show a clear spatial pattern of high co-activity scores. It is clear that the pattern of high hit ratios for conjunctive cells is proximate to the rat's current location and "points" downstream, in the direction that the rat is heading. We conclude that high hit ratios are found exclusively in a subset of connections among conjunctive cells. These connections share three properties: (1) they connect conjunctive cells with identical or similar heading preferences, (2) they connect conjunctive cells with nearby spatial excitability peaks, and (3) they connect origin conjunctive cells with cells whose excitability peak is in the direction the rat is facing.

### *Time window and the learning rule*

The *hit ratio* learning rule is a form of Hebbian association, in that the *hit ratio* will be high when pre-synaptic firing "predicts" a post-synaptic spike. *Hit ratio* computations perform almost exactly as a binomial correlation. When *correlation 1* (a binomial correlation between presynaptic cell firing in a time window and post-synaptic firing) was computed for three sessions the correlations between the *correlation 1* and *hit ratio* scores were 0.992, 0.994, and 0.992. We have used a long (500 ms) pre-synaptic window in most analyses in order to observe the overall pattern of interaction. Physiological data suggests shorter window times, in the order of 50 ms, may be more appropriate for LTP (Bi and Poo, 1998). Shorter windows have two effects on patterns of synaptic strengthening: the error of angular estimation increases and the distance offset decreases (**Figure 12**). Although the selective enhancement in the direction of heading preference decreases, after a 60 min training session, directionally selective enhancement remains statistically significant down to 50 ms. Finally, we implemented a form of spike-time dependent plasticity (STDP), with two temporal firing windows: an enhancement window, if firing preceded the post-synaptic spike, and a decrement window if pre-synaptic firing followed the post-synaptic spike (Bi and Poo, 1998). STDP enhances the sensitivity of conjunctive cells to look-ahead plasticity, both in terms of the minimum time window for effective plasticity and the length of the downstream displacement.

## PART 3: LINEAR LOOK-AHEAD WITH CONJUNCTIVE CELLS

In Part 2 we established high pre-to-post-synaptic correlations between the firing of pairs of conjunctive cells whose SIVs point in the direction the rat is facing. The final question we will address is whether transforming these firing correlates, via Hebbian mechanisms, to synaptic strength is sufficient to produce linear look-ahead. Specifically, we activate a set of conjunctive cells as if a rat is in a fixed location and head-direction and see if this sets up a step-by-step activation of conjunctive cell cohorts (F groups) that represent a linear sequence in the direction the rat is facing. There are four steps to the simulation. First, the hit ratios calculated during training (Part 2, above) are transformed into "connection strengths." Second, the vRat is placed at an arbitrary location in the environment with a particular head orientation, and the corresponding subset of the location and directionally tuned cells activated (firing set F1). Third, the cells that fire in F1 activate their outflow connections. Fourth, each downstream cell summates the F1 inputs to produce a level of excitation. Fifth, the downstream cells are rank-ordered by their excitation state, with the top X% (typically 2%) set to fire (F2). This process is iterated, with each iteration producing a subsequently activated cohort of neurons (F2, F3, etc.). The prediction is that each cohort of firing neurons will form a circular cluster, with the centroid of the cluster proceeding in a step-wise manner in the direction of the initial head orientation. A confirmation of this prediction is illustrated in **Figure 13**. A series of six step activations is illustrated. In each the set of activated conjunctive cells forms a neat circle

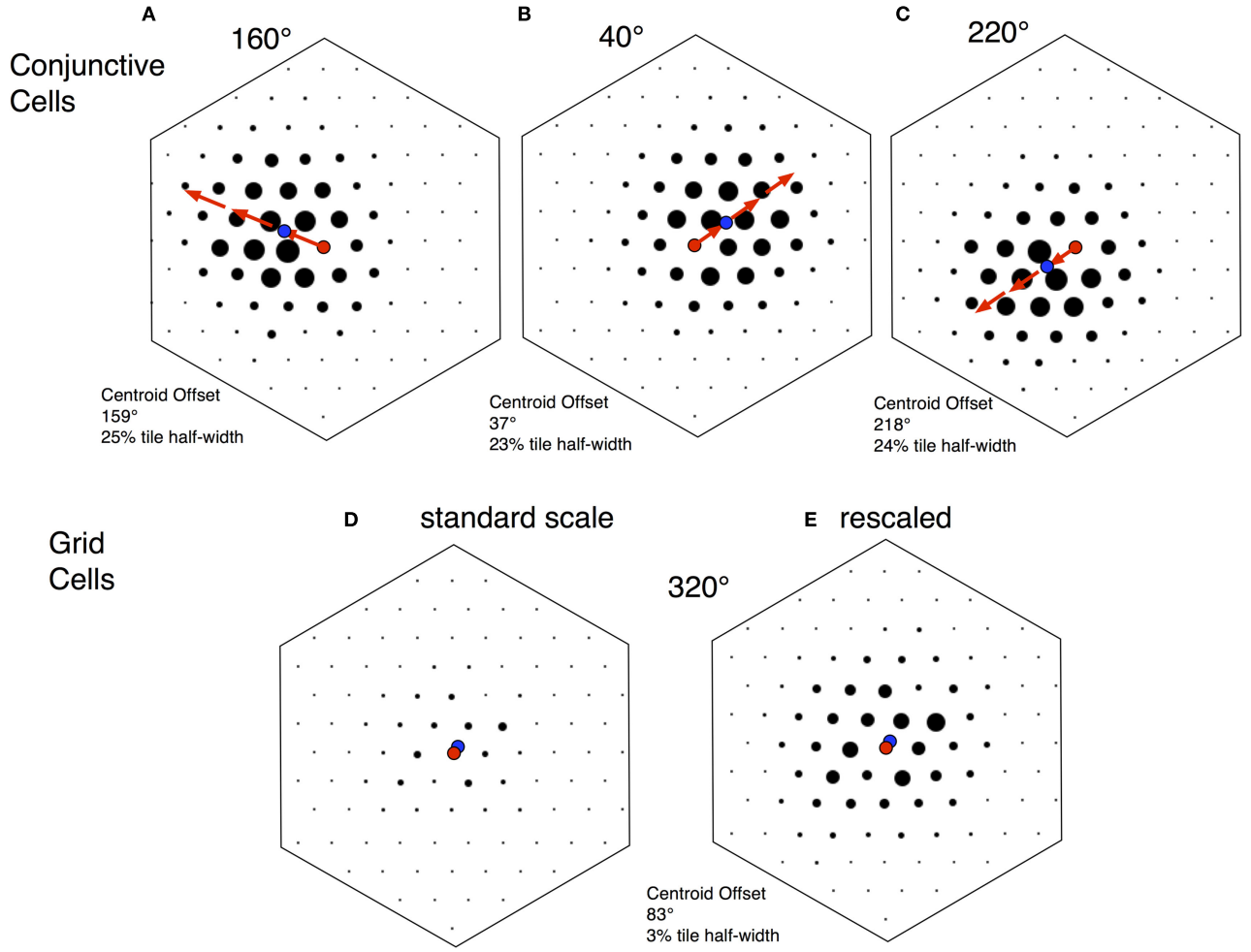


**FIGURE 10 | Connection strength plots.** Each plot represents a conjunctive cell or grid cell tile with a single cell at the center, represented by a red circle. Surrounding dots represent connections from the central neuron to other neurons, with the strength of connection depicted by the size of the circle. The location of each circle represents the shortest interbump vector (SIV; or phase difference) between the central neuron and other depicted neurons. For conjunctive cells, all of the neurons depicted share the same heading preference. These plots come from rigid modules with 100 evenly spaced phases, with a single cell at each phase location. As noted above (**Figure 5**) since we are plotting the set of SIVs from a single cell, the surface described is a hexagon. Note that each plot represents a very small subset of total connections in a rigid module. In these examples 100 connections out of a total of 3,238,200 connections are shown. The connections are restricted to those: (1) with a particular cell as an origin (out of 1800) and (2) with terminations on cells with the same heading preference (out of 18 at each phase location). The plots selected are representative out of 1800 alternatives. The top three panels **(A–C)** are from a simulated 30 min session with 1800 conjunctive cells distributed across 100 phases with 18 heading preferences at each phase. The bottom two panels **(D,E)** are from a simulated 30 min session with 1800 grid cells in a rigid module. These cells were distributed across 100 phases. For each phase location, 18 arbitrary directional identifiers were assigned that had no influence on the cell's behavior. **(A–C)** are plots from origin cells with heading preferences of 160°, 40°, and 220° respectively. The noteworthy feature of each plot is that the density of strong connections is near the center, but displaced from the center. The direction and distance of displacement is calculated by computing a centroid (center of mass) for the connections (blue dot). The distance of centroid displacement was ∼25% of the maximal distance to the edge of the hexagon. The direction of displacement for all three plots is very close to the direction of the common heading preference for the conjunctive cells. **(D)** Is a similar plot from a single grid cell. The directional preference is an arbitrary assignment made to each cell and does not reflect firing preferences. The point to note is that all of the connection strengths (black circles) are low. **(E)** Is a remapping of the same data, but increasing the dot-scale by a factor of three. This shows that relatively stronger connections are close to the central cell. Both panels show that the magnitude of displacement of centroid from center is almost imperceptible.

with a centroid. The progression of centroid locations produces a vector moving away from the start location at the angle of the initial heading direction.

Once F2 is activated, will it set off a chain reaction, a series of activations progressing in a straight line in the initial heading direction? The answer is a partial yes. In almost all cases, the

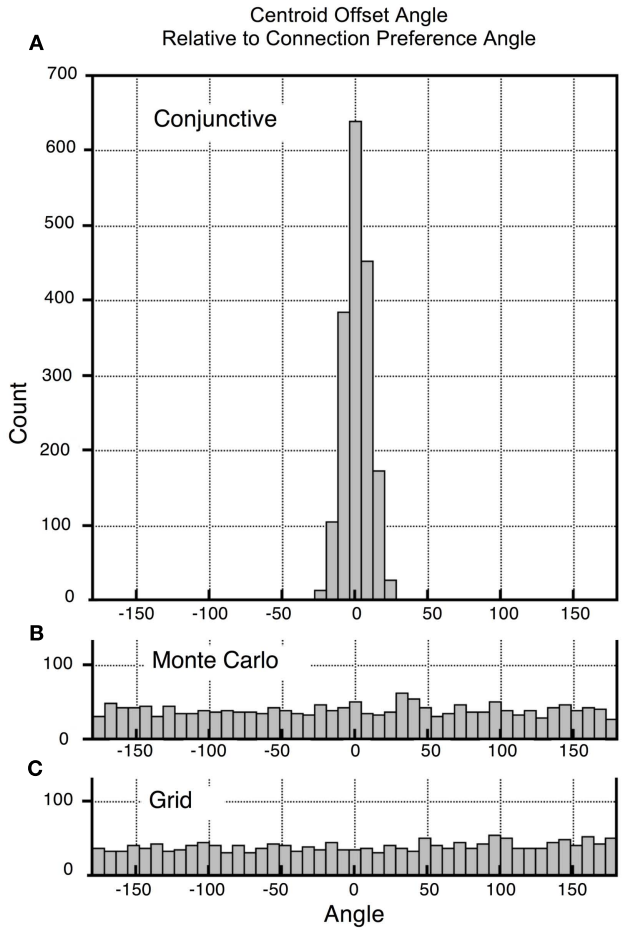


**FIGURE 11 | Histograms of centroid offset angles for all cells in a simulation.** Recall that **Figure 10** illustrates that the displacement centroid for 3 groups of connections are in the direction of the common heading preference of the cells. To prepare this figure similar centroid offset calculations were made for all 1800 possible subsets. Each centroid-offset-angle was subtracted from the common heading preference and the results plotted as a histogram. As predicted, common heading preference and offset angle are very similar. **(A)** For the conjunctive cell module, the angle difference clustered around 0, with a maximal deviation of 27°. Mean unsigned deviation was 6.7°. **(B,C)** Perform similar calculations on Monte Carlo simulations of direction pairs **(B)** and grid cell pairs where heading preference was randomly assigned. For each of these "random" simulations produced flat distributions, with deviations from 0 averaging ∼90°.

first set of activation steps remain linear, as seen in **Figure 13**. In extended series, however, there can be drift, as seen in **Figure 14A**. Most commonly, when drift occurs, the trajectory locks in on a nearby direction. When a single training session is used, certain directions are preferred. We feel that these directional preferences are due to inhomogeneities in the 30-min training session.

Adding a steady head-direction signal at each step is a straightforward method that appears to eliminate drift. In the experiments described above, location and head-direction inputs were turned "on" to initiate activity, but were "off" in subsequent activity steps. We feel it is reasonable to leave the head-direction signal "on" throughout the look-ahead process. This is postulating that the rat is stationary during look-ahead, with its head pointed in the look-ahead-direction. Since head-direction cells maintain firing during stationary behavior (Taube et al., 1990), it seems reasonable to surmise a tonic head-direction input to the conjunctive cell module. With head-direction input maintained during each iterative step in the look-ahead process, drift is effectively eliminated. This is illustrated in **Figures 14B–D** where an unchanging head-direction factor was added to the summed excitation at each step. In each case, trajectories remained steady for up to 40 steps. We conclude that a tonic head-direction input may be essential for the look-ahead process.

## DISCUSSION

Before discussing the implications of the current work, we would like to address some of the limitations and qualifications. First, the model is based on imagined connections among conjunctive cells and between grid cells and conjunctive cells. As noted above, there is very little experimental work addressing connectivity within and across layers of entorhinal cortex. For example, there is no definitive evidence for layer II stellate cell to layer III pyramidal cell connections (grid cell to conjunctive cell) nor is there evidence for-or-against conjunctive cell to conjunctive cell connections. Although each of these connections seems likely, experimental work is needed.

Second, it should be clear that this model performs "linear look-ahead" for a single rigid grid cell module. Since, as we have described, each rigid module is tiled across accessible space, the result of each step in the linear look-ahead process is not unique; rather, each step identifies a number of locations corresponding to the number of tiles. Unique locations can be identified if linear look-ahead is performed synchronously across several modules with different grid scales. We are in the process of doing this work.

Third, most of the simulations done for this paper were done with integration times of 500 ms, far longer than the estimated 50 ms pre-spike integration time for LTP. Shorter pre-spike integration time windows work, but with decreasing apparent effectiveness. Preliminary tests with a combination of a pre-spike LTP window and a post-spike LTD window (STDP) suggest these may be essential for look-ahead plasticity with realistic (shorter) integration times. It is important to note that Zhou et al. (2005) have shown both LTP and LTD in slice preparations of entorhinal layer II/III pyramidal neurons.

Finally, It should be noted that the notion of "linear look-ahead" is not unique to our work and may be effected through other mechanisms. Specifically, Erdem and Hasselmo (2012) have devised a "linear look-ahead" model based on the phase-interference mechanisms of entorhinal grid cells, with no involvement of conjunctive cells. The Erdem and Hasselmo model can solve complex navigational problems, such as taking shortcuts and dealing with detours. An interesting similarity is that both models require continual head-direction cell firing for optimal operation. We note that the two mechanisms are not in conflict and may operate separately or together to add to navigational prowess. In addition, Navratilova et al. (2012) explore the possibility that conjunctive cell inputs to grid cells and hippocampal place cells produce the "look-ahead" component of phase precession. In

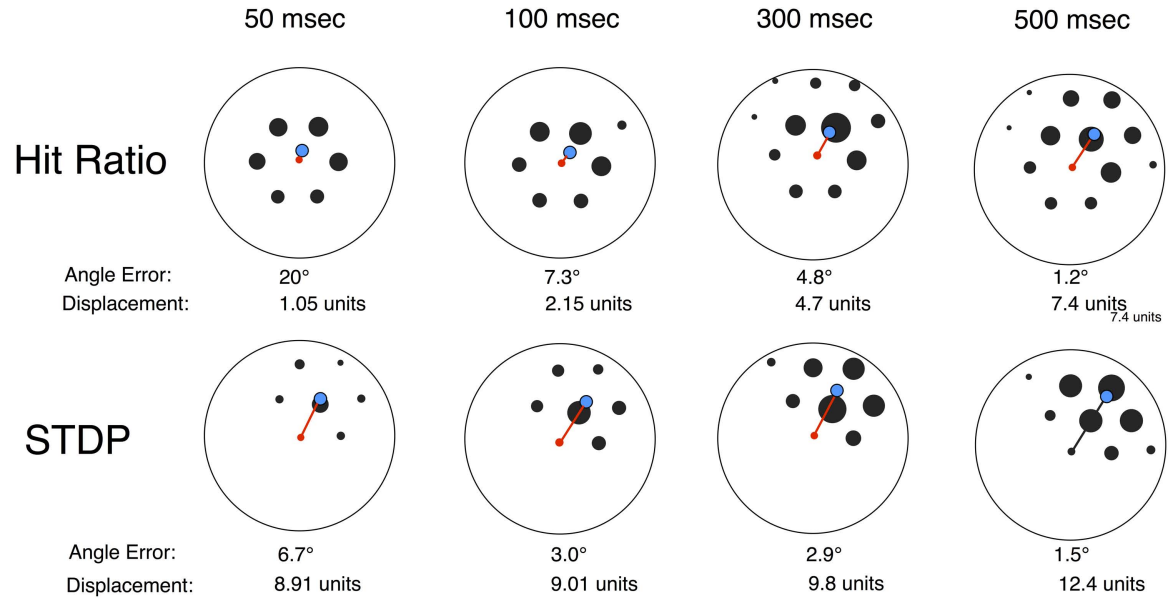


**FIGURE 12 | Effects of pre-synaptic spike window and spike-time dependent plasticity (STDP) patterns on connection strength.** The top row uses the *hit ratio* synaptic weighting method while the bottom row uses a STDP method. All plots are for an identical 60 min Training session. The preference angle for all cells is 60˚, so a perfect displacement will be at a 60˚ angle from center. Each plot depicts the centroid (center of mass) for the strength of connection between one neuron and 48 other neurons with the same heading preference (60˚). The set of depicted weightings for each plot is truncated to a circle, and cells with connection strengths below a threshold are not displayed. The central cell is a red dot, and the centroid is a blue circle. For this representative set, the angle of centroid offset improves with greater pre-synaptic integration time, but all are less than chance (90˚). The distance of centroid displacement also increases with integration time. The second row depicts the connection strengths of the same neuron pairs, where strength is a produced by a spike-time dependent plasticity rule (LTP–LDP). With a STDP learning rule errors are generally smaller, centroid displacement distances are larger, and are less affected by integration time.

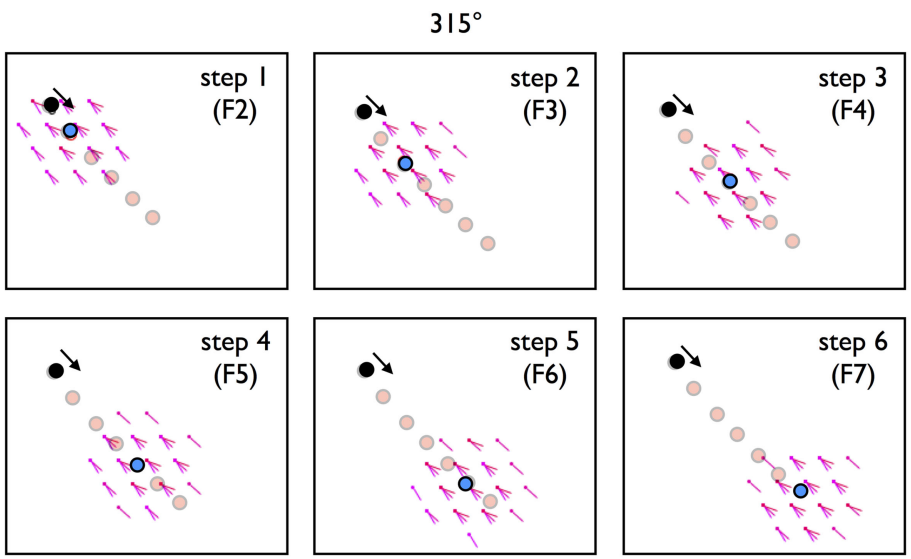


**FIGURE 13 | A trained module of 1800 conjunctive cells was tested for linear look-ahead.** As described in methods, F1 is a set of conjunctive cells that fire in the rat's initial orientation, in this case the upper left of a rectangular tile, with a head orientation of 315˚ (black dot). Panels labeled Steps 1 through 6 are the sets of conjunctive cells activated from the previous set of firing neurons. F2 is activated from F1 (initial conditions), F3 from F2, etc. Each violet dots represents a conjunctive cell that fires in that step, with the protruding line representing the cell's preferred heading direction. (Multiple lines represent multiple cells). Note that for each step, the set of firing cells remains a circular cluster. The blue dot is the centroid (center of mass) of the firing cells. Faint red dots are the entire path for the six steps. It's clear that with each step the centroid progress in the direction of head orientation.

line with our thinking, the authors of each of these studies propose an entorhinal-based look-ahead process as a mechanism for anticipating future locations.

The motivation for this work was an effort, stated in a previous paper, to find mechanisms for computing vectors – straight line paths – between an animal's current location and a previously visited goal (Kubie and Fenton, 2009). The constraints were that the animal must have performed journeys connecting these two locations, but the animal need not have visited locations along the direct path. **Figure 2** (modified from a figure in the earlier paper) represents these constraints, and shows how a vector-navigational system could, in principle take efficient paths across unvisited regions of space. The vector-navigation system hypothesized in the Kubie and Fenton (2009) model relied on path integration and speculated that such a mechanism might reside in entorhinal cortex. The current study explores the possibilities of vector-based navigation among known neuronal types in entorhinal cortex. With only two key additional assumptions, specifically that grid-like cells are organized in rigid modules and that the synaptic connections within a module are established in accord with Hebbian learning rules, we explored how grid cells and conjunctive cells could produce a mechanism termed "linear look-ahead." The reason for this is that the regular arrangement of grid cell and conjunctive cell firing bumps implicitly fills unvisited regions of space with predicted firing patterns. **Figure 2** illustrates a spatial pattern that covers both visited and unvisited regions of space. Implicit is that both grid cells and conjunctive cells have predicted firing properties as animal first explores, or vicariously explores, unvisited regions of space.

Exploiting linear look-ahead, an animal can, in principle, sit in one spot and take a hypothetical path across unvisited regions of space in search of goals. The process might go something like this. The animal sits in one region of space with a goal, represented by place cell activation and an associated sensory input also activated. In the start location the rat can explore potential direct paths to the goal. Through the process of linear look-ahead it can activate a series of conjunctive cells, grid cells, and place cells to see if any of the patterns matches the goal pattern. If a goal match is found in the look-ahead process then the current state of "look-ahead" would represent the direct path to the goal. In brief, the linear look-ahead process implemented in conjunctive cells is a viable candidate for vector-based navigation.

**Figure 15** is a simplified schema of layers 2 and 3 of entorhinal cortex illustrating how these two cell types might interact. According to this scheme:

1. Grid cells (predominantly layer II) and conjunctive cells (layer III) have reciprocal connections, such that there are corresponding grid cell/conjunctive cell sets. "Descending" and "ascending" connections can be activated independently (as far as we know, reciprocal connections have not been physiologically established, although cell morphology makes the connections likely (Lorente deNo, 1933; Canto et al., 2008).
2. Conjunctive cells have network processing that can produce linear look-ahead.
3. Grid cells have (indirect) reciprocal interactions with hippocampal place cells such that grid cells can update place cell firing and sensory information from place cells can update grid cell firing (van Strien et al., 2009).
4. Each of these connection sets is gated. That is, connection sets can be turned off or on such that some processes can operate without the interference of others.

With this scheme in mind, we can envision several functions for linear look-ahead. First, "long-distance" linear look-ahead, as described above, would be described as: (1) initial activation of

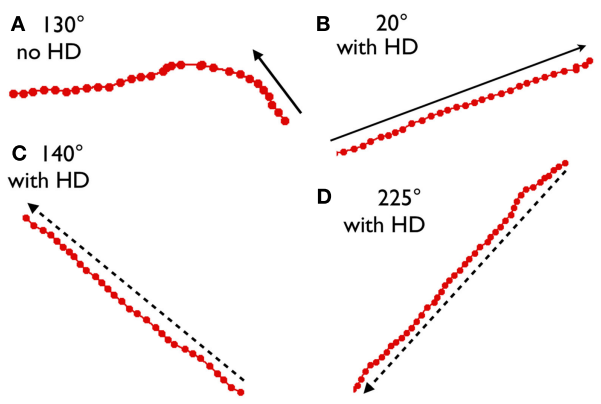


**FIGURE 14 | In panel (A) the initial position had a head orientation of 130°.** For the first eight steps the centroid location progressed at approximately a 130° angle, but in subsequent steps the direction drifted and stabilized at about 180°. In **(B–D)** head-direction stabilization was added (see Materials and Methods). We find that with head-direction stabilization the linear look-ahead mechanism progresses continuously in the initial heading direction.

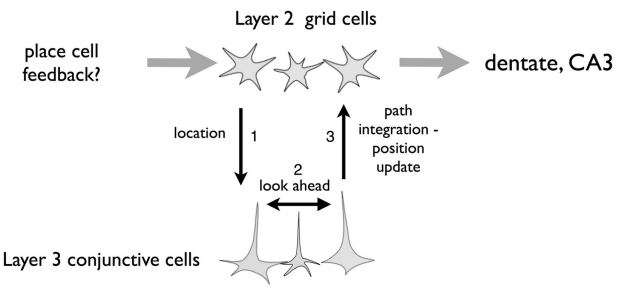


**FIGURE 15 | Schematic of grid cells (layer 2 EC) and conjunctive cells (layer 3 EC).** We hypothesize vertical integration and interaction between overlying layer 2 grid cells and deeper layer 3 conjunctive cells. Additionally, the conjunctive cells are interconnected to provide the "linear look-ahead" described in the paper. Each of the arrows can operate independently. The grid cell projection to conjunctive cells "sets up" the conjunctive cells to be in register with grid cells and sensory cues from the environment. If this influence is reduced and inter conjunctive cell interaction turned on (along with head-direction input) the conjunctive cell layer can process linear look-ahead, to predict locations ahead of the animal's nose. Finally, the conjunctive cell layer projects to the grid cell layer, permitting the grid cells to reflect the look-ahead mechanism. We see three functions of linear look-ahead. First, the mechanism can do long-distance look-ahead while the animal is stationary to predict distance locations. Second, the mechanism can do short-distance look-ahead, providing continual update while the rat is in motion. Finally, the mechanism can add to the cohesion of both conjunctive cells and grid cells, making a rigid network even more rigid.

conjunctive cells from grid cells at the start location followed by a disconnection (arrow 1); (2) simultaneous activation of conjunctive cell linear look-ahead (arrow 2); and the conjunctive-to-grid cell connection (arrow 3) to look for a match at the goal.

"Short-distance linear look-ahead" might be the mechanism for continuously updating the conjunctive cell/grid cell representation during active navigation. According to this notion, during navigation, when there is a velocity signal, there is a constant cycle of arrows 1, 2, and 3 in **Figure 15**. The grid cells representing the rat's current location (which may be reinforced by sensory cues) excite a corresponding set of conjunctive cells; (2) conjunctive cells trigger a set of "downstream" conjunctive cells in advance of the animal's current location on its path; (3) the "downstream" conjunctive set excites the corresponding "downstream" set of grid cells. In support of this notion is the stationary property of attractor networks. Several authors have noted that if the grid cell networks functions as an attractor system it require an external drive to update during locomotion (McNaughton et al., 2006; Giocomo et al., 2011; Sreenivasan and Fiete, 2011). An asymmetrical input, such as provided by conjunctive cells, could provide that drive.

A third function is that linear look-ahead might contribute to establishing and maintaining the rigidity of grid cell and conjunctive cell modules. In creating patterns of synaptic strengthening among conjunctive cells, we assumed *a priori* rigid modules. What if the modules were initially only slightly rigid? We imagine that it might take extensive experience for sufficient co-incidence of the firing patterns for rigidity to emerge based on Hebbian learning rules, but nonetheless the patterns would still emerge (Langston et al., 2010; Wills et al., 2010). After synaptic strengthening occurs, the short-distance linear look-ahead mechanism will reinforce rigid relationships among conjunctive cells. Even partially implemented linear look-ahead will reinforce the SIV patterns of neighborliness and direction. This will, in turn, strengthen conjunctive cell mediated linear look-ahead.

In summary, linear look-ahead operating within the hippocampal formation may have utility at three distinct spatio-temporal scales. First, the long spatial and temporal time scales are in accord with our goal of understanding how linear look-ahead could be implemented to navigate environments with unfamiliar expanses. Second, on the shorter scales of the next locomotor steps, linear look-ahead may provide a means for overcoming representational inertia by updating the representation as the animal moves through space. The third scale is that of synaptic plasticity and may be most relevant for the development of grid-like cell modules. Beyond our initial intent, linear look-ahead may have fundamental importance to the operations of the spatial representation system.

## METHODS

### GRID CELLS AND CONJUNCTIVE CELLS

The computational method is organized around a set, or sets, of neurons in a rigid module. The end result is that the program produces an excitability map for each grid cell or conjunctive cell that covers the surface of the apparatus. Grid bump size, grid scale, and grid orientation can be varied. Excitability maps are organized around the tile. Although a number of tile shapes are equivalent (parallelogram, rectangle, hexagon) the program uses a rectangular tile with a 0.86 × 1.0 aspect ratio. Grid scale sets the width of the tile. Grid cell distribution is the number of distinct phases per tile, with each phase occupying a single unique tile position. In the current study, phases were evenly distributed across the tile surface in 49 (7 × 7), 64 (8 × 8), or 100 (10 × 10) locations. For a given neuron, phase can be thought of as a rectangular tile with a dot at the phase location.

A single "bump surface" is used for all excitability maps in a simulation. This surface is a 2D Gaussian with a value 1.0 at center that drops to a cut-off at 0.05. The fall-off rate of the Gaussian determines the size of grid bumps.

A neuron's excitability map is created in two steps. First, the tile with the neuron's phase is tessellated across the surface of the apparatus; the tessellation pattern has alternate rows offset by half the tile width creating a "brick wall" of the rectangular tile pattern (**Figure 4A**). Next, the "bump surface" is repeatedly added, centered on the phase location of each tile. The resulting excitability map resembles a smooth grid cell rate map. Values vary from 1.0 at bump centers to 0 between bumps.

Each conjunctive cell, in addition to having an excitability map, has a preferred heading direction. Typically, preferred heading directions are grouped in 20° bins, but all directions are possible.

Paths are computed in a virtual rectangular enclosure 1.8 m × 1.8 m. The enclosure is divided into 25600 × 25600 square pixels with sides of 0.7 mm. Virtual rats move at a constant running speed of 20 cm/s. The vRat's location is sampled at 10 ms, making each step 28 pixels in the vRat's current direction. After each step current direction is updated by a random factor ranging between +3°. When the vRat encounters a wall, direction is updated as a random direction that takes the rat to a position within the apparatus.

During path execution the firing of grid cells, conjunctive cells, and head-direction cells is updated with each virtual step, based on the rat's location and head-direction. For a grid cell, firing is determined by an excitation equation:

$$\text{Excitation} = \text{excitability}\,(x, y) \times \text{RF}$$

where
$x$ and $y$ are the rat's location
*excitability()* = the apparatus excitability map for that cell
*RF* = a uniform random value between 0 and 1.0

A grid cell fires if

$$\text{Excitation} > \text{GridCellThreshold}$$

where *GridCellThreshold* is a value set to obtain a mean firing rate of 5 AP/s for grid cells.

For conjugate cells, an additional factor, the "heading direction factor" (*HDfactor*) is also computed.

$$a' = \left|\text{CurrentHeadingAngle} - \text{Heading PrefenceAngle}\right|$$

*hw* = "heading width": changes the width of the curve. Default is 0.5.
HDfactor – heading direction factor is a value ranging from 0 to 1
if($a'/hw$) > 180 then *HDfactor* = 0 else
HDfactor = $\cos(a'/\text{hw} + 1)/2$

With a "heading width" (*hw*) of 0.5 the cosine fall-off will reach zero 90° from peak. Lower *hw* values create sharper tuning curves.

Adding the *HDfactor* to the excitation equation:

$$\text{Excitation} = \text{excitability}(x, y) \times \text{RF} \times \text{HDfactor}$$

where *HDfactor* is computed as defined above.
a conjunctive cell fires if

$$\text{Excitation} > \text{ConjCellThreshold}$$

where *ConjCellThreshold* is a value set to obtain a mean firing rate of 5 AP/s.

Finally, head-direction cell firing is computed identically to conjunctive cells, but without an excitability map.

*Connections* are objects that connect neurons. A connection has an "origin" cell and a "termination" cell. A connection can also store values of "hits" and "misses." During path execution, when a cell fires, all of the connections that have the cell as a "termination" are queried. If the origin cell has fired within the set time window (typically 500 ms) the *hits* value is incremented; if the origin cell did not fire within the time window, the connection's *misses* parameter is incremented. In simulations, all cells of a module are connected; therefore, if there are 882 Grid Cells (49 phase locations; 18 cells per location), there are 777,924 connections. During training sessions, connections do not influence neuronal firing; they simply collect information. A connection with a high hit ratio [hits/(hits + misses)] has high correlated firing. If Hebbian learning rules are applied, connections with high hit ratios will be strengthened.

Connections are depicted in hit ratio maps. Hit ratio maps have a single cell at center and connections depicted spreading from the center. The distribution of connections is determined by the SIV from center cell to the connected cell. The surface formed by the set of these connections is a hexagonal tile. (This is because the set of SIVs from a single cell is a hexagonal tile with the cell at center). The magnitude of the hit ratio is depicted as the radius of a circle. For conjunctive cells hit ratio maps are typically limited to the set of conjunctive cells sharing a single directional preference. For grid cells, the distribution of connections can be made for a single grid cell, for each SIV, or as the average of identical SIVs emanating from the central cell.

Three methods have been used for computing connection strengths: *Hit ratio*, *Correlation 1*, and a *STDP* (spike-timing dependent plasticity). The *hit ratio* method is as described above. The computed *hit ratio* for a connection is used as connection strength. *Correlation 1* is a binomial correlation between the firing of the pre-synaptic cell in the pre-spike-time window and the firing of the post-synaptic cell. (Empirically, the correlation between Correlation 1 and *hit ratio* is consistently above 0.99). To compute the STDP value we calculate Correlation 2, a correlation between the firing of pre-synaptic cell in a time window *after* the post-synaptic cell fires. STDP for a given connection is (Correlation 1–Correlation 2). The STDP measure is conceptually equivalent to LTP–LTD, for a given synapse, where the LTP and LTD time windows have identical length (Bi and Poo, 1998).

After training sessions have been completed, connections can be turned on and used to drive conjunctive cells. Two methods have been used. The first is a conjunctive cell-only mechanism.

1. Initial state. A vRat with a set of conjunctive cells is placed in a location in the environment with its head pointing in a particular direction. Using the mechanism described above, the set of conjunctive cells that fire is determined. A "set of firing cells" is called a firing set (FS). This first set is FS(1).
2. cyclic firing
   a. The connections that have FS(1) as origin are queried. For each of these, the strength of the hit ratio is added to a value in the termination cell called "excitation."
   b. The cells in the module are sorted based on their stored "excitation value."
   c. The top 2% of cells with highest excitation values are set to fire. The threshold value is typically 3%. These become the next set of firing cells [FS(2)].
   d. All excitations are reset to 0 and the process is repeated, starting at 2a, with FS($n+1$) replacing FS($n$).

The second mechanism is termed "conjunctive plus head-direction stabilization." As the name suggests, a head-direction value is included in calculating the excitation of each cell at as part of step 2b. The head-direction factor uses the formula above for computing the deviation of head-direction preference from head-direction in the initial state.

For each step in the cycle, the vRat's represented location is computed in a two-step process. First, the rat's last location is taken as a first estimate. We compute the center of mass for the SIVs from the first estimated location to each cell in the current firing set and term this the "correction vector." The computed location is the "first estimate" + the "correction vector." This gives both the estimate of the animal's location on the tile and in the full environment.

## ACKNOWLEDGMENTS

NIH grant R21 NS072891 to John L. Kubie contributed to the support of this work.

## SUPPLEMENTARY MATERIAL

The Movie S1 for this article can be found online at http://www.frontiersin.org/Neural_Circuits/10.3389/fncir.2012.00020/abstract

**Movie S1 | video simulation of the firing from 1800 conjunctive cells, all from a single module.** The phases are distributed to 100 different locations (10 rows, 10 columns) distributed evenly across a rectangular tile. The path map on the right shows the vRat's location within a 1.8 m square chamber at the time of the frame. Rectangular "tiles" are superimposed on the chamber floor. The firing of cells is depicted on the left, with an individual cell's spikes distributed in phase-space on the rectangular tile. When a cell fires within a 200 m of the frame time, a circular dot is placed in the cell's phase location. The color and the direction of the "stick" emerging from the dot indicate the cell's heading preference. When several cells with the same phase fire in a time sample, several "sticks" emerge from the dot. Gray half-tiles are replicated around the central tile to enhance visualization of the circular firing cluster. When the movie is viewed, the set of cells firing cells forms a circular cluster that travel across the tile like a swarm of bees. The heading preference within the cluster falls within a tight range.

## REFERENCES


Alarcon, J. M., Barco, A., and Kandel, E. R. (2006). Capture of the late phase of long-term potentiation within and across the apical and basilar dendritic compartments of CA1 pyramidal neurons: synaptic tagging is compartment restricted. *J. Neurosci.* 26, 256–264.

Barry, C., Hayman, R., Burgess, N., and Jeffery, K. J. (2007). Experience-dependent rescaling of entorhinal grids. *Nat. Neurosci.* 10, 682–684.

Bi, G. Q., and Poo, M. M. (1998). Synaptic modifications in cultured hippocampal neurons: dependence on spike timing, synaptic strength, and postsynaptic cell type. *J. Neurosci.* 18, 10464–10472.

Brown, M. A., and Sharp, P. E. (1995). Simulation of spatial learning in the Morris water maze by a neural network model of the hippocampal formation and nucleus accumbens. *Hippocampus* 5, 171–188.

Canto, C. B., Wouterlood, F. G., and Witter, M. P. (2008). What does the anatomical organization of the entorhinal cortex tell us? *Neural. Plast.* 2008, 381243.

Erdem, U. M., and Hasselmo, M. (2012). A goal-directed spatial navigation model using forward planning based on grid cells. *Eur. J. Neurosci.* 35, 916–931.

Fuhs, M. C., and Touretzky, D. S. (2006). A spin glass model of path integration in rat medial entorhinal cortex. *J. Neurosci.* 26, 4266–4276.

Fyhn, M., Hafting, T., Treves, A., Moser, M. B., and Moser, E. I. (2007). Hippocampal remapping and grid realignment in entorhinal cortex. *Nature* 446, 190–194.

Giocomo, L. M., Moser, M. B., and Moser, E. I. (2011). Computational models of grid cells. *Neuron* 71, 589–603.

Giocomo, L. M., Zilli, E. A., Fransen, E., and Hasselmo, M. E. (2007). Temporal frequency of subthreshold oscillations scales with entorhinal grid cell field spacing. *Science* 315, 1719–1722.

Hafting, T., Fyhn, M., Molden, S., Moser, M. B., and Moser, E. I. (2005). Microstructure of a spatial map in the entorhinal cortex. *Nature* 436, 801–806.

Jeffery, K. J., and Burgess, N. (2006). A metric for the cognitive map: found at last? *Trends Cogn. Sci. (Regul. Ed.)* 10, 1–3.

Kjelstrup, K. B., Solstad, T., Brun, V. H., Hafting, T., Leutgeb, S., Witter, M. P., Moser, E. I., and Moser, M. B. (2008). Finite scale of spatial representation in the hippocampus. *Science* 321, 140–143.

Kubie, J. L., and Fenton, A. A. (2009). Heading-vector navigation based on head-direction cells and path integration. *Hippocampus* 19, 456–479.

Langston, R. F., Ainge, J. A., Couey, J. J., Canto, C. B., Bjerknes, T. L., Witter, M. P., Moser, E. I., and Moser, M. B. (2010). Development of the spatial representation system in the rat. *Science* 328, 1576–1580.

Lorente deNo, R. (1933). Studies on the structure of the cerebral cortex. *J. Psychol. Neurol.* 45, 381–438,

McNaughton, B. L., Battaglia, F. P., Jensen, O., Moser, E. I., and Moser, M. B. (2006). Path integration and the neural basis of the "cognitive map." *Nat. Rev. Neurosci.* 7, 663–678.

Minsky, M., and Papert, S. (1969). *Perceptrons.* Cambridge, MA: MIT Press.

Navratilova, Z., Giocomo, L. M., Fellous, J.-M., Hasselmo, M. E., and Mcnaughton, B. L. (2012). Phase precession and variable spatial scaling in a periodic attractor map model of medial entorhinal grid cells with realistic after-spike dynamics. *Hippocampus* 22, 772–789.

O'Keefe, J., and Burgess, N. (2005). Dual phase and rate coding in hippocampal place cells: theoretical significance and relationship to entorhinal grid cells. *Hippocampus* 15, 853–866.

O'Keefe, J., and Nadel, L. (1978). *The Hippocampus as a Cognitive Map.* Oxford: Clarendon Press.

Ranck, J. B. Jr. (1985). "Head direction cells in the deep cell layer of dorsal presubiculum in freely moving rats," in *Electrical Activity of the Archicortex*, ed. C. H. Buzsáki GaV (Budapest: Akadémiai Kiadeo), 217–220.

Sargolini, F., Fyhn, M., Hafting, T., McNaughton, B. L., Witter, M. P., Moser, M. B., and Moser, E. I. (2006). Conjunctive representation of position, direction, and velocity in entorhinal cortex. *Science* 312, 758–762.

Solstad, T., Boccara, C. N., Kropff, E., Moser, M. B., and Moser, E. I. (2008). Representation of geometric borders in the entorhinal cortex. *Science* 322, 1865–1868.

Solstad, T., Moser, E. I., and Einevoll, G. T. (2006). From grid cells to place cells: a mathematical model. *Hippocampus* 16, 1026–1031.

Sreenivasan, S., and Fiete, I. (2011). Grid cells generate an analog error-correcting code for singularly precise neural computation. *Nat. Neurosci.* 14, 1330–1337.

Stensola, H., Stensola, T., Frøland, K., Moser, M.-B., Moser, E. (2011). *Modular Organization of Grid Scale*, Program No. 726.15, 2011 Neuroscience Meeting Planner. Washington, DC: Society for Neuroscience.

Taube, J. S., Muller, R. U., and Ranck, J. B. Jr. (1990). Head-direction cells recorded from the postsubiculum in freely moving rats. I. Description and quantitative analysis. *J. Neurosci.* 10, 420–435.

van Strien, N. M., Cappaert, N. L., and Witter, M. P. (2009). The anatomy of memory: an interactive overview of the parahippocampal-hippocampal network. *Nat. Rev. Neurosci.* 10, 272–282.

Wills, T. J., Cacucci, F., Burgess, N., and O'Keefe, J. (2010). Development of the hippocampal cognitive map in preweanling rats. *Science* 328, 1573–1576.

Zhou, Y.-D., Acker, C. D., Netoff, T. I., Sen, K., and White, J. A. (2005). Increasing $Ca^{2+}$ transients by broadening postsynaptic action potentials enhances timing-dependent synaptic depression. *Proc. Natl. Acad. Sci. U.S.A.* 102, 19121–19125.


**Conflict of Interest Statement:** The authors declare that the research was conducted in the absence of any commercial or financial relationships that could be construed as a potential conflict of interest.

*Received: 11 December 2011; accepted: 06 April 2012; published online: 26 April 2012.*

*Citation: Kubie JL and Fenton AA (2012) Linear look-ahead in conjunctive cells: an entorhinal mechanism for vector-based navigation. Front. Neural Circuits **6**:20. doi: 10.3389/fncir.2012.00020*

frontiers in
NEURAL CIRCUITS

ORIGINAL RESEARCH ARTICLE
published: 29 March 2012
doi: 10.3389/fncir.2012.00009

# Head direction maps remain stable despite grid map fragmentation

***Jonathan R. Whitlock*[1] *and Dori Derdikman*[2]*** 

[1] *Kavli Institute for Systems Neuroscience and the Centre for the Biology of Memory, Norwegian University of Science and Technology, Trondheim, Norway*
[2] *Rappaport Faculty of Medicine, Technion – Israeli Institute of Technology, Haifa, Israel*

***Edited by:***
*Lisa M. Giocomo, Norwegian University of Science and Technology, Norway*

***Reviewed by:***
*John L. Kubie, The State University of New York, USA*
*Benjamin J. Clark, University of Lethbridge, Canada*

***Correspondence:**
*Dori Derdikman, Rappaport Faculty of Medicine, Technion – Israel Institute of Technology, Bat Galim, Haifa 31096, Israel.*
*e-mail: derdik@technion.ac.il*

Areas encoding space in the brain contain both representations of position (place cells and grid cells) and representations of azimuth (head direction cells). Previous studies have already suggested that although grid cells and head direction cells reside in the same brain areas, the calculation of head direction is not dependent on the calculation of position. Here we demonstrate that realignment of grid cells does not affect head direction tuning. We analyzed head direction cell data collected while rats performed a foraging task in a multi-compartment environment (the hairpin maze) vs. an open-field environment, demonstrating that the tuning of head direction cells did not change when the environment was divided into multiple sub-compartments, in the hairpin maze. On the other hand, as we have shown previously (Derdikman et al., 2009), the hexagonal firing pattern expressed by grid cells in the open-field broke down into repeating patterns in similar alleys when rats traversed the multi-compartment hairpin maze. The grid-like firing of conjunctive cells, which express both grid properties and head direction properties in the open-field, showed a selective fragmentation of grid-like firing properties in the hairpin maze, while the head directionality property of the same cells remained unaltered. These findings demonstrate that head direction is not affected during the restructuring of grid cell firing fields as a rat actively moves between compartments, thus strengthening the claim that the head direction system is upstream from or parallel to the grid-place system.

**Keywords: entorhinal cortex, head direction cells, grid cells, hippocampus, remapping, cognitive map**

## INTRODUCTION

The ancient Greek philosopher Heraclitus observed thousands of years ago that everything flows (Πάντα ῥεῖ). The world is constantly changing, and no two sensory stimuli are totally alike. In order to accommodate to the perpetual change of the world, the brain must extract invariant aspects of stimuli it senses (Gibson, 1979). Two examples of such invariants which can be extracted are *place* and *head direction*. It is thus not too surprising that the brain has evolved two separate systems: one for the representation of self-location, and another for the representation of head direction. We will overview the two systems below and then describe an experiment demonstrating their separability.

### SPATIAL REPRESENTATION IN THE HIPPOCAMPUS AND ENTORHINAL CORTEX

Our understanding of the neural representation of spatial location began with the discovery of "place cells" in area CA1 of the hippocampus in 1971 (O'Keefe and Dostrovsky, 1971). As their name suggests, place cells were found to exhibit the striking behavioral correlate of discharging selectively when rats occupied a particular location in a recording arena. The remarkable spatial specificity and stability exhibited by place cells suggest that they are key elements of the brain's spatial memory system (see O'Keefe, 2007 for review), and may provide the neural substrate for a "cognitive map" which provides "an objective spatial framework within which the items and events of an organism's experience are located and interrelated" (Tolman, 1948; O'Keefe and Nadel, 1978).

Studies in the decades since the discovery of place cells, however, suggest that spatial representations in the hippocampus are neither immutable nor absolute. Some of the first evidence for this came with the observation that place cells fire at different locations and at different firing rates in response to changes in visual cues or in the shape of the recording arena (Muller and Kubie, 1987; Bostock et al., 1991). Later termed hippocampal "remapping," this phenomenon can take one of two forms in the spatial domain—"rate remapping" and "global remapping" (Leutgeb et al., 2005). Rate remapping refers to a condition wherein place cells change their firing rate but maintain the same spatial location and has been shown to occur following non-spatial manipulations of the environment (e.g., reversing the colors of the walls and cue card in a recording arena) (Leutgeb et al., 2005) (**Figure 1A**). Global remapping, in which the combination of co-active cells changes and place fields undergo a complete reorganization of firing locations and firing rates, occurs following more profound changes in spatial inputs such as changing recording rooms or substantially altering the features of a recording arena (Leutgeb et al., 2005; Wills et al., 2005; Jezek et al., 2011) (**Figure 1B**).

A precise and more generalized spatial code was recently discovered one synapse upstream of the hippocampus in the form of grid cells in the medial entorhinal cortex (MEC) (Hafting et al.,

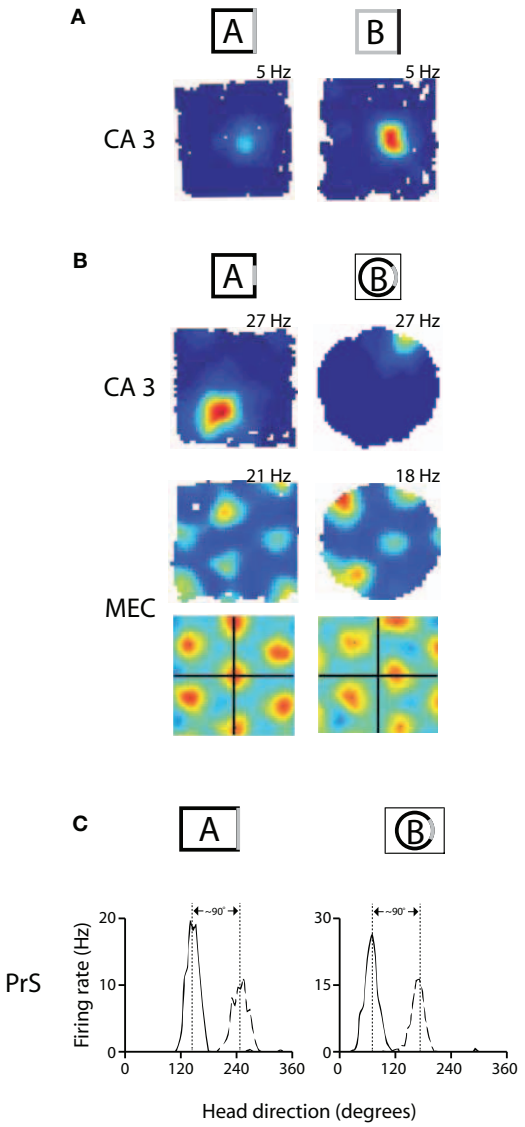


**FIGURE 1 | Remapping experiments have shown that spatial maps in hippocampus and MEC are coordinated, while head direction preferences are coordinated across cells in presubiculum. (A)** An example of rate remapping in area CA3 of the hippocampus. During rate remapping, place fields maintain a constant position but change firing rate; grid maps do not change during rate remapping. Left: Rate map of a CA3 place cell when the rat is in a box with three black walls and one white wall. Right: The same cell has a higher firing rate when the color scheme of the walls is reversed. **(B)** Switching recording enclosures elicits global remapping in the hippocampus, in which place cells change both their firing rate and position, and causes gird cells to undergo a shift in X-Y spatial phase that is apparent in the spatial cross-correlations beneath the rate maps [the cross-correlations are a comparison of rate maps at all overlapping spatial shifts for the grid cell in environment A vs. A' (left) or in A vs. B (right)] (adapted from Fyhn et al., 2007). **(C)** Changing recording enclosures causes head direction cells in the dorsal presubiculum (PrS) to change their preferred directions, but the relative difference in the cells' preferred directions is conserved across environments. Left: Head direction tuning for a pair of cells recorded from PrS in a rectangle. Right: the cells shift their directional tuning when the rat is placed in a cylinder, but the relationship between the cells' preferred firing directions is nearly the same (adapted from Taube et al., 1990b).

2005). Unlike place cells, grid cells have multiple firing fields arranged in an iterative triangular array which covers the entire environment explored by a rat, and the same stereotypic pattern is expressed irrespective of local landmarks and non-spatial cues (Fyhn et al., 2007; Solstad et al., 2008). Although grid cells express similar hexagonal firing patterns in different open recording arenas, switching recording enclosures was shown to cause grid maps to shift their X-Y spatial phase and to rotate to a new orientation (Fyhn et al., 2007) (**Figure 1B**, bottom).

Recent studies comparing simultaneously recorded place cells and grid cells suggest that spatial maps in the hippocampus and MEC may be linked causally. In the study of Fyhn et al., 2007, for example, it was shown that global remapping (but not rate remapping) in the hippocampus was always attended by the reorientation and realignment of grid maps in MEC. Later work showed that place cells and grid cells underwent a comparable restructuring of their firing fields when animals were moved from an open recording arena into a compartmentalized maze consisting of a series of interconnected alleys (i.e., a hairpin maze; **Figure 2A**) (Derdikman et al., 2009). It was found that the hexagonal structure of grid cells fragmented into a series of submaps that repeated across alleys in which the animals ran in the same direction, and that the firing fields of place cells repeated across alternating alleys in a similar manner. It was concluded that spatial maps in both areas were transformed into repeating submaps which reset at the turning point from one alley to the next (Derdikman et al., 2009; Derdikman and Moser, 2010). Together, these findings support the view that changes in the configuration of spatial maps in one area are attended by changes in the maps expressed in the other area, suggesting that the hippocampus and MEC comprise an integrated circuit within which self-location signals are generated.

## HEAD DIRECTION REPRESENTATION IN THE MAMMALIAN BRAIN

Head direction cells, which discharge when an animal is facing a particular direction irrespective of spatial location, were first reported in the 1980s by Ranck (1985), and have since been observed in many different brain regions, including the anterior dorsal thalamus (Taube, 1995), the dorsal presubiculum (Taube et al., 1990a; Boccara et al., 2010), retrosplenial cortex (Chen et al., 1994) and MEC (Sargolini et al., 2006). All known areas which contain grid cells also contain head direction cells (Sargolini et al., 2006; Boccara et al., 2010). Furthermore, it has recently been shown that there are orderly anatomical connections between patches of head direction cells and patches of putative grid cells in the MEC (Burgalossi et al., 2011). Consistent with the anatomical comingling of these cell types, there is evidence that grid cell maps and head direction signals in MEC are linked in that both follow the rotation of visual landmarks as a coherent ensemble (Solstad et al., 2008). There is, however, a substantial literature supporting the notion that head direction signals may be computed upstream from cells encoding spatial location, and that the two types of representations can change at least partly in parallel with one another.

Shortly after the discovery of head direction cells, Taube and colleagues demonstrated that head direction cells respond differently than place cells in circumstances which cause hippocampal

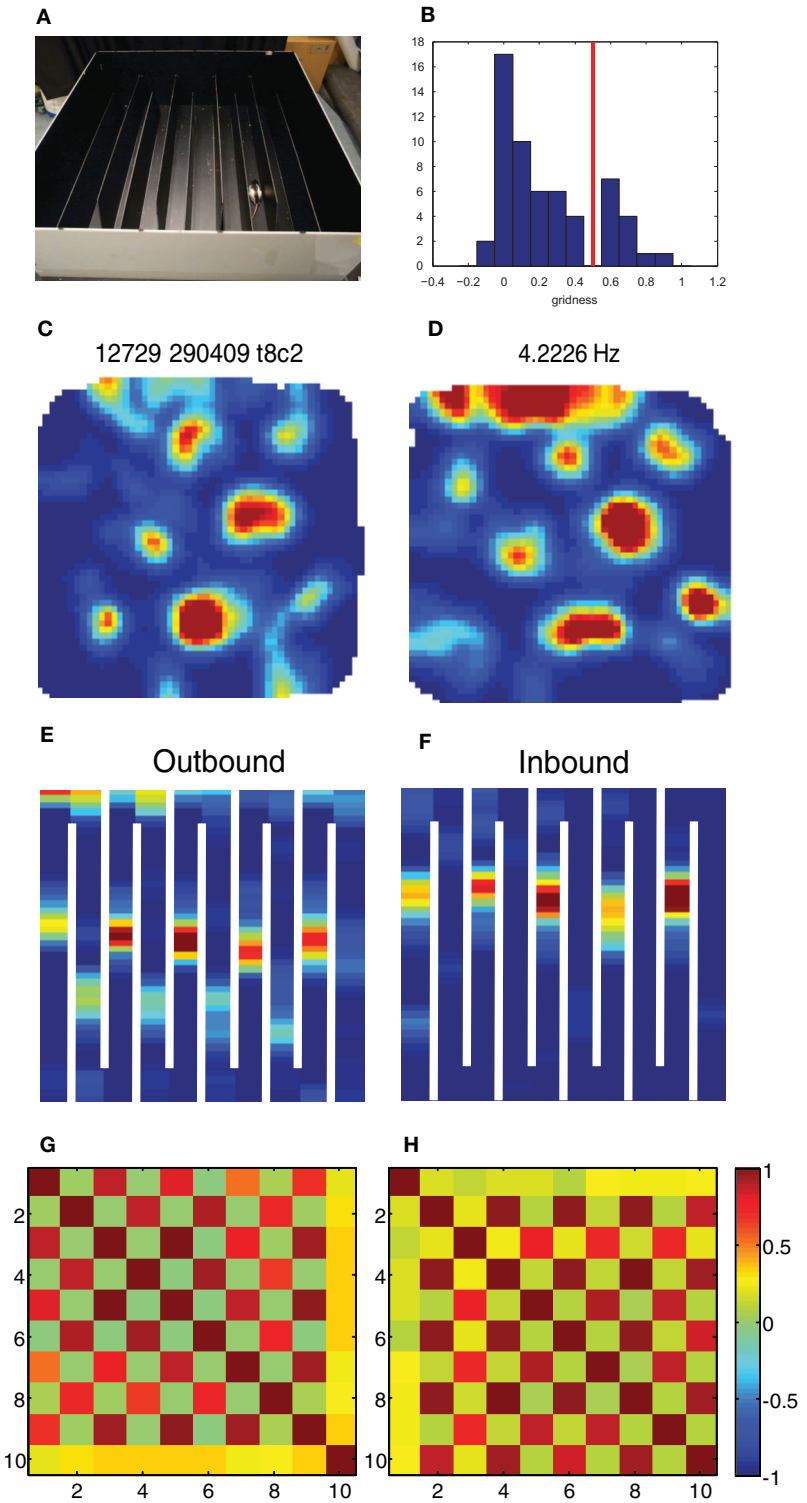


**FIGURE 2 | Break-down of grid cells in the hairpin maze. (A)** The hairpin maze setup, as used in the Derdikman et al. (2009): the rat ran first in the open-field, then in the hairpin maze, and then finally in the open-field again. **(B)** Grid score histogram (value averaged for first and second open-field sessions) for all 61 cells. Chosen threshold for conjunctive cells (0.5) is marked in red. **(C–F)** Example of a conjunctive cell when the rat is in the open-field **(C)**, when the rat is running outbound on the hairpin maze **(E)**, when it is running inbound in the same maze **(F)** and when it is put for a second time into the open-field **(D)**. **(G,H)** Correlation matrix between rate maps from the population of conjunctive cells in this study ($N = 13$) during outbound **(G)** and inbound **(H)** runs. The checkboard pattern results from the higher correlation between every second arm for both inbound and outbound runs.

remapping (Taube et al., 1990b). Namely, it was found that moving an animal from one arena to another caused simultaneously recorded head direction cells to shift to new directions, but that the angular distance between the cells' preferred directions was conserved in the different environments (i.e., the cells remained in register, **Figure 1C**). Subsequent studies showed that place cells could undergo partial spatial remapping independently of head direction cells in the anterior thalamus (Knierim et al., 1995), and that head direction signals and grid maps rotate arbitrarily with regard to one another in different recording rooms (Solstad et al., 2008). More recently it was found that inactivation of the medial septum caused a loss of the spatial structure of grid cells in the MEC while head direction cells were unaffected (Brandon et al., 2011; Koenig et al., 2011), suggesting that head direction cells do not depend on grid cells for their directional selectivity. This idea is further supported by developmental studies in rats showing that head direction signals are already mature before place cells and grid cells begin to show adult-like specificity (Langston et al., 2010; Wills et al., 2010).

In the current study we provide new analyses of data from head direction cells and grid cells published previously by Derdikman et al. (2009). In a subset of experiments from that study we monitored head direction of rats in both the open-field and the hairpin maze and found that head direction signals did not change between the tasks despite the total restructuring of grid maps in MEC. Our findings strengthen the argument that head direction signals are expressed upstream from spatial maps, such that representations of spatial location can change without affecting representations of head direction.

## MATERIALS AND METHODS

As this paper performs analysis of previously collected data, behavioral, and electrophysiological methods for these experiments were described in more detail in Derdikman et al. (2009). In short, neuronal activity was recorded from MEC in five male Long-Evans rats (3–5 months old, 350–450 g at implantation and testing), using an Axona data-acquisition system. Tetrodes were inserted above the dorsocaudal part of MEC. Rats collected crumbs of chocolate cereal thrown randomly into a black 1.5- × 1.5- × 0.5-m open-field arena surrounded by a black curtain. A white cue card (95 × 45 cm) was placed on the curtain 110 cm above the floor. Training in the hairpin maze began when the rat regularly covered the entire open-field on a 20-min trial. Nine opaque Perspex walls were inserted into parallel grooves carved into the underlying floor. The walls were 135 cm × 30 cm × 1 cm. The rats were trained to run from east to west (outbound) and from west to east (inbound) on alternating trials without interruption. During testing, the rats ran for 20-min in the open-field, followed by two 20-min runs in the hairpin maze, followed by another 20-min run in the open-field. Between runs, the rats rested in a flower pot next to the maze or in their home cage.

Spike sorting was performed offline using graphical cluster-cutting software. Position estimates were based on tracking of one LED on the headstage. The tracked positions were smoothed offline with a 15-point mean filter. Tracking errors were removed offline by an interactive MATLAB script that assumed that the path did not cross walls. The position data were sorted into 1 × 1 cm bins and the firing rate was determined for each bin in the open-field and in the hairpin maze. Following the experiments, the rats underwent perfusion, histological sectioning, and Nissl staining, in order to determine the electrode positions.

In the current paper we used the subset of the data from Derdikman et al. (2009) in which we tracked the position of two LEDs in the hairpin maze ($N = 5$ rats), so that we could derive the head direction of the rat both in the open-field and in the hairpin maze.

The grid score of the cells was calculated using a rotational-symmetry score (Sargolini et al., 2006; Boccara et al., 2010; Langston et al., 2010). Briefly, spatial autocorrelation maps were calculated for each rate map. The degree of spatial periodicity (gridness) was determined for each recorded cell by taking a circular sample of the autocorrelogram, centered on the central peak, and comparing rotated versions of this sample. The Pearson correlation of this circle with its rotation in α degrees was obtained for angles of 60° and 120° on one side and 30°, 90°, and 150° on the other. "Gridness" was defined as the minimum difference between any of the elements in the first group and any of the elements in the second. For each cell the grid score calculation was made on multiple circular samples surrounding the center of the autocorrelogram, with circle radii increasing in steps of 5 cm from 20 cm, up to the width of the box. Gridness was defined as the best score from these successive samples. The distribution of grid scores (averaged over both open-field sessions) in our study was bi-modal (**Figure 2B**), and thus we chose the gridness threshold at the trough of the bi-modal distribution (Gridness > 0.5).

In order to calculate the preferred head direction for each cell, we constructed a head direction histogram for each cell, and then calculated the direction and length of the Rayleigh vector for each head direction histogram (Boccara et al., 2010). In the Head direction histogram calculations we used bins of 6° without smoothing for display purposes (**Figure 3**), and 30° without smoothing for the population analyses. We note that the use of different bins for head direction calculation did not have a substantial effect on head direction estimates (derived from the angle of the Rayleigh vector), apart for the cases of very low firing rates. Data analysis was carried out using MATLAB. The $p$-value of correlation coefficients was computed by transforming the correlation to create a $t$ statistic having $n$–2 degrees of freedom. Each instance of monte-carlo shuffling of head direction data was done by permuting the order of the cells in one condition when comparing it to the other condition.

## RESULTS

As described in Derdikman et al. (2009), the rats were first trained to run randomly in an open-field, 1.5- × 1.5-m box. When the rats had covered the entire arena repeatedly across trials, they were trained to run in a multi-compartment hairpin maze constructed from Perspex walls inserted into the open-field box (**Figure 2A**). The rats ran outbound (west) and inbound (east) in an alternating manner. Daily sessions consisted of a 20-min trial in the open-field, two 20-min trials in the hairpin maze and a second 20-min trial in the open-field. Recording electrodes were placed in the MEC. In Derdikman et al. (2009) we found that grid cells formed a discrete spatial representation for each sub-environment when

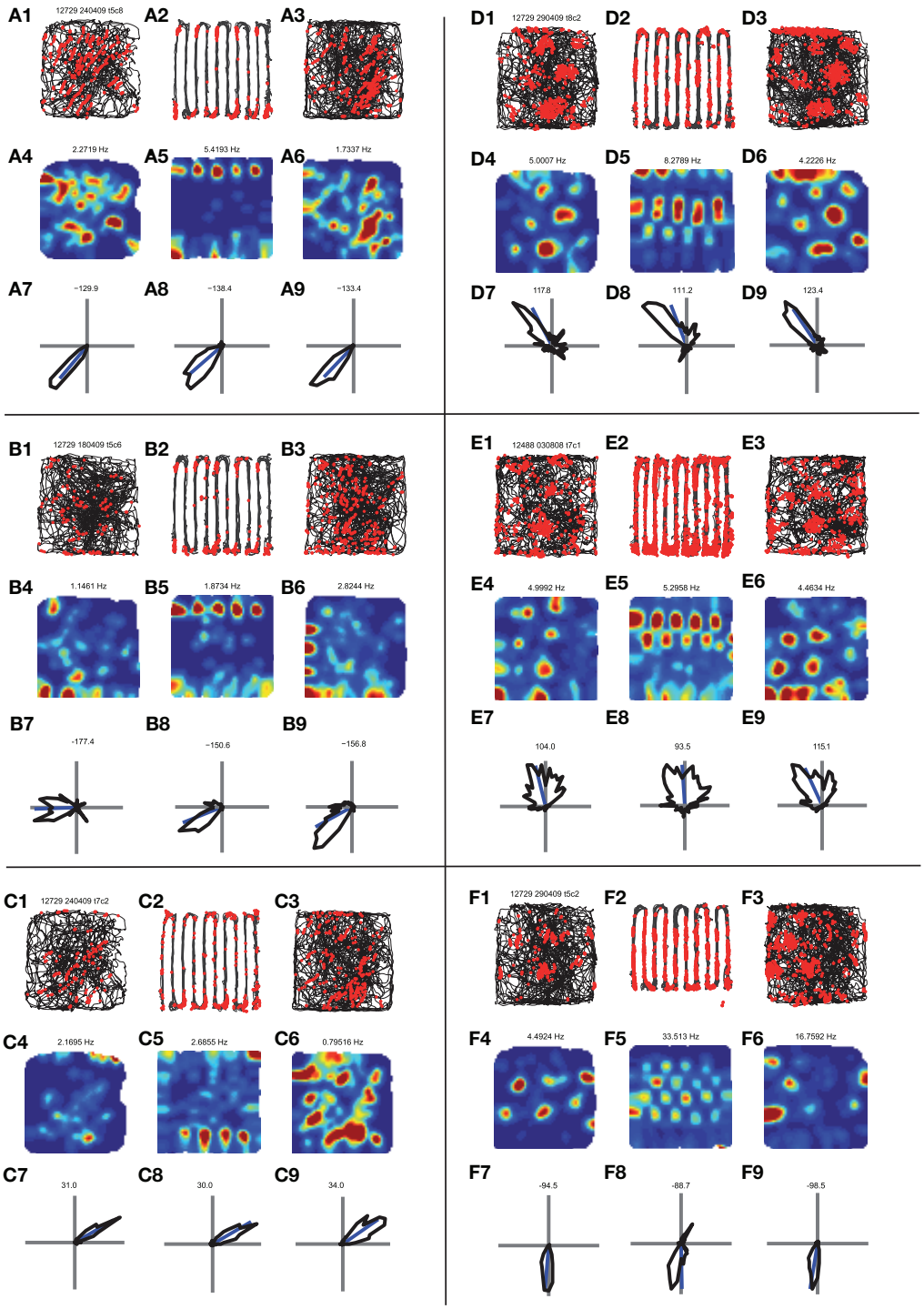


**FIGURE 3 | Comparison of the behavior of head direction cells in the open-field vs. the hairpin maze. (A)** A head direction cell. **(A1)** Path and spikes in first open-field trial. **(A2)** Path and spikes in hairpin trial **(A3)** path and spikes in second open-field trial. **(A4)** Rate map in first open-field trial (generated from **A1**). **(A5)** rate map in hairpin trial (generated from **A2**). **(A6)** Rate map in second open-field trial (generated from **A3**). **(A7)** Head direction polar histogram in first open-field. Blue line is the preferred direction of the cell. **(A8)** Head direction polar histrogram in hairpin trial. **(A9)** head direction polar histogram in second open-field. Note the similar head direction between the open-field and hairpin trials. **(B,C)** Two additional examples of head direction cells. Panels organized as in **A**. **(D,E,F)** Examples of the behavior of conjunctive {head direction × grid} cells. Note that for all of these examples the grid pattern seen in the open-fields **(D4,D6,E4,E6,F4,F6)** breaks down inside the hairpin maze **(D5,E5,F5)**, and repetitive patterns are seen between arms, as described in Derdikman et al. (2009), and in **Figure 2** above. However, head direction remains constant between the open-field conditions **(D7,D9,E7,E9,F7,F9)** and the hairpin condition **(D8,E8,F8)**.

the open environment was divided into multiple compartments. There was no master grid spanning across the alleys of the hairpin maze; instead the grid cell representation reset sharply each time the rat turned from one compartment to the next.

We extracted from the data 61 head direction cells (Rayleigh vector length $> 0.25$ in at least one of the open-field conditions), out of which 13 were clearly conjunctive head direction $\times$ grid cells (grid score $> 0.5$, **Figure 2B**), and wanted to check what transformation the grid pattern and head direction signal underwent between the open-field and the hairpin maze. As demonstrated already in Derdikman et al. (2009), the hexagonal firing pattern seen in grid cells in the open-field broke down within the hairpin maze (**Figures 2C–F**). Furthermore, also on this subset of the data, every second alley correlated in the hairpin, and the firing was different during outbound and during inbound runs of the rat, creating a check-board pattern when comparing arm-to-arm rate correlations, similar to the check-board patterns found in Derdikman et al. (2009) (**Figures 2G,H**).

Single examples of head direction cells (**Figures 3A–C**) demonstrated that the preferred direction of the cells was quite constant between the open-field and hairpin conditions. For example, one cell had a preferred direction of $-129.9°$ in the first open-field condition (**Figure 3A7**), a preferred direction of $-138.4°$ in the hairpin maze (**Figure 3A8**), and a preferred direction of $-133.4°$ in the second open-field condition (**Figure 3A9**). Similar results were seen in other head direction cells as well (**Figures 3B,C**). Furthermore, for a cell that had conjunctive grid $\times$ head direction properties (**Figures 3D–F**), the grid pattern broke-up in the hairpin maze (compare **Figures 3D4–D6**) while the preferred head direction remained quite constant between conditions (**Figures 3D7–D9**). This phenomenon repeated itself in additional conjunctive cell examples (**Figures 3E,F**).

We wished to quantify this phenomenon across the whole head direction and conjunctive cell population in our data. We compared the preferred head direction of the cells in the different conditions (**Figures 4A–D**). As expected, the head direction cells did not change their preferred direction much between the first and second open-field conditions. The median absolute value of angle change was 9.2°, (**Figure 4C**) which was lower than 100,000 runs of shuffled data (i.e., $p < 10^{-5}$; see Methods). Next, we compared the preferred direction of the cells between the first open-field and the hairpin conditions. Also in this case, the preferred head direction between the first open-field and hairpin did not change much. The median absolute value of angle change was 8.8° (**Figure 4D**), which was lower than 100,000 runs of shuffled head direction data (**Figure 4E**). Furthermore, the head direction angle of each cell did not change significantly between different arms (**Figures 4F–H**). The median difference between the head direction angle in a specified arm of the hairpin maze and the mean head direction angle for all arms together was 11.97° for all cells (**Figure 4G**), which was lower than 100,000 runs of shuffled data (e.g., **Figure 4H**). Thus we found that the preferred head direction did not change significantly between the open-field and hairpin conditions, and was similar in different subcompartments within the hairpin maze.

In Derdikman et al. (2009), the grid cells broke-up in the hairpin-maze. These results were also reproduced in the subset of conjunctive grid $\times$ head direction cells used in this study. Cells with high grid scores ($\geq 0.5$, $N = 13$; **Figure 4I**, red stars) had highly correlated rate maps between the first and second open-field conditions (mean $r = 0.535 \pm 0.049$), but failed to maintain a similar spatial correlation between the open-field and hairpin rate maps (mean $r = 0.081 \pm 0.035$), implying that, as expected from Derdikman et al. (2009), the conjunctive cells did not have a grid representation in the hairpin maze. Thus, spatial representations broke-up between the open-field and the hairpin maze in this cell sample as well (similar to the entire cell sample, reported in Derdikman et al., 2009). However, the subset of conjunctive cells did not change their preferred head direction from the open-field to the hairpin maze. The median absolute value of angle change for conjunctive cells was 11.7°, which was higher than only 17 instances out of 100,000 runs of shuffled data (i.e., $p \approx 0.00017$).

We conclude that while the grid pattern disintegrated in the hairpin maze, both head direction cells and conjunctive grid cells did not change their preferred head direction between the different conditions.

## DISCUSSION

In this paper we demonstrate that head direction cells and conjunctive head direction $\times$ grid cells conserve their preferred head direction between the open-field and hairpin maze despite the fragmentation of grid cell maps, and that the head direction signal within the hairpin maze remains constant across individual alleys despite the alternation between distinct submaps in the MEC. These findings show that the representation of head direction is unaffected by the restructuring of grid cell spatial maps and imply that head direction may be computed upstream of spatial location signals.

### COMPARISON WITH PRIOR STUDIES

The first set of data in this study show that head direction signals in MEC were the same regardless of whether rats ran in the open-field or the hairpin maze. This invariance of head direction representation with regard to the spatial layout of the tasks suggests that the animals oriented themselves using either idiothetic cues or visual landmarks outside the arena (in this case, a large white cue card was suspended above the south wall), and speaks against the view that heading orientation is derived purely from environmental geometry (Cheng, 1986). Rather, our observations are in line with recent studies showing that head direction signals in a variety of brain areas are unaffected by changes in environmental geometry, either in differently shaped recording enclosures (Knight et al., 2011) or as rats moved from one compartment to the next in a 14-unit T-maze (Yoder et al., 2011). These studies and ours support the view that idiothetic cues, distal visual landmarks or the combination of both play a primary influence in setting an animal's sense of orientation in environments with differing geometries (see also Goodridge and Taube, 1995; Blair, 1996).

Despite the stability of the head direction signal in MEC between the open-field and hairpin maze, the compartmentalization of the environment caused hexagonal grid maps to fragment into non grid-like submaps (Derdikman et al., 2009).

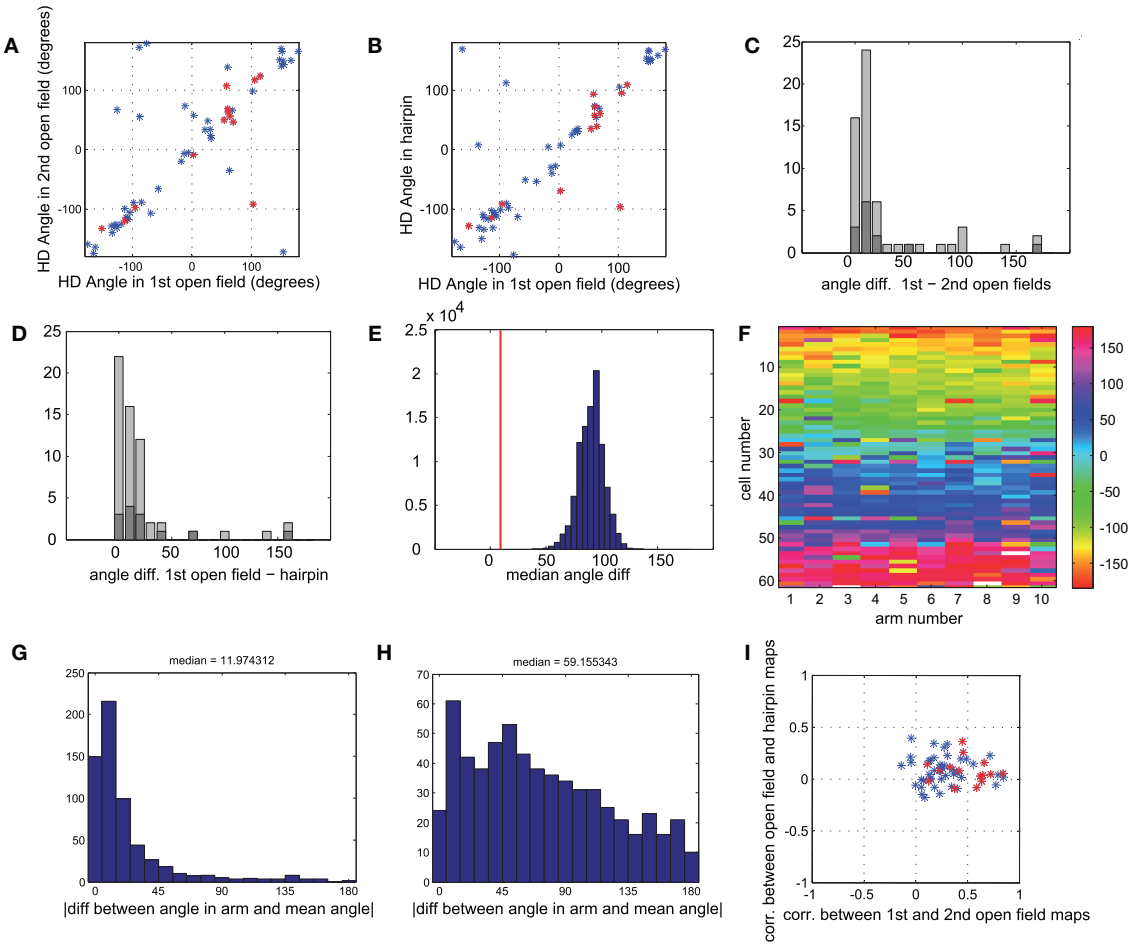


**FIGURE 4 | Head direction is similar for all conditions. (A)** Head direction angle preference for each cell, calculated from the direction of the Rayleigh vector, in the first vs. second open-field conditions. Red points mark sub-populations of conjunctive grid × head direction cells (gridness > 0.5 in open-fields). **(B)** Head direction angle preference in first open-field vs. hairpin maze. Red points as in A. **(C)** Histogram of absolute angle differences between head direction preferences in first and second open-field conditions. Dark gray bars mark conjunctive cells. Absolute angle difference can range between 0° and 180°, with an expected median of 90°, as can be seen in shuffled data (panel **E**). **(D)** Histogram of absolute angle differences between head direction preferences in first open-field condition vs. hairpin condition. Dark gray bars mark cells with high grid scores. **(E)** Real value of median angle difference between head direction in open-field vs. hairpin maze (shown in **E**) was 8.8°, lower than 100,000 monte-carlo angle differences generated from shuffled data. **(F)** Color-coded matrix of head direction preferences of each cell in each arm of the hairpin-maze. Cells are ordered according to the circular mean of their preferred head direction angle. **(G)** Histogram of absolute value of difference between head direction in each arm and mean head direction in all arms for all cells. The median difference between the head direction preference in a single arm and the mean for all arms is 11.97° **(H)** Similar histogram as in **G**, but with shuffled head directions **(I)** Comparison of spatial correlation between the two open-field rate maps (such as in **Figure 3**, **A4** correlated with **A6**) vs. correlation between open-field rate maps and rate maps generated from hairpin (such as in **Figure 3, A4** correlated with **A5**). Conjunctive cells (red points) show a higher correlation (x-axis) between two open-field conditions than between open-field and hairpin conditions (y-axis), demonstrating the breakup of the map in the hairpin maze, as described more thoroughly in Derdikman et al. (2009). However, the very same cells (dark gray bars in panels **C,D)** show strikingly similar head direction preferences between hairpin and open-field conditions.

This observation demonstrates that head direction tuning is expressed upstream from spatial signals in MEC, and is consistent with anatomical data suggesting that head direction cells in the deeper layers of MEC serve as inputs to grid cells in superficial layers (Canto et al., 2008). Though input from head direction cells may play a critical role in the etiology of grid cell firing patterns, as posited by oscillatory-interference models (Burgess et al., 2007) and attractor-network models (Fuhs and Touretzky, 2006; McNaughton et al., 2006) of grid map formation, the profound structural transformation of grid maps between the open-field and the hairpin maze (despite the unchanging directional signals) suggests that other inputs must also be at play in determining the geometric organization of grid maps.

We also found that head direction cells in MEC did not change within the hairpin maze when the rats passed from one compartment to the next, or between east- and westbound trajectories. This result contrasts somewhat with earlier studies showing that head direction cells change firing preferences readily in different recording enclosures (Taube et al., 1990b). A key methodological feature of the Taube et al. study, however, was that the animals

were passively transported between the two recording environments, allowing the subjects to become disoriented and for the head direction cells to change their preferred azimuth to a different one. It is now appreciated that head direction signals are maintained across different environments when animals are able to move actively between them, even when one of the recording enclosures is novel (Taube and Burton, 1995; Stackman et al., 2003), or when the arenas are connected but in separate rooms (Yoder et al., 2011). Thus, the continuity of self-motion signals, presumably related to path integration, is sufficient to anchor the frame of reference for the head direction system even when the pattern of sensory inputs has changed completely. Such a mechanism would allow the rats in the present study to maintain a constant representation of head direction in the hairpin maze since the animals maintained continuous motor control over their trajectory.

Given that head direction cells maintained a similar heading throughout the hairpin maze, it is again striking that spatial submaps expressed by nearby grid cells and conjunctive cells were different depending on north-south running direction and during east- and westbound traversals. In the absence of changes in directional inputs, the alternating firing patterns we observed may have arisen due to a combination of idiothetic cues and differences in the precise visual inputs available to the animals as they made north- and southward laps. The causal relationship between representations in grid cells and head direction could perhaps be further elucidated if head direction signals were re-anchored to a new set of visual landmarks between recording sessions in the hairpin maze, and it could then be determined whether the grid cell submaps showed a similar realignment. Recordings in the dark would also help isolate the precise contribution of path-integration cues.

### INHERITANCE OF HEAD DIRECTION AND SPATIAL PROPERTIES FROM UPSTREAM AREAS

The observation that head direction cells and grid cells in MEC behaved strikingly differently when the rats were transferred from the open-field to the hairpin maze demonstrates that spatial and directional signals can be disentangled from one another, even amongst co-localized cells. The fact that spatial maps in conjunctive cells were totally restructured while their directional tuning remained unchanged demonstrates that the two types of information can be computed separately, and may imply that the neural signals used to compute head direction and spatial location are conveyed from independent upstream pathways. For instance, it is known that conjunctive cells in MEC receive direct and indirect spatial input from place cells in the hippocampus as well as grid cells in MEC, presubiculum, and parasubiculum (Canto et al., 2008; Boccara et al., 2010). Precise spatial tuning in these structures, in turn, likely depends on visuo-spatial and self-motion signals from cortical afferents which include postrhinal, parietal, and retrosplenial areas (Burwell et al., 1998; Jones and Witter, 2007). The head direction signal, on the other hand, is most likely dependent on robust input from head direction cells in the presubiculum and parasubiculum, and may also depend partly on input from retrosplenial cortex (van Groen and Michael Wyss, 1990; Jones and Witter, 2007; Boccara et al., 2010; Canto and Witter, 2010). Directional tuning in the presubiculum itself sits atop a hierarchy of subcortical relays which propagate heading signals that originate primarily in the medial vestibular nuclei (see Taube, 2007, for review).

While lesioning or inactivating the vestibular apparatus results in a profound impairment in head direction representation (Stackman and Taube, 1997; Stackman et al., 2002), lesions to more downstream areas such as retrosplenial cortex or the presubiculum cause more specific impairments in the stability or landmark control of otherwise intact directional signals (Goodridge and Taube, 1997; Clark et al., 2010). In contrast, lesioning or inactivating areas outside of the head direction cell circuit, such as posterior parietal cortex, medial septum, or hippocampus has no effect on the expression of head direction signal in the anterior dorsal thalamus or in MEC, but causes a substantial disruption of the spatial structure of grid cells (Golob and Taube, 1997; Calton et al., 2008; Bonnevie et al., 2010; Whitlock et al., 2010; Brandon et al., 2011; Koenig et al., 2011). Furthermore, it seems that the head direction property is not related to the network mechanisms which supposedly can induce remapping in the hippocampal-entorhinal system (Samsonovich and McNaughton, 1997; McNaughton et al., 2006). Thus, the existing data point to the interpretation that head direction and spatial location signals each rely on contributions from several brain areas which constitute at least partially parallel systems. Ultimately, the head direction system may influence the grid-place system (Calton et al., 2003), but the data presented here and elsewhere (Clark and Taube, 2011) suggest that head direction signals are not affected by the grid-place system in return, and rather maintain a constant and robust reading of direction in all environments.

### GEDANKEN ARGUMENTS FOR THE INDEPENDENCE OF THE HEAD DIRECTION SYSTEM FROM THE PLACE SYSTEM

The supposed separation between the two systems can be understood also from more general arguments. While many idiothetic sensory channels can give clues about both spatial position and head direction, we point out here that, in principle, head direction information should be easier to estimate from such inputs. Two major sources believed to influence path integration (although others exist) are vestibular inputs and optic flow. It is known that we can gain information about our self-movement from our vestibular sense, through the semicircular canals which transduce mostly rotational movements, and through the otolith organs, which transduce mostly linear accelerations, although the functions of the two organs may be mixed (Taube, 2007). But note a major difference: in order to derive the linear position from the vestibular sense, the brain needs to perform a double integration, from linear acceleration (transduced mostly by the otolith organs), to linear velocity and then from linear velocity to linear position. While in order to derive angular head direction from the vestibular sense, the brain needs to perform only a single integration, from angular velocity to angular direction. This is because angular velocity is transduced directly by sensing the centrifugal force (which, as known from physics, is proportional to velocity and not to acceleration), in the otolith

organs and/or the semicircular canals. The necessity for double integration ($\int\int$acceleration $\rightarrow$ $\int$velocity $\rightarrow$ position) in the linear case *vs.* the need for only a single integration ($\int$angular velocity $\rightarrow$ angular position) in the angular case suggests that computing linear position from the vestibular sense is harder and more prone to noise than computing angular position. Thus, path integration mechanisms relying on the vestibular sense may be used more easily to derive angular position (Skaggs et al., 1995) than linear position (McNaughton et al., 1996; Samsonovich and McNaughton, 1997). It is, therefore, not too surprising that removing vestibular inputs to the head direction system has a strong effect on head direction cells (Stackman and Taube, 1997; Stackman et al., 2002) and, perhaps as a consequence, impairs path-integration abilities in a variety of species including cats, dogs, humans, and rodents (Beritoff, 1965; Mittelstaedt and Mittelstaedt, 1980).

A second important source of positional information can be gained from optic flow (Gibson, 1979; Horn, 1986). It is not known how this information is utilized by the brain in order to compute position. However, similar to the case of the vestibular sense, the brain has an easier task in computing angular self-motion *vs.* linear self-motion. Assuming no large eye-movements, such as in the case of the rat, turning the head causes a uniform optic flow of the image on the retina. On the other hand, a linear change of head position has a more complex effect on optic flow: distant items move fast while close items move slowly. Furthermore, there is an ambiguity: a distant object moving fast can have a similar effect on optic flow as a proximal object moving slowly, and the brain needs some estimate of the distances of different objects in order to compute linear optic flow (Horn, 1986). To sum up, it is conceptually not surprising that different brain mechanisms and different sensory inputs have evolved in order to estimate spatial position *vs.* head direction, and that the two systems are anatomically separable, consistent with the findings in this paper.

## ACKNOWLEDGMENTS

We thank Edvard Moser for reading and commenting on the manuscript, and May-Britt and Edvard Moser for giving their consent for the use of this data. We thank all of the people in the Kavli Institute for Systems Neuroscience and the Centre for the Biology of Memory in Trondheim for being both friendly and helpful all along. We thank the members of the Ulanovsky lab in the Weizmann Institute of Science for useful discussions. This work was supported by the Kavli Foundation and a Centre of Excellence grant from the Norwegian Research Council. Dori Derdikman is a David and Inez Myers Career Advancement Chair in Life Sciences fellow.

## REFERENCES

Beritoff, J. S. (1965). *Neural Mechanisms of Higher Vertebrate Behavior*. Boston: Little, Brown.

Blair, H. T. (1996). "A thalamocortical circuit for computing directional heading in the rat," in *Advances in Neural Information Processing Systems*, eds D. S. Touretzky, M. C. Moser, and M. E. Hasselmo (Cambridge: MIT press), 152–158.

Boccara, C. N., Sargolini, F., Thoresen, V. H., Solstad, T., Witter, M. P., Moser, E. I., and Moser, M.-B. (2010). Grid cells in pre- and parasubiculum. *Nat. Neurosci.* 13, 987–994.

Bonnevie, T., Fyhn, M., Hafting, T., Derdikman, D., Moser, E. I., and Moser, M. B. (2010). Hippocampal contribution to maintenance of entorhinal grid fields. *Soc. Neurosci. Abstr*. 101.4. San Diego, CA.

Bostock, E., Muller, R. U., and Kubie, J. L. (1991). Experience-dependent modifications of hippocampal place cell firing. *Hippocampus* 1, 193–205.

Brandon, M. P., Bogaard, A. R., Libby, C. P., Connerney, M. A., Gupta, K., and Hasselmo, M. E. (2011). Reduction of theta rhythm dissociates grid cell spatial periodicity from directional tuning. *Science* 332, 595–599.

Burgalossi, A., Herfst, L., von Heimendahl, M., Förste, H., Haskic, K., Schmidt, M., and Brecht, M. (2011). Microcircuits of functionally identified neurons in the rat medial entorhinal cortex. *Neuron* 70, 773–786.

Burgess, N., Barry, J., O-Keefe, J. (2007). An oscillatory interference model of grid cell firing. *Hippocampus* 17, 801–812.

Burwell, R. D., Shapiro, M. L., O'Malley, M. T., and Eichenbaum, H. (1998). Positional firing properties of perirhinal cortex neurons. *Neuroreport* 9, 3013–3018.

Calton, J. L., Stackman, R. W., Goodridge, J. P., Archey, W. B., Dudchenko, P. A., and Taube, J. S. (2003). Hippocampal place cell instability after lesions of the head direction cell network. *J. Neurosci.* 23, 9719–9731.

Calton, J. L., Turner, C. S., Cyrenne, D. L. M., Lee, B. R., and Taube, J. S. (2008). Landmark control and updating of self-movement cues are largely maintained in head direction cells after lesions of the posterior parietal cortex. *Behav. Neurosci.* 122, 827–840.

Canto, C. B., and Witter, M. P. (2010). Convergence of presubicular and parasubicular inputs on medial entorhinal cortex neurons in rat. *FENS Abstr.* vol. 5, 087.26. Amsterdam, Netherlands.

Canto, C. B., Wouterlood, F. G., and Witter, M. P. (2008). What does anatomical organization of entorhinal cortex tell us? *Neural Plast.* 2008, 381243.

Chen, L. L., Lin, L.-H., Green, E. J., Barnes, C. A., and McNaughton, B. L. (1994). Head direction cells in the rat posterior cortex. *Exp. Brain Res.* 101, 8–23.

Cheng, K. (1986). A purely geometric module in the rat's spatial representation. *Cognition* 23, 149–178.

Clark, B. J., Bassett, J. P., Wang, S. S., and Taube, J. S. (2010). Impaired head direction cell representation in the anterodorsal thalamus after lesions of the retrosplenial cortex. *J. Neurosci.* 30, 5289–5302.

Clark, B. J., and Taube, J. S. (2011). Intact landmark control and angular path integration by head direction cells in the anterodorsal thalamus after lesions of the medial entorhinal cortex. *Hippocampus* 21, 767–782.

Derdikman, D., and Moser, E. I. (2010). A manifold of spatial maps in the brain. *Trends Cogn. Sci.* 14, 561–569.

Derdikman, D., Whitlock, J. R., Tsao, A., Fyhn, M., Hafting, T., Moser, M.-B., and Moser, E. I. (2009). Fragmentation of grid cell maps in a multicompartment environment. *Nat. Neurosci.* 12, 1325–1332.

Fuhs, M. C., and Touretzky, D. S. (2006). A spin glass model of path integration in rat medial entorhinal cortex. *J. Neurosci.* 26, 4266–4276.

Fyhn, M., Hafting, T., Treves, A., Moser, M. B., and Moser, E. I. (2007). Hippocampal remapping and grid realignment in entorhinal cortex. *Nature* 446, 190–194.

Gibson, J. J. (1979). *The Ecological Approach to Visual Perception*. Boston, MA: Houghton Mifflin.

Golob, E. J., and Taube, J. S. (1997). Head direction cells and episodic spatial information in rats without a hippocampus. *Proc. Natl. Acad. Sci. U.S.A.* 94, 7645–7650.

Goodridge, J. P., and Taube, J. S. (1995). Preferential use of the landmark navigatioal system by head direction cells in rats. *Behav. Neurosci.* 109, 49–61.

Goodridge, J. P., and Taube, J. S. (1997). Interaction between the postsubiculum and anterior thalamus in the generation of head direction cell activity. *J. Neurosci.* 17, 9315–9330.

Hafting, T., Fyhn, M., Molden, S., Moser, M. B., and Moser, E. I. (2005). Microstructure of a spatial map in the entorhinal cortex. *Nature* 436, 801–806.

Horn, B. (1986). *Robot Vision*. Cambridge, MA: MIT Press.

Jezek, K., Henriksen, E. J., Treves, A., Moser, E. I., and Moser, M. B. (2011). Theta-paced flickering between place cell maps in the hippocampus. *Nature* 478, 246–249.

Jones, B. F., and Witter, M. P. (2007). Cingulate cortex projections to the parahippocampal region and hippocampal formation in the rat. *Hippocampus* 17, 957–976.

Knierim, J. J., Kudrimoti, H. S., and McNaughton, B. L. (1995). Place cells, head direction cells, and the learning of landmark stability. *J. Neurosci.* 15, 1648–1659.

Knight, R., Hayman, R., Lin Ginzberg, L., and Jeffery, K. (2011). Geometric cues influence head direction cells only weakly in nondisoriented rats. *J. Neurosci.* 31, 15681–15692.

Koenig, J., Linder, A. N., Leutgeb, J. K., and Leutgeb, S. (2011). The spatial periodicity of grid cells is not sustained during reduced theta oscillations. *Science* 332, 592–595.

Langston, R. F., Ainge, J. A., Couey, J. J., Canto, C. B., Bjerknes, T. L., Witter, M. P., Moser, E. I., and Moser, M.-B. (2010). Development of the spatial representation system in the rat. *Science* 328, 1576–1580.

Leutgeb, S., Leutgeb, J. K., Barnes, C. A., Moser, E. I., McNaughton, B. L., and Moser, M. B. (2005). Independent codes for spatial and episodic memory in hippocampal neuronal ensembles. *Science* 309, 619–623.

McNaughton, B. L., Barnes, C. A., Gerrard, J. L., Gothard, K., Jung, M. W., Knierim, J. J., Kudrimoti, H., Qin, Y., Skaggs, W. E., Suster, M., and Weaver, K. L. (1996). Deciphering the hippocampal polyglot: the hippocampus as a path integration system. *J. Exp. Biol.* 199, 173–185.

McNaughton, B. L., Battaglia, F. P., Jensen, O., Moser, E. I., and Moser, M. B. (2006). Path integration and the neural basis of the "cognitive map". *Nat. Rev. Neurosci.* 7, 663–678.

Mittelstaedt, M. L., and Mittelstaedt, H. (1980). Homing by path integration in a mammal. *Naturwissenschaften* 67, 566–567.

Muller, R. U., and Kubie, J. L. (1987). The effects of changes in the environment on the spatial firing of hippocampal complex-spike cells. *J. Neurosci.* 7, 1951–1968.

O'Keefe, J. (2007). "Hippocampal neurophysiology in the behaving animal," in *The Hippocampus Book,* eds P. Andersen, R. Morris, D. Amaral, T. Bliss, and J. O'Keefe (Oxford, NY: Oxford University Press), 475–540.

O'Keefe, J., and Dostrovsky, J. (1971). The hippocampus as a spatial map. Preliminary evidence from unit activity in the freely-moving rat. *Brain Res.* 34, 171–175.

O'Keefe, J., and Nadel, L. (1978). *The Hippocampus as a Cognitive Map*. Oxford, NY: Clarendon Press, Oxford University Press.

Ranck, J. B. (1985) "Head direction cells in the deep cell layer of dorsal presubiculum in freely moving rats," in *Electrical Activity of the Archicortex,* eds G. Buzsaki and C. H. Vanderwolf (Budapest: Akademiai Kiado), 217–220.

Samsonovich, A., and McNaughton, B. L. (1997). Path integration and cognitive mapping in a continuous attractor neural network model. *J. Neurosci.* 17, 5900–5920.

Sargolini, F., Fyhn, M., Hafting, T., McNaughton, B. L., Witter, M. P., Moser, M. B., and Moser, E. I. (2006). Conjunctive representation of position, direction, and velocity in entorhinal cortex. *Science* 312, 758–762.

Skaggs, W. E., Knierim, J. J., Kudrimoti, H. S., and McNaughton, B. L. (1995). A model of the neural basis of the rat's sense of direction. *Adv. Neural Inf. Process. Syst.* 7, 173–180.

Solstad, T., Boccara, C., Kropff, E., Moser, M. B., and Moser, E. I. (2008). Representation of geometric borders in the entorhinal cortex. *Science* 322, 1865–1868.

Stackman, R. W., Clark, A. S., and Taube, J. S. (2002). Hippocampal spatial representations require vestibular input. *Hippocampus* 12, 291–303.

Stackman, R. W., and Taube, J. S. (1997). Firing properties of head direction cells in the rat anterior thalamic nucleus: dependence on vestibular input. *J. Neurosci.* 17, 4349–4358.

Stackman, R. W., Golob, E. J., Bassett, J. P., and Taube, J. S. (2003). Passive transport disrupts directional path integration by rat head direction cells. *J. Neurophysiol.* 90, 2862–2874.

Taube, J. S. (1995). Head direction cells recorded in the anterior thalamic nuclei of freely moving rats. *J. Neurosci.* 15, 70–86.

Taube, J. S. (2007). The head direction signal: origins and sensory-motor integration. *Annu. Rev. Neurosci.* 30, 181–207.

Taube, J. S., and Burton, H. L. (1995). Head direction cell activity monitored in a novel environment and during a cue conflict situation. *J. Neurophysiol.* 74, 1953–1971.

Taube, J. S., Muller, R. U., and Ranck, J. B. (1990a). Head direction cells recorded from the postsubiculum in freely moving rats.1. Description and quantitative-analysis. *J. Neurosci.* 10, 420–435.

Taube, J. S., Muller, R. U., and Ranck, J. B. (1990b). Head direction cells recorded from the postsubiculum in freely moving rats.2. Effects of environmental manipulations. *J. Neurosci.* 10, 436–447.

Tolman, E. C. (1948). Cognitive maps in rats and men. *Psychol. Rev.* 55, 189–208.

van Groen, T., and Michael Wyss, J. (1990). Connections of the retrosplenial granular a cortex in the rat. *J. Comp. Neurol.* 300, 593–606.

Whitlock, J. R., Derdikman, D., Pfuhl, G., Moser, M. B., and Moser, E. I. (2010). Effects of parietal cortical inactivation on representations in entorhinal cortex. *Soc. Neurosci. Abstr*. 101.13. San Diego, CA.

Wills, T. J., Cacucci, F., Burgess, N., and O'Keefe, J. (2010). Development of the hippocampal cognitive map in preweanling rats. *Science* 328, 1573–1576.

Wills, T. J., Lever, C., Cacucci, F., Burgess, N., and O'Keefe, J. (2005). Attractor dynamics in the hippocampal representation of the local environment. *Science* 308, 873–876.

Yoder, R. M., Clark, B. J., Brown, J. E., Lamia, M. V., Valerio, S., Shinder, M. E., and Taube, J. S. (2011). Both visual and idiothetic cues contribute to head direction cell stability during navigation along complex routes. *J. Neurophysiol.* 105, 2989–3001.

**Conflict of Interest Statement:** The authors declare that the research was conducted in the absence of any commercial or financial relationships that could be construed as a potential conflict of interest.

*Received: 22 November 2011; accepted: 22 February 2012; published online: 29 March 2012.*

*Citation: Whitlock JR and Derdikman D (2012) Head direction maps remain stable despite grid map fragmentation. Front. Neural Circuits **6**:9. doi: 10.3389/fncir.2012.00009*

frontiers in
NEURAL CIRCUITS

ORIGINAL RESEARCH ARTICLE
published: 21 February 2012
doi: 10.3389/fncir.2012.00006

# Experience-dependent firing rate remapping generates directional selectivity in hippocampal place cells

***Zaneta Navratilova[1,2], Lan T. Hoang[3], C. Daniela Schwindel[1], Masami Tatsuno[1] and Bruce L. McNaughton[1]****

[1] *Canadian Centre for Behavioural Neuroscience, University of Lethbridge, Lethbridge, AB, Canada*
[2] *Graduate Interdisciplinary Program in Neuroscience, University of Arizona, Tucson, AZ, USA*
[3] *Evelyn F. McKnight Brain Institute, University of Arizona, Tucson, AZ, USA*

***Edited by:***
*Lisa M. Giocomo, Norwegian University of Science and Technology, Norway*

***Reviewed by:***
*Alessandro Treves, Scuola Internazionale Superiore di Studi Avanzati (SISSA), Italy*
*Caswell Barry, UCL, UK*

***Correspondence:**
*Bruce L. McNaughton, Department of Neuroscience, Canadian Centre for Behavioural Neuroscience (Room EP1242), The University of Lethbridge, 4401 University Dr W, Lethbridge, AB T1K 3M4, Canada.*
*e-mail: bruce.mcnaughton@uleth.ca*

When rodents engage in irregular foraging in an open-field environment, hippocampal principal cells exhibit place-specific firing that is statistically independent of the direction of traverse through the place field. When the path is restricted to a track, however, in-field rates differ substantially in opposite directions. Frequently, the representations of the track in the two directions are essentially orthogonal. We show that this directionally selective firing is not hard-wired, but develops through experience-dependent plasticity. During the rats' first pass in each direction, place fields were highly directionally symmetric, whereas over subsequent laps, the firing rates in the two directions gradually but substantially diverged. We conclude that, even on a restricted track, place cell firing is initially determined by allocentric position, and only later, the within-field firing rates change in response to differential sensory information or behavioral cues in the two directions. In agreement with previous data, place fields near local cues, such as textures on the track, developed less directionality than place fields on a uniform part of the track, possibly because the local cues reduced the net difference in sensory input at a given point. Directionality also developed in an open environment without physical restriction of the animal's path, when rats learned to run along a specified path. In this case, directionality developed later than on the running track, only after the rats began to run in a stereotyped manner. Although the average population firing rates exhibited little if any change over laps in either direction, the direction-specific firing rates in a given place field were up-or down-regulated with about equal probability and magnitude, which was independent in the two directions, suggesting some form of competitive mechanism (e.g., LTP/LTD) acting coherently on the set of synapses conveying external information to each cell.

**Keywords: CA1, CA3, rate remapping, directional place fields, navigation, path integration**

## INTRODUCTION

Principal neurons in the hippocampus proper exhibit activity correlated with the location in which an animal is located (O'Keefe and Dostrovsky, 1971). In an open environment, when an animal is moving around in a random path, such as while foraging for food, the majority of place cells fire at rates that are independent of the direction in which the animal is passing through the cell's "place field" (Muller et al., 1987). These findings are consistent with the predominant view of the hippocampus encoding an allocentric representation of space (O'Keefe and Nadel, 1978). It is clear that the hippocampus is necessary for spatial memory (e.g., Morris et al., 1982); however, the degree to which this structure encodes changes in sensory cues or behavioral contingencies occurring in a single spatial environment is still debated (e.g., Eichenbaum et al., 1999).

One view is that the selection of which hippocampal cells fire at a given location is initially determined by path integration mechanisms (McNaughton et al., 1996), whereas sensory information that may vary at that location may become associatively linked to the selected cells, thus enabling future correction of path integrator errors. Such associative linking would typically not involve changing the membership of the active population (which would be considered "global remapping"), but could affect their relative firing rates ("rate remapping"; Leutgeb et al., 2005). Global remapping is typically induced when a rat is transferred between separate, distinct, recording rooms (Leutgeb et al., 2004), when the rat locomotes between two boxes (Skaggs and McNaughton, 1998; Colgin et al., 2010), or when a large mismatch is introduced between its path-integrated heading direction and familiar visual landmarks (Knierim et al., 1998; Fuhs et al., 2005). In addition to local sensory information, internal information such as working memory, current goals, behavioral set, and possibly even circadian rhythms may also affect firing rates without significantly changing the locations at which the hippocampal cells fire (O'Keefe and Conway, 1978; Hetherington and Shapiro, 1997; Wood et al., 2000; Leutgeb et al., 2005, 2006; Sparks et al., 2010).

A long unresolved problem with the mainly allocentric view of hippocampal place cells has been that whereas, in an open environment, a large majority of place cells exhibit firing that is not

direction specific (Muller et al., 1994; Markus et al., 1995), on a track that is repeatedly traversed along a specific path, the activity of place cells in each direction differs substantially (McNaughton et al., 1983; Muller et al., 1994). In addition to the configuration of the traversable portion of the environment, the task the animal is performing also affects directionality of place cells: if the animal is repeatedly running a path between specified goal locations even in an open environment, the place cells show distinct directional firing (Markus et al., 1995). Interestingly, the presence of many local cues on the track reduces the difference in firing between the two running directions (Battaglia et al., 2004), but the complexity of distal room cues appears not to affect directionality (Markus et al., 1995).

Recent findings suggest that the firing of "grid cells" in the medial entorhinal cortex is generated by path integration and is the primary source of relative position information to the hippocampus (Hafting et al., 2005; Fyhn et al., 2007). Also notably, under conditions that induce rate remapping in hippocampal cells, grid cells do not exhibit changes in firing location or relative firing rate; however, conditions that induce global remapping in hippocampal cells also induce global remapping in grid cells (Fyhn et al., 2007). Overall, current data suggest that path integration occurs in the medial entorhinal cortex (McNaughton et al., 2006), and this information is then passed on to the hippocampus, which can combine it with other information, such as landmarks or other spatial cues, and task demands or other internal state variables, to form a conjunctive code for locations and the events that occur there (Leutgeb et al., 2005).

Path integration by the medial entorhinal cortex does not, however, explain why the place cell activity in two running directions on a track is so different, while the activity in an open environment is essentially independent of direction of travel. In the current study, we recorded from hippocampal cells while a rat traversed a circular track in both directions, beginning with the very first time that the rat had experienced the track in a given spatial context. We observed that, while the track was novel to the animal, the two running directions were in fact highly correlated. During repeated traversals of the track, the firing rates of place cells changed in both running directions, becoming highly dissimilar by the end of the session, as previous studies had shown. We present evidence that, unlike the expression of place fields per se, directional selectivity is an experience-dependent phenomenon driven by gradual changes in the response of a cell to external sensory cues and/or internal variables such as goals or recent trajectories which occurs when the traversal of a path becomes stereotyped.

## METHODS

### SUBJECTS

Five male rats (four Brown Norway-Fisher hybrids and one Brown Norway) were used for this study. The rats were housed individually and kept on a 12 h dark/12 h light schedule. Training and experiments occurred during the dark phase. During pretraining, and then again during recording, they were kept at ∼85% of their free-feeding body weight, in order to be motivated to run for food rewards. All animal protocols complied with National Institutes of Health guidelines and Canadian Council for Animal Care (CCAC) regulations under the guidance of the University of Arizona Institutional Animal Care and Use Committee (IACUC) or the institutional animal care committee at the University of Lethbridge.

### "HYPERDRIVE" ASSEMBLY AND IMPLANT

Rats were implanted with a "hyperdrive" consisting of 14 individually movable tetrodes. Each tetrode consisted of four strands of insulated 13 μm nichrome wire twisted together, and was inserted in silica tubing and secured with cyanoacrylate glue to a drive cannula. The drive cannula was coupled by a plastic nut to a drive screw, so that rotation of the nut allowed vertical movement of the tetrodes through another (30 gauge) guide cannula. The 14 guide cannulae were placed within the inverted conical core of the hyperdrive, evenly spaced and angled at 30° from the vertical axis at the top, and bundled together and vertical to the brain surface at the bottom of the hyperdrive, where they would be contacting the brain. For rats 1–3, the guide cannulae were bundled into a 2 × 7 linear array, to be placed along the proximal-distal axis of dorsal CA1. The remaining two animals (rats 4 and 5) were implanted with hyperdrives with a bundle forming a circle, and lowered to dorsal proximal-mid CA3. A more detailed explanation of the hyperdrive, implantation, and recording techniques is published in Gothard et al. (1996b).

Surgery was performed under Isofluorane anesthesia. A 3 mm in diameter craniotomy was opened above the right dorsal hippocampus (coordinates of the center of the craniotomy differed slightly between rats, between 3.3–3.8 mm posterior and 2.0–3.0 mm lateral). The Dura was removed, the hyperdrive bundle was centered above the craniotomy, with guide tubes just touching the surface of the brain, and the craniotomy was sealed with Kwik-Sil and then cemented in place with dental acrylic anchored by dental screws spread over the rest of the dorsal surface of the skull. After surgery rats were administered 26 mg of acetaminophen orally for pain relief, and given Ampicillin in their food for 10 days or given subcutaneous injections of Metacam and Tribrissen to prevent infection. All tetrodes were lowered into the brain immediately following surgery by turning the screws three full turns (954 μm).

### RECORDING PROCEDURES

Twelve tetrodes were lowered over the course of 2–4 weeks to CA1 (rats 1–3) or CA3 (rats 4 and 5). The remaining two tetrodes were lowered to the corpus callosum, to serve as a reference, and the hippocampal fissure as an EEG recording probe. For recording, the hyperdrive was connected to a unity-gain headstage (Neuralynx, Bozeman, MT) which allowed low noise transmission of signals from each of the four channels of each tetrode, via a multi wire cable and a commutator mounted on the ceiling, to digitally programmable amplifiers and then to the Neuralynx Cheetah system. Local field potential activity was continuously sampled from one channel of each tetrode at 2.4 kHz, amplified 500–1000 times, filtered between 1 and 300 Hz, and recorded. For this analysis, only the LFP signal from the tetrode with the largest number of cells on each day (the one most likely to be in the cell body layer) was used (filtered off-line at 6–10 Hz to determine the theta signal). Spike signals from each channel of

the 12 hippocampal tetrodes were referenced against the corpus callosum electrode signal, amplified 1000–5000 times and filtered between 600–6000 Hz. Signals were digitized at 32 kHz, and a 1ms sample was recorded when the signal reached a pre-determined threshold. The thresholds were adjusted manually for each channel, depending on the noise level and spike amplitude on that channel. The headstage also contained a circular array of LEDs that were detected by an overhead camera and recorded by the Cheetah system along with the neural signals to allow tracking of the position of the rat on the maze. Video spatial resolution was approximately 3 pixels/cm.

After the completion of recordings, the location of the tetrodes was ascertained by creating a small electrolytic lesion at the tip of each tetrode (by passing 5 μA current for 10 s). Histological sections were Nissl stained to localize the lesions. Based on coronal sections from the 3 CA1 rats, it was determined that the recordings of rats 1 and 2 came from a wide range of proximal-distal coordinates in CA1, and rat 3 was found to have most tetrodes in proximal CA1, one tetrode in CA2, and 2 tetrodes in distal CA3. Thus, the day 1 recordings included 183 CA3 cells, 22 CA2 cells, and 83 CA1 cells (51 from the proximal half).

#### PRE-TRAINING AND BEHAVIORAL TASKS

All rats were pre-trained prior to hyperdrive surgery to run laps back and forth between food dishes on a circular track, as well as to forage for randomly sprinkled food rewards in an open-field environment. All pre-training sessions occurred in a different room than the room in which recording took place. The track used during recording was usually different from the one used during pre-training, or when the same track was used, a different surface was placed on the track.

The first behavioral task involved the rats running on a circular track. Two rats ran on a track 120 cm in diameter, one rat on a 115 cm track and one on a 152 cm diameter track. A barrier was placed at one end of the track, with food dishes on either side of it, so the rat would have to turn around and run back to get the next food reward. Small objects and textures were placed on half of the track ("cue-rich"), and the other half had a uniform surface with no nearby objects ("cue-poor"). Each running session lasted 25–30 min, and was preceded and followed by 30 min–1 h of rest in a small pot near the track. Because the rats were pre-trained to perform this task, three of the rats showed good enough behavior during their very first exposure to the track to allow us to analyze individual laps. Rat 3, however, did not run on the track during his very first exposure, and ran too slowly and too few laps (6) during his second exposure for that data to be analyzed. Thus, the data analyzed as rat 3's "session 1" is actually his third day being placed on the track. Nevertheless, this data showed very similar results to the actual first exposure of the other three animals, and so was included in this study. The second task involved the rats running on a circular open platform. One rat ran on a platform 115 cm in diameter, and the other rat on a 142 cm platform. A three-walled box was placed at the edge of the platform, and the rat was acclimated to this environment for 5 min prior to each running session, by being confined to the box with a barrier placed along the opening. Once the barrier was removed, the rat was expected to run to the food dish on the opposite edge of the platform, pick up a food reward, and return to the box to eat the reward. The task was designed to be able to manipulate the speed of the rat as he returned with food rewards of different sizes. That aspect of the task, however, was not important to this study. Each running session lasted 30 min. The rats also foraged for randomly distributed food rewards in the same environment every day for 30 min (prior to the shuttle task, with a 30 min rest between tasks). It took the rats 2–4 days to learn the shuttle task, but once they learned it, they were running over 20 laps per session, most of them directly between the box and the food dish. Only the spikes occurring along a direct path were analyzed, and laps in which the rat diverged from a direct path to the food dish for more than 20% of the run in either direction were excluded from the analysis.

#### SPIKE SORTING

Spikes recorded during the entire recording session (2–3 rest periods and 1–2 running epochs) were sorted based on energies and first two principal components of the waveforms recorded on each electrode of a tetrode, using a semi-automated procedure. An automated algorithm (KlustaKwik, K. D. Harris, http://klustakwik.sourceforge.net/) was used to find clusters, which were then merged and adjusted manually using a modified version of MClust 3.1 (A. D. Redish, http://redishlab.neuroscience.umn.edu/MClust/MClust.html).

#### POSITION TRACKING

The position during the running epochs was extracted at each video frame by fitting a circle to the ring of LEDs on the headstage. The position determined during previous frames was used to eliminate active pixels at a distance of greater than 20 pixels, which could not have been from the headstage, but were a result of other spurious light sources. This 2D position was then deconstructed into a 1D representation along the track. For the circular track task, a circle was fit to the position data, and the coordinate along the diameter of the track was determined for each frame (with the barrier assigned a position of 0). For the shuttling task, principal component analysis on the XY coordinates was used to find the axis of the "track" and the coordinates along that axis were used (with the outer edge of the home box assigned a position of 0). Periods when the rat was stopped on the track were removed, by finding any periods when the rat was moving at less than 2 cm/s. Velocity was calculated by smoothing XY position with a 1-s hamming window, and then calculating the distance moved between subsequent frames. For the shuttling task, periods when the rat diverged from the track (the coordinates along the axis orthogonal to the "track" crossed a threshold value in either direction) were also removed from the analysis. If the rat diverged from the "track" for more than 20% of the distance in either direction, the whole lap (both directions) was removed from the analysis. Laps were identified by finding the turn-around points at the ends of the track.

#### FIELD ANALYSIS

Individual fields were delineated by smoothing (with a hanning window of five bins) the firing rate in (2 cm) position bins and automatically finding the peaks and troughs on either side of

those peaks. Peaks at a minimum of 0.8 Hz were considered fields, and the first trough away from the peak that had a firing rate of less than 0.05 of the peak rate was considered the field boundary. Fields that had two peaks that were separated by a trough of at least 0.6 of the smaller peak rate were split in two. Fields were outlined individually in each running direction, and then combined if the majority of the field overlapped with the field in the opposite direction. This way all the spikes from fields that had shifted in the forward running direction would be considered. If a field was not found in the opposite direction, the spikes occurring in the same position bins were considered as the opposite direction field. All field boundaries were checked manually on a phase precession plot (**Figure 1**), and overlapping fields, fields that did not show phase precession in at least one running direction, or overlapped with food dish locations were excluded. Approximately 30% of the fields found by the automated algorithm were deleted in the manual step, most of these because they included few spikes and did not show phase precession, or they overlapped with a food dish location. The phase precession criterion was not applied very stringently, instead it was used in conjunction with the other criteria, for example to differentiate low firing rate fields from spurious spikes, or to determine if overlapping fields could be successfully separated with a single boundary or should not be used. The boundaries of approximately 30% of the remaining fields were adjusted manually, because the automated algorithm did not identify the full phase precession of a field (especially low firing rate fields), or it included some noise spikes from outside of a field. Spikes occurring within the boundaries thus set were then considered for the lap-by lap analysis of each field. See **Table 1** for the number of cells and fields analyzed from each animal.

### DIRECTIONALITY INDEX

The directionality of cells was determined by counting the number of spikes fired in each direction within each field, because this measures rate remapping better than a correlation. Spatial correlations are also influenced by the fact that fields are often offset in the two running directions (Battaglia et al., 2004). Thus, we calculated a "directionality index," which was the difference in number of spikes fired in each running direction divided by the total spikes in both directions on each lap, based on the rate remapping difference ratio in Leutgeb et al. (2005). The difference between the higher firing rate direction (on average over the whole session) and the lower firing rate direction was used instead of the absolute value of the difference, because this way the same direction is being subtracted for all laps. Negative DI values resulted when the running direction in which more spikes occur switched between laps. When a cell spiked only in one running direction, the DI was 1.

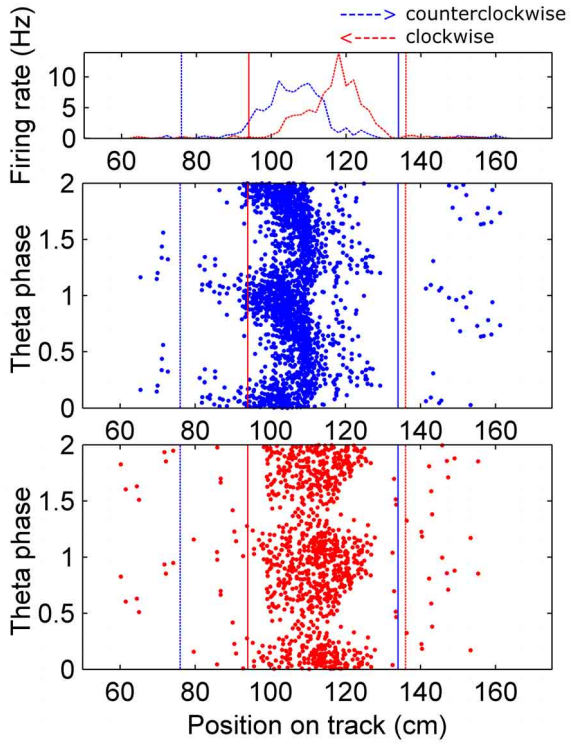


**FIGURE 1 | Assigning boundaries around fields. Top:** Occupancy normalized firing rate for an example cell is plotted on the coordinates of the circular track (the barrier was at 0 cm, which wraps around to 361.3 cm, and the food dishes were near that, at ~10 cm and 351 cm). The firing rate in the clockwise direction (right to left on this plot) is colored red, and the counter-clockwise direction is in blue. Fields were identified by an automated algorithm, which found peaks (in each direction separately) in the smoothed version of this plot, and set boundaries at the troughs around those peaks. If the majority of the field found in one direction overlapped with a field in the opposite direction the two fields were combined, and the spikes within the boundaries outlined in each direction were considered for further analysis. The boundaries were set separately for each direction to account for the shifting of fields in the backwards running direction. If a field did not overlap with one in the opposite direction, any spikes occurring in the same position bins were considered as the opposite direction field. Dotted vertical lines indicate the beginning and solid lines the end of the field. **Bottom:** All fields identified were visualized on a theta phase plot, to ensure they exhibited phase precession. Fields that did not show complete phase precession in at least one direction, overlapped with another field, or showed truncated phase precession because of overlap with a food dish location were eliminated from the analysis.

## RESULTS

To study whether and how the directionality of place cells changes during initial experience on a track, we compared firing rates during passes through place fields in either direction across laps during the animal's first session on the track. For each cell, each place field was delineated (see **Figure 1** and Methods), and all spikes that occurred within the field boundaries on each lap were counted. The "directionality index" (DI) of each field was calculated for each lap. The "higher firing rate direction" is defined as the direction in which, over the whole session, the number of spikes fired is greater. The DI is the number of spikes fired in the higher firing rate direction minus the lower firing rate direction, divided by the total number of spikes in both directions, and is the same as the rate remapping difference ratio used by Leutgeb et al. (2005). The average DI increased from a very low value (cells show almost identical firing in both directions) to a high value in about five laps of experience on the track (**Figure 2**), even though the average firing rates of the population stayed the same (**Figure 4A**). During the second and third sessions of experience on the track, the DI was already high on the first

**Table 1 | Statistics of each session analyzed.**

| Rat | Session | Full, direct laps run | Cells | Fields in analysis |
|---|---|---|---|---|
| **CUE-RICH CUE-POOR CIRCULAR TRACK** | | | | |
| 1 | 1 | 24 | 50 | 63 |
| | 2 | 12 | 72 | 80 |
| | 3 | 15 | 74 | 82 |
| 2 | 1 | 14 | 13 | 20 |
| | 2 | 7 | 43 | 39 |
| | 3 | 11 | 26 | 33 |
| 3 | 1 | 25 | 69 | 79 |
| | 2 | 7 | 65 | 28 |
| | 3 | 20 | 69 | 45 |
| 5 | 1 | 34 | 156 | 32 |
| | 2 | 20 | 175 | 22 |
| | 3 | 19 | 137 | 42 |
| **SHUTTLING TASK** | | | | |
| 3 | 1 | 13 | 47 | 9 |
| | 2 | 53 | 48 | 13 |
| | 3 | 77 | 39 | 18 |
| 4 | 1 | 20 | 94 | 15 |
| | 2 | 21 | 69 | 10 |
| | 3 | 29 | 81 | 14 |

*Two tasks were performed by five rats. Each rat ran a task for at least three days, and the first three sessions were analyzed. (Rat 1 ran on the circular track twice a day, so the afternoon session of day 1 was considered session 2 and analyzed with the other rats' day 2, and the morning session of day 2 was session 3). The numbers of laps completed by the rat, cells recorded, and fields analyzed are displayed for each rat and session. The smallest number of laps traversed by any of the rats during a given session was analyzed.*

lap, but still increased slightly during the next few laps (**Figure 2**). There was a significant difference between the DI on the first lap compared to the last lap on all three days (paired $t$-tests, day 1: $p < 0.0001$, day 2: $p < 0.05$, day 3: $p < 0.01$). This was true for both the CA1 and CA3 cells in our analysis, although, consistent with the more robust rate remapping in CA3 reported by Leutgeb et al. (2005), the CA3 cells showed higher directionality at the end of the session (CA1 DI during last lap: 0.42, ± SEM 0.056, CA3 DI during last lap: 0.66 ± SEM 0.074, $t$-test: $p < 0.05$). We cannot, however, rule out individual differences between rats in this case, because the CA3 and CA1 samples came largely from different animals. While the average pattern clearly shows that the directionality of place cells increases from the first few laps to the end of the first session, individual cells showed different patterns of firing rate changes within different fields (discussed below). Some examples of firing rate changes in individual fields are shown in **Figure 3**.

The average running speed of the rats tended to increase throughout the session, as the rats explored the track relatively slowly during the first few laps and later ran faster, now purely to receive their rewards (from 14.2 cm/s, SEM = 0.25 on lap 1 to 26.7 cm/s, SEM = 0.78 on lap 10). It is known that the firing rate of place cells increases with running speed (McNaughton et al., 1983); however, as the rat runs faster, he passes through each field more quickly, which compensates for the higher firing rate, and the total number of spikes fired during the pass through the field is approximately the same (Ekstrom et al., 2001). In our results, the number of spikes fired during each pass through a field actually decreased slightly with running speed (analysis of variance of the effect of velocity rank on number of spikes: $F = 7.3$, $p < 0.01$; **Figure 4B**). A decrease in the number of spikes in both directions would not, however, affect the DI, because this measure compensates for the total number of spikes. The number of spikes did, in fact, decrease with velocity similarly in both running directions (interaction between running direction and velocity rank: $F = 0.2$, $p > 0.1$; **Figure 4B**), but changed in opposite directions with chronological lap number (interaction between running direction and chronological lap number, $F = 9.53$, $p < 0.01$; **Figure 4A**). Thus, the observed change in firing rates over the first few laps cannot be accounted for by the effects of different running speeds seen during those laps.

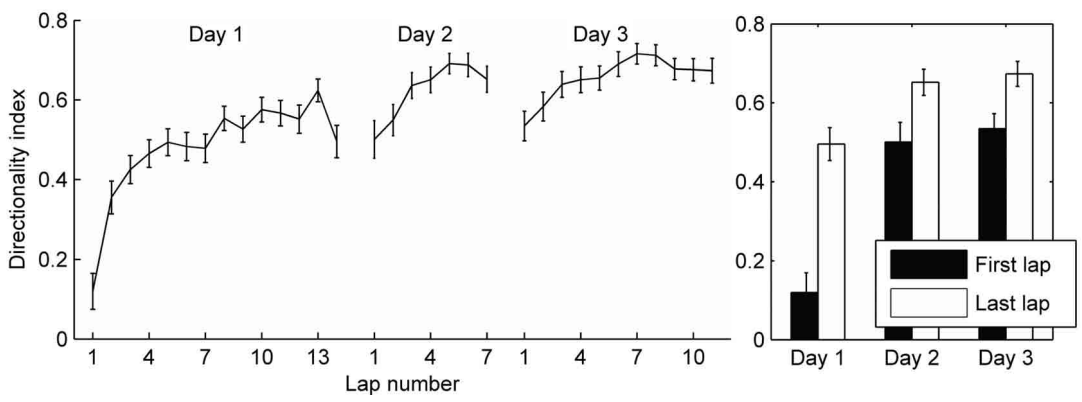


**FIGURE 2 | Development of directionality on a circular track.** The number of spikes occurring within the field boundaries in each running direction was analyzed. The directionality index was calculated for each field on each lap as the difference in number of spikes fired in the preferred and non-preferred running directions divided by the total spikes in both directions (see Methods). The mean directionality index for all fields is plotted for each lap and each session. Error bars represent standard error of the mean. Laps are cut off at the least number of laps run by the four rats in a given session. Right: Comparing the directionality index during the first lap and the last lap in each session shows a significant increase from beginning to the end of each session.

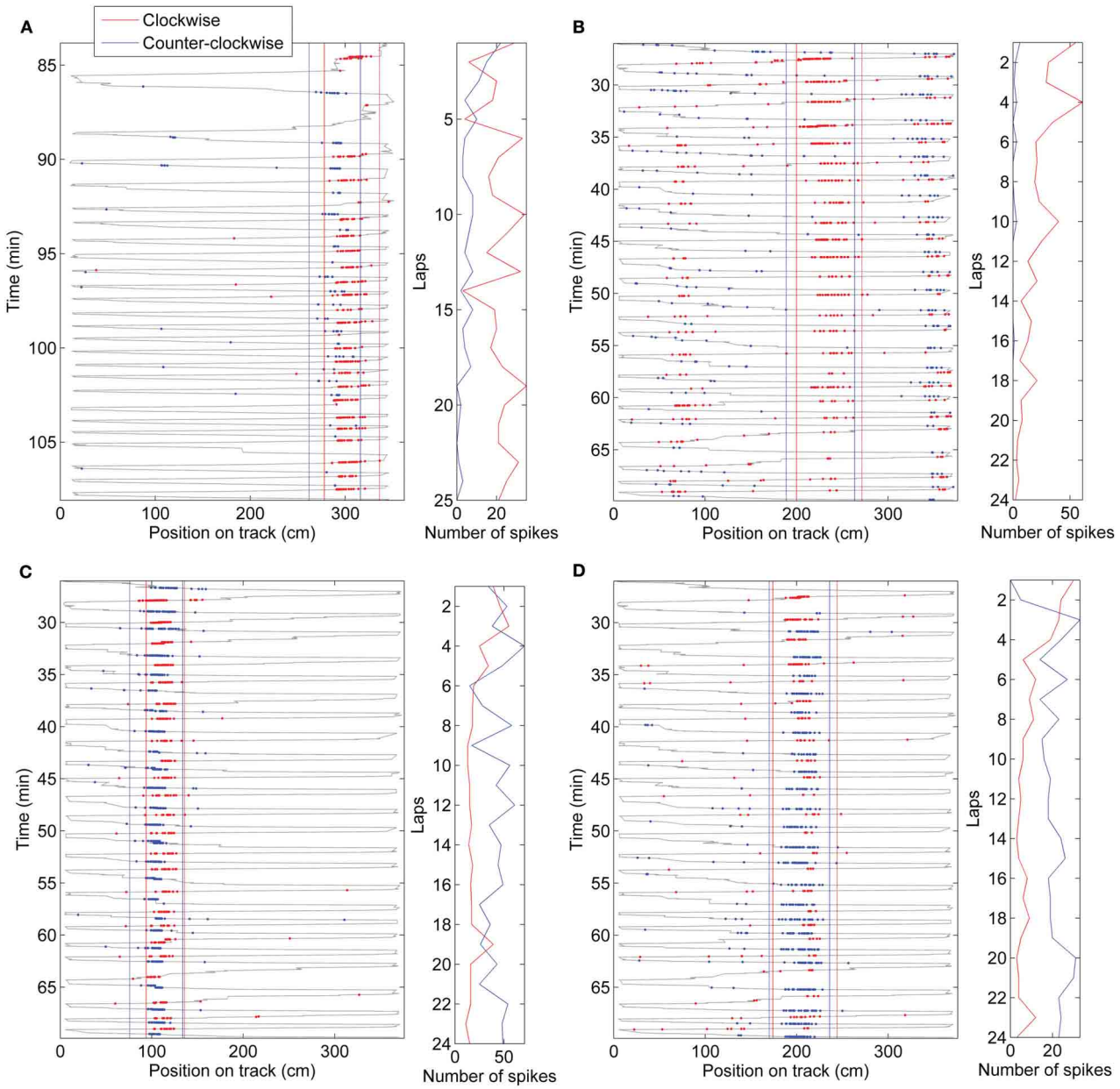


**FIGURE 3 | Examples of firing rate changes in individual cells on day 1.** **(A)** A proximal CA1 cell from rat 3 expressing a field on the cue-rich side of the track showed a typical pattern of directionality increase. Many cells (those falling in the category shown in **Figure 5B**) showed a directionality increase such as this. **(B)** Some cells expressed fields that started with significant directionality in the first few laps, such as the highlighted field of the intermediate CA1 cell shown here. Like this example, many cells in the category shown in **Figure 5C** increased their directionality even more after the first few laps. **(C)** An intermediate CA1 cell from rat 1 expressing a field on the cue-rich part of the track showed a small directionality increase. Many cells remained bi-directional throughout the session. **(D)** A few cells started directional and became less so, or reversed their preferred direction of firing (cells in the categories in **Figure 5E,F**). This intermediate CA1 cell from rat 1 didn't start firing until the return (clockwise) direction on the first lap, and then, over the next two laps, increased its firing rate in the counter-clockwise direction, eventually firing more spikes in that direction.

Even though the track was narrow (∼10 cm), it is possible the rats were following slightly different paths in the clockwise vs. counter-clockwise directions. To study whether a possible difference in paths could have affected place cell firing rates and contributed to the DI, we analyzed the effect of the difference in paths taken through a field on the DI. The difference in position along the width of the track of paths taken on two subsequent passes through a single field was on average 1.67 cm, and varied with a standard deviation of 1.86 cm. We found that the difference between position along the width of the track during passes in either direction accounted for only 0.2% of the variability in directionality indexes ($R^2 = 0.0023$, $p = 0.015$) on day 1. During

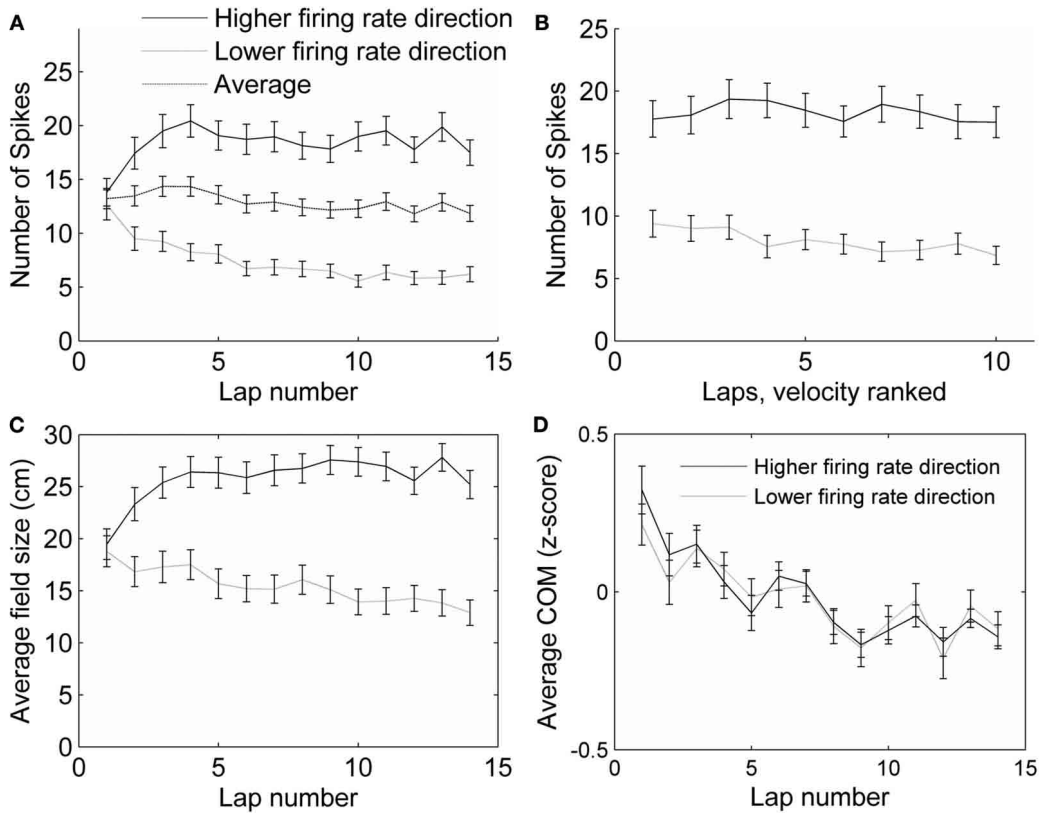


**FIGURE 4 | Control analyses. (A)** The average number of spikes fired in all fields did not change with lap number, even though the firing rates in each direction did. **(B)** The number of spikes fired within a field decreased slightly with running speed, but not differentially for the two running directions. The average number of spikes fired on the slowest pass through each field, the next slowest, and so on until the fastest pass, was calculated. The first four laps were excluded from this analysis, because the running speed was highly correlated with lap number in these laps. The slowest passes through each field (excluding the first four laps) were on average 17.7 cm/s (SEM = 0.53), and the fastest passes were on average 31.0 cm/s (SEM = 0.75), covering a range of the same size to the range of the passes during laps 1–10. **(C)** Average field size (measured as the distance from the first spike to the last spike) changed in each running direction across laps by about 35%, but not as much as the number of spikes fired (**A**). **(D)** The center of mass (COM) of place fields shifted backwards, in both preferred (higher firing rate) and non-preferred (lower firing rate) directions.

subsequent days, when the DI was greater, the effect of difference in position between passes on DI was not significant (day 2: $R^2 = 0.00017$, $p = 0.1$; day 3: $R^2 = 0.00036$, $p = 0.1$). Thus, the differences in firing rates in the two running directions are barely, if at all, affected by differences in paths traversed.

The change in relative firing rate within place fields in the two running directions has the characteristics of rate remapping, because changes in rate occurred without overall changes in firing location. To confirm this assessment, we analyzed several parameters that would indicate global remapping. First, global remapping would predict that many fields would appear in a novel location which did not show firing during the first few laps. During the first three laps, no spikes were fired only in 10 fields (5.2 percent), and six or fewer spikes were fired in 26 (13 percent) fields in those first three laps. When these fields were removed from the analysis, the average DI did not change noticeably (DI on lap 1 including all fields: 0.12 ± SEM 0.045, including only fields that exhibited more than six spikes in the first three laps: 0.14 ± SEM 0.045). Second, global remapping would predict that many cells stopped firing completely in one running direction; however, even during rate remapping the changes in rate can be sufficient to cause a few cells to have firing probabilities that approach zero in a given location in one or other condition (Leutgeb et al., 2005). Forty-eight fields (25 percent) ended with no spikes in at least one running direction. Removing these fields from the analysis reduced the DI both at the beginning and end of the session, but the change in directionality was still significant, both for the fields that ended with spikes in both directions, and for the fields that ended with no spikes in one direction (paired $t$-test between DI on first and last lap, $p < 0.001$ in both cases). Additionally, the size of each place field was measured on each lap, as the distance between the first and last spike (within the field boundaries) during that lap. The average field sizes did not change very much (about 35%—**Figure 4C**, compared to a 50% change in firing rates—**Figure 3A**, and only 20% when fields with no spikes are not included). To check for stability in the locations of place fields, we analyzed the center of mass (COM) of each field on each lap. The average COM of the fields shifted in the direction opposite to the direction of running, as has been observed previously (Mehta et al., 1997), but no other shifting of individual

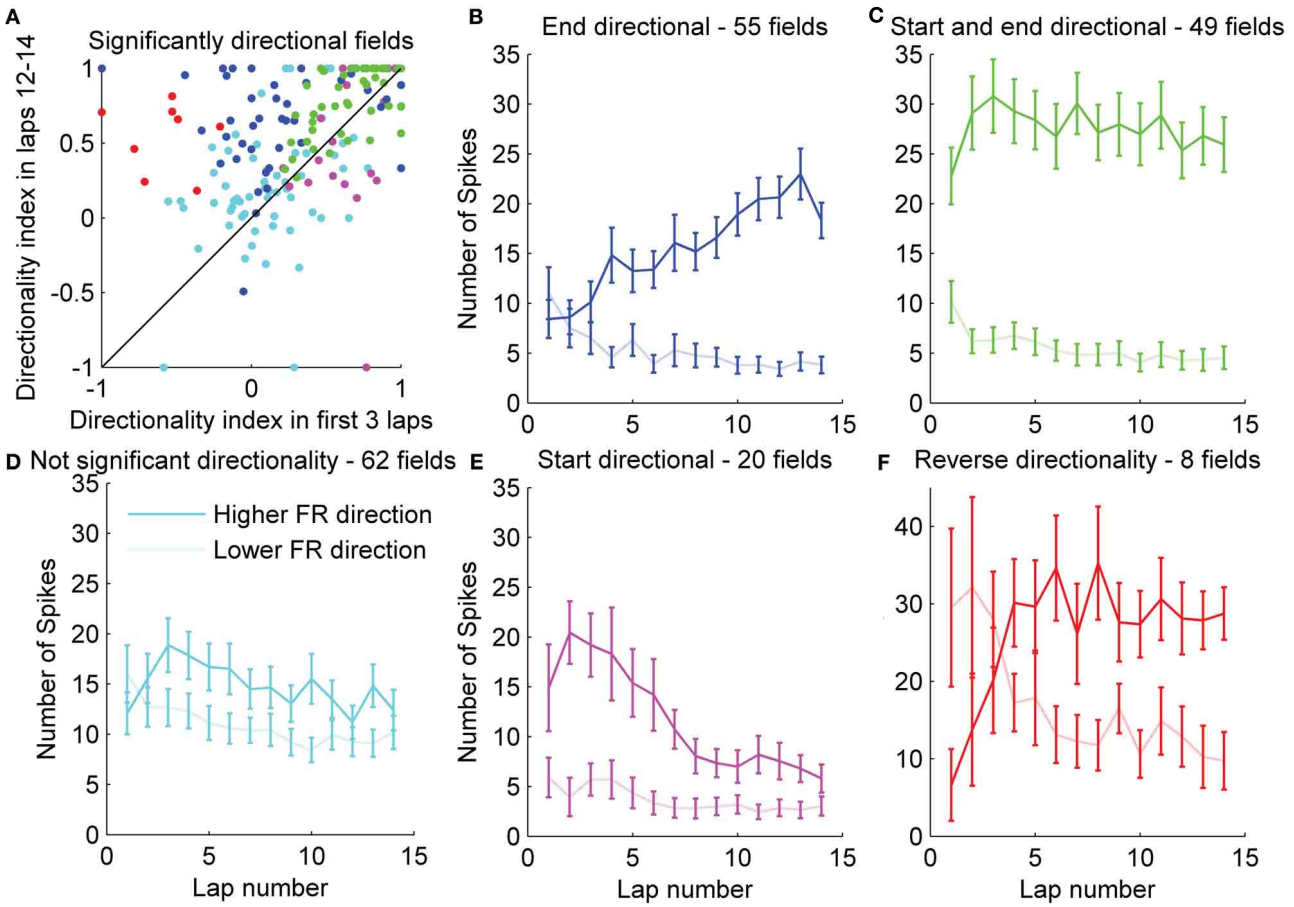


**FIGURE 5 | Remapping in individual fields. (A)** To observe the amount of rate remapping exhibited within individual fields, the directionality index during the first three laps was plotted against the directionality index during the last three laps. Significance of the directionality in individual fields was assessed with a $\chi^2$ test. Fields were classified based on whether they exhibited significant ($p < 0.05$) directionality at the beginning or end of the session or both, and are color-coded based on this classification. **(B–F)** For each group of fields, the average firing rates in each running direction are also displayed. Error bars represent standard error of the mean. Additionally, eight fields were identified that showed significant directionality in the non-preferred direction at the beginning of the session.

fields was observed (average COM shift from first to last lap was $4.6 \pm 12.6$ cm, SEM $= 0.83$; **Figure 4D**). Interestingly, the experience-dependent backwards COM shift was observed both in the direction in which the field was becoming stronger, as well as in the direction in which the field was becoming weaker. The COM shift was observed for both CA3 and CA1 cells on day 1, and also observed on days 2 and 3 in the preferred firing direction of CA1 cells, but not CA3 cells (similar to previous data of Lee et al., 2004).

To understand how individual fields changed as the rat gained experience in the environment, we plotted the DI during the first three laps versus the DI during the last three laps for each individual field (**Figure 5A**). This plot shows that while, on average, the DI increased with lap number, individual fields exhibited a wide range of directionality indices both at the start of exposure to the environment as well as after repeated runs. Consistent with the average results, many fields showed a substantial increase in DI during the behavior session, while many fewer fields showed a decrease in DI. To check the significance of the DI for each individual field, we calculated the chi square statistic comparing the number of spikes in each running direction for each field, both in the first three laps, and in the last three laps. Of the 194 total fields expressed on day 1, 77 showed significantly directional firing during laps 1–3, and 111 showed significant directionality during the last three laps. Fifty-six of these showed directional firing both at the beginning and end of the session. Of those 56 fields, 42 showed an increase in DI from the first three to the last three laps. The last 62 fields did not show significant directionality at the beginning or end of the session. Interestingly, of the 77 fields that showed significantly directional firing at the start of the session, eight exhibited a reversal in the preferred firing direction. At the beginning of the session, the firing rate in these eight fields was higher in the direction that became the lower firing rate direction when averaged over the session (the "lower firing rate," or "non-preferred" direction). By the end of the session, seven of these fields showed a significant directionality in the preferred direction, while one of them did not show significant directionality. We plotted the number of spikes per lap

separately for each of five categories of fields: fields that showed directional firing only at the end of the session (**Figure 5B**, blue), fields that showed directional firing (in the preferred direction) both at the start and end of the session (**Figure 5C**, green), fields that never showed directional firing (**Figure 5D**, cyan), fields that showed significant directional firing (in the preferred direction) only at the start of the session (**Figure 5E**, magenta), and fields that showed significant directional firing in the non-preferred (lower firing rate) direction at the start of the session (**Figure 5F**, red). Separating the fields into groups that exhibit similar directionality changes during the first session shows that even though different cells exhibit different amounts of directionality throughout the session, there was an average tendency to increase their firing rate in the preferred direction and decrease their firing rate in the non-preferred direction during the first few laps. A substantial number of cells, however, exhibited decreases in firing in the preferred direction or increases in firing in the non-preferred direction while nevertheless increasing overall directionality, due to even greater changes in the opposite direction.

We addressed the question of whether there may be some form of competition involved in the change in firing rates over the first few laps by assessing whether directionality tended to increase in the direction that was preferred on lap 1. In other words, we tested the hypothesis that initially stronger inputs tended to get stronger while initially weaker ones tended to get weaker. The average directionality during lap 1 was small, but significant ($0.12 \pm$ SEM 0.045, $t$-test: $p < 0.05$). We computed the signed DI (CW rate – CCW rate)/(CW rate + CCW rate) for each field for laps 1 and 14 on day 1 and performed a regression analysis. There was a weak tendency for directionality to increase in the direction of the initial bias ($R^2 = 0.084$, $F = 13.1$, $p < 0.001$). This tendency was true even for the three rats that were actually visiting the track for the first time ($R^2 = 0.081$, $F = 8.05$, $p < 0.01$).

Place cells are known to express more bidirectional place fields when local cues are present on the track (Battaglia et al., 2004). To assess how local cues affected the development of directional firing in our experiment, half of the track had small objects or textures on it, and the other half was bare. During the first lap, fields on either side of the track did not differ significantly ($t$-test, $p = 0.16$), but by the end of the first session, fields expressed on the cue poor half of the track showed higher directionality than fields expressed on the half of the track rich in cues ($t$-test, $p < 0.001$; **Figure 6**). An analysis of variance showed a significant effect of cue condition on the DI ($F = 4.39$, $p < 0.05$), and a significant interaction between lap number and cue condition ($F = 5.93$, $p < 0.05$). Another possible difference between the two halves of the track was the rats' behavior: they ran slower on the cue-rich part of the track, and stepped over and around certain objects and textures in stereotyped ways (running speed through fields on cue-rich part of the track: $18.2 \pm 4.56$ cm/s, cue-poor part of track: $29.5 \pm 7.99$ cm/s, $t$-test: $p < 0.001$). The specific stereotyped movements and the sequence of movements, however, was different between the two running directions on the cue-rich part of the track, and more similar (involving fewer specialized movements) on the cue-poor part of the track.

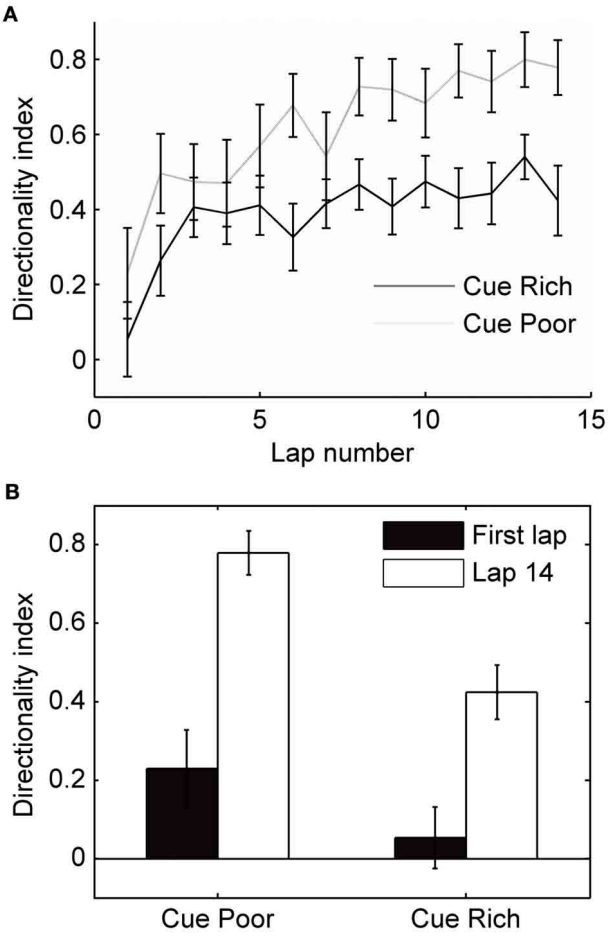


**FIGURE 6 | Local cues and the development of directionality.** Half of the circular track was enriched with small objects and textures (local cues). **(A)** The mean directionality index is plotted for fields expressed on the cue-rich and cue-poor halves of the track. **(B)** During the first lap, field directionality on the cue-rich and cue-poor halves of the track did not differ significantly ($t$-test, $p = 0.16$). Over the session, fields on both parts of the track became significantly more directional (paired $t$-tests, $p < 0.01$); however, fields on the cue-rich part of the track increased directionality less than fields on the cue-poor side, and directionality was significantly different between regions on the last lap ($t$-test, $p < 0.001$).

Directional firing of place cells has also been shown when a rat's path was not physically restricted to a track, but the rat was trained to run a specified path in order to receive rewards at known locations (Markus et al., 1995). To determine whether directional firing in this case also develops from initially omnidirectional place fields, we trained rats to run back and forth between a home-box location and a food dish on a circular open-field platform. It took the rats 2–4 days to learn the task, but as soon as they were running >20 laps, we analyzed the directionality of their place fields. On the first day the rats ran more than 20 laps, the DI of the fields was low and did not significantly change during the session (**Figure 7A**). The day after that, however, the DI started low and increased by the end of the session (**Figure 7A,B**; paired $t$-test between first three laps and last three

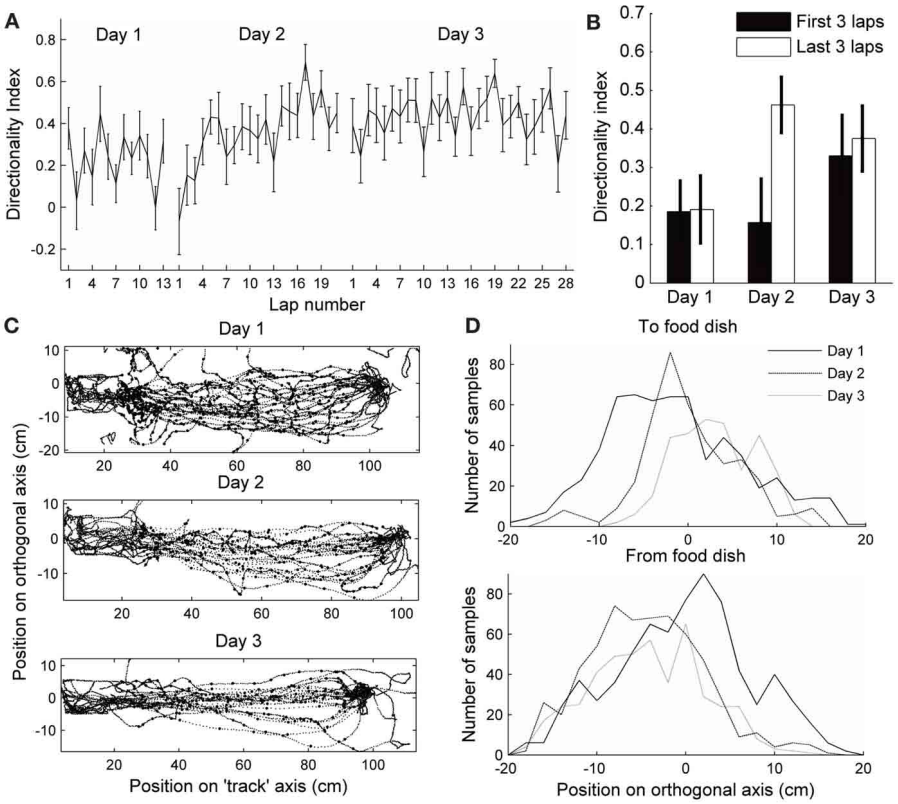


**FIGURE 7 | Directionality in an open-field. (A–B)** Directionality index in fields expressed on an open-field platform during performance of a shuttle task. Day 1 is the first day each rat ran more than 20 laps (This was actually day 2 in the environment for one rat, and day 4 for the other rat. On this day, rat 3 ran 22 laps, 13 of which were direct, and rat 4 ran 25, 20 of which were direct). The day after that, the rats ran 53 and 21 direct laps, respectively, and the directionality index started low and increased by laps 18–21. On the following day (3), the directionality index started as high as at the end of day 2, and did not change throughout the session. **(B)** Directionality index during the first three and last three laps of each session. **(C)** Paths run by one of the rats during the first 13 direct passes between the start box (left) and the food dish (right). The position was sampled five times per second, excluding the times when the rat was in the box or at the food dish, to test for variability (large dots). **(D)** Distribution of positions along the axis orthogonal to the direct path from food dish to box at the sampled times is plotted for both rats. Paths toward the food dish and away from the food dish are plotted separately. The distribution is wider on day 1 in both directions.

laps: $p < 0.01$). The following days the DI started as high as at the end of day 2, and did not change throughout the session. As in the circular track task, the speed of running through a field affected the number of spikes fired during that pass slightly, but did not affect passes in the two directions differentially. To determine why directionality only developed on the second day of performing the shuttling task, we analyzed the variability of the paths the rats took to the food dish (the paths for one rat are plotted in **Figure 7C**). The first 13 direct laps were analyzed on each day for each rat. The position was sampled five times per second during traverses to and from the food dish (excluding times the rat was in the box or at the food dish). The position along the axis orthogonal to the most direct path from home box to food dish (the "track" axis) was analyzed. On the first day, the distribution of positions visited by both rats during their runs was wider than on the following days (Brown–Forsythe test for equality of variances: $p < 0.001$, multiple comparison test shows that day 1 is significantly different from days 2 and 3, but day 3 is not different from day 2). Even though the paths were more stereotyped when directionality developed, and were different between the two running directions, the difference in the paths did not predict the DI, as in the circular track data. These results show that the differential rate remapping in opposite running directions can develop not only on tracks that constrain the animal's trajectory, but also in an open-field environment that is repeatedly traversed along a particular path. In an open-field environment, however, the rate remapping develops only once behavior becomes stereotyped.

## DISCUSSION

The main finding is that, in rats running on a track, the firing of hippocampal place cells is initially bidirectional, and gradually becomes highly unidirectional. This large increase in directional selectivity involves gradual changes in firing rates in either or both running directions, during approximately the first 5–10 laps on the first day of exposure to the track. This effect is almost entirely due to positive and negative changes in direction-specific firing rates of the neurons, and not to changes in the locations in

which the neurons fire (i.e., rate remapping). Thus, while retaining information about the allocentric location of the animal, the network gradually differentiates the direction in which it is traveling on the track. This finding clarifies a long standing question of why the firing of hippocampal neurons is different in different directions when the rat is following a specified path (McNaughton et al., 1983; Muller et al., 1994), but the same in each direction when the rat is following random paths (Muller et al., 1987).

The formation of place fields has been hypothesized to depend on one of two separate mechanisms: learning of the sensory details of the environment to construct a map and triangulate one's location in it, or a continuous updating of one's movement trajectory to calculate allocentric position in the environment (path integration), or some combination of the two mechanisms. Models relying on the first mechanism rely on the learning of associations between place cells and their sensory inputs in order to form non-directionally specific place fields. For example, Sharp (1991) modeled a network with sensory inputs relating to the egocentric distance and direction of landmarks projecting to entorhinal and then hippocampal cells, and used competitive learning to establish place fields. A prediction of this model was that place fields would initially be directional, but become direction-independent after exploration in multiple directions. Because exploration was restricted to two directions on a track, place fields on a track would never become omni-directional in this model. Our data, however, show a pattern opposite to that predicted by this model; place fields are initially omni-directional, and increase their direction-specificity with experience. The current findings are more consistent with models that rely on some form of path integration to determine the initial location of place fields.

The assertion that path integration determines the formation of place fields is well supported with previous experimental evidence (reviewed in McNaughton et al., 1996, 2006). For example, symmetry of sensory cues in an environment does not result in symmetrical place cell firing (Sharp et al., 1990) and identical sensory environments located at 180° rotated orientations (Fuhs et al., 2005), or in different rooms (Leutgeb et al., 2005) result in global remapping of place representations. Further, place fields do not change location when lights are turned on or off (O'Keefe and Speakman, 1987; Quirk et al., 1990; Markus et al., 1994). The inhibition (Kentros et al., 1998) or deficiency (Barnes et al., 1997) of LTP does not disrupt the formation of place fields, but does disrupt the recall of place cell associations with previously visited environments. Global remapping is instantaneous when a large mismatch between sensory cues and vestibular information occurs (Knierim et al., 1998), as is place field realignment to moved landmarks (Gothard et al., 1996a), further supporting that learning is not necessary for the establishment of novel or changed place cell representations.

In the framework of path integration models, earlier hypotheses to account for directionality along restricted paths involved a switch of "reference frames" or maps (now referred to as global remapping) at the arm ends; however, attempts to observe the predicted complete discontinuity in firing patterns at arm-ends were generally unsuccessful (Redish et al., 2000). The symmetrical firing observed during the first traversal of a path, is consistent with typical, non-directional firing during random foraging behavior, and also with the evidence that the selection of which hippocampal neurons are able to fire at a given location is determined on the basis of path integration rather than exteroceptive cues (presumably by inputs from the medial entorhinal cortex). When the animal travels the same route multiple times, however, it appears that the firing of hippocampal cells gradually becomes conjunctive for the path integrator coordinates and the direction-specific "local view" (McNaughton et al., 1991).

The most plausible source of external landmark information to the hippocampus proper is via the lateral entorhinal cortex (LEC) (Burwell and Amaral, 1998; Si and Treves, 2009; Renno-Costa et al., 2010; Deshmukh and Knierim, 2011). LEC projects to the outer portions of the dendrites of DG and CA3 uniformly along the transverse axis of hippocampus, and to the distal (i.e., nearest to subiculum) CA1 cells. We observed strong increases in directional tuning in both CA3 and CA1 (including the cells located in proximal CA1, which only get direct inputs from MEC and CA3), raising the possibility that the directionality increase in CA1 is largely driven by changes in CA3 itself or in Schaffer collateral synapses.

At present, one can only speculate about the possible mechanisms of the increased directionality. The data appear to be generally compatible with the observation that LEC inputs are capable of bidirectional weight changes (LTP/LTD; McNaughton et al., 1978; Abraham and Goddard, 1983) and support the hypothesis that the LEC to CA3 (and/or DG) connections which are active in a given direction either increase or decrease according to some form of competition. Plausibly, the initial mean weights of synapses driven by the novel cues, being drawn effectively at random from an existing weight distribution, would be approximately equal in the two directions (central limit theorem). Whether the mean weights would increase or decrease might depend on some form of competition (e.g., BCM rule), by which inputs causing strong activation are strengthened whereas those causing weaker activation are weakened. We did observe a slight tendency for directionality to increase in the direction of initial preference, but it accounted for only 8% of the directionality variance by the end of session 1. It is also possible that competition is influenced by the timing of inhibitory inputs from interneurons driven at short-latency by other pyramidal cells (Csicsvari et al., 1998; Marshall et al., 2002; Maurer et al., 2006). In addition, the firing rates of some hippocampal interneurons are strongly modulated by novelty (Wilson and McNaughton, 1993; Nitz and McNaughton, 2004), which may have an important impact on plasticity over the first few laps. In any case, if the magnitude and direction of weight change is a random variable that is correlated over the active population of inputs onto a given hippocampal cell for a given running direction, then the firing in opposite directions would tend to diverge, resulting in increased directional bias.

On average, there was about a 50% increase or decrease in firing rate over time in a given direction (**Figure 4A**); however, there were cases of cells either starting out or ending up with zero spikes in one direction. If the observed changes in firing are indeed due to changes in LEC synaptic efficacy, the complete lack of firing

in one direction implies that, at least in some cells, MEC inputs alone are not sufficient to drive spiking. Since MEC inputs are also known to exhibit plasticity, however, it is also possible that both sets of inputs may undergo experience-dependent changes. The effect of local cues on the track, however, which would likely reduce the net difference in external input in the two directions, appears to indicate that the main changes are driven by external inputs.

Other studies have shown that rate remapping occurs when the behavioral goals or context, or internal state of the animal changes (e.g., Frank et al., 2000; Wood et al., 2000; Bower et al., 2005). By teaching the rats a shuttling task, we modified their behavioral goals. This change in behavioral context could explain why remapping occurred in the same environment when the task changed from foraging for randomly placed rewards and running between predictable reward locations (Markus et al., 1995). In our results, this rate remapping didn't occur until the task was so well learned that it was performed stereotypically. This indicates that the development of directionality in the hippocampus does not drive the change in behavioral strategy; instead it may be driven by the shift to a different behavioral state. Some of the studies of rate remapping at identical locations during running toward different goals have been interpreted to mean that mnemonic coding, when it is task-relevant, exists in the hippocampus in addition to spatial coding (Berke et al., 2009). Another interpretation, based on our results, is that the "context" encoded by the hippocampus can include the particular trajectory being traversed, if traversal of the trajectories becomes highly stereotyped. Studies of the initial place cell activity in these tasks should be performed to differentiate between these two hypotheses. If the rate remapping occurs after the task is well learned, it would suggest that task demands, including goal locations, are actually learned by a different structure, such as the striatum, and remapping in the hippocampus is driven later by input relating to the task context. Some findings support this second hypothesis, including that Berke et al. (2009) did not see rate remapping in the initial learning trials of their cued goal maze task, even though in those trials the rat was using its prior positions to plan a future route. Additionally, rate remapping of overlapping positions in a sequence task does not occur when the overlapping parts of the trajectories include more than one arm (Lenck-Santini et al., 2001; Bower et al., 2005), and is not necessary for a rat to learn complex sequences (Bower et al., 2005).

Mehta et al. (1997) reported an experience-dependent place field expansion in CA1, with a COM shift in the direction opposite the direction of travel, when rats ran unidirectionally around a track. This effect was subsequently shown to occur also in CA3, in a more long lasting form (Lee et al., 2004) and to be dependent (at least in CA1) on NMDA receptor function (Ekstrom et al., 2001). The accepted view of the mechanism of this experience-dependent expansion and shift is that it reflects the development of what Hebb (1949) referred to as a "phase sequence." Synapses from cells that fire earlier in a sequence onto cells firing later become asymmetrically strengthened through spike-timing dependent LTP. In their discussion, Mehta et al. (1997) commented: "A natural question is whether the observed asymmetry would cancel out if the rat ran repeatedly back and forth along a route in both directions. It turns out that this experiment is not possible because, under such circumstances, the hippocampus encodes the forward and return journeys using different sets of place cells." The present results show that this conjecture was incorrect; the forward and return journeys apparently are encoded by the same set of place cells, but with substantially direction-dependent firing rates, and we did observe a COM shift in both the preferred and the non-preferred directions, on the first day. The fact that field expansion in both directions didn't cancel out the asymmetric COM shift, could be explained by local feedback inhibition, an after-hyperpolarizing current, or another form of depression in each place cell that does not allow a place cell that has recently fired to be activated by connections from other currently active place cells. Another possible implication of this result is that the synapses that mediate rate remapping are not the same as the synapses that mediate the place field shift. Rate remapping typically resulted in fewer spikes fired in the non-preferred direction, suggesting a synaptic depression, yet the field shift is generally attributed to synaptic enhancement.

On the second and third days on the track, place field shift occurred only in CA1 cells, and only in the preferred direction, while directionality increased only slightly, and in both CA1 and CA3 cells. The fact that place field expansion does not occur in CA3 on later days is consistent with previous results (Lee et al., 2004) which suggest that the underlying plasticity is more persistent in CA3 than CA1. A possible explanation for the lack of expansion in the non-preferred direction in CA1 on days 2 and 3 may be that there was insufficient depolarization on the cells to induce LTP in the feed-forward synapses from CA3. Of course, the foregoing proposals are speculative. Understanding the specific mechanisms involved in these phenomena await further study.

In summary, during the first few traverses of a fixed route in space, place cell activity is almost entirely determined by allocentric position; later the activity becomes modulated by other factors, without significantly affecting the position dependence (rate remapping). The shift is likely due to sensory information at a given position, but could also be partially driven by internal state variables such as memory or goals, or the behavior of the animal at particular locations. We presented evidence that directionality does not develop until behavior becomes stereotyped, suggesting that the performance of a specific task in an environment contributes to changes in place cell activity. Both sensory and motor information makes its way into the hippocampus, in a highly processed form, however. Recordings from the input structures to the hippocampus (especially MEC and LEC) during performance of directional tasks in a novel environment are needed to elucidate what drives the development of directionality of place cells.

## ACKNOWLEDGMENTS

We would like to thank J. L. Valdes for early involvement in the recordings, V. Bouquet, K. Bohne, J. Wang, and J. Bohanick for technical assistance, and C. A. Barnes for access to facilities and resources. Supported by NS20331 and AHFMR Polaris award.

## REFERENCES


Abraham, W. C., and Goddard, G. V. (1983). Asymmetric relationships between homosynaptic long-term potentiation and heterosynaptic long-term depression. *Nature* 305, 717–719.

Barnes, C. A., Suster, M. S., Shen, J., and McNaughton, B. L. (1997). Multistability of cognitive maps in the hippocampus of old rats. *Nature* 388, 272–275.

Battaglia, F. P., Sutherland, G. R., and McNaughton, B. L. (2004). Local sensory cues and place cell directionality: additional evidence of prospective coding in the hippocampus. *J. Neurosci.* 24, 4541–4550.

Berke, J. D., Breck, J. T., and Eichenbaum, H. (2009). Striatal versus hippocampal representations during win-stay maze performance. *J. Neurophysiol.* 101, 1575–1587.

Bower, M. R., Euston, D. R., and McNaughton, B. L. (2005). Sequential-context-dependent hippocampal activity is not necessary to learn sequences with repeated elements. *J. Neurosci.* 25, 1313–1323.

Burwell, R. D., and Amaral, D. G. (1998). Cortical afferents of the perirhinal, postrhinal, and entorhinal cortices of the rat. *J. Comp. Neurol.* 398, 179–205.

Colgin, L. L., Leutgeb, S., Jezek, K., Leutgeb, J. K., Moser, E. I., McNaughton, B. L., and Moser, M. B. (2010). Attractor-map versus autoassociation based attractor dynamics in the hippocampal network. *J. Neurophysiol.* 104, 35–50.

Csicsvari, J., Hirase, H., Czurko, A., and Buzsaki, G. (1998). Reliability and state dependence of pyramidal cell-interneuron synapses in the hippocampus: an ensemble approach in the behaving rat. *Neuron* 21, 179–189.

Deshmukh, S. S., and Knierim, J. J. (2011). Representation of non-spatial and spatial information in the lateral entorhinal cortex. *Front. Behav. Neurosci.* 5, 69. doi: 10.3389/fnbeh.2011.00069

Eichenbaum, H., Dudchenko, P., Wood, E., Shapiro, M., and Tanila, H. (1999). The hippocampus, memory, and place cells: is it spatial memory or a memory space? *Neuron* 23, 209–226.

Ekstrom, A. D., Meltzer, J., McNaughton, B. L., and Barnes, C. A. (2001). NMDA receptor antagonism blocks experience-dependent expansion of hippocampal "place fields". *Neuron* 31, 631–638.

Frank, L. M., Brown, E. N., and Wilson, M. (2000). Trajectory encoding in the hippocampus and entorhinal cortex. *Neuron* 27, 169–178.

Fuhs, M. C., Vanrhoads, S. R., Casale, A. E., McNaughton, B., and Touretzky, D. S. (2005). Influence of path integration versus environmental orientation on place cell remapping between visually identical environments. *J. Neurophysiol.* 94, 2603–2616.

Fyhn, M., Hafting, T., Treves, A., Moser, M. B., and Moser, E. I. (2007). Hippocampal remapping and grid realignment in entorhinal cortex. *Nature* 446, 190–194.

Gothard, K. M., Skaggs, W. E., and McNaughton, B. L. (1996a). Dynamics of mismatch correction in the hippocampal ensemble code for space: interaction between path integration and environmental cues. *J. Neurosci.* 16, 8027–8040.

Gothard, K. M., Skaggs, W. E., Moore, K. M., McNaughton, B. L. (1996b). Binding of hippocampal CA1 neural activity to multiple reference frames in a landmark-based navigation task. *J. Neurosci.* 16, 823–835.

Hafting, T., Fyhn, M., Molden, S., Moser, M. B., and Moser, E. I. (2005). Microstructure of a spatial map in the entorhinal cortex. *Nature* 436, 801–806.

Hebb, D. O. (1949). *The Organization of Behavior: A Neuropsychological Theory*. New York, NY: Wiley.

Hetherington, P. A., and Shapiro, M. L. (1997). Hippocampal place fields are altered by the removal of single visual cues in a distance-dependent manner. *Behav. Neurosci.* 111, 20–34.

Kentros, C., Hargreaves, E., Hawkins, R. D., Kandel, E. R., Shapiro, M., and Muller, R. V. (1998). Abolition of long-term stability of new hippocampal place cell maps by NMDA receptor blockade. *Science* 280, 2121–2126.

Knierim, J. J., Kudrimoti, H. S., and McNaughton, B. L. (1998). Interactions between idiothetic cues and external landmarks in the control of place cells and head direction cells. *J. Neurophysiol.* 80, 425–446.

Lee, I., Rao, G., and Knierim, J. J. (2004). A double dissociation between hippocampal subfields: differential time course of CA3 and CA1 place cells for processing changed environments. *Neuron* 42, 803–815.

Lenck-Santini, P. P., Save, E., and Poucet, B. (2001). Place-cell firing does not depend on the direction of turn in a Y-maze alternation task. *Eur. J. Neurosci.* 13, 1055–1058.

Leutgeb, S., Leutgeb, J. K., Barnes, C. A., Moser, E. I., McNaughton, B. L., and Moser, M. B. (2005). Independent codes for spatial and episodic memory in hippocampal neuronal ensembles. *Science* 309, 619–623.

Leutgeb, S., Leutgeb, J. K., Moser, E. I., and Moser, M. B. (2006). Fast rate coding in hippocampal CA3 cell ensembles. *Hippocampus* 16, 765–774.

Leutgeb, S., Leutgeb, J. K., Treves, A., Moser, M. B., and Moser, E. I. (2004). Distinct ensemble codes in hippocampal areas CA3 and CA1. *Science* 305, 1295–1298.

Markus, E. J., Barnes, C. A., McNaughton, B. L., Gladden, V. L., and Skaggs, W. E. (1994). Spatial information content and reliability of hippocampal CA1 neurons: effects of visual input. *Hippocampus* 4, 410–421.

Markus, E. J., Qin, Y. L., Leonard, B., Skaggs, W. E., McNaughton, B. L., and Barnes, C. A. (1995). Interactions between location and task affect the spatial and directional firing of hippocampal neurons. *J. Neurosci.* 15, 7079–7094.

Marshall, L., Henze, D. A., Hirase, H., Leinekugel, X., Dragoi, G., and Buzsaki, G. (2002). Hippocampal pyramidal cell-interneuron spike transmission is frequency dependent and responsible for place modulation of interneuron discharge. *J. Neurosci.* 22, RC197.

Maurer, A. P., Cowen, S. L., Burke, S. N., Barnes, C. A., and McNaughton, B. L. (2006). Phase precession in hippocampal interneurons showing strong functional coupling to individual pyramidal cells. *J. Neurosci.* 26, 13485–13492.

McNaughton, B. L., Barnes, C. A., Gerrard, J. L., Gothard, K., Jung, M. W., Knierim, J. J., Kudrimoti, H., Qin, Y., Skaggs, W. E., Suster, M., and Weaver, K. L. (1996). Deciphering the hippocampal polyglot: the hippocampus as a path integration system. *J. Exp. Biol.* 199(Pt 1), 173–185.

McNaughton, B. L., Barnes, C. A., and O'Keefe, J. (1983). The contributions of position, direction, and velocity to single unit activity in the hippocampus of freely-moving rats. *Exp. Brain Res.* 52, 41–49.

McNaughton, B. L., Battaglia, F. P., Jensen, O., Moser, E. I., and Moser, M. B. (2006). Path integration and the neural basis of the "cognitive map". *Nat. Rev. Neurosci.* 7, 663–678.

McNaughton, B. L., Chen, L. L., and Markus, E. J. (1991). "Dead reckoning," landmark learning, and the sense of direction: a neurophysiological and computational hypothesis. *J. Cogn. Neurosci.* 3, 190–202.

McNaughton, B. L., Douglas, R. M., and Goddard, G. V. (1978). Synaptic enhancement in fascia dentata: cooperativity among coactive afferents. *Brain Res.* 157, 277–293.

Mehta, M. R., Barnes, C. A., and McNaughton, B. L. (1997). Experience-dependent, asymmetric expansion of hippocampal place fields. *Proc. Natl. Acad. Sci. U.S.A.* 94, 8918–8921.

Morris, R. G., Garrud, P., Rawlins, J. N., and O'Keefe, J. (1982). Place navigation impaired in rats with hippocampal lesions. *Nature* 297, 681–683.

Muller, R. U., Bostock, E., Taube, J. S., and Kubie, J. L. (1994). On the directional firing properties of hippocampal place cells. *J. Neurosci.* 14, 7235–7251.

Muller, R. U., Kubie, J. L., and Ranck, J. B. Jr. (1987). Spatial firing patterns of hippocampal complex-spike cells in a fixed environment. *J. Neurosci.* 7, 1935–1950.

Nitz, D., and McNaughton, B. L. (2004). Differential modulation of CA1 and dentate gyrus interneurons during exploration of novel environments. *J. Neurophysiol.* 91, 863–872.

O'Keefe, J., and Conway, D. H. (1978). Hippocampal place units in the freely moving rat: why they fire where they fire. *Exp. Brain Res.* 31, 573–590.

O'Keefe, J., and Dostrovsky, J. (1971). The hippocampus as a spatial map. Preliminary evidence from unit activity in the freely-moving rat. *Brain Res.* 34, 171–175.

O'Keefe, J., and Speakman, A. (1987). Single unit activity in the rat hippocampus during a spatial memory task. *Exp. Brain Res.* 68, 1–27.

O'Keefe, J., and Nadel, L. (1978). *The Hippocampus as a Cognitive Map*. Oxford: Oxford University Press.

Quirk, G. J., Muller, R. U., and Kubie, J. L. (1990). The firing of hippocampal place cells in the dark depends on the rat's recent experience. *J. Neurosci.* 10, 2008–2017.

Redish, A. D., McNaughton, B. L., and Barnes, C. A. (2000). Place cell firing shows an inertia-like process. *Neurocomputing* 32–33, 235–241.

Renno-Costa, C., Lisman, J. E., and Verschure, P. F. M. J. (2010). The mechanism of rate remapping

in the dentate gyrus. *Neuron* 68, 1051–1058.

Sharp, P. E. (1991). Computer simulation of hippocampal place cells. *Psychobiology* 19, 103–115.

Sharp, P. E., Kubie, J. L., and Muller, R. U. (1990). Firing properties of hippocampal neurons in a visually symmetrical environment: contributions of multiple sensory cues and mnemonic processes. *J. Neurosci.* 10, 3093–3105.

Si, B., and Treves, A. (2009). The role of competitive learning in the generation of DG fields from EC inputs. *Cogn. Neurodyn.* 3, 177–187.

Skaggs, W. E., and McNaughton, B. L. (1998). Spatial firing properties of hippocampal CA1 populations in an environment containing two visually identical regions. *J. Neurosci.* 18, 8455–8466.

Sparks, F. T., Mandkin, E. A., Slayyeh, B., Sutherland, R. J., and Leutgeb, J. K. (2010). *Coding of temporal context in the hippocampus: do rate codes offer insight into a time-of-day signature*? Program No. 203.9.2010. Abstract Viewer/ Itinerary Planner. San Diego, CA: Society for Neuroscience. Online.

Wilson, M. A., and McNaughton, B. L. (1993). Dynamics of the hippocampal ensemble code for space. *Science* 261, 1055–1058.

Wood, E. R., Dudchenko, P. A., Robitsek, R. J., and Eichenbaum, H. (2000). Hippocampal neurons encode information about different types of memory episodes occurring in the same location. *Neuron* 27, 623–633.

**Conflict of Interest Statement:** The authors declare that the research was conducted in the absence of any commercial or financial relationships that could be construed as a potential conflict of interest.

*Received: 14 December 2011; accepted: 06 February 2012; published online: 21 February 2012.*

*Citation: Navratilova Z, Hoang LT, Schwindel CD, Tatsuno M and McNaughton BL (2012) Experience-dependent firing rate remapping generates directional selectivity in hippocampal place cells. Front. Neural Circuits* ***6****:6. doi: 10.3389/ fncir.2012.00006*

frontiers in
NEURAL CIRCUITS

ORIGINAL RESEARCH ARTICLE
published: 27 April 2012
doi: 10.3389/fncir.2012.00021

# The abrupt development of adult-like grid cell firing in the medial entorhinal cortex

**Thomas J. Wills[1], Caswell Barry[2,3] and Francesca Cacucci[3]***

[1] Department of Cell and Developmental Biology, Division of Biosciences, University College London, London, UK
[2] Institute of Neurology, University College London, London, UK
[3] Institute of Behavioural Neuroscience, Division of Psychology and Language Sciences, University College London, London, UK

**Edited by:**
Yasser Roudi, Norwegian University of Science and Technology, Norway

**Reviewed by:**
Hugh T. Blair, UCLA, USA
Edvard I. Moser, Norwegian University of Science and Technology, Norway

***Correspondence:**
Francesca Cacucci, Institute of Behavioural Neuroscience, Division of Psychology and Language Sciences, University College London, 26 Bedford Way, London WC1H 0AP, UK.
e-mail: f.cacucci@ucl.ac.uk

Understanding the development of the neural circuits subserving specific cognitive functions such as navigation remains a central problem in neuroscience. Here, we characterize the development of grid cells in the medial entorhinal cortex, which, by nature of their regularly spaced firing fields, are thought to provide a distance metric to the hippocampal neural representation of space. Grid cells emerge at the time of weaning in the rat, at around 3 weeks of age. We investigated whether grid cells in young rats are functionally equivalent to those observed in the adult as soon as they appear, or if instead they follow a gradual developmental trajectory. We find that, from the very youngest ages at which reproducible grid firing is observed (postnatal day 19): grid cells display adult-like firing fields that tessellate to form a coherent map of the local environment; that this map is universal, maintaining its internal structure across different environments; and that grid cells in young rats, as in adults, also encode a representation of direction and speed. To further investigate the developmental processes leading up to the appearance of grid cells, we present data from individual medial entorhinal cortex cells recorded across more than 1 day, spanning the period before and after the grid firing pattern emerged. We find that increasing spatial stability of firing was correlated with increasing gridness.

**Keywords: development, grid cell, entorhinal cortex, hippocampus**

Grid cells in the medial entorhinal cortex (mEC) are active when the animal's position coincides with the vertices of a triangular grid covering the whole of the local environment (Hafting et al., 2005). The regularly spaced and repeating nature of grid cell firing, along with the findings that the mEC also contains neural representations of direction, speed and local boundaries (Sargolini et al., 2006; Solstad et al., 2008), suggests that it is a critical brain structure for navigation, combining path integration with local cue information in order to calculate an animal's position.

Since the discovery of grid cells in 2005, a sustained effort has been made toward modeling the neural circuits that produce grid firing in adult rats. Two major categories of theories have become prominent: those positing that grid cells are wired to form a continuous attractor representation of space (Fuhs and Touretzky, 2006; McNaughton et al., 2006; Burak and Fiete, 2009; Navratilova et al., 2011; Sreenivasan and Fiete, 2011), and those which suggest that the regularly repeating patterns of firing of grid cells emerge from the summation of distinct oscillators beating at differing frequencies (Burgess et al., 2007; Giocomo et al., 2007; Blair et al., 2008; Burgess, 2008; Zilli and Hasselmo, 2010). Despite this progress, less emphasis has been placed on understanding how either of these network architectures might be set up during the organism's ontogenetic development (see McNaughton et al., 2006; Welinder et al., 2008; Widloski and Fiete, 2010, for exceptions), leaving open the question of how the grid cell circuit is wired during brain development.

In recent work, we and others have characterized the developmental timeline of the emergence of spatially responsive cells in the hippocampal formation of pre-weanling rats (Langston et al., 2010; Scott et al., 2010; Wills et al., 2010). These studies indicate that head-direction cells are the earliest developing spatial response, appearing fully mature at postnatal day 16 (P16). Rudimentary place cell firing is also present at this age, but continues to improve gradually as the animals age (until at least P45; Scott et al., 2010). Grid cells emerged later, with adult-like grid cell firing present around 3–4 weeks of age. Although the different spatial responses follow distinct developmental trajectories, all the basic components of the hippocampal navigation system are in place by 3 weeks of age, coinciding with the time when weanlings first start to leave their nest (Gerrish and Alberts, 1996).

However, beyond noting the first appearance of grid cell firing and the spatial stability of grid fields, the Wills et al. (2010) and Langston et al. (2010) studies did not offer a detailed investigation of the development of grid cell firing in immature rats. For instance, it is still an open question whether all the aspects that define the adult grid cell system are present from the first appearance of grid firing or if, similarly to place cells, grid cells follow a gradual developmental trajectory. The focus of this study, therefore, is to provide a fuller characterization of grid cell development. With minor exceptions, we find that, as soon as grid cells

are present, the grid cell network possesses all of the characteristic properties observed in the adult. We also present data from a small number of mEC cells that were recorded across 2 days, both before and after stable grid firing emerged. We found that different cells display different patterns of development, and that increasing spatial stability of firing may be an important factor in grid cell development.

## METHODS

### IMPLANTATION OF EXTRACELLULAR RECORDING ELECTRODES IN MEDIAL ENTORHINAL CORTEX

The data used for analyses in this paper have previously been presented in Wills et al. (2010): detailed methods relating to extra-cellular recording of mEC cells in awake and behaving pre-weanling rats were described in that study. For methods relating to adult control data, see Barry et al. (2007). In summary, 28 male Lister Hooded rat pups, aged P14–P23 at the time of surgery, were chronically implanted with microdrives loaded with 4 tetrodes (HM-L coated 90% platinum-10% iridium 17 μm diameter wire). Microelectrodes were aimed at the mEC using co-ordinates 3.8 mm lateral to the midline and 0.2–0.3 mm anterior to the transverse sinus, with electrodes angled 9° tip anterior. After surgery rats were placed in a heated chamber until they had fully recovered from the gas anesthetic (1% isofluorane; 30 min recovery time), and were then returned to the dam and littermates. After completion of the experiments, rats were perfused transcardially with saline followed by 4% paraformaldehyde. Brains were sliced parasagitally into 30 μm thick sections and Nissl stained to aid visualization of the electrode track.

### SINGLE-UNIT RECORDING IN BEHAVING RATS

Rats were allowed a 1 day postoperative recovery, after which microelectrodes were advanced ventrally by 60–250 μm/day. When mEC cells were found, recording sessions began. Single unit data was acquired using the Axona DACQ system (Axona, UK). Two LEDs spaced 7 cm apart and placed in a fixed orientation with respect to the animal's head were used to track the position and directional heading of the animal. Isolation of single units from multi-unit data was performed manually on the basis of peak-to-trough amplitude. Cells were selected for further analysis if they had: (a) spike width >200 μs, (b) an overall mean rate less than 10 Hz, and (c) fired at least 100 spikes during the trial.

### BEHAVIORAL TESTING

Single-unit recording trials took place in a square-walled (62 cm sides, 50 cm high) light-gray wooden box, placed on a black platform, while the rat searched for drops of soya-based infant formula milk randomly scattered on the floor of the environment. The floor was not washed between trials. Trials were 15 min long. Distal visual cues were available in the form of the fixed apparatus of the laboratory. Rats were kept in a separate holding box (30 × 30 cm, 30 cm high walls) between recording trials (inter-trial intervals were 15 min). Cells were used for analysis if they were recorded in a trial where total path length exceeded 45 m, and the recording session involved at least two trials (to assess for reproducibility of firing).

### FIRING RATE MAPS

Firing rate maps were constructed by sorting position data into 2 × 2 cm bins. The binned position and spike data were then smoothed using the adaptive smoothing rule described in (Skaggs and McNaughton, 1998), where the smoothing radius for each bin was expanded until the amount of dwell time (in seconds) multiplied by square root of the number of spikes within the radius was greater than 200. Firing rates in each bin were then calculated by dividing the total number of action potentials during occupancy of the bin by the total duration of occupancy. The ten colors of the firing-rate maps were auto-scaled to represent 10% of the peak rate—red (top 10%) to dark blue (bottom 10%). Unvisited bins are shown in white.

### AUTO-CORRELOGRAMS AND GRIDNESS SCORE

Following Hafting et al. (2005), the spatial autocorrelogram of the firing rate map was calculated as:

$$r(\tau_x, \tau_y) = \frac{n\sum \lambda_1(x,y)\lambda_2(x-\tau_x, y-\tau_y) - \sum \lambda_1(x,y)\sum \lambda_2(x-\tau_x, y-\tau_y)}{\sqrt{n\sum \lambda_1(x,y)^2 - \left(\sum \lambda_1(x,y)\right)^2} \times \sqrt{n\sum \lambda_2(x-\tau_x, y-\tau_y)^2 - \left(\sum \lambda_2(x-\tau_x, y-\tau_y)\right)^2}}$$

where $r(\tau_x, \tau_y)$ is the autocorrelation between bins with spatial offset of $\tau_x$ and $\tau_y$. $\lambda_1(x, y)$ and $\lambda_2(x, y)$ are equivalent for an autocorrelation and indicate the mean firing rate in bin $(x, y)$ and $n$ is the number of bins over which the estimate was made. The six central peaks of the autocorrelogram were defined as the six local maxima, with $r > 0.3$, closest to (but excluding) the central peak. Gridness was calculated by defining a mask on the spatial autocorrelogram centered on the central peak, but excluding the peak itself ($r > 0.5$), bounded by a circle defined by the mean distance from the center of the six closest peaks, multiplied by 1.25. Gridness was then expressed as the lowest correlation obtained for rotations of 60° and 120°, versus the unrotated mask, minus the highest correlation obtained at 30°, 90°, or 150°. Grid cell wavelength was calculated as the mean distance from the central peak to the six surrounding peaks in the spatial autocorrelogram (expressed in cm). Grid field size (radius) was calculated as the square root of the area of the central peak of the autocorrelogram ($r > 0.5$) divided by π.

### CLASSIFICATION OF mEC CELLS AS GRID CELLS

Grid cells were identified by comparing gridness scores of mEC cells to a threshold value calculated as the 95 percentile value of the gridness scores of a shuffled data null population (for more details see Wills et al., 2010). For any single trial, randomized data was generated by shifting the whole spike train with respect to the position data by a random amount (>20 s). This process was repeated a sufficient number of times for there to be 20,000 shuffled rate maps for each age. The gridness thresholds obtained in this study were 0.36 for young rats, and 0.29 for adults. In order to reduce the influence of false positive grid classifications (expected as 5% of a total 727 cells = 36 cells in this study), data was only included in further analyses if at least one cell in the recording session was classified as a grid cell on more than one trial.

Cells shown in **Figure 5** were selected by the following criteria: (1) electrodes were not moved between Day N and Day N + 1; (2) clusters were identifiable between Day N and Day N + 1; (3) the waveform of the cell in question had not substantially changed; (4) the cell met the grid cell criterion (see above) on at least one trial on Day N + 1; (5) the cell's mean gridness increased between Day N and Day N + 1.

#### CROSS-CORRELOGRAMS AND GRID FIELD PHASE OFFSET

Cross-correlograms between two rate maps were calculated as for autocorrelograms, with the exception that $\lambda_1(x, y)$ and $\lambda_2(x, y)$ indicate the mean firing rate in bin $(x, y)$ in the two different rate maps. The phase offset of the grid fields was defined as the vector between the center of the cross-correlogram and the closest local maxima of the cross-correlogram ($r > 0.3$). Gridness was calculated from cross-correlograms (**Figure 1A**) or population vector cross-correlograms (**Figure 2D**) by offsetting the cross-correlogram such that the local maxima closest to the center is placed at the center of the cross-correlogram, and then calculating gridness as described above.

#### DIFFERENT ENVIRONMENT PROBE, PHASE OFFSET VARIABILITY, AND POPULATION VECTOR CROSS-CORRELOGRAMS

Young rats were exposed to a different environment which was in the same room as the standard testing environment, but completely enclosed within black curtains, such that there were no common visual cues. The second environment was a 62 × 62 cm square, with interior walls coated in brown masking tape. The floor was translucent Perspex overlaid on a black surface, which was washed before every trial. In all data shown, rats had been exposed at least three times to this environment. To test whether phase offsets were significantly clustered, we calculated the variability of a group of phase offsets, defined as the mean length of the vectors connecting the phase offset coordinates with the center-point of the group (mean $x$ and $y$ coordinate). To take account of the sixfold symmetry of the autocorrelogram, all phase offsets were first mapped onto the range 0–60°, by taking the remainder modulo 60 of the offset vector angle. The offset variabilities of the three ensembles in the environment A versus environment B condition (A–B) were compared to the offset variabilities for environment A versus a repeat trial of the same environment (A–A′). The A–B ensemble variabilities were then further compared to the variability between all cells (i.e., from across ensembles) in the A–B condition. Population vector cross-correlograms were calculated following Fyhn et al. (2007). Briefly, rate maps from simultaneously recorded cells were stacked into a three-dimensional matrix with the two spatial dimensions on the $x$ and $y$ axes and cell identity on the z axis. Each vector in the $z$-dimension of the matrix, therefore, described the set of firing rates from all simultaneously recorded cells in one trial, in one particular spatial 2 × 2 cm bin. The cross-correlation between two different trials was defined as the mean of all dot products between vectors from spatially corresponding bins in different trials (dot products were first normalized to vector length to yield a number between 0 and 1). Then, to compute a spatial cross-correlogram, one matrix was shifted in 2 cm steps in the $x$ and $y$ dimensions, to cover all possible offsets between the two matrices in $x$ and $y$, and the mean population vector cross-correlation at each offset was re-calculated. Cross-correlations at each offset were only used in the cross-correlogram if the number of overlapping bins at each offset was >50. To test for rotations of grid firing, one matrix was rotated in 3° increments and the cross-correlogram recalculated. The rotation yielding the maximum gridness score is shown in **Figure 2C** (rightmost column).

#### IDENTIFICATION OF CONJUNCTIVE CELLS

For all grid cells, directional data was sorted into 1° bins and smoothed with 14.5° boxcar window. Firing rate polar plots were computed by dividing the number of spikes that the cell fired when the animal was pointing its head in a specific direction by the time spent facing that direction. The Rayleigh vector was defined as the length of the mean resultant vector derived from the binned, smoothed directional rate map. Grid cells were classified as conjunctive cells if the length of the Rayleigh vector exceeded the threshold of the 95th percentile value of the Rayleigh vector lengths of a shuffled data null population (obtained similarly to gridness classification, see above). The resulting threshold values were 0.18 for young rats and 0.15 for adults. The stability of directional tuning was assessed by (1) correlating rate values of spatially corresponding bins from two consecutive trials, and (2) testing whether the inter-trial differences between preferred firing directions (defined as the circular means of the firing rate maps), significantly differed from 0°.

#### SPEED MODULALTION OF FIRING RATE AND INTRINSIC FREQUENCY

Position and spike data from trials in which grid cells were recorded were filtered by running speed into eight bins, using the following boundary values (in cm/s): 2.5, 3.5, 4.5, 5.5, 7, 8.5, 10, 12.5, 15, 20. Data in which running speed was less than 2.5 cm/s or greater than 20 cm/s were discarded. Each bin represented a 10 ± 1% percentile range of the entire speed data set. The mean rate for each speed bin was defined as the number of spikes divided by the dwell time in each speed bin. Linear regression was used to test for a significant relationship between speed and mean rate. Adult data was analyzed using both the same speed bins as above (**Figure 4G**) and a set of percentile-matched bins to account for greater running speed in adult rats (**Figure 4F**). The boundary values for these were (cm/s): 5, 7.54, 10.03, 12.44, 15.75, 18.87, 21.83, 26.37, 30.69, 39.12. To estimate the intrinsic frequency of the cell, data was filtered into slow (2.5–8 cm/s) or fast (8–20 cm/s) speed bins. The spike train autocorrelogram for each segment of data (with duration ≥ 0.5 s after filtering) was calculated, segments were then combined (weighted by the duration of the segment of data) and mean normalized. The power spectrum for the combined autocorrelogram was then obtained using the fast Fourier transform, smoothed (Gaussian kernel with standard deviation 0.375 Hz), and the intrinsic frequency was defined as the peak value in the 4–10 Hz band. The theta modulation of a cell was defined as the ratio between the mean power ±0.5 Hz from the intrinsic frequency peak, and the mean power of the remaining power spectrum between 2 and 125 Hz. Only cells with theta modulation >5 were used for analysis of intrinsic frequency modulation with speed.

## RESULTS

The data used for analyses in this paper have previously been presented in Wills et al. (2010). 727 mEC cells were recorded in rats aged between postnatal day 16 and 30 (P16–P30). Of these, 65 cells were classified as grid cells, which were recorded between the ages of P19 and P30 (see Methods for details).

### GRID CELL FIRING FIELDS ARE ADULT-LIKE FROM THEIR FIRST APPEARANCE IN DEVELOPMENT

In the adult rat, most grid cells in the same local patch of mEC share the same wavelength and orientation, but are offset in spatial phase (Hafting et al., 2005). The population of grid cells in a local patch of mEC, therefore, forms a coherent neural representation of space, in which the firing fields of a relatively small number of cells tessellate the whole surface of the environment. We have previously shown that in young rats, similarly to what observed in adults, the wavelength and orientation of simultaneously recorded grid cells are clustered together (**Figure 1A**; see also Wills et al., 2010 supporting figure 16). Here we also asked whether grid fields exhaustively tessellate the whole environment: if so, phase offset vectors should be evenly distributed between 0 (overlapping fields) and 50% of ensemble wavelength (maximum offset). This was found to be the case for all simultaneously recorded grid cell ensembles (P19–P30; **Figure 1B**; $\chi^2$ goodness-of-fit of uniform distribution: $\chi^2_{(11)} = 14.3$, $p = 0.21$), and also for those ensembles recorded at the earliest stages of grid development (P19–P22; **Figure 1C**; $\chi^2_{(11)} = 12.6$, $p = 0.32$). From this data we can infer that local groups of grid cells, as soon as they appear, form a coherent map covering the entire environment.

In adults, the size of individual grid firing fields is closely related to the spacing between fields (Hafting et al., 2005). We found that this was true also in young rats: there was a close correlation between the field size and the wavelength of the grid (**Figure 1D**; linear regression between wavelength and field size: $R^2 = 0.49$, $p < 0.001$). This was also true when just those grid cells from the youngest animals (P19–P22) were considered ($R^2 = 0.37$, $p < 0.001$). Are grid fields more diffuse in rat pups compared to adults? Field size as a proportion of wavelength was found to be slightly, but significantly larger than that in adults (**Figure 1E**; $t$-test P19–P30 versus adult: $t = 3.00$,

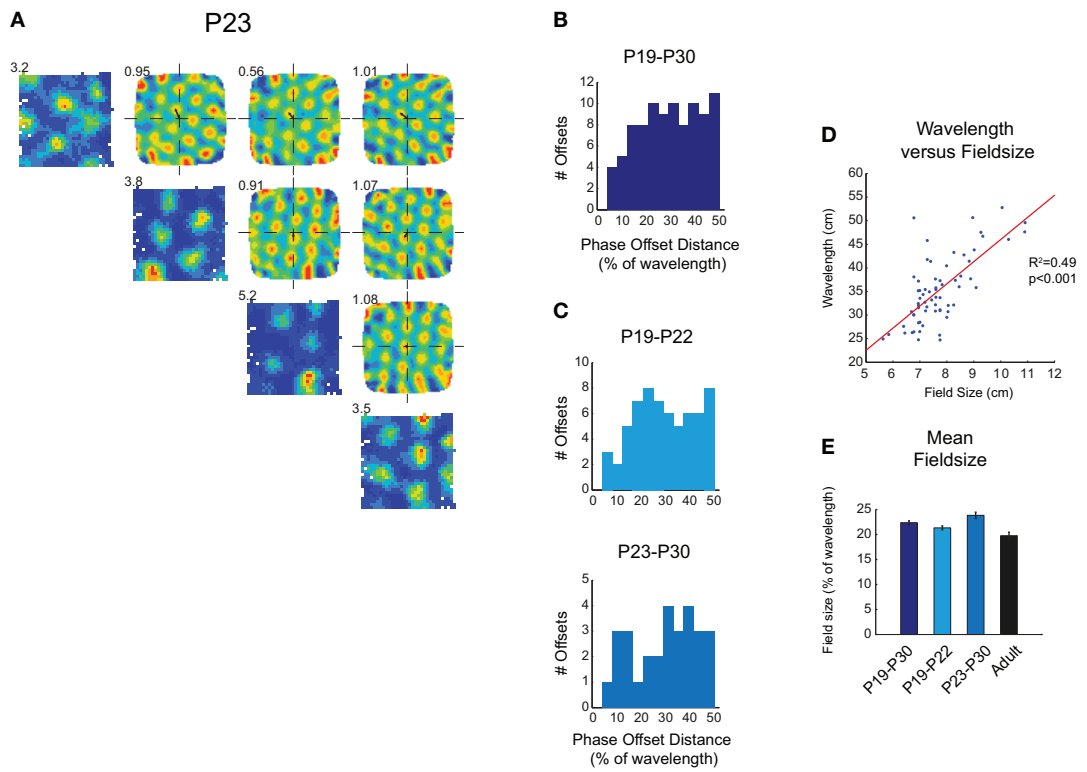


**FIGURE 1 | (A–C)** Simultaneously recorded grid fields in immature rats share the same wavelength and orientation, and tessellate to cover the whole environment surface. **(A)** Diagonal row shows firing rate maps for four grid cells simultaneously recorded at P23. Peak firing rate is shown at top left of map. Top-right quadrant of **(A)** shows spatial cross-correlograms which compare firing rate maps. These show clear hexagonal symmetry, demonstrating a repeating grid structure that is shared between different cells. The distance between the center of the cross-correlogram and the closest peak (small black arrow) represents the phase offset between different firing fields. Numbers on the top-left of cross correlograms show the gridness score calculated from the cross-correlogram. **(B)** Phase offsets for all simultaneously recorded grid cells from P19 to P30. Offsets are evenly distributed between 0% and 50% of grid wavelength **(C)** Phase offsets are equally distributed in both younger (light blue) and older (blue-gray) developing rats. **(D)** Scatter plot showing the wavelength for each grid cell (ages P19–P30) versus the field size. Red line shows significant linear regression between wavelength and field size, $R^2$ and $p$-values for regression are shown to left of plot. **(E)** Mean field size as a percentage of wavelength, ±SEM. Field size in pups is slightly larger than that in adults, but there is no trend for field size to decrease during the period P19–P30.

df = 282, $p = 0.003$), though there was no trend for field size to decrease between the ages of P19 and P30 (**Figure 1E**). The grid circuit in rat pups, therefore, has the same internal structure as that in the adult, although grid firing fields appear to be slightly more diffuse in young rats.

### THE GRID CELL MAP OF SPACE MAINTAINS ITS INTERNAL STRUCTURE IN DIFFERENT ENVIRONMENTS

If adult rats are exposed to different testing environments grid cell fields will rotate and shift their spatial phase. Simultaneously recorded local groups of cells will shift and rotate in unison, such that the internal structure of the grid cell map is maintained (Fyhn et al., 2007). We asked whether local groups of grids cells have the same fixed phase structure early in development. If the internal structure of the grid network is not fixed, cells could adopt different phase offsets when introduced into a different environment. **Figure 2A** shows firing fields for five simultaneously recorded cells from a 22-day-old animal introduced into two different testing environments (Env A and Env B). The spatial cross-correlograms for the Env A rate map versus the Env B rate map show that all cells share the same phase offset. **Figure 2B** similarly shows that phase offset vectors for all cells recorded from this animal are closely clustered together. To quantify whether phase offset vectors were significantly clustered for all simultaneously recorded cells, we tested whether the variability between phase offsets within ensembles increased when animals were placed in Env B (A-B condition, see Methods), and found no such effect (2-sample $t$-test: $t = -0.70$, df = 4, $p = 0.52$). Furthermore, the offset variability across ensembles (in the A–B condition) was significantly greater than that within ensembles (1-sample $t$-test: $t = -5.23$, df = 2, $p = 0.034$). To further quantify whether local groups of grid cells

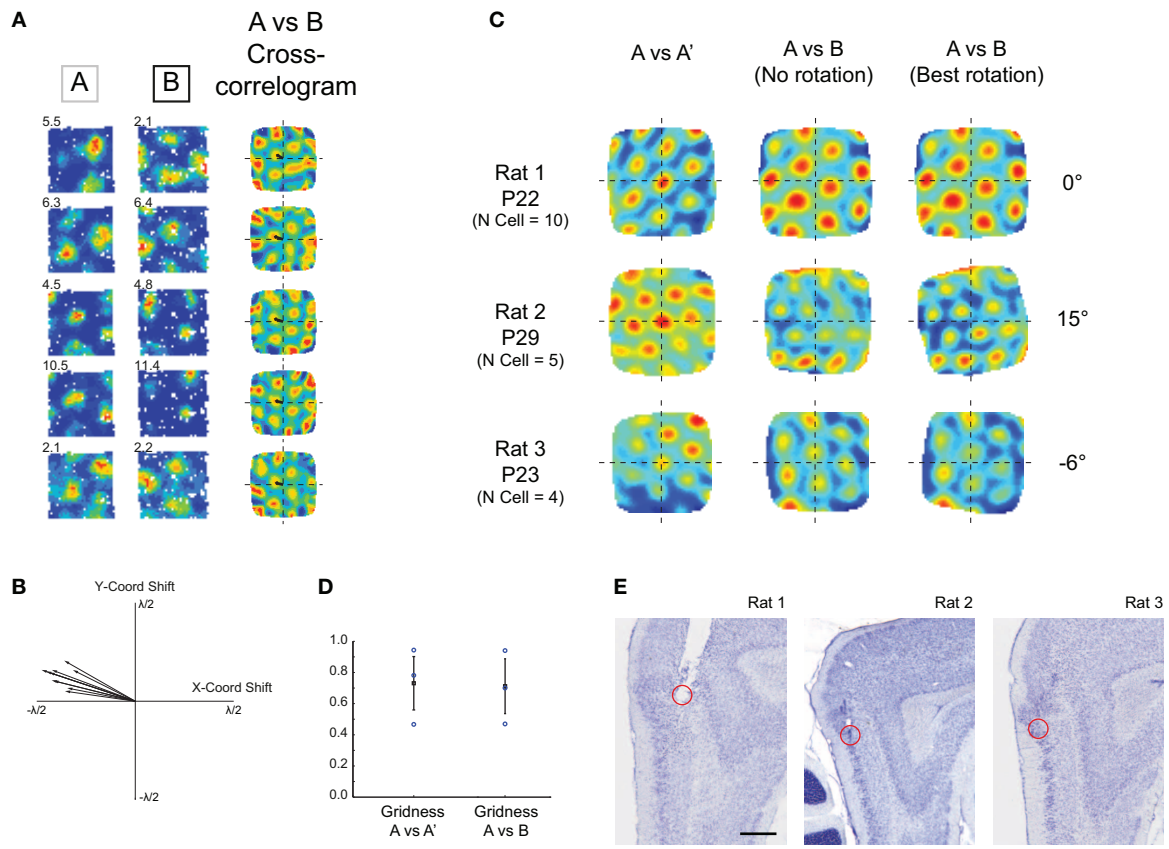


**FIGURE 2 | Grid cells simultaneously recorded in young rats maintain their relative spatial structure in different environments. (A)** Example cells recorded at P22 in two different environments. Left-hand column: rate map for cell in Env A, middle column: rate map for cell in Env B, right-hand column: cross-correlogram for Env A rate map vs. Env B rate map. Note that all cross-correlograms show the same hexagonal symmetry and the same phase offset (small black arrow), indicating that all cells have shifted their firing fields coherently between Env A and Env B. **(B)** Phase offset vectors for all grid cells recorded in experiment shown in **(A)** are clustered together. **(C)** Population vector cross-correlograms for three simultaneously recorded grid cell ensembles. Left-column: population vector cross-correlogram for two different trials in Env A. Hexagonal structure shows repeatable grid firing in two consecutive trials in the same environment. Middle column: population vector cross-correlogram for Env A versus Env B. Two ensembles (P29 and P23) show some degradation in the hexagonal symmetry. Right column: cross-correlogram after rotation of Env B rate maps. Hexagonal symmetry is restored in the P29 and P23 ensembles, demonstrating a coherent rotation of grid cell firing fields between Env A and Env B. **(D)** Gridness scores calculated from population vector cross-correlograms, for within-environment and across-environment comparisons. **(E)** Estimated recording locations for the three ensembles of simultaneously recorded cells. Ensembles from Rats 2 and 3 were most likely recorded from mEC LII, the ensemble from Rat 1 was most likely recorded from just below the mEC/Parasubiculum border zone. Scale bar = 0.5 mm.

maintain their fixed phase structure in different environments, we compared activity of the entire grid cell ensemble using population vector-based cross-correlograms (Fyhn et al., 2007; see Methods). **Figure 2C** (left-hand column) shows the population cross-correlogram comparing two different trials in Env A. The symmetrical hexagonal structure, with a strong peak in the center of the correlogram demonstrates stable, fixed grid cell activity upon exposure to the same environment during two temporally contiguous trials. When the Env A ensemble firing is compared to that of Env B (**Figure 2C** middle column), the cross-correlogram for Rat 1 shows an equally strong hexagonal symmetry, although offset in spatial phase, indicating a coherent shift in grid firing. Rat 2 and Rat 3 ensembles show some degradation of hexagonal symmetry when compared directly (**Figure 2C** middle column), but this degradation is rescued when Env B firing rate maps are rotated (all maps being rotated by the same angle), demonstrating that grid ensemble firing has coherently rotated and shifted between Env A and Env B. **Figure 2C** right-hand column shows the population cross-correlogram for the rotation that resulted in the highest gridness score for each rat. After rotation, there was no significant difference between the gridness scores calculated from the population cross-correlogram for the A–A′ condition and the A–B condition (**Figure 2D**, $t$-test: $t = 0.11$, $\mathrm{df} = 4$, $p = 0.91$). At the earliest stages of grid cell development, therefore, local groups of grid cells maintain a stable phase offset structure upon exposure to distinct environments.

## CONJUNCTIVE REPRESENTATION OF DISTANCE AND DIRECTION IN THE EARLIEST GRID CELLS

The entorhinal cortex encodes a combined representation of distance, direction and speed, which allows the computation of position based on heading direction and distance travelled (Sargolini et al., 2006). Previous work has shown that head direction cells recorded from both the mEC and the Presubiculum have adult-like properties very early on during postnatal development (P16; Langston et al., 2010; Wills et al., 2010). In adult rats, representations of direction and distance are encoded in single cells, the so called "conjunctive cells," found throughout the parahippocampal cortices (Sargolini et al., 2006). It is not known when conjunctive cells emerge during development. We analyzed our grid cell data set to look for directional tuning, quantified by the length of the mean resultant vector ("Rayleigh vector") of the directional firing rate map. **Figure 3A** shows three examples of conjunctive cells recorded from three different rats aged between P20 and P23. The preferred direction of the cells' firing is stable over two consecutive trials in the same environment. This was

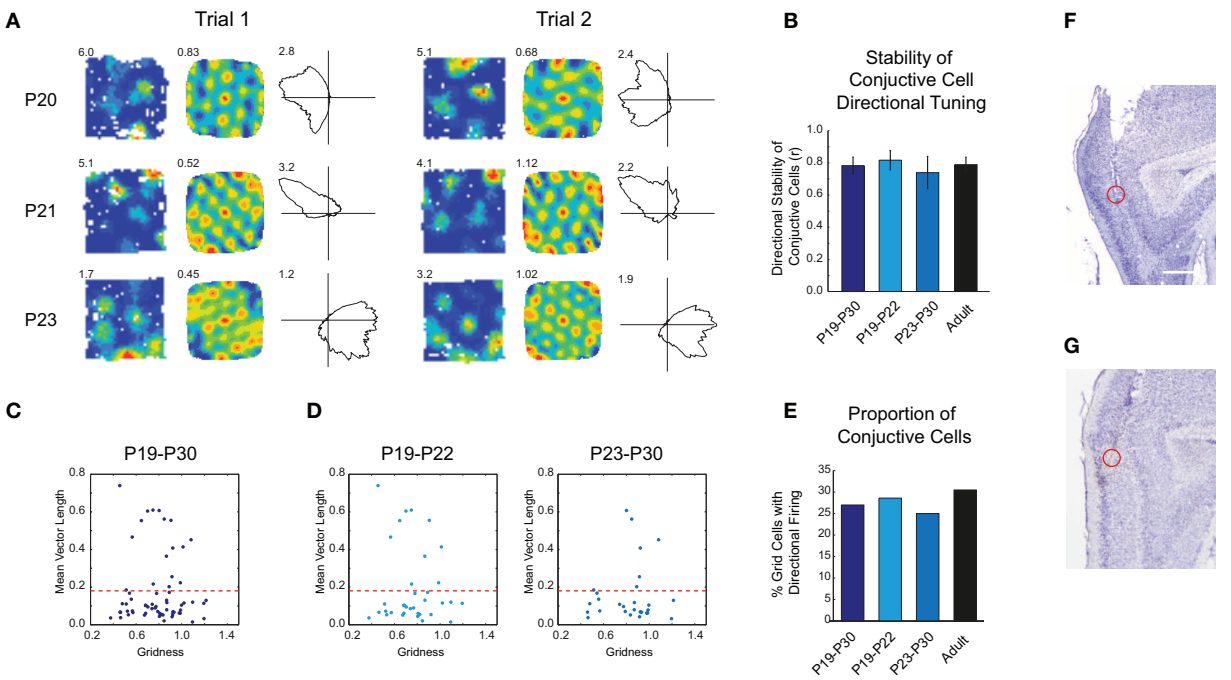


**FIGURE 3 | Conjunctive grid-head direction cells exist at the earliest stages of grid cell development. (A)** Three example of conjunctive cells recorded from three different rats at P20, P21, and P23, for two consecutive trials. For each trial, the left-hand column shows the firing rate map with peak firing rate, the middle column the auto-correlogram with the gridness score, and the right-hand column the directional firing rate map, with the peak directional firing rate. The directional firing correlate is stable between consecutive trials. **(B)** The mean stability of the directional correlate of conjunctive cells is at adult levels from the earliest emergence of conjunctive cell firing. Bar chart shows mean inter-trial stability of the directional component of conjunctive cell firing for different age groups, ±SEM. **(C)** Scatter plot showing gridness versus the mean vector length of the directional rate map. The red dashed line shows the threshold for classifying cells as directional, based on the 95th percentile of a shuffled data null distribution. **(D)** Distributions of gridness and mean vector lengths are similar for both young (P19–P22) and older developing rats (P23–P30) rats. **(E)** The proportions of grid cells classified as conjunctive do not significantly change during development. **(F,G)** Representative recording location for conjunctive cells, which were most likely recorded from mEC LIII. Scale bar = 0.5 mm.

assessed by computing the correlation between the two firing rate maps (**Figure 3B**; *t*-test young versus adult correlation: $t = 0.29$, $df = 22$, $p = 0.77$), and by calculating the inter-trial differences in the preferred firing directions: these were closely clustered around 0° (all young rats mean difference = 3°, 95% confidence interval ±8°; P19–P22 group mean difference = 1°, 95% confidence interval ±8.5°). **Figure 3C** shows the distribution of directionality versus gridness for all mEC cells that were classified as grid cells. All grid cells with a mean vector length greater than the 95th percentile of a null distribution from spatially shuffled data (red dashed line) were classified as conjunctive cells. Do conjunctive cells emerge abruptly and at the same time as grid cells, or is there an extended period during which they gradually emerge? When the data was split into two groups, P19–P22 and P23–P30, there were no significant differences in the proportions of grid cells with directional correlates across these age groups, and compared to adults (**Figures 3D,E**; $\chi^2 = 0.44$, $df = 2$, $p = 0.80$). The combined representation of distance and direction in single mEC cells is, therefore, present from the earliest ages at which grid cells emerge.

## GRID CELLS IN IMMATURE RATS SHOW RATE MODULATION BY RUNNING SPEED

Is grid cell firing in young rats also affected by the running speed of the animal? To test how many grid cells showed modulation of firing rate by running speed in young rats, we calculated the overall mean firing rates at different running speeds for each cell. No attempt was made to separate within-field from out-of-field firing. After finding the mean firing rate for each of the seven speed bins (see Methods for details), we tested whether there was a significant linear correlation between firing rate and running speed. In 70% of grid cells recorded from young rats (44/63), we found a significant rate-speed relationship. Four examples are shown in **Figures 4A–C**. In each case, when rate maps are constructed from data filtered for fast running speeds, grid field firing rates are higher than when rate maps are constructed from data filtered for low running speeds (**Figure 4B**). The increase in mean rate (combined in- and out- of field firing rate) with speed for these cells can be seen in **Figure 4C**. Note that both the slope and the intercept of the relationship between rate and speed differ between cells, but the large majority increase rate with speed: the distributions of slope and intercept values for all cells are shown in **Figure 4D**. Between the ages of P19–P22 and P23–P30, there is a trend for both slope and intercept to decrease, though these trends reach significance only for intercepts (**Figure 4E**, *t*-test slopes: $t = 1.42$, $df = 42$, $p = 0.16$; intercepts: $t = 2.23$, $df = 42$, $p = 0.03$).

How similar is the speed modulation of immature rat grid cells to that seen in adults? When adult cells are tested using a set of speed bins scaled to match faster running speeds in adults (5–39 cm/s, see Methods), 42% of adult cells (85/208) had a significant linear relationship between firing rate and running speed. **Figure 4E** shows the distributions of slope and intercept values for these 85 cells. Although there was no difference between immature and adult intercepts ($t = 0.39$, $df = 127$, $p = 0.69$), adult slope values are significantly lower than those in immature rats (Adult mean = 0.0162, Immature mean = 0.0284; $t = 4.90$, $df = 127$, $p < 0.001$). Does this difference truly reflect a greater degree of speed modulation in young rat firing rates, or does it instead reflect the different speed ranges covered by adults and immature rats? To check this, we re-ran the analysis on the adult data, this time using the same absolute values of speed bin as for immature rats (2.5–20 cm/s). Using these speeds, fewer cells showed significant modulation (50/208), but those that were modulated had slope values similar to those seen in young rats (Adult mean slope = 0.0263; adult versus immature *t*-test: $t = 0.23$, $df = 92$, $p = 0.81$). Over the range of speeds covered by immature rats, therefore, the percentage of adult cells modulated by speed is considerably lower, but the degree of speed modulation of firing rate in those cells appears to be similar.

Oscillatory interference models of grid cell firing predict that the frequency of intrinsic oscillation should increase with running speed (Burgess et al., 2007). Does the modulation of rate by speed reflect an increase in the intrinsic frequency of grid cells with faster running speed? We calculated an estimate of intrinsic frequency from the spike train autocorrelogram of grid cells (see Methods), for both slow (2.5–8 cm/s) and fast (8–20 cm/s) runs. Intrinsic frequency increases with running speed in young rats (**Figure 4H**, *t*-test slow versus fast: $t = 2.71$, $df = 44$, $p = 0.009$). This pattern holds true also for the younger and older groups of rats (**Figure 4H**, middle and right). At the earliest ages at which grid cells appear, therefore, the grid cell network also contains an adult-like representation of the speed of the animal.

## THE EMERGENCE OF GRID FIRING IN INDIVIDUAL mEC CELLS

From the data presented so far it appears that the grid cells recorded from immature rats are adult-like as soon as they appear. The abrupt emergence of adult-like grid cell firing at around P19 poses an experimental conundrum: how is one to study the development of grid cells if, upon their first emergence, they appear to be mature in most respects? In other words, in the absence of a reliable physiological identifier (as in the case of CA1 pyramidal cells), how are we to know what is the activity of nascent grid cells, if they are fully developed as soon as they can be detected? To begin to answer this question, we looked at whether we could track the same cell across different days. Electrodes were moved after most recording sessions, and this, combined with the natural growth of the brain, meant that stably tracked cells were rarely found. However, we have identified six grid cells from our dataset which we can track across 2 days on the basis of their extracellular waveform characteristics. Crucially we recorded these cells on the day *before* they exhibited a recognizable grid firing pattern. In all six cells, the mean gridness score increased between the first day ("Day N") and second day ("Day N + 1") of recording. **Figures 5A,B** show these six cells, recorded on two consecutive trials on the first (A), and the second day of recording (B). The ages at which grid firing first emerged in these cells ranged from P20 to P24. Cells 1 and 2 show multiple, discrete firing fields on Day N (P19), though these are not arranged hexagonally, and show a degree of instability between trials. On Day N + 1, their firing fields become more stable, and hexagonally arranged. Cells 3–5, by contrast, show more diffuse firing patterns on Day N, which "sharpens up," on Day N + 1, increasing their in- to out-of field firing ratio. However, some hexagonal symmetry can also

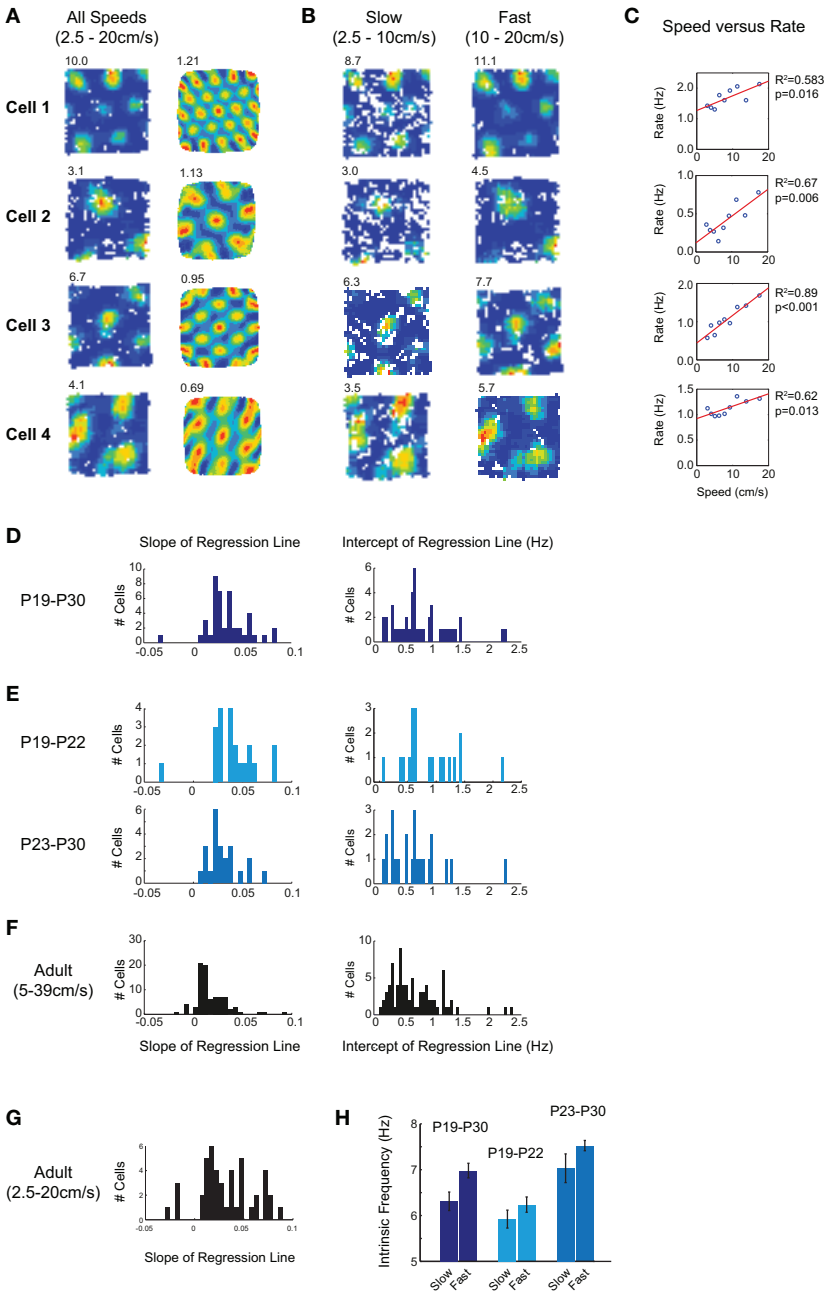


**FIGURE 4 | Grid cell firing rate in young rats is modulated by running speed. (A)** Firing rate maps and autocorrelograms for four grid cells. Peak firing rate is top left of rate map, gridness score is top left of autocorrelogram. Firing rate maps are constructed from data in which the running speed was 2.5–20 cm/s. **(B)** Firing rate maps for the same four cells, with data filtered by either slow (2.5–10 cm/s; left column) or fast (10–20 cm/s; right column) running speeds. The grid firing field is preserved at both fast and slow speeds, but firing rates increase with running speed. **(C)** Scatter plots of mean firing rate versus running speed for the same four grid cells. The mean rates shown include both in- and out- of field firing. The red lines show linear regression fits to the speed versus firing rate data: $R^2$ and $p$ values for these fits are shown to the right of the plots. **(D)** Distribution of regression line slopes and intercepts for all grid cells with a significant linear fit between speed and firing rate. Most cells increase firing rate with running speed, and all intercept values are positive. **(E)** Distribution of regression line slopes for younger (P19–P22; top) and older (P23–P30; bottom) developing rats. Grid cells are speed modulated when they first emerge during development, though the slope and the intercept of the regression line tends to decrease with age. **(F,G)** Speed modulation of grid cell firing in adults. **(F)** When regression lines are fitted over a range of speeds scaled to reflect the faster running of adults, regression slopes are significantly lower than those seen in young rats. **(G)** When the same absolute speed range as for young rats is used, fewer grid cells show a significant speed modulation, but those which do show similar slope values to those seen in young rats. **(H)** Intrinsic frequency of grid cell firing increases with running speed. Bars show mean intrinsic frequency of theta-modulated grid cells, ±SEM. "Slow" bars show data where speed lies between 2.5 and 8 cm/s, "Fast" bars from 8 and 20 cm/s. Dark blue shows all young rats, light blue P19–P22, and gray P23–P30.

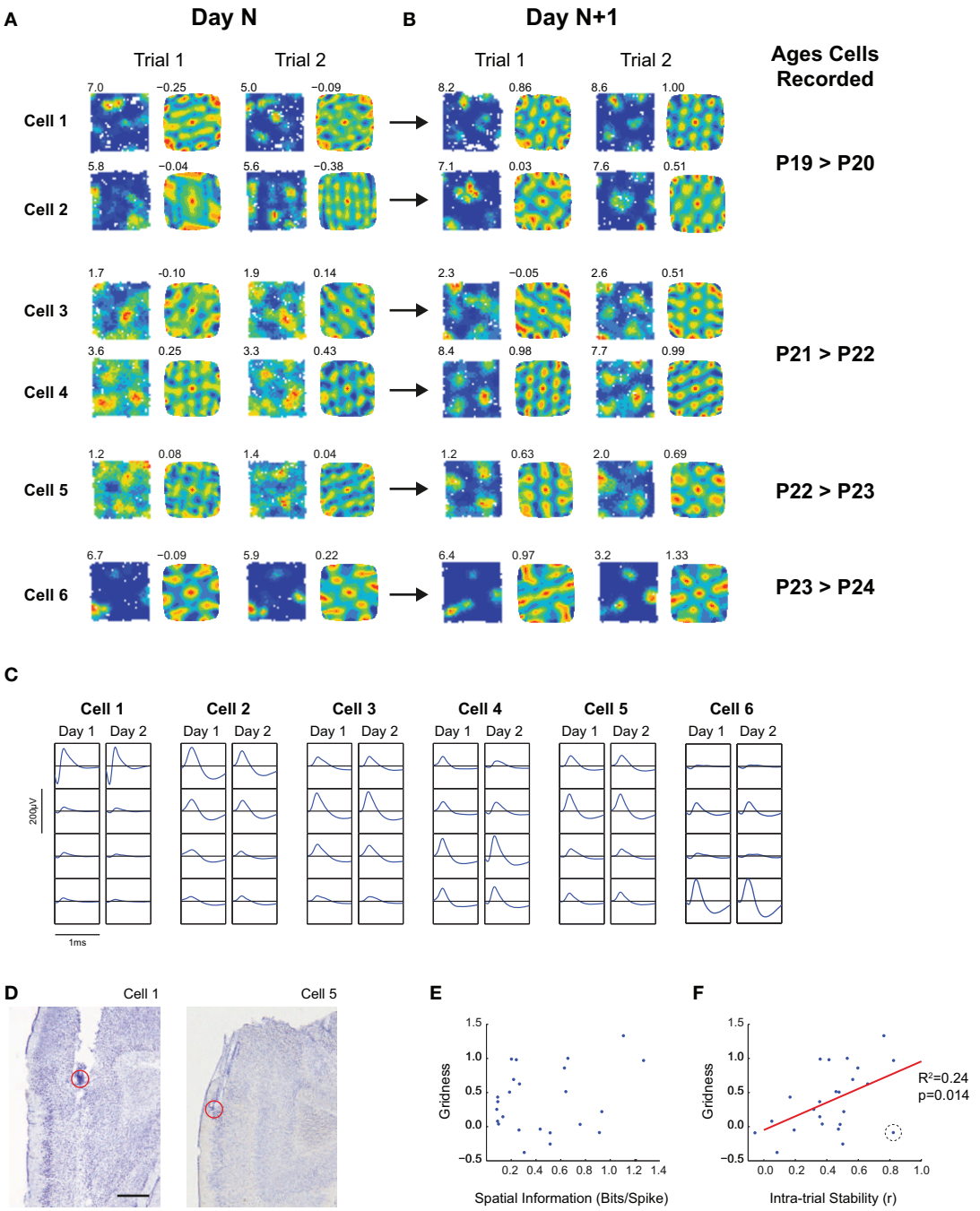


**FIGURE 5 | The development of grid firing in individual mEC cells. (A,B)** Firing rate maps and autocorrelograms for six mEC cells which were tracked for more than 1 day, and which developed stable grid cell firing patterns on the second day of recording. Text top left of firing rate maps shows peak firing, top-left of autocorrelogram shows gridness score for the trial. **(A)** shows two consecutive trials on the first day for which the cell was recorded ("Day N"), **(B)** shows two consecutive trials for the second day of recording ("Day N + 1"). The ages, in postnatal days, corresponding to Day N and Day N + 1 are shown to the right of **(B)**. **(C)** Extracellular waveforms for the six mEC cells shown in **(A,B)**. Each column shows the waveforms on the four wires of the tetrode on which the cell was recorded. For each cell, the left column shows the waveform for the last recording trial of Day N, the right column shows the recording trial of Day N + 1 with the highest gridness score. The vertical and horizontal scale bars (200 μV and 1 ms, respectively) apply to all waveform plots. **(D)** Estimated recording locations for cells shown in **(A)** for which recording locations are not shown elsewhere in the paper. For the recording location of Cell 2, see **Figure 3G**; for Cell 3–4, see **Figure 2E**, "Rat 1"; and for Cell 6 see **Figure 3F**. Scale bar = 0.5 mm. **(E,F)** Scatter plots of Spatial Information **(E)** and Intra-trial stability **(F)** against Gridness. Each point represents a trial on Day N or Day N + 1 [i.e., all trials shown in **(A)**]. There is a significant relationship between Gridness and Intra-trial Stability ($R^2$ and $p$ value for linear regression shown to right of plot), but not for Gridness and Spatial Information. The data point in **(F)** highlighted by a black dashed circle, which has a high stability but low gridness, corresponds to Cell 6, Trial 1 on P23 (see text for details).

be observed on Day N, despite the diffuse firing. Cell 6 seems to be different again: sharply peaked firing fields with hexagonal symmetry are already present on the first day. However, time is needed for the south-western field to detach itself from the wall, such that a precise equilateral triangle, consistent with grid cell firing, is formed.

Is it possible to make any generalizations about the mechanisms of grid cell development based on these 6 examples? We looked at the development of two fundamental properties of spatial firing: spatial specificity (measured by spatial information) and spatial stability (measured as the correlation between firing in the first and second halves of each trial), and tested for correlations between these two measures and gridness on a trial-by-trial basis (**Figures 5E,F**). We found a significant relationship between stability and gridness (linear regression; $R^2 = 0.24$, $p = 0.014$), but no significant relationship between spatial information and gridness ($R^2 = 0.06$, $p = 0.21$). **Figure 5F** shows one outlier with high stability but low gridness (circled in black), and removing this point strengthens the relationship between stability and gridness ($R^2 = 0.40$, $p = 0.001$). This data point corresponds to Cell 6 Trial 1 on Day N: in this case, the environment wall may have stabilized the firing field, despite grid firing had not yet fully developed. The increases in gridness and stability likely reflected developmental processes rather than increased familiarity with the environment: there was no significant relationship between either of these measures and the total number of exposures to the environment (Gridness: linear regression, $R^2 < 0.001$, $p = 0.98$; Stability: linear regression, $R^2 = 0.03$, $p = 0.39$). On the basis of this limited dataset, therefore, we can conclude that there may be different patterns of maturation for different grid cells, but that increasing spatial stability of firing may be an important factor in grid cell development.

This data can also tell us about the time course of grid cell development in individual cells. In several cells, a rudimentary hexagonal symmetry is present on the day preceding mature grid firing, suggesting that, at the single cell level, the transition from rudimentary to fully mature grid cell firing takes place over the time course of approximately 24 h.

## DISCUSSION

In this study, we have attempted to provide a full characterization of the emergence of grid cell firing during rat post-natal development. We have shown that grid cells first emerge around 3 weeks of age, and that the development of their functional properties occurs rapidly. Indeed, as soon as grid cells can be detected, they possess almost all of the properties that characterize adult grid cell firing. Grid fields in immature rats evenly cover the whole explored environment, exhaustively mapping it (c.f. Hafting et al., 2005 for adult grid cells). These neural maps appear to be universal even in young rats: different grid cells maintain their phase offsets in different environments, even though absolute firing field positions shift and rotate (c.f. Fyhn et al., 2007), similarly to the rigid relationships seen in simultaneously recorded head direction cells (Taube et al., 1990). Conjunctive representations of place and direction co-exist in grid cells in immature rats, and these grid cells are also modulated by the running speed of the animal (c.f. Sargolini et al., 2006). The emergence of stable, adult-like grid firing fields appears to be relatively abrupt, occurring around the beginning of the fourth week of life in the rat (see also Wills et al., 2010). Individual grid cells may mature over the course of approximately 1 day, though we cannot rule out that the time needed for the maturation of the whole mEC grid cell network is longer than this. Although early grid cells share most of the properties of their adult counterparts, it should be noted that some properties of the grid cell network at P19–P30 differ from those of adults. For example, the proportion of grid cells with a significant speed modulation is higher in pups, and the overall proportion of grid cells in the mEC is slightly lower in pups than in adults (see Wills et al., 2010).

One other previous study has characterized the timeline of grid cell development in the hippocampal formation (Langston et al., 2010). In agreement with Wills et al. (2010), grid cells were also found to be the slowest to develop with respect to head direction and place cells, with no adult-like grids seen until P19 at the earliest. Langston et al also reported an abrupt change to adult-like values for the proportion of grid cells, the levels of mean gridness and the grid spatial stability (though this occurred somewhat later than observed in our data, at around P28). However, consistent with what we report here and in Wills et al. (2010), Langston et al. show clear examples of adult like grid cells at P19 and P23. Furthermore, the abrupt appearance, at P22, of sub-threshold membrane synchrony in mEC stellate cells reported by Langston et al. (2010) is suggestive of a sudden maturational step occurring in mEC circuits around this age.

We have also presented data tracking the patterns of development in individual nascent grid cells. Grid cells represent a sub-set of all spatially modulated responses reported in the adult mEC (Fyhn et al., 2004; Sargolini et al., 2006), and there is no extracellular physiological signature unique to grid cells. Tracking the development of individual cells is, therefore, the only way to investigate the developmental stages leading up to the expression of grid cell firing using our current technology. In the data presented, cells showed diverse patterns of development, suggesting more than one mechanism for grid cell development. Despite the differences between cells, one common theme was that grid cell firing correlated with increased spatial stability. Although grid firing clearly could not occur in the complete absence of stability, it is noteworthy that stability is correlated with the development of gridness, whereas the spatial information conveyed by the cells' firing is not, and furthermore, that spatial stability does occur in the absence of grid firing. Increasing spatial stability in mEC could be due to increasing quality of the sensory information available to the mEC, for example through developmental of the visual or vestibular systems (Lannou et al., 1979; Fagiolini et al., 1994), or an increase in the spatial stability of the place signaling feeding into the mEC. Further technological developments will be required in order to track the development of larger numbers of cells through optogenetic and/or *in vivo* imaging means (Dombeck et al., 2010; Osakada et al., 2011).

Can the developmental programme of grid cells inform us about mechanisms of grid cell firing in adults? More specifically, is the pattern of grid cell development shown here consistent with the two major classes of theories seeking to explain grid cell firing

(the attractor network and oscillatory interference models)? The early emergence of a universal fixed phase relationship between grid cells is consistent with the early development of recurrent connections between cells of similar phases, as required by continuous attractor models (Fuhs and Touretzky, 2006; McNaughton et al., 2006; Burak and Fiete, 2009), whilst not being predicted by oscillatory interference models. The development of subthreshold membrane synchrony across stellate cells at P22 (Langston et al., 2010) also suggests that recurrent connectivity is set up in the mEC around this age, though whether such recurrent connections are direct or indirect remains an open question (Dhillon and Jones, 2000; Quilichini et al., 2010). Tracking the anatomical development of intra-mEC connectivity, ideally in combination with the functional correlates of the cells (Ko et al., 2011), would be necessary to fully understand the role of recurrent connectivity in grid cell development. The presence of head direction- and speed-modulation of grid firing at the earliest stages of development is also consistent with attractor network models, according to which these cells' function is to shift the network activity "bump" depending on the animals' velocity (Fuhs and Touretzky, 2006; McNaughton et al., 2006; Burak and Fiete, 2009; Navratilova et al., 2011).

In this and other studies (Wills et al., 2010) we have also tested whether the temporal dynamics of grid cells during early development are consistent with the oscillatory interference class of models. We have previously shown that grid cell firing is temporally modulated at a frequency slightly higher than the theta-band LFP at all stages of development (Wills et al., 2010; as predicted in Burgess et al., 2007; Giocomo et al., 2007). In the present study, we have also shown that the intrinsic frequency of grid cells in young rats increases with running speed at all ages, consistent with a central concept of oscillatory inference models, that a velocity-modulated oscillator is used to integrate displacement over time (Burgess et al., 2007; Hasselmo et al., 2007; Blair et al., 2008; Burgess, 2008). Also consistent with oscillatory inference models is the finding that theta-band sub-threshold oscillations in mEC stellate cells, proposed to be one of the two oscillatory components (Burgess et al., 2007; Giocomo et al., 2007), emerge shortly before grid cells, at P18 (Burton et al., 2008). One outstanding question for both types of model is the nature of the velocity signal which grid cells use to track distance. This question is particularly pertinent to weanling rats, in which body size, and associated motor and proprioceptive systems, are scaled down by a factor of approximately 3, but grid field spacing is only 20–25% less than the smallest grids seen in adults (Hafting et al., 2005; Wills et al., 2010).

Do our results support any of the theories proposed for the mechanisms of grid cell development? McNaughton et al. (2006) suggested that patterns of recurrent connectivity in the mEC could be created by waves of spontaneous cortical activity in the first 2 weeks of life. The resulting network would be topographically arranged (with cells anatomically proximal sharing similar spatial phases, in contrast to what is seen in mEC grid cells), and would act as a teaching network for mEC grid cells. The later emergence of grid cell firing at 3 weeks of age (Langston et al., 2010; Wills et al., 2010) argues against this model (for further objections, see Welinder et al., 2008), though it remains possible that the correct internal mEC connectivity pre-exists the emergence of stable grid cell firing, and that the critical developmental step is the stabilization of grid fields through the maturation of afferent projections conveying speed, visual or other sensory information. Welinder et al. (2008; see also Widloski and Fiete, 2010) proposed that patterns of recurrent activity needed for an attractor network could be achieved through a self-organizing process, in which velocity signals signifying speed and direction, and local position cues from place cells, set up mEC network connectivity using a combination of symmetric and asymmetric spike-timing dependent plasticity rules. An experience-dependent learning process is consistent with the emergence of grid cells after a period of exploratory behavior (Langston et al., 2010; Wills et al., 2010), but further work is needed to fully test this hypothesis. Finally, it has been pointed out that the 60° symmetry of grid cells could be achieved through a self-organizing integration of one-dimensional band-like firing patterns (Mhatre et al., 2010; see also Burgess et al., 2007), though whether such one-dimensional bands are observed in immature mEC firing will require further investigation (see also Krupic et al., 2011).

Can studying the development of spatially responsive cells in the hippocampal formation help to explain the ontogeny of spatial learning and exploratory behavior? Various lines of evidence suggest that the ability to construct and use a cognitive map of the environment (Tolman, 1948; O'Keefe and Nadel, 1978) emerges around 3 weeks of age. Young rats will learn to find a hidden platform in a water maze using only distal cues ("place learning") at P20–P21 (Schenk, 1985; Rudy et al., 1987; Brown and Whishaw, 2000; Akers et al., 2007). Learning the position of a platform marked by a proximal visual cue precedes place learning by 1 or 2 days (Rudy et al., 1987; Akers et al., 2007; although see Brown and Whishaw, 2000), suggesting that the physical demands of the task are not the limiting step delaying the emergence of place learning. Likewise, rats will learn a delayed alternation T-maze task at P21, but not at P15 (Green and Stanton, 1989), and spontaneous alternation in the T-maze appears around P25 (Kirkby, 1967). Young rats also show an abrupt increase in the tendency to explore the environment away from the "huddle" of their littermates on P20, and furthermore, have the ability to "home" directly back to their littermates after exploration, suggesting that path integration is already in place at this age (Loewen et al., 2005). Interestingly, there is evidence that spatial competence emerges abruptly in individual animals (Kirkby, 1967; Nadel, 1990), mirroring the abrupt emergence of adult like grid cells described here.

Convergent evidence, therefore, points to the appearance of place learning and exploration at around P20, coinciding with the sudden development of grid cell firing in our data. By contrast, the gradual developmental trajectory of CA1 place cells is not marked by any corresponding step change at this age. This suggests that the functional maturation of the mEC at this age is a critical factor for the expression of spatial behavior. However, it should also be noted that, despite the first evidence for spatial learning appearing at around 3 weeks, levels of performance on several spatial tasks do not reach adult levels until much later (Schenk, 1985; Rossier and Schenk, 2003) consistent with the protracted development of hippocampal CA1 spatial responses

(Scott et al., 2010). It is, therefore, plausible that the full complement of spatial cognitive ability requires both mEC and hippocampus proper networks to be fully mature. Furthermore, if spatial stability is key for grid cell development, then it may be that an increasingly stable spatial signal originating in CA1 represents the critical developmental ingredient needed in order to set up spatially stable grid cell firing (Burgess et al., 2007; Hasselmo, 2008). More experimental effort will be needed to address these questions.

## ACKNOWLEDGMENTS

We would like to acknowledge the following funding: The Royal Society (Fellowship to Thomas J. Wills), Research Councils UK (Fellowship to Francesca Cacucci), EU FP7 ("SPACEBRAIN" grant), an ERC fellowship ("DEVSPACE"; to Francesca Cacucci), the BBSRC. Caswell Barry and Thomas J. Wills were additionally supported by the Wellcome Trust. We also thank John O'Keefe and Neil Burgess for helpful discussions regarding the manuscript.

## REFERENCES

Akers, K. G., Candelaria, F. T., and Hamilton, D. A. (2007). Preweanling rats solve the Morris water task via directional navigation. *Behav. Neurosci.* 121, 1426–1430.

Barry, C., Hayman, R., Burgess, N., and Jeffery, K. J. (2007). Experience-dependent rescaling of entorhinal grids. *Nat. Neurosci.* 10, 682–684.

Blair, H. T., Gupta, K., and Zhang, K. (2008). Conversion of a phase- to a rate-coded position signal by a three-stage model of theta cells, grid cells, and place cells. *Hippocampus* 18, 1239–1255.

Brown, R. W., and Whishaw, I. Q. (2000). Similarities in the development of place and cue navigation by rats in a swimming pool. *Dev. Psychobiol.* 37, 238–245.

Burak, Y., and Fiete, I. R. (2009). Accurate path integration in continuous attractor network models of grid cells. *PLoS Comput. Biol.* 5:e1000291. doi: 10.1371/journal.pcbi.1000291

Burgess, N. (2008). Grid cells and theta as oscillatory interference: theory and predictions. *Hippocampus* 18, 1157–1174.

Burgess, N., Barry, C., and O'Keefe, J. (2007). An oscillatory interference model of grid cell firing. *Hippocampus* 17, 801–812.

Burton, B. G., Economo, M. N., Lee, G. J., and White, J. A. (2008). Development of theta rhythmicity in entorhinal stellate cells of the juvenile rat. *J. Neurophysiol.* 100, 3144–3157.

Dhillon, A., and Jones, R. S. (2000). Laminar differences in recurrent excitatory transmission in the rat entorhinal cortex *in vitro*. *Neuroscience* 99, 413–422.

Dombeck, D. A., Harvey, C. D., Tian, L., Looger, L. L., and Tank, D. W. (2010). Functional imaging of hippocampal place cells at cellular resolution during virtual navigation. *Nat. Neurosci.* 13, 1433–1440.

Fagiolini, M., Pizzorusso, T., Berardi, N., Domenici, L., and Maffei, L. (1994). Functional postnatal development of the rat primary visual cortex and the role of visual experience: dark rearing and monocular deprivation. *Vision Res.* 34, 709–720.

Fuhs, M. C., and Touretzky, D. S. (2006). A spin glass model of path integration in rat medial entorhinal cortex. *J. Neurosci.* 26, 4266–4276.

Fyhn, M., Hafting, T., Treves, A., Moser, M. B., and Moser, E. I. (2007). Hippocampal remapping and grid realignment in entorhinal cortex. *Nature* 446, 190–194.

Fyhn, M., Molden, S., Witter, M. P., Moser, E. I., and Moser, M. B. (2004). Spatial representation in the entorhinal cortex. *Science* 305, 1245–1246.

Gerrish, C. J., and Alberts, J. R. (1996). Environmental temperature modulates onset of independent feeding: warmer is sooner. *Dev. Psychobiol.* 29, 483–495.

Giocomo, L. M., Zilli, E. A., Fransen, E., and Hasselmo, M. E. (2007). Temporal frequency of subthreshold oscillations scales with entorhinal grid cell field spacing. *Science* 315, 1719–1722.

Green, R. J., and Stanton, M. E. (1989). Differential ontogeny of working memory and reference memory in the rat. *Behav. Neurosci.* 103, 98–105.

Hafting, T., Fyhn, M., Molden, S., Moser, M. B., and Moser, E. I. (2005). Microstructure of a spatial map in the entorhinal cortex. *Nature* 436, 801–806.

Hasselmo, M. E. (2008). Grid cell mechanisms and function: contributions of entorhinal persistent spiking and phase resetting. *Hippocampus* 18, 1213–1229.

Hasselmo, M. E., Giocomo, L. M., and Zilli, E. A. (2007). Grid cell firing may arise from interference of theta frequency membrane potential oscillations in single neurons. *Hippocampus* 17, 1252–1271.

Kirkby, R. J. (1967). A maturation factor in spontaneous alteration. *Nature* 215, 784.

Ko, H., Hofer, S. B., Pichler, B., Buchanan, K. A., Sjostrom, P. J., and Mrsic-Flogel, T. D. (2011). Functional specificity of local synaptic connections in neocortical networks. *Nature* 473, 87–91.

Krupic, J., Burgess, N., and O'Keefe, J. (2011). Periodic bands are the building blocks of locational firing in the Parahippocampal Formation. *Soc. Neurosci. Abstr.* 729.13.

Langston, R. F., Ainge, J. A., Couey, J. J., Canto, C. B., Bjerknes, T. L., Witter, M. P., Moser, E. I., and Moser, M. B. (2010). Development of the spatial representation system in the rat. *Science* 328, 1576–1580.

Lannou, J., Precht, W., and Cazin, L. (1979). The postnatal development of functional properties of central vestibular neurons in the rat. *Brain Res.* 175, 219–232.

Loewen, I., Wallace, D. G., and Whishaw, I. Q. (2005). The development of spatial capacity in piloting and dead reckoning by infant rats: use of the huddle as a home base for spatial navigation. *Dev. Psychobiol.* 46, 350–361.

McNaughton, B. L., Battaglia, F. P., Jensen, O., Moser, E. I., and Moser, M. B. (2006). Path integration and the neural basis of the 'cognitive map'. *Nat. Rev. Neurosci.* 7, 663–678.

Mhatre, H., Gorchetchnikov, A., and Grossberg, S. (2010). Grid cell hexagonal patterns formed by fast self-organized learning within entorhinal cortex. *Hippocampus* 22, 320–334.

Nadel, L. (1990). Varieties of spatial cognition. Psychobiological considerations. *Ann. N.Y. Acad. Sci.* 608, 613–626.

Navratilova, Z., Giocomo, L. M., Fellous, J. M., Hasselmo, M. E., and McNaughton, B. L. (2011). Phase precession and variable spatial scaling in a periodic attractor map model of medial entorhinal grid cells with realistic after-spike dynamics. *Hippocampus* 22, 772–789.

O'Keefe, J., and Nadel, L. (1978). *The Hippocampus as a Cognitive Map*. Oxford, UK: Oxford University Press.

Osakada, F., Mori, T., Cetin, A. H., Marshel, J. H., Virgen, B., and Callaway, E. M. (2011). New rabies virus variants for monitoring and manipulating activity and gene expression in defined neural circuits. *Neuron* 71, 617–631.

Quilichini, P., Sirota, A., and Buzsaki, G. (2010). Intrinsic circuit organization and theta-gamma oscillation dynamics in the entorhinal cortex of the rat. *J. Neurosci.* 30, 11128–11142.

Rossier, J., and Schenk, F. (2003). Olfactory and/or visual cues for spatial navigation through ontogeny: olfactory cues enable the use of visual cues. *Behav. Neurosci.* 117, 412–425.

Rudy, J. W., Stadler-Morris, S., and Albert, P. (1987). Ontogeny of spatial navigation behaviors in the rat: dissociation of "proximal"- and "distal"-cue-based behaviors. *Behav. Neurosci.* 101, 62–73.

Sargolini, F., Fyhn, M., Hafting, T., McNaughton, B. L., Witter, M. P., Moser, M. B., and Moser, E. I. (2006). Conjunctive representation of position, direction, and velocity in entorhinal cortex. *Science* 312, 758–762.

Schenk, F. (1985). Development of place navigation in rats from weaning to puberty. *Behav. Neural Biol.* 43, 69–85.

Scott, R. C., Richard, G. R., Holmes, G. L., and Lenck-Santini, P. P. (2010). Maturational dynamics of hippocampal place cells in immature rats. *Hippocampus* 21, 346–353.

Skaggs, W. E., and McNaughton, B. L. (1998). Spatial firing properties of hippocampal CA1 populations in an environment containing two visually identical regions. *J. Neurosci.* 18, 8455–8466.

Solstad, T., Boccara, C. N., Kropff, E., Moser, M. B., and Moser, E. I. (2008). Representation of geometric borders in the entorhinal cortex. *Science* 322, 1865–1868.

Sreenivasan, S., and Fiete, I. (2011). Grid cells generate an analog error-correcting code for singularly precise neural computation. *Nat. Neurosci.* 14, 1330–1337.

Taube, J. S., Muller, R. U., and Ranck, J. B. Jr. (1990). Head-direction cells recorded from the postsubiculum in freely moving rats. II. Effects of environmental manipulations. *J. Neurosci.* 10, 436–447.

Tolman, E. C. (1948). Cognitive maps in rats and men. *Psychol. Rev.* 55, 189–208.

Welinder, P. E., Burak, Y., and Fiete, I. R. (2008). Grid cells: the position code, neural network models of activity, and the problem of learning. *Hippocampus* 18, 1283–1300.

Widloski, J., and Fiete, I. (2010). Spike time-dependent synaptic plasticity can organize a recurrent network to generate grid cell responses. *Soc. Neurosci. Abstr.* 100.4.

Wills, T. J., Cacucci, F., Burgess, N., and O'Keefe, J. (2010). Development of the hippocampal cognitive map in preweanling rats. *Science* 328, 1573–1576.

Zilli, E. A., and Hasselmo, M. E. (2010). Coupled noisy spiking neurons as velocity-controlled oscillators in a model of grid cell spatial firing. *J. Neurosci.* 30, 13850–13860.

**Conflict of Interest Statement:** The authors declare that the research was conducted in the absence of any commercial or financial relationships that could be construed as a potential conflict of interest.

*Received: 12 December 2011; accepted: 09 April 2012; published online: 27 April 2012.*

*Citation: Wills TJ, Barry C and Cacucci F (2012) The abrupt development of adult-like grid cell firing in the medial entorhinal cortex. Front. Neural Circuits* ***6****:21. doi: 10.3389/fncir.2012.00021*

frontiers in
NEURAL CIRCUITS

ORIGINAL RESEARCH ARTICLE
published: 01 March 2012
doi: 10.3389/fncir.2012.00008

# Ontogeny of neural circuits underlying spatial memory in the rat

***James A. Ainge*** [1] ***and Rosamund F. Langston*** [2] ***

[1] *School of Psychology, University of St. Andrews, St. Mary's Quad, St. Andrews, Fife, Scotland, UK*
[2] *Division of Neuroscience, Medical Research Institute, University of Dundee, Ninewells Hospital and Medical School, Dundee, Scotland, UK*

***Edited by:***
*Lisa M. Giocomo, Norwegian University of Science and Technology, Norway*

***Reviewed by:***
*Paul A. Dudchenko, University of Stirling, UK*
*Giorgio Ascoli, George Mason University, USA*

***Correspondence:**
*Rosamund F. Langston, Division of Neuroscience, Medical Research Institute, University of Dundee, Ninewells Hospital & Medical School, Dundee DD1 9SY, Scotland, UK.*
*e-mail: r.f.langston@dundee.ac.uk*

Spatial memory is a well-characterized psychological function in both humans and rodents. The combined computations of a network of systems including place cells in the hippocampus, grid cells in the medial entorhinal cortex and head direction cells found in numerous structures in the brain have been suggested to form the neural instantiation of the cognitive map as first described by Tolman in 1948. However, while our understanding of the neural mechanisms underlying spatial representations in adults is relatively sophisticated, we know substantially less about how this network develops in young animals. In this article we briefly review studies examining the developmental timescale that these systems follow. Electrophysiological recordings from very young rats show that directional information is at adult levels at the outset of navigational experience. The systems supporting allocentric memory, however, take longer to mature. This is consistent with behavioral studies of young rats which show that spatial memory based on head direction develops very early but that allocentric spatial memory takes longer to mature. We go on to report new data demonstrating that memory for associations between objects and their spatial locations is slower to develop than memory for objects alone. This is again consistent with previous reports suggesting that adult like spatial representations have a protracted development in rats and also suggests that the systems involved in processing non-spatial stimuli come online earlier.

**Keywords: hippocampus, memory and learning, postnatal development, entorhinal cortex, spatial representation, place cell, grid cell, head direction cell**

## INTRODUCTION

The ability of animals to internally represent external space and use this representation to guide navigation-based behavior was first suggested by Tolman in his proposal of the cognitive map theory in 1948 (Tolman, 1948; O'Keefe and Nadel, 1978). Since then a number of systems within the hippocampus and surrounding regions of the medial temporal lobe have been discovered which provide the basic building blocks that could support such a system. Place cells in the hippocampus (O'Keefe and Dostrovsky, 1971) combined with grid cells (Hafting et al., 2005), head direction cells (Taube et al., 1990; Sargolini et al., 2006) and border cells (Savelli et al., 2008; Solstad et al., 2008), which have been found in other areas of the medial temporal lobe, provide all the information that an animal would need to navigate efficiently within familiar environments. Some aspects of these systems have been extensively studied. A large amount of research has been carried out to examine the properties of place cells including how they respond to different familiar environments (Muller, 1996; Lever et al., 2002; Leutgeb et al., 2005a,b; Wills et al., 2005; Colgin et al., 2008), changes in physical characteristics of environments (Muller and Kubie, 1987; Bostock et al., 1991; O'Keefe and Burgess, 1996) and changes in cognitive demands within an environment (Wood et al., 2000; Ferbinteanu and Shapiro, 2003; Lee et al., 2006; Smith and Mizumori, 2006; Ainge et al., 2007a,b, 2012; Griffin et al., 2007). These studies have significantly enhanced our understanding of how place cells contribute to our ability to represent familiar spatial locations. Head direction cells have also been widely studied and their properties are well documented (for review see Taube, 2007). Grid cells and border cells have been discovered more recently and as such are much less well understood, although this situation is changing rapidly. However, a number of factors, such as the interdependence of these systems, remain to be addressed. Here we discuss a novel approach to this question, namely examining the ontogeny of the neural circuits for spatial representations. We present new data suggesting that the systems that support navigation and spatial memory come on line at similar points on the developmental timescale.

## ONTOGENY OF SPATIAL MEMORY

Following the discovery of place cells, much research was directed toward spatial memory and the mechanisms underlying it in adult rodents. However, relatively little research has examined how this type of memory develops in young animals. Those studies that have examined this development have used the same behavioral paradigms as used in adults, primarily the Morris water maze.

One of the most comprehensive studies of spatial memory in young rats was carried out by (Schenk, 1985) in which rats of different ages were trained to navigate to a hidden platform in the Morris water maze using either distal environmental cues

(place learning) or a proximal cue marking the location of the escape platform (cue and place learning). Rats began training at Postnatal day 21 (P21), P28, P35, P42, or as adults (P64) and were tested for 5 days. All age groups learned to escape from the pool more quickly when trained with the additional proximal cue compared to just using distal room cues, although all age groups learned the location of the escape platform in both the cue and place conditions. What was noticeable about the younger animals (P21 and P28 groups) was that if they were trained in the place only condition, they benefitted more from the later addition of a proximal cue than did older animals. Conversely, if they were trained with the additional proximal cue and this was later removed, their ability to find the hidden escape platform was impaired much more than that of older animals. These data imply that during the fourth and fifth postnatal weeks, rats are reliant on the presence of local visual cues in the environment to perform optimally, but after postnatal week 6, they are much less affected by the manipulation of the local environment and are capable of using solely distal environmental cues to navigate effectively.

Akers et al. (2007) examined the development of navigation-based on directional headings. In their study, P24 rats were trained using a place strategy to find a hidden platform in the Morris water maze and then their memory for this location was tested in a series of probe tests. During the probe tests the physical location of the water maze was changed in relation to the distal cues in the environment (which the rats had used to learn the task). This manipulation aimed to discover whether the rats would use the distal cues in the room to navigate to the trained platform position as an absolute location in space or whether they would use the directional heading information they had learned from their starting point in the previous pool location and swim to the same platform location relative to the pool walls and start point. The authors found that the weanling rats used directional heading to navigate to the platform location, ignoring the distal room cues.

Other studies have gone on to examine further the extent to which even younger rats can navigate using cued locations or adult like allocentric memory. These studies demonstrated that rats as young as P17 were able to learn to navigate to an escape platform marked by a proximal cue (equivalent to the "cue and place" condition of Schenk, 1985) but that rats at this age showed no learning in a place only condition (Rudy et al., 1987). Rats aged P21 however already showed significant learning of the location of the escape platform in the place only condition. This experiment did not use adult control animals for comparison so does not indicate when cue and place learning reach adult levels but does show a differential ontogeny of the two types of learning, with place learning developing later than cue learning. These findings were disputed by Brown and Whishaw (2000) whose findings indicated that both place and cue learning can be displayed in rats as early as P19 (Brown and Whishaw, 2000). They do, however, concede that their measures of place learning revealed lower levels of performance relative to cued learning, therefore supporting Schenk's (1985) data that younger animals are more reliant on proximal visual cues than distal environmental cues.

## ONTOGENY OF SPATIAL REPRESENTATIONS

Clearly rats' ability to learn and remember spatial locations is not present from birth but rather develops through adolescence into early adulthood. If place cells, grid cells and the other cell types in the medial temporal lobe are the critical mechanisms that underlie rats' ability to navigate and remember spatial locations then these should develop on a similar timescale to their spatial memory. In a recent study we addressed this issue by examining the timescale upon which place cells, grid cells, and head direction cells develop in very young rats (Langston et al., 2010). Rats typically start to explore their surroundings after they have opened their eyes on approximately P15. After this they start to make longer and more frequent journeys away from the nest to explore their external environment. This is consistent with the behavioral data which suggests that at the beginning of this exploration process (P17) rats have poor spatial memory but that this improves in the next 2–3 postnatal weeks. We used *in vivo* single unit electrophysiology to record place cells in the CA1 region of hippocampus, grid cells from MEC and head direction cells from presubiculum. By examining the timescale upon which these systems develop and comparing the spatial information that they convey with that conveyed by the adult system in the same environments we were able to see whether these systems develop on a timescale that is consistent with them being the critical mechanism underlying spatial memory. We were also able to address the interesting philosophical question of whether an understanding of space is an innate psychological capability or whether it develops with experience of the world. Finally we were able to ask questions about the hierarchy and interdependence of the place cell, grid cell, and head direction cell systems.

The results from our study are illustrated in **Figure 1**. Head direction cells were present in presubiculum in the very earliest recordings that were made (**Figure 1A**). These animals were 15 days old and had usually opened their eyes during the previous 24 h. The particularly noteworthy properties of these head direction cells were that they conveyed as much directional information as head direction cells recorded from adult rats in the same environment and that the preferred direction of firing was consistent across sessions. To examine consistency we examined head direction information in two 10 min sessions. The rat was removed from the box between sessions and so by correlating the head direction information between the sessions we were able to examine how consistently individual head direction cells represented a directional heading within a familiar environment. The results showed that rats have an adult like ability to remember a directional heading as soon as they open their eyes. While it remains a possibility that only a very small amount of visual experience was necessary to form this directional representation these data suggest that this psychological capability may be innate.

We then went on to look at place cells during the same developmental period. Place cells had some adult properties in the very young rats but other properties took longer to develop. As shown in **Figure 1**, place cells that had specific spatial firing patterns were present at the earliest time point that we were able to sample (P17; **Figure 1B**). These cells conveyed similar amounts of spatial information to place cells in adult rats in the same environment.

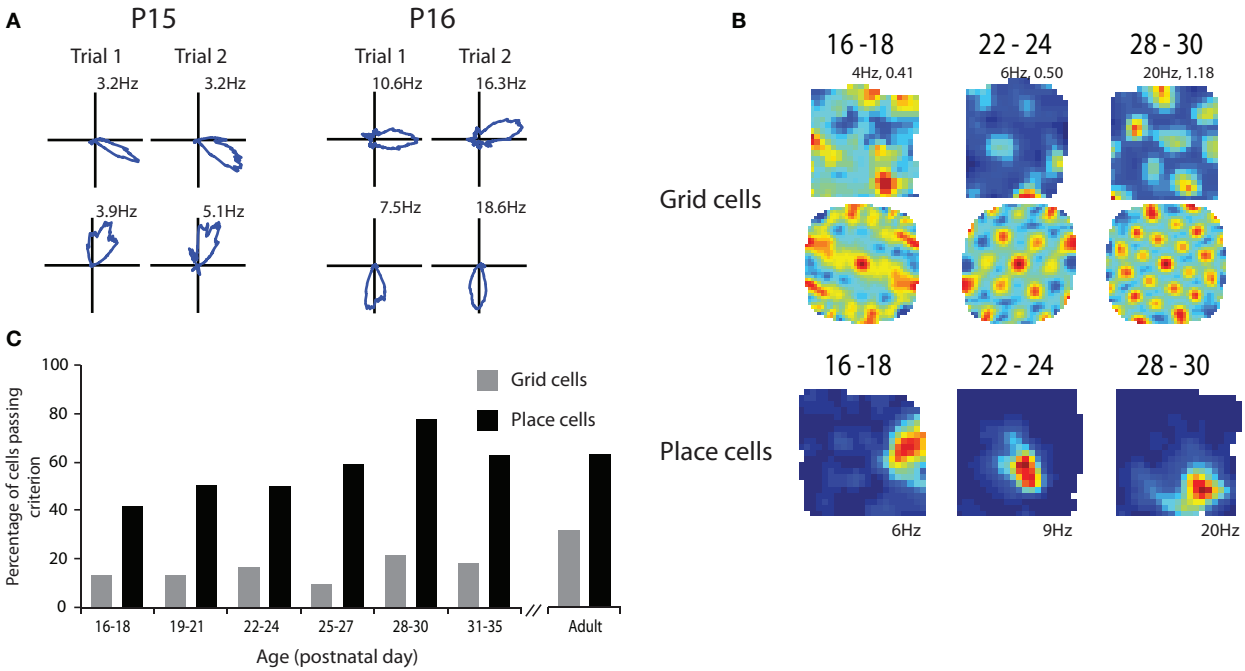


**FIGURE 1 | Spatial representations at the outset of navigational experience. (A)** Head direction cells show adult like directional coding and stability at P15. **(B)** Grid cells show grid like characteristics in their rate maps (top row) and spatial autocorrelations (middle row) from P16 to 18 but the regularity and specificity of the grid increases with age. Examples of adult like place cells from P16 to 18 (bottom row). **(C)** Percentage of cells passing criterion for being place and grid cells through development. Note that the proportion of both place and grid cells that pass the criterion increases with age. Adapted from Langston et al. (2010).

However, the proportion of cells that conveyed enough spatial information to satisfy our criterion for being place cells increased through the first 4–5 post natal weeks (**Figure 1C**). This suggests that the network takes some time to develop an adult like representation of space. When the consistency of place cell firing across sessions was examined it was again clear that while very young rats had some place cells that showed consistent firing location across trials the proportion of these cells increased to adult levels through the first 4–5 postnatal weeks. This finding is consistent with the studies showing that rats' use of allocentric cues from the environment to guide navigation is immature until at least the third or fourth postnatal week (Schenk, 1985; Rudy et al., 1987).

Finally we examined grid cell firing through the course of development. As with the other two cell types we examined it was clear from the earliest recordings that some cells with grid like properties were present at this very early stage of development (**Figure 1B**). However, when we measured how regular grid cell firing was it was clear that grid cell regularity increased throughout the first 4–5 weeks of postnatal development (**Figure 1B**). This was combined with an increase in the number of cells that had regular enough firing to pass our criterion for being a grid cell. As with the place cell data, grid cell consistency across sessions also increased across the first 4–5 postnatal weeks. These data suggest that while some grid like cells are present from a very early age the adult like grid cell representation takes a long time to develop. This seems to give a clear hierarchy of cell types within the hippocampal-entorhinal system. Head direction cells develop first followed by place cells and finally grid cells. This hierarchy would be consistent with some computational models which suggest that grid cells are formed from inputs from head direction cells and that their stability is reliant on projections from the place cell system in the hippocampus and information about environmental boundaries (Burgess et al., 2007; Hasselmo et al., 2007). However, at first glance these data appear to be at odds with other models that suggest that place cell firing patterns are derived from the spatial information in the grid cells (Solstad et al., 2006; Monaco and Abbott, 2011). Given that grid cells develop adult like properties relatively slowly it seems unlikely that they are the source of the spatial information needed to form adult like place cells. However, this interpretation may be somewhat simplistic. It is entirely conceivable that place cells could be formed from fairly coarse spatial information from grid cell like firing patterns such as those seen in the very early recordings. It is also the case that lesions of the hippocampus do not abolish grid cell firing in the MEC which suggests that grid cells are not reliant on place cell input (Fyhn et al., 2004) or can at least compensate for the absence of the majority of place cell input. Inactivation of place cells does, however, disrupt grid cell firing and in some cases cells that used to have grid like properties become head direction cells (Bonnevie et al., 2006). This would be consistent with the hypothesis that grid cells are formed by combining inputs from head direction cells and that the grid representation is stabilized by place cell input.

The fine-tuning of the spatial signal in the medial entorhinal cortex suggests that some properties of the system mature during the time period when the rat starts to explore its external surroundings. To attempt to identify these properties we went on to record from groups of 3–4 unconnected stellate cells in slices from littermates of the rats in the *in vivo* recording study at the same age. Spontaneous changes in the subthreshold membrane potentials were then examined and correlated across pairs of simultaneously recorded cells. At the early time points between P16–P21 there were relatively few pairs of cells with significantly correlated subthreshold changes in membrane potential. However, the proportion of cell pairs with significantly correlated subthreshold membrane potential changes increased to between 30% and 40% by P29. In contrast the strong inputs to MEC from presubiculum have adult like properties from 2 weeks of age. This suggests that the maturation of the grid cell signal in MEC is dependent on the intrinsic connectivity of MEC rather than just reflecting a maturation of its afferent connections.

Our data are largely consistent with other reports of spatial representations throughout the postnatal developmental period. Wills et al. (2010) reported similar findings in that directional firing properties were present at very early ages while place cells and grid cells develop more slowly in the third and fourth postnatal week. As in our study Wills et al. showed robust theta activity in the local field potential from the very earliest recordings although the frequency of the theta did increase significantly with age independently of running speed. Two other studies have examined place cells during development (Martin and Berthoz, 2002; Scott et al., 2011). These data are somewhat contrasting with our own and that of Wills et al. in that they suggest that place cells carry on developing for much longer. Indeed it was suggested that place cells do not fully mature until approximately P40–P45. The findings of Martin and Berthoz are based on very few cells and as such are hard to interpret as the variability in the sample is large. Scott et al., however, recorded from a large population of place cells across a range of ages. There is some agreement across studies in that all of the available data suggest that some properties of place cells (stability in particular) are relatively slow to mature. However, the data from Wills et al. combined with our own clearly demonstrate that place cells that provide adult like levels of spatial information are present from as young as P17 and indeed the spatial information content of the cells that pass criterion for being place cells does not increase with age.

## DIFFERENTIAL ONTOGENY OF OBJECT AND ASSOCIATIVE SPATIAL MEMORY IN THE JUVENILE RAT

These electrophysiology data have demonstrated that rudiments of the network of systems that support representations of external space are present in young rats at the outset of navigational experience. While some aspects of these systems have adult like qualities from the day that the rats open their eyes, other aspects take longer to mature and do not reach adult levels of specificity and stability until the fourth or fifth postnatal week. These data are consistent with studies showing that rats can navigate using direction information from very young ages but the ability to use allocentric spatial memory does not develop until after some experience of exploring the world. These studies have concentrated on spatial memory and navigation but the same neural systems have been suggested to have a critical role to play in more general memory processes, specifically episodic memory, in both humans and rats (Vargha-Khadem et al., 1997; Eichenbaum et al., 1999; Gelbard-Sagiv et al., 2008; Langston and Wood, 2010). It has been suggested that the role of the hippocampus is to bind features of events we have experienced, including spatial location, together to form episodic memories (Eichenbaum et al., 2011). We have recently addressed this issue using the developing rat as a model to examine whether memory for single features of an event (objects) is evident earlier in development than associative memory for multiple features of an event (object in location). The evidence reviewed so far suggests that rats' ability to represent space takes a while to reach adult levels of maturity and consequently we would predict that memory for objects within specific spatial locations will be equally slow to develop. Memory for object identity has been demonstrated to be dependent on the perirhinal cortex (Brown and Aggleton, 2001). As this memory is not dependent on the hippocampus or entorhinal cortex it remains a possibility that this type of memory will not show the same slow emergence during development.

Memory for specific features of an environment can be tested using the object recognition paradigm in which rats are presented with novel junk objects and given the opportunity to explore them. Rats have been shown to have a propensity to preferentially explore novel objects relative to familiar objects within a familiar environment (Ennaceur and Delacour, 1988). This task has been adapted in a number of ways to examine different types of memory and studies have shown that rodents will preferentially explore familiar objects within novel locations in preference to the same objects presented in familiar locations. This demonstrates a memory for the combination of object and spatial location in which it was presented (Dix and Aggleton, 1999). To examine memory for objects within spatial locations through development we used tests of object recognition and object in place recognition at different postnatal ages.

## MATERIALS AND METHODS

### SUBJECTS

Twelve Lister Hooded rats were used as subjects. Six rats were tested on postnatal day (P) 24 and six rats were tested on P30. After being weaned from their mother at P21 they were housed in single sex groups of 3–6, and kept on a 12 h light/12 h dark cycle ("sunrise" 5–6 a.m., "sunset" 5–6 p.m.). All rats had unrestricted access to food and water throughout the experiment. Compliance was ensured with national (Animals [Scientific Procedures] Act, 1986) and international (European Communities Council Directive of 24 November 1986 [86/609/EEC]) legislation governing the maintenance of laboratory animals and their use in scientific experiments.

### APPARATUS

All testing was carried out in a square arena measuring 70 × 70 cm with walls 40 cm in height. The arena was constructed of wood and painted with brown matt floor paint (Johnstone's, UK).

Two 3 cm strips of Dual-Lock (3M, UK) reusable adhesive were attached to the floor in the two locations in which objects were to be presented in the arena, in order to secure the objects to the arena floor and prevent the rats from displacing them. These locations were 10 cm from the box walls, at the north-west and north-east points. The arena was placed on a table approximately 50 cm high to allow ease of access for the experimenter. The arena was open to the room to allow the rats access to distal visual room cues. There were also two proximal cues situated above the north-west and north-east corners of the arena. These were a plastic plant pot approximately 10 cm diameter and 15 cm high and a plastic model of a tree approximately 15 cm high. These proximal cues were suspended from the ceiling of the testing room using string so that they hung with their bases just inside the top of the walls of the arena, with the aim that the rats could use them as visual cues but not physically reach them and interact with them. There was a holding container approximately 40 cm high with a floor area of 15 × 25 cm covered by a 2 cm layer of woodchip bedding (as used in the rats' home cages) which was used to house the rats in between the different stages of testing (described in the next section) placed in a corner of the room approximately 2 meters away from the testing arena. The room was lit by two fluorescent strip lights on the ceiling, approximately equidistant from the testing arena. There was a radio in the testing room which was kept on at a constant location, frequency and volume during testing with the aim of providing low-level background noise in the room to minimize the possibility of the rats becoming startled by noises in adjacent rooms and corridors.

Objects for exploration were collected from a variety of sources but had to fulfill the criteria of being easily cleaned, made from non-porous materials and having a suitable flat base where a reusable adhesive strip could be attached. Object size and shape varied but followed the guidelines that objects should either be larger than the rat in one or more dimensions or have complex surfaces/features. These guidelines were formed from previous experience and observations (unpublished) of rats interacting with three-dimensional objects.

## BEHAVIORAL TESTING

We shortened a previously published protocol for novel object recognition and associative spatial recognition memory testing which is normally carried out over 2 weeks in adult rats (Langston and Wood, 2010) into a 2 day protocol in order to be able to test specific time points during development in juvenile rats. All behavioral testing was carried out in the light phase between 8 a.m. and 5 p.m.

### *Handling*

Each rat was handled for three daily sessions prior to commencing the experiment. The aim of this stage was to familiarize the rats with the experimenter and the procedure of being removed from and replaced in the home cage. The handling consisted of the experimenter picking up, holding, manipulating and replacing each rat multiple times each day with the total contact time for each rat being around 2 min per day. For the older group of rats (P30), handling was carried out on P26, P27, and P28. For the younger group of rats (P24), handling was carried out on P20 (while the rats were still housed with their parents), P21 (weaning day) and P22.

### *Habituation*

One group habituation session and one individual habituation session were carried out on the day after the last handling session, when the rats were aged P29 (older group) and P23 (younger group). There were no objects in the arena during the habituation sessions.

The group habituation session was carried out in the morning and consisted of all rats who were housed in a cage together being placed into the testing arena together for 15 min. The arena was cleaned between cage groups using lemon scented cleaning wipes (Tesco, UK) to minimize distracting odors from the previous occupants of the arena and provide a consistent olfactory environment within the arena. The aim of this stage was to begin to familiarize the rats with the testing arena and to reduce stress by allowing them to remain with their cagemates. The individual habituation session was carried out in the afternoon of the same day. Each rat was individually placed into the testing arena for 5 min. The arena was cleaned between each rat using lemon scented cleaning wipes. The aim of this stage was to further familiarize the rats with the testing arena and give them the experience of being in the arena alone.

On both habituation sessions, the rats entered the testing arena from the south, and were placed in to the arena facing the south wall.

### *Novel object recognition*

The day after habituation (P30 and P24 for the older and younger groups respectively), the rats were tested on a standard novel object recognition task during the morning (**Figure 2A**, upper schematics). Each rat was removed from its home cage and placed in the holding container while the apparatus was configured. Two copies of the same object were cleaned with lemon scented cleaning wipes and attached at the north-west and north-east locations in the testing arena (**Figure 2A**, top left schematic). The rat was placed into the arena from the south side, facing the south wall, for the sample phase. The sample phase consisted of the rat being allowed to explore the two identical objects in the testing arena for 2 min Exploration was defined as the rat being within 2 cm of an object, directing its nose at the object and being involved in active exploration such as sniffing or whisking. Sitting on or next to an object without any signs of active exploration was not included. After 2 min the rat was removed from the arena at the same point from which it entered and placed in the holding container for a 1–2 min intertrial interval while the arena was reconfigured for the test phase. The floor and walls were cleaned and new objects were cleaned and placed in the arena. For the test phase one object was a third copy of the two objects seen in the sample phase while the other object was completely novel (**Figure 2A**, top right schematic, novel object marked by an arrow). The test phase was carried out using exactly the same procedures as the sample phase. After the test phase, the rat was returned to its home cage. The location and identity of the novel object was counterbalanced across each age group of rats.

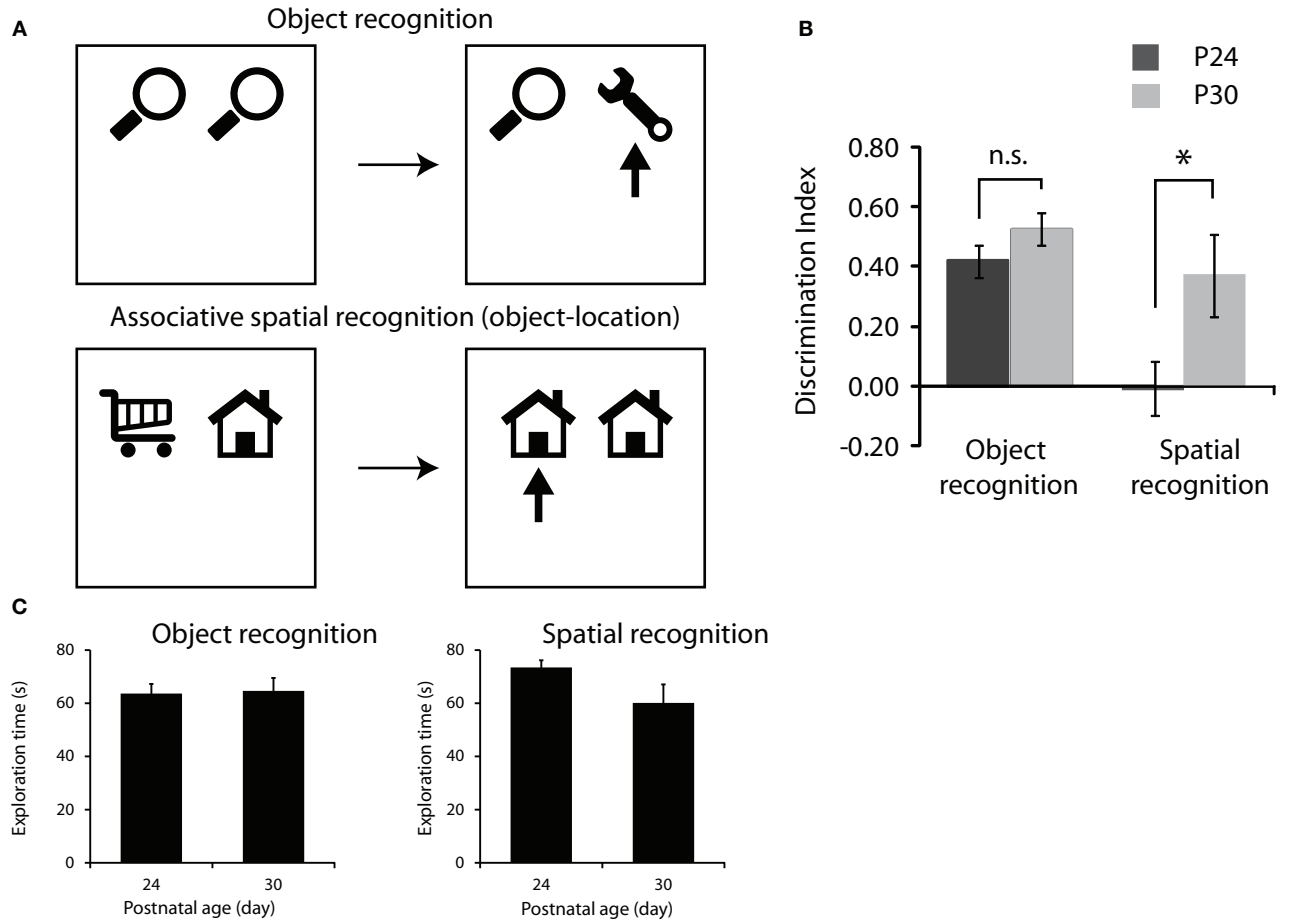


**FIGURE 2 | Development of memory for objects and objects in location. (A)** Object recognition protocol (top row) and associative spatial recognition protocol (bottom row). Both tasks consist of a sample phase where rats are presented with two objects to explore (left schematics) followed by a 2 min delay and a test phase (right schematics) where rats are given different combinations of objects to test memory for object or object in location. Arrows in test phase schematics represent the novel object or combination of object and location that we would expect the rats to preferentially explore. **(B)** Performance on the object recognition and associative spatial recognition tasks. P30 rats showed significantly greater preference for the novel object-location association than the P24 rats ($p < 0.05$) while the groups did not differ in standard object recognition performance. **(C)** Total exploration of the objects in the sample phase of the two tasks. Note no significant difference between the groups and the trend is toward P24 rats showing greater levels of exploration.

### *Associative spatial recognition (object-location task)*

In the afternoon of the same day as the novel object recognition task the rats were tested on an associative spatial recognition task. The procedure for the rats in this task was the same as that used in the novel object recognition task, except that the objects used in the sample and test phases were manipulated in the opposite way (**Figure 2A** lower schematics). During the sample phase, two different objects were present in the testing arena (**Figure 2A**, bottom left schematic). During the test phase, a further two copies of one of the objects from the sample phase were present. Thus, during the test phase, one of the objects was presented in the same location as it had been in the sample phase, whereas the other was in a location which had previously been occupied by a different object (**Figure 2A**, bottom right schematic, novel object-location configuration marked by an arrow). In this situation, both the objects and the two locations had been experienced during the sample phase, and so were familiar, but for one object, the object-location configuration was the same as in the sample phase, but for other it was novel. The location and identity of the novel configuration was counterbalanced across each age group of rats.

## DATA COLLECTION

An overhead black and white camera was used to monitor the movement of the rat around the testing arena. The video signal was fed into a TV monitor on the desk of the experimenter. A computer ran an in-house timing program whereby depression of a key on the computer keyboard would activate a timer. This was performed manually by the experimenter who observed the behavior of the rat via the TV monitor and recorded the amount of time the rat was engaged in exploration. Key presses activated timers which differentially timed exploration at the left and right objects. The raw data from sample and test phases were recorded as times that rats spent exploring the left and right objects. Video

files of all data were recorded on to a hard drive connected to the TV monitor so that a random selection of the tests could be rescored and checked for accuracy by an experimentally blind second analyst.

### DATA ANALYSIS

Data from the novel object recognition and associative spatial recognition tasks were analyzed in the same way. The raw exploration times at each object were converted into a discrimination index for each rat on each task using the formula *(time at novel − time at familiar)/(time at novel + time at familiar)* where novel refers to the novel object, or the novel configuration of object in place in the associative spatial recognition task, and familiar refers to the other object. A value of zero indicates no preference, whereas a positive value indicates preferential exploration of the novel configuration and a negative value indicates preferential exploration of the familiar configuration.

Statistical analyses of the discrimination index values were run in SPSS. A repeated measures ANOVA was performed with age group (P24 vs. P30) as the between subjects factor, task (object vs. spatial recognition) as the within subjects factor and discrimination index as the dependent variable. *Post hoc* tests (independent samples *t*-tests) were carried out to examine whether rats of different ages differed in their preference for the novel object (object recognition) or novel configuration of object and location (associative spatial recognition). Performance of each group was compared to chance level performance using 1-sample *t*-tests. Data collected during the sample phases of each task was also analyzed to examine the total amount of time spent exploring objects. Repeated measures ANOVA were performed for the sample and test phases of the tasks, with age group (P24 vs. P30) as the between subjects factor, task (object vs. spatial recognition) as the within subjects factor and total exploration time as the dependent variable.

## RESULTS

The main result is illustrated in **Figure 2B**. We found that at P24, rats could successfully perform the novel object recognition task but performed at chance levels on the associative spatial recognition task. By P30 however, rats could successfully perform both memory tasks. Repeated measures ANOVA showed significant main effects of both group [P24 vs. P30; $F(1, 10) = 10.84$, $p < 0.008$] and task [object recognition vs. associative spatial memory; $F(1, 10) = 8.79$, $p < 0.014$] and a significant group × task interaction [$F(1, 10) = 6.24$, $p < 0.032$]. *Post hoc* 1-sample *t*-tests revealed that rats of both ages spent significantly longer exploring the novel object than would be expected by chance ($p < 0.05$) in the object recognition task and that preference for the novel object did not differ between P24 and P30. In the associative spatial recognition task P30 rats showed a significantly greater preference for the novel configuration of object in location than the P24 rats [$t(10) = -3.263, p < 0.009$]. P30 rats spent significantly longer exploring the novel configuration of object and location than would be expected by chance while the P24 rats' preference for the novel configuration did not differ from chance.

In order to check whether differences in memory performance (discrimination index) between P24 and P30 could be explained by variation in baseline exploratory levels, the total amounts of exploration in both the sample and test phases of each task were analyzed using repeated measures ANOVA. Analysis of both sample and test phase data indicated no significant main effect of task or group and no task × group interaction (**Figure 2C**).

## DISCUSSION

In summary, rats of both ages showed a preference for exploring the novel object in the standard test of object recognition. Clearly even young rats are capable of remembering objects that they have previously encountered over short periods of time. Rats at P30 also showed a preference for the copy of the object in the novel location in the associative spatial memory test. These rats showed a clear memory for the association between object and spatial location that they saw in the sample phase. However, P24 rats showed no preference for either object in the associative spatial memory test suggesting that they have no memory for where they have previously encountered familiar objects. These data fit with previous data in that they suggest that P24 rats do not have a fully functioning representation of external space into which event information, such as objects encountered, can be incorporated. By P30, however, rats can remember where familiar objects have been previously encountered suggesting that they do have a spatial framework that allows them to remember where they were when they encountered specific stimuli. One potential caveat is that young rats might show generally lower levels of interaction with the objects due to fatigue, anxiety, or lack of motivation. However, as illustrated in **Figure 2C** the P24 rats actually showed more total exploration of the objects than the P30 rats, although this difference was not significant. This argues against the lack of novelty preference being due to non-mnemonic factors such as fatigue or lack of motivation.

Interestingly these data are not consistent with a previous study of this type of memory in adolescent mice. Ricceri et al. (2000) tested mice at 18, 28, 46, and 90 days old to see whether they could remember familiar objects in unfamiliar locations. Surprisingly it was reported that mice could not remember this form of associative spatial memory until they were 90 days old. These data are not consistent either with the current data or the studies examining navigation and spatial memory reviewed in the introduction This suggests that either mice develop spatial memory much later than rats or that the exact protocol used in this study is not sensitive enough to detect spatial memory at younger ages. Ricceri et al. presented mice with four objects at a time, some of which were replaced and some of which moved position between trials. This placed a much greater memory load on the system and as such the delay in associative spatial memory may have been due to task difficulty rather than a difference in the fundamental mechanisms supporting spatial memory across species. The data we have reviewed present a consistent picture that some ability to internally represent external space is present in rats even before they have any navigational experience of the world. This is consistent with behavioral data suggesting that rats can use simple navigational strategies to solve spatial memory tasks even at very young ages (P17). However, adult like representations of space throughout the hippocampal-entorhinal network do not develop until the fourth or fifth postnatal week. Again this is consistent

with behavioral data showing that rats do not learn to solve allocentric spatial memory tasks based on distal visual cues until later in development (4 weeks postnatal). We have also presented data that suggests that rats' ability to bind features of events or episodes that they have experienced into a spatial framework also takes some time to develop. This memory is present in P30 rats but absent in rats aged P24.

The current data combined with the previous electrophysiology and behavior studies begin to elucidate the timescale upon which spatial representations develop. These types of studies are important for a number of reasons. Philosophers have debated for hundreds of years whether or not our ability to represent external space is innate or must be learned through experience. This longstanding debate can be captured by contrasting two philosophical schools of thought; rationalism and empiricism. Rationalists, such as Immanuel Kant, suggest that our understanding of concepts such as spatial representation go beyond that which can be gained from sensory experience. Kant argued that our sense of time and space are innate constraints of thought rather than the result of experience of the world (Kant, 1781). This view is at odds with empiricists, such as David Hume, who argue that all of our knowledge and concepts come through experience (Hume, 1777). While this oversimplified explanation does not do justice to the philosophical complexities of the arguments it does demonstrate that our ability to internally represent external space has been a controversial subject for many years. In recent years modern neuroscience techniques have allowed us to address these issues empirically for the first time.

While these extreme views are interesting from a philosophical perspective, one other possibility is that some aspects of our neural representation of space are present at birth but that these mature with experience to an adult level of complexity. Assuming that the system undergoes some kind of improvement or refinement during development, then understanding the timescale upon which this happens is of importance for many reasons. Creating age appropriate models for basic science is one of these. One of the key milestones in systems neuroscience research has been the discovery and examination of long-term potentiation (LTP) as a neural mechanism underlying learning and memory (Bliss and Lomo, 1973). LTP has been studied extensively in many neural systems and the detailed molecular mechanisms underlying it are now well understood (Martin et al., 2000; Malenka and Bear, 2004). However, one aspect of much of this research that is problematic is that the animals from which the slices are taken are very young, typically 2–3 weeks of age (McCutcheon and Marinelli, 2009). The reason for this is that recording from brain slices taken from older animals has proved to be technically challenging with stable electrophysiological signals difficult to isolate and maintain. Consequently much of our knowledge of the mechanism that is widely cited as the molecular basis of memory comes from the brains of very young animals and yet this is used to make predictions about the learning and memory capabilities of adult animals. Given the problems of recording from slices taken from adult animals, one way of reconciling this problem is to examine the behavioral and psychological capabilities of very young animals. If young animals are capable of adult like learning and memory then the study of the molecular mechanisms in slices taken from young animals is a valid experimental approach. In contrast if very young animals are incapable of learning new information in an adult like manner then this discrepancy in the literature must be addressed.

It is also interesting to characterize the time course of the development of spatial representations and the cognitive map in terms of developmental disorders. There are a number of clinical conditions involving abnormalities of learning and memory during childhood including autism, attention deficit hyperactivity disorder, schizophrenia, developmental amnesia, and Down syndrome. In creating animal models to study these disorders we need to take into consideration the ages of the human patients at onset of the disorders we wish to study and therefore the equivalent ages of our animal models. Many animal models of childhood or developmental diseases are modeled in adult animals. This approach may miss crucial information regarding the changes occurring during development which potentially contribute to these disorders and putative therapeutic targets may consequently go undiscovered.

## USING THE POWER OF YOUTH TO RESTORE THE WISDOM OF OLD AGE

Another very interesting reason to characterize the ontogeny of spatial representations is that it may be possible to use development as a tool to investigate the cellular and network mechanisms underlying certain types of learning and memory. We propose that an ideal system in which to examine spatial memory, for example, is one in which you can study an individual organism in a longitudinal fashion at time points before and after which the organism has acquired the capability that you want to study. It would then be possible to define a critical time window in which a particular memory capability develops and then study the neural mechanisms during that window in order to define what properties of the network are changing. This approach allows researchers to characterize the critical rate limiting steps in development and correlate these neural mechanisms with learning and memory capabilities. The majority of research that examines critical mechanisms underlying psychological function involves producing lesions or temporary pharmacological inactivations in the brain to examine functional deficits. However, this approach is not ideal as the system is damaged and the level of compensation from other networks is hard to quantify. By using the developing rat as a model it is possible to examine these functions in a healthy brain and to use a longitudinal, within subjects design. The search for critical mechanisms underlying spatial memory is particularly important as it is a component of episodic memory, deficits in which are a key early symptom of Alzheimer's disease and other neurodegenerative disorders (Salmon and Bondi, 2009). Discovering the critical networks and mechanisms underlying formation of episodic memory would provide putative therapeutic targets for disorders in later life.

## ACKNOWLEDGMENTS

This research was supported by a Tenovus small project grant to RFL. The authors would like to thank Ms. Frances R. Butterworth, a Carnegie Vacation Scholarship student in the laboratory of Rosamund F. Langston, for assistance with behavioral data collection.

## REFERENCES


Ainge, J. A., Tamosiunaite, M., Worgotter, F., and Dudchenko, P. A. (2012). Hippocampal place cells encode intended destination, and not a discriminative stimulus, in a conditional T-maze task. *Hippocampus* 22, 534–543.

Ainge, J. A., Tamosiunaite, M., Woergoetter, F., and Dudchenko, P. A. (2007a). Hippocampal CA1 place cells encode intended destination on a maze with multiple choice points. *J. Neurosci.* 27, 9769–9779.

Ainge, J. A., van der Meer, M. A., Langston, R. F., and Wood, E. R. (2007b). Exploring the role of context-dependent hippocampal activity in spatial alternation behavior. *Hippocampus* 17, 988–1002.

Akers, K. G., Candelaria, F. T., and Hamilton, D. A. (2007). Preweanling rats solve the Morris water task via directional navigation. *Behav. Neurosci.* 121, 1426–1430.

Bliss, T. V., and Lomo, T. (1973). Long-lasting potentiation of synaptic transmission in the dentate area of the anaesthetized rabbit following stimulation of the perforant path. *J. Physiol.* 232, 331–356.

Bonnevie, T., Fyhn, M., Hafting, T., Moser, M. B., and Moser, E. I. (2006). Misalignment of entorhinal grid fields after hippocampal inactivation. *Society for Neuroscience Abstracts*, 68.1.

Bostock, E., Muller, R. U., and Kubie, J. L. (1991). Experience-dependent modifications of hippocampal place cell firing. *Hippocampus* 1, 193–205.

Brown, M. W., and Aggleton, J. P. (2001). Recognition memory: what are the roles of the perirhinal cortex and hippocampus? *Nat. Rev. Neurosci.* 2, 51–61.

Brown, R. W., and Whishaw, I. Q. (2000). Similarities in the development of place and cue navigation by rats in a swimming pool. *Dev. Psychobiol.* 37, 238–245.

Burgess, N., Barry, C., and O'Keefe, J. (2007). An oscillatory interference model of grid cell firing. *Hippocampus* 17, 801–812.

Colgin, L. L., Moser, E. I., and Moser, M. B. (2008). Understanding memory through hippocampal remapping. *Trends Neurosci.* 31, 469–477.

Dix, S. L., and Aggleton, J. P. (1999). Extending the spontaneous preference test of recognition: evidence of object-location and object-context recognition. *Behav. Brain Res.* 99, 191–200.

Eichenbaum, H., Dudchenko, P. A., Wood, E. R., Shapiro, M. L., and Tanila, H. (1999). The hippocampus, memory, and place cells: is it spatial memory or a memory space? *Neuron* 23, 209–226.

Eichenbaum, H., Sauvage, M., Fortin, N., Komorowski, R., and Lipton, P. (2011). Towards a functional organization of episodic memory in the medial temporal lobe. *Neurosci. Biobehav. Rev.* Jul 23 [Epub ahead of print].

Ennaceur, A., and Delacour, J. (1988). A new one-trial test for neurobiological studies of memory in rats. 1: behavioral data. *Behav. Brain Res.* 31, 47–59.

Ferbinteanu, J., and Shapiro, M. L. (2003). Prospective and retrospective memory coding in the hippocampus. *Neuron* 40, 1227–1239.

Fyhn, M., Molden, S., Witter, M. P., Moser, E. I., and Moser, M. B. (2004). Spatial representation in the entorhinal cortex. *Science* 305, 1258–1264.

Gelbard-Sagiv, H., Mukamel, R., Harel, M., Malach, R., and Fried, I. (2008). Internally generated reactivation of single neurons in human hippocampus during free recall. *Science* 322, 96–101.

Griffin, A. L., Eichenbaum, H., and Hasselmo, M. E. (2007). Spatial representations of hippocampal CA1 neurons are modulated by behavioral context in a hippocampus-dependent memory task. *J. Neurosci.* 27, 2416–2423.

Hafting, T., Fyhn, M., Molden, S., Moser, M. B., and Moser, E. I. (2005). Microstructure of a spatial map in the entorhinal cortex. *Nature* 436, 801–806.

Hasselmo, M. E., Giocomo, L. M., and Zilli, E. A. (2007). Grid cell firing may arise from interference of theta frequency membrane potential oscillations in single neurons. *Hippocampus* 17, 1252–1271.

Hume, D. (1777). *Inquiries Concerning Human Understanding and Concerning the Principles of Morals*. Oxford: Clarendon Press.

Kant, I. (1781). *Kritik Der Reinen Vernunft*. Riga, Latvia: Hartknoch.

Langston, R. F., Ainge, J. A., Couey, J. J., Canto, C. B., Bjerknes, T. L., Witter, M. P., Moser, E. I., and Moser, M. B. (2010). Development of the spatial representation system in the rat. *Science* 328, 1576–1580.

Langston, R. F., and Wood, E. R. (2010). Associative recognition and the hippocampus: differential effects of hippocampal lesions on object-place, object-context and object-place-context memory. *Hippocampus* 20, 1139–1153.

Lee, I., Griffin, A. L., Zilli, E. A., Eichenbaum, H., and Hasselmo, M. E. (2006). Gradual translocation of spatial correlates of neuronal firing in the hippocampus toward prospective reward locations. *Neuron* 51, 639–650.

Leutgeb, S., Leutgeb, J. K., Barnes, C. A., Moser, E. I., McNaughton, B. L., and Moser, M. B. (2005a). Independent codes for spatial and episodic memory in hippocampal neuronal ensembles. *Science* 309, 619–623.

Leutgeb, S., Leutgeb, J. K., Moser, M. B., and Moser, E. I. (2005b). Place cells, spatial maps and the population code for memory. *Curr. Opin. Neurobiol.* 15, 738–746.

Lever, C., Wills, T., Cacucci, F., Burgess, N., and O'Keefe, J. (2002). Long-term plasticity in hippocampal place-cell representation of environmental geometry. *Nature* 416, 90–94.

Malenka, R. C., and Bear, M. F. (2004). LTP and LTD: an embarrassment of riches. *Neuron* 44, 5–21.

Martin, P. D., and Berthoz, A. (2002). Development of spatial firing in the hippocampus of young rats. *Hippocampus* 12, 465–480.

Martin, S. J., Grimwood, P. D., and Morris, R. G. (2000). Synaptic plasticity and memory: an evaluation of the hypothesis. *Annu. Rev. Neurosci.* 23, 649–711.

McCutcheon, J. E., and Marinelli, M. (2009). Age matters. *Eur. J. Neurosci.* 29, 997–1014.

Monaco, J. D., and Abbott, L. F. (2011). Modular realignment of entorhinal grid cell activity as a basis for hippocampal remapping. *J. Neurosci.* 31, 9414–9425.

Muller, R. U. (1996). A quarter of a century of place cells. *Neuron* 17, 979–990.

Muller, R. U., and Kubie, J. L. (1987). The effects of changes in the environment on the spatial firing of hippocampal complex-spike cells. *J. Neurosci.* 7, 1951–1968.

O'Keefe, J., and Burgess, N. (1996). Geometric determinants of the place fields of hippocampal neurons. *Nature* 381, 425–428.

O'Keefe, J., and Dostrovsky, J. (1971). The hippocampus as a spatial map. Preliminary evidence from unit activity in the freely moving rat. *Brain Res.* 34, 171–175.

O'Keefe, J., and Nadel, L. (1978). *The Hippocampus as a Cognitive Map*. New York: Oxford University Press.

Ricceri, L., Colozza, C., and Calamandrei, G. (2000). Ontogeny of spatial discrimination in mice: a longitudinal analysis in the modified open-field with objects. *Dev. Psychobiol.* 37, 107–118.

Rudy, J. W., Stadler-Morris, S., and Albert, P. (1987). Ontogeny of spatial navigation behaviors in the rat: dissociation of "proximal"- and "distal"-cue-based behaviors. *Behav. Neurosci.* 101, 62–73.

Salmon, D. P., and Bondi, M. W. (2009). Neuropsychological assessment of dementia. *Annu. Rev. Psychol.* 60, 257–282.

Sargolini, F., Fyhn, M., Hafting, T., McNaughton, B. L., Witter, M. P., Moser, M. B., and Moser, E. I. (2006). Conjunctive representation of position, direction, and velocity in entorhinal cortex. *Science* 312, 758–762.

Savelli, F., Yoganarasimha, D., and Knierim, J. J. (2008). Influence of boundary removal on the spatial representations of the medial entorhinal cortex. *Hippocampus* 18, 1270–1282.

Schenk, F. (1985). Development of place navigation in rats from weaning to puberty. *Behav. Neural Biol.* 43, 69–85.

Scott, R. C., Richard, G. R., Holmes, G. L., and Lenck-Santini, P. P. (2011). Maturational dynamics of hippocampal place cells in immature rats. *Hippocampus* 21, 347–353.

Smith, D. M., and Mizumori, S. J. (2006). Hippocampal place cells, context, and episodic memory. *Hippocampus* 16, 716–729.

Solstad, T., Boccara, C. N., Kropff, E., Moser, M. B., and Moser, E. I. (2008). Representation of geometric borders in the entorhinal cortex. *Science* 322, 1865–1868.

Solstad, T., Moser, E. I., and Einevoll, G. T. (2006). From grid cells to place cells: a mathematical model. *Hippocampus* 16, 1026–1031.

Taube, J. S. (2007). The head direction signal: origins and sensory-motor integration. *Annu. Rev. Neurosci.* 30, 181–207.

Taube, J. S., Muller, R. U., and Ranck, J. B. (1990). Head-direction cells recorded from the postsubiculum in freely moving rats. I. Description and quantitative analysis. *J. Neurosci.* 10, 420–435.

Tolman, E. C. (1948). Cognitive maps in rats and men. *Psychol. Rev.* 55, 189–208.

Vargha-Khadem, F., Gadian, D. G., Watkins, K. E., Connelly, A., Van Paesschen, W., and Mishkin, M. (1997). Differential effects of early hippocampal pathology on episodic and semantic memory. *Science* 277, 376–380.

Wills, T. J., Cacucci, F., Burgess, N., and O'Keefe, J. (2010). Development of the hippocampal cognitive map in preweanling rats. *Science* 328, 1487–1488.

Wills, T. J., Lever, C., Cacucci, F., Burgess, N., and O'Keefe, J. (2005). Attractor dynamics in the hippocampal representation of the local environment. *Science* 308, 873–876.

Wood, E. R., Dudchenko, P. A., Robitsek, R. J., and Eichenbaum, H. (2000). Hippocampal neurons encode information about different types of memory episodes occurring in the same location. *Neuron* 27, 623–633.

**Conflict of Interest Statement:** The authors declare that the research was conducted in the absence of any commercial or financial relationships that could be construed as a potential conflict of interest.

*Received: 10 December 2011; accepted: 17 February 2012; published online: 01 March 2012.*

*Citation: Ainge JA and Langston RF (2012) Ontogeny of neural circuits underlying spatial memory in the rat. Front. Neural Circuits* ***6****:8. doi: 10.3389/fncir.2012.00008*